

Lecture Notes in Bioengineering

Doraiswami Ramkrishna
Subhabrata Sengupta
Sudipta Dey Bandyopadhyay
Avijit Ghosh *Editors*

Advances in Bioprocess Engineering and Technology

Select Proceedings ICABET 2020

 Springer

Lecture Notes in Bioengineering

Advisory Editors

Nigel H. Lovell, Graduate School of Biomedical Engineering, University of New South Wales, Kensington, NSW, Australia

Luca Oneto, DIBRIS, Università di Genova, Genova, Italy

Stefano Piotto, Department of Pharmacy, University of Salerno, Fisciano, Italy

Federico Rossi, Department of Earth, University of Salerno, Fisciano, Siena, Italy

Alexei V. Samsonovich, Krasnow Institute for Advanced Study, George Mason University, Fairfax, VA, USA

Fabio Babiloni, Department of Molecular Medicine, University of Rome Sapienza, Rome, Italy

Adam Liwo, Faculty of Chemistry, University of Gdansk, Gdansk, Poland

Ratko Magjarevic, Faculty of Electrical Engineering and Computing, University of Zagreb, Zagreb, Croatia

Lecture Notes in Bioengineering (LNBE) publishes the latest developments in bioengineering. It covers a wide range of topics, including (but not limited to):

- Bio-inspired Technology & Biomimetics
- Biosensors
- Bionanomaterials
- Biomedical Instrumentation
- Biological Signal Processing
- Medical Robotics and Assistive Technology
- Computational Medicine, Computational Pharmacology and Computational Biology
- Personalized Medicine
- Data Analysis in Bioengineering
- Neuroengineering
- Bioengineering Ethics

Original research reported in proceedings and edited books are at the core of LNBE. Monographs presenting cutting-edge findings, new perspectives on classical fields or reviewing the state-of-the art in a certain subfield of bioengineering may exceptionally be considered for publication. Alternatively, they may be redirected to more specific book series. The series' target audience includes advanced level students, researchers, and industry professionals working at the forefront of their fields.

Indexed by SCOPUS and Springerlink. The books of the series are submitted for indexing to Web of Science.

More information about this series at <http://www.springer.com/series/11564>

Doraiswami Ramkrishna · Subhabrata Sengupta ·
Sudipta Dey Bandyopadhyay · Avijit Ghosh
Editors

Advances in Bioprocess Engineering and Technology

Select Proceedings ICABET 2020

 Springer

Editors

Doraiswami Ramkrishna
Department of Chemical Engineering
Purdue University
West Lafayette, Indiana, USA

Subhabrata Sengupta
Former Scientist
Indian Institute of Chemical Biology (IICB)
Kolkata, India

Sudipta Dey Bandyopadhyay
Department of Biotechnology
Heritage Institute of Technology
Kolkata, India

Avijit Ghosh
Department of Chemical Engineering
Heritage Institute of Technology
Kolkata, India

ISSN 2195-271X

Lecture Notes in Bioengineering

ISBN 978-981-15-7408-5

<https://doi.org/10.1007/978-981-15-7409-2>

ISSN 2195-2728 (electronic)

ISBN 978-981-15-7409-2 (eBook)

© Springer Nature Singapore Pte Ltd. 2021

This work is subject to copyright. All rights are reserved by the Publisher, whether the whole or part of the material is concerned, specifically the rights of translation, reprinting, reuse of illustrations, recitation, broadcasting, reproduction on microfilms or in any other physical way, and transmission or information storage and retrieval, electronic adaptation, computer software, or by similar or dissimilar methodology now known or hereafter developed.

The use of general descriptive names, registered names, trademarks, service marks, etc. in this publication does not imply, even in the absence of a specific statement, that such names are exempt from the relevant protective laws and regulations and therefore free for general use.

The publisher, the authors and the editors are safe to assume that the advice and information in this book are believed to be true and accurate at the date of publication. Neither the publisher nor the authors or the editors give a warranty, expressed or implied, with respect to the material contained herein or for any errors or omissions that may have been made. The publisher remains neutral with regard to jurisdictional claims in published maps and institutional affiliations.

This Springer imprint is published by the registered company Springer Nature Singapore Pte Ltd. The registered company address is: 152 Beach Road, #21-01/04 Gateway East, Singapore 189721, Singapore

Preface

Bioprocess engineering and technology is primarily associated with the commercial application of living organisms on large scale. Commercialization of biological discoveries requires substantial engineering work. Bioprocess engineering and technology is an interdisciplinary subject which brings disciplines of biology and engineering on the same platform. A large number of disciplines like microbiology, genetics, chemistry, biochemistry, engineering mathematics, modelling and simulation and computer science have contributed significantly in achieving the target of delivering product and process to the society. In this spectrum, a large number of research findings are accumulating every day from all these disciplines. Many of these findings require proper scrutiny to find their place to the initiative for bioprocess development for future commercialization. The collection of data for scrutiny and review are primarily required by the experts for any further promotion of bioprocess to the next phase. It is true that global young generation is trying hard to generate data in this domain and aimed at the production of biopharmaceuticals, bio fuels and, development of biosensors, pollution control technologies, such as, mineral recovery, bioremediation of soil and water and so on. With the objective to assemble these data, Heritage Institute of Technology, Kolkata (HITK), India, hosted the 1st International Conference on Advances in Bioprocess Engineering and Technology on 20–22 January, 2016. The grand success in the effort tempted the institute to arrange second such conference: 2nd International Conference on Advances in Bioprocess Engineering and Technology on 20–22 January, 2020 (ICABET 2020). Department of Biotechnology and Department of Chemical Engineering of HITK successfully organized the conference. The conference aimed to highlight areas like fermentation technology and bioreactor; environment and agriculture; food, pharmaceutical and health care; sustainable energy; nanomaterials and nanotechnology. Each session was well participated, particularly by young generation of researchers. Many of them got the opportunity to meet and discuss

their research with expert seniors. I personally appreciate the objective and success of the conference and hope continuation of such conference in future with balance participation of senior and junior researchers.

Kolkata, India

Subhabrata Sengupta

Introduction

Biotechnology covers a broad segment of science and technology and commands worldwide research because of its potential impact on the improvement of quality of life. A bioprocess is the technology to obtain desired product or process with the help of living cells or their component or products like enzymes. Bioprocess engineering is a sub discipline within Biotechnology that is necessary for the translation of discoveries of this field into usable products, and processes deliverable to the society. Bioprocess technology was initiated in the first half of 20th century with the production of penicillin and citric acid by classical fermentation processes and later on fortified significantly by recombinant DNA technology, plant and mammalian cell culture techniques. Nano biotechnology, as a promising technology is also progressing, classically for cancer targeted drug development. Bioprocessing today became a major part of biotechnology domain involved in the production of huge number of human health care products, as well as products for agriculture, industries, and food processing. Apart from these, development of biosensors, detoxification of environmental pollutants, biofuel generation are major focused research in this domain.

In earlier days putting the biology in bottle took much longer time. It took almost 15 years for penicillin from discovery to application as drug. Glucose isomerase for high fructose syrup commercialization took 10 years or more. Products, that are now under development, demands novel bioprocess techniques which is more efficient and more economic, so as to reduce the time gap between discovery and application. Bioprocess Engineering by its very nature is interdisciplinary subject and thus requires more coherent approach to cross disciplinary research and education. Although bioprocess industries have successfully translated many basic research in biological science and molecular biology into valuable products, but more intense research is needed for the development of more effective biopharmaceuticals for many catastrophic diseases like cancer, heart diseases and kidney diseases. A second generation products should be available whose price-cost difference is low. Bioprocess for the generation of alternative energy source like ethanol, biohydrogen, biomethane, bioelectricity from renewable biomass should reach to consumer within a reasonable time period at affordable cost. Utilization of

renewable resources for production of renewable energy through bioprocess route has tremendous impact on lowering our energy budget. At the juncture of novel process development, the cost effectiveness and cost input for a bioprocess should be given importance for successful delivery to the society. Bioprocess engineering must carefully consider more economic route for the production, not only for new products but also for older products so that the larger fraction of society gets benefitted.

The major challenge in achieving optimal benefit from the technology is to bring about the synergistic combination of skills of biology, biotechnology, chemical engineering, bioprocess engineering and computer science on a single platform. In future, nanotechnology and information technology will see substantial progress and expansion of bioprocess engineering and technology.

Finally, it may be added that engineering in the traditional sense of scale up and cost reduction is not enough. Significant advances and efforts are required for implementing new ideas other than traditional pathways. An academic policy maker should take more responsibility of educating young generation of students in different cross fields of bioprocess engineering in a comprehensive manner from a single platform.

Contents

Fermentation Technology and Bioreactor

Isolation of Cellulose-Degrading Bacteria and to Use Their Cellulolytic Potential for Production of Bioethanol from Paper Waste	3
Sayan Chatterjee, Kalyani Tripathi, and Ram Singh Purty	

Bioconversion of Mandarin Orange Peels by <i>Aspergillus oryzae</i> and <i>Penicillium</i> sp.	13
Debarati Roy and Jayati Bhowal	

Utilization of Low-Cost Fatty Acid Sources by Bacterial Isolate for Improved Production of Valuable Prodigiosin	21
Dalia Dasgupta Mandal, Subhasree Majumdar, Sovan Dey, Sourav Dutta, and Tamal Mandal	

Simplified Detection of Serotonin by FET-Based Sensor	29
Koel Sinha, Rabindranath Majumder, and Chitragada Das Mukhopadhyay	

Production of Lactose-Free Cheese Using Partially Purified β-Galactosidase from <i>Enterobacter aerogenes</i> st KCTC2190	39
Manisha Maity, D. K. Bhattacharyya, and Jayati Bhowal	

Fungal Production of Single Cell Oil Using Defatted Oilseed Meals as Feedstock	51
Ruma Dutta, D. K. Bhattacharyya, and Jayati Bhowal	

Food, Pharmaceuticals and Health Care

Synergistic Effect of Quercetin with Allicin from the Ethanolic Extract of <i>Allium cepa</i> as a Potent AntiQuorum Sensing and Anti-Biofilm Agent Against Oral Biofilm	69
Dibyajit Lahiri, Moupriya Nag, Bandita Dutta, Sudipta Dash, Shreyasi Ghosh, and Rina Rani Ray	

Development of Micellized Antimicrobial Thiosulfinate: A Contemporary Way of Drug Stability Enhancement	83
Souptik Bhattacharya, Deepanjali Gupta, Dwaipayan Sen, and Chiranjib Bhattacharjee	
Production and Characterization of Functional Lipid and Micronutrient Rich Health Beneficial Mayonnaise	91
Satarupa Ghosh, D. K. Bhattacharyya, and Minakshi Ghosh	
Computer-Aided Drug Design Against Dopamine D2 Receptor for Antischizophrenia Drug Development.	101
Dipankar Chaudhuri and Pradipta Bhattacharjee	
Biodegradation of Dyes by Laccase from Isolated Strain <i>Aspergillus flavus</i> PUF5	109
Priyanka Ghosh and Uma Ghosh	
Effect of <i>Saccharomyces cerevisiae</i> Fermentation Process on the Phenolic Content, Flavonoid Content and Antioxidant Properties of Flaxseeds.	119
Saheli Ghosal, D. K. Bhattacharyya, and Jayati Bhowal	
Study on the Antioxidant and Cytotoxic Properties of Pyocyanin Extracted from <i>Pseudomonas aeruginosa</i>	133
Sucharita Sengupta and Jayati Bhowal	
Effect of Metabolic Risk Factors, Gene Polymorphisms and Family History Among T2DM Population in Asian Indians.	143
Plaban Chaudhuri, Riju Ghosh, Mithun Das, Indrani Lodh, and Riddhi Goswami	
Composition and Antioxidant Activity of Vapours from Clove Bud During Roasting	151
Moumita Dev, D. K. Bhattacharyya, and Minakshi Ghosh	
Characterization, Purification and Immobilization of an Acid Invertase from <i>Mentha Spicata</i> (Pudina) for the Production of Invert Syrup	159
Abhishek Mukherjee	
Identification of Aqueous Extract of Red Amaranth Leaves by HPLC and LC-MS	167
Arjuma Sultana and Uma Ghosh	
Preparation and Utilization of Hydroxy Fatty Acid Rich Soyphospholipid for Emulsifier Application in Food Products	177
Gargi Saha, D. K. Bhattacharyya, and Minakshi Ghosh	

Effect of Medicinal Plants on Biofilm-Forming <i>Staphylococcus aureus</i> from Tertiary Health Care Hospital and Characterization of Biofilm-Associated Extracellular Polymeric Substances (EPS)	189
Rimashree Baishya and Soma Banerjee	
Synthesis and Characterization of MgO Nanoparticle and Its In Vitro Cytotoxic Effect on Erythrocytes	199
Bitopan Boro, Anup Kr. Nath, Manash Barthakur, and Pankaj Kalita	
Formulation, Production, and Characterization of Nutritionally Enriched Spread Product with Blends of Fish Skin (<i>Labeo rohita</i>) Oil and Chia Seed (<i>Salvia Hispanica</i>) Oil	209
Nabanita Ghosh, Monalisa Roy, and D. K. Bhattacharyya	
Application of Used Tea as Solid Matrix for Immobilization of Alkaline Protease by OVAT Method	219
Tapasi Polley and Uma Ghosh	
Environment and Agriculture	
Isolation and Characterization of Arsenic Tolerant Bacteria from Industrial Soil and Analysing Its Metal Removal Potency	233
Aishwarya Das, Ranjana Das, and Chiranjib Bhattacharjee	
Application of <i>Bacillus</i> sp. NITD 19 for Utilization of Cyanide as Nutrient Source	241
Abhilasha Rai, Sanket Mukherjee, Agradeep Mukherjee, Jitamanyu Chakrabarty, Pinaki Bhattacharya, and Susmita Dutta	
Degradable Plastic Composite Film—A Comparison Between Photocatalytic and Biodegradation	249
Parbatee Nag, Aniruddha Mukhopadhyay, Amrita Debnath, Anirban Roy, and Sampa Chakrabarti	
Optimization of Energy-Proficient Infrared Radiated Rapid Hydrolysis of Pineapple Skin to Reducing Sugar	257
Swapnendu Chatterjee, Sayan Kumar Bhattacharjee, Rajdip Roy, and Rajat Chakraborty	
Value Addition of Agricultural Wastes for Improved Production of Industrially Important Enzymes by Employing Co-cultivation of Fungi	265
Sayari Majumdar and Jayati Bhowal	
Cost-Effective and Eco-Friendly Method for Decolorization of Malachite Green by <i>Kocuria marina</i> DAGII	277
Daiji Brahma and Debjani Dutta	

Isolation of a Most Potent Bacterial Strain from Soil for Bioremediation of Phenol	287
Debapriya Maity, Pradyut Kundu, and Sunita Adhikari (Nee Pramanik)	
Study on Application of Novel Synthesized Silver Metallosurfactant for Membrane Cleaning	297
Ankita Mazumder, Zinnia Chowdhury, Dwaipayan Sen, and Chiranjib Bhattacharjee	
Effect of Calcium Salts on Salinity Stress on Morphology and Biochemical Estimation of Rice Seedlings	305
Banhishikha Singh and Soma Banerjee	
Synthesis and Characterization of TiO₂ Nanoparticle and Checking Its Antimicrobial Activity Against <i>Escherichia coli</i> and <i>Staphylococcus aureus</i>	317
Ram Singh Purty, Ishant Shakya, and Sayan Chatterjee	
Taguchi-Based Process Optimization for Improving Iron Removal from Water Using Electrocoagulation Technique	327
Krishti Biswas and Mehabub Rahaman	
Kinetics Study of a Suspended Growth System for Biological Treatment of Bakery and Confectionery Wastewater	339
Biswajit Chakraborty, Pradyut Kundu, Joydeep Mukherjee, and Somnath Mukherjee	
Role of Metallothionein and Phytochelatin in Combating Abiotic Stress Imparted by Copper-Induced Toxicity in Brinjal (<i>Solanum melongena</i>)	349
Pratik Talukder	
Optimization of Process Parameters for Biodegradation of Resorcinol in Presence of Toxic Heavy Metals by Response Surface Methodology (RSM)	359
Sonali Hazra Das, Ayimyaba R. Longkumer, Rayanee Chaudhuri, Srabanti Basu, Sudipta Dey Bandyopadhyay, and Bhaswati Chakraborty	
An Environmentally Benign Green Approach for the Reduction of Graphene Oxide by Apple Extract: Spectroscopic and Thermal Interpretation	373
Shweta Mitra, Saswata Bose, and Mehabub Rahaman	
Performance and Kinetic Studies of Dairy Effluent Using Mixed Culture in a Suspended Growth Batch Reactor	383
Dipankar Raha, Pradyut Kundu, and Somnath Mukherjee	

Sustainable Energy

Optimization of TiO₂-KMnO₄ Composites with Natural Dyes for Solar Cell Application	397
Shyamal Datta and Subhasis Roy	

Production of Hydrogen by Steam Reforming of Methanol Over Novel Nano-Nickel Oxide-Based Catalyst	405
Barnali Bej, N. C. Pradhan, and Swati Neogi	

Performance Enhancement of Dye-Sensitized Solar Cell Using Extracted Photo-Sensitized Organic Molecules in Addition with Dielectric Nanomaterial	415
Argha Dey, Subhasis Roy, and Sourav Mondal	

Simulation of Biomagnetic Fluid Flow in a Lid-Driven Cavity Under Steady Localized Magnetic Field	423
Sumanta Banerjee and Ranjan Ganguly	

Systems Biology Approach to Screen and Identify Algae-Based Alkaline Phosphatases as Heavy Metal-Detecting Biosensors	431
Dipankar Ghosh, Kalyanee Bera, Poulami Bera, Megha Bhattacharya, Bijaya Samanta, Somashree Mondal, Mamta Das, Bishal Maity, Sanjit Das, Surjata Haobam, Anwesa Das, and Pritha Mondal	

Origin of Enantioselectivity: A Model Study of Sharpless Epoxidation	439
Nabanita Paul	

Electron Momentum Distribution Around Vacancy Cluster in CdO Nanoparticles	449
Anjan Das	

Isolation, Screening, and Evaluation of Cellulase-Producing Bacteria from the Soil of Similipal Biosphere Reserve for Biofuel Production from Lignocellulosic Biomass	457
Manish Paul, Soumya Ranjan Meher, Subhadarshini Giri, and Hrudayanath Thatoi	

Nanomaterials and Nanotechnology

Reduced Graphene Oxide (RGO)-Based Nanocatalyst for Inhibition of Pathogenic Bacteria Toward Enhancement of Water Purification	469
Shubhanwita Saha, Debashis Roy, and Chiranjib Bhattacharjee	

Wound Healing and Antimicrobial Property of Phytofabricated Silver Nanoparticle by <i>Saraca asoca</i> Bark Extract on Diabetic Wound In Mice	475
Baishakhi Bairagi and Debjani Nath	

Anti-adhering Property Study of Green Nanotechnology Based Modified Chitin Flakes: A Novel Approach Towards Biofilm Eradication	485
Anindita Chatterjee, Rimashree Baishya, and Soma Banerjee	
Modern Advancement of Nanotechnology Over Conventional Drug Therapies	493
Tania Pal, Bhuban Ruidas, and Chitragada Das Mukhopadhyay	

About the Editors

Prof. Doraiswami Ramkrishna is currently Harry Creighton Peffer Distinguished Professor of Chemical Engineering at Purdue University. He obtained B. (Chem) Eng., from University of Bombay (1960) and Ph.D. in Chemical Engineering from University of Minnesota (1965). Prof. Ramkrishna's research group is motivated by ideas in the application of mathematics to solving problems in chemical and biochemical reaction engineering, biotechnology and biomedical engineering. He is the recipient of many prestigious Awards and Honors, a few of them are: Award for Outstanding Graduate Faculty Mentor (2019), Balwant S. Joshi Distinguished Professorship, ICT, Mumbai, (2017–2018), Sigma Xi Faculty Research Award (Purdue Chapter, 2013), College of Science, Team Award, (2012), Foreign Fellow, Indian National Academy of Engineering (2011), M. M. Sharma Distinguished Professor, Institute of Technology, University of Mumbai (2010), Mumbai Institute of Technology Platinum Award (2009), Member, US National Academy of Engineering (2009), Fellow of the American Institute of Chemical Engineers (2008) and many more. He has published more than 260 papers in international journals and authored 8 books and book chapters. More than 45 students were awarded PhD under his guidance. He has served as a Consultant to General Mills, Inc. Minneapolis, Minnesota, Pillsbury Co., Minneapolis, MN, and to American Oil Company, Naperville, IL, and Ciba-Corning, MA. He is also Member of Technology Advisory Board (2005), Member Advisory Council to Pacific Northwest National Laboratory, Richland, WA, on Microbial Community Initiative (2010–2013). He has carried out consultation activity with Pillsbury Company, Amoco, Ciba-Corning, Abbot Laboratories and Eli Lilly. He is the First Chairman of Area 10D on Applied Mathematics of CAST Division of the American Institute of Chemical Engineers (1987–1991). He has Chaired several sessions in the annual meetings of the A.I.Ch.E. on applied mathematics. He is on the Editorial Board member of Journals: Latin American Journal of Chemical Engineering, International Journal of Applied Engineering Research, The World Journal of Chemical Engineering, Current Opinion in Chemical Engineering, International Journal of Chemical Engineering. He was honored with Guest Editorship of journals: Chemical Engineering Communications, Journal of Biotechnology, and Processes.

Prof. Subhabrata Sengupta is former scientist of Indian Institute of Chemical Biology (CSIR-IICB), Kolkata. He has joined IICB in 1972, retired from the institute as Director Grade Scientist on January, 2006 and was immediately invited by Heritage Institute of Technology, Kolkata (HITK) to join as Professor and Head, Department of Biotechnology. Since then, he is working as Professor, then as Dean (Post Graduate & Research) and retired on January, 2016. He was graduated with Hons. in chemistry (1964), Post graduated with Biochemistry (1966), and awarded D.Sc (1973), all under Calcutta University, India. He carried out Post-doctoral research at Herriot-Watt University, Edinburgh, UK (1981) and Osaka University, Osaka, Japan (1983). His research was focused in the area of antibiotics, enzyme technology, bioprocess development, therapeutic and commercial enzymes and glycosidase inhibitors of plant origins. He has R&D experience of 44 years at Indian Institute of Chemical Biology (CSIR), Kolkata and at HITK. He Acted as Adjunct Professor, Department of Biotechnology, Jadavpur University (1990–2000), Visiting Professor (2003–2006) and Full professor (2006–2016), HITK. He is the recipient of many prestigious awards. A few of them to mention: Silver Medal in M.Sc. Examination (2nd position) by Calcutta University (1966), Young Scientist Medal by Indian National Science Academy (1974) presented by the then Prime Minister Smt Indira Gandhi, British Council – CSIR Exchange Program Fellowship (1980), Japan Academy of Science & INSA Exchange Program Fellowship (1984), Sankar Prasad Ghosh Memorial Award by the Department of Biochemistry, Calcutta University (1985), Prof. A. K. Chanda Memorial Award by the Department of Botany, Calcutta University (2003), 7th SR Bose Memorial Award, by Indian Mycological Society, 2007. He is a Fellow of West Bengal Academy of Science & Technology (FASc&T), Institute of Chemists India, (FIC). He has 17-Indian and 2-US patents in his name. He has published 117 journal papers, authored 17 book chapters and guided total 15 students for PhD He was Sectional President (New Biology): 90th Indian Science Congress Association (2002) and selected as Fellow, West Bengal Academy of Science & Technology and Institute of Chemists (India). He was also the associate editor of Journal of Indian Chemical Society (1991–93) and reviewer of many scientific journals.

Dr. Sudipta Dey Bandyopadhyay is currently an Assistant Professor at Department of Biotechnology, Heritage Institute of Technology, Kolkata. She obtained B.Tech in Chemical Engineering from Vidyasagar University, M.Tech in Biotechnology and Ph.D in Engineering from Jadavpur University, Kolkata. Her area of research includes bioprocess development, bioreactor design and scale up, modeling and simulation of bioprocess, downstream processing of biological products, environmental biotechnology, biological wastewater treatment and bioremediation of polycyclic aromatic hydrocarbons. She has research and teaching experience of total 15 years at Indian Institute of Chemical Biology, Jadavpur University and Heritage Institute of Technology, Kolkata. In addition to many conference publications (international and national), she has published many full papers in reputed peer reviewed international journals. Currently she is reviewer of

journals: Desalination and Water Treatment, Journal of Taiwan Institute of Chemical Engineers, Chemical Engineering Journal, International Journal of Environment and Waste Management, African Journal of Microbiology Research, International Journal of Emerging Technology & Advanced Engineering, Current Journal of Applied Science and Technology, Industrial & Engineering Chemistry Research. She is the life member of Indian Science Congress Association (ISCA) and life associate member of Indian Institute of Chemical Engineers (IICChE).

Dr. Avijit Ghosh is currently an Assistant Professor at Department of Chemical Engineering, Heritage Institute of Technology, Kolkata. He obtained B.Tech in Chemical Engineering from Heritage Institute of Technology, WBUT, M.Tech in Chemical Engineering from Calcutta University and Ph.D from Indian Institute of Technology, Guwahati, India. His major area of research includes Carbon nano-materials synthesis and characterization, polymer nano-composite for fuel cell application, fuel cells, noble metal free electrocatalyst, hydrogen production, hydrogen storage, solar cells, energy management. In addition to many international and national conference publications, he has published 12 full papers in peer reviewed journals. He has authored one book chapter (CRC press, Handbook of Graphene Science) and one monograph (Scholars' Press, Germany). He is member of the reviewer board of the Splendid Journals in the field of engineering and technology (2018) and editorial board member of International Journal of Nanomaterials and Nanostructures published by Journal Pub (2018). He is also reviewer of the Royal Society of Chemistry: RSC Advance. Recently, he has received Best Reviewer Award from International Journal of Hydrogen Energy (2017), Elsevier.

Fermentation Technology and Bioreactor

Isolation of Cellulose-Degrading Bacteria and to Use Their Cellulolytic Potential for Production of Bioethanol from Paper Waste



Sayan Chatterjee, Kalyani Tripathi, and Ram Singh Purty

Abstract In the present scenario, solid waste management has emerged as a huge problem for the environment and mankind. Most of the wastes are generated from the plant source that is made up of cellulose. Cellulose can serve as the source of glucose by various methods of degradation that can be chemical or enzymatic. The cellulase enzyme of the bacterial system can also be used for cellulose degradation. In the present study, cellulose-degrading bacteria have been isolated from soil obtained from wood habitat. To indicate the cellulase activity of the organisms, the diameter of clear zone around the colony and hydrolytic value on cellulose Congo Red agar media were measured. The strain with maximum cellulolytic potential was selected on the basis of DNS assay. The selected strain was further characterized at the molecular level using 16S RNA sequencing. The characterized strain was later used for the production of glucose by degrading the tissue paper. The glucose such produced was used for the production of bioethanol using *Saccharomyces cerevisiae*. The production of ethanol was positively tested after 6 days by iodoform test and amount of alcohol produced was obtained by distillation of the fermented mash.

Keywords Cellulose · Cellulolytic bacteria · Paper waste · Bioconversion · Bioethanol

S. Chatterjee · K. Tripathi · R. S. Purty (✉)
University School of Biotechnology, Guru Gobind Singh Indraprastha University, New Delhi,
India

e-mail: rspurty@ipu.ac.in

S. Chatterjee

e-mail: sayan@ipu.ac.in

K. Tripathi

e-mail: kalyanitripathi8@gmail.com

1 Introduction

Human activities create wastes and these wastes are handled, stored, collected, and disposed of so that they do not become a risk for the health and environment. With the rapid increase in urbanization and population, the nature of solid waste has become complexed. Municipal solid waste (MSW) is generally categorized as degradable and nondegradable (Mehta et al. 2018). Wastes like paper, textile, fiber, food all those composed of plant components are degradable in nature and other wastes like plastic, metals, glass, e-wastes are termed as nondegradable. Characterization of MSW indicated that the waste consists of 30–45% organic matter, 6–10% recyclables, and the rest as inert matter (Kumar et al. 2009). The nature of waste suggests that the main content of waste is cellulose, which is the component of plant cell wall.

Cellulose is a complex carbohydrate or polysaccharide consisting of several glucose units linked together by β -1,4 glycosidic bond (Klemm et al. 2005). Abundant availability and accessibility of cellulose make it a long-term raw material for producing many industrially important commercial products that will be cost-effective and eco-friendly. But in the present juncture, much of the cellulose are disposed of as waste all over the globe. Cellulose is mainly obtained from plants hence if we are concerned about the environment and global warming, we must find ways to utilize the cellulosic waste generated. This can be done by using cellulolytic system, by which cellulose can be converted into glucose, which is a multiutility product and has industrial value. Cellulolysis is a biological process for the degradation of cellulose that is effectively done by the cellulase enzyme system (Kumakura 1997).

The microbial system is the best source for the extraction of cellulose-degrading enzyme. There is a large range of microorganisms that are responsible for cellulase production including aerobic and anaerobic bacteria, white rot and soft rot fungi, and anaerobic fungi (Lynd et al. 2002). The cellulase enzymes isolated from microbes can be used to degrade cellulose to produce glucose that can be further utilized for the production of several industrially important products such as bioethanol. Bioethanol is a striking alternative fuel as it is a renewable bio-based resource, and it is oxygenated and hence provides the opportunity to reduce particulate emissions in compression-ignition engines (Balat 2007). Therefore, in the present investigation, focus has been made to isolate cellulose-degrading bacteria and utilizes its cellulolytic potential for degradation of paper waste for the production of bioethanol. Several studies showed the production of bioethanol from paper waste using hydrolysis and fermentation (Wang et al. 2013; Maceiras et al. 2016).

2 Materials and Methods

2.1 Sample Collection

For isolation of cellulose-degrading bacteria (CDB), the soil samples were collected from location of wood habitat manufacturing industry of Bawana, New Delhi, India

(28.7884° N, 77.0301° E). After collection, the soil samples were stored at 4 °C in sterile containers.

2.2 Screening of Cellulose-Degrading Bacteria

For screening of cellulose-degrading bacteria (CDB), around 2 g of soil sample was homogenized in 0.9% saline solution and serially diluted ranging from 10^{-1} to 10^{-3} under sterile condition. Around 100 μ l of each serially diluted sample was spread plate on carboxymethyl cellulose (CMC) agar media composed of KH_2PO_4 , 0.5 g; MgSO_4 , 0.25 g; cellulose, 2 g; agar, 15 g; gelatin, 2 g; distilled water, 1 L; pH, 6.8–7.2. The plates were incubated at 37 °C for 24 h. Colonies obtained were maintained on CMC agar plate and preserved at 4 °C.

2.3 Cellulolytic Ability Assay

Cellulose-degrading ability was analyzed by streaking the isolated bacterial strains on Congo Red agar media composed of CMC agar media supplemented with Congo Red 0.2 g/l. The formation of a clear zone of hydrolysis indicated cellulose degradation ability of the isolated bacterial strain. The colony showing maximum degradation was selected and used for further study.

2.4 Estimation of Carboxymethyl Cellulase (CMCase) Activity

Using the 3, 5-dinitrosalicylic acid (DNS) method, CMCase activity was determined (Miller 1959). Supernatant obtained from overnight-grown culture after centrifugation at 5000 rpm for 10 min at 4 °C was used as crude enzyme source. Assay was carried out by adding around 0.5 ml of crude enzyme to 0.5 ml of 1% CMC (solubilized in 0.05 M phosphate buffer, pH 8) followed by incubation at 50 °C in water bath for 30 min. The reaction was stopped by the addition of 1.5 ml of DNS reagent followed by boiling the reaction mixture for 10 min. Sugars liberated were estimated by measuring absorbance at 540 nm. A unit of activity is defined as the amount of enzyme required to liberate 1 mol of glucose per minute under the assay conditions.

2.5 Molecular Identification and Phylogenetic Analysis

The bacterial strain that showed maximum cellulose activity was used for molecular characterization using 16S rRNA sequencing. The isolated bacterial strain streaked

on CMC agar plate was deposited and sequenced at Microbial Type Culture Collection and Gene Bank (MTCC), CSIR-IMTECH, Chandigarh, India. The sequence obtained was compared using BLASTN program and the members of the closely related genera were retrieved from EzTaxon server (Chun et al. 2007) and aligned using the MEGA software version 6.0 (Tamura et al. 2013). Phylogenetic trees were constructed using the neighbor-joining as well as maximum parsimony algorithms. Bootstrap analysis was performed to assess the confidence limits of the branching.

2.6 Production of Bioethanol

The isolated CDB strain was grown in two sets, one in CMC media and another in basal salt media composed of KH_2PO_4 , 2 g; MgSO_4 , 0.2 g; NaCl , 0.2 g; NaNO_3 , 2.5 g; $\text{CaCl}_2 \cdot 6\text{H}_2\text{O}$, 0.1 g; Whatman No. 1 filter paper, 2.5 g; distilled water, 1 L; pH 6.8–7.2, for 4 days at 37 °C with constant shaking of 150 rpm. The supernatant obtained from the first set of culture was used as the source of enzymes for saccharification process, where as the broth obtained from the second culture was used for fermentation using *Saccharomyces cerevisiae* (NCIM Accession No: 3594, NCL, Pune, India). Simultaneous saccharification and fermentation processes were carried out at 27 °C for 6 days as described by Jain et al. 2014. Preparation of yeast growth medium was done using yeast extract 5.0 g, peptone 5.0 g, diluted saccharified slurry to attain an overall sugar percentage of 1%, volume made up to 1000 ml with pH 5.0.

Post fermentation, iodoform test was done to confirm the presence of ethanol. The fermented mash was distilled and alcohol percentage was estimated (Ghosal et al. 2013).

2.7 Iodoform Test

The presence of ethanol in the culture broth was confirmed by iodoform test (Lieben 1870). Around 10 drops of methanol, ethanol, and the culture broth were taken in three separate test tubes. The methanol and ethanol were taken as negative and positive control, respectively. Around 10 drops of diluted NaOH solution were added to each test tube along with 30 drops of iodine solution. The color developed was later analyzed.

3 Results and Discussion

3.1 Isolation of Cellulose-Degrading Bacteria

Cellulose-degrading bacteria were isolated from the soil sample on CMC agar medium using serial dilution. Serial dilution ranging from 10^{-1} to 10^{-3} under sterile

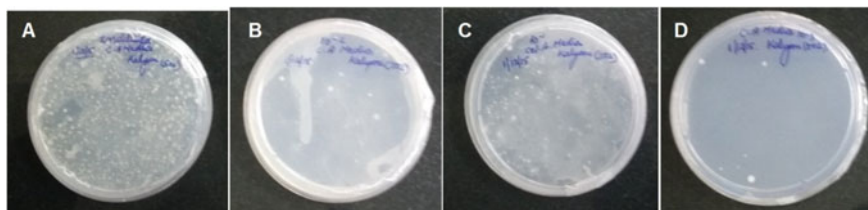


Fig. 1 Screening of cellulose-degrading bacteria from the soil sample using serial dilution on carboxymethyl cellulose (CMC) agar medium. **a** Undiluted, **b** 10^{-1} , **c** 10^{-2} , and **d** 10^{-3}

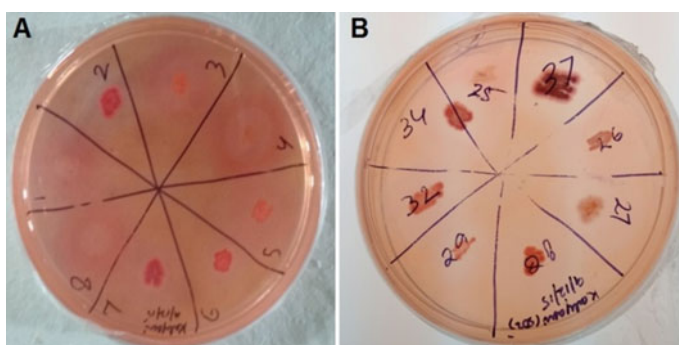


Fig. 2 a, b Cellulolytic potential of selected six bacteria, namely, CDB1, CDB4, CDB29, CDB32, CDB34, and CDB37, showing halo zones around the colony on CMC agar medium

condition was performed to obtain the isolated colonies (Fig. 1). A total of 37 isolated colonies were selected and named as cellulose-degrading bacteria, CDB 1–37. Isolation of CDB was also reported from the other sources like guts of invertebrates (Gupta et al. 2012), kitchen waste (Kaur 2012), and sheep rumen (Guder and Krishna 2019).

3.2 Cellulolytic Ability Assay

Cellulose degrading ability was analyzed by streaking the isolated bacterial strains on Congo Red agar media. Based on the morphology, six morphologically distinct bacterial isolates that were giving halo zones in CMC agar medium were selected, namely, CDB1, CDB4, CDB29, CDB32, CDB34, and CDB37 (Fig. 2).

3.3 Carboxymethyl Cellulase (CMCase) Activity

Production of cellulase enzyme by six bacterial isolates was analyzed using the 3, 5-dinitrosalicylic acid (DNS) method. The cellulase production ability of the bacterial isolates in the production medium was in the following order, CDB-37 < CDB-32 <

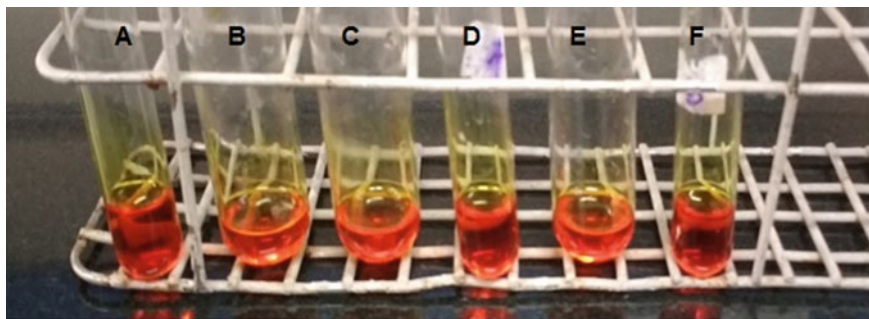


Fig. 3 Carboxymethyl cellulase activity of six bacterial isolates using 3, 5-dinitrosalicylic acid (DNS) assay. **a** CDB1, **b** CDB4, **c** CDB29, **d** CDB32, **e** CDB34, and **f** CDB37

CDB-4 < CDB-29 < CDB-34 < CDB-1 (Fig. 3). Among these two bacterial isolates, CDB-1 and CDB-34 showed maximum cellulase production ability. Out of these strains, CDB-1 was chosen for molecular characterization.

3.4 Molecular Identification of Cellulolytic Bacteria

The strain CDB-1 that showed maximum cellulose activity was further subjected to molecular characterization. The 16S rRNA gene sequence obtained was compared using BLASTN program, which showed the strain CDB-1 to be *Streptomyces albo-griseolus*. Multiple sequence alignment analysis with all the closely related genera showed 99–98% similarities at the sequence level. Phylogenetic tree analysis showed that the strain CDB-1 is closely related to other *Streptomyces* species available in the database (Fig. 4). Several actinomycetes are known to degrade cellulose (Saini et al. 2015).

3.5 Production of Bioethanol from Tissue Paper

The strain CDB-1 was used for its cellulolytic potential to degrade tissue paper to obtain glucose as the product that was, for further, used for fermentation. The strain *Saccharomyces cerevisiae* was used in the fermentation process for the conversion of glucose to ethanol. The fermentation product was obtained from the broth that was further confirmed by iodoform test (Fig. 5). After distillation of the fermented mash, the percentage of alcohol in distillate was calculated to be 7.8%.

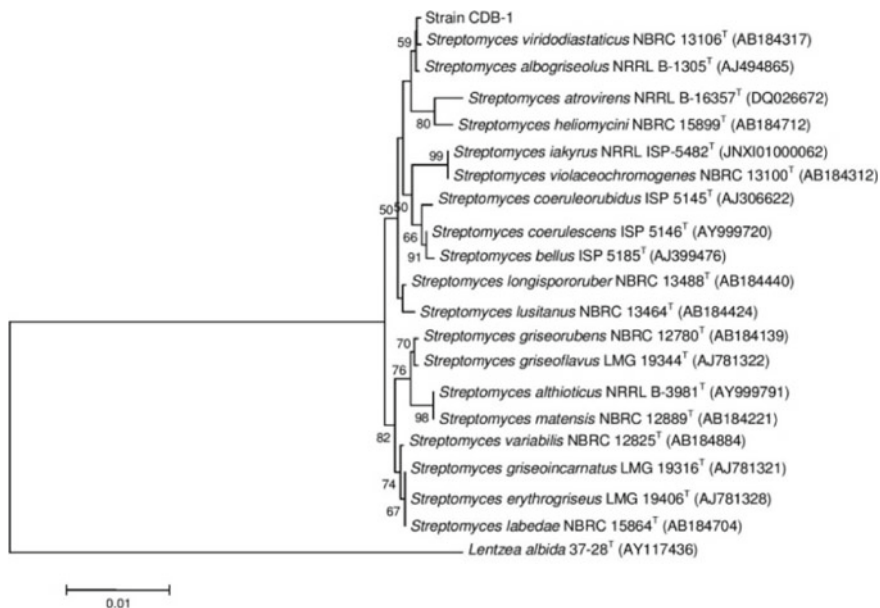


Fig. 4 Phylogenetic tree analysis showed the strain CDB-1 is closely related to other *Streptomyces* species available in the database

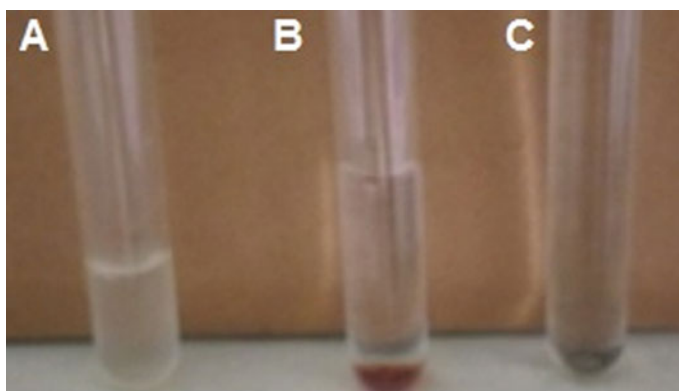


Fig. 5 Confirmation of fermentation product using iodoform test **a** broth, **b** methanol as negative control, and **c** ethanol as positive control

4 Conclusion

Rapid increase in population and urbanization has led to the generation of huge municipal solid waste. The percentage of cellulose waste is around 17%, which mainly consists of woods, papers, old furniture, etc. Using biotechnology tools,

research has been accelerated to find ways to convert cellulose into industrial important products. Due to its cellulolytic potential, microbes are the excellent system for the degradation of cellulose. Therefore, in the present investigation, we have screened and isolated cellulose-degrading bacteria (CBD) from the soil sample. Out of 37 bacterial strains, 6 showed cellulose-degrading ability. The cellulase production ability of the six was in the following order—CDB-37 < CDB-32 < CDB-4 < CDB-29 < CDB-34 < CDB-1. Molecular characterization of CBD-1 showed that the strain is closely related to *Streptomyces* species. The isolated CBD-1 bacterial strain was later used for the saccharification along with *S. cerevisiae* during fermentation. After distillation of the fermented mash, the production of alcohol was confirmed using iodoform test. Thus, the biodiversity of microbes like bacteria, fungi gives us the chance to identify and isolate strains that could assist in the biological conversion of cellulose into glucose, which can later be used for the production of some industrial useful products.

Acknowledgements SC, KT, and RSP like to thank GGS Indraprastha University, New Delhi for all the laboratory space and financial support provided.

Conflict of Interest The authors declare that they have no conflict of interest.

Declaration by authors Appropriate permissions were obtained from responsible authorities for collecting soil samples for the study from manufacturing industry of Bawana, New Delhi.

References

- Balat M (2007) Global bio-fuel processing and production trends. *Energ Explor Exploit* 25(3):195–218. <https://doi.org/10.1260/014459807782009204>
- Chun J, Lee JH, Jung Y et al (2007) EzTaxon: a web-based tool for the identification of prokaryotes based on 16S ribosomal RNA gene sequences. *Int J Syst Evol Microbiol* 57(10):2259–2261. <https://doi.org/10.1099/ijs.0.64915-0>
- Ghosal A, Banerjee S, Chatterjee S (2013) Biofuel precursor from potato waste. *Int J Res Eng Technol* 2(3):213–219
- Guder DG, Krishna MSR (2019) Isolation and characterization of potential cellulose degrading bacteria from sheep rumen. *J Pure Appl Microbiol* 13(3):1831–1839. <https://doi.org/10.22207/jpam.13.3.60>
- Gupta P, Samant K, Sahu A (2012) Isolation of cellulose-degrading bacteria and determination of their cellulolytic potential. *Int J Microbiol* 2012:1–5. <https://doi.org/10.1155/2012/578925>
- Jain M, Gupta AK, Chatterjee S (2014) To optimize the process of alcohol production from banana peel. *Recent Adv Bioenergy Res* 3:208–217
- Kaur M (2012) Isolation and Screening of cellulose degrading bacteria in kitchen waste and detecting their degrading potential. *IOSR J Mech Civil Eng* 1(2):33–35. <https://doi.org/10.9790/1684-0123335>
- Klemm D, Heublein B, Fink HP et al (2005) Cellulose: fascinating biopolymer and sustainable raw material. *Angew Chem Int Edit* 44:3358–3393. <https://doi.org/10.1002/anie.200460587>
- Kumakura M (1997) Preparation of immobilized cellulase beads and their application to hydrolysis of cellulosic materials. *Process Biochem* 32(7):555–559. [https://doi.org/10.1016/s0032-9592\(97\)00011-3](https://doi.org/10.1016/s0032-9592(97)00011-3)

- Kumar S, Bhattacharyya JK, Vaidya AN et al (2009) Assessment of the status of municipal solid waste management in metro cities, state capitals, class I cities, and class II towns in India: An insight. *Waste Manag* 29(2):883–895. <https://doi.org/10.1016/j.wasman.2008.04.011>
- Lieben A (1870) The formation of iodoform and the application of this reaction in the chemical analysis. *Liebigs Ann Chem Suppl* 7:218. <https://doi.org/10.1002/9780470114735.hawley09809>
- Lynd LR, Weimer PJ, Van Zyl WH et al (2002) Microbial cellulose utilization: fundamentals and biotechnology. *Microbiol Mol Biol Rev* 66(3):506–577. <https://doi.org/10.1128/mnbr.66.3.506-577.2002>
- Maceiras R, Alvonsin V, Poole JE (2016) Bioethanol production from waste office paper. *J Environ Sci* 6(7)
- Mehta YD, Shastri Y, Joseph B (2018) Economic analysis and life cycle impact assessment of municipal solid waste (MSW) disposal: a case study of Mumbai, India. *Waste Manag Res* 36(12):1177–1189
- Miller GL (1959) Use of dinitrosalicylic acid reagent for determination of reducing sugar. *Anal Chem* 31(3):426–428
- Saini A, Aggarwal NK, Sharma A et al (2015) Actinomycetes: a source of lignocellulolytic enzymes. *Enzym Res* 2015:1–15. <https://doi.org/10.1155/2015/279381>
- Tamura K, Stecher G, Peterson D et al (2013) MEGA6: molecular evolutionary genetics analysis version 6.0. *MolBioE* 30(12):2725–2729 <https://doi.org/10.1093/molbev/mst197>
- Wang L, Sharifzadeh M, Templer R, Murphy RJ (2013) Bioethanol production from various waste papers: economic feasibility and sensitivity analysis. *App Energy* 111:1172–1182. <https://doi.org/10.1016/j.apenergy.2012.08.048A>

Bioconversion of Mandarin Orange Peels by *Aspergillus oryzae* and *Penicillium* sp.



Debarati Roy and Jayati Bhowal

Abstract The present study deals with the identification and determination of flavor compounds present in the essential oils of mandarin (*Citrus reticulata*) peel and fungal bioconverted mandarin peel. The essential oils of citrus fruits contain volatile chemical compounds enriched with various medicinal properties. The peel oils were extracted through solvent distillation method and analyzed by gas chromatography–mass spectrometry. The predominant aroma compounds were o-xylene, alpha pinene, beta pinene, sabinene, limonene, limonene oxide, and decanal in fresh mandarin peel oil. After bioconversion due to fungal infection, the infected peel oils contained various newly produced volatile components such as perillen, citral, carveol, terpineol, verbenone, and carvone.

Keywords Flavor · Mandarin peels · Gas chromatography–mass spectrometer · Bioconversion · Limonene

1 Introduction

Citrus fruits are one of the fruits that are mostly used in food, cosmetic industries due to their contributions to flavors and antimicrobial activities. The peels are mainly responsible for the essence of citrus fruits (Beltran et al. 2006). The essential oils of citrus fruits are prepared by steam distillation, cold-pressing, or solvent extraction. Citrus essential oils are obtained by cold-pressing or distillation from fruit peels. There are several studies that have been concerned with the identification of aroma compounds of mandarin peel oils. The cold-pressed essential oils of mandarin peel contained a huge number (116) of aroma molecules and it also represented the highest presence of limonene (80.3% w/w) along with gamma terpinene and myrcene (Choi

D. Roy · J. Bhowal (✉)

Department of SOCSAT, Indian Institute of Engineering Science and Technology, Shibpur, Howrah, India

e-mail: jayatibhowal@gmail.com

D. Roy

e-mail: roydebarati90@gmail.com

© Springer Nature Singapore Pte Ltd. 2021

D. Ramkrishna et al. (eds.), *Advances in Bioprocess Engineering and Technology*, Lecture Notes in Bioengineering,

https://doi.org/10.1007/978-981-15-7409-2_2

et al. 2013). There has been no published research work on identification of volatile aroma components present in spoiled mandarin peel of fruits of Darjeeling district. Therefore, this present work focuses to investigate the production of valuable flavor compounds from peel oils of spoiled mandarins collected from Darjeeling district and it also helps to understand whether spoilage of mandarin peel can influence the bioconversion of the aroma particles (limonene, alpha pinene) to produce new flavor compounds such as carvone, perillen, carveol, terpineol, verbenone.

2 Materials and Methods

2.1 Collection of Plant Sample (Mandarin Fruits)

Healthy mature ripe mandarin oranges were collected from Darjeeling District in West Bengal. The fruits were plucked from the trees during January–February. They were transported to the experimental lab in sterile bags and the peels were analyzed within 4 days after plucking.

2.2 Chemicals

The chemicals (different analytical standards and other reagents) were purchased from Sigma-Aldrich Chemical Company (USA) and MERCK (Emerck India Ltd., Mumbai, India).

2.3 Extraction of Oils from Fresh Mandarin Peel

The mature and healthy fruits were cleaned with tap water to wash away the dust and other foreign particles. The peels of the mandarin were removed and cut into small pieces with the help of sterile sharp knife. Mandarin peel of 100 g was weighed and smashed. The smashed peels were kept into a sterile 250-ml Erlenmeyer flask and stirred with 40–60 petroleum ether for 1 day. Extraction of volatile compounds from mandarin peel oil was done by direct solvent extraction method (Nwobi et al. 2006). The light yellow-colored essential oil (5 ml) was recovered. To remove the water from extracted oil, anhydrous sodium sulfate was added. The sample was concentrated through rotary evaporator and then collected in a sterile brown bottle closed tightly until GC-MS analysis.

2.4 Gas Chromatography–Mass Spectrometry (GC–MS) Analysis of Essential Oils of Fresh Mandarin Peel

After extraction of essential oil, the sample was diluted with HPLC-grade 40–60 petroleum ether in 1:100 ratio (v/v). The separation of aroma compounds was carried out by using an Agilent 7890 GC system with 575C triple axis equipped with selective mass detector Agilent 5973. A capillary column of HP-5MS (30 m × 0.25 μm × 10 m duraguard column film thickness) and an automatic injection system were used. The initial oven temperature was 60 °C. In the splitless mode, the column was held at 60 °C for 5 min followed by an increase to 150 °C at 3 °C/min temperature rate and held for 2 min. Finally, the oven temperature was increased to 200 °C at a rate of 5 °C/min and held for 2 min. Finally, column temperature was increased to 260 °C at a rate of 10 °C/min and then held for 2 min.

2.5 Identification of Volatiles Present in Essential Oils of Fresh Peel of Mandarin Orange

Individual chromatographic peak identification of volatile components was carried out by comparing their mass spectra with the mass spectra from NIST 05 library and WILEY L-built library (Ibrahim et al. 2011). The results were also confirmed by comparing with previous studies and reviews (Elmaci and Altug 2012). The fragmentation of mass spectra of specific compounds was also identified by comparing with chromatograms and retention times of the analytes with those from analytical standards (Adams 1995).

2.6 Spoilage of Mandarin Peel Infected by *Aspergillus* sp. (*Aspergillus oryzae*) and *Penicillium* sp.

About 100 g of peels from fresh Mandarin mandarins was weighed and smashed. Then the smashed peel was homogenized at 8000 rpm by homogenizer (REMI MOTORS-RQ-122). The pH of the resulting mixture solution was adjusted according to the pH optima of specific fungus. Two sterilized 100-ml Erlenmeyer flasks were taken and 30 ml of homogenized peel was poured into each of the flasks. Then one of the flasks was inoculated with the pure fungal strain *Aspergillus* sp. (*Aspergillus oryzae*) and another flask inoculated with the pure fungal strain *Penicillium* sp. at a level of 10⁷ cells or spores per ml of homogenized peel sample. The flasks were then incubated at 28 °C for 5 days in incubator.

2.7 Extraction of Oil from Spoiled Mandarin Peel

Extraction of oil from soiled mandarin peel was performed by direct solvent extraction method (Nwobi et al. 2006). The method of *extraction of oil from spoiled mandarin peel* was performed as the method described in Sect. 2.3.

2.8 Bioconversion of Standard Limonene by *Aspergillus sp.* (*Aspergillus oryzae*)

In a 100-ml Erlenmeyer flask, 30 ml of Potato Dextrose Broth was prepared and autoclaved at 121 °C for 15 min. After that one loopful pure fungal strain of *Aspergillus sp.* was inoculated into the sterile PDA broth, then 0.1 ml of analytical standard limonene was added into the flask, and the flask was incubated for 2 days at 28 °C. After incubation period, fungal mat was developed. The mat was collected and the liquid residual part of the media was filtered. About 10 ml of HPLC-grade pet ether solvent was added and stirred continuously for 1 day on a magnetic stirrer. The sample was then centrifuged at 5000 rpm and the supernatant was recovered. The concentrated liquid sample was allowed to rotary evaporation to concentrate the sample and was then analyzed by GC-MS.

2.9 Bioconversion of Standard α -Pinene by *Aspergillus sp.* (*Aspergillus oryzae*)

The bioconversion of standard α -Pinene by *Aspergillus sp.* was performed as described earlier in Sect. 2.8.

2.10 Bioconversion of Standard Limonene by *Penicillium sp.*

The bioconversion of standard by limonene by *Penicillium sp.* was performed as described earlier in Sect. 2.8.

2.11 GC–MS Analysis of Flavors Obtained from Spoiled Mandarin Peel Oils and Bioconversion of Standard Aromatic Volatiles

Flavor compounds obtained from fungus-infected mandarin peel oils and bioconversion of standard aromatic volatiles were extracted by direct solvent extraction method (Nwobi et al. 2006) and determined by GC–MS analysis as described earlier in Sects. 2.4 and 2.5.

3 Results and Discussion

3.1 Gas Chromatography–Mass Spectrometry (GC–MS) Analysis of Essential Oils of Fresh Mandarin Peel

The chromatogram of essential oils of fresh mandarin peel was evaluated and presented in Table 1. Based on the observation, it was shown that the essential oil derived from fresh peel of mandarin orange retained six terpene compounds and one aldehyde (o-xylene, alpha pinene, beta pinene, sabinene, limonene, copaene limonene oxide, and decanal). It was found that limonene was highest dominant compound (85%). The study of Brat et al. (2001) also revealed that mandarin peel oil has limonene as major compound and other terpenes, aldehydes, alcohols (pinene, myrcene, terpineol, citronellol, nerals). The aroma constituents of mandarin essential oils were recorded and they were α -pinene, β -pinene, β -myrcene, d-limonene, linalool, m-cymene, and 4-terpineol (Bozkurt et al. 2017).

Table 1 GC–MS Data of the aroma components of peel oil of fresh mandarin

Component	Quantity (%)
O-xylene	0.008
Alpha pinene	0.006
Beta pinene	0.008
Sabinene	14.21
Limonene	85.26
Limonene oxide	0.40
Decanal	0.10
Copaene	0.03

Table 2 GC–MS Data of peel oil of spoiled mandarin

Sample name	Identified flavor compounds
<i>Penicillium</i> sp.-infected peel oil	Beta myrcene (27.19%), beta pinene (30.06%), 3-carene (6.58%), limonene (32.29%), perillen (0.62%), geranyl alpha terpinene (2.30%), citral (0.50%), carvone (0.46%)
<i>Aspergillus</i> sp.-infected mandarin peel oil	Beta pinene (10.21%), 3-carene (3%), limonene (79.11%), carveol (2.68%), isocarveol (1.72%), trans-carveol (0.69%), linalool (1.02%), verbenone (1.49%)

3.2 GC–MS Analysis of Flavors Obtained from Fungus-Infected Mandarin Peel Oils and Bioconversion of Standard Aromatic Volatiles

Table 2 shows that the essential oils derived from fungus-infected mandarin peel contained different types of terpenes and alcohols and aldehydes.

When healthy mandarin peels were infected with *Penicillium* sp., various flavor compounds were newly produced, such as beta myrcene, 3-carene, perillen, geranyl alpha terpinene, citral, carvone. The *Aspergillus* sp.-infected mandarin peel oil showed the presence of 3-carene, carveol, linalool, verbenone that were absent in peel oils of fresh mandarin. The study of Crowell (1999) reported that the newly produced aroma components such as carvone, perillen, and a-terpineol could scavenge DPPH radicals. Antioxidant potential and antiproliferative effect of three monoterpenoids (carvone, perillyl alcohol, and a-terpineol) showed cytostatic effect against five cancers (breast, lung, prostate, ovarian, and leukemia).

The results of this study also revealed that due to the bioconversion of limonene by *Aspergillus* sp. alpha pinene, beta pinene, linalool, verbenol, carveol, isocarveol, cis- trans-carveol were produced (Table 3). It was also found that the bioconversion of alpha pinene by *Aspergillus* sp. alpha pinene was transformed into d-limonene, trans-beta-ocimene, 2-carene, verbenol, D-verbenone. The present study revealed that *Penicillium* sp. can cause the bioconversion of standard D-limonene into D-carvone, germecrene-D, and trans-carveol. Several previous research works revealed that *Aspergillus* sp. and *Penicillium* sp. are very much able to bioconvert different flavor compounds such as limonene, pinene, myrcene, vanillin, etc. The study of

Table 3 GC–MS Data of the aroma components identified from fungal bioconverted standard aromatic volatiles

Bioconversion of limonene by <i>Aspergillus</i> sp.	Bioconversion of limonene by <i>Penicillium</i> sp.	Bioconversion of alpha pinene by <i>Aspergillus</i> sp.
Alpha pinene, beta pinene, linalool, verbenol, carveol, isocarveol, cis- trans-carveol	D-carvone, germecrene D, and transcarveol	D-limonene, trans-beta ocimene, 2-carene, verbenol, D-verbenone

Marostica and Pastore (2007) stated that cassava wastewater can be used in bioflavor production by using fungi species like *Aspergillus* sp. or *Penicillium* sp. *Penicillium digitatum* can convert (R)-(+)-limonene to pure (R)-(+)- α -terpineol in 8 h with a yield of up to 93% (Adams et al. 2003). Citral was bioconverted into thymol, geraniol, and nerol by *Penicillium digitatum* (Esmaili and Tavassoli 2010). Fungi species like *Aspergillus* sp. or *Penicillium* sp. grown in cassava wastewater could biotransform R-(+)-limonene to R-(+)- α -terpineol. The microbial transformation of ferulic acid is a great alternative source for natural vanillin (Zheng et al. 2007). *Aspergillus niger* is used for biotransformations of different terpene compounds (Parshikov and Sutherland 2014). The products of biotransformation of flavor compounds showed good results of total antioxidant capacity, DPPH radical scavenging assay, and it revealed good activity against cultured leukemic cells (Mario et al. 2009).

4 Conclusion

Peel oils of mandarin fruits contain so many flavor compounds that have various antimicrobial and medicinal properties. This study may be helpful to reuse the fungi-infected peels of mandarin fruits as cheap substrate in the production of natural identical flavor compounds that are less toxic than chemical flavors. Some fungal strains showed that the biotransformation of limonene, pinene yields several flavor components with economic value. This study is a new promising area in the production of natural aromas.

References

- Adams RP (1995) Identification of essential oil components by gas chromatography/mass spectrometry. Allured Publishing Corporation, Carol Stream
- Adams A, Demyttenaere JCR, De Kimpe N (2003) Biotransformation of (R)-(+)- and (S)-(-)-limonene to α -terpineol by *Penicillium digitatum*—investigation of the culture conditions. *Food Chem* 80(4):525–534
- Beltran F, Perez-Lopez AJ, Jose Lopez-Nicolas M, Carbonell-Barrachina AA (2006) Effects of mandarin cultivar on quality of mandarin juice. *Food Sci Tech Int* 14(4):307–313
- Bozkurt T, Gulnaz O, Kacar YA (2017) Chemical composition of the essential oils from some citrus species and evaluation of the antimicrobial activity. *IOSR J Environ Sci Toxicol Food Technol (IOSR-JESTFT)* 11(10):29–33
- Brat P, Gancel AL, Reynes RM, Brillouet JM (2001) Essential oils obtained by flash vacuum-expansion of peels from lemon, sweet orange, mandarin and grapefruit. *Fruits* 56(6):395–402
- Choi IS, Kim J-H, Wi SG, Kim KH, Bae H-J (2013) Bioethanol production from mandarin (*Citrus unshiu*) peel waste using popping pretreatment. *Appl Energy* 102:204–210
- Crowell PL (1999) Prevention and therapy of cancer by dietary monoterpenes. *J Nutr* 129:775–778
- Elmaci Y, Altug T (2012) Mandarin peel aroma: Estimation by using headspace/GC/MS and descriptive analysis techniques. *Acta Aliment* 41(1):131–139
- Esmaili A, Tavassoli A (2010) Microbial transformation of citral by *Penicillium* sp. *Acta Biochim Pol* 57(3):265–268

- Ibrahim AD, Hussaini H, Aliero AA, Yakubu SE (2011) Volatile metabolites profiling to discriminate diseases of tomato fruits inoculated with three toxigenic fungal pathogens. *Res Biotechnol* 2(3):14–22
- Junior MM Jr, Rocha e Silva TAA, Franchi GC et al (2009) Antioxidant potential of aroma compounds obtained by limonene biotransformation of orange essential oil. *Food Chem* 116(1):8–12
- Marostica MR, Pastore GM (2007) Production of R-(+)- α -terpineol by the biotransformation of limonene from orange essential oil, using cassava waste water as medium. *Food Chem* 101(1):345–350
- Nwobi BE, Ofoegbu O, Adesina OB (2006) Extraction and qualitative assessment of African sweet mandarin seed oil. *Afr J Food Agric Nutr Dev* 10(8):245–253
- Parshikov IA, Sutherland JB (2014) The use of *Aspergillus niger* cultures for biotransformation of terpenoids. *Process Biochem* 49(12):2086–2100
- Zheng L, Zheng P, Sun Z, Bai Y (2007) Production of vanillin from waste residue of rice bran oil by *Aspergillus niger* and *Pycnoporus cinnabarinus*. *Biores Technol* 98(5):1115

Utilization of Low-Cost Fatty Acid Sources by Bacterial Isolate for Improved Production of Valuable Prodigiosin



Dalia Dasgupta Mandal, Subhasree Majumdar, Sovan Dey, Sourav Dutta, and Tamal Mandal

Abstract Prodigiosin, a bright pinkish-red bioactive compound, has enormous pharmacological significance as anti-cancer, anti-microbial, anti-oxidant and immunosuppressive agents. This is produced by several bacterial species such as *Serratia*, *Pseudomonas* and *Streptomyces*. It is one of the most conspicuous bacterial pigments extant in the microbial world. In the present work, cost-effective production of prodigiosin from *Serratia marcescens* NITDPER1 an indigenous bacterial strain isolated from paper mill effluent was studied. The pigment yield from this isolate was much less in nutrient broth media and peptone glycerol media $0.047 \pm 0.001 \text{ g L}^{-1}$ and $0.02 \pm 0.003 \text{ g L}^{-1}$, respectively, at 30 °C, pH 7 and 120 rpm. To increase production, fatty acid as carbon source, such as peanut oil, peanut powder and palm oil, was used that gave better yield compared with common media. Among these three, peanut oil gave the highest yield ($5.36 \pm 0.81 \text{ g L}^{-1}$) followed by palm oil ($4.43 \pm 0.72 \text{ g L}^{-1}$) and peanut powder ($3 \pm 0.45 \text{ g L}^{-1}$). From economical perspectives, palm oil as a low-cost fatty acid source showed noticeable production and

D. Dasgupta Mandal (✉) · S. Dey · S. Dutta
Department of Biotechnology, National Institute of Technology Durgapur, Mahatma Gandhi Avenue, Durgapur, West Bengal 713209, India
e-mail: dalia.dasgupta@bt.nitdgp.ac.in

S. Dey
e-mail: deysovan97@gmail.com

S. Dutta
e-mail: kittu.sd79@gmail.com

S. Majumdar
Department of Biotechnology, National Institute of Technology Durgapur, Durgapur, India
e-mail: subhasree.majumdar1987@gmail.com

Department of Zoology, Sonamukhi College, Sonamukhi, Bankura, West Bengal 722207, India

T. Mandal
Department of Chemical Engineering, National Institute of Technology Durgapur, Mahatma Gandhi Avenue, Durgapur, West Bengal 713209, India
e-mail: tamal.mandal@che.nitdgp.ac.in

thus can be thought of an alternative nutrient source. The extracted pigment characterized by UV–visible spectroscopy ($\lambda_{\max} = 535 \text{ nm}$), TLC ($R_f = 0.9$), HPLC (RT = 2.865), FTIR and NMR confirmed it as prodigiosin. The kinetic parameters of Luedeking–Piret model for pigment production in different fatty acid media revealed growth-associated production.

Keywords Prodigiosin · Fatty acid · Peanut powder · Peanut oil · Palm oil

1 Introduction

Secondary metabolites of bacterial origin are of great importance to mankind in many ways, which include various pigments, enzymes, antibiotics and many other valuables. Prodigiosin, a bright red pigment produced by several bacterial species such as *Serratia*, *Pseudomonas* and *Streptomyces* (Giri et al. 2004) is one of the most conspicuous bacterial pigments extant in the microbial world (Venil et al. 2013). The attention on prodigiosin increased when different studies certified it to possess anti-bacterial, anti-malarial, anti-oxidant and anti-neoplastic properties (Darshan and Manonmani 2015). It has gained much research attention among microbial pigments because of its good thermostability and bright colour (Ren et al. 2018). However, one of the major constraints in pigment production from bacterial cells is the high cost of synthetic medium used (Venil et al. 2013). This limitation along with the parallel high-potential commercial value of prodigiosin has kindled the demand of cost-effective bioprocesses for this biopigment. From different studies, fatty acids as carbon source such as peanut, sesame, sunflower, and so on have shown their potential in enhancing prodigiosin production by bacterial species not only in their powdered forms but also through extracted oils (Giri et al. 2004). These oil sources are, however, costly that lead to the usage of cheap fatty acid sources in demand to enhance prodigiosin production with minimum production cost. Palm oil is such a low-cost oil source that contains 50% of saturated fatty acids (Montoya et al. 2014) and may prove its potential as a cost-effective carbon source for prodigiosin production.

In the present study, *Serratia marcescens* NITDPER1 (GenBank accession number MN380036), an indigenous bacterial strain isolated in our laboratory from paper mill effluent was explored for prodigiosin production using conventional synthetic media as well as different fatty acid sources to compare maximum pigment production. The extracted reddish-pink pigment was characterized to ascertain its nature as prodigiosin. The kinetic parameters of growth and pigment production were analysed to relate growth associatedness of the process. This study aimed at an alternate low-cost source of nutrition for *S. marcescens* NITDPER1 for improved prodigiosin production from economic perspective and commercial use.

2 Materials and Methods

2.1 *Microorganism and Chemicals*

Paper mill wastewater was collected from Raniganj area, West Bengal, India, from where *S. marcescens* NITDPER1 was isolated and maintained in laboratory conditions. All the reagents were from Sigma-Aldrich, Merck and Himedia unless otherwise mentioned and were of analytical grade.

2.2 *Batch Studies for Pigment Production*

Five different media, namely, nutrient broth, peptone glycerol broth, peanut powder broth (2%), peanut oil broth (2%) and palm oil broth (2%) were prepared (100 ml) and autoclaved at 121 °C, 105 kPa for 20 min followed by inoculation with 5% overnight-grown bacterial culture. The flasks were kept in an incubator at a shaking speed of 120 rpm and 30 °C temperature for 96 h. At regular interval, 10 ml culture was taken out from the flask, and pigment was extracted with 2 ml acidified ethanol following Suryawanshi et al. (2014). Growth was monitored at regular intervals spectrophotometrically by withdrawing 1 ml culture volume and drying the pellet biomass.

2.3 *Characterization of the Extracted Pigment*

The extracted pigment was characterized by UV-vis spectrophotometry (200–800 nm) and TLC using chloroform:methanol (9:1) as the solvent system (de Araújo et al. 2010). The HPLC profile was analysed using acetonitrile: HPLC water (60:40) as solvent system (Faraag et al. 2017). FTIR spectra were recorded between scanning ranges of 400 and 4000 cm^{-1} and ^1H NMR (125 MHz) spectroscopy (Bruker Advance 500 NMR) was done using chloroform-d₂ (CDCl_3) as the solvent.

2.4 *Kinetic Analysis of Growth and Pigment Production*

Growth- and production-associated kinetic parameters such as specific growth rate (μ), generation time (T_G) and growth-associated (α) and non-growth-associated (β) kinetic constants for product formation were determined. Production kinetics was studied using Luedeking–Piret model (Luedeking and Piret 1959), which is given as

$$dp/dt = \alpha dx/dt + \beta x \quad (1)$$

3 Results and Discussion

3.1 Pigment Production in Batch Studies

The growth profile of bacterial isolate from Fig. 1a reveals that the bacterial isolate has preferred fatty acid-containing powders and oils as carbon source in comparison to nutrient broth and peptone glycerol media for growth and pigment production. Nutrient broth and peptone glycerol broth yielded only 0.047 ± 0.001 g/L and 0.02 ± 0.003 g/L productivity, respectively, after 60 h of incubation. It is important to note that compared with this study, much higher productivity of prodigiosin in nutrient broth (0.35 g/L) and peptone glycerol media (0.56 g/L) in similar process conditions have been reported by Giri et al. (2004), using other strains of *Serratia*. The variations in production may be due to the preferential nutritional choice of the selected strain as certain carbon source may be responsible for catabolite repression (Kalivoda et al. 2010). In the presence of fatty acid source-containing media, the bacterial growth and prodigiosin production were considerable. There was time-dependent enhancement in production in correlation with growth with maximum yield observed at 60 h for peanut oil and palm oil and 72 h for peanut powder, beyond that there was no significant yield enhancement. The highest productivity was observed in case of peanut oil (5.36 ± 0.81 g/L) followed by palm oil (4.43 ± 0.72 g/L) and peanut powder media (3 ± 0.45 g/L). Similar findings were reported by Giri et al. (2004) where fatty acid as carbon source showed improved prodigiosin production compared with conventional media. Further, this can be supported by the finding of Aruldass et al. (2014) for prodigiosin production by *S. marcescens* UTM1 where complex media were deemed to be poorly nutritious compared with chemically defined simple media such as brown sugar. Palm oil as an alternate source of fatty acids showed promising results in comparison with peanut oil that gave only 1.2-fold higher production. However, peanut oil is the costliest edible oil in India (Economic Times 2015), so, on economic point of view, palm oil as nutrient can be thought as

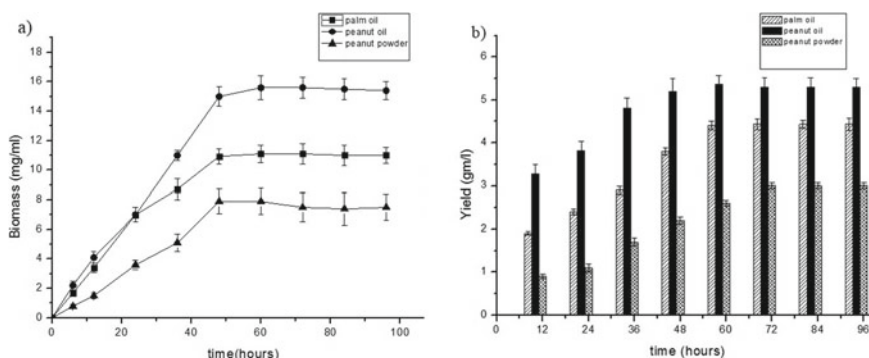


Fig. 1 a Growth of bacterial isolate in different fatty acid media and b pigment production

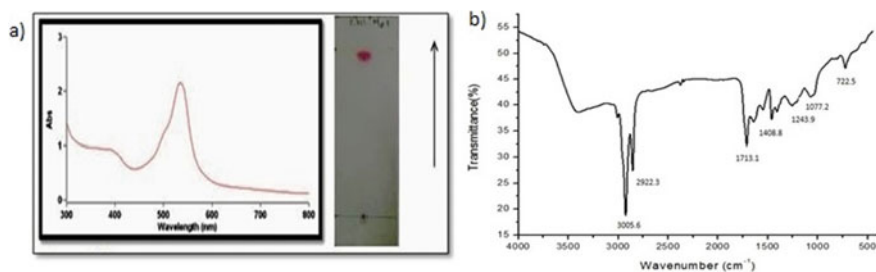


Fig. 2 a UV-vis scan and TLC, b FTIR spectra of extracted pigment

an alternative. This is the first report as per our knowledge related to the production of prodigiosin using low-cost palm oil source revealing an economically feasible alternate to peanut oil without hampering much productivity.

3.2 Characterization of the Extracted Pigment

The characterization of extracted pigment revealed lambda max at 535 nm and R_f value of 0.9 (Fig. 2a). The HPLC profile revealed a single clear peak at retention time of 2.865 that is close to the reports of Faraag et al. (2017) for prodigiosin.

The FTIR absorption spectra of the pigment for the location of various peak intensities at different wavenumbers (cm⁻¹) indicating the presence of different functional groups in its structure (Fig. 2b). Bands were located at 3005.6, 2922.3, 2853.8, 1713.1, 1643.7, 1547.1, 1408.8, 1243.9, 1077.2 and 722.5. These characteristic spectra showed similarity with the already reported FTIR data of prodigiosin pigment (Sumathi et al. 2014; Suryawanshi et al. 2014) certifying its nature to be prodigiosin.

The NMR spectral analysis of extracted pigment (not shown) via ¹H NMR (500 MHz, CDCl₃) showed δ values at 7.26, 6.95, 4.01, 3.08, 2.54, 2.35, 2.2, 1.54, 1.28, 1.257, 0.88, 0.89, 0.87, 0.86, 0.85, 0.83 ppm similar to patterns with other prodigiosin spectra reported by Faraag et al. (2017) and Arivizhivendhan et al. (2015). The high degree of similarity thus confirms extracted pigment to be prodigiosin.

3.3 Growth and Production Kinetics

In batch studies using fatty acid sources, the specific growth rate (μ) of the bacterial isolate was 0.1923, 0.2715 and 0.1586 h⁻¹ and generation time (T_G) was 3.6 h, 2.55 h and 4.37 h in peanut oil, palm oil and peanut powder media, respectively. Kinetic study carried out using Luedeking–Piret model is shown in Fig. 3 that reveals growth-

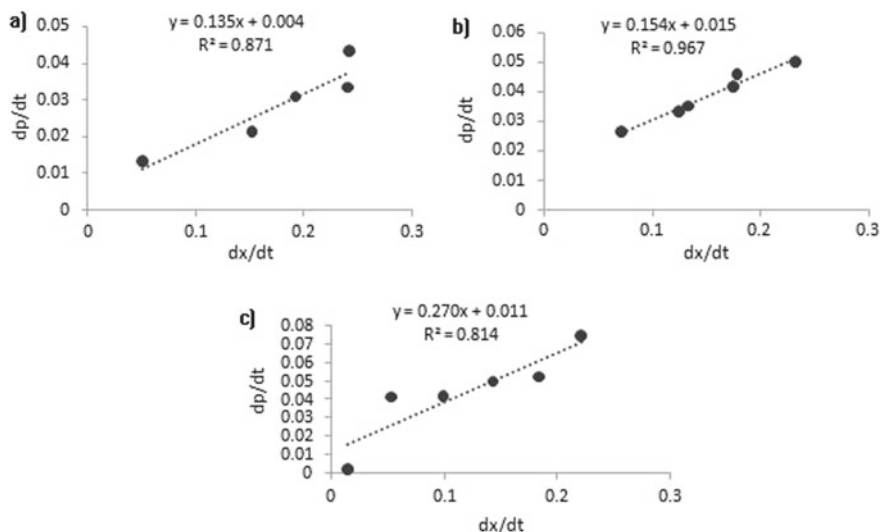


Fig. 3 Luedeking–Piret model for production using **a** peanut oil, **b** peanut powder, **c** palm oil

associated pigment yield coefficient (α) of 0.2707, 0.1358, 0.1547 and a minor non-growth-associated constant (β) of 0.0117, 0.0047 and 0.015 for palm oil, peanut oil and peanut powder, respectively. The non-growth-associated production means production during stationary phase that was very less, so it could be said that in this case, prodigiosin production process is growth associated. Similar findings of growth-associated pigment production and substrate consumption were found for *Monascus purpureus* red pigment production in shake flasks (Musaalbakri et al. 2006). Whereas, Lu et al. (2009) reported non-growth-associated violacein pigment production by *Janthinobacterium lividum* XT1 using sucrose as the carbon source. So, depending on the microbe being used, production kinetics may vary. In the present study, growth associatedness emphasizes the importance of fatty acids as carbon source for growth and related production.

4 Conclusion

This study determined the efficacy of palm oil as a carbon source for the growth and prodigiosin production by *S. marcescens* NITDPER1. Prodigiosin as a promising drug and biocolour has enormous market value for which economically feasible media are highly demanded. Here, the isolated bacterial strain shows celebrated productivity of prodigiosin using a cheap fatty acid carbon source paving the path for low-cost productivity.

Acknowledgements The authors convey their sincerest gratitude to the Department of Biotechnology and Department of Chemical Engineering, National Institute of Technology Durgapur, India for providing the necessary instrumental and infrastructural support.

References

- Araújo HWC, Fukushima K, Campos-Takaki GM (2010) Prodigiosin production by *Serratia marcescens* UCP 1549 using renewable-resources as a low cost substrate. *Molecules* 15:6931–6940
- Arivizhivendhan KV, Mahesh M, Mary RR, Sekaran G (2015) Bioactive prodigiosin isolated from *Serratia marcescens* using solid state fermenter and its bactericidal activity compared with conventional antibiotics. *Microbial Biochemical Technol* 7(5):305–312
- Aruldass CA, Venil CK, Zakaria ZA, Ahmad WA (2014) Brown sugar as a low-cost medium for the production of prodigiosin by locally isolated *Serratia marcescens* UTM1. *Int Biodeterior Biodegrad* 95:19–24
- Darshan N, Manonmani HK (2015) Prodigiosin and its potential applications. *J Food Sci Technol* 52:5393–5407
- Economic times (2015) <http://m.economictimes.com/markets/commodities/groundnut-oil-now-the-most-expensive-cooking-oil-in-india/articleshow/47777970.cms>
- Faraag AH, El-Batal AI, El-Hendawy HH (2017) Characterization of prodigiosin produced by *Serratia marcescens* strain isolated from irrigation water in Egypt. *Nature and Science* 15(5):55–68
- Giri AV, Anandkumar N, Muthukumaran G, Pennathur G (2004) A novel medium for the enhanced cell growth and production of prodigiosin from *Serratia marcescens* isolated from soil. *BMC Microbiol* 4(11):1–10
- Kalivoda EJ, Stella NA, Aston MA, Fender JE, Thompson PP, Kowalski RP, Shanks RMQ (2010) Cyclic AMP negatively regulates prodigiosin production by *Serratia marcescens*. *Res Microbiol* 161(2):158–167
- Lu Y, Wang L, Xue Y, Zhang C, Xing X, Lou K, Zhang Z, Li Y, Zhang G, Bi J, Su Z (2009) Production of violet pigment by a newly isolated psychrotrophic bacterium from a glacier in Xinjiang, China. *Biochem Eng J* 43:135–141
- Luedeking E, Piret L (1959) A kinetic study of the lactic acid fermentation: batch process at controlled pH. *J Biochem Microbiol Technol Eng* 4:231–241
- Musaalbakri AM, Ariff A, Rosfarizan M, Ismail AKM (2006) Kinetics and modelling of red pigment fermentation by *Monascus purpureus* FTC 5391 in 2-litre stirred tank fermenter using glucose as a carbon source. *J Trop Agric Fd Sc* 33(2):277–284
- Montoya C, Cochard B, Flori A, Cros D, Lopes R (2014) Genetic architecture of palm oil fatty acid composition in cultivated oil palm (*Elaeis guineensis* Jacq.) compared to its wild relative *E. oleifera* (H.B.K) Cortés. *PLoS One* 9(5):e95412. <https://doi.org/10.1371/journal.pone.0095412>
- Ren Y, Gong J, Fu R, Zhang J, Fang K, Liu X (2018) Antibacterial dyeing of silk with prodigiosins suspension produced by liquid fermentation. *J Clean Prod* 201:648–656. <https://doi.org/10.1016/j.jclepro.2018.08.098>
- Sumathi C, MohanaPriya D, Swarnalatha S, Dinesh MG, Sekaran G (2014) Production of prodigiosin using tannery fleshing and evaluating its pharmacological effects. *Sci World J*. <https://doi.org/10.1155/2014/290327>
- Suryawanshi RK, Patil CD, Borase HP, Salunke BK, Patil SV (2014) Studies on production and biological potential of prodigiosin by *Serratia marcescens*. *Appl Biochem Biotechnol* 173:1209–1221
- Venil CK, Zakaria ZA, Ahmad WA (2013) Bacterial pigments and their applications. *Process Biochem* 48:1065–1079

Simplified Detection of Serotonin by FET-Based Sensor



Koel Sinha, Rabindranath Majumder, and Chitragada Das Mukhopadhyay

Abstract Qualitative and quantitative detection of neurotransmitter is crucial in many areas, ranging from early clinical diagnosis to homeland security. Due to various advantages such as the ultralow limit of detection, fast readout, low cost, and easy method of fabrication over traditional detection systems, semiconductor nanorod-based electronic devices have emerged out to be a potential sensing platform. In the present study, we synthesized biologically active ZnO nanorod field-effect transistor (FET)-based biosensor for the detection of different concentrations of serotonin (5-HT) solution. In addition, serotonin ranging from lower to higher concentration resulted in the change in electrical current with an increase in gate voltage. The ZnO nanorod FET-based biosensor could easily detect as low as 1 fM serotonin, which implied that the detection limit of the biosensor can be as low as 1 fM.

Keywords Neurotransmitter · Field-effect transistor · Biosensor · Serotonin

1 Introduction

Serotonin is one of the principal neurotransmitters and is regarded as the molecule of contentment as it participates actively in controlling a number of behavioral as well as cognitive activities (Godoy-Reyes et al. 2018). It is majorly produced by the brain under the normal physiological condition where it functions in passing the information to various organs through the central nervous system (Lacasse and

K. Sinha · R. Majumder · C. Das Mukhopadhyay (✉)
Centre for Healthcare Science and Technology, Indian Institute of Engineering Science and Technology, Shibpur, Howrah, West Bengal 711103, India
e-mail: chitragadadas@yahoo.com

K. Sinha
e-mail: ksinha2110@gmail.com

R. Majumder
e-mail: dr.rabindranath.majumder@gmail.com

© Springer Nature Singapore Pte Ltd. 2021
D. Ramkrishna et al. (eds.), *Advances in Bioprocess Engineering and Technology*,
Lecture Notes in Bioengineering,
https://doi.org/10.1007/978-981-15-7409-2_4

Leo 2005). In addition, the gastrointestinal tract has also been reported for secreting serotonin to control the intestinal movement (Camilleri 2009). Its abnormal levels have been related not only with various disorders namely neurodegenerative diseases, autism, inflammatory syndromes but also linked with a number of psychotic states including attention-deficit hyperactivity disorder (Carver et al. 2009). In addition, altered serotonin levels have been reported to be associated with sudden death symptoms of infant and an influence on phenomenon of natural aging (Paterson et al. 2006). This implies that it is highly important to quickly detect serotonin for health care and clinical treatment. However, serotonin concentration in body fluid is ~ 15 nM whereas, in urine it is around 295–687 nM, thus, the detection of serotonin is often applied by specific techniques that are complicated strategies, high cost, and time-consuming (Artigas et al. 1985; Huang et al. 2012; Tekes 2008; Umeda et al. 2005). In this regard, high-quality electrocatalyst-based electrochemical sensor would be a valuable clinical diagnostic tool to permit the simple, sensitive, accurate, rapid, and reliable detection of low serotonin levels.

Recently, numerous detection methods have been developed to monitor serotonin, but still several problems exist. For instance, several detection techniques such as solvent extraction and ion-exchange chromatography require extensive sample preparation and are aspecific with respect to other indole species (Tonelli et al. 1982). Comparably, this can be overcome by high-performance liquid chromatography (HPLC), which can distinguish between different indoles. Therefore, it is currently the most common technique in the field, but it is especially costly and requires sophisticated equipment, making it unsuitable for routine tests (Anderson 1991; Patel et al. 2005; Kema et al. 2000). Hence, another alternative detection system must be needed to overcome these problems of the conventional serotonin detection systems.

Recently, a semiconducting nanorod field-effect transistor (FET)-based biosensors have gained much interest owing to its outstanding properties and efficiency. As sensing elements, the FET device serves to overcome many obstacles faced by current sensing technologies. For example, significant advantages such as portability, high sensitivity, fast response, low manufacturing cost, and label-free detection procedure have provided a clear aspect to develop FET-based biosensors for analyzing biological/chemical molecules. To this end, in this study, zinc oxide nanorod FET device, was utilized for the first time to develop a highly sensitive biosensor for detecting serotonin molecule in a fast response manner. Different concentrations of serotonin molecule (range from 1 fM to 1 μ M) in a wide range were sensitively analyzed by current change based on the immunoreactions.

2 Materials and Methods

2.1 Fabrication of ZnO FET

ZnO FET-based biosensor with lateral electrode configuration has been fabricated using hydrothermal technique involving the ZnO seed layer preparation. Contacts have been installed on one side of the glass substrate by photolithography. Here, positive photoresist S1813 was spin-coated on top of glass surface by centrifugation at 2500 rpm for 30 s. First, the ZnO precursor solution was prepared by mixing 50 mM zinc nitrate hexahydrate [$\text{Zn}(\text{NO}_3)_2 \cdot 6\text{H}_2\text{O}$] with 100 ml of deionized (DI) water. The solution bath has been placed on a magnetic stirrer and was heated. Next, 4 ml of ammonium hydroxide [NH_4OH] solution has been added in the solution as soon as the bath temperature rises to 60 °C, followed by stirring up to 30 min. Then, the solution was kept uninterrupted for 24 h. ZnO film is obtained from the precursor solution and has been spin-coated on glass surface. After that, for evaporation of the remaining solvent, ZnO sample has been kept on a hot plate at 250 °C for 10 min. Next step involves the hydrothermal growth of ZnO nanorod on the seeded surface area following the procedure as reported earlier. About 50 mM zinc nitrate hexahydrate [$\text{Zn}(\text{NO}_3)_2 \cdot 6\text{H}_2\text{O}$] with 50 ml DI water, whereas, on another beaker, 50 mM hexamethylenetetramine [HMTA, $\text{C}_6\text{H}_{12}\text{N}_4$] has been blended with 50 ml DI water and was stirred for 10 min respectively. Then both the solutions have been mixed with one another and stirred at 260 rpm. The ZnO-seeded glass platform has been suspended into the solution bath for 2 h. After this step, the glass platform has been taken out from the solution and washed with DI water. To achieve better crystallization, the ZnO nanorod has been thereby annealed at 350 °C using the rapid thermal annealing method for 5 min.

2.2 Functionalization of ZnO

For proper antibody immobilization, silanization process was followed by cross-linker attachment. The silane solution has been prepared by the addition of 0.4 ml mercaptopropyltrimethoxysilane (MTS) and 9.258 ml ethanol with 0.341 ml DI water and was pipetted on the sensor surface. The sensor was sealed and was left in the nitrogen environment for 24 h. The sample was washed with ethanol and then ultrasonicated for 5 min along with a drying session in the nitrogen environment. Thereafter, the cross-linker attachment was achieved by 2 mM N- γ -maleimidobutyryloxysuccinimide (GMBS) solution on the ZnO surface and was kept for 24 h. The sample was then ultrasonicated in ethanol for 5 min and thereafter the activated ZnO surface is now suitable for covalent attachment of antibody. Therefore, all the surface modification steps have been performed in room temperature following the reported protocol (Corso et al. 2008).

2.3 Preparation of Serotonin Solution

Serotonin hydrochloride (1 mg/ml) has been utilized as the target molecule purchased from Sigma-Aldrich, USA. For the purpose of electrical measurements, several serial dilutions of serotonin hydrochloride have been performed with phosphate buffer saline (PBS) (pH 7.2) and 20 mM ionic strength to produce concentration ranging from 1 fM to 1 μ M. Thereafter, to carry out further measurements in physiological sample, serotonin hydrochloride has been spiked in human blood serum. The blood samples were kept at room temperature to separate the serum following the standard protocol. The selectivity of the fabricated FET biosensor has been examined with dopamine and uric acid molecules by separately spiking each of the samples.

2.4 Electrical Measurement

Each sensor chip has been used to interface with the PC through a sensor holder setup. In the setup, the bond pads of the sensors have been set just below the probes of the sensor holder. The probes of the sensor holder are connected with drain and source electrodes and are spring loaded and the adjustment screws are provided to align with the bond pads. The gate electrode has been inserted by a small gap in the setup and soldered to a metal connector. The gate electrode has been fixed to a DC power supply (Keysight technologies). A high-frequency signal of 20 mV amplitude in the frequency range of 200–1000 kHz has been applied through a signal generator (Agilent 33521A) at the drain electrode. The high-frequency signal with a reference signal of 1.43kHz has been modulated using a lock-in amplifier (Stanford Research, SR 830) and provided to the ZnO FET at the source terminal.

2.5 Characterization Techniques

To characterize the surface morphology of the ZnO nanorods, growth was recorded with field emission scanning electron microscopy (FESEM) (ZEISS SUPRA-40). The X-ray diffraction (XRD) was employed using RIGAKU diffractometer to confirm the crystal structure of ZnO nanorod.

2.6 Real Sample Analysis

Human blood samples were collected from Nashipur Block Primary Health Centre, West Bengal and were used for the experiment. They were kept in sterilized containers and were centrifuged for 10 min at approximately 3000 rpm. The obtained serum was

kept in sterilized containers for further experimentation. The study has been approved by the appropriate institutional ethics committee (No. NBPHC/187 dated 11th May, 2019), and blood sampling and experimentation have been performed in accordance with the 1964 Helsinki Declaration and its later amendments or comparable ethical standards.

3 Results and Discussion

3.1 Structural Characterization

The surface morphological study has been conducted with high-resolution FESEM with an operating voltage of 10 kV and magnification of 100 K. The top view of FESEM micrograph of the ZnO samples is shown in Fig. 1. Therefore, film continuity has been confirmed from the FESEM micrograph. Average grain size has been found to be around 60 nm. The XRD pattern of the rapidly grown ZnO nanorod exhibited diffraction peak along (002) plane at $2\theta \approx 34.4^\circ$ (Fig. 2). The diffraction peak (002) denoted the unit cell of the crystal to be hexagonal in growth with its c -axis perpendicular to that of the glass substrate. Besides, clear sharpness and no impurity diffraction peaks indicate the crystallinity along with the high purity of the fabricated ZnO nanorod.

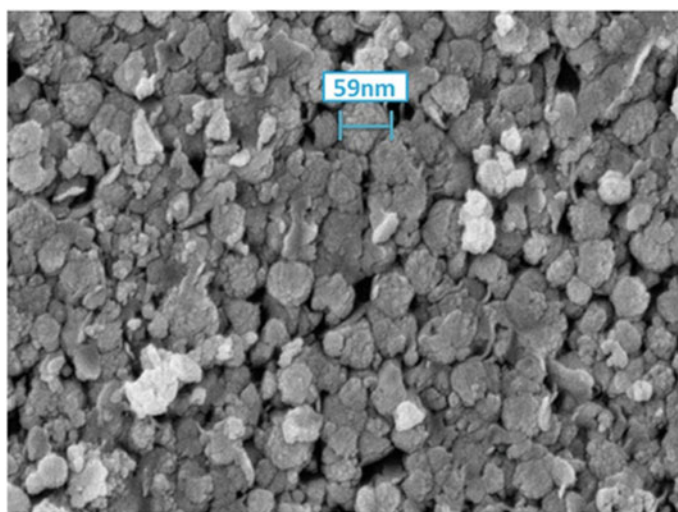


Fig. 1 FESEM micrograph of ZnO seed layer

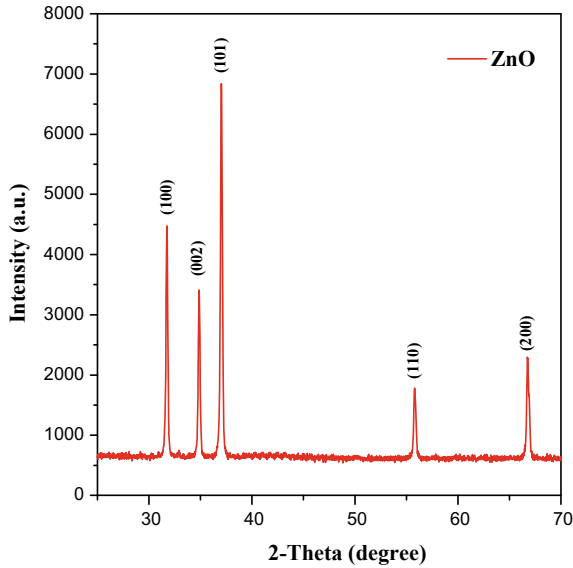


Fig. 2 XRD pattern of ZnO nanorod

3.2 Electrical Characterization of the Fabricated Sensor

The FET-based systems are prone to miniaturization, along with small sample volume, high sensitivity (femtomolar level), real-time analyte detection, quantification, and the possibility of in-site analysis (He et al. 2012). The change of I_d with V_{gs} before and after antibody functionalization and after serotonin capture in the presence of 20 mM PBS buffer at pH 7.2 and V_{ds} of 5 V has been examined (Fig. 3). It can be evidenced that the increment in the drain current (I_d) with V_{gs} denotes the n -type intrinsic doping on the surface of the synthesized ZnO nanorod. It has also been observed that the current increases significantly for a change in V_{gs} from 0 to 5 V, which indicates high transconductance. For lateral electrode configuration, conduction of current mostly takes place through the ZnO seed layer. It has been observed that the current decreases significantly after antibody functionalization followed by an increment after serotonin capture. This may be attributed due to the negative charges of antibody molecules at pH 7.2, which leads to modulation of the applied gate voltage, resulting in carrier depletion within the ZnO seed layer and decrease in I_d .

Variation of sensitivity with different serotonin concentrations at V_{gs} 5 V for 1 MHz frequency has been plotted in Fig. 4. From this plot, it can be noted that sensitivity around 6.42% can be achieved at 1 fM serotonin concentration in biological matrix namely serum with this fabricated sensor. It can be observed that the sensitivity gets decreased for serum in comparison with buffer solution (7.85%).

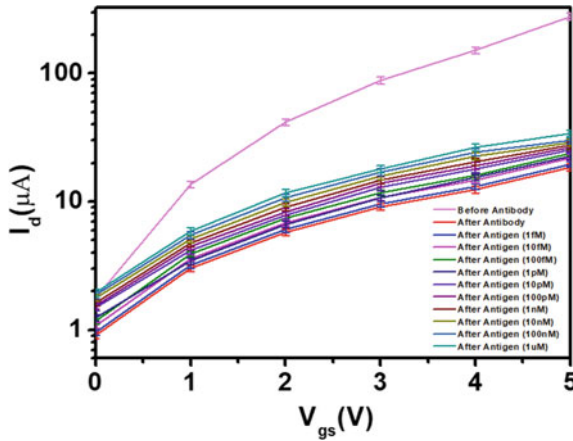


Fig. 3 Variation of I_d with V_{gs} before and after antibody functionalization and after serotonin (antigen) capture

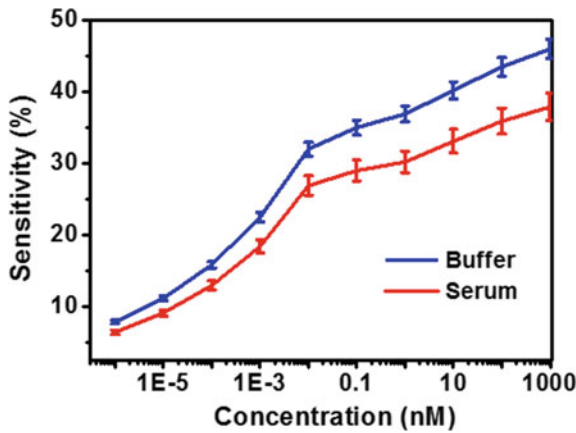


Fig. 4 Variation of sensitivity with different serotonin concentrations in buffer and serum

This phenomenon has been justified due to the lower number of target biomolecules are being captured for the equal quantity of pipetted solution.

4 Conclusion

This present study describes the development of fast, label-free, economical, ZnO nanorod FET-based biosensor for serotonin detection in serum. The fabrication of the sensor was characterized by FESEM and XRD. The selection of FET-based sensor for

electrical detection of serotonin was demonstrated for the first time in a ZnO nanorod matrix to the best of our knowledge, where the sensitivity was achieved at a very lower level. The limit of detection of the proposed biosensor is 1 fM – $1 \text{ } \mu\text{M}$, which is suitable for discriminating the control serum from the case serum at point of collection without using any additional instrument. The biosensor was highly selective toward serotonin detection and shows 6.42% sensitivity of serotonin from serum samples. Based on the sensing principle, a miniaturized device can be developed for serotonin detection in real biological samples, indicating its real clinical benefits and prospective industrial potential. In the future, the sensing platform or principle described here in the study can be extended toward the detection of various molecules in different matrices.

Compliance with Ethical Standards **Funding** This work was not supported by any grant from funding agencies.

Conflict of Interest The authors declare that they have no conflict of interest.

Research involving Human Participants and/or Animals **Ethical approval:** All procedures performed in studies involving human participants were in accordance with the ethical standards of the institutional and/or national research committee and with the 1964 Helsinki Declaration and its later amendments or comparable ethical standards.

References

- Anderson GM (1991) Signal-to-noise optimization of HPLC-fluorometric systems and their application to the analysis of indoles. *Adv Exp Med Biol* 294:51–61
- Artigas F, Sarrias MJ, Martinez E et al (1985) Serotonin in body fluids: characterization of human plasmatic and cerebrospinal fluid pools by means of a new HPLC method. *Life Sci* 37:441–447
- Camilleri M (2009) Serotonin in the gastrointestinal tract. *Curr Opin Endocrinol Diabetes Obes* 16:53
- Carver CS, Johnson SL, Joormann J (2009) Two-mode models of self-regulation as a tool for conceptualizing effects of the serotonin system in normal behavior and diverse disorders. *Curr Dir Psychol Sci* 18:195–199
- Corso CD, Dickherber A, Hunt WD (2008) An investigation of antibody immobilization methods employing organosilanes on planar ZnO surfaces for biosensor applications. *Biosens Bioelectron* 24:805–811
- Godoy-Reyes TM, Llopis-Lorente A, Costero AM et al (2018) Selective and sensitive colorimetric detection of the neurotransmitter serotonin based on the aggregation of bifunctionalised gold nanoparticles. *Sens. Actuators B Chem* 258:829–835
- He RX, Lin P, Liu ZK et al (2012) Solution-gated graphene field-effect transistors integrated in microfluidic systems and used for flow velocity detection. *Nano Lett* 12:1404–1409
- Huang H, Chen Z, Yan X (2012) Simultaneous determination of serotonin and creatinine in urine by combining two ultrasound-assisted emulsification microextractions with on-column stacking in capillary electrophoresis. *J Sep Sci* 35:436–444
- Kema IP, De Vries EGE, Muskiet F (2000) Clinical chemistry of serotonin and metabolites. *J Chromatogr B Analyt Technol Biomed Life Sci* 747:33–48
- Lacasse JR, Leo J (2005) Serotonin and depression: a disconnect between the advertisements and the scientific literature. *PLoS Med* 2:392

- Patel BA, Arundell M, Parker KH et al (2005) Simple and rapid determination of serotonin and catecholamines in biological tissue using high performance liquid chromatography with electrochemical detection. *J Chromatogr B Analyt Technol Biomed Life Sci* 818:269–276
- Paterson DS, Trachtenberg FL, Thompson EG et al (2006) Multiple serotonergic brainstem abnormalities in sudden infant death syndrome. *J Am Med Assoc* 296:2124–2132
- Tekes K (2008) HPLC determination of serotonin and its metabolites from human platelet-rich plasma; shift to 5-hydroxytryptophol formation following alcohol consumption. *J Chromatogr Sci* 46:169–173
- Tonelli D, Gattavecchia E, Gandolfi M (1982) Thin-layer chromatographic determination of indolic tryptophan metabolites in human urine using Sep-Pak C18 extraction. *J Chromatogr B Analyt Technol Biomed Life Sci* 231:283–289
- Umeda S, Stagliano GW, Borenstein MR et al (2005) A reverse-phase HPLC and fluorescence detection method for measurement of 5-hydroxytryptamine (serotonin) in *Planaria*. *J Pharmacol Toxicol Methods* 51:73–76

Production of Lactose-Free Cheese Using Partially Purified β -Galactosidase from *Enterobacter aerogenes* st KCTC2190



Manisha Maity, D. K. Bhattacharyya, and Jayati Bhowal

Abstract β -galactosidase has numerous applications in milk and other dairy industries including treatment of lactose intolerance. It catalyzes the hydrolysis of milk sugar lactose into monosaccharides, namely, D-galactose and D-glucose. In this present study, *Enterobacter aerogenes* st KCTC2190 was isolated from soil around cattle shed area, which was capable of producing intracellular β -galactosidase. Extracted β -galactosidase was partially purified by cold acetone method. After partial purification, specific activity and purification fold increased to 10.64 ± 1.12 U/mg and 1.28 fold. Partially purified β -galactosidase was then applied on cheese to produce lactose-free soft cheese. Physicochemical analysis such as moisture, ash, fat, carbohydrates, proteins of raw material, control cheese (without enzyme treatment), and cheese from β -galactosidase-treated milk was almost same except lactose content. This partially purified β -galactosidase displayed hydrolytic effect on cheese lactose. Lactose hydrolysis of 81.90% occurred after 4 h of treatment of milk with this partially purified enzyme at 40 °C. After 4 h of enzymatic treatment, lactose hydrolysis became constant.

Keywords β -galactosidase · Lactose hydrolysis · Cheese

M. Maity · D. K. Bhattacharyya · J. Bhowal (✉)
School of Community Science and Technology, Indian Institute of Engineering Science and Technology, Shibpur, Howrah, West Bengal 711103, India
e-mail: jayatibhowal@gmail.com

M. Maity
e-mail: manisha.maity04@gmail.com

D. K. Bhattacharyya
e-mail: dkb_oiltech@yahoo.co.in

1 Introduction

β -galactosidase has important application in food and medical industries due to their ability of both hydrolytic and transglycosylation activities (Qi et al. 2017). This enzyme can be used in milk and milk derivatives to decrease their lactose content and thus solving the problem of low lactose solubility and its low degree of sweetening (Kumar et al. 2015). Inadequate production of β -galactosidase leads to discomforts such as cramps, gas, in digestion, diarrhea. β -galactosidase enhances the color, aroma, and flavor of milk products. The creaminess of the ice cream increases due to lactose hydrolysis (Erich et al. 2015). Regular milk and lactose-free milk have differences in viscosity and whiteness. The lactose contents of milk and milk products are a matter of concern for lactose-intolerant people. Technologies have to be applied for the production of lactose-free milk and milk products from the regular milk. β -galactosidase can commercially be applied in dairy industry to produce products of low lactose content (Bosso et al. 2016). Factors such as pH, temperature, time, lactose concentration, and presence of some activators alter the enzymatic hydrolysis process (Triose et al. 2016). The present work was aimed at lactose hydrolysis of milk by β -galactosidase obtained from soil bacteria and production of lactose-free cheese.

2 Materials and Methods

2.1 Chemicals

Cow milk and starter culture tablet (Lactobacil_{plus}) were purchased from local market, Shibpur, Howrah, India. Chemicals used in this study were of analytical grade and purchased from Merck, Germany and Sigma-Aldrich, USA. Bacteriological media were procured from HiMedia laboratory Pvt. Ltd., India. The test kit of oxidase–peroxidase for glucose estimation was purchased from Robonik (Prietest).

2.2 Screening and Isolation of β -Galactosidase-Producing Microorganism

The β -galactosidase-producing bacteria were screened, isolated, and purified from soil samples collected from cattle shed area. Soil samples were serially diluted and plated on presterilized petriplates containing lactose media. Lactose medium was containing per liter lactose 5 g, peptone 5 g, beef extract 3 g, agar 15 g, and pH at 6.5 along with chromogenic substance 5-bromo-4-chloro-3-indolyl- β -D-galactopyranoside (X-gal) and incubated at 37 °C for 24 h. Strain was characterized and identified using biochemical and morphological studies and verified by MTCC

(Microbial Type Culture Collection & Gene Bank), Chandigarh. 16S rRNA amplification and phylogenetic tree analysis were developed and verified by BioAxis DNA Research Centre (P) Ltd., Hyderabad.

2.3 β -Galactosidase Production and Purification

Fermentation for β -galactosidase production was carried out into 150-ml Erlenmeyer flask containing 50-mL presterilized modified lactose broth containing nutrients (g/L) lactose 10, peptone 10, yeast extract 10, $(\text{NH}_4)_2\text{SO}_4$ 5, NaH_2PO_4 1, MgSO_4 0.5, $7\text{H}_2\text{O}$, MnCl_2 0.5, potato starch 10, and pH 7 at 37 °C for 32 h at static condition. Microbial cells were harvested, suspended in 0.05 mM phosphate buffer, lysed by sonicator (250 W, Piezo-U-Sonic Ultrasonic Cleaner) for 20 min at 4 °C and centrifuged at 6000 rpm for 15 min. Crude intracellular β -galactosidase thus obtained was concentrated by lyophilization and was assayed according to Iqbal et al. (2010) with some modifications. β -galactosidase was further purified through cold acetone precipitation method according to Sumathy et al. (2012).

$$\text{Specific activity (U/mg of protein)} = \text{Enzyme activity/protein concentration}$$

2.4 Lactose-Free Soft Cheese Preparation

Lactose-free cheese preparation involved the preparation of lactose-free milk and later on conversion of this treated milk to cheese.

2.4.1 Lactose-Free Milk Preparation and Optimization of Process Parameters for Lactose Hydrolysis

Cow milk was hydrolyzed by this partially purified β -galactosidase for 6 h before cheese production. Effects of temperature (35–60 °C) and pH (5–7.5) on the hydrolysis of lactose present in cow milk were evaluated. Liberated glucose was measured for both untreated cow milk and β -galactosidase-treated cow milk by glucose oxidase kit, and lactose hydrolysis efficiency (Eh%) was measured.

$$\begin{aligned} & \text{Lactose hydrolysis efficiency (Eh\%)} \\ &= \frac{\text{Glucose concentration} \times \text{Molar mass of lactose}}{\text{Initial lactose concentration} \times \text{Molar mass of glucose}} \times 100 \end{aligned}$$

2.4.2 Preparation of Cheese from β -Galactosidase-Treated and Untreated Cow Milk

Lactose-free soft cheese was prepared as described by Yossef and El Beltagey (2014) with some modifications. Partially purified β -galactosidase was added to cow milk at a ratio of 1:10 (v/v). Then milk was stirred gently at 25–30 °C for 20 min. After that milk was heated at 60–70 °C for 30 min and cooled immediately to 30–40 °C. About 0.02% calcium chloride was added and kept for 15 min. Then 1% starter culture was mixed and kept for 3 h. Whey was discarded after adding rennet and pressed by cheese mold. Disc-shaped cheese was stored in the refrigerator. Similarly, control cheese was prepared with untreated (without β -galactosidase) cow milk.

2.4.3 Proximate Analysis of Cheese from β -Galactosidase-Treated and Untreated Cow Milk

Physicochemical analyses such as moisture, ash, fat, carbohydrates, and proteins of cow milk, control cheese, and cheese from β -galactosidase-treated milk were analyzed according to standard replication AOAC (Association of Official Agricultural Chemists 2011) methods.

2.4.4 Estimation of Antioxidant Activity of Cheese from β -Galactosidase-Treated and Untreated Cow Milk

Estimation of antioxidant activity involved at first the preparation of water-soluble extract of cheese from β -galactosidase-treated and untreated milk. Water-soluble cheese extract was prepared according to Huma et al. (2018) with slight modification. Prepared cheese was mixed with distilled water at a ratio of 1:2 and homogenized (1000 rpm/min) for 20 min. pH of this homogenized mixture was adjusted at 4.6 by 1 M HCl. Slurry was heated in water bath (40 °C) for 1 h, followed by centrifugation (5000 rpm, 15 min) at 4 °C. Then the supernatant was filtered and taken as a water-soluble extract for antioxidant determination. Antioxidant activities such as 2,2'-azino-bis(3-ethylbenzothiazoline-6-sulphonic acid) (ABTS) radical scavenging activity, 2,2-diphenyl-1-picrylhydrazil (DPPH) radical scavenging activity, and ferric reducing antioxidant power (FRAP) assay of aqueous extract of cheese from β -galactosidase-treated milk and cheese from non-treated milk were estimated according to Rahmawati and Suntornsuk (2016) and Huma et al. (2018).

2.4.5 Microbial Load Analysis of Cheese from β -Galactosidase-Treated and Untreated Cow Milk

Microbial load analysis was carried out for both the cheeses during storage condition (stored for 0–30 days at 4 °C). The amount of total viable organisms, lactic acid

bacteria, yeast, and coliform bacteria was estimated using plate count agar, potato dextrose agar, and violet red bile agar, respectively, by the processes described by American Public Health Association (2005).

2.5 Statistical Analysis

All samples were analyzed in triplicates. One-way analysis of variance (ANOVA) of data was analyzed by Tukey test at a significance level of 5% ($P < 0.05$).

3 Results and Discussion

3.1 Screening, Isolation, and Identification

During screening of microorganisms, 43 strains were observed on modified lactose agar media. Among them, 16 strains showed blue colonies on lactose agar media in the presence of X-gal and indicated the ability to produce β -galactosidase activity by these respective strains. Among them, the highest β -galactosidase activity-producing isolate had been identified as *Enterobacter aerogenes* st KCTC2190 on the basis of morphological, biochemical characterization, and 16S rRNA sequence analysis. Figure 1 depicts the phylogenetic tree analysis of this organism. The sequence obtained was 100% identical to the partial gene sequence of 16S rRNA of *Enterobacter aerogenes* st KCTC2190. Accession number of the sequence was KP941761.1.

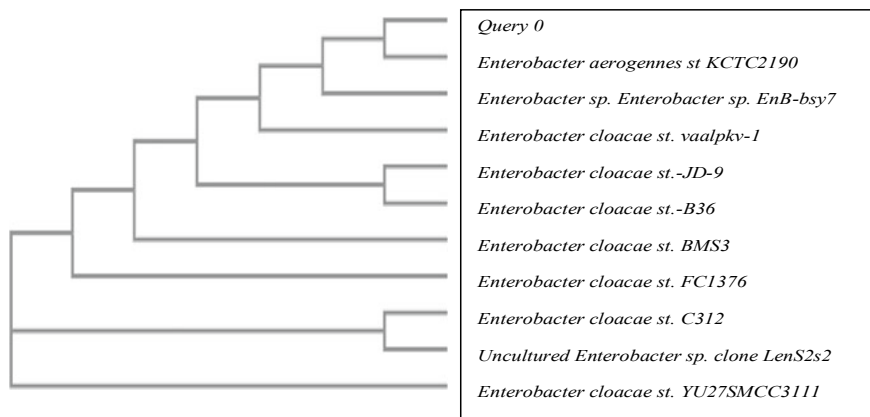


Fig. 1 Diagram representing the estimated phylogenetic relationship on the basis of 16S rRNA sequences of bacteria isolated from cattle shed area

Table 1 Partial purification of β -galactosidase by cold acetone method

Purification steps	Volume (ml)	Total protein concentration (mg)	Total enzyme activity (U)	Specific activity (U/mg)	Recovery (%)	Purification fold
Crude enzyme extract	30	11.21	92.59	8.26 ± 0.57	100	1
Acetone precipitation	10	3.1	32.98	10.64 ± 1.12	35.61	1.28

3.2 β -Galactosidase Production and Enzyme Assay from *Enterobacter aerogenes* st KCTC2190

Enterobacter aerogenes st KCTC2190 was cultivated on modified lactose media and an appreciable amount of intracellular β -galactosidase was produced in process. Crude β -galactosidase from *Enterobacter aerogenes* st KCTC2190 had a specific activity of 8.26 ± 0.57 U/mg as shown in Table 1.

3.3 Partial Purification of β -Galactosidase

Table 1 indicates that partial purification of intracellular β -galactosidase extracted from *Enterobacter aerogenes* st KCTC2190 by cold acetone precipitation method caused a slight increase in specific activity of the enzyme and purification fold was increased up to 1.28 fold.

3.3.1 Optimization of Process Parameters for Lactose Hydrolysis of Cow Milk

Temperature and pH are the two most important factors related to lactose hydrolysis to the extent. Without proper temperature and pH maximum, hydrolysis cannot be achieved. Table 2 exhibits the effect of temperature on lactose hydrolysis efficiency of cow milk. It was observed that maximum lactose hydrolysis efficiency of milk ($73.23 \pm 1.38\%$) was achieved at 50 °C. Dutra Rosolen et al. (2015) studied that lactose hydrolysis efficiency was 30.70% for milk and 44.38% for cheese whey at 55 °C using 9 U/ml β -galactosidase from *Aspergillus oryzae*. According to Panesar (2007), β -galactosidase from alginate-entrapped yeast cells was able to generate 84.8% lactose hydrolysis at 30–35 °C. Bosso et al. (2016) investigated that at 35–40 °C, β -galactosidase from *K. lactis* showed the maximum lactose hydrolyzing activity on ultrahigh-temperature milk.

Table 2 Effect of different temperature and pH on lactose hydrolysis efficiency of milk

Temperature (°C)	35	40	45	50	55	60
Lactose hydrolysis efficiency (%)	60.34 ± 1.52 ^a	66.26 ± 3.87 ^b	73.09 ± 1.13 ^c	73.23 ± 1.38 ^{ac}	61.94 ± 0.67 ^{db}	39.01 ± 1.43 ^e
pH	5	5.5	6	6.5	7	7.5
Lactose hydrolysis efficiency (%)	30.63 ± 0.88 ^a	66.78 ± 1.22 ^b	69.45 ± 0.75 ^{cb}	73.8 ± 0.59 ^d	79.23 ± 0.20 ^e	51.82 ± 0.77 ^f

Samples were analyzed in triplicate. Values are calculated as mean ± SD. Values displayed by different letters in the same row are significantly different ($P < 0.05$) from each other

Table 3 Effect of β -galactosidase on lactose hydrolysis (%) of cheese

Sample	Lactose hydrolysis efficiency%	
	3 h	4 h
Control cheese	7.47 \pm 0.31 ^a	7.89 \pm 1.34 ^a
Cheese from β -galactosidase-treated milk	72.60 \pm 2.15 ^a	81.90 \pm 0.34 ^a

Samples were analyzed in triplicate. Values are calculated as mean \pm SD. Values displayed by same letters in the same column are significantly different ($P < 0.05$) from each other

Table 2 exhibited the effect of pH on lactose hydrolysis efficiency of cow milk. It was observed that maximum lactose hydrolysis efficiency of milk (79.23 \pm 0.20%) was achieved at pH 7. β -galactosidase from *Kluveromyces marxianus* leads to 86.8% dairy whey lactose hydrolysis at pH 7 (Rajakala and Selvi 2006).

3.3.2 Estimation of Lactose Hydrolysis After Cheese Preparation

Cheese can be made from various sources of milk (cow, buffalo, goat, and sheep). Depending on source, the appearance, color, and flavor of cheese vary. The main sugar in milk is lactose. This partially purified β -galactosidase displayed hydrolytic effect on milk lactose. Table 3 showed that 81.90% lactose hydrolysis occurred after 4 h of treatment of milk before cheese production with this partially purified β -galactosidase at 50 °C. After 4 h of enzymatic treatment, lactose hydrolysis became constant. It is already an established fact that hardness of cheese increases with the increasing lactose content in it. Also it is known that fresh cheese contains more lactose than aged one. Generally, during the cheese-making process, lactose is mostly drained off with the whey. The small amount that remains in the curd is changed to lactic acid during ripening of cheese. Only a trace amount of lactose remains. In this study, the prepared cheese was not aged. The lactose content as well as hardness of this unripe cheese was reduced after enzyme treatment. Apricot seed β -galactosidase was able to hydrolyze 99.66% lactose of buffalo milk cheese (Yossef and El Beltagey 2014).

3.3.3 Proximate Analysis

Proximate analysis of cow milk and that of cheese from β -galactosidase-treated and untreated milk are presented in Table 4. Proximate analysis was almost similar for both cheeses.

Table 4 Proximate analysis of cow milk, control cheese, and β -galactosidase-treated cheese

Characteristics	Moisture (%)	Protein (%)	Fat (%)	Ash (%)	Carbohydrate (%)
Cow milk	88.11 \pm 0.85 ^a	3.59 \pm 0.16 ^a	3.21 \pm 0.08 ^a	0.78 \pm 0.07 ^a	4.90 \pm 0.45 ^a
Control cheese	52.82 \pm 1.36 ^b	14.86 \pm 0.11 ^b	6.50 \pm 0.45 ^b	6.73 \pm 1.34 ^b	2.74 \pm 0.41 ^b
Cheese from β -galactosidase-treated milk	55.11 \pm 1.72 ^{cb}	14.93 \pm 0.27 ^{cb}	6.72 \pm 1.17 ^{cb}	4.58 \pm 0.35 ^c	2.67 \pm 0.20 ^{cb}

Samples were analyzed in triplicate. Values are calculated as mean \pm SD. Values displayed by different letters in the same column are significantly different ($P < 0.05$) from each other

Table 5 Antioxidant activity of control- and β -galactosidase-treated cheese

Sample	Day	ABTS (%)	DPPH (%)	FRAP ($\mu\text{mol/g}$)
Control cheese	0	10.26 \pm 0.24 ^a	42.63 \pm 1.28 ^b	112.16 \pm 0.73 ^c
	10	10.95 \pm 0.48 ^a	41.30 \pm 1.43 ^b	113.02 \pm 2.64 ^c
	20	13.21 \pm 0.55 ^a	40.99 \pm 1.82 ^b	116.20 \pm 0.20 ^c
	30	13.88 \pm 0.97 ^a	36.33 \pm 1.01 ^b	119.29 \pm 0.25 ^c
Cheese from β -galactosidase-treated milk	0	10.33 \pm 0.19 ^a	52.19 \pm 1.25 ^b	123.35 \pm 0.21 ^c
	10	11.15 \pm 1.07 ^a	51.26 \pm 1.68 ^b	121.28 \pm 1.76 ^c
	20	12.62 \pm 0.60 ^a	50.03 \pm 0.34 ^b	129.93 \pm 1.46 ^c
	30	14.70 \pm 0.51 ^a	49.01 \pm 1.99 ^b	131.33 \pm 1.43 ^c

Samples were analyzed in triplicate. Values are calculated as mean \pm SD. Values displayed by different letters in the same row are significantly different ($P < 0.05$) from each other

3.3.4 Antioxidant Activity

Hydrophilic and lipophilic character of antioxidants can be measured by ABTS radical scavenging activity. From Table 5, it can be noted that ABTS radical scavenging activity increased with increasing storage time. Almost similar results were found between enzyme-treated and untreated cheese. Hydrogen donating activity was measured by DPPH radical scavenging activity. Enzyme-treated cheese showed higher ABTS and DPPH activity than untreated one. But with increasing storage duration, the activity increased.

Always full-fat cheese shows higher FRAP values than low-fat cheese. In this study, full-fat milk was used for cheese production. A slight increase in FRAP value was observed in cheese from β -galactosidase-treated milk after 30 days under 4 °C storage condition. Antioxidant activity of lactose-free cheese as obtained in the present study had not been reported in the literature.

3.3.5 Microbial Load Analysis

Almost similar result was achieved for the both cheeses. Table 6 showed that control cheese had slight higher colony count than cheese from β -galactosidase-treated milk after 30 days of storage condition within standard value. According to Sharma et al. (2018), microbiological load of cottage cheese produced with kiwi fruit was raised with increasing storage duration, which corroborates the present observation. According to Haddad and Yamini (2017), standard plate count was average 8.3 cfu/g of different traditionally produced soft cheese of Jordan.

Table 6 Microbial load at storage condition in control cheese and cheese from β -galactosidase-treated milk

Microorganism	Day 0		Day 10		Day 20		Day 30	
	CC	BTC	CC	BTC	CC	BTC	CC	BTC
Standard plate count (log cfu/g)	8.92	8.41	9.46	8.62	10.19	9.29	10.66	9.60
Lactic acid bacteria (log cfu/g)	8.12	8.39	8.62	8.14	8.59	8.23	8.91	8.66
Yeast (log cfu/g)	2.66	2.29	2.82	3.16	3.21	4.21	4.72	4.33
Coliform (log cfu/g)	3.63	4.58	4.26	4.67	5.11	4.72	5.66	4.79

CC—control cheese, BTC—cheese from β -galactosidase treated milk

4 Conclusion

From the present results, it can be concluded that *Enterobacter aerogenes* st KCTC2190 is a potent producer of β -galactosidase and this enzyme can be used to degrade the lactose content of dairy food products. Partial purification is an important aspect in improving the activity of crude enzyme for a better yield of mono sugar from lactose. Enzymatic hydrolysis of cheese with β -galactosidase decreases the hardness of cheese by degrading the lactose content. The ability of this enzyme in reducing lactose percentage enhances its acceptability in the food industry.

Acknowledgements Authors acknowledge the facilities given by School of Community Science and Technology, Indian Institute of Engineering Science and Technology, Shibpur, India to carry out this work. Authors are also thankful to Indian Council of Medical Research, New Delhi, India for providing financial assistance in form of Senior Research Fellowship.

References

- American Public Health Association (2005) Standard methods for the examination of water and waste water, 21 st edn. Washington, DC USA
- AOAC (2011) Official methods of analysis international. Association of official analytical chemists, 18th edn. Washington DC USA
- Bosso A, Morioka LRI, Santos LFD, Suguimoto HH (2016) Lactose hydrolysis potential and thermal stability of commercial β -galactosidase in UHT and skimmed milk. *Food Sci Technol* 36(1):159–165
- Erich S, Kuschel B, Schwarz T, Ewert J, Böhmer N, Niehaus F, Eck J, Lutz-Wahl S, Stressler T, Fischer L (2015) Novel high-performance metagenome β -galactosidases for lactose hydrolysis in the dairy industry. *J Biotechnol* 210:27–37
- Haddad MA, Yamini MI (2017) Microbiological quality of soft white cheese produced traditionally in Jordan. *J Food Process Technol* 8(12):706–712
- Huma N, Rafiq S, Sameen A, Pasha I, Khan MI (2018) Antioxidant potential of buffalo and cow milk Cheddar cheeses to tackle human colon adenocarcinoma (Caco-2) cells. *Asian-Australas J Anim Sci* 31(2):287–292

- Iqbal S, Nguyen TH, Nguyen TT, Maischberger T, Haltrich D (2010) β -Galactosidase from *Lactobacillus plantarum* WCFS1: biochemical characterization and formation of prebiotic galacto-oligosaccharides. *Carbohydr Res* 345:1408–1416
- Kumar T, Sourirajan A, Dev K (2015) Isolation and characterization of psychrotolerant *Serratia quinivorans* strains secreting β -D galactosidase. *Univers J Microbiol Res* 3(1):1–9
- Panesar PS (2007) Lactose hydrolysis in whole milk using immobilized *Kluveromyces marxianus* cells. *Am J Food Technol* 2(4):288–294
- Qi T, Gu G, Xu L, Xiao M, Lu L (2017) Efficient synthesis of tyrosol galactosides by the β -galactosidase from *Enterobacter cloacae* B5. *Appl Microbiol Biot* 101(12):4995–5003
- Rahmawati IS, Suntornsuk W (2016) Effects of fermentation and storage on bioactive activities in milks and yoghurts. *Procedia Chem* 18:53–62
- Rajakala P, Selvi PK (2006) The Effects of pH, temperature and alkali metal Ions on the hydrolysis of whey lactose catalyzed by β -galactosidase from *Kluveromyces marxianus*. *Int J Dairy Sci* 1(2):167–172
- Dutra Rosolen M, Gennari A, Volpato G, Volken de Souza CF (2015) Lactose hydrolysis in milk and dairy whey using microbial β -Galactosidase. *Enzyme Res*
- Sharma S, Vidya D, Chauhan N (2018) Microbiological analysis and nutritional evaluation of cottage cheese produced with kiwifruit enzyme. *Int J Curr Microbiol App Sci* 7(2):1–7
- Sumathy R, Vijayalakshmi M, Deecaraman M (2012) A study on β -galactosidase of *Lactobacillus* sp from milk products and its applications. *Int J Appl Biol Pharm* 3(4):138–148
- Triose AD, Bandini E, De Donno R, Meijer G, Trezzi M, Fogliano V (2016) The quality of low lactose milk is affected by the side proteolytic activity of the lactase used in the production process. *Food Res Int* 89:514–525
- Yossef HD, El Beltagey AED (2014) Extraction, Purification and characterization of apricot seed β -galactosidase for producing free lactose cheese. *J Nutr Food Sci* 4(2):1–5

Fungal Production of Single Cell Oil Using Defatted Oilseed Meals as Feedstock



Ruma Dutta, D. K. Bhattacharyya, and Jayati Bhowal

Abstract In the present study, the production of single cell oil by three soil isolated strains of *Aspergillus* sp. was investigated in various basal lipid production media and by adding defatted oilseed (flaxseed, mustard, and rice bran) meal as supplements. Microorganisms were identified after screening from rice bran oil industry-drained soil, and their growth and lipid production rate were investigated in various fermentation media. The organisms were incubated with various oilseed cakes for higher oleic acid (18:1) and linoleic acid (18:2) contents. Growth and lipid production were monitored for 10 days, in which the 7th day showed optimum results. An increase in lipid yield from 24 to 55% was observed when supplemented with defatted oilseed meals. The maximum lipid content was observed in potato dextrose medium when the microorganism was supplemented with 3% flaxseed meal for 7 days. Gas chromatography (GC) analysis showed that the major fatty acids produced were palmitic (16:0), palmitoleic (16:1), stearic (18:0), oleic (18:1), linoleic (18:2), and linolenic (18:3).

Keywords Single cell oil · Meal supplements · *Aspergillus* sp. · Oleic acid · Linoleic acid

R. Dutta · D. K. Bhattacharyya · J. Bhowal (✉)
School of Community Science and Technology, Indian Institute of Engineering Science and Technology, Shibpur, Howrah, West Bengal 711103, India
e-mail: jayatibhowal@gmail.com

R. Dutta
e-mail: lrumadutta@gmail.com

D. K. Bhattacharyya
e-mail: dkb_oiltech@yahoo.co.in

1 Introduction

Single cell oils (SCOs) are oils produced from oleaginous microorganisms. Such microbes have the ability to utilize carbon, nitrogen, and other nutrients present in the medium and transform them into oils, accumulated into their cell membrane. SCOs having different fatty acid compositions from plant seed oils and fish oils, which are valuable for human life (Sakuradani 2010). The microorganisms such as bacteria, yeasts, molds, and microalgae that accumulate more than 25% of their biomass as microbial oil are generally termed as oleaginous due to the similarity of their oils in fatty acid composition to vegetable oil (Bayizit et al. 2014). Recently, published studies reported that lignocellulose biomass could be bioconverted into lipids by oleaginous microorganisms (Qiao et al. 2018). Lignocellulosic feedstocks such as rice straw, husks, wheat straw, sugarcane bagasse, molasses, oil cakes, and corn stover are some of such well-recognized substrates that have already proved their worth in industrial-scale production of several contemporary microbial products (Diwan et al. 2018).

The biotechnology industry has also focused on the ability of oleaginous fungi to convert agricultural waste streams and residues into specialty lipids containing polyunsaturated fatty acids of nutraceutical and pharmaceutical importance, such as γ -linolenic acid (Chan et al. 2018). Linoleic acid has effects on mitochondria, cancer, and aging (Eldor 2018). Although vegetable oils such as virgin olive oil and safflower oil contain edible oleic acid and linoleic acid, by breeding of an oleaginous fungus, it is expected to stably supply fermented microbial oils and to develop new functional lipids using these breeding fungi (Sakamoto et al. 2017).

2 Materials and Methods

2.1 Materials

All chemicals used were analytical grade, purchased from Merck. FAME standard was purchased from Supelco.

2.2 Collection of Soil

Soil sample was collected from drained waste of rice bran oil industry situated in Saktigarh, Burdwan and stored at 4 °C under refrigeration immediately until use.

2.3 Screening and Isolation of Oleaginous Fungi

Oleaginous fungi were isolated from the collected soil sample by serial dilution using 0.9% sterile saline water and plating in potato dextrose agar (PDA) medium and incubated at 28 °C for 2–4 days. The isolated colonies were further screened for their lipid producing abilities by qualitative analysis with the Sudan Black B staining technique (Thakur et al. 1988).

2.4 Identification of Fungi

Fungal strains were identified by 18s rDNA amplification followed by denaturation, annealing, and extension by Bio Axis DNA Research Centre (P) Ltd., Hyderabad.

2.5 Preparation of Oilseed Meals

About 25 g of each flaxseed, black mustard seed, and rice bran were collected from the market and dried to reduce the moisture content and subjected to oil extraction by Soxhlet after grinding.

2.6 Proximate Composition of the Meals

Proximate composition of the deoiled meals, such as moisture, carbohydrate, protein, ash, and fiber, was determined by standard AOAC methods (2000).

2.7 Inoculation of Filamentous Fungi in Fermentation Media for Oil Production

The activated seed cultures of oleaginous fungi were transferred into preculture medium consisted of (in g/L): glucose 30 g, peptone 5 g, yeast extract 5 g with initial pH of 5.0 and grown at 28 °C for 2–3 days. Ten percent of precultures were added to two different fermentation media for determination of highest growth and lipid production. Medium I contained (in g/L): glucose 50 g, (NH₄)₂SO₄ 3 g, KH₂PO₄ 0.8 g, K₂HPO₄ 0.2 g, MgSO₄ · 7H₂O 0.5 g and Medium II contained 100 mL of potato dextrose broth. The fermentation media were incubated at 28 °C and biomass growth and lipid production were measured for 10 days. In another experiment, 1, 2,

and 3% each of deoiled flaxseed meal, mustard meal, and rice bran meal were added to medium II as supplementation for biomass growth and lipid production.

2.8 Fungal Dry Mass Determination

The biomasses from all the experimental media were harvested by filtering and then freeze-dried (Eyela FDU-1110, Japan) to constant mass and weighted dry cell weight. The amount of biomass yield with respect to the substrate consumption, in the term of, growth yield efficiency, $Y_{X/C}$, is calculated using Eq. 1.

$$Y_{X/C} = \frac{X}{(C_i - C_f)} \quad (1)$$

Biomass yield with respect to carbon substrate consumed, g biomass/g substrate; where, X , fungal biomass yield at time t , g/L; C_i , initial carbon substrate concentration, g/L; and C_f , carbon substrate concentration after fermentation, g/L.

2.9 Residual Glucose Analysis

Residual glucose present in the media after fermentation was analyzed using the DNS method (Miller 1959).

2.10 Extraction of Lipid Compounds from Fungal Dried Biomass

The dried fungal biomasses were subjected to lipid extraction according to the method described by Bligh and Dyer (1959) with methanol, water, and chloroform in a ratio of 2:1:1. The lipid content in biomass, in the term of SCO productivity, $Y_{L/X}$, was calculated using Eq. 2.

$$Y_{L/X} = \frac{L_{\max}}{X} \quad (2)$$

where L_{\max} is maximum lipid yield, g/L, and X is biomass yield corresponding to the maximum lipid yield, g/L.

The lipid yield with respect to carbon substrate consumption, $Y_{L/C}$, was calculated using Eq. 3.

$$Y_{L/C} = \frac{L_{\max}}{(C_i - C_f)} \quad (3)$$

Every fungal oil sample was methylesterified according to the method described by Metcalfe and Schmitz (1961) to evaluate the content and composition of fatty acids by gas chromatography with mass spectrometry (GC–MS) and gas chromatography with flame ionized detector (GC–FID).

2.11 Determination of Fatty Acid Composition of Oil Extracted from Fungal Biomass

FAME was analyzed by an Agilent 6890 N; J&W Scientific, computerized gas chromatograph (network GC system—G 1530 N), fitted with a DB-wax capillary column (30 m × 0.32 mm × 0.25 μm) and a flame ionization detector. Fatty acids were identified using Supelco FAME-35 mix standard. For mass spectrometry, an Agilent 7890A gas chromatograph was used and fitted with HP-5 capillary column (30 m × 0.25 mm × 0.25 μm) with mass detector.

3 Results and Discussion

3.1 Isolation and Identification of the Fungal Strain

Three fungal strains (designated primarily as fungus 1, 2, and 3) were isolated from the soil and identified.

The molecular analysis of fungus 1 shows 100% identity to *Aspergillus heteromorphus* CBS 117.55, fungus 2 shows 100% identity to *Aspergillus niger* st YLAC-69, and fungus 3 shows 100% identity to *Aspergillus fumigatus* st SZJO1.

3.2 Variation of the Culture Medium for Growth and Lipid Production by the Fungi

Biomass growth and lipid production were measured in both media (medium I and II) without any supplementation. The results are illustrated in Table 1.

All three *Aspergillus* sp. strains produced oils in both media. *A. niger*, *A. heteromorphus*, and *A. fumigatus* produced 0.96 g/L, 0.77 g/L, and 1.01 g/L oil from 5.23 g/L, 4.59 g/L, and 5.61 g/L biomass respectively in medium I. Growth and production rate of these fungi were increased in medium II, where 8.96, 6.29, and 7.20 g/L biomass were produced, and from them, 2.15, 1.33, and 1.64 g/L lipid were

Table 1 Biomass and lipid production in various media by the fungi

Fungus	Medium I			Medium II		
	Biomass (g/L)	Lipid yield (g/L)	Lipid content (%)	Biomass (g/L)	Lipid yield (g/L)	Lipid content (%)
<i>A. niger</i>	5.23 ± 0.6	0.96 ± 0.02	18.37 ± 1.2	8.96 ± 0.7	2.15 ± 0.1	24 ± 0.03
<i>A. heteromorphus</i>	4.59 ± 0.2	0.77 ± 0.01	16.91 ± 0.9	6.29 ± 0.4	1.33 ± 0.1	21.2 ± 0.02
<i>A. fumigatus</i>	5.61 ± 0.7	1.01 ± 0.04	18.02 ± 1.5	7.20 ± 0.8	1.64 ± 0.2	22.9 ± 0.02

Values are calculated as mean ± SD ($n = 3$)

extracted. Though oil was produced in both media, the isolated fungi showed their oleaginous property (production of >20% lipid) in only medium II, as highest utilization and conversion of glucose to lipids were found in the PD medium. Similar result was found in a study, where various filamentous fungi were incubated in five different culture media including PD broth, Czapek–Dox medium and yeast extract, molasses, and wheat bran added with PD broth medium. It was found that PD broth medium was the highest biomass and lipid-producing medium for *Trichoderma viride* NRC 314 (Ali and El-Ghonemy, 2014). As PD medium (medium II) showed highest biomass and lipid production, further study was carried out in this culture media.

3.3 Fatty Acid Analysis of Oil Produced in Different Culture Media

Analysis of the methyl esters (FAME) of oils extracted from dried biomass produced by the fungi in both media (medium I and II) was done by GC–MS. The results are given in Table 2. It showed a distinctive feature of these fungi. All cultures produced similar kind of fatty acid profile in both media. They mainly contained palmitic

Table 2 Fatty acid composition of oil produced in different fermentation media

Fermentation medium	Fungus	Fatty acid profile (%)				
		16:0	18:0	18:1	18:2	18:3
Medium I	<i>A. niger</i>	19.88 ± 0.1	20.86 ± 0.3	39.76 ± 0.6	19.46 ± 0.2	–
	<i>A. heteromorphus</i>	35.91 ± 0.5	11.00 ± 0.3	23.05 ± 0.5	29.72 ± 0.5	–
	<i>A. fumigatus</i>	36.78 ± 0.5	15.54 ± 0.4	21.09 ± 0.2	22.63 ± 0.3	3.69 ± 0.1
Medium II	<i>A. niger</i>	24.75 ± 0.2	5.56 ± 0.1	34.31 ± 0.7	33.56 ± 0.6	1.80 ± 0
	<i>A. heteromorphus</i>	21.87 ± 0.4	4.84 ± 0.1	41.68 ± 0.9	31.59 ± 0.2	–
	<i>A. fumigatus</i>	38.72 ± 0.7	4.71 ± 0	41.56 ± 0.7	14.29 ± 0.1	0.70 ± 0

Values are calculated as mean ± SD ($n = 3$)

(16:0), stearic (18:0), oleic (18:1), linoleic (18:2), and some amounts of linolenic (18:3) acid.

As the nitrogen, mineral sources, and nutrient content varied, they trigger the production of fatty acids in various percentages. The result showed that medium I helped to produce oleic acid in *A. niger*, whereas, more amount of palmitic and linoleic acids were found in *A. heteromorphus* and *A. fumigatus* and Medium II produced highest amount of oleic acid in *A. heteromorphus* and *A. fumigatus* and a little amount of linolenic acid was produced in *A. niger*. But the most common and abundant fatty acids extracted were palmitic (C16:0), stearic (C18:0), oleic (C18:1), and linoleic (C18:2), which often corresponded to 95% of the *Aspergillus* sp. total FA content (Fraga et al. 2008). These fatty acid profiles can be used as reliable biomarkers for these cultures (Devi et al. 2006).

3.4 Effect of Incubation Time on Biomass and Lipid Production by the Fungal Isolates

It was observed that both biomass production and their corresponding lipid production increased simultaneously up to the 7th day of incubation and then went lower as day passed, whereas glucose exhaust day by day for lipid production. After 7th day, glucose concentration in the media became limited, resulting in deterioration in biomass and lipid production. Similar kind of growth curve was noted in *Aspergillus oryzae* on PDA, having optimal harvesting time of 5 days (Pinasthika et al. 2018) (Table 3).

3.5 Growth and Lipid Production by the Isolated Fungus

The growth yield efficiency, lipid productivity, and lipid coefficient with their corresponding sugar consumption by the fungus are shown in Table 4.

The Y_{LC} values of the fungi were ranging from 6 to 11 g lipids/100 g of glucose consumed. In a similar study, Y_{LC} values of fungal isolates were ranged from 4.7 to 14.0 g lipids/100 g of glucose consumed. The higher Y_{LC} values demonstrate the higher substrate conversion efficiency of the isolated oleaginous fungi (Muniraj et al. 2017).

3.6 Proximate Analysis of Defatted Oilseed Meal

Total carbohydrate, crude protein, moisture content, ash, and fiber content were measured after total extraction of oil from flaxseed, black mustard seed, and rice

Table 3 Growth and lipid production of the fungal isolates in PD broth medium

Days	Residual sugar (g/L)			Weight of biomass (g/L)			Weight of lipid production (g/L)		
	<i>A. niger</i>	<i>A. hetromorphus</i>	<i>A. fumigatus</i>	<i>A. niger</i>	<i>A. hetromorphus</i>	<i>A. fumigatus</i>	<i>A. niger</i>	<i>A. hetromorphus</i>	<i>A. fumigatus</i>
0	21.7 ± 2.4	21.7 ± 2.4	21.7 ± 2.4	0 ± 0	0 ± 0	0 ± 0	0 ± 0	0 ± 0	0 ± 0
3	10.1 ± 2	13.0 ± 2.8	11.2 ± 2.1	2.3 ± 0.1	1.0 ± 0	1.7 ± 0	0.18 ± 0	0.05 ± 0	0.11 ± 0
5	7.40 ± 1.9	10.6 ± 2	8.0 ± 2.1	5.49 ± 0.3	3.74 ± 0.2	4.83 ± 0.1	0.93 ± 0.1	0.59 ± 0.1	0.86 ± 0.1
7	5.53 ± 1.6	8.45 ± 1.9	6.01 ± 1.8	7.96 ± 1	6.29 ± 0.7	7.2 ± 1	1.91 ± 0.5	1.33 ± 0.1	1.64 ± 0.4
8	4.0 ± 0.8	6.0 ± 1.1	5.28 ± 1.8	7.03 ± 1	5.94 ± 0.5	6.98 ± 1	1.52 ± 0.2	1.02 ± 0.1	1.18 ± 0.2
9	3.01 ± 0.1	5.01 ± 0.3	3.21 ± 0.9	6.48 ± 0.8	5.13 ± 0.2	6.19 ± 1	0.90 ± 0	0.56 ± 0	0.68 ± 0
10	2.8 ± 0.1	3.88 ± 0.3	2.96 ± 0.6	5.93 ± 0.4	4.36 ± 0.2	5.98 ± 0.7	0.54 ± 0	0.34 ± 0	0.47 ± 0

Values are calculated as mean ± SD (*n* = 3)

Table 4 Characterization of the fungal isolates grown on medium II

Fungus	(Y_{LX}) g/g	Sugar consumed (g/L)	(Y_{XC}) g/g	(Y_{LC}) g/g
<i>A. niger</i>	0.24 ± 0.03	16.17 ± 1.2	0.55 ± 0.02	0.13 ± 0.01
<i>A. heteromorphus</i>	0.21 ± 0.02	13.25 ± 1.5	0.47 ± 0.01	0.10 ± 0
<i>A. fumigatus</i>	0.22 ± 0.02	15.69 ± 1.0	0.45 ± 0.01	0.10 ± 0

Values are calculated as mean ± SD ($n = 3$)

Table 5 Proximate composition of defatted seed meal

Seed meal	Carbohydrate (%)	Protein (%)	Moisture (%)	Ash (%)	Fiber (%)
Flaxseed meal	29.78 ± 2.3	28.27 ± 1.7	12.70 ± 2.6	3.2 ± 0.9	6.4 ± 1.7
Mustard meal	18.39 ± 1.8	31.46 ± 3.4	7.2 ± 1.1	8.6 ± 1.0	9.8 ± 1.2
Rice bran meal	47.1 ± 4.1	17.8 ± 1.2	8.3 ± 1.4	11.7 ± 2.1	13.2 ± 2.8

Values are calculated as mean ± SD ($n = 3$)

bran, which were brought from the local market. Percentages of these compositions are illustrated in Table 5.

From the proximate analysis experiment, it was observed that defatted flaxseed meal contained 28.27% protein along with 6.4% fiber, 3.2% ash, and 12.7% moisture contents. Similar result containing 27.78% protein, 7.20% fiber, 3.4% ash, and 10.65% moisture was reported by Gutiérrez et al. (2010). It was observed that deoiled mustard meal contained high protein (31.46%) and fiber (9.8%). Higher protein (41.03%), carbohydrate (32.73%), and ash (10.23%) contents, with similar moisture (8.07%) and fiber (10.63%) contents to our result, were reported by Bandikari et al. (2017). Deoiled rice bran meal composed of high amount of carbohydrate (47.1%) and fiber (13.2%) along with 17.8% protein, 11.7% ash, and 8.3% moisture content. A study reported similar fiber (13.1%) and ash (11.6%) with higher carbohydrate (61.46%) and lower protein content (13.8%) than our study (Kumari et al. 2018).

3.7 Effect of Seed Meal Supplementation on Lipid Production

Lipid production was measured by adding various concentrations (1, 2, and 3%) of supplements (deoiled seed meals) to the PD media. It was observed that the oil production by the fungus increased up to 50–55% than in control media (22–24%), when supplements were added to the media. The highest SCO production by *A. niger* was found to be 55% when 3% deoiled flaxseed meal was added. The biomass, lipid yield, and productivity of oil by the fungi are given in Table 6. *A. heteromorphus* and *A. fumigatus* showed higher biomass production, respectively, 12.03 g/L and 15.30 g/L and lipid production, respectively, 35.9 and 44.9% in supplemented media.

Mustard meal showed maximum 33–36% lipid production, with the highest biomass production being 9.43, 9.00, and 15.20 g/L in *A. niger*, *A. heteromorphus*,

Table 6 Biomass, oil content, and oil productivity by the fungus with meal supplements

Supplements	Fungus	Meal added (%)	Biomass weight (g/L)	Oil content (g/L)	SCO (%)
Deoiled flaxseed meal	<i>A. niger</i>	1	11.80 ± 0.9	5.90 ± 0.3	50.0 ± 2.2
		2	14.80 ± 1.2	7.99 ± 0.7	53.9 ± 2.6
		3	17.00 ± 1.7	9.35 ± 0.9	55.0 ± 2.9
	<i>A. heteromorphus</i>	1	8.40 ± 0.5	2.10 ± 0.1	25.0 ± 1.7
		2	9.50 ± 0.3	2.85 ± 0.1	30.0 ± 1.2
		3	10.6 ± 1.1	3.49 ± 0.2	33.0 ± 2.2
	<i>A. fumigatus</i>	1	9.27 ± 0.8	3.05 ± 0.1	32.9 ± 1.9
		2	12.40 ± 1.6	4.96 ± 0.3	40.0 ± 2.1
		3	15.30 ± 1.5	6.42 ± 0.3	41.9 ± 1.3
Deoiled mustard meal	<i>A. niger</i>	1	5.23 ± 0.4	1.56 ± 0.1	29.8 ± 1.1
		2	7.98 ± 0.4	2.55 ± 0.1	31.9 ± 1.0
		3	9.43 ± 0.8	3.21 ± 0.1	34.0 ± 1.5
	<i>A. heteromorphus</i>	1	8.21 ± 0.4	2.47 ± 0.1	30.1 ± 1.1
		2	9.00 ± 0.7	2.88 ± 0.1	32.0 ± 1.4
		3	9.48 ± 0.7	3.21 ± 0.1	33.9 ± 1.6
	<i>A. fumigatus</i>	1	8.95 ± 0.8	2.80 ± 0.1	31.3 ± 1.1
		2	10.78 ± 1.1	3.66 ± 0.2	33.9 ± 2.0
		3	15.20 ± 1.7	5.62 ± 0.4	36.9 ± 2.0
Deoiled rice bran meal	<i>A. niger</i>	1	11.90 ± 1.1	4.99 ± 0.3	41.9 ± 1.8
		2	15.01 ± 1.8	6.46 ± 0.7	43.1 ± 2.7
		3	16.82 ± 1.1	7.55 ± 0.5	44.9 ± 1.3
	<i>A. heteromorphus</i>	1	11.21 ± 0.4	3.87 ± 0.1	34.6 ± 2.0
		2	11.94 ± 0.3	4.19 ± 0.1	35.1 ± 2.2
		3	12.03 ± 0.4	4.31 ± 0.2	35.9 ± 1.9
	<i>A. fumigatus</i>	1	10.41 ± 0.9	4.56 ± 0.2	43.9 ± 1.1
		2	13.24 ± 1.4	5.86 ± 0.7	44.3 ± 2.1
		3	12.59 ± 1.2	5.65 ± 0.5	44.9 ± 1.9

Values are calculated as mean ± SD ($n = 3$)

and *A. fumigatus*, respectively. It was observed that the fungus utilized rice bran meal better than mustard meal. They accumulate 45–47% lipid in their biomass. The highest biomass production was measured to be 15.01 g/L, 6.94 g/L, and 13.24 g/L in *A. niger*, *A. heteromorphus*, and *A. fumigatus* respectively. Another study reported the production of 9.2% lipid from 13.6 g/L of biomass in *A. fumigatus* and 17.9% lipid from 14 g/L biomass in *A. niger* (Ali and El-Ghonemy 2014) similar to our study.

3.8 Analysis of Fatty Acids

Lipids extracted from the biomass were analyzed by gas chromatography (GC–FID). The retention time of the fatty acids identified showed perfect similarity with previous GC–MS data of this study. Fatty acid contents and their ratios are shown in Table 7.

Linolenic acid was produced in a variety of range but maximum 13% was observed in 3% flaxseed meal media in *A. niger*. Highest linoleic content (48.57%) was found in added flaxseed meal medium, whereas rice bran meal supplementation enhanced the stearic acid percentage (19.88%) in the oils produced by the fungus. The oils produced by the fungi were more or less similar to rice bran oil in their fatty acid composition.

Ratio of total polyunsaturated fatty acids (PUFA; 18:2 + 18:3), monounsaturated fatty acids (MUFA; 18:1), and saturated fatty acids (SFA; 16:0 + 18:0) was calculated and observed that it is similar to the balanced diet ratio as suggested by all dietetic associations, which is 1:1:1.

Yao et al. (2019) showed the relationship between lipid productivity and different organic carbon and nitrogen sources. They showed that soybean meal was the best nitrogen source for *Mortierella alpine* TSM-3, producing 16.60 g/L biomass containing 23.68% total fatty acids when glucose was used as the only carbon source. High protein content of flaxseed, mustard, and rice bran meal supplements the media with rich nutrients. The effect is reflected in the fatty acid composition of the oil. High linoleic content of flaxseed may have an influence on the fungus to produce higher linoleic acid in the oils.

4 Conclusion

In this study, *Aspergillus* sp produced oils in various lipid-producing media. The fatty acid content of all oils in all media remained same, which is a remarkable finding for assuring that these fatty acids are biomarkers for these three *Aspergillus* strains. The oil produced by the fungi contained high amounts of oleic and linoleic acids. High oleic content gives a beneficial effect. Better production of oil with better fatty acid composition was shown in meal-supplemented media. Hence, it can be concluded that defatted seed meals helped the isolates to improve both the quality and quantity of oil production. The oils have an ideal PUFA, MUFA, and SFA ratio of 1:1:1. These oils have nutritional significance and resemblance with vegetable oils. So, if refining and toxicity checking are done, then the oils can be used as better substitute for cooking oil.

Table 7 Fatty acid composition of SCOs produced by fungal isolates in the supplemented medium

Fungus	Supplements	Meal added (%)	Fatty acid profile (%)						PUFA:MUFA:SFA
			16:0	18:0	18:1	18:2	18:3		
<i>A. niger</i>	Deoiled flaxseed meal	1	20.09 ± 0.1	5.08 ± 0.1	31.73 ± 0.5	40.02 ± 0.7	2.80 ± 0.1	1.70:1.26:1	
		2	20.01 ± 0.1	6.75 ± 0.2	33.30 ± 0.5	32.71 ± 0.5	7.21 ± 0.2	1.49:1.24:1	
		3	19.73 ± 0.2	8.49 ± 0.1	22.13 ± 0.6	35.75 ± 0.9	13.87 ± 0.2	1.75:0.7:1	
	Deoiled mustard meal	1	27.76 ± 0.4	3.59 ± 0.1	38.09 ± 0.5	24.33 ± 0.2	6.21 ± 0.1	0.9:1.21:1	
		2	19.87 ± 0.2	3.86 ± 0	31.46 ± 0.6	40.28 ± 0.6	4.50 ± 0.1	1.88:1.32:1	
		3	22.09 ± 0.3	3.37 ± 0	36.93 ± 0.6	32.33 ± 0.4	4.49 ± 0.2	1.44:1.45:1	
	Deoiled rice bran meal	1	20.15 ± 0.3	13.69 ± 0.2	32.30 ± 0.3	31.49 ± 0.4	2.33 ± 0.2	0.99:0.95:1	
		2	18.00 ± 0.2	17.10 ± 0.2	33.68 ± 0.2	30.23 ± 0.2	0.97 ± 0.1	0.88:0.95:1	
		3	16.94 ± 0.1	18.08 ± 0.1	34.33 ± 0.5	29.27 ± 0.1	0.68 ± 0	0.85:0.98:1	
<i>A. heteromorphus</i>	Deoiled flaxseed meal	1	23.56 ± 0.4	5.00 ± 0.1	37.74 ± 0.4	32.69 ± 0.2	0.08 ± 0	1.14:1.32:1	
		2	24.08 ± 0.5	5.06 ± 0	35.21 ± 0.2	34.31 ± 0.4	1.32 ± 0.1	1.22:1.20:1	
		3	26.30 ± 0.3	5.49 ± 0.2	30.22 ± 0.2	36.48 ± 0.5	1.09 ± 0	1.18:0.95:1	
	Deoiled mustard meal	1	28.55 ± 0.7	4.09 ± 0.1	36.26 ± 0.5	28.74 ± 0.2	1.30 ± 0.1	0.92:1.11:1	
		2	27.39 ± 0.6	3.85 ± 0	33.41 ± 0.1	31.28 ± 0.2	1.06 ± 0	1.03:1.06:1	
		3	26.56 ± 0.6	3.49 ± 0	37.72 ± 0.3	29.43 ± 0.1	0.89 ± 0	1:1.25:1	
	Deoiled rice bran meal	1	20.82 ± 0.3	19.88 ± 0.3	32.37 ± 0.5	25.56 ± 0.1	1.33 ± 0.1	0.66:0.79:1	
		2	18.89 ± 0.2	18.56 ± 0.2	35.41 ± 0.6	26.10 ± 0.1	1.02 ± 0	0.72:0.94:1	
		3	16.49 ± 0.2	16.20 ± 0.2	37.31 ± 0.6	27.19 ± 0.3	0.84 ± 0	0.85:1.14:1	
<i>A. fumigatus</i>	Deoiled flaxseed meal	1	36.08 ± 0.7	4.69 ± 0	39.22 ± 0.5	18.78 ± 0.1	1.21 ± 0.1	0.49:0.96:1	
		2	30.22 ± 0.5	3.98 ± 0	36.54 ± 0.5	26.44 ± 0.3	2.23 ± 0.1	0.83:1.06:1	

(continued)

Table 7 (continued)

Fungus	Supplements	Meal added (%)	Fatty acid profile (%)				PUFA:MUFA:SFA		
			16:0	18:0	18:1	18:2		18:3	
	Deoiled mustard meal	3	14.65 ± 0.1	4.73 ± 0.1	26.81 ± 0.2	48.57 ± 0.7	5.21 ± 0.3	2.77:1.38:1	
		1	38.24 ± 0.5	5.02 ± 0.1	32.46 ± 0.4	23.03 ± 0.4	3.52 ± 0.2	0.61:0.75:1	
		2	32.79 ± 0.3	5.54 ± 0.3	31.01 ± 0.3	28.41 ± 0.4	2.22 ± 0.2	0.79:0.80:1	
	Deoiled rice bran meal	3	30.20 ± 0.7	5.69 ± 0.2	30.27 ± 0.3	31.47 ± 0.6	1.38 ± 0.1	0.91:0.84:1	
		1	22.67 ± 0.3	16.30 ± 0.1	30.88 ± 0.3	28.79 ± 0.3	1.09 ± 0	0.76:0.79:1	
		2	20.53 ± 0.2	17.79 ± 0.3	31.20 ± 0.1	27.74 ± 0.3	0.89 ± 0	0.74:0.81:1	
			3	18.37 ± 0.1	16.39 ± 0.1	34.76 ± 0.5	29.05 ± 0.3	1.02 ± 0	0.86:1:1

Values are calculated as mean ± SD (*r* = 3)

Acknowledgements I sincerely thank and express my gratitude to IEST, Shibpur for supporting me throughout my work. I am also thankful to Sethia Oil Ltd., Burdwan, for giving me permission to use the soil of the industrial drained waste for my research work and for supplying the same. I am also grateful to the Lipidomics Department of Ballygunj Science College and Chemical Engineering Department of Rajabazar Science College for the analysis of FAME.

Conflict of Interest None.

References

- Ali TH, El-Ghonemy DH (2014) Optimization of culture conditions for the highest lipid production from some oleaginous fungi for biodiesel preparation. *Asian J Appl Sci* 2(5):600–609. <https://www.researchgate.net/publication/271215318>
- A.O.A.C. (2000) Official methods of analysis, 17th edn. Association of Official Analytical Chemists, Gaithersburg MD USA
- Bayazit AA, Ozcan T, Ersan YL, Basoglu F (2014) Single cell oil (SCO) production by *Fusarium* species using cheese whey as a substrate. *Mljekarstvo* 64(2):111–118
- Bandikari R, Katike U, Seelam NS, Obulam VSR (2017) Valorization of de-oiled cakes for xylanase production and optimization using central composite design by *Trichoderma koenigi* isolate. *Turk J Biochem* 42(3):317–328. <https://doi.org/10.1515/tjb-2016-0290>
- Bligh EG, Dyer WJ (1959) A rapid method of total lipid extraction and purification. *Can J Biochem Physiol* 37(8):911–917. <https://doi.org/10.1139/o59-099>
- Chan GL, Cohen LJ, Ozturk G, Hennebelle M, Taha AY, De Moura Bell JMLN (2018) Bioconversion of cheese whey permeate into fungal oil by *Mucor circinelloides*. *J Biol Eng* 12(25). <https://doi.org/10.1186/s13036-018-0116-5>
- Devi P, Divya-Shridhar MP, D'souza L, Naik CG (2006) Cellular fatty acid composition of marine derived fungi. *Indian J Mar Sci* 35(4):359–363
- Diwan B, Parkhey P, Gupta P (2018) From agro-industrial wastes to single cell oils: a step towards prospective biorefinery. *Folia Microbiol.* <https://doi.org/10.1007/s12223-018-0602-7>
- Eldor J (2018) Linoleic acid: the code of life? *J Health Sci Dev* 1(2):18–32
- Fraga ME, Santana DMN, Gatti MJ, Direito GM, Cavaglieri LR, Rosa CLR (2008) Characterization of *Aspergillus* species based on fatty acid profiles. *Mem I Oswaldo Cruz* 103(6):540–544
- Gutiérrez C, Rubilar M, Jara C, Verdugo M, Sineiro J, Shene C (2010) Flaxseed and flaxseed cake as a source of compounds for food industry. *J Soil Sci Plant Nutr* 10(4):454–463
- Kumari N, Vinita NK, Rani P (2018) Nutrient composition of full fat and defatted rice bran. *Asian J Dairy Food Res* 37(1):77–80
- Metcalf LD, Schmitz AA (1961) The rapid preparation of fatty acid esters for gas chromatographic analysis. *J Anal Chem* 33(3):363–364. <https://doi.org/10.1021/ac60171a016>
- Miller GL (1959) Use of dinitrosalicylic acid reagent for the determination of reducing sugar. *Anal Chem* 31(3):426–428. <https://doi.org/10.1021/ac60147a030>
- Muniraj IK, Xia L, Hu Z, Zhan X (2017) Screening and characterization of oleaginous fungi from Irish soil for growth under low carbon substrates. *Int J Curr Microbiol Appl Sci* 6(12):772–781. <https://doi.org/10.20546/ijcmas.2017.612.082>
- Pinasthika NP, Arbianti R, Utami TS, Hermansyah H (2018) Effect of medium and incubation time on production of AA, DHA and EPA from *Aspergillus oryzae* by solid state fermentation. *IOP Conf Ser Earth Environ Sci* 105:012104. <http://dx.doi.org/10.1088/1755-1315/105/1/012104>
- Qiao W, Tao J, Luo Y, Tang T, Miao J, Yang Q (2018) Microbial oil production from solid-state fermentation by a newly isolated oleaginous fungus, *Mucor circinelloides* Q531 from mulberry branches. *R Soc Open Sci* 5:180551. <https://doi.org/10.1098/rsos.180551>

- Sakamoto T, Sakuradani E, Okuda T, Kikukawa H, Ando A, Kishino S, Izumi Y, Bamba T, Shima J, Ogawa J (2017) Metabolic engineering of oleaginous fungus *Mortierella alpina* for high production of oleic and linoleic acids. *Bioresour Technol* . <https://doi.org/10.1016/j.biortech.2017.06.089>
- Sakuradani E (2010) Advances in the production of various polyunsaturated fatty acids through oleaginous fungus *Mortierella alpina* breeding. *Biosci Biotech Biochem* 74(5):908–917. <https://doi.org/10.1271/bbb.100001>
- Thakur MS, Prapulla SG, Karanth NG (1988) Microscopic observation of Sudan Black B staining to monitor lipid production by microbes. *J Chem Technol Biotechnol* 42:129–134. <https://doi.org/10.1002/jctb.280420206>
- Yao Q, Chena H, Wang S, Tang X, Gu Z, Zhang H, Chen W, Chen YQ (2019) An efficient strategy for screening polyunsaturated fatty acid-producing oleaginous filamentous fungi from soil. *J Microbiol Methods* 158:80–85. <https://doi.org/10.1016/j.mimet.2018.12.023>

Food, Pharmaceuticals and Health Care

Synergistic Effect of Quercetin with Allicin from the Ethanolic Extract of *Allium cepa* as a Potent AntiQuorum Sensing and Anti-Biofilm Agent Against Oral Biofilm



Dibyajit Lahiri, Moupriya Nag, Bandita Dutta, Sudipta Dash, Shreyasi Ghosh, and Rina Rani Ray

Abstract The organism predominantly obtained from the oral biofilm was identified as *Bacillus cereus* which was observed to be one of the root causes of pharyngeal infections. It was found that when the biofilm was treated with $16 \times \text{MIC}$ ($2.24 \pm 0.12 \mu\text{g/mL}$) there was an eradication of $62.78 \pm 1.26\%$ when treated with the ethanolic extract of *Allium cepa* as compared to $41.12 \pm 0.98\%$ when treated with antibiotic azithromycin. The in silico studies of identified bioactive compounds from the extracts depicting the synergism of the above two phytochemicals on the target biofilm-forming protein. The binding energy of synergistic interaction was found to be -33.521 kcal/mol , whereas antibiotic showed a value of -27.568 kcal/mol which in turn implied that through synergism a better antibiofilm activity could be obtained on *B. cereus*. It was observed that the viability of bacterial cells showed a marked reduction of 9.3% when challenged with $16 \times \text{MIC}$ of ethanolic extract of *A. cepa* for a time period of 0–48 h with respect to control and standard antibiotic Azithromycin. The quantification of individual components of extracellular carbohydrates, proteins and nucleic acids showed maximum reduction in presence of ethanolic extract of *A. cepa*. Comparative quantification of the total concentration of bacterial genomic

D. Lahiri and M. Nag: Both the authors has equal contributions

D. Lahiri · M. Nag · S. Dash · S. Ghosh
Department of Biotechnology, University of Engineering & Management, Kolkata, India
e-mail: dibyajit.lahiri@uem.edu.in

M. Nag
e-mail: moupriya.nag@uem.edu.in

S. Ghosh
e-mail: shreyasighosh1807@gmail.com

B. Dutta · R. R. Ray (✉)
Department of Biotechnology, Maulana Abul Kalam Azad University of Technology, Haringhata, West Bengal, India
e-mail: raypumicro@gmail.com

B. Dutta
e-mail: bandita2611@gmail.com

DNA and RNA showed maximum reduction in the presence of phytoextract. Thus this study clearly indicated by utilizing the synergistic properties of bioactive components of *A. cepa*, an effective substitute for conventional antibiotics can be developed which can be used for treatment against the biofilm-associated infections.

Keywords Biofilm · Quercetin · Allicin · Antibiofilm · Azithromycin

1 Introduction

Rapid use of antibiotics over various bacteria influenced the development of antibiotic-resistant strains of bacteria leading to a new threat to human health. One of the major reasons for this resistance is the formation of biofilms by microorganisms. Biofilms are a coherent cluster of bacterial cells embedded in a matrix known as extra polymeric substances (EPS), which is more tolerant of most antimicrobials and host defences compared with planktonic bacterial cells (Waters and Bassler 2005). This development of EPS makes the biofilm impermeable to antibiotics and drugs resulting in the development of multidrug-resistant organisms (Olson et al. 2002). Bacterial growth is characterized by two phenotypes, single cells (planktonic) or sessile aggregates responsible for the biofilm mode of growth (Nazzaro et al. 2013). Recently, it has been observed that throat infections are becoming more resistant to antibiotic treatment leading to failure in eradicating the diseases such as chronic rhinosinusitis [CRS], chronic otitis media [COM] and otitis media with effusion [OME] (Vlastarakos et al. 2007). Thus, treatment of these bacterial infections has become indispensable by application of more than one conventional drug or higher concentrations of the drugs. But this has its own flaws. First of all, synthetic antibiotics or antimicrobial agents are generally narrow spectrum in nature. Secondly, increase in concentration may cause severe health threat by serious side effects. Hence, there is a need of an alternative method and development of modern drugs that can deal with infections efficiently by not increasing the resistivity of the bacteria.

Fortunately, it has been seen that the traditional medicinal plants having a wide range of bioactive compounds such as alkaloids, terpenoids, saponin, quercetin, anthocyanin, flavonoids and essential oils can effectively treat the bacterial infection (Sánchez et al. 2016). Moreover, these herbal treatments, unlike synthetic medicines, do not cause severe health threat. The current project was performed as a comparative analysis to study the efficacy of *Allium cepa*, extracts and the common antibiotics (Azithromycin) used in throat infection treatment with an objective to find out whether plant extracts can be a potential alternative to the selected antibiotic for throat infection and a solution to fight the formation of bacterial biofilms.

2 Materials and Methods

2.1 *Microorganism*

The biofilm-forming bacterial strain was collected from infected throat and was cultivated in LB broth at 37 °C for 24 h. Characterization of the isolated organism was done by performing 16S rRNA sequencing.

2.2 *Preparation of Plant Extract*

The ethanolic extract of the plant *A. cepa* (onion) was prepared by mixing 8 gm of pulverized rhizome of the plant with 8 ml of 30% ethanol, followed by a treatment with 700 μ L of 80% H₂SO₄. After 24 h, the sample was filtered out using cotton gauge filter and the filtrate was stored at 0–4 °C.

2.3 *Biochemical Assay of Plant Extract*

Biochemical assays of ethanolic extract of *A. cepa* were done for estimating total flavonoid, total phenol, hydroxyl scavenging and hydrogen peroxide scavenging activity (Debiyi and Sofowora 1978; Roopashree et al. 2008).

2.4 *Minimum Inhibitory Concentration (MIC) and MBEC Assay by Crystal Violet Method*

The bactericidal and bacteriostatic effects of the bioactive compounds of *A. cepa* (Onion) were detected on LB Agar spread plates for the strain of *Bacillus cereus* using Azithromycin as standard antibiotic (Tang et al. 2011).

The antibiofilm effect of the ethanolic extract of *A. cepa* on *B. cereus* was checked by microdilution method where bacterial cells (1×10^6 CFU/ml) were grown on the wells (96 well-plate) leaving the control at 37 °C for 72 h to allow the formation of biofilm (Tang et al. 2011). Diluted plant extract or antibiotic (Azithromycin) were added with 3-[4,5-dimethyl-2-thiazolyl]-2,5-diphenyl-2H-tetrazolium bromide (MTT dye) to quantify the viability of the bacterial cells in the presence of the challenge using ELISA plate reader (2018 GEN-NET). The percentage inhibition was determined using the following equation:

$$[1 - (A_{570} \text{ of the test} / A_{570} \text{ of non-treated control}) \times 100] \text{ (Gomes et al. 2012)}$$

2.5 Phenol Coefficient

The phenol coefficient was measured spectrophotometrically at 540 nm by treating the culture of *B. cereus* with 5 mL of ethanolic extract of *A. cepa* and phenol for different time periods (Eliasa et al. 2013).

2.6 Study of the Quorum Sensing of the Isolated Bacteria from Throat

The supernatant of bacterial culture broth filtered through 0.2 μm membrane filter was mixed with ethyl acetate and shaken for 10 min for phase separation. The upper part of the solution was mixed with 1:1 mixture of 2 M hydroxyl amine and 3.5 M NaOH and later with 10 μl of 1:1 Ferric Chloride and 95% ethanol. OD was measured at 520 nm (Yang et al. 2006).

2.7 Determination of Viability Count of the Biofilm Forming Isolated Bacterial Cells

The colonies of working strains were scrapped from the biofilm formed on the surface of chitin flakes and were inoculated in LB broth having 0.1% (W/V) of chitin flakes to re-grow for a period of 72 h. After adequate washing, the planktonic cells were removed and the cultures of the working strains were treated with the required concentration of ethanolic extract of *A. cepa* and standard antibiotic Azithromycin in three different flasks and the data were noted in 2–24 h of time challenge (Gomes et al. 2012).

2.8 Scanning Electron Microscopy (SEM)

Biofilms were grown on glass coverslips by the treated and untreated cultures of isolated bacteria from throat. The effect of plant extract on biofilm formation was visualized under a scanning electron microscope (Model-ZEISS EVO-MA 10) (Andersson et al. 2009; Singh et al. 2013).

2.9 Fluorescence Confocal Microscopy

The biofilm formation in the presence and absence of extract of *A. cepa* and *Azithromycin* were observed by fluorescence microscopy. The biofilm was formed on glass slides for a period of 72 h, and then the samples were challenged with the extract for 2 h keeping the control untreated. Then the samples were treated with 10 mg/mL of acridine orange solution and were incubated at 37 °C for 1 h. Stained cells were observed using an Axioplan Fluorescence Microscope equipped with digital camera (d × m 1200, Nikon, Japan).

2.10 FTIR Analysis of Biofilm Formation

Biofilm was formed upon Chitin flakes for a period of 72 h at 37 °C, and challenged with plant extract and kept for drying at 37 °C for 48 h. The FTIR spectra were recorded in the range of 450–4000 cm⁻¹ using Spectrum 100 FTIR Spectrophotometer.

2.11 GC–MS Analysis

The study of Gas Chromatography–Mass Spectrometry is the process of optimization that includes the process of introducing the plant extract into the column followed by the separation of the constituents being present and the target molecules are analyzed including the process of Mass Spectrometry. The chromatographic analysis of the methanolic extract of the *A. cepa* was done using GC Model—Trace GC Ultra, MS model—POLARISQ (Thermoscientific). The data obtained were searched using NIST Library. The spectra formed as a result of GC-MS were linked with their existing library.

2.12 Protein Structure Preparation and Ligand Search from Online Database

Bioactive compounds from *A. cepa*, i.e. allicin and quercetin were found from PubChem Database (Morris et al. 1998). Molecular docking studies were carried out to elucidate the interaction of allicin and quercetin with biofilm-forming protein. 3-D atomic co-ordinate of the protein is not available in the protein data bank (PDB) so homology modelling and fold recognition was employed to model the protein. Protein intimin from *E coli*. was found to have maximum sequence identity. So, the

structure of intimin has been used as a template to model the structure of biofilm-forming protein using SWISS-MODEL online server. PHYRE2 online server has been used to model protein structure using fold recognition. The best models were further used in the docking study.

2.13 Protein-Ligand Docking Using Schrodinger

2.13.1 Ligand Docking

The docking calculations were performed with Schrödinger 2015 suite of softwares. All non-bonded heteroatoms and water molecules were removed and hydrogen bonds were added to optimize the structure. The biofilm protein grid file and quercetin were docked using Glide standard precision. This docked structure was again used as the receptor grid file and allicin was docked to understand the synergistic mechanism of binding. Glide score was used to infer the affinity and binding energy values (Guex and Peitsch 1997).

2.14 Statistical Analysis

All the data were of sample size 5 and were represented as Mean \pm SE.

3 Results and Discussion

3.1 Biochemical Estimation of Plant Compounds

3.1.1 Total Phenolic (TPC) and Flavonoid Content (TFC)

The total flavonoids and polyphenol content of *A. cepa* extract were determined using quercetin and gallic acid as standard samples by colorimetric assays (Fig. 1a). The high flavonoid content ($6.54 \pm 0.02 \mu\text{g/ml}$) and total polyphenol content ($102.819 \pm 0.05 \mu\text{g/ml}$) of *A. cepa* indicated the antioxidant potential of the plant extract (Fig. 1).

3.1.2 Hydrogen Peroxide and Hydroxyl Radical Scavenging Activity

Hydrogen peroxide activity and IC_{50} value of the extract of *A. cepa* compared to the control Ascorbic acid revealed the fact that the efficacy of the plant extract was better

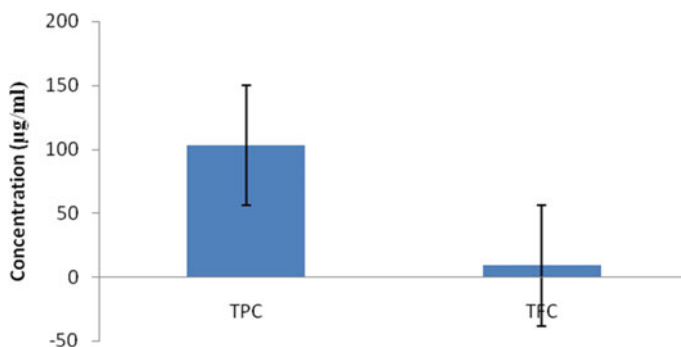


Fig. 1 Total polyphenol content (TPC) and total flavonoid content (TFC) in *A. cepa*

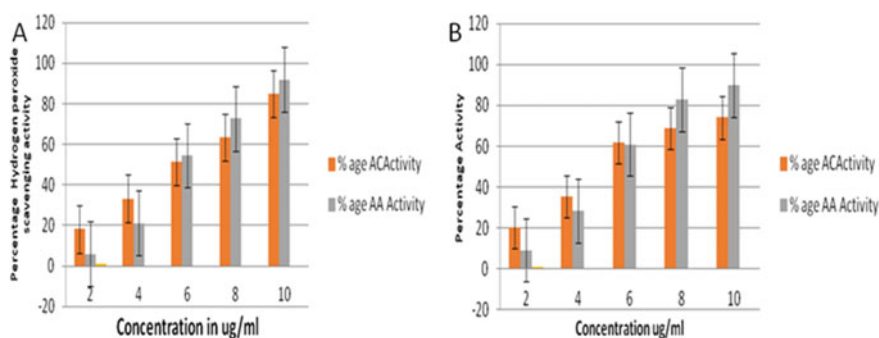


Fig. 2 a Hydroxyl radical scavenging activities of *A. cepa* and the standard, ascorbic acid (AA). All data expressed as mean \pm SE ($n = 5$). The data were statistically significant ($P < 0.01$). **b** Hydrogen peroxide scavenging activities of *A. cepa* and the standard, ascorbic acid (AA). All data expressed as mean \pm SE ($n = 5$). The data were statistically significant ($P < 0.01$)

than ascorbic acid, a standard antioxidant up to a concentration of 4 $\mu\text{g/ml}$ of the plant extract (Fig. 2). The effect of *A. cepa* on the inhibition of free radical-mediated deoxyribose damage was assessed by means of the hydroxyl radical scavenging assay. The IC_{50} value of the AC was almost that of standard, showing better ability in hydroxyl radical scavenging up to a concentration of 6 $\mu\text{g/ml}$ of the plant extract (Fig. 2).

3.2 Minimum Biofilm Eradication Concentration

Although antibiotic and plant extracts showed inhibition of biofilm formation, maximum inhibition of biofilm formation was brought about by the ethanolic extract of *A. cepa* followed by azithromycin, respectively (Fig. 3).

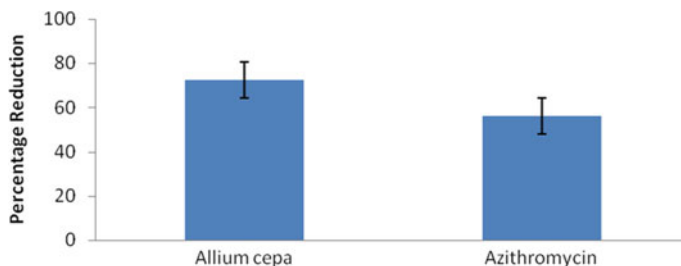


Fig. 3 Effect of treatment of *A. cepa* on the biofilm formation of *B. cereus*

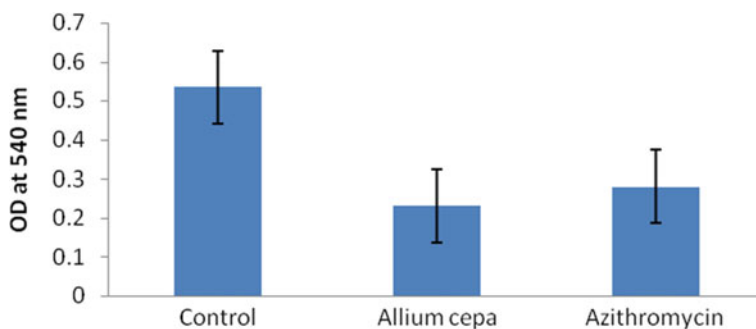


Fig. 4 Effects of treatment with ethanolic extract of *A. cepa* on the quorum sensing activity of oral isolates

3.3 Effect of Treatment on Quorum Sensing

Since quorum sensing (QS) used to play critical role in regulating biofilm formation, the concentration of acyl homoserine lactone (AHL), the autoinducer molecule in QS could be used as a marker. It was observed that there was a marked diminution (around 50%) in the concentration of AHL in both the working strains after being treated with extracts of *A. cepa* and azithromycin (Fig. 4). However, the extract of *A. cepa* was found to be more effective than azithromycin in inhibiting AHL dependent quorum sensing.

3.4 Effect of Treatment on Viability and Revival of the Biofilm Forming Bacterial Cells

It was observed that the count of sessile bacterial cells from the biofilms of *B. cereus*, treated with herbal compounds and antibiotics showed marked reduction with time. This reduction was higher in extract-treated cells than those of antibiotic-treated cells. It was observed that the viability of bacterial cells showed a marked reduction of 9.3%

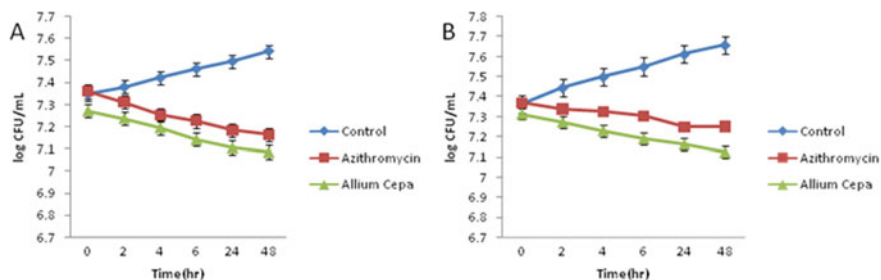


Fig. 5 **a** The viability kinetics of the sessile group of oral isolate cells after treatment with ethanolic extract of AC and azithromycin. **b** The kinetics of revival of treated cells of *B. cereus*

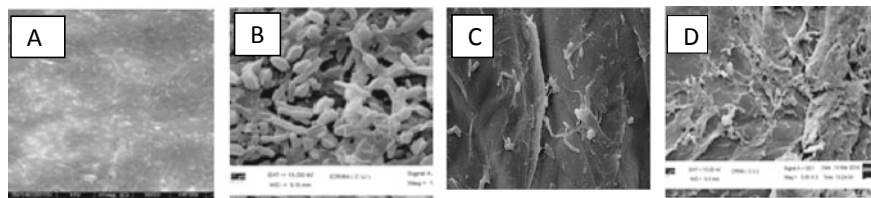


Fig. 6 SEM images of biofilms developed by oral isolates. SEM images illustrating the effect of *A. cepa* and azithromycin extract (1 mg/ml) on biofilm formation. **a** Normal chitin flakes without any biofilm formation. **b** Biofilm established on chitin flakes by oral isolates. **c** Shrinkage of EPS matrix of oral isolates due to the addition of plant extract of *A. cepa*. **d** Shrinkage of EPS matrix of oral isolates due to the addition of plant extract of azithromycin

when challenged with $16 \times$ MIC of ethanolic extract of *A. cepa* for a time period of 0–48 h with respect to control and standard antibiotic Azithromycin (Fig. 5b).

3.5 SEM Analysis

The topography of the biofilm developed by oral isolates and the effect of *A. cepa* extract and azithromycin treatment on it was analyzed by SEM. A well-grown biofilm along with adhering bacterial cells were observed in controls (normal biofilm developed by bacterial isolate) in the SEM analysis, whereas dispersed bacterial cells were observed in treated samples (Fig. 6).

3.6 Fluorescent Microscopy Analysis

Fluorescence microscopic observations provide useful information on biofilms. In the control experiment, a thick coating of biofilms was detected in absence of plant

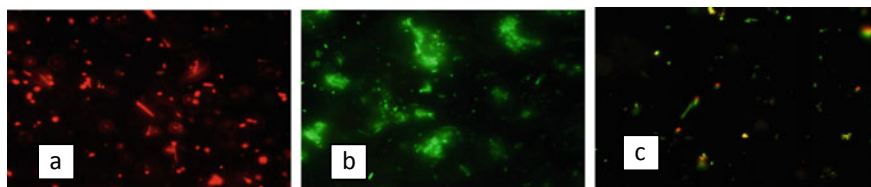


Fig. 7 FCM images of bacterial biofilms grown in the absence and presence of *A. cepa* extract. Fluorescence microscopic images of **a** Sessile form of *B. cereus* as control sample without *A. cepa* extract, respectively **b, c** Sessile form of *B. cereus* in presence of *A. cepa* extract and azithromycin, respectively

extract (Fig. 7a). As shown in Fig. 7b and c, treatment with 1 mg mL^{-1} of *A. cepa* extract showed significant reduction in the microbial attachment to the glass surface compared to controls.

3.7 FTIR Analysis

FTIR spectra of bacterial biofilm formed in presence and absence of ethanolic extract of *A. cepa* are shown in Fig. 8, which showed peak at $1080, 1675, 2974, 3532 \text{ cm}^{-1}$ that confirmed the presence of carboxylic group, C–H stretching of sugar molecules, C–H functional groups and hydroxyl group, respectively. The absorption bands from 1668 to 1540 cm^{-1} corresponded to amide I and II in proteins. The bands at $830.65, 650.63$ and 700.51 cm^{-1} represent the presence of =CH in aromatic compounds in the plant extract. The gradual decrease or disappearance of peaks revealed the reduction of protein and carbohydrate content in the EPS of various bacteria when treated with *A. cepa* and Azithromycin.

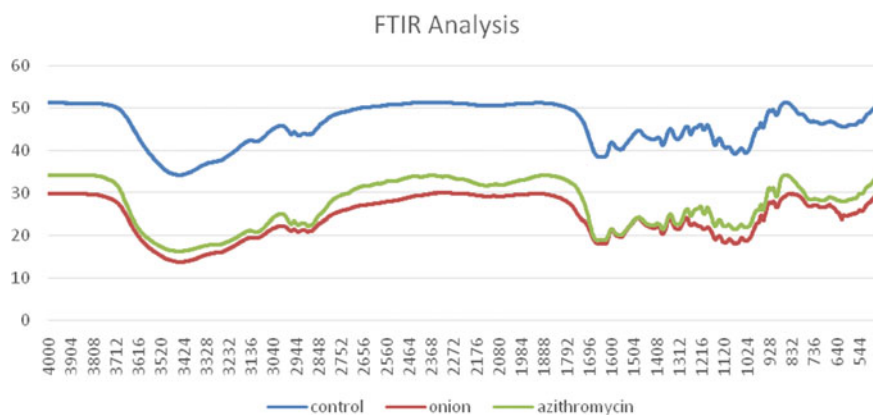


Fig. 8 FTIR spectrum of *B. cereus* biofilm in presence and absence of *A. cepa* and azithromycin

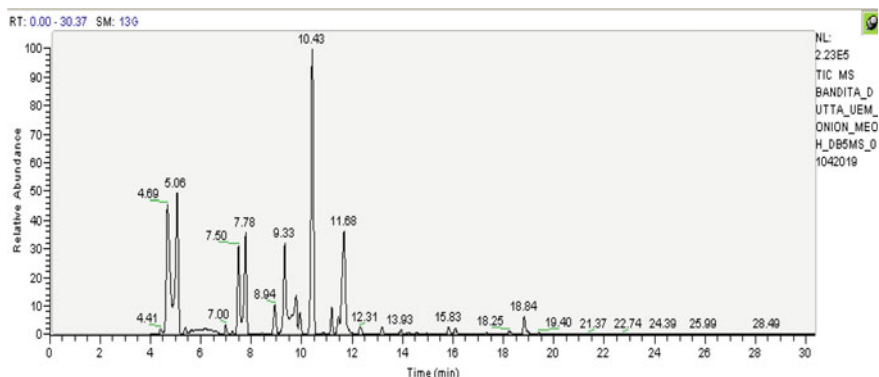


Fig. 9 GC-MS Data for *A. cepa*

3.8 GC-MS Analysis

The mass spectrum of unknown component was compared with the spectrum of the known component stored in the database of National Institute Standard and Technology (NIST) library. The mass spectrometer analyzes the compounds eluted at different times (retention time) to identify the nature and structure of the compounds. The GC-MS study of the ethanolic extract of *A. cepa* had shown the presence of essential bioactive compounds. Two such bioactive compounds *viz.* Quercetin and Allicin were chosen for the synergistic effect on bacterial biofilm-forming protein compared to antibiotic azithromycin (Fig. 9).

3.9 Molecular Docking Studies

3.9.1 Docking Between Biofilm Forming Protein and Bioactive Compounds Present in *A. cepa*

Phytochemicals were synergistically docked in silico with the receptor proteins, and docking sites were compared with antibiotics for its subsequent use as putative drugs. The best-docked poses were selected based on the lowest energy and good interaction to the active site residues via H-bonds, electrostatic interactions or pi-pi interactions (Fig. 10; Table 1).

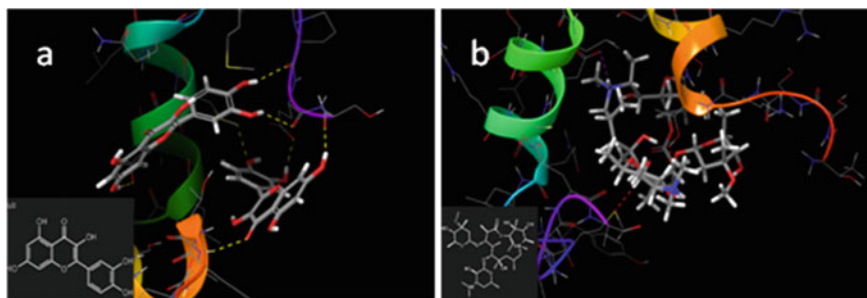


Fig. 10 **a** shows the synergistic effect of Quercetin and allicin on the target biofilm-forming protein. **b** shows the effect of Azithromycin on the biofilm-forming protein

Table 1 Synergistic docking of bioactive compounds Quercetin and Allicin showed the highest binding energies (Kcal/mol) with comparison to antibiotic azithromycin while docking with Receptor proteins of oral biofilm-forming bacteria

Ligands	Gibbs free energy of docked ligand and biofilm-forming protein of oral bacteria (ΔG)
Quercetin + allicin	-33.521 kcal/mol
Azithromycin	-27.568 kcal/mol

3.10 Conclusion

This study clearly indicated that the synergistic properties of bioactive components like Allicin and Querecetin in *A. cepa* show a newer arena of drug development, which could be used as an effective substitute for conventional antibiotics to target against the biofilm-associated infections.

Ethical Clearance Informed consent was obtained from all individual participants included in the study. The study was performed under the guidelines of Institutional Ethics Committee MAKAUT: IEC-(18-19)/02 dated 30 December 2019.

Conflict of Interest There is no conflict of interest among the co-authors involved in the study.

Funding Information No funding received for this study from any agencies.

References

- Andersson S, Dalhammar G, Land C, Rajarao G (2009) Characterization of extracellular polymeric substances from denitrifying organism *Comamonas denitrificans*. *Appl Microbiol Biotechnol* 82:535–543
- Debiyi OO, Sofowora FA (1978) Phytochemical screening of medical plants. *Iloyidia* 3:234–246

- Eliasa EA, Samuel O, Emmanuela N, Abrahama O (2013) Evaluation of efficacy of disinfectants using standard methods in healthcare facilities in Kogi state. North central Nigeria, *AJBPS* 03(27):34–38
- Gomes F, Teixeira P, Ceri H, Oliveira R (2012) Evaluation of antimicrobial activity of certain combinations of antibiotics against in vitro *Staphylococcus epidermidis* biofilms. *Indian J Med Res* 135(4):135542–135547
- Guex N, Peitsch MC (1997) SWISS-MODEL and the Swiss-Pdb viewer: An environment for comparative protein modeling. *Electrophoresis* 18:2714–2723
- Morris GM, Goodsell DS, Halliday RS, Huey R, Hart WE, Belew RK, Olson AJ (1998) Automated docking using a Lamarckian genetic algorithm and an empirical binding free energy function to compute its bulk and surface properties. *J Comput Chem* 19(14):1639–1662
- Nazzaro F, Fratianni F, Coppola R (2013) Quorum sensing and phytochemicals. *IJMS* 14(6):12607–12619
- Olson ME, Ceri H, Morck DW, Buret AG, Read RR (2002) Biofilm bacteria: formation and comparative susceptibility to antibiotics. *Can J Vet Res* 66(2):86–92
- Roopashree TS, Dang R, Rani RHS, Narendra C (2008) Antibacterial activity of antipsoriatic herbs: cassia tora, Momordica charantia and calendula officinalis. *Int J Appl Res Nat Prod* 1(3):20–28
- Sánchez E, Rivas Morales C, Castillo S, Leos-Rivas C, García-Becerra L, Martínez ODM (2016) Antibacterial and antibiofilm activity of methanolic plant extracts against nosocomial microorganisms *ECAM*, 1–8
- Singh VK, Kavita K, Prabhakaran R, Jha B (2013) Cis-9-octadecenoic acid from the rhizospheric bacterium *Stenotrophomonas maltophilia* BJ01 shows quorum quenching and anti-biofilm activities. *Biofouling* 29(7):855–867
- Tang HJ, Chen CC, Ko WC, Yu WL, Chiang SR, Chuang YC (2011) In vitro efficacy of antimicrobial agents against high-inoculum or biofilm-embedded methicillin-resistant *Staphylococcus aureus* with vancomycin minimal inhibitory concentrations equal to 2 µg/mL (VA2-MRSA). *Int J Antimicrob Agents* 38(1):46–51
- Vlastarakos PV, Nikolopoulos TP, Maragoudakis P, Tzagaroulakis A, Ferekidis E (2007) Biofilms in ear, nose, and throat infections: How important are they? *The Laryngoscope* 117:668–673
- Waters CM, Bassler BL (2005) Quorum sensing: cell-to-cell communication in bacteria. *Annu Rev Cell Dev Biol* 21:319–346
- Yang YH, Lee TH, Kim JH, Kim EJ, Joo HS, Lee CS, Kim BG (2006) High-throughput detection method of quorum-sensing molecules by colorimetry and its applications. *Anal Biochem* 356(2):297–299

Development of Micellized Antimicrobial Thiosulfinate: A Contemporary Way of Drug Stability Enhancement



Souptik Bhattacharya, Deepanjali Gupta, Dwaipayan Sen,
and Chiranjib Bhattacharjee

Abstract Over the past few decades, the development of bacterial resistance of antibiotics and dose-related toxicity of modern aggressive antibiotics has attracted attention to the dire need of new antibiotic discovery, which is efficient, cost-effective, and biocompatible. The ancient Indian medicinal system (*Ayurveda*) provided concepts of plant-based pharmacotherapy to treat infectious diseases. Medicinal plant parts contain numerous types of nutraceutical phytochemicals like flavonoids, phenols, thiosulfinate, quinones, alkaloids, terpenes, etc., which deliver significant antimicrobial properties and are known to be effective, edible, and nontoxic drugs. Their mode of action includes DNA inhibition, enzyme inactivation, cell wall and membrane damage, protein misfolding, denaturation, etc. of microorganisms. Several research works successfully demonstrated that these extracts are very effective against a wide range of pathogens and multidrug resistant (MDR) bacteria such as Methicillin-Resistant *Staphylococcus aureus* (MRSA), uropathogens, *Klebsiella*, *Escherichia*, etc. However, low extraction yield and unstable nature of phytochemicals pose major constraints in their commercial utilization. Micellization using biocompatible surfactants can be employed for enhanced drug delivery and stability. Naturally derived plant compounds can provide useful and low-cost source of antimicrobials to mitigate the challenges of drug discovery process required for antimicrobial chemotherapy.

Keywords Antimicrobial · Ayurveda · Nutraceutical · MDR · Polysorbate

S. Bhattacharya · D. Gupta · C. Bhattacharjee (✉)

Department of Chemical Engineering, Jadavpur University, Kolkata, West Bengal 700032, India
e-mail: c.bhatta@gmail.com

S. Bhattacharya

e-mail: souptikjduv@gmail.com

D. Gupta

e-mail: deepanjali15@gmail.com

D. Sen (✉)

Department of Chemical Engineering, Heritage Institute of Technology, Kolkata, West Bengal 700107, India

e-mail: dwaipayanju@gmail.com

© Springer Nature Singapore Pte Ltd. 2021

D. Ramkrishna et al. (eds.), *Advances in Bioprocess Engineering and Technology*,
Lecture Notes in Bioengineering,

https://doi.org/10.1007/978-981-15-7409-2_8

1 Introduction

Despite the discovery of modern antibiotics, the resurgence of bacteria-mediated infectious diseases continues to pose a threat toward human health due to bacterial resistance toward antibiotics. This emerging trend is concerning and is considered by the World Health Organization (WHO) and among the most urgent issues worldwide. This has directed present research trends toward alternative traditional medicines based on combinational therapies. Approximately, 80% of the developing world relies on medicines retrieved from medicinal plants as their primary health-care method (Moslamy and Shahira 2018). Medicinal plants are less expensive, abundant in bioactive compounds, safer to use in terms of side effects, and more readily available in comparison to their synthetic counterparts. These bioactive phytochemicals include tannins, alkaloids, terpenoids, steroids, thiosulfates, flavonoids, and coumarins (Bhattacharya et al. 2019). These plant-based compounds are of particular clinical value as their bioactivity generally does not induce bacterial resistance. The thiosulfate *allicin* is a plant defensin mimetic compound present in *Allium sativum* (garlic) extract, capable of high bacteriostatic properties. It is a major pharmaceutically important phytochemical that is capable of several potential biological activities including wide spectrum antibiotic action and synergy. However, the most crucial issue with the compound is its stability. Biocompatible polymeric surfactant system brings some advantages to the drug stability and delivery, particularly for oral phytodrug delivery. Several nonionic surfactants/polymers like polyethylene glycols (PEGs), polysorbate (tween), alkyl ethers, lauryl ether (Brij 30), etc. are often used for medicinal purposes. They allow (1) the extraction, stabilization, and delivery of poorly water-soluble drugs; (2) the targeting of drugs to specific parts of the gastrointestinal tract (GI); (3) the transcytosis of drugs across the tight intestinal barrier; and (4) the intracellular and transcellular delivery of large macromolecules (Grillo et al. 2018). Recently, this technique has been widely focused worldwide for its superiority in increasing efficacy, specificity, tolerability, and therapeutic index of corresponding drugs. Polymeric surfactant micelles (PSMs) have gained ample attention as a delivery system for poorly water-soluble drugs. Due to their nanoscopic size, PSM can obtain desirable biopharmaceutical and pharmacokinetic properties of drugs and enhance their bioavailability. In this present chapter, the importance of plant-based antimicrobial phytodrug stabilization using micellization and its bioprocessing development will be discussed (Sharmeen et al. 2018).

2 Challenges and Issues with Modern Antibiotics and Bacterial Virulence

The indiscriminate usage of antibiotics has led to a situation of the limited effectiveness of modern antibiotics. Multiple and total drug-resistant (MDR and TDR) microbes have developed diverse methods to resist antibiotic actions. The challenges regarding infectious diseases are increasing the rate of human morbidity and

mortality worldwide at an alarming rate. Bacteria often develop antibiotic-resistant genes through spontaneous mutation, thereby enhancing their chances of survival in unfavorable circumstances. These genes code for efflux pump activation that dislodges antibiotics from the cells, inhibit permeability of antibiotics through the cell membrane, and produce enzymes (e.g., β -lactamase) that nullify the action of antibiotics or revert the antibiotic target (Moslamy and Shahira 2018). *Staphylococcus aureus*, a Gram-positive bacterial species became resistant to penicillin treatment by developing penicillinase-type counter enzyme. Methicillin was introduced in the defense against this challenge. However, methicillin-resistant *S. aureus* developed extended-spectrum β -lactamases (ESBLs) to resist the modified β -lactams to render it unable to bind adequately with its target. *Klebsiella pneumonia*, a Gram-negative pathogen is the major cause of community-acquired infection, was found to have genes like *AmpC* that encodes for β -lactamases, thus rendering it unresponsive to wide-spectrum β -lactam drugs. The MDR strain of *K. pneumonia* is sensitive to *Colistin*, an aggressive last-resort antibiotic. However, new mutant strain of *Klebsiella* is found to have *mcr-1* gene that provides its enzymatic mechanism to resist against Colistin, thereby making this particular strain Total Drug Resistant (TDR) (Ankri et al. 1999). Such a significant rise of MDR and TDR strains necessitates the discovery, design, and development of novel aggressive antibiotics. Dose-related toxicity in juvenile and elderly population is a result of this new advancement. Fatal situations are found commonly in terminal patients with end-of-life care facilities. This present challenging scenario has uplifted the approach for holistic medicines or complementary and alternative medicine (CAM).

3 Plant-Based Pharmacotherapy and Bioprocessing: A Possible Solution

Plants remain a central source of drug to medical practices like *Ayurveda* (traditional Indian medicinal system). A recent report by the WHO indicated medicinal plants as one of the best potential sources of the novel drugs (Rao et al. 2006). Plant cell-based bioprocessing aims to produce phytochemicals with anti-tumor, antiviral, hypoglycemic, anti-inflammatory, antiparasite, antimicrobial, and immunomodulating properties. The detailed steps are presented in Fig. 1. Numerous Indian medicinal plants used in folkloric medicine possess significant antimicrobial properties against both Gram-positive and Gram-negative bacteria. Multiple studies have reported that allicin from garlic possesses relatively high levels of antimicrobial activity (Pool et al. 2006). Such plant-derived antimicrobials (PDAs) have particular pharmaceutical value because bacterial virulence does not confer resistance against PDAs.

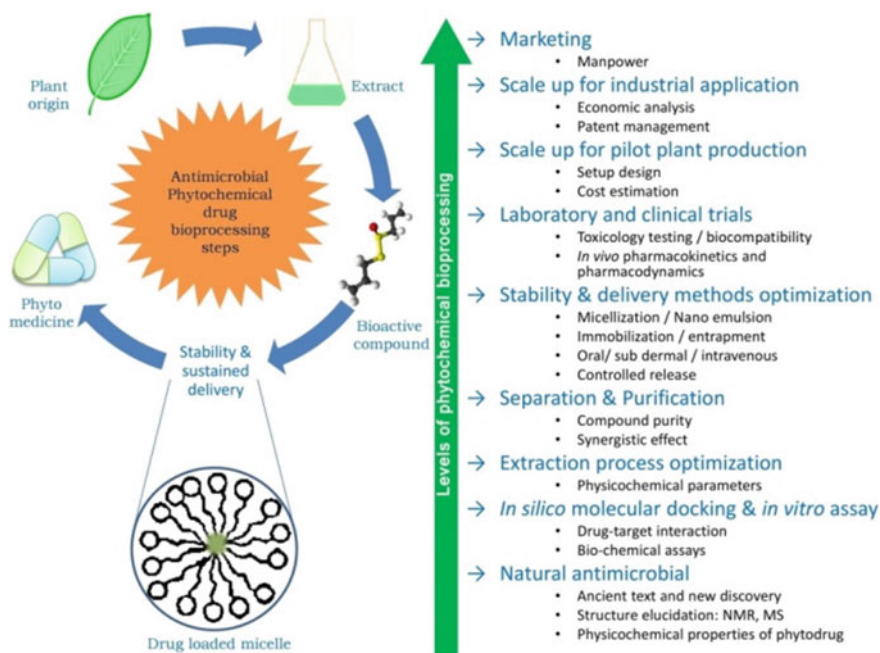


Fig. 1 Phytochemical drug bioprocessing steps

4 Advantages and Limitations of Herbal Drugs

The use of plant-derived drugs (PDD) for herbal medicine especially in the field of countering bacterial pathogenesis is increasing worldwide. Phytomedicine demonstrates promising results with lower dose-related toxicity and maximum effectiveness. The past two decades have witnessed a tremendous surge in acceptance and public interest in natural product therapies worldwide. The use of herbal remedies is now becoming mainstream in Europe, North America, India, and Australia. This can be attributed to the facts that PDD are cheap, have fewer side effects than their synthetic analogs, environment-friendly, and act as an effective antioxidant (Bhattacharya et al. 2019). Bioactive compounds in PDD such as tannins, alkaloids, flavonoids, thiosulfonates, glycosides, etc. act as natural immunostimulants and are known to provide nonspecific defense against pathogens. Sharmeen et al. tested 20 MDR strains of *Klebsiella* sp. against several aqueous herbal extracts and synthetic antibiotics (Sharmeen et al. 2018). The strains were reported to be sensitive to three herbal extracts while it developed resistance against 70% of the common antibiotics, though none of the strains was found to be resistant against any of the herbal extracts (Cui et al. 2009). Allicin is volatile and poorly soluble in aqueous solutions. Allicin exhibits antimicrobial activity against a wide variety of microbes, including

species of *Escherichia*, *Salmonella*, *Klebsiella*, *Bacillus*, and *Clostridium*. Antibacterial activity of allicin is due to the apparent inability of most bacteria to develop resistance to it because the mode of action is completely different from that of other antibiotic substances. Allicin acts by inhibiting the thiol-containing enzymes in the microorganisms (Miron et al. 1998). However, there are several constraints in the development of herbal drugs, the most significant of them being their nonspecific mode of action and poor bioavailability. Moreover, most of the bioactive compounds are highly unstable in nature, which makes the extraction process very complicated and expensive. However, researchers are constantly stressing to develop advanced techniques for stabilization, extraction, and sustained delivery of PDD for better bioavailability.

5 Micellization: A Contemporary Way of Drug Stability Enhancement

PDDs such as thiosulfonates, eugenol, essential oil, etc. are volatile and unstable in nature. They are sparingly soluble in commonly accepted pharmaceutical solvents. Therefore, one of the major challenges in the development of these herbal drugs is to enhance their solubility, thereby facilitating their extraction process. The earlier procedures applied to enhance drug stability and extractions were pH adjustment, cosolvent addition, complexation, and surfactant addition. In aqueous solution, surfactant molecules above their critical micelle concentration (CMC) self-assemble into nearly spherical clusters of micelles due to phase separation guided by the hydrophilic heads and hydrophobic tail groups of the surfactant molecules (Grillo et al. 2018). The hydrophobic micellar core provides an apt environment for solubilization of the hydrophobic drug of interest, hence leading to entrapment of drugs. The drug is incorporated into the micellar core employing noncovalent bonds, which causes steric hindrance to the drug molecule. This phenomenon effectively hinders the interaction of the PDDs with surrounding entities, thus augmenting the drug's pharmacokinetic and pharmacodynamic properties, thereby renders the stability. When administered, the release of the entrapped drug occurs at the target site through the dissolution of the micelle at the low intestinal pH (1.5–3). Curcumin, a slightly water-soluble drug with very poor bioavailability was stabilized and solubilized using a self-microemulsifying drug delivery system (SMEDDS). SMEDDS was formulated by using a surfactant, cosurfactant, and an oil into which curcumin was incorporated. The best result was obtained when SMEDDS was formulated with emulsifier OP and Cremophor EL as surfactant, cosurfactant PEG, and ethyl oleate oil. With this SMEDDS formulation, curcumin was reported to be stable for 3 months when stored at 4 °C (Akula et al. 2014).

6 Recent Application: Micellization of Allicin in Tween 20

Allicin was self-micellized in the Tween 20 surfactant system to prevent the degradation. The stabilization achieved at around $2 \times$ CMC of Tween 20 (500 mg/L) concentration. The short-term stability of allicin was studied over a period of 7 days. Allicin was extracted in aqueous solution as mentioned elsewhere (Bhattacharya et al. 2019) and self-micellized in the presence of Tween 20 and stored in refrigerator and room temperature during the time of the study. A second sample of extracted allicin was also stored without surfactant. The concentration of allicin in these stored samples was checked using the 4-mercaptopyridine method (Miron et al. 1998). The extracted allicin kept in presence of tween 20 at 4 °C was found to be stable up to 74.22% of the initial concentration after the test duration where only allicin was found degraded completely.

7 Conclusion

Herbal medicines have been recognized for their better therapeutic value as they have fewer adverse effects as compared with modern medicines. MDR and TDR microbes are a leading cause of human mortality in the modern world. Aggressive last-resort antibiotics are the only option in these situations and can be fatal for infants, elderly, immune-compromised and terminal patients. The drugs of *Ayurveda* origin had shown promising effectiveness upon various infectious diseases and can be commercialized in a better state with enhanced efficacy by incorporating in the modern engineered carrier system. Micelle-based carrier system has achieved massive consideration in the field of modern sustainable drug delivery process. Nonionic surfactants (Tween 20) are often used in upstream and downstream processing of drug formulation. They increase the stability, solubility, blood circulation, retention, bioavailability, intestinal absorption, and percutaneous absorption of phytomedicines. In this present investigation, the phytopharmaceutical allicin was self-micellized by tween 80 above its CMC concentration, and after 7 days, a significantly enhanced amount of allicin (74.22%) was found stable than raw allicin. Application of this stabilization method can be used during plant-based bioprocessing for production and commercialization of similar phytopharmaceuticals such as flavonoids, phenols, quinones, alkaloids, etc. This nontoxic, less expensive carrier system will fulfill the consumer demands and compliance with herbal drugs.

Acknowledgements The authors acknowledge the fellowship (SRF) provided by CSIR, India [file no. 09/096(0879)/2017-EMR-I], and GATE scholarship by AICTE, India.

Conflict of Interest None

References

- Akula S, Gurram AK, Devireddy SR (2014) Self-microemulsifying drug delivery systems: an attractive strategy for enhanced therapeutic profile. *Int Sch Res Notices* 2014:1–11. <https://doi.org/10.1155/2014/964051>
- Ankri S, Mirelman D (1999) Antimicrobial properties of allicin from garlic. *Microbe Infect* 1(2):125–129. [https://doi.org/10.1016/S1286-4579\(99\)80003-3](https://doi.org/10.1016/S1286-4579(99)80003-3)
- Bhattacharya S, Sen D, Bhattacharjee C (2019) In vitro antibacterial effect analysis of stabilized PEGylated allicin-containing extract from *Allium sativum* in conjugation with other antibiotics. *Process Biochem* 87(12):221–231. <https://doi.org/10.1016/j.procbio.2019.09.025>
- Cui J, Yu B, Zhao Y et al (2009) Enhancement of oral absorption of curcumin by self-microemulsifying drug delivery systems. *Int J Pharm* 371(1):148–155. <https://doi.org/10.1016/j.ijpharm.2008.12.009>
- Grillo I, Morfin I, Prévost S (2018) Structural characterization of Pluronic micelles swollen with perfume molecules. *Langmuir* 34(44):13395–13408. <https://doi.org/10.1021/acs.langmuir.8b03050>
- Miron T, Rabinkov A, Mirelman D et al (1998) A spectrophotometric assay for allicin and Alliinase (*Alliin lyase*) activity: reaction of 2-nitro-5-thiobenzoate with thiosulfates. *Anal Biochem* 265(2):317–325. <https://doi.org/10.1006/abio.1998.2924>
- Moslamy EL, Shahira H (2018) Bioprocessing strategies for cost-effective large-scale biogenic synthesis of nano-MgO from endophytic *Streptomyces coelicolor* strain E72 as an anti-multidrug-resistant pathogens agent. *Sci Rep* 8(1):1–22. <https://doi.org/10.1038/s41598-018-22134-x>
- Pool R, Bolhuis PG (2006) Prediction of an autocatalytic replication mechanism for micelle formation. *Rev Phys* 97(1):1–4. <https://doi.org/10.1103/PhysRevLett.97.018302>
- Rao VM, Nerurkar M, Pinnamaneni S et al (2006) Co-solubilization of poorly soluble drugs by micellization and complexation. *Int J Pharm* 319(1):98–106. <https://doi.org/10.1016/j.ijpharm.2006.03.042>
- Sharmeen R, Hossain MN, Rahman MM et al (2018) In-vitro antibacterial activity of herbal aqueous extract against multi-drug resistant *Klebsiella* sp isolated from human clinical samples. *Int Curr Pharm J* 1(6):133–137. <https://doi.org/10.3329/icpj.v1i6.10534>

Production and Characterization of Functional Lipid and Micronutrient Rich Health Beneficial Mayonnaise



Satarupa Ghosh, D. K. Bhattacharyya, and Minakshi Ghosh

Abstract The present study involved the production of mayonnaise by using a binary blend of flaxseed oil and rice bran oil (1:1) as the oil phase. Lemon juice was used instead of vinegar and egg yolk was used as an emulsifier. This study also included a comparative analysis of antioxidant activity by DPPH test, FRAP, and ABTS assay methods. Oxidative stability tests were based on acid value, peroxide value, TBA and anisidine value, and phytochemical contents (total phenolic and flavonoid content). Functional group detection (by FTIR analysis) of both sample mayonnaise (mayonnaise made by binary oil blend) and market mayonnaise was made. Sample mayonnaises were rich in both antioxidant and phytochemical content than market mayonnaise. Both sample mayonnaise and market mayonnaise were oxidatively stable after storage for one month at 15 °C temperatures in refrigerator.

Keywords Flaxseed oil · Rice bran oil · Antioxidant activity · Oxidative stability test · FTIR analysis

1 Introduction

Mayonnaise is very popular emulsified product in all over the world. It was first commercially produced in 1900s centuries in western countries and became very popular in America since 1917 (Depree and Savage 2001). It is an oil in water emulsion and can be produced by mixture of different vegetable oils, egg yolk, vinegar, and some spices. It consists of different phases: 70–80% oil (dispersed phase), vinegar

S. Ghosh · D. K. Bhattacharyya · M. Ghosh (✉)
School of Community Science and Technology, Indian Institute of Engineering Science and Technology, Shibpur, Howrah, West Bengal 711103, India
e-mail: g_minakshi2000@yahoo.com

S. Ghosh
e-mail: satarupa.ghosh8@gmail.com

D. K. Bhattacharyya
e-mail: dkb_oiltech@yahoo.co.in

(continuous phase), and egg yolk is used as an emulsifier (Li et al. 2014). Due to high-fat content of mayonnaise, there is a greater chance for the development of lipid oxidation. As a result, there is a possibility for the production of toxic chemicals and undesirable off-flavor and it decreases the shelf life of mayonnaise. One of the most common ways to retard lipid oxidation is the addition of antioxidants. In market mayonnaise, different types of synthetic antioxidants like butylated hydroxy anisole (BHA), ethylene diamine tetraacetic acid (EDTA), and butylated hydroxyl toluene (BHT) are used. But these products have a negative impact for their toxic and carcinogenic effects in high concentration. There is a growing demand from the customers for the production of mayonnaise using natural ingredients instead of chemical products. Incorporation of natural antioxidant into food products has great potential for improving the oxidative stability of food products and also beneficial for our health and nutrition (Hermund et al. 2016). Low pH and high-fat content of mayonnaise are more resistant to microbial spoilage (Depree and Savage 2001).

The use of binary blending of flaxseed oil and rice bran oil (1:1) for the production of mayonnaise and lemon is used instead of vinegar. Salt is added for taste and to reduce the microbial load also. Black pepper is also used as a spice.

Flaxseed oil is very well known for its nutritional and health benefits. It contains 53% alpha-linolenic acid (ALA), 17% linoleic acid (LA), 19% oleic acid, 3% stearic, and 5% palmitic acid. Omega 3 fatty acids help to prevent several diseases like ulcer, migraine headache, eating disorders, psoriasis, glaucoma, lyme disease (Harper et al. 2006). Flaxseed protein contains a favorable ratio of amino acids with Lysine, Threonine, and Tyrosine as the limiting amino acids. It is also very good source of sulfur-containing amino acids such as methionine and cysteine and branched chain amino acids like BCAA, Isoleucine, Leucine, and Valine, etc. (Oomah et al. 2007). It also contains several bioactive compounds like phenolic compounds, flavonoids, lignans, phenolic acids, etc. (Basavaraj 2009).

Rice bran oil is most popular among the cooking oils due to its nutritional composition, increased shelf life, well balanced fatty acids composition and antioxidants, and phytochemicals content that include squalene, oryzanol, phytosterol, and triterpene alcohols. It contains high amount of vitamin E both tocopherol and tocotrienols. The oil exhibits high antioxidant, anti carcinogenic, anti-diabetic, hypocholesterolemic, anti-inflammatory activities. It also has low viscosity and high-melting point which makes the oil healthier while cooking (Ali and Devarajan 2017).

Lemon juice is not only the richest source of vitamin C, it also contains fair amount of potassium, calcium, phosphorus, and magnesium. It helps to improve our immune system.

The main objective of the present study is to formulate a new kind of emulsion product (mayonnaise) by using binary blend of flaxseed oil and rice bran oil to provide functional fatty acids and antioxidants such as oryzanol, tocopherol, squalene and to analyze its antioxidant, oxidative stability as well as functional group content compared to market mayonnaise.

Table 1 Composition of ingredients including oil blend (binary) in the preparation of mayonnaise sample

Ingredients	Amount (g)
Flaxseed oil	30
Rice bran oil	30
Egg yolk	26
Salt	1
Sugar	1
Lemon juice	1.5
Black pepper	0.5

2 Materials and Methods

2.1 Samples and Chemicals

Rice bran oil was provided by M/S Sethia oil mill, West Bengal, India. All products including flaxseed, egg, lemon, spices were purchased from local market of Kolkata (West Bengal, India). All chemicals were brought from MERK, India.

2.2 Preparation of Mayonnaise

Mayonnaise sample was prepared by flaxseed oil, rice bran oil (1:1) blend, egg yolk, salt, sugar, lemon juice, and black pepper using the formula as shown in Table 1. Here egg yolk is used as an emulsifier and black pepper as a flavor enhancer spice.

Salt, sugar, black pepper were first mixed with the egg yolk and vinegar with the help of electric mixer for 5–10 s. After that the binary blended oil (flaxseed oil and rice bran oil) was added to the mixture. All the ingredients were mixed in a blender for 5 min. Then the sample mayonnaise was kept in a screw cap glass reagent bottle and stored in a refrigerator at 10 °C temperature for ten days. After ten days the sample mayonnaise was analyzed.

2.3 Antioxidant Activity

Antioxidant activity of the mayonnaises were measured by the following standard assay methods:

2.3.1 DPPH Free Radical Scavenging Activity Assay

The mayonnaises were assessed using 1, 1-diphenyl 2-picrylhydrazyl (DPPH) radical scavenging assay (Gorinstein et al. 2007). 0.1 mM solution of DPPH in methanol was prepared. An aliquot of 0.2 ml of sample was added to 2.8 ml of this solution and kept in the dark place for 30 min. The absorbance was measured at 517 nm. The ability to scavenge the DPPH radical was calculated with the following equation. Inhibition percentage ($I\%$) = $(A_0 - A_1)/A_0$ (A_0 = Absorbance of the control, A_1 = Absorbance of the sample.)

2.3.2 Ferric Reducing Antioxidant Power (FRAP)

The FRAP assay of the test samples was determined (Benzie and Strain 1996). The FRAP reagent consists of 10 mM TPTZ in 40 mM HCL, 250 mM sodium acetate buffer (pH -3.6), and 20 mM FeCl_3 . The reagent was freshly prepared by mixing TPTZ solution, FeCl_3 solution, and acetate buffer in a ratio of 1:1:10. An extract solution (100 μl) was mixed with 900 μl of FRAP reagent. The mixture was incubated at 37 °C temperature for 4 min and the absorbance was measured at 593 nm.

2.3.3 ABTS Free Radical Scavenging Activity

ABTS assay of mayonnaises were measured using the following method (Fatma et al. 2016). A solution of ABTS (7 μM) was prepared in distilled water and mixed with the solution of potassium per sulfate (2.45 μM). The mixture was kept in the dark place for 16 h at room temperature. The resulting intense color matches the ABTS radical cations. The solution subsequently diluted with distilled water and absorbance was measured at 734 nm. 1 ml of ABTS diluted solution was mixed with 10 μl of sample at different concentration and the reaction mixture was kept for 6 min before measuring the absorbance. ABTS scavenging activity was calculated by the following equation. Inhibition Percentage ($I\%$) = $(1 - A/A_0) \times 100$. (A = Absorbance of the sample. A_0 = Absorbance of the ABTS solution.)

2.4 *Fourier-Transformed Infrared Spectroscopy (FTIR) Analysis*

The functional groups, present in both sample and market mayonnaise, was analyzed by FTIR (Siregar et al. 2018) equipped with a tri glycine sulfate (TGS) detector. Absorbance intensity was measured at 4 cm^{-1} resolution. 2–3 mg of sample was

placed in the cell of FTIR. Sample analyzing was done at 27 °C temperature. All spectra were recorded from 600 to 3600 cm^{-1} .

2.5 Oxidative Stability Test

Oxidative stability of the mayonnaises was measured by the following standard assay methods:

2.5.1 Acid Value (AV)

This analysis has been conducted according to the following method (AOCS Ca 5a-40 official method). 1 gm of oil was mixed with hot ethyl alcohol and 2–3 drops phenolphthalein indicator was added to this mixture. The mixture was titrated with standard aqueous solution of alkali (0.1 N), shaking the solution vigorously during titration. Titration was continued till the solution turns pink.

2.5.2 Peroxide Value (PV)

This analysis has been conducted according to the following method (AOCS Cd 8-53). 5 gm oil was mixed with 30 ml acetic acid-chloroform solution (3:2). 0.5 ml potassium iodide (KI) solution was added to the oil solution and then the conical flask allowed to stand exactly 1 min. 30 ml distill water was added to the solution. Then titration was done against 0.1(N) sodium thiosulphate ($\text{Na}_2\text{S}_2\text{O}_3$) solution. Then the titration was continued until the yellow color of the solution almost disappeared. Then 0.5 ml starch solution was added to this mixture and continued the titration until the blue color appeared.

2.5.3 Anisidine Value

This analysis was done according to the following method (AOCS Cd 18-90). 1 ml of 0.25% of p-anisidine in glacial acetic acid made up to 100 ml with iso-octane, 1 gm of oil was dissolved in the mixture and allowed to react for 10 min at room temperature and absorbance was measured at 350 nm.

2.5.4 TBA Value

This analysis was carried out according to the method (Patton and Kurtz 1951). Thio barbituric acid (TBA) reagent was prepared by dissolving 200 mg TBA in 100 ml 1-butanol and left it for one night. Then it was filtered to remove the undissolved

Table 2 Antioxidant activity of sample mayonnaise prepared and market mayonnaise

Test	Mayonnaise made by using binary blended oil	Market mayonnaise
DPPH (%)	76% \pm 0.37	69% \pm 0.57
FRAP (μ mol/ml)	10 \pm 0.56	8 \pm 0.43
ABTS (%)	40% \pm 0.37	33% \pm 0.67

Correlation is significant at the $p \leq 0.05$ level

residue and makeup the filtrate to 100 ml with 1-butanol. 50–200 mg sample was taken in a volumetric flask (25 ml), dissolved in small amount of 1-butanol and made up to volume with the same solvent. 5 ml sample solution was mixed with 5 ml reagent solution, and the solution was placed into a thermostat bath at 95 °C temperature. After 120 min the solution was removed from thermostat and cooled under running water and absorbance was measured at 530 nm.

2.6 Statistical Analysis

Results were expressed as mean value \pm standard deviation of three replications. Statistical differences were analyzed using one way ANOVA followed by post hoc Tukey HSD (Honestly Significant Difference) at level $p \leq 0.05$.

3 Results and Discussion

3.1 Antioxidant Activity

The antioxidant activity of sample mayonnaise and market mayonnaise were evaluated using DPPH, FRAP, ABTS assay, and the results are shown in Table 2. Mayonnaise made by using binary oil blends shows maximum antioxidant activity (DPPH –76%, FRAP-10 μ mol/ml, ABTS –40%) as compared to market mayonnaise.

3.2 FTIR Analysis

From the above report, it can be stated that sample mayonnaise contains aromatic C–H bending, alkenyl C=C stretch, alkane C–H bond, and primary amine groups. Market mayonnaise contains aromatic C–H bending, aromatic C=C bending, aldehyde C=O stretch, and carboxylic acid group. FTIR reports are included in Table 3 (Figs. 1 and 2).

Table 3 FTIR analysis of Mayonnaise samples

Absorption (cm^{-1})	Functional group	Mayonnaise prepared by using binary oil blends	Market mayonnaise
3467.70	O–H stretch hydrogen bond	Present	–
3411.30	O–H stretch hydrogen bond	–	–
3050.83	=C–H stretch carbon hydrogen bond	–	Present
3009.37	=C–H stretch carbon hydrogen bond	–	Present
2925.50	C–H stretch bond	Present	–
2921.63	C–H stretch bond	–	Present
2854.30	C–H stretch bond	Present	–
2852.00	C–H stretch bond	–	Present
2761.56	H–C = O stretch bond	–	Present
2126.80	Alkynyl C=C stretch	–	–
1766.70	C=O stretch aliphatic aldehyde	Present	–
1747.00	C=O stretch aliphatic aldehyde	–	Present
1745.90	C=O stretch aliphatic aldehyde	–	–
1650.60	C = O stretch α , β unsaturated ketone	Present	–
1549.50	Aromatic ring	Present	–
1465.30	C–C stretch bond	–	–
1461.78	C–C stretch bond	–	Present
1460.20	C–C stretch bond	Present	–
1245.79	C–O stretch bond	–	Present
1230.60	C–O stretch bond	–	–
1159.80	C–O stretch bond	Present	–
1158.04	C–O stretch bond	–	Present
1156.70	C–O stretch bond	–	–
1094.40	C–O stretch bond	–	Present
855.27	Aromatic C–H bending	–	Present
717.39	Aromatic C–H bending	–	Present

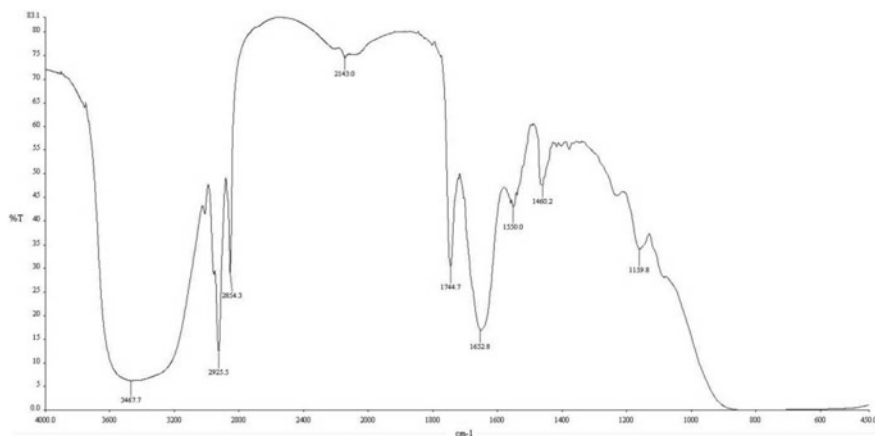


Fig. 1 Mayonnaise prepared by binary oil blend

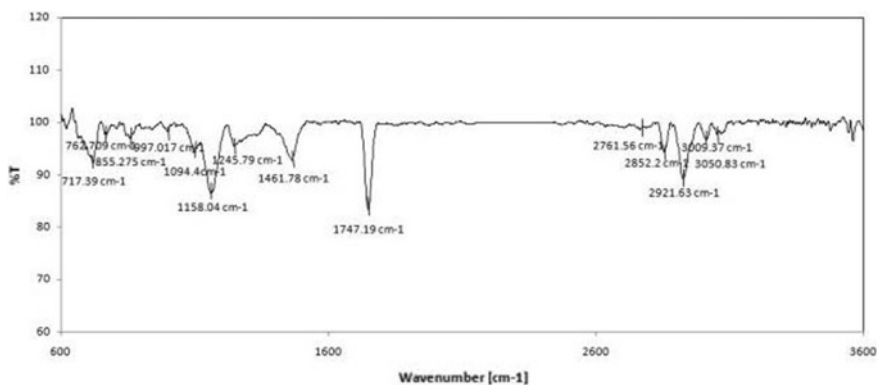


Fig. 2 Market mayonnaise

FTIR REPORT

3.3 Oxidative Stability

To evaluate oxidative stability such as acid value, peroxide value, anisidine value, and TBA test were performed and the results are shown in Table 4. Both sample and market mayonnaises are stable at room temperature.

Table 4 Oxidative stability test of mayonnaises samples

Test	Mayonnaise made by using binary blended oil	Mayonnaise made by using ternary blended oil
Acid value (mg KOH/gm oil)	0.67 ± 0.69 ^a	0.72 ± 0.93
Peroxide value (mequivalent/kg oil)	0.71 ± 0.53 ^a	0.85 ± 0.37
Anisidine test	3.37 ± 0.91	3.53 ± 0.43 ^b
TBA value	2.92 ± 0.39 ^a	2.97 ± 0.81 ^b

The data are presented as mean value ± standard deviation of triplet analyses. Different letters in the same column indicate statistically significant values ($p \leq 0.05$)

^{a, b} Mean values

4 Conclusion

From the present study, it can be concluded that the sample mayonnaise (mayonnaise produced by using binary oil blend) contained more phytochemicals than market mayonnaise because flaxseed oil contains several phytochemicals like phenolic compound, saponin, glycoside, flavonoid, alkaloid, and rice bran oil that also contains huge amount of oryzanol, squalene, phytosterol, etc. All the mayonnaises contained aldehyde, ketone, and alkene group. Both the sample mayonnaise and market mayonnaise are having nearly the same oxidative stability after storage of one month at 10 °C temperature.

Acknowledgements Firstly, I would like to acknowledge my institute Indian Institute of Engineering Science and Technology (IEST), Shibpur, Howrah, West Bengal, India for providing laboratory facilities. I also want to acknowledge Bose Institute, Kolkata for performing FTIR analysis.

References

- Ali A and Devarajan S (2017) Book—rice brown. Springer publication. Chapter—nutritional and health benefit of rice bran oil pp 135–158
- AOCS (1997a) Official method Ca 5a-40: free fatty acids, American oil chemists society sampling and analysis of commercial fats and oils
- AOCS (1997b) Official method Cd 8–53: peroxide value acetic acid-chloroform method, American oil chemists society sampling and analysis of commercial fats and oils
- AOCS (1997c) Official method Cd 18-90: p-Anisidine value, American oil chemists society sampling and analysis of commercial fats and oils
- Basavaraj M (2009) Potential benefits of flaxseed in health and disease—a perspective. *Agriculturae Conspectus Scientificus* 74(2):67–72
- Benzie IFF, Strain JJ (1996) The ferric reducing ability of plasma (FRAP) AS A MEASURE OF “antioxidant power” the FRAP assay. *Anal Biochem* 239:70–76

- Depree JA, Savage GP (2001) Physical and flavor stability of mayonnaise. *Trends Food Sci Technol* 12:157–163
- Fatma B, Mohamed KF, Barba SR, Semia EC (2016) Antioxidant properties of water soluble gum from flax seed hull. *Antioxidants (Basel)* 5(3):26
- Gorinstein OJ, Medina V, Nicolas JO, Simon T (2007) The total polyphenols and the antioxidant potentials of some selected cereals and pseudocereals. *Eur Food Res Technol* 225(3):321–328
- Harper CR, Edwards MJ, DeFilippis AP, Jacobson TA (2006) Flaxseed oil increases the plasma concentrations of cardioprotective (n-3) fatty acids in humans. *J Nutr* 136(1):83–87
- Hermund DB, Karadağ A, Andersen U et al (2016) Oxidative stability of granola bars enriched with multilayered fish oil emulsion in the presence of novel brown seaweed based antioxidants. *J AGR FOOD CHEM* 64(44):8359–8368
- Li C-Y, Kim H-W, Li H, Lee D-C, Rhee H-I (2014) Antioxidative effect of purple corn extracts during storage of mayonnaise. *Food Chem* pp 1s52:592-6
- Oomah BD, Berekoff B, Li-Chan ECY, Mazza G, Kenaschuk EO, Duguid SD (2007) Cadmium-binding protein components of flaxseed: influence of cultivar and location. *Food Chem* 100(1):318–325
- Patton S, Kurtz GW (1951) 2-Thiobarbituric acid as a reagent for detecting milk fat oxidation. *J Dairy Sci* 34:669–674
- Siregar C, Martono S, Rohman A (2018) Application of fourier transform infrared (FTIR) spectroscopy coupled with multivariate calibration for quantitative analysis of curcuminoid in tablet dosage form. *J App Pharma Sci* 8(08):151–156

Computer-Aided Drug Design Against Dopamine D2 Receptor for Antischizophrenia Drug Development



Dipankar Chaudhuri and Pradipta Bhattacharjee

Abstract Schizophrenia is a long term psychosis caused by dysregulation of dopamine D2R. Existing antipsychotic drugs that alleviate positive symptoms of schizophrenia exhibit varied side effects for which designing antipsychotic drugs with reduced side effects remains an important therapeutic goal. This research project has been designed to develop potential amino acid and small molecule-based lead compounds for the reduction of schizophrenic symptoms using in silico drug design tools and methods. Use of LIGDREAM resulted in generation of 100 analogues of Eticlopride. Those with better ADMET properties were subjected to molecular docking against D2R receptor using AutoDock Vina and iGEM dock which yielded two analogues that had more substantial binding affinities for D2R than Eticlopride. NCS-1 is a signalling protein that desensitizes Dopamine D2R. Hence, a protein-based therapeutic compound for schizophrenia was being developed by conserved mutations of two amino acid residues on NCS1 (Phe55 and Leu189) by more hydrophilic and hydrophobic substituent, respectively. Protein-protein docking using the CLUSPRO docking portal and subsequent energy analysis have shown that increased hydrophilicity one had enhanced stabilization. Results obtained from both the modified Eticlopride leads and NCS1 mutations indicate that they can be collectively taken further downstream in anti-schizophrenia drug development.

Keywords Schizophrenia · D2 receptor · Eticlopride · Small molecule-protein docking · Protein-protein docking

1 Introduction

Schizophrenia is a complex debilitating psychological ailment that manifests its symptoms through decades of an afflicted patient's lifetime. Schizophrenia is considered by medical practitioners and scientists to be a type of psychosis (Ajinkya et al.

D. Chaudhuri (✉) · P. Bhattacharjee
Department of Biotechnology, Heritage Institute of Technology, Chowbaga Road P.O, Anandapur,
East Kolkata Township, Kolkata, West Bengal 700107, India
e-mail: dipankar.chaudhuri@heritageit.edu

© Springer Nature Singapore Pte Ltd. 2021
D. Ramkrishna et al. (eds.), *Advances in Bioprocess Engineering and Technology*,
Lecture Notes in Bioengineering,
https://doi.org/10.1007/978-981-15-7409-2_10

101

2015). Research into cause and treatment of schizophrenia proposes a complex combination of physical, hereditary, mental and ecological components which can combine to develop the condition. Antipsychotic drugs are the key mode of treatment for major symptoms of Schizophrenia (Patel et al. 2014). Present antipsychotic drugs can show tardive dyskinesia as side effects in the patients who consume such drugs for long period of time (Carbon et al. 2018). Other side effects include irregular heartbeat and muscle instability.

A hypothesis exists regarding dysregulation of neurotransmitters like dopamine and over-stimulation of dopamine D2 receptors (D2R) in subcortical and limbic brain schizophrenia development. This hypothesis is referred as the Dopamine Hypothesis (Brisch et al. 2014). This hypothesis postulates that the maximum numbers of antipsychotic drugs that are used to treat symptoms of Schizophrenia are antagonists with respect to targeting the Dopamine D2R (Li et al. 2016). Neuronal calcium sensor-1 (NCS-1) is one of the important members of calcium-myristoyl-switch proteins that have been known to act as calcium-ion sensors. NCS-1 binds in the signalling site for synaptic activity and desensitizes the D2 receptors. Since D2-NCS1 interaction modulates D2 mediated neurotransmission signalling pathway, this interaction has been chosen as an important focus area for the development of new antipsychotic drugs (Kabbani et al. 2012). Computer-aided drug design assists in determination of binding affinity and selectivity of lead candidate binding to the receptor. Aside from binding affinity determination, computer-aided drug design methodology also incorporates determination of pharmacokinetic and pharmacodynamics properties of the lead and uses the techniques of molecular docking and scoring, molecular diversity and combinatorial chemistry. These techniques reduce the cost of drug discovery and development as well as reduce the time needed for new, modified or repurposed lead candidate drug development (Makhouri and Ghasemi 2018). It has been determined that there is urgent need for the development of more potent targeted drugs against schizophrenia. This computational drug design project centres around (i) modification of an existing well-known drug named Eticlopride to yield analogues with better pharmacological properties and (ii) develop protein-based therapeutic molecules by introducing mutations in the NCS-1 protein with better binding efficacy and introducing reduce side effects and improving stability of mutant.

2 Materials and Methodology

2.1 Generation of Novel Lead Compounds

Eticlopride is an important antagonist drug with high affinity towards dopamine D2 receptors and used as lead for designing antipsychotic drugs. A shape decoding tool LigDream was used to derive 100 novel leads had been derived from the parent compound Eticlopride. SWISSADME and ADMETLab database were used to estimate physicochemical characteristics of Eticlopride and other newly designed

Table 1 Mutations introduced in NCS1 (Neuronal calcium sensor-1)

Control NCS1	Mutated towards hydrophilic	Mutated towards hydrophobic
PHE 55	ARG 55	ILE 55
LEU 189	ARG 189	ILE 189

PHE Phenylalanine, *LEU* Leucine, *ARG* Arginine, *ILE* Isoleucine

compounds. Compounds with better ADMET values than that of Eticlopride were docked with Dopamine D2 receptor for estimating binding efficacy.

2.2 Docking with AutoDock Vina and iGEM Docking

For molecular docking AutoDock Vina uses a hybrid scoring function of empirical and knowledge-based functions in calculation of X-Score to determine the best poses. iGEMDOCK, on the other hand, uses energy-based scoring function that is composed of electrostatic, hydrogen bonding and Van der Waals interaction between protein and ligand molecules. Henceforth in this research work both docking tools have been utilized for cross-validation of the binding affinity of newly derived leads towards D2R.

2.3 Introduction of Mutation in Ncs1 Docking

Docking has been performed between wild type NCS1 (Phyre2 id d1g8ia) and D2R (PDBID 6CM4). Posts docking the binding hotspot and total stabilizing energy have been analyzed with the help of PPCHECK. Hydrophobic amino acid residues present in the HOTSPOT have been mutated to introduce hydrophilic and more hydrophobic amino acids with the SWISSPDB VIEWER and the structural stability estimated. Docking has been done with the help of CLUSTER PRO DOCKING tool between mutated NCS1 and D2R. ΔG , K_d values and total stabilizing energy values were determined with the help of computational tools like PP CHECK and PRODIGY (Table 1).

3 Result and Discussion

3.1 Physicochemical Property

From ADMET lab report, the hepatotoxicity probability of compound 36th (C₁₆H₂₄ClN₃O₃) and compound 96th (C₁₆H₂₁ClF₂N₂O₃) are 0.66 and 0.62,

Table 2 Structure and physicochemical properties of new lead compounds with the help of public domain tools

Compound	MW	C LOG P	Aqueous solubility ($\mu\text{g/ml}$)	PSA (\AA^2)	Hbond acceptor	Hbond donor
C16H24ClN3O3 (36th compound)	341.839 Dalton	2.41	344	51.42	4	2
C16H21ClF2N2O3 (96th compound)	362.804 Dalton	2.82	129	50.46	5	2

MW Molecular weight, *PSA* Polar surface area, *HBOND* Hydrogen bond

respectively. These are less than that of parent lead Eticlopride, i.e. 0.71. Estimation of the hepatotoxic potential of drug leads is an important part of drug development process. This is especially applicable since a large number of drugs can exhibit adverse side effects that are often hepatotoxic. LD50 values for 36th and 96th compound were found to be 976.836 and 1193.087 mg/kg which are higher than that of Eticlopride which is 789.886 mg/kg. According to ADMETlab LD50 value for High-toxicity = 1–50 mg/kg; Toxicity = 51–500 mg/kg; low-toxicity = 501–5000 mg/kg (Dong et.al. 2018). Hence it can be concluded that both of the new compounds have lower toxicity profile than that of Eticlopride. To become a potent CNS Drug, a lead compound must not be potent CYP3A4 inducer. According to ADMETlab report probability of P450 CYP3A4 inhibition for our 36th and 96th compound found to be 0.637 and 0.245, respectively. These are higher than that of Eticlopride, i.e. 0.069. It can therefore be stated that new compounds have less significant potency to induce P450 CYP3A4 (Table 2).

All these physicochemical properties of the new lead molecules have proven that these two compounds proper attributes to penetrate the CNS according to Lipinski Rules. CNS penetration is a characteristic antipsychotic drug due to the presence of D2 receptors in central nervous system. Ideally orally mediated CNS penetrating drugs should have lesser polar surface area (PSA) (<60–70 \AA) because these leads increase passive permeability. Henceforth the PSA of these new compounds is lower as well. To increase the bioavailability, CNS drug is designed as less flexible with less than 8 rotatable bonds (Pajouhesh and Lenz 2005). The number of rotatable bonds for 36th and 96th compound have been found to be 6 and 5, respectively, with the help of cheminformatics software like Molinspiration. Finally, the GPCR ligand bioactivity score for 36th and 96th compound was found to be 0.26 and 0.27 which are higher than that of Eticlopride, i.e. 0.20. This implies that these two compounds have more favourable physicochemical properties.

Table 3 AutoDock Vina result for all compounds

Compound	RMSD	Affinity score with respect to lower RMSD (kcal/mol)
ETICLOPRIDE	1.15	-7.4
C16H24CIN3O3 (36th compound)	0.277	-8
C16H21CIF2N2O3 (96th compound)	0.699	-8.7

RMSD Root mean square division

Table 4 iGEM Docking result for total energy Eticlopride and other two newly derived lead compounds

Compound	Total energy (kJ/mol)
C16H24CIN3O3 (36th compound)	-98.46
C16H21CIF2N2O3 (96th compound)	-92.32
Eticlopride	-82.93

3.2 Docking (AutoDock Vina and IGEM)

According to AutoDock Vina, the affinity score is equivalent to the ΔG value. So lower the ΔG value and lower RMSD values are the two key factors to determine the binding efficiency of lead compounds towards receptor. From AutoDock Vina result, the RMSD values are estimated on energy involved in protein-ligand interaction. Difference between two RMSDs (ub-lb) was taken as indication of best pose with respect to high affinity for comparison between modified leads and Eticlopride with respect to Dopamine D2 receptor. For 36th and 96th compound, the RMSD values were found to be 0.277 and 0.699, respectively, which are lower in comparison to Eticlopride whose RMSD found to be 1.15. This can be stated hypothetically that new compounds are more capable to form stable complex with dopamine d2 than that of eticlopride (Tables 3 and 4).

iGEMDOCK ranks all the screening compounds based on the energy involved and pharmacological scoring function and clusters the compounds on the basis of their chemical composition. According iGEMDOCK standard report 36th compound has ranked first with total energy 1, 96th compound as second with total energy and Eticlopride as third with total energy which implies that both of the new compounds have higher efficiency to bind with D2R.

3.3 Docking (Cluspro)

After doing docking between NCS1 (wild type) and D2R in CLUSPRO docking tool, the hotspot of NCS1 has been found to be PHE55, LEU189 and GLU142 with help of PPCHECK web server (Table 5).

Table 5 PPCHECK web server analysis report for total stabilizing energy between protein-protein docking complexes

Protein complex	Total stabilizing energy (kJ/mol)
D2R-NCS1 mutated towards hydrophilic	-488.33
D2R-NCS1 mutated towards more hydrophobic	-428.63
D2R-NCS1 (control)	-393.49

D2R Dopamine D2 Receptor

Table 6 PRODIGY analysis report for ΔG and K_d values for all protein-protein docking complexes

Protein complex	ΔG (kcal mol ⁻¹)	K_d
D2R- NCS1 mutated towards hydrophilic	-17.1	2.0E-13
D2R- NCS1 mutated towards more hydrophobic	-16.5	7.9E-13
D2R-NCS1(control)	-15.7	2.9E-12

According to PPCHECK web server analysis report both the mutated NCS1 have shown better stabilizing energy than the control NCS1. However, NCS1 mutated towards hydrophilic formed more stable complex with D2R than one the mutated towards hydrophobic. In the protein-based drug design experiments affinity is considered as the initial criteria to estimate the potency of that protein for binding with the target protein/DNA/RNA. If the stabilizing energy is of negative value that means the ligand binds spontaneously without consuming energy and when binding energy is a positive value that implies the binding is energy consuming and would occur only if the required energy is available (Table 6).

ΔG values for both mutated NCS1 (hydrophilic and hydrophobic) are lower than that of control which indicates greater stabilization. Lower K_d indicates greater stabilization. On the basis of K_d , PPIs have been divided into three groups such as high ($K_d \leq 10^{-9}$ M), medium (10^{-9} M < $K_d \leq 10^{-6}$ M) and low affinities ($K_d > 10^{-6}$ M) (Erijman et al. 2014) In this case K_d values for mutated NCS1 are lower than that of control NCS1. Ramachandran plot analysis showed 1.6% of amino acids are present in disallowed regions both control and mutated NCS1 proteins. However, 66% of the total amino acids in disallowed region are glycines. The flexibility of Glycine makes it present over large area in RM plot. Thus they always found in loop region where polypeptide chain needs to make a sharp turn. From the above discussion, it can be concluded that the protein stability of control protein has not been compromised for the interest of protein modification towards hydrophilicity/more hydrophobicity and better druggability.

4 Conclusion

This project was designed with the aim of developing therapeutic compounds (chemical and protein based) for the treatment of Schizophrenia by (i) modification of the chemical structure of Eticlopride using Bioisosterism and QSAR-based methods and (ii) mutation of the wild type human NCS1 protein using computational mutational sensitivity analysis and in silico drug design techniques in both cases. The ultimate conclusions of this research centred around designing more therapeutically potent lead compounds than Eticlopride in the small molecule antagonist category as well as mutated forms of NCS1 wild type that computationally have more stable binding energetics than wild type NCS1 thereby indicative of being usable for further lead development/optimization for the treatment of positive symptoms of schizophrenia like antipsychotic effects.

References

- Ajinkya SA, Jadhav P R, Rajamani S (2015) Which is a more debilitating disorder schizophrenia or dysthymia?—a comparative study. *J Clin Diagn Res JCDR* 9(5):VC01–VC03. <https://doi.org/10.7860/JCDR/2015/11935.5926>
- Brisch R, Saniotis A, Wolf R et al (2014) The role of dopamine in schizophrenia from a neurobiological and evolutionary perspective: old fashioned, but still in vogue. *Front Psychiatry* 5:47. <https://doi.org/10.3389/fpsy.2014.00047>
- Carbon M, Kane JM, Leucht S et al (2018) Tardive dyskinesia risk with first- and second-generation antipsychotics in comparative randomized controlled trials: a meta-analysis. *World Psychiatry: Official J World Psychiatric Assoc (WPA)* 17(3):330–340. <https://doi.org/10.1002/wps.20579>
- Dong J, Wang NN, Yao ZJ et al (2018) ADMETlab: a platform for systematic ADMET evaluation based on a comprehensively collected ADMET database *J Cheminformatics* 10(1):29. <https://doi.org/10.1186/s13321-018-0283-x>
- Erijman A, Rosenthal E, Shifman JM (2014) How structure defines affinity in protein-protein interactions. *PLoS ONE* 9(10):e110085. <https://doi.org/10.1371/journal.pone.0110085>
- Kabbani N, Woll MP, Nordman JC et al (2012) Dopamine receptor interacting proteins: targeting neuronal calcium sensor-1/D2 dopamine receptor interaction for ANtipsychotic Drug Devel. *Curr Drug Targets* 13(1):72–79. <https://doi.org/10.2174/138945012798868515>
- Li P, Snyder GL, Vanover KE (2016) Dopamine Targeting Drugs for the Treatment of Schizophrenia: Past, Present and Future. *Curr Top Med Chem* 16(29):3385–3403. <https://doi.org/10.2174/1568026616666160608084834>
- Makhouri FR, Ghasemi JB (2018) In silico studies in drug research against neurodegenerative diseases. *Curr Neuropharmacol* 16(6):664–725. <https://doi.org/10.2174/1570159X15666170823095628>
- Pajouhesh H, Lenz GR (2005) Medicinal chemical properties of successful central nervous system drugs. *NeuroRx* 2:541–553. <https://doi.org/10.1602/neurorx.2.4.541>
- Patel KR, Cherian J, Gohil K et al (2014) Schizophrenia: overview and treatment options. *P & T: A peer-Rev J formulary Manage* 39(9):638–645

Biodegradation of Dyes by Laccase from Isolated Strain *Aspergillus flavus* PUF5



Priyanka Ghosh and Uma Ghosh

Abstract Synthetic dyes are very difficult to degrade for their complex structure. During dyeing process in industry, a huge amount of dyes are lost as effluents. Degradation of these effluents by physical and chemical processes is the most problematic issues nowadays. Enzymatic oxidation of these dyes using oxidoreductase such as laccase has received a great attention in recent years for decolorization of dyes in effluent. In the present study, an isolated fungus *Aspergillus flavus* PUF5 was used to produce laccase enzyme and employed for degradation of five commercially used textile dyes, phenol red, methyl orange, malachite green, bromophenol blue and Congo red. The investigations were made with the effect of redox mediators (1 mM), temperature (25–45 °C), pH (4–8) and incubation time (0–24 h) in the dye decolorization by laccase. Highest efficiency in dye decolorization was found with redox mediator 1-hydroxy-benzotriazole (HBT). The interactions between four variable factors were statistically studied using response surface methodology. Optimized states of selected variables were dye concentration (6.04 μM), enzyme concentration (78.8 U/ml), pH (5.6) and redox mediator (1.07 mM) with predicted and observed activity of laccase 85.94 and 86.3 U/ml, respectively. These results suggest that laccase is a potential enzyme for removal of dyes present in wastewater of textile industry.

Keywords *Aspergillus flavus* PUF5 · Laccase · Textile dyes · RSM · HBT

1 Introduction

Laccases (benzenediol: oxygen oxidoreductase, EC 1.10.3.2) is a multicopper oxidase that reduces molecular oxygen to water and simultaneously performs one-electron oxidation in a large range of inorganic and organic substrates, including

P. Ghosh · U. Ghosh (✉)
Food Technology & Biochemical Engineering Department, Jadavpur University, Kolkata,
West Bengal 700032, India
e-mail: ughoshftbe@yahoo.co.in

P. Ghosh
e-mail: priyankaghsh288@yahoo.in

© Springer Nature Singapore Pte Ltd. 2021
D. Ramkrishna et al. (eds.), *Advances in Bioprocess Engineering and Technology*,
Lecture Notes in Bioengineering,
https://doi.org/10.1007/978-981-15-7409-2_11

mono-, di- and polyphenols, methoxyphenols, aromatic amine and aminophenols. In the recent decades, it has been reported that a number of fungal laccases could decolorize and degrade industrial dyes which are widely used in the dyeing fabric, printing paper, leather, food process industries, colour photography and as additives in petroleum-based products. Synthetic dyes are different types like azo, triaryl-methane, indigoid and anthra-quinonic, used in dyeing process. The textile industry stands out, as it produces a large amount of effluents which can cause serious environmental problems like affect photosynthetic activity in aquatic life by reducing light penetration intensity and may also be toxic to some aquatic fauna and flora due to the presence of aromatics, metals, chlorides, etc. (Chacko and Subramaniam 2011). It is estimated that about 10–15% of dyes are released into processing water during dyeing and subsequent washing steps of procedure (Selvam et al. 2003). Traditional processes are usually costly, complex and produced a large number of slush but enzymatic process give an eco-friendly and capable substitute for decolorizing of dyes and also detoxify before discharging into the environment (Blanquez et al. 2004). The enzymatic approach deals mainly with ligninolytic enzymes, of which laccases are the most preferred enzymes for this purpose since they act oxidatively and less particularly on aromatic rings, thus having prospective to degrade a various range of compound. The use of mediator compounds permits an expansion of the reactivity of laccase to include such unnatural laccase substrates by generating high redox potential species. Using mediator, laccase can indirectly oxidize large molecules and even nonphenolic substrates also. 1-hydroxybenzotriazole (HBT) is one of the most important laccase mediators (Moldes and Sanroman 2006), but the prime issue of HBT using is its limited biodegradability and possible toxicity (Murugesan et al. 2007). Hence, HBT concentration optimization is much more important for efficient decolourization. In this present work, we have investigated degradation/decolourization of textile dyes, Bromophenol blue, phenol red, malachite green, methyl orange and Congo red by laccase enzyme which is produced from an isolated and identified fungus *Aspergillus flavus* PUF5. The aim of this study is to optimize the HBT, pH, enzyme and dyes concentrations in order to obtain the best possible results in dye decolourization by laccase.

2 Materials and Methods

2.1 Fungal Strain

The laccase producing fungi *A. flavus* PUF5 (GenBank accession number KX181714.1) was maintained on potato dextrose agar slants. A suspension containing about 5×10^9 spores/ml was used as an inoculum.

2.2 Laccase Enzyme Production by Solid-State Fermentation

Agricultural waste substrate ribbed gourd peel was moistened with water and auto-claved in 250 ml Erlenmeyer flasks up to 7 days with 7-day-old culture at 30 °C. After fermentation, the supernatant was collected, stored and used as enzyme source of laccase.

2.3 Enzyme Assay

Free laccase activity was determined using the process as described by Desai et al. (2011) where guaiacol was used as substrate. Laccase activity was expressed in U/ml.

2.4 Effect of Laccase and Dye Concentrations on Decolorization Efficiency

The effect of laccase concentration on decolorization efficiency was determined by incubating the synthetic dyes with varying concentrations of laccase (20–100 U/ml) for 24 h. To study the effect of dye concentrations with varying concentrations (5, 10, 15, 20, 25 μ M) were used for 24 h. Immediate after incubation the dye degradation efficiency was expressed in percentage (%).

2.5 Effect of Temperature, PH, Incubation Time and Laccase Mediator on Dye Decolorization Efficiency

During optimization of dye decolorization efficiency by laccase, the enzyme and dyes were incubated at varying temperatures (25–45 °C), pH (4.0–8.0) and incubation time (0–24 h). 1-hydroxybenzotriazole (HBT) (1 mM) was added in the reaction mixture as redox mediator and observed up to 24 h. Dye degradation efficiency was expressed in percentage (%).

2.6 Box–Behnken Response Surface Methodology

The effects of dye concentration (mM), enzyme concentration (U/ml), pH, HBT (%) on dye decolorization efficiency were evaluated. These factors were chosen as they showed influencing effects in one variable at a time (OVAT) optimization. Levels

of these factors were optimized for maximum decolorization of dye using Box–Behnken statistical design (Box and Behnken 1960). Table 1 represents different selected factors where each variable was tested in three different coded levels: low (−1), middle (0) and high (+1). Table 2 represents a 29-trial of the experimental design.

Table 1 Box–Behnken experiments design matrix with experimental and predicted values for dye decolorization by laccase enzyme

Run	Dye concentration (mM)	Laccase concentration (U/g)	pH	HBT (mM)	Observed response (U/ml)	Predicted response (U/ml)
1	8	100	5.5	1.0	26.3	26.29
2	4	80	5.5	1.5	36.4	36.35
3	4	80	6.5	1.0	33	32.52
4	6	100	4.5	1.0	57.7	56.65
5	6	80	5.5	1.0	85.3	85.94
6	8	80	4.5	1.0	29.6	31.10
7	8	80	5.5	0.5	37	36.53
8	4	60	5.5	1.0	24.8	24.31
9	6	60	4.5	1.0	51.2	50.59
10	6	60	6.5	1.0	63.6	64.13
11	6	100	5.5	0.5	63.6	63.37
12	6	80	5.5	1.0	86.3	85.94
13	6	80	6.5	0.5	68.6	68.95
14	6	80	4.5	1.5	68.2	67.36
15	6	80	5.5	1.0	85.5	85.94
16	4	80	5.5	0.5	32.2	31.86
17	6	80	5.5	1.0	86.3	85.94
18	8	80	6.5	1.0	35.7	35.98
19	6	60	5.5	0.5	54.2	54.64
20	8	60	5.5	1.0	33.6	32.48
21	6	80	4.5	0.5	57.1	57.36
22	6	60	5.5	1.5	68	69.25
23	6	100	5.5	1.5	55.86	56.44
24	4	80	4.5	1.0	25.8	26.53
25	6	100	6.5	1.0	53.9	53.99
26	6	80	5.5	1.0	86.3	85.94
27	6	80	6.5	1.5	67.4	66.64
28	8	80	5.5	1.5	39.9	39.72
29	4	100	5.5	1.0	25.8	26.42

Table 2 Analysis of variance (ANOVA) for dye decolorization in second-order polynomial model

Source	Sum of square	df	Mean square	F-value	p-value Prob > F	
Model	12,345.22	14	881.80	1054.38	<0.0001	Significant
A-Dye concentration	48.40	1	48.40	57.87	<0.0001	
B-Laccase concentration	12.48	1	12.48	14.93	0.0017	
C-pH	88.56	1	88.56	105.90	<0.0001	
D-HBT	44.31	1	44.31	52.99	<0.0001	
AB	17.22	1	17.22	20.59	0.0005	
AC	0.30	1	0.30	0.36	0.5572	
AD	0.42	1	0.42	0.51	0.4889	
BC	65.61	1	65.61	78.45	<0.0001	
BD	115.99	1	115.99	138.69	<0.0001	
CD	37.82	1	37.82	45.22	<0.0001	
A2	11,271.17	1	11,271.17	13,477.08	<0.0001	
B2	1847.68	1	1847.68	2209.29	<0.0001	
C2	1049.92	1	1049.92	1255.40	<0.0001	
D2	429.79	1	429.79	513.91	<0.0001	
Residual	11.71	14	0.84			
Lack of fit	10.72	10	1.07	4.32	0.0856	Not significant
Pure error	0.99	4	0.25			
Cor total	12,356.93	28				

2.7 Statistical Analysis

Statistical analyses were performed using statistical software Design Expert (version 8.2; STATEASE Inc., Minneapolis, MN, USA).

3 Results and Discussion

3.1 Effect of PH and Temperature on Decolorization of Dye

Congo red, bromophenol blue and malachite green were decolorized after 12 h of incubation (15–28%), at around pH 4.8–5.8. On the other hand, methyl orange and phenol red were most decolorized (60–75%) at pH 5, above which the decolorization process decreased remarkably. These observations are shown in (Fig. 1a) indicated

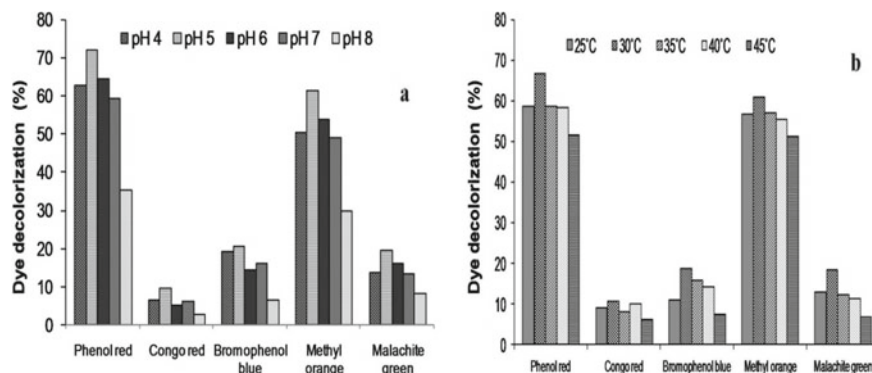


Fig. 1 a Effect of pH on dye decolorization b Effect of temperature on dye decolorization

that the optimum pH is mostly 5 for laccase catalyzed oxidation (Nyanhongo et al. 2002).

The effects of temperature (25–45 °C) on decolorization are shown in (Fig. 1b). Over the examined range, decolorization rate increased at 30 °C after this certain degree dye decolorization decreased as a result of the fact that the enzymatic catalysis rate becomes lower than the rate of enzyme inactivation at high temperature (Nyanhongo et al. 2002).

3.2 Effect of Laccase and Dye Concentration on Decolorization of Dye

The effect of laccase concentration on decolorization of dye found out that the optimum concentration of laccase required for maximum decolorization was 100 U/ml (Fig. 2a). The effect of dye concentration (5–25 μ M) on decolorization

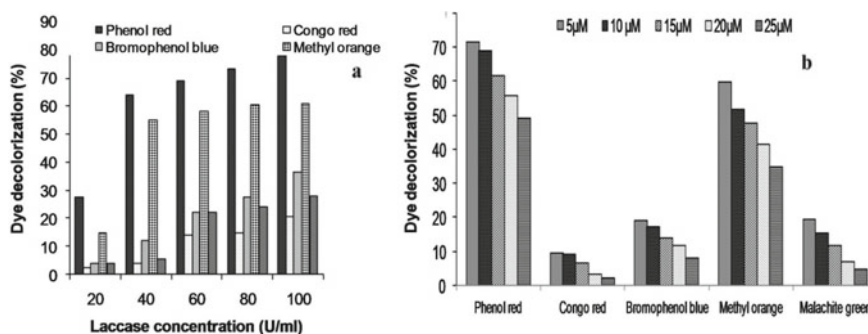


Fig. 2 a Effect of laccase concentration on dye decolor b Effect of dye concentration on dye decolor

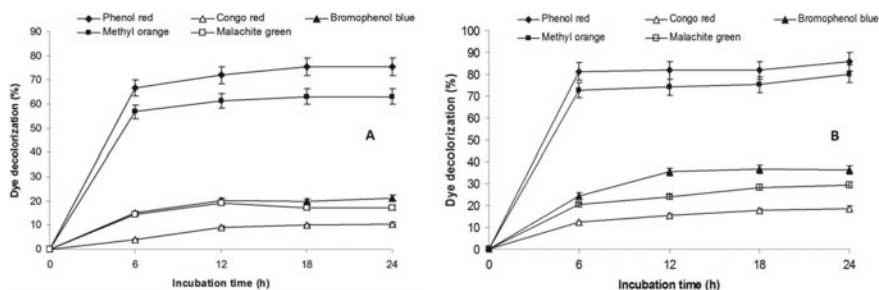


Fig. 3 a and b Effect of dye decolorization by laccase enzyme without mediator and with mediator (HBT)

of dyes by laccase observed that the percentage of decolorization was gradually decreased after 24 h on increasing the concentration of dye (Fig. 2b). Sathishkumar et al. (2010) had reported that when concentration of laccase increased then rate of dye decolorization also increased and concentrations of the dye when higher, then effectiveness of the enzyme gradually reduced but did not diminish completely.

3.3 Effect of Incubation Time and Mediator on Dye Decolorization

Facilitating electron transfer from O_2 to laccase substrate is the main mechanism behind HBT assisted oxidation of different substrates (Forootanfar et al. 2012). Figure 3a showed that phenol red (73%), methyl orange (68%), bromophenol blue, congo red and malachite green less than 30% were decolorized after 24 h (Ado et al. 2019). In the presence of HBT as a laccase mediator Fig. 3b showed that 10–20% positive influence on decolorization percentages of all studied dyes. Maalej-Kammoun et al. 2009 reported in their study that among ten laccase mediators, HBT showed the maximum decolorization of malachite green.

3.4 Optimization of Parameters for Dye Decolorization Through Box–Behnken Response Surface Design

The optimal level of the key factors and the effect of their interactions on dye decolorization were explored by the Box–Behnken response surface methodology. By applying multiple regression analysis on the experimental data, the following second-order polynomial equation was established to explain the decolorization of dye:

$$\begin{aligned}
 Y = & +85.94 + 2.01A - 1.02B + 2.72C + 1.92D \\
 & - 2.08AB - 0.28AC - 0.32AD - 4.05BC - 5.39BD \\
 & - 3.07CD - 41.69A^2 - 16.88B^2 - 12.72C^2 - 8.14D^2
 \end{aligned}$$

where Y is the predicted yield of dye decolorization; A, B, C, D are the coded values of dye concentration (mM), enzyme concentration (U/ml), pH, HBT (%), respectively. The analysis of variance (ANOVA) was conducted to test the significance of the fit of the second-order polynomial equation for the experimental data as shown in Table 2.

The Model F -value of 1054.38 implies the model is significant. There is only a 0.01% chance that a “Model F -value” could occur due to noise. Model P -value in this study was <0.0001 which also indicates that the model was significant. The coefficient of variation ($R^2 = 0.999$) indicates a good agreement between experimental and predicted values, which implies that the model was reliable for dye decolorization and statistically sound. The response surface plots and the contour plots are shown in Fig. 4. Shapes of response surfaces and contour plots indicate the nature and extent

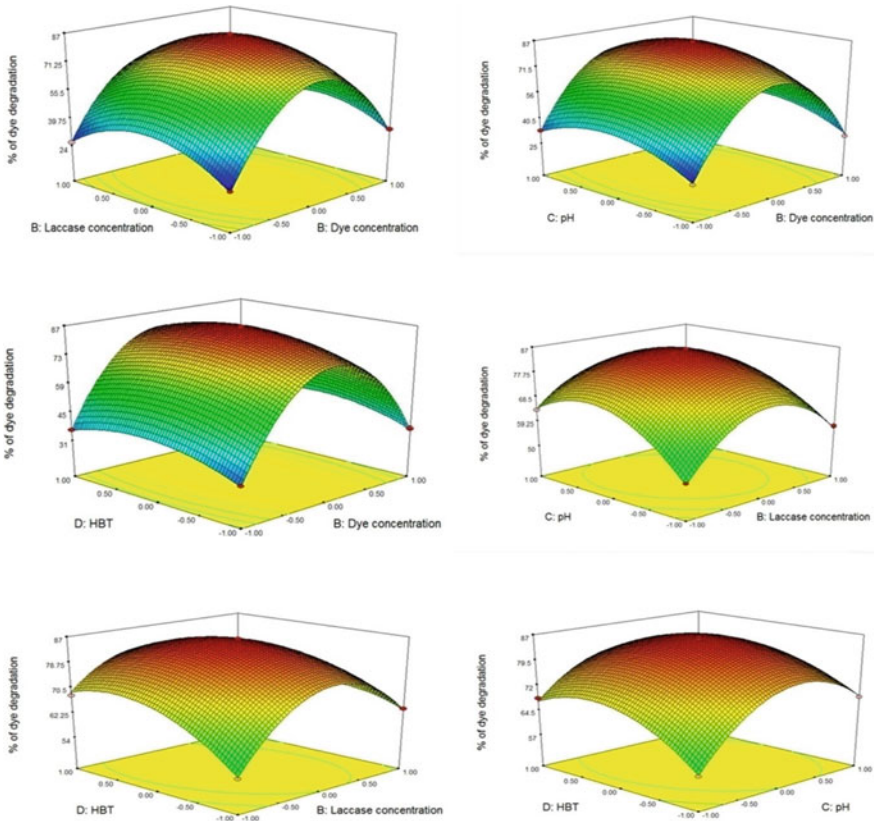


Fig. 4 3D response surface graphical representation of effective parameters

of the interaction between different factors (Prakash et al. 2008). Ferreira et al. (2009) also showed that the smallest ellipse in the contour diagram is indicating the maximum predicted value. On the basis of parameters optimization, the quadratic model predicted that the maximum decolorization of dyes was 86.30% when the dye concentration, enzyme concentration, pH and HBT were 6.04 μM , 78.8 U/ml, 5.6 and 1.07 mM, respectively.

3.5 Validation of the Optimized Condition

To verify the predicted result, validation experiment was performed in triplicate tests. Under the optimized condition, experimental and predicted values 86.3 and 85.94 U/ml of laccase yield were in good agreement. The predicted value and the effectiveness of the model, indicating that the optimized medium favours the dye decolorization ability of laccase.

4 Conclusion

The results implement that laccase was produced by *A. flavus* PUF5 through solid-state fermentation presented a highly decolorizing ability, for azo and triphenyl-methane dyes. Further statistically optimized dye decolorization efficiency of laccase. All results advice that laccase and laccase-mediator systems are valuable biocatalysts for the management of effluents from printing, textile and dye industries. This will enable its prompt removal from the effluent before discharge.

Acknowledgements The authors are thankful to the University Grant Commission [Sanction no: F/2016-17/NFO201517OBCWES 32372/(SAIII/Website)], Government of India for the financial assistance in this study.

References

- Ado BV, Onilude AA, Oluma HOA et al (2019) Production of fungal laccase under solid state bioprocessing of agroindustrial waste and its application in decolorization of synthetic dyes. *Biol Biotechnol* 21:1–17. <https://doi.org/10.9734/jabb/2019/v21i430100>
- Blanquez P, Casas N, Font X et al (2004) Mechanism of textile metal dye biotransformation by *Trametes versicolor*. *Water Res* 38:2166–2172. <https://doi.org/10.1016/j.watres.2004.01.019>
- Box GEP, Behnken DW (1960) Simplex-sum designs: a class of second order rotatable designs derivable from those of first order. *Ann Math Statist* 31(4):838–864. <https://doi.org/10.1214/aoms/1177705661>
- Chacko JT, Subramaniam K (2011) Enzymatic degradation of azo dyes—a review. *Int J env sci* 1:1250–1260

- Desai SS, Tennali GB, Channur N et al (2011) Isolation of laccase producing fungi and partial characterization of laccase. *J Biotechnol Bioinfo Bioengg* 1:543–549
- Ferreiraa S, Duartea AP, Ribeiro MHL et al (2009) Response surface optimization of enzymatic hydrolysis of *Cistus ladanifer* and *Cytisus striatus* for bioethanol production. *Biochem Eng* 45:192–200. <https://doi.org/10.1016/j.bej.2009.03.012>
- Forootanfar H, Moezzi A, Aghaie-Khozani M et al (2012) Synthetic dye decolorization by three sources of fungal laccase. *IJEHSE* 9:27. <https://doi.org/10.1186/1735-2746-9-27>
- Maalej-Kammoun M, Zouari-Mechichi H, Belbahri L et al (2009) Malachite green decolourization and detoxification by the laccase from a newly isolated strain of *Trametes* sp. *Int Biodeter Biodegr* 63:600–606. <https://doi.org/10.1016/j.ibiod.2009.04.003>
- Moldes D, Sanroman MA (2006) Amelioration of the ability to decolorize dyes by laccase: relationship between redox mediators and laccase isoenzymes in *Trametes versicolor*. *World J Microbiol Biotechnol* 22:1197–1204. <https://doi.org/10.1007/s11274-006-9161-1>
- Murugesan K, Dhamija A, Nam IH et al (2007) Decolourization of reactive black 5 by laccase: optimization by response surface methodology. *Dyes Pigment* 75:176–184. <https://doi.org/10.1016/j.dyepig.2006.04.020>
- Nyanhongo GS, Gomesa J, Gubitz GM et al (2002) Decolorization of textile dyes by laccases from a newly isolated strain of *Trametes modesta*. *Water Res* 36:1449–1456. [https://doi.org/10.1016/S0043-1354\(01\)00365-7](https://doi.org/10.1016/S0043-1354(01)00365-7)
- Prakash O, Talat M, Hasan SH et al (2008) Factorial design for the optimization of enzymatic detection of cadmium in aqueous solution using immobilized urease from vegetable waste. *Bioresour Technol* 99:7565–7572. <https://doi.org/10.1016/j.biortech.2008.02.008>
- Sathishkumar P, Murugesan K, Palvannan T (2010) Production of laccase from *Pleurotus florida* using agro-wastes and efficient decolorization of reactive blue 198. *J Basic Microbiol* 50:360–367. <https://doi.org/10.1002/jobm.200900407>
- Selvam K, Swaminathan K, Keo-Sang C (2003) Microbial decolourization of azo dyes and dye industry effluent by *Fomes lividus*. *World J Microbiol Biotechnol* 19:591–593. <https://doi.org/10.1023/A:1025128327853>

Effect of *Saccharomyces cerevisiae* Fermentation Process on the Phenolic Content, Flavonoid Content and Antioxidant Properties of Flaxseeds



Saheli Ghosal, D. K. Bhattacharyya, and Jayati Bhowal

Abstract The importance of flaxseeds as nutrient sources for human consumption has received considerable attention in recent years to provide health benefits. Nowadays fermentation procedure is used in food industry for producing and enhancing micronutrient with superior properties from nutrition aspect. Various microbes such as lactic acid bacteria or *Saccharomyces cerevisiae* are commonly used to ferment edible seed. The present study was undertaken to investigate the effect of *S. cerevisiae* on phytochemicals and antioxidant activity of whole and defatted flaxseed extracts. The phytochemical screening of unfermented and fermented flaxseed extracts showed positive result for alkaloid, saponin, flavonoid and phenolic. Fermentation also increase antioxidant activity of flaxseed extracts. This study established that the fermentation by *S. cerevisiae* improved nutritional quality of flaxseed extracts.

Keywords Flaxseed · Fermentation · *Saccharomyces cerevisiae* · Antioxidant

1 Introduction

Flax, scientifically known as *Linum usitatissimum* is the common name for an herb of the Linaceae Family (Amin and Thakur 2014). Today, consumers turn to flax for its nutritional benefits. Flaxseed is one of the functional foods which are key sources of phytochemicals (Hussain et al. 2006). These phytochemicals are antioxidants which inhibit or delay the oxidation of molecules by inhibiting the initiation of

S. Ghosal · D. K. Bhattacharyya · J. Bhowal (✉)

School of Community Science and Technology, Indian Institute of Engineering Science and Technology, Shibpur, Howrah, West Bengal 711103, India

e-mail: jayatibhowal@gmail.com

S. Ghosal

e-mail: ghosalsaheli1991@gmail.com

D. K. Bhattacharyya

e-mail: dkb_oiltech@yahoo.co.in

© Springer Nature Singapore Pte Ltd. 2021

D. Ramkrishna et al. (eds.), *Advances in Bioprocess Engineering and Technology*,
Lecture Notes in Bioengineering,

https://doi.org/10.1007/978-981-15-7409-2_12

oxidizing chain reaction (Badarinath et al. 2010). Flax is also a good source of phenolic compounds which have multiple biological functions such as antioxidants, antiinflammatory, anticancer and antimicrobial activities (Amin and Thakur 2014).

In recent days, fermentation processing step is gaining much importance in food market of both developing and industrialized countries, not only for the benefit of preservation and safety, but also for their highly appreciated sensory attributes. Fermented foods enhance nutritional quality and digestibility, improve food safety and are traditionally acceptable and accessible (Holzapfel 2002; Rolle and Satin 2002). The principal objectives of fermentation are preservation and safeguarding of foods and beverages.

Saccharomyces is a species of yeasts and it is known as baker's yeast. It is used in food processing industry to improve the nutritional quality of food and also better shelf life. The purpose of this study is to investigate the phenolic content, flavonoid content and antioxidant activity of *Saccharomyces cerevisiae* fermented flaxseed extracts on a comparative basis of unfermented flaxseed extracts. It is quite important to note that no reports are available to this kind of investigation.

2 Materials and Methods

Flaxseeds were procured from local market of Sealdah, Kolkata, West Bengal, India. All chemicals and solvents were obtained from Sigma-Aldrich (MA, USA) and Merck (Germany). *S. cerevisiae* was provided by food technology laboratory, Jadavpur University, Kolkata, India.

2.1 Sample Preparation

Flaxseeds were sorted cleaned to remove the impurities. The seeds were grounded by mixer grinder. Half of the powder soaked in n-hexane 1:10 ratio for 24 h and filtered by What-man No.1 filter paper (removed oil with n-hexane). After filtration the residue was dried at room temperature for 24 h. The whole and defatted flaxseeds flour was packed in airtight container and stored at desiccators (30 °C) until required for use.

2.2 Preparation of Unfermented and Fermented Flaxseed Extract

5 grams of flaxseed powder was mixed with 100 ml of distilled water and autoclaved. After autoclaving, the sample was cooled at room temperature. For unfermented

preparation, the sample was subjected to centrifugation at 6000 rpm for 15 min and the supernatant was collected and stored at 18 °C until use.

However, for fermented preparation the sample was inoculated with *S. cerevisiae*. The fermentation process was then carried out for a period of 24 h at 35 °C. The sample was subjected to centrifugation at 6000 rpm for 15 min. The supernatant was collected and stored at 18 °C until use.

2.3 Phytochemical Screening

The phytochemical screening was assessed by using a standard procedure described by Bekal et al. (2015). Phytochemical screening was done to identify the major phytochemical constituents such as tannins, saponins, flavonoids, phenols, alkaloids and glycosides.

2.4 Determination of Total Phenolic (TPC)

The determination of total phenolic contents (TPC) of fermented and unfermented extracts was based on Skerget et al. (2005). An aliquot of the extract (0.2 ml) was mixed with 2.5 ml of Folin-Ciocalteu reagent and 2 ml of Na₂CO₃ (7.5%) and incubated for 30 min at room temperature. Absorbance was measured at 760 nm using distilled water as blank. The amounts of TPC were calculated using gallic acid for calibration.

2.5 Determination of Total Flavonoid (TFC)

Flavonoids in flaxseed extracts were quantified by AlCl₃ method described by Sultana et al. (2007). Total flavonoid content was expressed as catechin equivalents (CE). Briefly, 1 ml of extract, 5 ml of distilled water, 0.3 ml of 5% NaNO₂ were added and mixed well, after 5 min 0.6 ml of 10% AlCl₃ was added. After another 5 min 1 ml of 1 M NaOH was added and volume made up to 10 ml with distilled water. The solution was mixed well. Absorbance was recorded at 510 nm.

2.6 Free Radical Scavenging Activity Using DPPH Method

The free radical scavenging activity of the extracts was measured by 1, 1-diphenyl-2-picrylhydrazyl (DPPH) method (Kaur et al. 2008). In a brief, 0.1 Mm solution of DPPH was prepared. 1 ml DPPH working solution was mixed with 1 ml of extract

solution at different concentrations. The absorbance was measured at 517 nm using a spectrophotometer after 30 min. A solution of DPPH was used as a negative control. The DPPH radical scavenging activity was calculated with the following equation: DPPH Scavenging activity (%) = $(A_c - A_s) / A_c \times 100$ (where A_c is the absorbance of negative control and A_s is the absorbance of sample, respectively).

2.7 *Fe²⁺ Chelating Activity*

Metal Chelating activity was measured by the method of Hsu et al. (2003). Different concentrations of flaxseed extracts were mixed with 0.1 ml of 2 mM $\text{FeCl}_2 \cdot 4\text{H}_2\text{O}$, 0.2 ml of 5 mM ferrozine solution and 3.7 solvent were mixed in a test tube. After 10 min the absorbance was measured at 562 nm. Mixture without extract was used as the control. The percentage of metal chelating activity was calculated using the following equation: Iron chelating activity (Inhibition %) = $[(A_c - A_s) / A_c] \times 100$ (where A_c = the absorbance of the control reaction and A_s = the absorbance in the presence of the flaxseed extract.)

2.8 *ABTS Radical Scavenging Activity*

ABTS radical scavenging activity was measured by the method described by Re et al. (1999), with modification. ABTS solution was prepared by mixing 5.0 mL of 7 mM ABTS solution with 88 of 140 mM potassium persulfate, and keeping in the dark at room temperature for 16 h. Different concentrations of samples were mixed with ABTS radical working solution and incubated for 15 min at room temperature in dark. Absorbance was measured at 734 nm. ABTS radical scavenging activity was calculated according to the following equation: ABTS (%) = $(1 - \text{Absorbance of sample} / \text{Absorbance of control}) \times 100$.

2.9 *Ferric Reducing Antioxidant Power Activity (FRAP)*

Ferric reducing antioxidant power (FRAP) activity was based on the method of Benzie and Strain (1996). Different concentrations of samples were mixed with 3 ml of FRAP reagent and the mixture was incubated at 37 °C for 4 min. The absorbance was measured at 593 nm. Fresh working solutions of FeSO_4 were used for calibration. The result was expressed as $\mu\text{mol FeSO}_4$ equivalents per ml of sample.

2.10 Reducing Power Activity

The reducing power was assessed by the method of Oyaizu (1986). Different concentrations of extracts (1 ml) were mixed with 2.5 ml of 0.2 M sodium phosphate buffer (pH 6.6) and 2.5 ml of 1% potassium ferricyanide, and then the mixture was incubated at 50 °C for 20 min. Then 2.5 ml of 10% trichloroacetic acid was mixed with each test tube and centrifuged at 1000 rpm for 10 min. The upper layer (2.5 ml) was mixed with 2.5 ml distilled water and 0.5 ml of 0.1% of ferric chloride, and the absorbance was recorded at 700 nm. BHT was used as standards.

2.11 Identification of Phenolic and Flavonoid Compounds by HPLC

Separation and identification of phenolic and flavonoid compounds were carried out by High-Performance Liquid Chromatography. The HPLC was equipped with 2487 dual λ absorbance detector, column symmetry C18, reversed phase (4.6 \times 250 mm, 5 μ m) (Alliance, model-2695 from Waters). A constant flow rate of 1 ml/min was used with two mobile phases: (A) 0.1% trifluoroacetic acid in HPLC grade water; and solvent (B) 0.5% phosphoric acid in 90% acetonitrile. The chromatograms were recorded at 280, 210 and 370 nm. The identification was carried out by retention time using external and internal standards of the individual phenolic acids and flavonoid compounds. The concentration of an individual compound was calculated on the basis of peak area measurements. All solutions were HPLC grade and were filtered prior to HPLC analysis.

Statistical Analysis

All experiments were conducted in triplicates. Results were reported as their mean values \pm standard deviation. One-way analysis of variance (ANOVA) of the data was carried out using the Tukey HSD test. $P \leq 0.05$ was considered statistically significant.

3 Results and Discussions

3.1 Phytochemical Screening

The result of phytochemical analysis was presented in Table 1. Phytochemical analysis for unfermented and fermented flaxseed extracts showed the presence of glycerides, saponins, alkaloids and flavonoids. Tests for Sterols, terpenoids and tannins were found to be negative. The presence of different phytochemicals in the extract may be responsible for the therapeutic properties of flaxseed. Bekal et al. (2015)

Table 1 Phytochemical screening of unfermented and fermented flaxseed extracts

Phytochemicals	Whole unfermented extracts	Defatted unfermented extracts	Whole fermented extracts	Defatted fermented extracts
Alkaloid	+	+	+	+
Glycoside	–	–	–	–
Saponin	+	+	+	+
Flavonoid	+	+	+	+
Phenolic	+	+	+	+
Tannin	–	–	–	–

in their study on phytochemical analysis of aqueous flaxseed extract showed the presence of glyceride, saponin, flavonoid and alkaloid.

3.2 Total Phenolic Content

The total phenolic contents of whole and defatted fermented flaxseed extracts were found to be 8.21 mg GAE/g and 9.93 mg GAE/g, respectively. The content is higher than the phenolic contents of whole and defatted unfermented flaxseed extracts. The result of total phenolic content was demonstrated in Table 2. The total phenolic content results obtained in our study are higher than the results reported by Monica and Joseph 2016, who reported 3.4 mg GAE/g for unfermented flaxseed extracts and 4.5 mg GAE/gm for *Lactobacillus* fermented extracts. The total phenolic content of *Lactobacillus plantarum* fermented myrtus communis berries was found to be significantly higher than the unfermented berries (Curiel et al. 2015), is also similar to this report.

3.3 Total Flavonoid Content

The result of total flavonoid content was represented in Table 2. The table reported that the flavonoid content of fermented whole and defatted flaxseed extracts were higher than the unfermented extracts. This observation was similar to the findings of other investigators, who reported that the total flavonoid content of *L. plantarum* fermented myrtus communis berries is higher than the unfermented berries (Curiel et al. 2015).

Table 2 Total Phenolic content, flavonoid content, antioxidant activity by DPPH, Fe²⁺ chelating activity, ABTS radical scavenging activity, Ferric reducing antioxidant power activity and reducing power activity of unfermented and fermented flaxseed extracts

Sample	Total Phenol Content (mg GAE/gm)	Total Flavonoid content (mg CE/gm)	IC ₅₀ value of Antioxidant activity by DPPH (mg/ml)	IC ₅₀ value (mg/ml) of Fe ²⁺ chelating activity	IC ₅₀ value (mg/ml) of ABTS radical scavenging activity	FRAP assay value (μM/ml)	Reducing power assay (mg/ml)
Whole unfermented flaxseed extracts	5.87±0.17 ^a	1.84±0.03 ^a	0.499±0.003 ^a	13.54±0.16 ^a	28.24±0.14 ^a	3.33±0.07 ^a	1.67±0.005 ^a
Whole fermented flaxseed extracts	8.21±0.22 ^b	2.58±0.05 ^b	0.455±0.004 ^b	11.28±0.25 ^b	20.93±0.20 ^b	3.52±0.04 ^b	1.71±0.006 ^b
Defatted unfermented flaxseed extracts	7.34±0.19 ^c	2.21±0.03 ^c	0.469±0.003 ^c	11.90±0.11 ^c	21.66±0.20 ^c	2.98±0.04 ^c	1.63±0.011 ^c
Defatted fermented flaxseed extracts	9.93±0.14 ^d	3.04±0.04 ^d	0.431±0.004 ^d	9.79±0.05 ^d	10.90±0.10 ^d	3.46±0.03 ^b	1.69±0.009 ^a

Results were expressed as mean ±SD (n = 3). Mean values having different superscript letters (a, b, c, d) in the same column were significantly different (p < 0.05) and values having same superscript letters were not significantly different (p < 0.05)

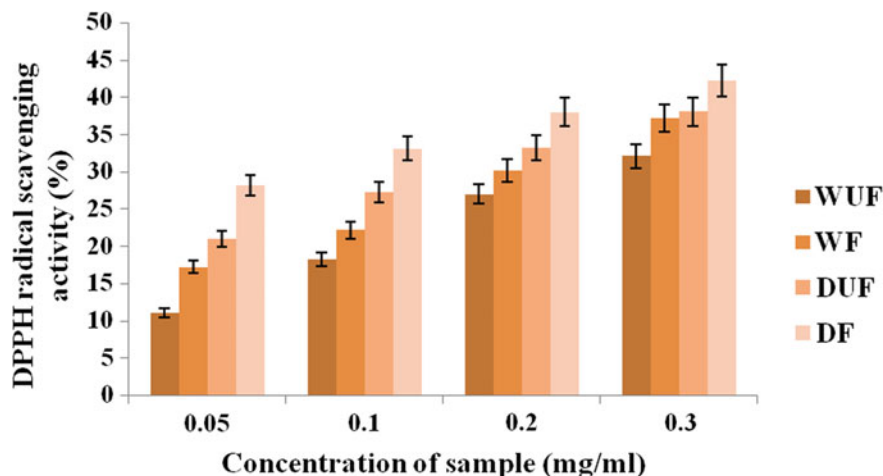


Fig. 1 DPPH free radical scavenging activity (%) of the sample (WUF—Whole unfermented sample, WF—Whole fermented sample, DUF—Defatted unfermented sample, DF—Defatted fermented sample)

3.4 Antioxidant Activity by DPPH

DPPH radical scavenging ability of the fermented and unfermented flaxseed extracts was presented in Figure 1. The IC_{50} value represents the concentration of sample extract required to decrease DPPH activity by 50%. The lower IC_{50} value indicates higher antioxidant activity in the sample. The defatted fermented sample showed maximum DPPH scavenging effect of $42.33 \pm 0.3\%$ in 0.3 mg/ml concentration with IC_{50} value of 0.431 ± 0.004 . The DPPH radical scavenging ability (IC_{50} value) of the unfermented and fermented flaxseed extracts were shown in Table 2. It showed that fermentation increased the scavenging ability of whole and defatted flaxseed extracts. The DPPH radical scavenging activity of *L. plantarum* fermented *Myrtus communis* berries higher than the unfermented berries (Curiel et al. 2015), similar to our results.

3.5 Fe^{2+} Chelating Activity

The chelating activity of the extracts is shown in Fig. 2. Chelation of transition metal is a mechanism of antioxidative action. Chelating agents help to disrupt the complex formation with the result that the red colour of the complex is decreased. The chelating activity is measured by the measurement of colour reduction. The metal chelating activity of the fermented and unfermented flaxseed extracts was presented

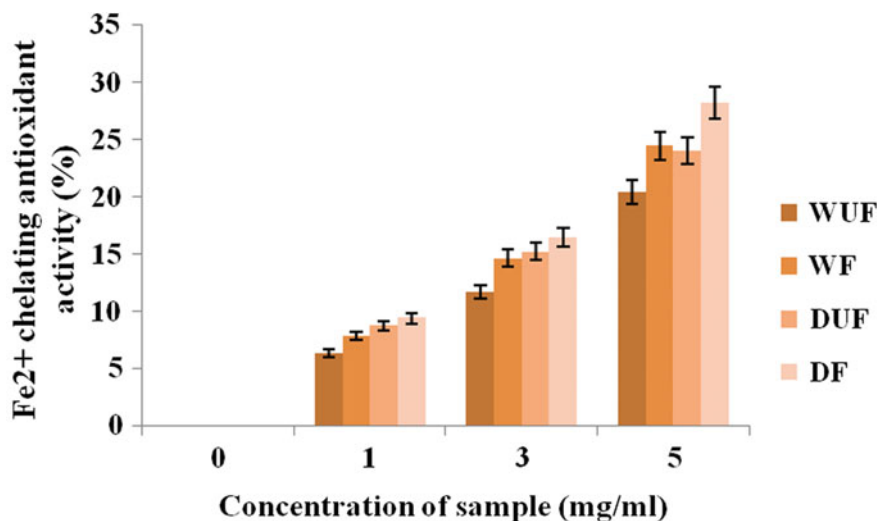


Fig. 2 Fe^{2+} chelating antioxidant activity (%) of the sample (WUF—Whole unfermented sample, WF—Whole fermented sample, DUF—Defatted unfermented sample, DF—Defatted fermented sample)

by IC_{50} value in Table 2. *Sachharomyces cerevisiae* fermented flaxseed extracts had higher metal chelating activity than unfermented flaxseed extracts.

3.6 ABTS Radical Scavenging Activity

The ABTS radical assay is a widely used method of screening for antioxidant activity and is reported as a decolorization assay. The scavenging effect of the extracts is showed in Figure 3. The ABTS scavenging activity of the fermented and unfermented flaxseed extracts was presented by IC_{50} value in Table 2. Defatted *S. cerevisiae* fermented flaxseed extracts had higher ABTS radical scavenging activity than unfermented and whole fermented seed extracts. Similar result has been reported on *L. plantarum* fermented myrtus communis berries (Curiel et al. 2015).

3.7 Ferric Reducing Antioxidant Power Activity (FRAP)

The ferric reducing antioxidant power activity of unfermented and fermented flaxseed extracts was presented in Table 2. It was clear from the results that the FRAP activity of fermented flaxseed extracts were the highest among the unfermented extracts.

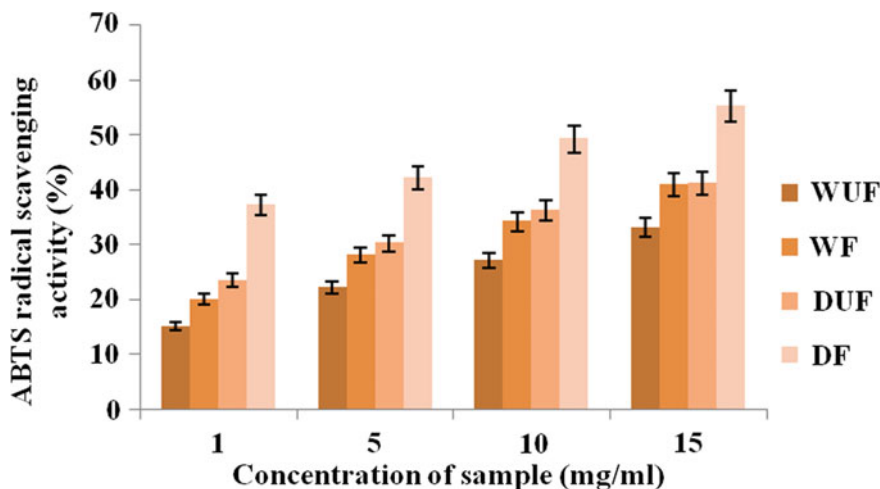


Fig. 3 ABTS radical scavenging activity (%) of the sample (WUF—Whole unfermented sample, WF—Whole fermented sample, DUF—Defatted unfermented sample, DF—Defatted fermented sample)

3.8 Reducing Power Activity

Reducing power assay measures the electron-donating capacity of an antioxidant (Yen and Chen 1995). The fermented flaxseed extracts had higher reducing power activity than unfermented seed extracts. Results were shown in Table 2.

3.9 Identification of Phenolic and Flavonoid Compounds for Defatted Unfermented and Fermented Flaxseed Extracts by HPLC

HPLC was done for defatted unfermented and fermented extracts because they contain higher total phenolic and flavonoid than whole unfermented and fermented sample. The chromatographic profile of defatted unfermented and fermented flaxseed extracts was presented in Table 3. Figure 4 and 5 showed the chromatograms of the defatted unfermented and fermented flaxseed extracts. In this study aspartic acid, gallic acid, valinic acid, vitamin-p, transcenamic acid, ferulic acid, elachic acid, quercetin, kamferol were detected for both samples. Lignan which is an important phytochemical had been identified in defatted fermented flaxseed extracts and it has antioxidant and anticancer properties.

Table 3 HPLC identification of phenolic and flavonoid compounds present in defatted unfermented and fermented flaxseed extracts

Sample	Aspartic acid (%)	Gallic acid (%)	Lignan (%)	Valinic acid (%)	Vitamin-P (%)	Transcenenamic acid (%)	Ferulic acid (%)	Elachic acid (%)	Quercetin (%)	Kamferol (%)
Defatted unfermented extracts	1.63	8.35	-	4.16	4.17	5.82	7.49	19.96	0.026	0.22
Defatted fermented extracts	5.43	8.65	1.12	0.67	11.08	16.24	6.00	12.91	0.20	0.06

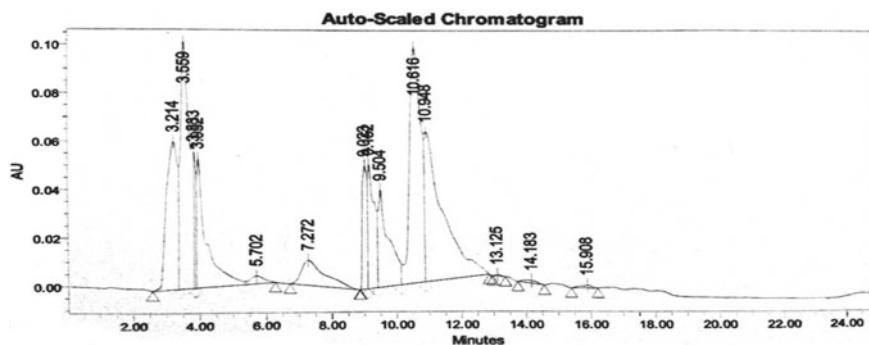


Fig. 4 HPLC chromatogram of unfermented flaxseed extracts

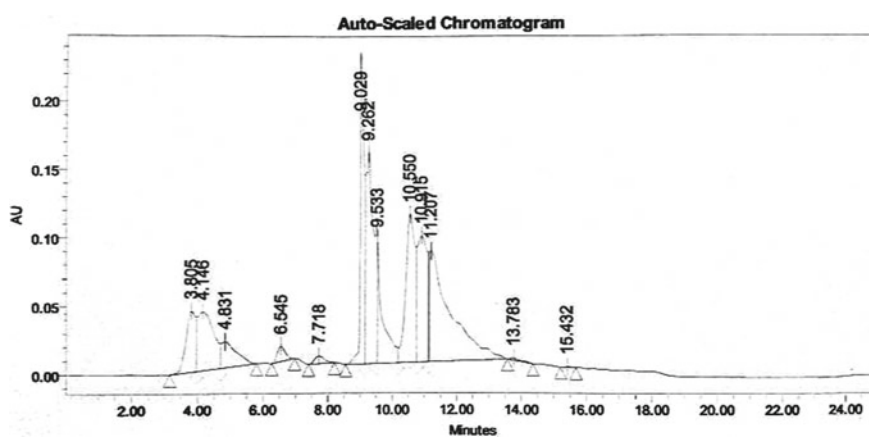


Fig. 5 HPLC chromatogram of fermented flaxseed extracts

4 Conclusion

The present study demonstrated that the antioxidant activity of fermented flaxseed extract is better than unfermented extract. Total phenolic content and flavonoid content are also high in fermented seed extracts. Defatted fermented flaxseed extracts enhanced DPPH radical scavenging effect; Fe^{2+} chelating antioxidant activity and ABTS radical scavenging activity, whereas whole fermented flaxseed extracts enhanced Ferric Reducing Antioxidant Power activity and reducing power activity.

Acknowledgements This work was supported by the Indian Institute of Engineering Science And Technology, Shibpur. I would also like to acknowledge Indian Institute of Chemical Biology, Kolkata for HPLC analysis during this work.

References

- Amin T, Thakur M (2014) A comparative study on proximate composition, phytochemical screening, antioxidant and antimicrobial activities of (*Linum usitatissimum* L.) flaxseeds. *Int J Curr Microbiol Appl Sci* 3(4):465–481
- Badarinath AV, Rao KM et al (2010) A review on invitro antioxidant methods: comparisons, correlations and considerations. *Int J PharmTech Res* 2(2):1276–1285
- Bekal M, Kumari S et al (2015) Preliminary phytochemical screening of flax seed and assessment of its in vitro antioxidant activity. *World J Pharm Pharm Sci* 4:952–958
- Benzie IF, Strain JJ (1996) The ferric reducing ability of plasma (FRAP) as a measure of “antioxidant power”: the FRAP assay. *Anal Biochem* 239:70–76
- Curiel JA, Pinto D et al (2015) Lactic acid fermentation as a tool to enhance the antioxidant properties of *Myrtus communis* berries. *Microb Cell Fact* 14:1–10. <https://doi.org/10.1186/s12934-015-0250-4>
- Holzapfel WH (2002) Appropriate starter culture technologies for small-scale fermentation in developing countries. *Int J Food Microbiol* 75(3):197–212. [https://doi.org/10.1016/S0168-1605\(01\)00707-3](https://doi.org/10.1016/S0168-1605(01)00707-3)
- Hsu CL, Chen W, Weng YM et al (2003) Chemical composition, physical properties, and antioxidant activities of yam flours as affected by different drying methods. *Food Chem* 83(1):85–92. [https://doi.org/10.1016/S0308-8146\(03\)00053-0](https://doi.org/10.1016/S0308-8146(03)00053-0)
- Hussain S, Anjum FM et al (2006) Physical and sensoric attributes of flaxseed flour supplemented cookies. *Turk J Biol* 30:87–92
- Kaur P, Singh B et al (2008) In vitro evaluation of free radical scavenging activity of *Rubia cordifolia* L. *J Chin Clin Med* 3(5):278–284
- Monica SJ, Joseph M (2016) Phytochemical screening of flaxseed (*Linum usitatissimum* L.). *Int J Sci Res* 5:218–220
- Oyaizu M (1986) Studies on products of browning reactions: antioxidative activities of products of browning reaction prepared from glucosamine. *Jap J Nutr* 44:307–315
- Re R, Pellegrini N et al (1999) Antioxidant activity applying an improved ABTS radical cation decolorization assay. *Free Radic Biol Med* 26:1231–1237
- Rolle R, Satin M (2002) Basic requirements for the transfer of fermentation technologies to developing countries. *Int J Food Microbiol* 75:181–187
- Skerget M, Kotnik P et al (2005) Phenols, proanthocyanides, flavones and flavonols in some plant materials and their antioxidant activities. *Food Chem* 89:191–198
- Sultana B, Anwar F, Przybylski R (2007) Antioxidant activity of phenolic components present in barks of *Azadirachta indica*, *Terminalia arjuna*, *Acacia nilotica*, and *Eugenia jambolana* Lam Trees. *Food Chem* 104:1106–1114
- Yen GC, Chen HY (1995) Antioxidant activity of various tea extracts in relation to their antimutagenicity. *J Agr Food Chem* 43:27–32

Study on the Antioxidant and Cytotoxic Properties of Pyocyanin Extracted from *Pseudomonas aeruginosa*



Sucharita Sengupta and Jayati Bhowal

Abstract Microbial pigments are a promising alternative source for natural pigments. They possess a great potential for application due to their natural color, safety, and low production cost. The present investigation is carried out on the antioxidant assays, namely, 2,2-di phenyl-1 picryl-hydrazyl (DPPH), 2,2'-azinobis-3-ehtylbenzthiazoline-6-sulfonate (ABTS), metal chelating activity, reducing power, and ferric reducing antioxidant power (FRAP) of pyocyanin produced from *Pseudomonas aeruginosa*. Principal antioxidant compounds present in pyocyanin were identified by HPLC. In vitro cytotoxicity study was carried out to evaluate the effect of pyocyanin on MG-63 osteosarcoma cell line.

Keywords *Pseudomonas aeruginosa* · Pyocyanin · Antioxidant activity · MTT assay · HPLC

1 Introduction

Microbes have been exploited for pigment production due to factors like relatively large and easily manipulated strands of genes, independent of weather conditions, etc. (Shaikh 2016). The increasing awareness of health and pollution hazards of chemical dye has led to the resurgence of interest in microbial color (Kant 2012). The most characteristic feature of *Pseudomonas aeruginosa* is the production of a water-soluble blue-green phenazine compound known as pyocyanin (Sudhakar et al. 2013).

S. Sengupta · J. Bhowal (✉)
School of Community Science and Technology, Indian Institute of Engineering Science and Technology, Shibpur, P.O. Botanic Garden, Howrah, West Bengal 711103, India
e-mail: jayatibhowal@gmail.com

S. Sengupta
e-mail: sucharitac66@gmail.com

© Springer Nature Singapore Pte Ltd. 2021
D. Ramkrishna et al. (eds.), *Advances in Bioprocess Engineering and Technology*,
Lecture Notes in Bioengineering,
https://doi.org/10.1007/978-981-15-7409-2_13

The current study aims at the exploitation of different antioxidant activities of pyocyanin, namely, 1,1-diphenyl-2-picrylhydrazyl (DPPH) free radical scavenging activity, ferric-reducing antioxidant power (FRAP) activity, 2,2'-azino-bis-3-ethylbenzthiazoline-6-sulphonic acid (ABTS) activity, reducing power assay (RPA), metal chelating activity, and total phenolic content (TPC) and total flavonoid content (TFC). In vitro cytotoxic effects of pyocyanin on osteosarcoma cell line MG-63 was also studied. An in-depth study on the various antioxidant activities of pyocyanin has been done. We reported for the first time, cytotoxic effect of pyocyanin on MG-63 osteosarcoma cell line.

2 Materials and Methods

2.1 Chemicals

Analytical grade chemicals and solvents were obtained from Sigma Aldrich, Sisco Research Laboratories Pvt. Ltd. (SRL) and Merck, India. Standards like ascorbic acid, ethylene diamine tetra acetic acid (EDTA), beta hydroxy toluene (BHT), gallic acid, and catechin were procured from Sigma Aldrich. MG-63 osteosarcoma cell lines were procured from National Centre for Cell Science (NCCS), Pune, India.

2.2 Screening of Pigment-Producing Microorganism

Screening of the pigment-producing microorganism from soil was previously performed by serial dilution and spread plate method on nutrient agar plates and incubated at 37 °C for 18–24 h. This study had earlier been reported in our previous publication, Chatterjee and Bhowal (2016).

2.3 Identification of the Pigment-Producing Microorganism

Standard biochemical tests and molecular characterization of the microorganism were done for the identification purpose (El-Fouly et al. 2015).

2.4 *Production and Extraction of Extracellular Microbial Pigment*

Extraction of the pigment was done by solvent (chloroform) extraction method and was stored in a dark-colored glass container at $-20\text{ }^{\circ}\text{C}$ for future experimental work. This work had already been reported in our previous publication (Chatterjee and Bhowal 2016).

2.5 *Antioxidant Activity of the Pigment*

Evaluation of antioxidant potentiality of the pigment was done by various antioxidant assays.

2.5.1 *2,2-Di Phenyl-1 Picryl-Hydrazyl (DPPH) Assay*

DPPH radical scavenging activity was carried out according to the method reported by Lamien-Meda et al. (2008). DPPH solution in methanol (1:1) served as control. Radical scavenging activity of the pigment was expressed in terms of percentage inhibition of DPPH radical.

$$\text{DPPH radical scavenging activity (\%)} = \frac{A_{\text{control}} - A_{\text{sample}}}{A_{\text{control}}} \times 100\%$$

where A_{control} is the absorbance of the DPPH+ methanol and A_{sample} is the absorbance of free radical solution with the pigment. Ascorbic acid was used as the positive control.

2.5.2 *2,2'-Azinobis-3-Ehtylbenzthiazoline-6-Sulfonate (ABTS) Assay*

The ABTS radical scavenging activity was determined by the method described by Miller and Rice-Evans (1997). α -tocopherol was used as the positive control. The scavenging activity on the ABTS radical was measured by the following equation:

$$\% \text{ scavenging activity} = \frac{A_{\text{control}} - A_{\text{sample}}}{A_{\text{control}}} \times 100\%$$

2.5.3 Ferric-Reducing Antioxidant Power (FRAP) Assay

The reducing power of the sample was done with the modified method of Benzie and Strain's (1996). Catechin was used as positive control. The FRAP value was determined from the standard curve of Fe^{2+} ($\text{FeSO}_4 \cdot 7\text{H}_2\text{O}$).

2.5.4 Reducing Power Assay (RPA)

This assay was carried out according to the method reported by Jayanthi and Lalitha (2011) with slight modifications. Ascorbic acid (AsA) and butylated hydroxy toluene (BHT) were used as a positive and negative controls, respectively.

2.5.5 Metal Chelating Activity

The ability of pyocyanin to chelate ferrous ion was performed according to the method reported by Dinis et al. (1994). EDTA was used as the positive control. The percentage inhibition was calculated as follows:

$$\text{Chelating ability (\%)} = \frac{A_{\text{control}} - A_{\text{sample}}}{A_{\text{control}}} \times 100$$

2.5.6 Total Phenolic Content (TPC)

The concentration of phenolic compounds was measured by the method described by Waterman and Mole (1994). Total phenolic content of the metabolite was calculated from standard curve of gallic acid ($1 \mu\text{g}/\mu\text{l}$). Total phenolic content of the sample was expressed as mg of gallic acid equivalents (GAEs) per gram of sample.

2.5.7 Total Flavonoid Content (TFC)

This assay was carried out according to the method reported by Quettier et al. (2000). The content of flavonoid was calculated on the basis of the calibration curve of catechin and the results were expressed as mg of catechin equivalents per gram of extract.

2.6 Identification of Principal Antioxidant Compounds by High-Performance Liquid Chromatography (HPLC)

The pigment extract was subjected to HPLC analysis. Ascorbic acid, phenolic acids (gallic acid and ferulic acid), and flavonoids (catechin, myricetin, quercetin and kaempferol) were used as standards. The gradient elution was conducted according to the Evaristo and Leitao (2001) method with minor modifications. Identification of the compounds was done by comparison of their retention's time and UV absorption spectrum with those of the standards.

2.7 In Vitro Cytotoxic Effect of Pyocyanin on MG-63 Osteosarcoma Cell Lines

The cell viability on MG-63 bone cancer cell lines was determined by standard [3-(4, 5-dimethylthiazol-2-yl)-2, 5-diphenyltetrazolium bromide] (MTT) assay (Hassani et al. 2012). Optical density was read at 540 nm with DMSO as blank. The results were expressed in terms of cell viability percentage.

$$\text{Cell viability (\%)} = \frac{A_{\text{control}} - A_{\text{sample}}}{A_{\text{control}}} \times 100$$

3 Results and Discussion

3.1 Screening of Pigment-Producing Microorganism

Among all the microorganisms that had been screened, a blue-green pigment-producing bacterium was selected for further studies.

3.2 Identification of the Pigment-Producing Microorganism

Standard biochemical tests were done and positive results were recorded with growth on MacConkeys agar medium, methyl red test, citrate test, nitrate reduction test, catalase test, oxidase test, esculine hydrolysis test, and Tween 40 test. The report of the molecular characterization revealed that the sequence obtained was 100% identical to the partial gene sequence of 16S rRNA of *P. aeruginosast Hema 10*. This strain was accessed in NCBI gene bank for MF419261.1. El-Fouly et al. (2015) found the 16S rRNA gene sequence analysis of two isolates, namely, *P. aeruginosa*

R₁ and *P. aeruginosa* U₃ which possessed 97% nucleotide sequence identity to those of *P. aeruginosa* FPVC 14 and 94% similarity with those of *P. aeruginosa* 13.A, respectively.

3.3 Production and Extraction of Extracellular Microbial Pigment

Blue-colored microbial pigment was obtained after solvent (chloroform) extraction.

3.4 Antioxidant Assays

3.4.1 DPPH (1,1-Diphenyl-2-Picrylhydrazyl) Free Radical Scavenging Activity

DPPH radical scavenging activity (%) was found to be $47.79 \pm 0.05\%$ and the IC₅₀ value was evaluated at 4.75 µg/ml. Ascorbic acid was used as standard. These results are significantly higher than in the study carried out by Dahah et al. (2016) who observed the IC₅₀ value of pyocyanin at 3.15 µg/ml.

3.4.2 Free Radical Scavenging Activity (%) Against ABTS+

The ABTS+ radical scavenging activity was significantly ($p \leq 0.05$) high, i.e., $43.63 \pm 0.3\%$ at 3.50 µg/ml concentration of pyocyanin which was comparable to that of standard, ascorbic acid. Pawar et al. (2015) reported that the bacterial pigment (PIGB 77) exhibited $38.9 \pm 1.98\%$ radical scavenging activity.

3.4.3 Ferric-Reducing Antioxidant Power (FRAP) Assay

FRAP value was recorded as 8.99 ± 0.23 for 1 mg/ml sample concentration. Ferric chloride was used as the standard. This was significantly higher than the results of Pawar et al. (2015) where it was reported that the FRAP value was 7.97 ± 0.12 for 1 mg/ml concentration of pigment produced by *Pseudomonas argentinensis* (PIGB 46) and 5.90 ± 0.13 for 1 mg/ml in case of the pigment produced by *Pseudomonas koreensis* (PIGB 77).

3.4.4 Reducing Power Assay (RPA)

RPA (mEq BHT/gm) of the pigment was found to be 34.8 ± 0.00 . BHT was used as the standard. Pawar et al. (2015) tested the reducing power activity with the pigment produced by *P. koreensis*. The highest activity was recorded at 15 mg/ml.

3.4.5 Metal Chelating Activity (MCA)

MCA (%) of the pigment was found to be 20.78 ± 0.02 at 1.36 mg/ml and it represents the greatest inhibition activity when compared to the standard, EDTA. Mani et al. (2015) observed in their study that FC1-3 showed the highest metal chelating activity at 1.53 mg/ml.

3.4.6 Total Phenolic Content (TPC)

TPC was found to be 26.47 ± 0.9 mg GAE/ml. Gallic acid was served as standard. In the study conducted by Mullick et al. (2015), it was reported that the TPC of the pigment extracted from *P. aeruginosa* MTCC 741 was 23.53 ± 2.5 mg GAE/ml.

3.4.7 Total Flavonoid Content (TFC)

TFC was found to be 32 ± 0.82 mg CAE/ml which is higher than in the study conducted by Mullick et al. (2015) who reported that the TFC of the pigment extracted from *P. aeruginosa* MTCC 741 was 30 ± 0.99 mg QE/ml.

3.5 Identification of Antioxidant Compounds Present in the Pigment Extract by High-Power Liquid Chromatography (HPLC) Analysis

The phenolic and flavonoid profiling of the pigment extract was identified by HPLC coupled to photodiode array detector (Fig. 1). Aspartic acid, gallic acid, dihydroxy benzoic acid (DHBA), trans cinnamic acid, and ferulic acid were identified as the principal antioxidant compounds present in the pigment extract. This has been reported for the first time.

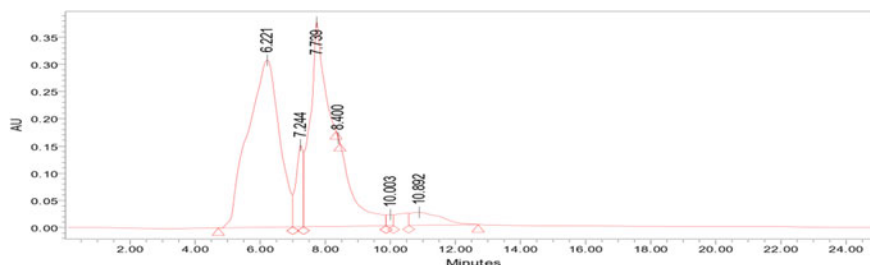
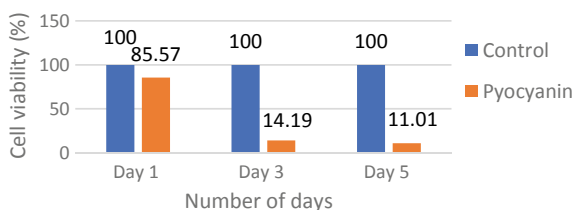


Fig. 1 Peaks of principal antioxidant compounds in pyocyanin by HPLC

Fig. 2 Effect of pyocyanin on MG-63 osteosarcoma cell



3.6 *In Vitro* Cytotoxic Effect of Pyocyanin on MG-63 Osteosarcoma Cell Lines

The gradual decline in cell viability percentage established the non-cytotoxic behavior of pyocyanin toward MG-63 osteosarcoma cell lines with respect to control (Fig. 2). On day 1, the cell viability percentage was recorded to be 85.57% and gradually decreased to 11.01% at the end of day 5. Moayed et al. (2018) reported that pyocyanin was able to reduce human pancreatic cancer (Panc-1) cells, inhibition rate being by $89.88 \pm 1.86\%$. He further added that pyocyanin could also induce dose-dependent apoptosis in Panc-1 cells after 24 h.

4 Conclusion

In vitro investigations showed that pyocyanin exhibits promising antioxidant capacity to scavenge free radicals in biological system. The pigment thus can be used as an alternative natural antioxidant after toxicological examination. This high percentage of free radical scavenging activity of the pigment at very minute concentrations gives us a positive indication for the safe use of the pigment. In addition to this, the pigment showed no cytotoxic effects on cultured MG-63 osteosarcoma cell lines.

Acknowledgements The authors express their sincere thanks to Indian Institute of Chemical Biology (IICB), Kolkata and Centre for Healthcare Science and Technology, IEST, Shibpur.

Conflict of Interest The authors declare that there is no conflict of interest.

Ethical Approval This chapter does not contain any studies with human participants or animals performed by any of the authors.

References

- Benzie IFF, Strain JJ (1996) The ferric reducing ability of plasma (FRAP) as a measure of 'antioxidant power': the FRAP assay. *Anal Biochem* 239:70–76
- Chatterjee S, Bhowal J (2016) Production of microbial color from soil microbes for food use. *Materials Today: Proc* 3(10):3388–3402
- Dahah H, Djibaoui R, Nemmiche S (2016) Antimicrobial, antioxidant and hemolytic effects of Pyocyanin produced by *Pseudomonas aeruginosa* isolated from saline soil of Mina river. Algeria *Int J Biosci* 9(5):134–143
- Dinis TCP, Madeira VMC, Almeida LM (1994) Action of phenolic derivatives (acetoaminophen, salicylate and 5aminosalicylate) as inhibitors of membrane lipid peroxidation and as peroxy radical scavengers. *J Architectural Biochem Biophysics* 315:161–169
- El-Fouly MZ, Sharaf AM, Shahin AAM et al (2015) Biosynthesis of pyocyanin pigment by *Pseudomonas aeruginosa*. *J Rad Res Appl Sci* 8(1):1–13
- Evaristo IM, Leitao MC (2001) Identification and quantification by DAD-HPLC of the phenolic fraction contained in the leaves of *Quercus suber* L. *Silva Lusitana* 9:135–141
- Hassani HH, Hasan HM, Al-Saadi A et al (2012) A comparative study on cytotoxicity and apoptotic activity of pyocyanin produced by wild type and mutant strains of *Pseudomonas aeruginosa*. *Euro J Exp Bio* 2(5):1389–1394
- Jayanthi P, Lalitha P (2011) Reducing power of the solvent extracts of Eichhorniacrassipes (Mart.) solms. *Int J Pharm Pharm Sci* 3:126–128
- Kant R (2012) Textile dyeing industry an environmental hazard. *Nat Sci* 4:22–26
- Lamien-Meda A, Lamien CE, Compaoré MM et al (2008) Polyphenol content and antioxidant activity of fourteen wild edible fruits from Burkina Faso. *Molecules* 13(3):581–94
- Mani VM, Priya MS, Dhaylini S et al (2015) Antioxidant and antimicrobial evaluation of bioactive pigment from *fusarium* sp. isolated from stressed environment. *Int J Curr Microbiol App Sci* 4(6):1147–1158
- Miller N, Rice-Evans C (1997) Factors influencing the antioxidant activity determined by the ABTS radical action assay. *Free Radic Res* 26:195–199
- Moayedi A, Nowroozi J et al (2018) Cytotoxic effect of pyocyanin on human pancreatic cancer cell line (Panc-1). *Iran J Basic Med Sci* 21:794–799
- Mullick A, Shah A, Sett SD (2015) Antimicrobial activity of cell free extract of *Pseudomonas aeruginosa* MTCC 741 towards opportunistic human pathogens. *Int J Pharm Bio Sci* 5(3):42–48
- Pawar R, Mohandass C, Sivaperuma E et al (2015) Epiphytic marine pigmented bacteria: a prospective source of natural antioxidants. *Braz J Microbiol* 46(1):29–39
- Quettier DC, Gressier B, Vasseur J et al (2000) Phenolic compounds and antioxidant activities of buckwheat (*Fagopyrum esculentum Moench*) hulls and flour. *J Ethnopharmacol* 72:35–42
- Shaikh Z (2016) Biosynthesis of prodigiosin and its applications. *IOSR-JPBS* 11(6):1–28
- Sudhakar T, Karpagam S, Shiyama S (2013) Analysis of pyocyanin compound and its antagonistic activity against phytopathogens. *Int J of Chem. Tech Res* 5:1101–1106
- Waterman PG and Mole S (1994) Analysis of phenolic plant metabolites. Blackwell Scientific Publication, pp 83–85

Effect of Metabolic Risk Factors, Gene Polymorphisms and Family History Among T2DM Population in Asian Indians



Plaban Chaudhuri, Riju Ghosh, Mithun Das, Indrani Lodh,
and Riddhi Goswami

Abstract Women with a family history of diabetes (FHD) are at significantly increased risk of developing gestational diabetes mellitus, which is itself an important risk factor of childhood obesity and type 2 diabetes mellitus (T2DM) in early age. Elevated C-reactive protein (CRP) is a marker of low-grade systemic inflammation and involved in the etiology of diabetes. Insulin receptor substrate (IRS) molecules are key mediators in insulin signaling and development of diabetes. The present study was conducted on 100 healthy (non-diabetic, normotensive) adult Asian Indian women, including 50 with and 50 without FHD, living in and around Kolkata, India. During the gestation period they were studied twice, and followed up till delivery. During delivery both mothers' venous blood and cord blood were collected to estimate serum CRP, glucose, and lipid profiles of the respective mothers and their newborns. Genotyping of IRS-1, IRS-2 and CRP polymorphisms was done from these blood samples. A comparison of the metabolic variables among the subjects with and without FHD revealed significant differences among them. We also found close association of several polymorphisms in case of all three genes for both mothers and their newborn babies. More specifically, genotyping results for mothers with FHD and their newborn babies show susceptibility to T2DM: (i) for IRS-1 via diseased A allele (57%) which is carried over to the newborn babies (43%), (ii) for IRS-2 via

P. Chaudhuri · R. Ghosh · R. Goswami (✉)
Department of Biotechnology, Heritage Institute of Technology, Kolkata, India
e-mail: riddhi.goswami@heritageit.edu

P. Chaudhuri
e-mail: plaban.chaudhuri@heritageit.edu

R. Ghosh
e-mail: rijughosh1992@gmail.com

M. Das
Department of Anthropology & Tribal Studies, Sidho-Kanho-Birsha University, Purulia, India
e-mail: mithundas01@yahoo.com

I. Lodh
Urvaraa IVF Clinic, Kolkata, India
e-mail: drindranilodh@yahoo.co.in

diseased D allele (80%) which is carried over to the newborn babies (65%), and (iii) for CRP via diseased G allele (70%) which is also carried over to the newborn babies (72%). This study leads to the conclusion that Asian Indian population are ethnically and genetically predisposed to the risk factors of diabetes, which is reflected in their gestational phase and it has a significant implication on their birth outcomes.

Keywords Asian indians · Type 2 diabetes · Family history of diabetes · Gene polymorphisms · Birth outcomes

1 Introduction

Metabolic syndrome (MetS) is the culmination of a number of risk factors which give rise to a variety of potentially harmful diseases such as cardiovascular disease (CVD) and more importantly development of type 2 diabetes mellitus (T2DM). Other factors which can give rise to MetS also include insulin resistance (IR), atherogenic dyslipidemia, obesity, genetic inheritance, and high blood pressure. MetS can cause a fivefold increase in T2DM (Borch-Johnsen 2007).

Diabetes mellitus (DM), one of the major contributing factors of MetS, is caused by dysregulation of blood glucose. T2DM is the most common type of diabetes with a frequency of 90-95% of all diabetic cases. This form of diabetes is caused by both genetic and lifestyle factors which results in insulin resistance or deficiency or both (Fraser and Lawlor 2014). According to International Diabetes Foundation (IDF 2006), India is currently placed behind China in terms of diabetes. Diabetes is spreading rapidly and consists of more than 62 million Indians with approximately 1 million Indians dying due to diabetes each year (Gale 2010).

T2DM is associated with a number of single nucleotide polymorphisms (SNPs) among which IRS-1, IRS-2 and CRP are very common genes in South Asian population. Among the two most common polymorphisms reported for IRS-1, Gly972Arg polymorphism is more pronounced in T2DM patients. Even though four other polymorphisms exist, the most prominent polymorphism which targets IRS-2 is Gly1057 substituted to aspartic acid and this SNP has been reported with T2DM (Waqar et al. 2009). Genetic factors account for 40% of variance in plasma CRP levels and +1059 G > C polymorphism in CRP gene has been considered to be contributing factor toward the progression of T2DM (Thalmaier et al. 2006).

Family history of diabetes (FHD) has been found to be most useful for predicting T2DM when the disease is premature and thus adding FHD could provide significant improvements in detecting undiagnosed diabetes (Yang et al. 2010). This study correlates how FHD and other metabolic risk factors are related to these SNPs and eventually lead to increased susceptibility toward T2DM and metabolic syndrome in the next generation.

2 Materials and Methods

In this study, 100 healthy adult Asian Indian women population, including 50 without FHD and 50 with FHD, were used to determine the risk for T2DM for both mothers and their future generation. For this purpose, both mothers' venous blood and cord blood of their babies were used to determine their risk associated with T2DM by taking biochemical measurements such as fasting blood sugar (7 ml), CRP for both mother and their babies, triglycerides, HbA1C, and HDL cholesterol by auto-analyzer (Robonik India) as per NECP ATP Panel-III (International Diabetes Federation 2006) guidelines. This study was approved by the "Institutional Ethics Committee of the Heritage Institute of Technology".

Genomic DNA for all samples was isolated using DNA purification spin kit and then amplified by using PCR (ABI Biosystems USA). For *IRS-1*, 221 bp PCR product containing the polymorphic site (Gly972Arg) was digested with *BstNI* (Ijaz et al. 2019) and obtained the following bands: wild type homozygotes (GG)—two bands at 31 and 190 bp, variant homozygotes (AA)—one band at 190 bp, and heterozygous (GA)—three bands at 31, 190, and 221 bp. For *IRS-2*, 291 bp PCR product containing the polymorphic site (Gly1057Asp) was digested with *HhaI* (Bodhini et al. 2007; Ijaz et al. 2019) and obtained the bands showed at 268 bp and 23 bp, respectively. For CRP, a 744 bp PCR product containing the polymorphic site (1059 G > C) was digested by *MaeIII* (Thalmaier et al. 2006) and obtained the following band: digestion of the less common 1059 C allele produced two smaller fragments with sizes of 434 and 310 bp. Digestion of the more common 1059G allele produced three fragments with sizes of 310, 233, and 201 bp, respectively. Amplified products were separated by electrophoresis on a 1.5% agarose gel containing ethidium bromide and bands were then visualized by UV transilluminator (Kodak Ultra-cam Imaging, Japan).

3 Results and Discussion

3.1 Biochemical Analysis of Metabolic Risk Factors

Statistical analysis of the comparison of group differences (with and without FHD) for all the variables (12 and 30 weeks of gestational period) was performed using t-test ($p < 0.05$). Table 1 shows the biochemical parameters which were considered during the study.

A comparison of the biochemical characteristics among the subjects with and without FHD by two-tailed t-test revealed that there were significant differences among them with respect to triglycerides (TG), total cholesterol (TC), fasting blood sugar (FBS), HDL cholesterol, HbA1c (glycated haemoglobin), and C-reactive protein (CRP), both at the gestational period of 12 and 30 weeks, respectively. This indicates that family history plays a pivotal role in influencing metabolic variables

Table 1 Baseline biochemical characteristics of the study population with respect to family history

	12 weeks		P-value (without FHD vs. with FHD)	30 weeks		P-value (without FHD vs. with FHD)
	Without FHD (n = 50)	With FHD (n = 50)		Without FHD (n = 50)	With FHD (n = 50)	
TG (mg/dl)	133.22 ± 18.47	207.50 ± 17.76	<0.05	133.94 ± 17.47	231.22 ± 29.86	<0.05
TC (mg/dl)	212.58 ± 20.12	324.64 ± 22.77	<0.05	210.40 ± 19.64	328.78 ± 38.55	<0.05
FBS (mg/dl)	91.00 ± 9.95	115.04 ± 8.52	<0.05	91.66 ± 9.62	128.10 ± 15.48	<0.05
HDL (mg/dl)	52.92 ± 20.62	42.38 ± 8.22	<0.05	53.54 ± 19.57	40.78 ± 8.38	<0.05
HbA1c (%)	4.81 ± 0.65	6.29 ± 0.39	<0.05	4.65 ± 0.68	6.26 ± 0.69	<0.05
CRP (mg/L)	0.86 ± 0.17	4.42 ± 0.63	<0.05	0.85 ± 0.14	3.73 ± 0.82	<0.05

and thus triggering the metabolic risk factors early in gestational phase eventually leading to complications such as T2DM leading to MetS in later life.

Comparison of subjects with respect to the CRP levels between the groups by contingency chi-square analysis also revealed a statistically significant difference ($p < 0.05$) in the number of subjects with FHD and without FHD (Table 2). It shows that there is a significant difference in CRP values between groups of mothers with and without FHD. This shows that mothers with FHD have a greater tendency toward a high inflammatory status.

Newborn babies were classified with respect to the family history and CRP levels of their mothers and then their CRP levels are compared in Table 3. Comparison of CRP levels between these groups by two-tailed t-test also revealed a statistically significant difference ($p < 0.05$) between the two groups of newborn babies. These findings suggest that family history and perturbations in the gestational period are

Table 2 Difference in C-reactive protein (CRP) with respect to family history

Family history of T2DM (FHD)	Classification with respect to C-reactive protein			P-value
	Number of mothers with normal CRP (0.3–1 mg/L)	Number of mothers with high CRP (> 1 mg/L)	Total	
Without FHD	45	5	50	< 0.05
With FHD	3	47	50	
Total	48	52	100	

Table 3 Differences in C-reactive protein (CRP) of the babies by mothers' CRP and FHD

	CRP of the babies of mothers without FHD and normal CRP (n = 45)	CRP of the babies of mothers with FHD and high CRP (n = 47)	P-value (without FHD vs. with FHD)
Mean	0.82	3.65	< 0.05
SD	±0.11	±0.58	

reflected in the CRP values of the newborn babies and thus may influence the inflammatory status in those newborns whose mothers are with FHD compared to their normal counterparts.

3.2 Genotyping of *IRS-1*, *IRS-2* and *CRP* Genes

Table 4 shows genotyping results of *IRS-1* genes of newborn babies with respect to their mothers' FHD and genotypes. This genotyping results of *IRS-1* show that there is a greater tendency for not only the mothers with FHD to progress to T2DM via the diseased A allele (57%), but also to carry on the A allele to their newborn babies (43%) in the next generation.

T2DM is classified as a heterogeneous disorder and genetic factors in terms of Gly972Arg *IRS-1* with environmental factors such as diet, physical activity and age playing a pivotal role in progression to diabetes. This polymorphism is linked with obesity-induced insulin resistance (IR) which can be proved by the fact that there is a 50% reduction in insulin sensitivity among obese non-diabetic with polymorphism versus obese without polymorphism (Clausen et al. 1995). Thus, Gly972Arg *IRS-1* is associated with higher frequency of T2DM and hyperlipidemia which has a strong susceptibility to metabolic syndrome (Baroni 1999). Based on a study on North Indian Population of Jammu and Kashmir, Sethi et al. (2015) concluded that dysregulation in *IRS-1* can lead to enhanced risk of T2DM. Yousuf et al. (2018) have observed in a study on Egyptian population that those who have *IRS-1* polymorphism are genetically predisposed to IR and hence T2DM. This is quite similar to our findings.

Table 4 Genotyping of *IRS-1* Gly972Arg polymorphism

<i>IRS-1</i>	Mother		Baby	
	Without FHD	With FHD	Without FHD	With FHD
GG	32 (64%)	12 (24%)	31 (62%)	19 (38%)
GA	17 (34%)	19 (38%)	19 (38%)	19 (38%)
AA	1 (2%)	19 (38%)	0 (0%)	12 (24%)
G	81 (81%)	43 (43%)	81 (81%)	57 (57%)
A	19 (19%)	57 (57%)	19 (19%)	43 (43%)

Table 5 Genotyping of IRS-2 Gly1057Asp polymorphism

IRS-2	Mother		Baby	
	Without FHD	With FHD	Without FHD	With FHD
GG	20 (40%)	5 (10%)	22 (44%)	10 (20%)
GD	22 (44%)	10 (20%)	15 (30%)	15 (30%)
DD	8 (16%)	35 (70%)	13 (26%)	25 (50%)
G	62 (62%)	20 (20%)	59 (59%)	35 (35%)
D	38 (38%)	80 (80%)	41 (41%)	65 (65%)

Genotyping results of IRS-2 genes of newborn babies with respect to their mothers' FHD and genotypes are shown in Table 5.

The genotyping results of IRS-2 (Table 5) show that there is a greater tendency not only for mothers with FHD to progress to T2DM via the diseased D allele (80%), but also to carry on the D allele to their newborn babies (65%) in the next generation. For IRS-2, this mutation plays a major role in β -cell development and regulation of β -cell mass which is evident in obese individuals. Aspartic acid is a charged amino acid and this exchange, i.e., glycine to aspartic acid, is located close to two tyrosine phosphorylation sites (1042 and 1072) (Cheatham and Kahn 1995) and this in turn alters downstream signaling from IRS-2 (Stefan et al. 2003). Bodhini et al. (2007) also reported the susceptibility of DD genotype toward T2DM risk in Asian Indians, which is in line with our findings.

Table 6 shows genotyping results of CRP genes of newborn babies with respect to their mothers' FHD and genotypes. Genotyping results of CRP show that there is a greater tendency for mothers with FHD to progress to T2DM via the diseased G allele (70%) and also to pass on the G allele to its newborn babies (72%) in the next generation. CRP is a potential biomarker for prediction of future risk for development of CVD in both diabetic and non-diabetic individuals as even a small increase in plasma CRP levels can lead to CVD. By taking into account the thrifty genotype hypothesis, the ancestral version of alleles now prove to be having a detrimental effect in present-day environment (Sharma 1998). Mahajan et al. (2009) had studied North Indian population for relation of CRP with T2DM and found out that those

Table 6 Genotyping of CRP +1059 G > C polymorphism

CRP	Mother		Baby	
	Without FHD	With FHD	Without FHD	With FHD
CC	25 (50%)	9 (18%)	23 (46%)	8 (16%)
CG	11 (22%)	12 (24%)	11 (22%)	12 (24%)
GG	14 (28%)	29 (58%)	16 (32%)	30 (60%)
C	61 (61%)	30 (30%)	57 (57%)	28 (28%)
G	39 (39%)	70 (70%)	43 (43%)	72 (72%)

who have increased CRP are more prone to T2DM risk. We have also found similar results in our study.

The above genotyping results of IRS-1, IRS-2 and CRP genes suggest that mothers with FHD tend to cause the progression of diseased alleles to the next generation: (i) for IRS-1 gene via GA genotypes, (ii) for IRS-2 gene via GD genotypes, and (iii) for CRP gene via GC genotypes, increasing their risk toward T2DM.

4 Conclusion

This study suggests that patients carrying A allele (IRS-1), D allele (IRS-2) and G allele (CRP) may contribute to GD and eventually to T2DM. The etiology of GD involves a complex interplay of multiple genes, and environmental and immunologic factors. Although no single theory can explain all cases, it seems that IRS-1 and IRS-2 gene polymorphisms might be associated with increased risk of GD and eventually T2DM, whereas the thrifty genotype hypothesis explains parental G allele to be recognized as diseased allele for CRP mutation. In conclusion, having observed that family history of diabetes (FHD) is indeed an important and independent risk factor for genomic studies of complex diseases like T2DM, efforts should be made toward translating this knowledge for use in public health programmers designed to detect and prevent diabetes.

Compliance with ethical standards

Conflict of Interest: The authors declare that they have no conflict of interest.

Research involving human participants and/or animals

- (a) **Statement of human rights:** The study was approved by “Institutional Ethics committee” of Heritage Institute of Technology. All procedures performed in studies involving human participants were in accordance with the ethical standards of the institutional and/or national research committee (Ethical Guidelines for Biomedical Research on Human Participants, issued by Indian Council of Medical Research 2006) and with the 1964 Helsinki declaration and its later amendments or comparable ethical standards.
- (b) **Statement on the welfare of animals:** This chapter does not contain any studies with animals performed by any of the authors.

Informed consent: Informed consent was obtained from all individual participants included in the study.

References

- Baroni MG (1999) A common mutation of the insulin receptor substrate-1 Gene is a risk factor for coronary artery disease. *Arterioscler Thromb Vasc Biol* 19:2975–2980
- Bodhini D, Radha V, Deepa R et al (2007) The G1057D polymorphism of IRS-2 gene and its relationship with obesity in conferring susceptibility to type 2 diabetes in Asian Indians. *Int J Obesity* 31:97–102
- Borch-Johnsen K (2007) The metabolic syndrome in a global perspective. *Danish Med Bull* 54(2):157–159
- Cheatham B, Kahn CR (1995) Insulin action and the insulin signaling network. *Endocrine Rev* 16(2):117–142
- Clausen JO, Hansen T, Bjorbaek C et al (1995) Insulin resistance: interactions between obesity and a common variant of insulin receptor substrate-1. *Lancet* 346:397–402
- Fraser A, Lawlor DA (2014) Long-term health outcomes in offspring born to women with diabetes in pregnancy. *Curr Diab Rep* 14:489
- Gale J (2010) India's diabetes epidemic cuts down millions who escape poverty. <https://www.bloomberg.com/news/articles/2010-11-07/india-s-deadly-diabetes-scourge-cuts-down-millions-rising-to-middle-class>. Accessed 12 Nov 2019
- International Diabetes Federation (2006) The IDF consensus worldwide definition of the metabolic syndrome. <http://www.idf.org/metabolicsyndrome>. Accessed 12 Nov 2019
- Ijaz A, Babar S, Sarwar S et al (2019) The combined role of allelic variants of *IRS-1* and *IRS-2* genes in susceptibility to type 2 diabetes in the Punjabi Pakistani subjects. *Diabetol Metab Syndr* 11:64
- Mahajan A, Tabassum R, Chavali S et al (2009) High-sensitivity C-reactive protein levels and type 2 diabetes in urban North Indians. *J Clin Endocrinol Metab* 94:2123–2127
- Sharma AM (1998) The thrifty-genotype hypothesis and its implications for the study of complex genetic disorders in man. *J Mol Med* 76:568–571
- Sethi S, Panjaliya RK, Kumar P et al (2015) Comprehensive SNP analysis of genes in cholesterol metabolism (PGC 1 Alpha), insulin signaling (IRS1), potassium channel (KCNJ11) and glucose homeostasis (PI3K) in three diversified groups. *J Diabetes Metab* 6:531. <https://doi.org/10.4172/2155-6156.1000531>
- Stefan N, Kovacs P, Stumvoll M et al (2003) Metabolic effects of the Gly1057Asp polymorphism in IRS-2 and interactions with obesity. *Diabetes* 52:1544–1550
- Thalmaier D, Dambacher J, Seiderer J et al (2006) The +1059G/C polymorphism in the C-reactive protein (CRP) gene is associated with involvement of the terminal ileum and decreased serum CRP levels in patients with Crohn's disease. *Aliment Pharmacol Ther* 24:1105–1115
- Waqar MA, Aijaz S, Shaikat S et al (2009) Malfunctioning of genes contributing towards diabetes mellitus 2. *J Chem Soc Pakistan* 31(2):339–356
- Yang Q, Liu T, Valdez R et al (2010) Improvements in ability to detect undiagnosed diabetes by using information on family history among adults in the United States. *Am J Epidemiol* 171:1079–1089
- Yousef AA, Behiry EG, Abd Allah WM et al (2018) IRS-1 genetic polymorphism (r.2963G > A) in type 2 diabetes mellitus patients associated with insulin resistance. *Appl Clin Genet* 11:99–106

Composition and Antioxidant Activity of Vapours from Clove Bud During Roasting



Moumita Dev, D. K. Bhattacharyya, and Minakshi Ghosh

Abstract The volatile chemical composition and antioxidant properties of essential oil of clove buds and vapour of roasted clove buds have been revisited together. The major bioactive compounds showed to be eugenol, β -caryophyllene, and eugenol acetate; their different quantitative contribution justifies the unequal aroma and antioxidant properties of clove products. Antioxidant activity of essential oil of clove bud oil and its roasted vapour was measured by 2,2'-azino-bis(3-ethylbenzthiazoline-6-sulfonic acid) (ABTS) radical scavenging activity, α, α -diphenyl- β -picryl-hydrazyl free radical (DPPH) scavenging activity, total reducing ability determination by Fe^{3+} - Fe^{2+} transformation method (FRAP) and total phenolic content by TPC. Antioxidant activity of the unroasted clove bud oil is greater than the vapours of the roasted clove bud. Original clove bud (unroasted) contains 89.77 ± 0.03 DPPH, 74.47 ± 0.04 ABTS, 11.1 ± 0.1 FRAP, and 1.15 ± 0.06 TPC, whereas vapours of roasted clove bud contain 60 ± 0.02 DPPH, 72.80 ± 0.03 ABTS, 1.56 ± 0.01 FRAP and 1.44 ± 0.07 TPC. Vapours of the roasted clove bud contain 74.19% eugenol whereas original clove bud (unroasted) contains 94.73% eugenol. Different types of compounds are present in vapours of the roasted clove bud oil.

Keywords Clove and its roasted vapour · Antioxidant activity · GC-MS

M. Dev · D. K. Bhattacharyya · M. Ghosh (✉)
School of Community Science and Technology, Indian Institute of Engineering Science and Technology, Shibpur, Howrah, West Bengal 711103, India
e-mail: g_minakshi2000@yahoo.com

M. Dev
e-mail: moumitadev.2013@gmail.com

D. K. Bhattacharyya
e-mail: dkb_oiltech@yahoo.co.in

1 Introduction

Spices are vegetable products used to provide seasoning, flavouring and aroma to foods (Peter and Babu 2012). They are commonly used to enhance the aroma of food and some of them have been described as strong antioxidants, having other beneficial qualities too. Spices used to have an important social role due to their ability to perpetuate life and to heal through their use as medicines and in dieting. Spices are able to enrich or alter the quality of food, for instance, changing the taste to give it zest or a piquant, pungency or lasting flavouring, or a relish (Nurdjannah and Bermawie 2001). The role of spices is related to the bioactivity of their constituents, namely, the antioxidant activity (Charles 2013; Shobana and Akhilender Naidu 2000; Lindberg Madsen 1995). Clove, the dried aromatic bud of the evergreen trees, *Eugenia caryophyllata* (= *Syzygium aromaticum*) (Myrtaceae), has been used in the food industry and domestic culinary purposes as a flavouring agent due to their medicinal attributes and antioxidant activity and intense flavour (Nurdjannah and Bermawie 2001; Kamatou et al. 2012).

Clove bud and other flavour materials when heated generate invariable flavour vapours which are normally lost during culinary preparation. The composition of such vapours and their antioxidant activities are likely to be different from the original material. Present study aims to characterize the composition and antioxidant activity of the vapours that are formed and then collected during roasting. Composition studies established by GC-MS and antioxidant activity by standard methods have been done.

2 Materials and Methods

Clove buds were purchased from local market of Kolkata, West Bengal, India. All the analytical grade chemicals and solvents were purchased from MERCK, INDIA.

2.1 Preparation of Samples

Roasting was carried from ground clove bud at around 80 °C in a round bottom pan and vapours condensed through a condenser and eventually collected by solubilization in petroleum ether (b.p. 40–60 °C) and later removing the solvent.

2.2 Determination of Total Polyphenols (TPC)

Total polyphenols content (TPC) was determined by Singleton et al. (1999) method.

2.3 Determination of Antioxidant Activity

2.3.1 DPPH Free Radical Scavenging Activity Assay

The total antioxidant capacity of two samples was determined spectrophotometrically, assessed using 1, 1-diphenyl 2-picryl-hydrazyl (DPPH) as followed by Shimada et al 1992. 0.1 m mol solution of DPPH in methanol was prepared. The *absorbance* was measured 30 min after the initial mixing of samples with 1 ml of DPPH solution at 517 nm. The ability to scavenge the DPPH radical was calculated with the following equation:

$$\text{Inhibition percentage (I\%)} = (A_0 - A_1)/A_0$$

(A_0 = absorbance of the control, A_1 = absorbance of the sample).

2.3.2 Ferric Reducing Antioxidant Power (FRAP)

The ferric ions (Fe^{3+}) reducing antioxidant power (FRAP) method was used to measure the reducing capacity of samples, described by Benzie and Strain 1996. The FRAP reagent consists of 10 mM TPTZ in 40 mM HCL, 250 mM sodium acetate buffer (pH-3.6) and 20 mM FeCl_3 . The reagent was freshly prepared by mixing TPTZ solution, FeCl_3 solution and acetate buffer in a ratio of 1:1:10. Samples (100 μl) were mixed with 900 μl of FRAP reagent. The mixture was incubated at 37 °C for 4 min and the absorbance was measured at 593 nm.

2.3.3 ABTS Free Radical Scavenging Activity

ABTS⁺ assays were done by modified procedure described by Re et al. 1999. ABTS⁺ (ABTS radical cation) was generated through the reaction between potassium per sulphate (2.45 μM) and ABTS stock solution. The mixture was kept in the dark place for 16 h at room temperature before use. The resulting intense colour matches the ABTS radical cations. The obtained solution was subsequently diluted with methanol and absorbance was measured at 734 nm. 1 ml of ABTS diluted solution was mixed with 10 μl of sample and the reaction mixture was kept for 6 min before measuring the absorbance at 734 nm. ABTS scavenging activity was calculated by the following equation:

$$\text{Inhibition Percentage (I\%)} = (1 - A/A_0) \times 100$$

(A = absorbance of the sample, A₀ = absorbance of the ABTS solution).

2.4 GC-MS Analysis

Two samples were analysed using GC-MS (Thermo Scientific). A fused silica capillary column DB5-MS (30 m × 0.25 mm, film thickness 0.25 μm) was used with helium as the carrier gas at constant pressure of 100 kPa, at a flow rate of 1 ml/min. The injector and detector temperature was 250 °C. The components of the essential oil were identified based on a comparison of their retention indexes (RI), mass spectra (NIST library) and literature data.

2.5 Statistic Analysis

Each analysis was carried out in triplicate. The results were expressed as mean values and standard deviation. One-way analysis of variance was performed by ANOVA with post hoc *Tukey HSD* (honestly significant difference) Test.

3 Results and Discussion

3.1 Antioxidant Activity of Clove Bud Oil and Roasted Vapour of Clove Bud Using Reducing Power Assay (FRAP)

3.1.1 Reducing Power Assay (FRAP) of Clove Bud Oil and Roasted Vapour of Clove Bud

The antioxidant activity of clove bud oil and roasted vapour of clove bud using reducing power assay is presented in Table 1. The ferric ions (Fe³⁺) reducing antioxidant power (FRAP) method was used to measure the reducing capacity of clove

Table 1 The antioxidant activity of clove bud oil and its roasted vapour

Antioxidant activity	Clove bud oil	Roasted vapour
DPPH (%)	89.77 ± 0.03 ^a	60 ± 0.02 ^a
ABTS (%)	74.47 ± 0.04 ^a	72.80 ± 0.03 ^a
FRAP (μM/ml)	11.10 ± 0.12 ^a	1.56 ± 0.01 ^a

^a Values are in terms of mean ± SD after triplicate analysis. Same letter in a row represents significant differences

bud oil and its roasted vapour. During roasting, there were decreased reducing power capacity. Both control clove oil and roasted vapour showed FRAP in the range of 11.10 $\mu\text{M/ml}$ –1.56 $\mu\text{M/ml}$ and vapour sample had significantly lower antioxidant activity than control.

3.1.2 DPPH Assay of Clove Bud Oil and Roasted Vapour of Clove Bud

The inhibitory effects of clove bud oil and roasted vapour of clove bud samples on the DPPH activity were given in Table 1. DPPH presented the highest scavenging power for clove bud oil (89.77%) among vapour sample. Clove bud oil, however, exhibited a very different profile wherein a progressive decrease in DPPH activity of roasted vapour samples (60%). There were significant differences observed between above two samples.

3.1.3 ABTS⁺ Assay of Clove Bud Oil and Roasted Vapour of Clove Bud

As seen in Table 1, clove bud oil had an effective ABTS⁺ radical scavenging activity (74.47%). Also, significant differences in ABTS⁺ scavenging potential could be determined among control clove bud oil (without heat) and roasted vapour (72.80%).

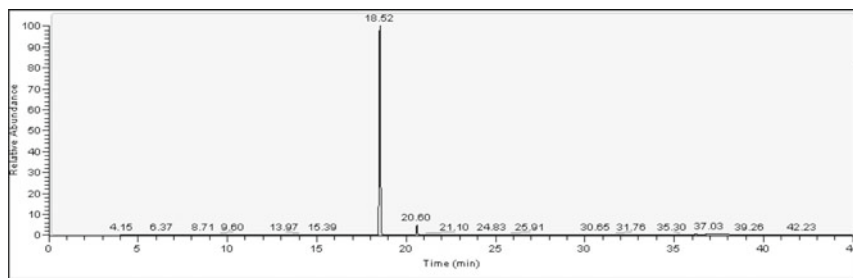
3.2 Total Phenolic Content of Clove Bud Oil and Roasted Vapour of Clove Bud

In present studies (Table 2), total phenol content (mgGAE/ml) in clove buds oil with no heat treatment was 1.15 mgGAE/ml which increased significantly in roasted vapour samples (1.44 mgGAE/ml).

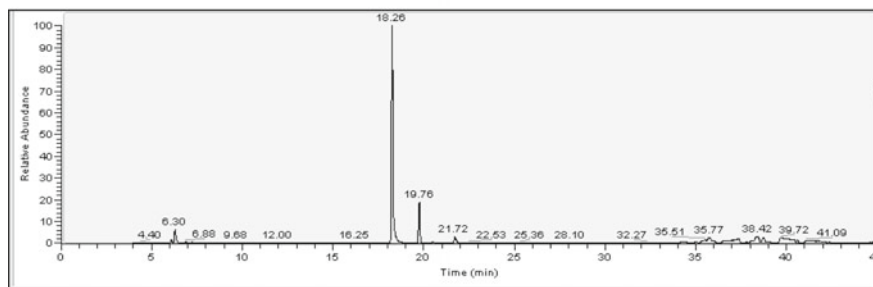
Table 2 Total phenolic content of clove bud oil and its roasted vapour

Antioxidant activity	Clove bud oil	Roasted vapour
TPC (mgGAE/ml)	1.15 \pm 0.06 ^a	1.44 \pm 0.07 ^a

^aValues are in terms of mean \pm SD after triplicate analysis. Same letter in a row represents significant differences



a. Clove bud oil



b. Roasted vapour

Fig. 1 GC-MS analysis of clove bud oil and its roasted vapour

3.3 GC-MS Analysis

The GC-MS running time for clove bud oil and its roasted vapour was 45 min and spectrum is shown in Fig. 1. Interpretation of mass spectrum was done using data base of National Institute Standard and Technology (NIST). The active principles with their retention time and concentration (%) are presented in Table 3. Thermal treatment strongly influenced the chemical constituents, flavour and percentage composition of the oils. The retention time for eugenol is nearly the same for vapour sample compared to control. Gas chromatographic analysis of essential oils revealed that the oils contained a complex mixture of compounds mainly monoterpene hydrocarbons, phytocompounds and sesquiterpenes. A total of seven compounds were identified in clove bud oil with no heat treatment and ten compounds identified for roasted vapour sample. Clove bud oil contains 0.03% deca-1, 9-diyne, 0.08% ethylbenzol, 94.73% eugenol, 0.17% caryophyllene and other minor compounds, whereas vapour sample contains 74.19% eugenol. During roasting alloaromadendrene, isoeugenol, O-xylene and other minor compounds are formed. Some of the compounds have been considered to be tentatively identified based on comparison in the NIST data and in the absence of particular standard molecule.

Table 3 GC-MS analysis of clove bud oil and its roasted vapour

Serial No.	Compounds name	Retention time	Percentage (%)	
			Clove bud oil (%)	Roasted vapour (%)
1.	Deca-1,9-diyne	4.15	0.03	
2.	Ethylbenzene	6.1		1.26
3.	O-Xylene	6.3		5.38
4.	Ethylbenzol	6.37	0.08	–
5.	3,5-heptadiyn-2-one	6.88	–	0.48
6.	5-Chloro-2-nitrobenzylalcohol, chloromethyldimethylsilyl ether	7.24	–	2.39
7.	Eugenol	18.26		74.19
8.	Eugenol	18.52	94.73	–
9.	Benzamide,3-methyl-N-(2,3-dimethoxyphenethyl)	18.79	–	0.14
10.	Alloaromadendrene	19.76	–	11.85
11.	Furylmethyl-2-methyl-3-furyl disulfide	20.52	–	0.51
12.	Sesquiterpene	20.91	0.01	–
13.	o-Anisic acid,undec-2-enyl ester	21.1	0.04	–
14.	Isoeugenol	21.72	–	3.03
15.	Caryophyllene	24.56	0.12	–
16.	Benzene,1-(1,5-dimethyl-4-hexenyl)-4-methyl-	24.83	0.17	
17.	Benzenepentacarboxylic acid	34.38		1.75

4 Conclusion

Natural clove bud when roasted generates flavour molecules in vapour state which on recovery shows significant changes in the composition as well as in antioxidant activity. However, results indicate that roasted vapours can be utilized as flavouring agent with great deal of antioxidant activity.

Acknowledgements I would like to acknowledge my institute Indian Institute of Engineering Science and Technology (IEST), Shibpur, Howrah, West Bengal, India and my supervisors Prof. D.K. Bhattacharyya and Dr. M. Ghosh. Thanks are extended to Smriti Ranjan Maji, Technical Officer, Bose Institute, for his wonderful technical support (GC-MS).

Conflict of interest There is no conflict of interest.

References

- Benzie I, Strain J (1996) The Ferric Reducing Ability of Plasma (FRAP) as a measure of "Antioxidant Power": the FRAP assay. *Anal Biochem* 239:70–76. <https://doi.org/10.1006/abio.1996.0292>
- Charles DJ (2013) Antioxidant properties of spices. *Herbs and Other Sources*. <https://doi.org/10.1007/978-1-4614-4310-0>
- Kamatou G, Vermaak I, Viljoen A (2012) Eugenol—from the remote Maluku Islands to the international market place: a review of a remarkable and versatile molecule. *Molecules* 17:6953–6981. <https://doi.org/10.3390/molecules17066953>
- Lindberg Madsen H (1995) Spices as antioxidants. *Trends Food Sci Technol* 6:271–277. [https://doi.org/10.1016/s0924-2244\(00\)89112-8](https://doi.org/10.1016/s0924-2244(00)89112-8)
- Nurdjannah N, Bermawie N (2001) Clove. *Handb Herbs Spices* 154–163. <https://doi.org/10.1533/9781855736450.154>
- Peter K, Babu KN (2012) Introduction to herbs and spices: medicinal uses and sustainable production. *Handb Herbs Spices* 1–16. <https://doi.org/10.1533/9780857095688.1>
- Re R, Pellegrini N, Proteggente A et al (1999) Antioxidant activity applying an improved ABTS radical cation decolorization assay. *Free Radical Biol Med* 26:1231–1237. [https://doi.org/10.1016/s0891-5849\(98\)00315-3](https://doi.org/10.1016/s0891-5849(98)00315-3)
- Shimada K, Fujikawa K, Yahara K, Nakamura T (1992) Antioxidative properties of xanthan on the autoxidation of soybean oil in cyclodextrin emulsion. *J Agric Food Chem* 40:945–948. <https://doi.org/10.1021/jf00018a005>
- Shobana S, Akhilender Naidu K (2000) Antioxidant activity of selected Indian spices. *Prostaglandins Leukotrienes Essential Fatty Acids (PLEFA)* 62:107–110. <https://doi.org/10.1054/plf.1999.0128>
- Singleton VL, Orthofer R, Lamuela-Raventós RM (1999) Analysis of total phenols and other oxidation substrates and antioxidants by means of folin-ciocalteu reagent. In: *Oxidants and antioxidants Part A methods in enzymology*, pp 152–178. [https://doi.org/10.1016/s0076-6879\(99\)99017-1](https://doi.org/10.1016/s0076-6879(99)99017-1)

Characterization, Purification and Immobilization of an Acid Invertase from *Mentha Spicata* (Pudina) for the Production of Invert Syrup



Abhishek Mukherjee

Abstract Invertase (β -fructofuranosidase), a commercially important enzyme, for the preparation of invert syrup, has gained importance due to its various biotechnological applications in food and pharmaceutical industry. The present study reports that a 68 kDa invertase (specific activity = 230 ± 25 U/mg protein), appreciably present in *Mentha spicata* stem (1900 ± 100 U/100 g fresh wt.), was purified by $(\text{NH}_4)_2\text{SO}_4$ precipitation, ion exchange chromatography, size exclusion chromatography and HPLC. The enzyme was stable in the pH range of 3.5–7.0 up to 55 °C, with a K_m of 7.9 mM sucrose. $\text{Hg}^{2+} > \text{PCMB} > \text{Ag}^+ > \text{Pb}^{2+} > \text{Cd}^{2+}$ inhibited the enzyme activity. Iodoacetic acid, iodoacetamide, DTNB and N-ethylmaleimide did not affect the invertase activity suggesting the non-thiol nature of the enzyme. The enzyme hydrolyzed sucrose, raffinose and inulin (slightly) with no maltose or levan hydrolyzing activities. The enzyme (3U/mL) completely hydrolyzed sucrose (8% w/v) to invert syrup in 5 h at 50 °C. Immobilization of the enzyme on oxidized bagasse (dialdehyde cellulose) increased its temperature optima (by 10 °C) and thermostability (retaining $45 \pm 2\%$ and $30 \pm 1\%$ activities at 70 and 80 °C, respectively). Immobilized enzyme system efficiently produced invert syrup from sucrose, remaining $80 \pm 1\%$ active after 20th cycle.

Keywords *Mentha spicata* · Invertase · Sucrose · Enzyme immobilization · Bagasse

1 Introduction

Invertase (EC 3.2.1.26) or β -fructofuranosidase catalyses the cleavage of sucrose to an equimolar mixture of glucose and fructose, known as invert syrup. Invert syrup is sweeter than sucrose and does not crystallize easily (remains in liquid form), and therefore widely used in food (as fondant filling for chocolates, confectioneries, jams

A. Mukherjee (✉)

Department of Biotechnology, Heritage Institute of Technology, Chowbaga Road
P.O.-Anandapur, East Kolkata Township, Kolkata, West Bengal 700107, India
e-mail: abhi.india79@gmail.com

© Springer Nature Singapore Pte Ltd. 2021

D. Ramkrishna et al. (eds.), *Advances in Bioprocess Engineering and Technology*,
Lecture Notes in Bioengineering,
https://doi.org/10.1007/978-981-15-7409-2_16

159

and candy making, artificial honey), beverage (in soft drinks) and pharmaceutical industries (Kulshrestha et al. 2013). The most successful commercial invertase is derived from Baker's yeast. Though phytoenzymes in food industry offer new means to address energy savings and increase in efficiency and sustainability, they have not been seriously commercialized except that of malt amylase (from barley), papain and bromelain. Production of enzymes from microbial sources requires maintained upstream process technology, which is cost-effective, but no such technology is required for extracting phytoenzymes. The source plant itself acts like a bioreactor producing the enzyme, which needs only to be harvested and extracted. Plant parts such as stems, producing appreciable amount of extracellular enzymes, are a cheap source, as these renewable parts can be harvested time to time (Mukherjee et al. 2012).

Mentha spicata L. (Lamiaceae) commonly known as spearmint, (in India as 'Pudina'), is known to be endowed with a variety of biological properties and is extensively used in culinary purpose and ayurvedic and folk medicines in the Indian subcontinent (Güney et al. 2006; Kumar et al. 2008). However, till date, no reports are available on the presence of macromolecules (enzymes) from the plant. This is the first report of the presence of appreciable amount of any enzymatic activity (invertase) in the stems of *Mentha spicata*.

2 Materials and Methods

2.1 Chemicals

Sucrose, bovine serum albumin (BSA, Fraction-V), DEAE-Sephadex (A50), Bradford reagent, pepsin, trypsin (porcine pancreas), chymotrypsin (porcine pancreas), proteinase-K, maltose, raffinose, inulin (chicory root), melezitose, levan, N-ethylmaleimide (NEM), p-chloromercuri benzoate (PCMB), iodoacetic acid, iodoacetamide and 1-ethyl-3-(3-dimethyl aminopropyl) carbodiimide-hydrochloride (EDAC) were all purchased from Sigma Chemicals, (St Louis, MO, USA). 3,5-dinitrosalicylic acid (DNSA) and 5,5'-dithiobis-2-nitrobenzoic acid (DTNB) were products of SRL.

2.2 Extraction of Enzyme

Mentha spicata stems (400 g) were chopped into small pieces (1–2 cm long) and dropped immediately in 400 ml of 0.1 M phosphate buffer, pH 6.0 kept at 37 °C. The mixture was blended for 5 min in a warring blender and the biomass squeezed through

a nylon cloth to collect the extract (370 ml) which was centrifuged at 10,000 rpm to obtain the clear supernatant (360 ml) which was subjected to ultra-filtration (using PM 10 KDa membrane; Sartorius, Germany) and finally used as the source of crude enzyme.

2.3 Determination of Enzyme Activity

Invertase activity was determined in 0.1 M acetate buffer, pH 5.0 at 50 °C using 2% (w/v) sucrose as substrate. Reducing sugars formed were estimated by DNSA method. One unit of enzyme activity was taken as the amount of enzyme that could produce 1 μ mole of reducing sugar/min under the assay conditions (Mukherjee et al. 2010). Protein was determined by coomassie brilliant blue protein assay reagent (Bradford 1976).

2.4 Purification of the Enzyme

Enzyme was purified by $(\text{NH}_4)_2\text{SO}_4$ precipitation (90% saturation), ion exchange chromatography using DEAE-Sephadex (A50) column (3 cm \times 25 cm), size exclusion chromatography using Sephacryl S-300-HR column (1.5 cm \times 60 cm) and HPLC [BioSep-SEC-S-2000 (300 mm \times 7.8 mm)]. Purified protein sample (40 μ g) was subjected to denaturing SDS-PAGE. The gels were also subjected to Periodic Acid-Schiff (PAS) stain.

2.5 Determination of Physicochemical Properties of the Enzyme

The pH optimum and stability of plant invertase was determined in the pH range of 3.0–9.0 using various buffer systems. The optimum temperature and thermostability of the enzyme was determined in the temperature range of 20–80 °C. Effect of different chemical modifiers on enzyme activity was determined by incubating 20 U of purified invertase separately (at 37 °C) with iodoacetic acid (50 mM), iodoacetamide (50 mM), NEM (50 mM), PCMB (1 mM), DTNB (5 mM) and EDAC (50 mM) at their respective recommended pH buffers (Mukherjee et al. 2010). Effect of various metal ions on purified invertase was determined by incubating 5 U/ml of enzyme (in 0.1 M acetate buffer, pH 5.0; 37 °C) in presence of different metal ions

(Hg^{2+} , Ca^{2+} , Mg^{2+} , Zn^{2+} , Fe^{2+} , Fe^{3+} , Cd^{2+} , Cu^{2+} , Ag^+ and Mn^{2+}) of 1 mM concentration. Effect of proteolytic enzymes on the stability of invertase was determined by pre-incubating (at 37 °C) purified invertase (25 U/ml) separately with pepsin (150 U/ml), trypsin (200 U/ml), chymotrypsin (132 U/ml) and proteinase-K (40 U/ml) in their respective buffers.

Activity of purified invertase on various substrates (sucrose, maltose, raffinose, melezitose, trehalose, inulin, levan, isomaltose) was determined in 0.1 M acetate buffer, pH 5.0 at 50 °C. The kinetics of sucrose hydrolysis was studied in terms of liberation of reducing sugars from the reaction mixtures (20 ml) containing 3–6 U/ml of purified invertase and 1%–8% (w/v) sucrose in 0.1 M acetate buffer, pH 5.0 at 50 °C.

2.6 Immobilization of *Mentha spicata* Invertase on Bagasse Dialdehyde Cellulose

Bagasse (1 kg), collected from the local market, was boiled thrice in distilled water, dried in a hot air oven (60 °C), chopped into small pieces (0.2–0.5 cm long), treated alternatively with 1.25% (v/v) sulphuric acid and 1.25% (w/v) sodium hydroxide, followed by thorough washing with distilled water and 95% (v/v) ethanol. The biomass was finally dried in a hot air oven to obtain purified bagasse which was oxidized (Varavinit et al. 2002) by soaking 40 g of biomass in 1 L of 0.03 M periodic acid (pH-3.0; 90 °C), followed by washing (with distilled water) and oven-drying to obtain cellulose-dialdehyde. 200 ml of crude concentrated enzyme solution (300 ± 50 U/ml) in 0.1 M phosphate buffer, pH 6.0 was coupled with 24 g cellulose-dialdehyde in four steps (using 6 g biomass each step). The treated bagasse was then vacuum filtered, washed twice in distilled water, press-dried on a blotting paper and stored at 4 °C in 0.1 M phosphate buffer, pH 6.0.

3 Results and Discussion

3.1 Yield and Storage Stability

Though invertase activity has been reported in plants, like potato tuber (Bracho and Whitaker 1990), carrot (Lee and Sturm 1996), apple fruit (Pan et al. 2005), cherry fruit (Krishnan and Pueppke 1990), chicory root (Van Den Ende and Van Laere 1993), *Tinospora cordifolia* stem (Mukherjee et al. 2012; Sengupta et al. 2013) etc., yet, except in *Tinospora cordifolia* (4500 ± 500 U/100 g fresh stem), the presence of appreciable amount of enzyme has not been reported. *Mentha spicata* stem yielded 1900 ± 100 U of acid stable invertase/100 g when extracted with 0.1 M phosphate buffer, pH 6.0 at 37 °C. Lyophilized stem powder yielded 8800 ± 400 U/100 g

while lyophilized aqueous extract yielded $15,000 \pm 350$ U/100 g of powder. It was observed that invertase activity in the plant stem pieces (stored at $0-4$ °C) rapidly decreased to $50 \pm 2\%$ of its original activity after 1 week of storage but the aqueous extract (from fresh stem) stored at $0-4$ °C retained $83 \pm 2\%$ of its activity till 90 days. Lyophilized plant stem pieces, powdered and stored at $0-4$ °C or at room temperature was found to be an excellent source of stable enzyme, retaining 90–95% of its activity till 10 months of the study. Lyophilized (to dryness) aqueous extract stored at $0-4$ °C retained $95 \pm 2\%$ of its original activity.

3.2 Purification

The purified enzyme was recovered to the extent of $30 \pm 1\%$ of its original activity with a specific activity of 274 ± 10 U/mg of protein (Table 1), displaying a molecular weight of 68 kDa, similar to that of mung bean invertase (67 kDa), while neutral invertase from carrot and mango invertase displayed a molecular weight of 57 kDa (Lee and Sturm 1996) and 45 kDa (Li et al. 2017) on SDS PAGE, respectively. Ion exchange chromatography on DEAE-Sepahdex column increased the specific activity of *Mentha* invertase to almost six times (Table 1). Size exclusion chromatography of the enzyme protein on Sephacryl S-300-HR column indicated presence of a non-sucrase protein contamination eluted separately in lower molecular weight range, thus increasing the specific activity of the enzyme (Table 1). The enzyme was homogenous in Native PAGE and gave a single band in SDS PAGE. Both the bands gave positive response to PAS staining indicating the enzyme to be a glycoprotein, similar to that of potato tuber invertase (10.9% carbohydrate content) (Bracho and Whitaker 1990).

Table 1 Steps of purification of invertase from *Mentha spicata* stem

Sample	Total enzyme activity (U)	Total protein (mg)	Specific activity (U/mg protein)	Fold purification	% Recovery
Crude extract (300 ml)	3300 ± 250	220 ± 20	12.2 ± 1.5	1	100
Concentrated (ultra-filtered and lyophilized) extract (60 ml)	3150 ± 75	203 ± 7	14.3 ± 0.80	1.25 ± 0.2	94 ± 2
(NH ₄) ₂ SO ₄ precipitation (90% saturation) (10 ml)	2650 ± 100	115 ± 12	25 ± 2.50	2.04 ± 0.1	80 ± 2
DEAE-Sephadex (3 ml)	1850 ± 125	25 ± 6	75 ± 3.5	6.14 ± 0.3	56 ± 1
Sephacryl S-300-HR (1 ml)	1100 ± 120	4.5 ± 0.4	230 ± 25	16 ± 1.2	33 ± 2
HPLC(BioSep-SEC-S-2000 column)	980 ± 20	3.6 ± 0.1	274 ± 10	22 ± 1	30 ± 1

3.3 Physicochemical Properties

Purified invertase was found to be optimally active in the pH range of 4.0–5.5, with optimal activity at 5.0, similar to that of *Tinospora cordifolia* invertase (Sengupta et al. 2013), potato tuber invertase (Bracho and Whitaker 1990) and cherry fruit invertase (Krishnan and Pueppke 1990). The enzyme retained $46 \pm 2\%$, $75 \pm 2\%$ and $83 \pm 1\%$ of its activity at pH 3.0, 4.0 and 5.0, respectively, after 3 h of incubation, displaying maximum stability at pH 6.0 but lost $62 \pm 2\%$ of its activity at pH 8.0. Enzyme activity increased with the increase in temperature till 60°C , being optimally active in the range of $50\text{--}60^\circ\text{C}$ and stable in the range of $0\text{--}55^\circ\text{C}$. pH and thermal stability of *Mentha spicata* invertase makes it an effective remedy (oral enzyme therapy) for sucrose intolerance. The enzyme need not be purified and can be used as a crude concentrated powder or liquid as the source plant is completely non-toxic (Güney et al. 2006; Kumar et al. 2008) and has been used since a long time in various traditional flavoured drinks and recipes throughout the Indian subcontinent.

Mentha spicata invertase was completely inhibited by 1 mM PCMB (within 10 min of incubation). On the other hand, DTNB, iodoacetamide, iodoacetic acid and NEM had no significant effect on enzyme activity thereby suggesting its non-thiol nature unlike that of papain, *T. cordifolia* amylase, bromelain and ficin (which are all thiol enzymes). However, water-soluble carbodimide decreased invertase activity by $49 \pm 2\%$ and $69 \pm 1\%$ in 2 and 4 h, respectively, suggesting the requirement of carboxyl group for its catalytic activity. The enzyme efficiently hydrolyzed sucrose, displayed much less activity on raffinose, hydrolyzed inulin slightly but was completely inactive on maltose, melezitose, trehalose, isomaltose and levan. Purified enzyme (3–6 U/ml) efficiently hydrolyzed 93–95% of 8% (w/v) sucrose in 5 h (Fig. 2a). Purified invertase displayed K_m and V_{max} of 7.9 mM (2.7 mg/ml) and 0.90 μmole of reducing sugar/min, respectively, using sucrose as substrate. Invertase was found to be strongly inhibited by heavy metal ions ($\text{Hg}^{2+} > \text{Ag}^+ > \text{Pb}^{2+} > \text{Cd}^{2+}$) at 1 mM concentration while Ca^{2+} , Mg^{2+} , Zn^{2+} had no significant effect on enzyme activity. However, Mn^{2+} slightly increased the enzyme activity. It was observed that the proteolytic enzymes (trypsin, chymotrypsin, proteinase-K) at their optimal pH did not lower the activity of *Mentha spicata* invertase till 2 h of incubation.

3.4 Immobilization

Immobilization of invertase (Fig. 1) on oxidized bagasse (% activity yield = $49 \pm 2\%$) improved its temperature optima (by 10°C) and thermostability. Immobilized invertase was found to be optimally active at 70°C (instead of at 60°C for soluble enzyme) and displayed $24 \pm 1\%$ more activity than soluble enzyme at 80°C . Soluble invertase was sharply inactivated beyond 65°C while the immobilized enzyme system remained fairly stable retaining $45 \pm 2\%$ and $30 \pm 1\%$ of its activity at 70 and 80°C , respectively. The immobilized enzyme system could efficiently run for 20 successive

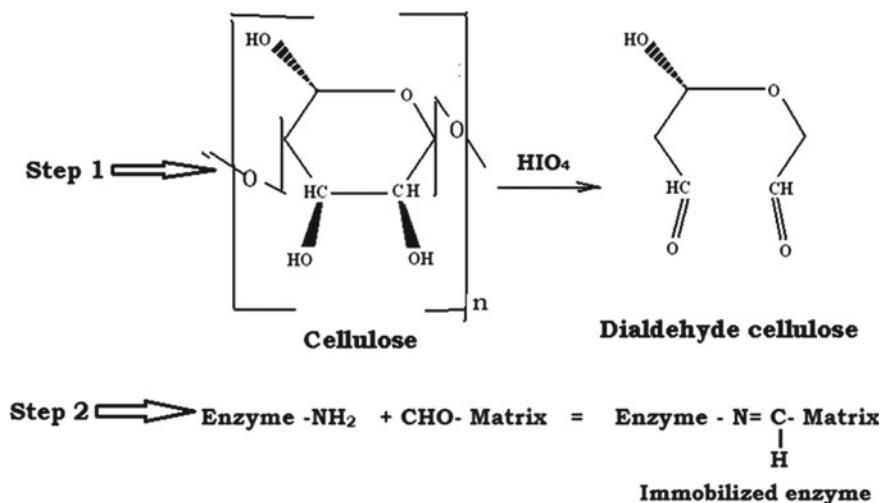


Fig. 1 Scheme of enzyme immobilization

cycles (each cycle of 4 h duration), producing invert syrup from sucrose, remaining $85 \pm 1\%$ and $80 \pm 1\%$ active after 10th and 20th cycles, respectively (Fig. 2a, b).

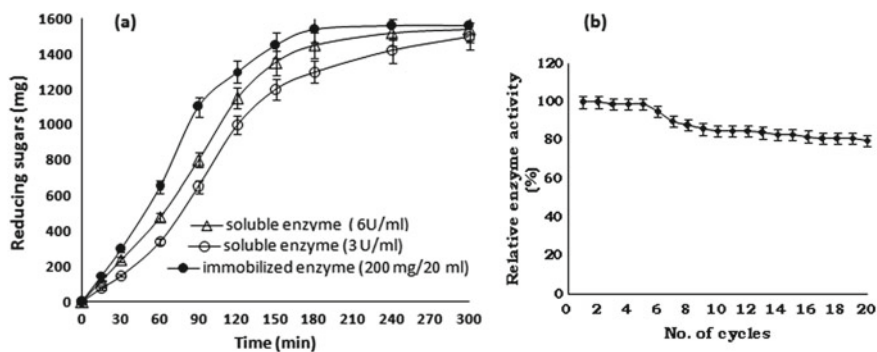


Fig. 2 **a** Kinetics of sucrose hydrolysis by soluble and immobilized enzyme. Reaction mixtures (20 ml) containing either purified (soluble) or immobilized enzyme were incubated separately with 8% (w/v) sucrose in 0.1 M acetate buffer, pH 5.0 at 50 °C. Aliquots were withdrawn at different time intervals and the amount of reducing sugars determined. **b** Efficiency of the immobilized enzyme system. Immobilized enzyme system was used for 20 successive cycles (4 h duration each) of sucrose hydrolysis (8% w/v of sucrose in 0.1 M acetate buffer, pH 5.0 at 50 °C) and the efficiency of the immobilized enzyme system was determined (in terms of % relative enzyme activity) after every cycle of operation

4 Conclusion

Mentha spicata seems to be a good source of acid stable invertase obtained from a non-toxic medicinal plant. The crude concentrated enzyme extract can effectively be used for the production of invert syrup and also as a useful and safe remedy for sucrose intolerance.

References

- Bracho GE, Whitaker JR (1990) Purification and partial characterization of potato (*Solanum tuberosum*) invertase and its endogenous proteinaceous inhibitor. *Plant Physiol* 92(2):386–394
- Bradford M (1976) A rapid and sensitive method for the quantitation of microgram quantities of protein utilizing the principle of protein dye binding. *Anal Biochem* 72(1–2):248–254
- Güney M, Oral B, Karahanli N et al (2006) The effect of *Mentha spicata* Labiatae on uterine tissue in rats. *Toxicol Ind Health* 22(8):343–348
- Krishnan HB, Pueppke SG (1990) Cherry fruit invertase: partial purification, characterization and activity during fruit development. *J Plant Physiol* 135(6):662–666
- Kulshrestha S, Tyagi P, Sindhi V et al (2013) Invertase and its applications—a brief review. *J Pharm Res* 7:792–797
- Kumar V, Kural MR, Pereira BM et al (2008) Spearmint induced hypothalamic oxidative stress and testicular anti-androgenicity in male rats—altered levels of gene expression, enzymes and hormones. *Food Chem Toxicol* 46(12):3563–3570
- Lee HS, Sturm A (1996) Purification and characterization of neutral and alkaline invertase from carrot. *Plant Physiol* 112(4):1513–1522
- Li R, Li J, Liao X et al (2017) Purification and characterization of soluble acid invertase from mango fruits. *Int J Food Sci Tech* 52(4):906–915
- Mukherjee A, Ghosh AK, Sengupta S (2010) Purification and characterization of a thiol amylase over produced by a non-cereal non leguminous plant, *Tinospora cordifolia*. *Carbohydr Res* 345(18):2731–2735
- Mukherjee A, Sengupta S, Ray L et al (2012) Evaluation of *Tinospora cordifolia* amylase as a commercial digestive enzyme of plant origin. *J Herbs Spices Med Plants* 18(1):58–76
- Pan QH, Zou KQ, Peng CC et al (2005) Purification, biochemical and immunological characterization of acid invertases from apple fruit. *J Integr Plant Biol* 47(1):50–59
- Sengupta S, Mukherjee A, Ray L et al (2013) *Tinospora cordifolia*, a novel source of extracellular disaccharidases, useful for human disaccharidase deficiency therapy. *Phytother Res* 27(5):725–730
- Varavinit S, Chaokasem N, Shobsngobb S (2002) Immobilization of a thermostable alpha-amylase. *Sci Asia* 28:247–251

Identification of Aqueous Extract of Red Amaranth Leaves by HPLC and LC-MS



Arjuma Sultana and Uma Ghosh

Abstract The demand for natural antioxidants in the upcoming years is set to rise exponentially due to increasing consumer awareness of harmful effects of synthetic antioxidants on human health. Fruits and vegetables are rich sources of bioactive compounds having antioxidant property. The natural dietary antioxidants of fruits and vegetables promote health effect. Various flavonoids and phenolic acids present in fruits and vegetables are responsible for prevention of several chronic diseases including cardiovascular disease, inflammation, and cancers due to their antioxidant properties. Red amaranth looks wonderful with purple or fully red in color. It is a good source of nutrients with high-quality proteins, vitamins, minerals, fibers, and bioactive compounds such as phenolics and pigments. Red amaranth leaves are the rich source of polyphenol and antioxidant. They are also helpful to increase the awareness of consumers in regards to the benefit of phyto-chemical. Solvent extraction is one of the most common conventional methods for extraction of color from leafy vegetables. The aim of the present study was to apply the conventional aqueous extraction procedure in extracting the color of red amaranth leaves. The aqueous extract was analyzed by high-performance liquid chromatography (HPLC) and liquid chromatography-mass spectrometry (LC-MS) for identification of the pigment. The result reveals the presence of anthocyanin pigment in red amaranth leaves.

Keywords Red amaranth leaves · Bioactive compounds · Antioxidant · HPLC · LC-MS

A. Sultana · U. Ghosh (✉)
Department of Food Technology and Biochemical Engineering, Jadavpur University, Kolkata
700032, India
e-mail: ughoshftbe@yahoo.co.in

A. Sultana
e-mail: asultana16ftbe@gmail.com

© Springer Nature Singapore Pte Ltd. 2021
D. Ramkrishna et al. (eds.), *Advances in Bioprocess Engineering and Technology*,
Lecture Notes in Bioengineering,
https://doi.org/10.1007/978-981-15-7409-2_17

1 Introduction

Amaranth leaves are nutritious leafy vegetables. They grow in the lowland tropics of Asia and Africa. They are of two types, namely, green amaranth and red amaranth. Red amaranth looks wonderful with purple or fully red in color. It is a rich source of calcium, iron, vitamin C, and protein (Khandaker et al. 2008). Because of these it acts as a natural antioxidant to fight against infectious diseases like heart disease, cancer, serious eye disease, and muscular degeneration (Dasgupta and De 2007; Kumar et al. 2017). Bioactive compounds are present in red amaranth leaves. Bioflavonoid was the most important topic for recent research mainly for their beneficial effects on human health and applications as potential sources of natural food dyes. Natural pigments are used as an eco-friendly alternative to synthetic dyes and also in textile industry. In recent years, color plays an important role in the consumer acceptability of food. Colorants are being used in food industry since centuries to enhance or at least restore original appearance of foods and ensure uniformity as an indicator of food quality. Color is the first characteristic perceived by the senses. Synthetic colorants have always been a question of controversy regarding their safety. Consumers prefer natural colorants than the synthetic ones, as they are increasingly concerned with the safety of synthetic colorants. Therefore, interest in natural colorants has significantly increased because of both legislative action and consumer awareness (Yousuf et al. 2016). The present study deals with aqueous extraction of color from red amaranth leaves and identification of the potent pigment by high-performance liquid chromatography (HPLC) and liquid chromatography-mass spectrometry (LC-MS).

2 Materials

Red amaranth leaves were purchased from market. HPLC grade acetonitrile, methanol, acetone, acetic acid, 36% pure hydrochloric acid, Millipore, and ferric chloride (FeCl_3) were purchased from Merck. 2,2-azinobis (3 ethylobenzothiazoline-6 sulphonate) (ABTS), triphenyltriazine (TPTZ), 2,4,6-tris(2-pyridyl)-1,3,5-triazine, 1,1-diphenyl-2-picrylhydrazyl (DPPH), 6-hydroxy-2,5,7,8-tetramethyl-2-carboxylic acid (trolox), sodium peroxy disulfate, Folin–Ciocalteu reagent, and gallic acid were purchased from Sigma-Aldrich. Laboratory-grade de-ionized water was used. All reagents were of analytical grade.

3 Methods

3.1 *Extraction Process*

Red amaranth leaves were dried at 50 °C for 5–6 h in a tray drier. Dried leaves were ground. Then 1 gm samples were dissolved in 100 ml of distilled water. Then the extract was poured in a bottle which was tightly capped later. After that it was kept in the water bath with continuous shaking at 80 °C temperature for an hour. Finally, extract was cooled and filtered and stored at 4 °C. Then the extract was concentrated by rotary evaporator and evaporates under reduced pressure and then lyophilized the concentrated extract to get powder.

3.2 *Determination of Moisture Content*

10 g sample of red amaranth leaves were weighed accurately in a dry Petri dish and dried at 105°C for 3 h. The sample is allowed to cool in desiccators, reweighed, and the weight is recorded. The drying–cooling–reweighing procedure is repeated until the weight is constant. The moisture content is measured using the following equation:

$$\text{Moisture content (\%)} = (A - B/B) * 100$$

where *A* is the weight of the moist sample and *B* is the weight of the dry sample.

3.3 *Determination of Ash Content*

Porcelain crucible was weighed accurately (*A* g). About 3 g of ground sample was put in the crucible and the crucible with the sample was weighed accurately (*B* g). The sample was ashes in an electric muffle furnace, which can maintain the temperature at 625 ± 25 °C overnight, cooled in the desiccators for 15 min, and the crucible containing the ash was weighed (*C* g). Completeness of ashing was checked by shaking with a platinum wire to discover whether there exist any unburnt particles and if so, ashing is to be continued until constant weight. The ash content is calculated using the following equation:

$$\text{Ash content (\%)} = (C - A)/(B - A) * 100$$

where

A = weight of empty crucible (gm),

B = weight of crucible and sample (gm), and

C = weight of crucible and ash (gm).

3.4 Determination of FRAP Activity

The FRAP assay was determined according to the method of Li et al. (2012). In this process, ferric (Fe^{3+}) ion was reduced to ferrous (Fe^{2+}) ion and the intensive blue color was observed because of the formation of ferrous-tripyridyl-s-triazine (TPTZ) at maximum absorbance of 593 nm. Absorbance was measured after 8 min and was proportional to the combined ferric reducing/antioxidant power of the antioxidants in the extracts. The percentage of inhibition of DPPH by the leaf extract was calculated according to the following equation:

$$\% \text{ of Inhibition} = (1 - A_{\text{test sample}}/A_{\text{blank}}) \times 100$$

where

A_{blank} = absorbance of the methanolic blank and

$A_{\text{test sample}}$ = absorbance of the leaf extracts.

3.5 Determination of Total Phenol Content

Total phenol content was determined by using Folin–Ciocalteu reagent as described by Li et al. (2012) and Pieroni et al. (2011). The absorbance of the reaction mixture was read at 765 nm using a (U-1800, HITACHI, Tokyo, Japan) spectrophotometer. The results were expressed as mg gallic acid equivalent/g dry weight (mg GAE/g DW). Results were expressed of three independent extractions.

3.6 Determination of Total Anthocyanin Content

The total anthocyanin pigment content was estimated by the pH differential method (Lee et al. 2005). 1 g of the defatted sample was extracted with 1 ml of acetonitrile containing 4% acetic acid. The absorbance was measured at 510 nm and 700 nm in buffers at different pH levels (pH 1.0 and 4.5). The total monomeric anthocyanin was calculated by using the following equation:

$$A = [(A_{510} - A_{700}) \times \text{pH}1.0 - (A_{510} - A_{700}) \times \text{pH}4.5]$$

Molar extinction coefficient of cyanidine-3-glucoside was 26,900 molar in L mol⁻¹ cm⁻¹. Results were expressed as milligrams of cyanidine-3-glucoside equivalent (CGE) 100 g₋₁ DW.

3.7 Identification of Red Amaranth Aqueous Extract by HPLC Methods

For removing the sugar and acid from the aqueous extract, 1% trifluoroacetic acid (TFA) in methanol was added to it and then it was pass through a supelclean LC-18 cartridge (María de Lourdes Vargas y Vargas et al 2013). A high-performance liquid chromatography (HPLC) (Alliance 2695 HPLC system; Waters Corporation, Massachusetts, MA) is equipped with a binary pump, a dual λ absorbance UV detector 2487, an inline degasser, and the Empower 2 software. The separations were performed using Symmetry C-18 reversed-phase column (250 mm \times 4.6 mm length, 5 μ m particle size) at 30 °C. Acidified water with 0.1% TFA (v/v) was used as mobile phase A and HPLC grade acetonitrile with 0.035% formic acid (v/v) was used as phase B. The injection volume was 20 μ l. The following gradients were used: 10%–11% of B in 12 min, 11%–12% in 8 min, 12%–13% in 5 min, 13%–18% in 10 min, and 18% of B maintained for 25 min. The anthocyanins were analyzed with a visible detector at 520 nm. Before injecting it, the sample was filtered through a 0.45 μ m acrodisc (Millipore, Bedford, MA). The flow rate was kept at 1 ml/min. For the identification of anthocyanin cyaniding-3-glucoside was used as a standard. The amount of phenolic compound was expressed as milligram per gram of the extract.

3.8 Qualitative and Quantitative Analysis of Aqueous Red Amaranth Leaves by LC-MS

Analyses were performed using a Waters Xevo-G2 XS Q-TOF mass C-18 column (100 \times 2.1 mm i.d.; particle size 5 μ m) and as mobile phase a gradient of 0.1% formic acid as eluent A and acetonitrile (LC-MS grade, J. T Becker) as eluent B. The flow rate was 0.250 ml/min and the amount injected was 10 μ l. Here, the column back pressure was used as 1490 bar and the temperature was set at 25 °C. An electro-spray ionization source (source block temperature 130 °C, desolvation temperature 300 °C, capillary voltage 3 kV, cone voltage 35 V) was used when the desolvation and cone gas flow rate were 650 and 50 L/h, respectively. The flow generated by chromatographic separation was directly injected into the electro-spray ion source for mass detection. Positive ion as well as negative ion mode was used for mass detection.

Table 1 Composition of fresh red amaranth leaves (dry basis)

Moisture content (%)	Ash content (%)	Total phenol content (μg FAE/g dw)	Antioxidant activity (% of inhibition)	Total anthocyanin content (mg/100 g of fresh sample)
89.39	1.25	161.29	35.13	161.9

4 Results and Discussion

4.1 Composition of Fresh Red Amaranth Leaves

From Table 1, the moisture content of red amaranth leaves is 89.39%. The ash content of the sample is 1.25% per gram of sample, which indicated the amount of micronutrient composition in red amaranth leaf. The total phenol content of red amaranth leaves is 161.29 μg FAE/g dw. Antioxidant content of red amaranth leaves is 35.13 (% inhibition). Results indicated that the extracted red amaranth leaves contained about 161.90 mg/100 g on fresh weight of anthocyanins pigments and declared that red amaranth leaves contained high concentration of total anthocyanins. These results are in agreement with that obtained by M.T.M. Assous *, M.M. Abdel-Hady, Ghada M. Medany (2014).

4.2 Identification of Red Amaranth Leaves Aqueous Extract by HPLC Methods

HPLC methods are applied for separation and purification of bioactive compounds in plant samples (Robbins et al. 2003; Zhang and Kou 2004). It also helps to identify the accurate structure of bioactive compound from natural sources (Patel et al. 2010). This analytical technique is used for the qualitative or quantitative analysis of non-volatile compounds like phenolics, terpenoids, and alkaloids (Harborne et al. 1973). These highly capable methods accelerate the analytical separation with higher sample loading capacity (Long et al. 2014; Chen et al. 2012). Estimation of qualitative analysis of the analyzed sample depends on the stability of retention time of the referred standard. When the standards are injected at different dilution levels quantitative estimation is performed by standard curve obtained (Pang et al. 2016). Five major peaks have been identified by HPLC for the aqueous red amaranth leaf extracts. Here, we are using cyanidin-3-glucoside as a standard. Cyanidin-3-glucoside gave a maximum absorption at 518 nm. Peonidin, delphinidin, petunidin, and malvidin had similar spectra with maximum absorption at wavelengths 524 nm, 530 nm, 532 nm, and 534 nm, respectively. Anthocyanins pigments extracted from red amaranth leaves were separated and identified by HPLC as shown in Fig. 1.

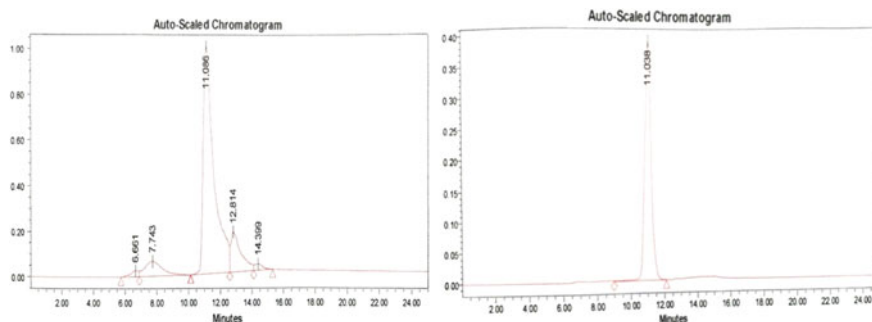


Fig. 1 HPLC chromatogram of red amaranth leaves aqueous extract and the standard curve of anthocyanin (cyaniding-3-glucoside): aspartic acid (6.7 min), gallic acid (7.0 min), protocatechuic acid (7.2 min), vanillic acid (8.4 min), anthocyanin (11.03), catechin (12.5 min), rutin (12.8 min), trans-cinnamic acid (13.0), ferulic acid (13.1 min), quercetin (13.9 min), and kampferol (14.5)

Figure 1 represents the HPLC of aqueous extract of red amaranth leaves and the standard curve of anthocyanin (cyanidin-3-glucoside). Five phenolic compounds from the aqueous red amaranth leaf extracts were separated and successfully identified by using a HPLC method (Fig. 1). Figure 1 shows five different peaks at different retention times (6.661, 7.743, 11.086, 12.814, and 14.399). This aqueous extract has aspartic acid, proto-catechuic acid, anthocyanin, rutin, and kampferol. From the standard curve of cyaniding-3-glucoside, we have to see the retention time of anthocyanin is 11.038. Therefore, from Fig. 1, we have to conclude that anthocyanin was present in the aqueous extract of red amaranth leaf.

4.3 LC-MS of Red Amaranth Leaves Aqueous Extract

A mass spectrometer combined with a liquid chromatography can detect mass characteristics of a compound or of a class of compounds. The system can selectively detect compounds of interest in a complex matrix, thus making it easy to find and identify suspected impurities at trace levels. Presently, LC-MS is the most popular identification method for bioactive compounds from natural sources. LC-MS provides the exact or predicted molecular weight of the extract sample. It also gives the structural identification by calculating the accurate mass-to-charge (m/z) ratio of the compounds (Stalikas et al. 2010). Polyphenols are the most common bioactive compounds in plant sample. LC-MS is the most efficient method for separation of flavonoids from natural sources. Flavonoids are detected depending on the chemical composition. UV absorption spectrum and the retention time of the reference standard indicated the chemical composition of the compounds. If the retention times of two components are nearly same then on the basis of multiple wavelength detection systems absorption spectra is separated. Flavonoids have O-glycoside and C-glycoside and as a result the substitution patterns of methoxy and hydroxyl groups are in small

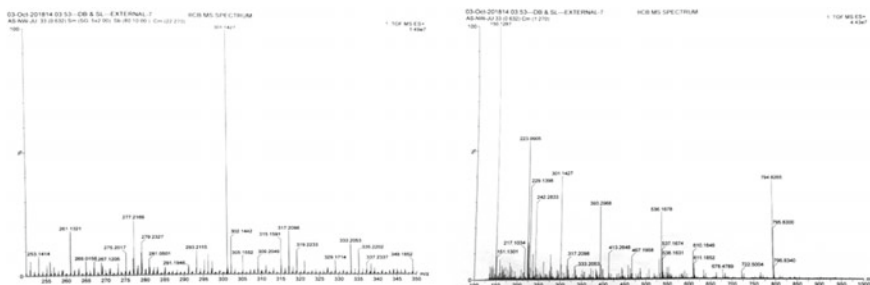


Fig. 2 These two corresponding figures represent the mass spectrum of aqueous red amaranth leaf extract

wavelength range of both bands. In flavonoids analysis, ESI and APCI are used as an ionization source. Mass spectrometry imparts structural information of phenolic compounds by identifying the distribution pattern of the components (Mandal et al. 2010). In several cases, due to the presence of impurity in the sample, the analyzed compound may not have reached the accurate corresponding fragment ion.

The volatile compounds are usually present in plant polyphenol as acylated with aliphatic and aromatic acids to the glycosidic part. So it is very difficult to identify the structure of acylated flavonoid glycosides. Figure 2 shows the LC-MS of aqueous extract of red amaranth leaves. The mass spectrum of this unknown compound contained some fragments at m/z 287, (cyanidin), m/z 303, (delphinidin), m/z 317 (petunidin), m/z 331 (malvidin), m/z 435 (cyaniding-3-arabinoside), m/z 449 (cyaniding-3-galactoside), m/z 465 (delphinidin-3-glucoside and delphinidin-3-galactoside), and m/z 493 (malvidin-3-glucoside). This result shows that anthocyanin was present in the aqueous extract of red amaranth leaves.

5 Conclusion

In comparison of phenolics and anthocyanin composition, red amaranth leaf has nutritional value as well as antioxidant property. On the basis of color characteristics, total phenol content, total antioxidant, total anthocyanin content, and composition of major phenolic and anthocyanin compounds will help with further scientific evaluation of red amaranth leaf. The strong positive correlations between the bioactive phytochemicals (TPC and TANC) and the antioxidant activities (FRAP) suggest that anthocyanin, rutin, catechin, quercetin, and other phenolic compounds as well as amarantines were the main antioxidants in red amaranth leaves. So we have to conclude that anthocyanin pigment is present in the aqueous extract of red amaranth leaf.

Acknowledgements The authors acknowledge financial support of Maulana Aazad National fellowship under the scheme UGC (Ref- F1-17.1/2017-18/MANF-2017-18-WES-80905/(SA-III/Website)), Government of India.

References

- Chen Q, Li Y, Chen Z et al (2012) Separation, identification, and quantification of active constituents in Fructus Psoraleae by high-performance liquid chromatography with UV, ion trap mass spectrometry, and electrochemical detection. *J Pharm Anal* 2(2):143–151. <http://www.elsevier.com/locate/jpa>
- Harborne BJ et al (1973) *Phytochemical methods: a guide to modern techniques of plant analysis*. Springer Netherlands. <https://doi.org/10.1007/978-94-009-5570-7>
- Khandaker L, Ali B, Oba SM et al (2008) Total polyphenol and antioxidant activity of red Amaranth (*Amaranthus tricolor* L.) as affected by different sunlight level. *J Jpn Soc Hortic Sci* 77(4):395–401. <https://www.researchgate.net/publication/250169525>
- Kumar RB et al (2017) Application of HPLC and ESI-MS techniques in the analysis of phenolic acids and flavonoids from green leafy vegetables (GLVs). *J Pharm Anal*. <http://dx.doi.org/10.1016/j.jpha.2017.06.005>
- Li H, Deng Z, Zhu H, Hu C, Liu R, Young JC, Tsao R (2012) Highly pigmented vegetables. Anthocyanin compositions and their role in antioxidant activities. *Food Res* 46:250–259. <https://doi.org/10.1016/j.foodres.2011.12.014>
- Long Y, Zhang W, Wang F, Chen Z et al (2014). Simultaneous determination of three curcuminoids in *Curcuma longa* L. by high performance liquid chromatography coupled with electrochemical detection. *J Pharm Anal* 4(5):325–330. <https://doi.org/10.1016/j.jpha.2013.10.002>
- Pang B, Zhu Y, Lu L, Gu F, Chen H et al (2016) The applications and features of liquid chromatography-mass spectrometry in the analysis of traditional Chinese medicine. Evidence-Based Complementary Alternative Med. <http://dx.doi.org/10.1155/2016/3837270>
- Patel NK, Patel KJ, Patel PM, Rajput CG, Patel AH (2010) Introduction to hyphenated techniques and their applications in pharmacy. *Pharm Methods* 1(1):2–13. <https://doi.org/10.4103/2229-4708.72222>
- Pieroni GL, Rezende DMF, Ximenes FV, Dokkedal LA et al (2011) Antioxidant activity and total phenols from the methanolic extract of miconia albicans (Sw.) triana leaves. *Molecules* 16:9439–9450. <https://doi.org/10.3390/molecules16119439>
- Robbins JR et al (2003) Phenolic acids in foods: an overview of analytical methodology. *J Agr Food Chem* 51:2866–2887. <https://doi.org/10.1021/jf026182t>
- Vargas M, Cortez J, Duch E, Lizama A, Méndez C et al (2013) Extraction and stability of anthocyanins present in the skin of the dragon fruit (*Hylocereus undatus*). *Int J Food Sci Nutr* 4:1221–1228. <https://doi.org/10.4236/fns.2013.412156>
- Zhang Z, Kou X et al (2004) Comparison of HPLC methods for determination of anthocyanin and anthocyanidins in bilberry extracts. *J Agr Food Chem* 52:688–691. <https://doi.org/10.1021/jf034596w>

Preparation and Utilization of Hydroxy Fatty Acid Rich Soyphospholipid for Emulsifier Application in Food Products



Gargi Saha, D. K. Bhattacharyya, and Minakshi Ghosh

Abstract Phospholipids have been used as an emulsifier in the food product industry for years because of its distinct surface-active properties. Modification of phospholipid can improve the surface-active property for better food applications. The study focuses on the modification of phospholipid in terms of their fatty acid composition introducing hydroxy fatty acid. The incorporation of hydroxy fatty acid in phospholipid was carried out by enzymatic interesterification reaction at 60 °C temperature for 6–24 h. The incorporation of hydroxy fatty acid in phospholipid was 29.99 ± 0.11%. The antioxidant property and surface-active property were determined and significant changes were measured. Antioxidant activity was improved and surface tension was reduced. The modified phospholipid shows the better surface-active property. As hydroxy fatty acids are unabsorbed in the human body, it may show some reduction of cholesterol level in blood as in terms of composition similar to sucrose polyester. The use of such emulsified products offers a new kind of usage for healthcare.

Keywords Soyphospholipid · Hydroxy fatty acid · Emulsifier · Margarine

1 Introduction

Soyphospholipid modification comprising fatty acyl groups interchange and incorporation of individual fatty acid has been studied generously. These modified products are already stated as nutritionally beneficial and virtuous emulsifier.

G. Saha (✉) · D. K. Bhattacharyya · M. Ghosh
School of Community Science and Technology, Indian Institute of Engineering Science and Technology, Shibpur, Howrah, West Bengal 711103, India
e-mail: gargish6@gmail.com

D. K. Bhattacharyya
e-mail: dkb_oiltech@yahoo.co.in

M. Ghosh
e-mail: g_minakshi2000@yahoo.com

During the incorporation of hydroxy and epoxy fatty acids in soyphospholipids by transesterification reaction using either a lipase catalyst or a chemical catalyst, the changes in surface properties such as effectiveness of interfacial tension reduction (γ_{CMC}), critical micelle concentration (CMC), maximum surface excess concentration (Γ_{max}), minimum area/molecule at the interface (A_{min}), and free energy change of micellization (ΔG°_{mic}) of modified soyphospholipids showed accented variances from original soyphospholipids (Das and Bhattacharyya 2006).

T. Vijeeta showed “1-Ricinoyleoyl-2-acyl-sn-glycero-3-phosphocholine was prepared by incorporating ricinoletic acid completely in the sn-1 position of egg and soya phosphatidylcholine (PC) using immobilized phospholipase A_1 as the catalyst.” The hydroxy fatty acids (also known as ricinoletic acids) in the phospholipids divulge hydrophilic properties to improve moisture retention of lecithin with increased water dispersibility (Vijeeta et al. 2004). These kind of modified (hydroxylated) phospholipids are suitable in baking applications where it can increase the dispersion of fats and impede staling (Schmidt and Orthoefer 1985).

The objective of this study is to suggest that the use of such modified phospholipid with hydroxy fatty acid may involve in reducing cholesterol level similar to sucrose polyester (SPE) or olestra. M. M. Chakrabarty showed that SPEs were considered as no calorie fat substitutes of some spreads or margarines which are indigestible for humans and often used to control plasma cholesterol levels as well as for slimming diet (Chakrabarty 2003).

Among most of the vegetable oils, an unusual chemical characteristic is present in castor oil. It is a triglyceride derived from ricinoletic acid (12-hydroxy-9-octadecenoic), constituted of 90% of a typical hydroxylated fatty acids and 10% of non-hydroxylated fatty acids, generally oleic and linoleic acids (Conceição et al. 2007). The oil is safe and biocompatible with viscous, pale yellow, non-volatile, and non-drying oil characteristics having a bland taste too. The shelf life of this oil comparatively to other oils is commendable and does not easily get rancid unless exposed to extreme climate. There are numerous medicinal uses of castor oil other than purgative or laxative since ancient times and it also becomes highly valuable for industrial purposes (Ogunniyi 2006).

A superior presence of hydroxy acid in the castor oil is revealed in its colligative properties, such as high values of viscosity and density (Conceição et al. 2007).

The modification of hydrophobic group of phospholipids is influenced by the nature and packing of phospholipids at oil–water interface for the emulsification. The unsaturated fatty acids present in phospholipid molecules make it more rigid and therefore obstructed negatively on its packing at the interface. The amount of the unsaturation was reduced through modification, which made the modified phospholipid less rigid and flexible. This flexible structure of phospholipid will effect in densely packed surfactant arrangement and the interaction between phospholipid molecules and aqueous film will increase at the oil–water interface. This supports to expand the interfacial activity of phospholipid (Nyankson et al. 2016). Therefore, the emulsion stability will enhance by improved interaction between surfactant and aqueous film at oil–water interface which may offer a strong barrier to droplets coalescence (Chiplunkar and Pratap 2017).

The present study investigates the modification of soyphospholipid with castor oil to produce hydroxy fatty acid or ricinoleic acid rich soyphospholipid which may open a new range of emulsifiers in food industry and produce fat-based margarine products.

2 Materials and Methods

2.1 Materials

Soyphospholipid (SPL): SPL has been collected from Ruchi Soya Industries Ltd., Nagpur, India.

Castor Oil (CO) and rice bran oil (RBO): CO and RBO have been collected from market.

Enzyme: Enzyme RM IM (*Rhizomucour miehei*) has been received as a gift from Novozymes A/S, Krogshoejvej 36, 2880 Bagsvaerd, Denmark.

Palm stearin: It has been collected from Budge Budge Refineries Limited, Kolkata, India.

2.2 Deoiling of Soyphospholipid

Deoiling of crude soyphospholipid was performed by acetone (in 1:7 w/v ratio) treatment repeatedly until the acetone layer was colorless. Acetone was removed under vacuum pressure and soyphospholipid was isolated (Saha et al. 2018). The yield of deoiled SPL was 86% with 95.56% purity based on phosphorus content of SPL (Chen et al. 1956).

2.3 Enzymatic Interesterification

The parameters studied were molar ratio and time. Different molar ratios such as 1:1, 1:2, 1:3, and 1:4 of SPL and castor oil were taken, whereas 1:4 ratio was suitable for reaction for experiments. Blend of SPL and castor oil was heated up to 60 °C temperature to obtain an even solution. Enzyme (10%) was then added as catalyst. After 6, 12, and 24 h of stirring at a constant speed of 300 rpm, samples were collected. The collected mixture was then cooled at room temperature. Chloroform was then added to it to separate the enzyme by filtration and the solvent was dried under vacuum. By repeated extraction with acetone the interesterified soyphospholipid and oil were separated (Saha et al. 2018).

2.4 Fatty Acid Analysis of Esterified Phospholipid and Oil

Isolated products were methylated by adding 1 mL diethyl ether and 1 mL of 0.5 N methanolic KOH, followed by shaking the mixture for 10 min vigorously. HCl (1 mL, 1 N) was added, and the methyl esters of fatty acids were extracted with petroleum ether (40–60 °C) (Litchfield 1972). Gas chromatographic analysis was next done as follows.

2.5 Gas Chromatography

Fatty acid methyl esters were analyzed on a Hewlett-Packard gas chromatograph (HP 5890A) (7890B GC system of Agilent Technologies), equipped with a flame ionization detector (FID) and capillary DB-Wax column (30 mL, 0.250 mm I.D., 0.25 μm FT). The column temperature was programmed between 150 and 240 °C. The different fatty acid methyl esters and the standard sample were separated on the same column under identical conditions. N₂ as a carrier gas was used at 25 mL/min (Saha et al. 2018).

2.6 Antioxidant Activity Determination by 1, 1-Diphenyl-2-Picrylhydrazyl (DPPH) Radical Inhibition Assay

DPPH assay was determined by method of Blois (1958) and modified by Saha et al. (2018). Each sample was added to 1 mL of 1 mM DPPH in chloroform. The decrease in absorbance was monitored at 517 nm until a constant reading was obtained. The readings were compared with the controls, which contained solvent (chloroform) instead of the extract. The percentage inhibition was calculated as follows:

$$\% \text{ inhibition} = \frac{\text{Absorbance of control} - \text{Absorbance of sample}}{\text{Absorbance of control}} \times 100$$

2.7 Total Phenolic Assay

The total phenolic content (TPC) was determined by the assay method modified by Yu et al. (2003) and then also modified by Saha et al. (2018). Briefly, 1 ml of solvent extract was transferred into a test tube and mixed with 1 mL of 95% ethanol and 5 mL of dH₂O. Folin–Ciocalteu reagent (50% v/v; 0.5 mL) was added to each

sample followed by thorough mixing using a vortex. After 5 min, 1 mL of 5% Na₂CO₃ was added to the reaction mixture and these were left to stand for 60 min at room temperature. The absorbance was read at 725 nm. The absorbance values were converted to total phenolics and were expressed in microgram equivalents of gallic acid per milliliter (mL) of the sample. Standard curves were established using various concentrations of gallic acid (5–30 µg mL⁻¹) in methanol.

2.8 Surface Tension Measurement

Surface tension of the esterified phospholipid was measured using dynamic contact angle meter and tensiometer (DCAT) (Sudheesh and Ahmad 2013).

2.9 Preparation of Margarine

Margarines were formulated using the following calculated ratio of ingredients (w/w %): fat phase 85% (including 0.2% SPL or modified phospholipid [MPL] and 0.2% GMS as emulsifier); aqueous phase 15% (including 0.5% salt as preservative and taste improver) (Pande et al. 2013). Oil, a blend of fraction of palm stearin with RBO (40:60) with a melting point of 35 °C, and emulsifiers were mixed and heated at 40 °C to remove any crystal into a blender. The temperature of the aqueous phase was also maintained at 40 °C. Then water was poured in dropwise to form a uniform and stable emulsion with continuous stirring. Then the temperature of the emulsion was cooled down at a rate of 2 °C/min until its crystallization temperature of 24 °C and kept for 5 min. The margarine was again reheated at 31 °C to remove any kind of crystal through vigorous mixing. The temperature was again cooled down and stored at refrigerator.

2.10 Physical Properties of Produced Margarine

2.10.1 Softness

Softness of margarine samples was determined by Haighton (1959) method as modified by Laia et al. (2000) with a penetrometer (Stanhope-Seta surrey, England) using the cone-form penetration body with an apical angle of 40°. The penetrating cone was placed just above the surface of the sample before it was released. The depth of the penetration in 0.1 mm increments was read on the dial after 5 s of contact.

2.10.2 Color

Color of margarine samples was measured using Konica Minolta Color reader CR-10 (Japan) portable colorimeter. Sample color was taken using condition of the standard illuminant D65 and 10 degree observer. Three different parameters were recorded named as **L** (lightness from black to white), **a** [green (–) and red (+)], and **b** [bluish color (+) and yellowish color (–)] (Yilmaz and Ögütçü 2014).

2.10.3 Free Fatty Acid (FFA)

FFA was determined according to the method of Cocks and van Rede (1966).

2.10.4 Crystal Morphology

Crystal morphology of margarine samples was observed using Nikon Eclipse E200 (Japan) polarizing light microscope (PLM) with an attached Nikon DS-Fi2 digital camera. The photomicrograph of the crystals was recorded at a 500× magnification and images were captured (Zhang et al. 2013).

2.11 Statistical Analysis

Statistical analysis was performed using analysis of variance (ANOVA) and the means were compared across groups by Tukey test. The significant differences were determined at $p \leq 0.05$.

3 Results and Discussion

3.1 Fatty Acid Composition (FAC)

Table 1 shows the fatty acid composition of original soyphospholipid (SPL) and castor oil (CO) while Table 2 shows the fatty acid composition of modified soyphospholipids with specific time interval.

There is an unusual drop in the hydroxy fatty acid in SPL at 12 h which is difficult to explain. The percentage incorporation of hydroxy fatty acid was increased again at 24 h reaction. There is a reduction of unsaturated fatty acid percentage in terms of oleic, linoleic, and linolenic acids which helps to improve the interfacial activity of SPL and magnify the emulsion ability.

Table 1 FAC of original soyphospholipid (SPL) and castor oil (CO)

Samples	FAC (Area %)					
	C _{16:0}	C _{18:0}	C _{18:1}	C _{18:2}	C _{18:3}	C _{18:1OH}
SPL	25.14	3.25	16.71	50.48	4.41	–
CO	1.13	1.30	3.71	4.52	0.42	88.92

C_{16:0}, palmitic acid; C_{18:0}, stearic acid; C_{18:1}, oleic acid; C_{18:2}, linoleic acid, C_{18:3}, linolenic acid; C_{18:1OH}, ricinoleic acid

3.2 Antioxidant Activity

Antioxidant property of MSPLs is improved in respect of DPPH and TPC (Table 3).

3.3 Surface Tension

The surface tension of MSPL is decreased in comparison with original SPL that indicates the surface activity or interfacial activity of MSPL should be considerably more improved for better emulsion (Table 4).

3.4 Physical Property of Produced Margarine

Produced margarine using hydroxy fatty acid rich SPL as emulsifier shows softer texture and lighter color than original one. The FFA content is not hampered in both cases (Table 5).

3.5 Crystal Morphology of Margarine

The crystal morphology by PLM has showed a smooth and homogenous mixture in both MSPL and SPL. A denser network-like structure shows better antioxidant property in MSPL because it entrapped large number of oil than SPL (Figs. 1 and 2).

Table 2 FAC of modified soyphospholipid (MSPL)

Samples	FAC (Area %)							
	C _{16:0}	C _{18:0}	C _{18:1}	C _{18:2}	C _{18:3}	C _{18:1OH}	C _{18:2OH}	C _{18:1OH}
MSPL (6 h)	17.05 ± 0.05 ^a	2.25 ± 0.06 ^a	12.7 ± 0.11 ^a	34.74 ± 0.08 ^a	2.91 ± 0.06 ^a	29.99 ± 0.11 ^a		
MSPL(12 h)	24.15 ± 0.06 ^b	3.45 ± 0.10 ^b	14.78 ± 0.09 ^b	47.33 ± 0.07 ^b	3.79 ± 0.08 ^b	6.49 ± 0.11 ^b		
MSPL(24 h)	16.65 ± 0.09 ^c	3.69 ± 0.07 ^c	13.70 ± 0.07 ^c	35.15 ± 0.04 ^c	2.91 ± 0.08 ^c	27.53 ± 0.05 ^c		

C_{16:0}, palmitic acid; C_{18:0}, stearic acid; C_{18:1}, oleic acid; C_{18:2}, linoleic acid; C_{18:3}, linolenic acid; C_{18:1OH}, ricinoleic acid. Results have been expressed as mean ± SD (*n* = 3). Mean values in the same row with same superscript letters indicate significantly different (*p* < 0.05)

Table 3 Antioxidant activity of original SPL, CO, and MPL by DPPH scavenging effect and TPC

Samples	DPPH scavenging effect (%)	TPC (mgGAE/g)
SPL	11.19 ± 0.15 ^a	4.45 ± 0.22 ^a
Castor oil	56.79 ± 0.34 ^a	2.39 ± 0.10 ^a
6 h MSPL	47.89 ± 0.40 ^a	1.24 ± 0.03 ^{a,b}
12 h MSPL	44.28 ± 0.55 ^a	1.41 ± 0.23 ^{a,b}
24 h MSPL	45.38 ± 0.45 ^a	0.77 ± 0.02 ^a

Results have been expressed as mean ± SD ($n = 3$). Mean values in the same column with same superscript letters indicate significantly different ($p < 0.05$)

Table 4 Surface tension of SPL and MSPL

Samples	Surface tension (mN/m)
Original SPL	24.589 ± 0.027 ^a
6 h MSPL	21.527 ± 0.026 ^a
12 h MSPL	22.092 ± 0.029 ^a
24 h MSPL	21.937 ± 0.027 ^a

Water = 69.634 ± 0.024. Mean values in the same column with same superscript letters indicate significantly different ($p < 0.05$)

Table 5 Softness (penetration), FFA, and color

Samples of margarine	Penetration (0.1 mm)	FFA (% as oleic acid)	Color L (Lightness)	Color a (Redness)	Color b (Yellowness)
Using SPL	54 ± 2.0 ^a	0.05 ± 0	78.46 ± 1.34 ^{a,c}	-0.7 ± 0.17 ^{a,c}	+15.46 ± 0.20 ^{a,c}
Using MSPL	72 ± 2.0 ^a	0.05 ± 0	76.8 ± 0.36 ^{a,b}	-1.03 ± 0.05 ^{a,c}	+12.06 ± 0.11 ^{a,c}

Results have been expressed as mean ± SD ($n = 3$). Mean values in the same row and same column with same superscript letters indicate significantly different ($p < 0.05$)

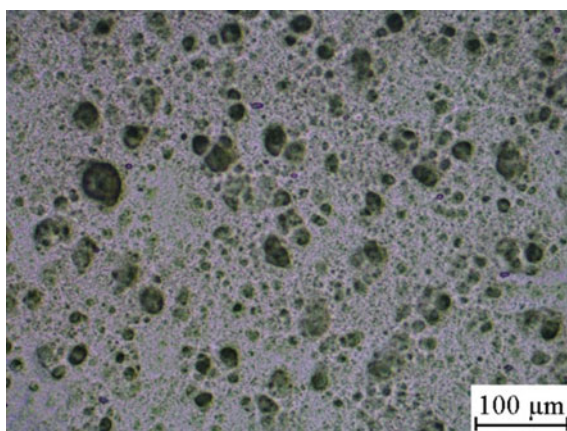
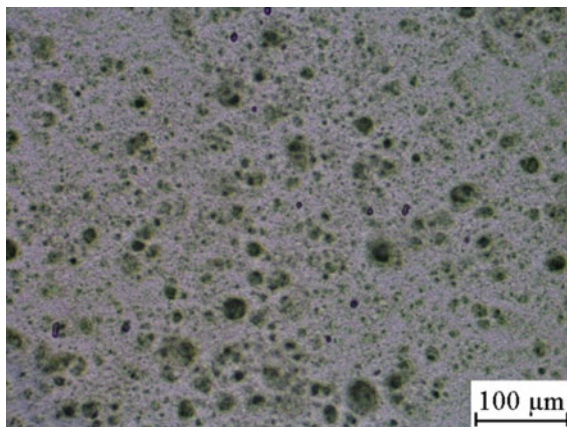
Fig. 1 MSPL

Fig. 2 SPL

4 Conclusion

The present study concerning the incorporation of hydroxy fatty acid or ricinoleic acid in SPL by enzymatic interesterification process with 1:4 molar proportion is expedient approach for producing better emulsifier in margarine preparation. The antioxidant property is significantly improved whereas the surface tension is decreased which defines the enhanced interfacial activity for better emulsion. The utilization of hydroxy acid rich SPL as emulsifier in margarine preparation indicates some differences in properties when compared with non-hydroxy acid SPL. The hydroxy acid rich SPL produces relatively much softer margarine and also lighter color due to transparency characteristics of hydroxy fatty acid.

Acknowledgements This work was financially supported by University Grants Commission under the scheme Rajiv Gandhi National Fellowship. I am also thankful to Department of Chemical Technology, University of Calcutta for analysis of surface tension and to HoD, Department of Geology, Presidency University for crystal morphology of my samples. The authors have declared no conflict of interest.

I express my deepest gratitude for the cooperation for providing me soyphospholipid from Ruchi Soya Industries Ltd., Nagpur, and palm stearin from Budge Budge Refineries Limited, Kolkata, India for my research work.

References

- Blois MS (1958) Antioxidant determinations by the use of a stable free radical. *Nature* 181(74):1199–1200
- Chakrabarty MM (2003) Margarine, shortenings, spreads. In: Chakrabarty MM (ed) *Chemistry and technology of oils and fats*. Allied Publishers Pvt. Limited, Delhi, India, pp 500–523
- Chen PS, Toribara TY, Warner H (1956) Microdetermination of phosphorus. *Anal Chem* 28(11):1756–1758

- Chiplunkar PP, Pratap AP (2017) Ultrasound assisted synthesis of hydroxylated soybean lecithin from crude soybean lecithin as an emulsifier. *J Oleo Sci* 66(10):1101–1108
- Cocks LV, van Rede C (1966) Laboratory handbook for oils and fats analyses. Academic Press, London, pp 113–117
- Conceição MM, Candeia RA, Silva FC, Bezerra AF, Fernandes VJ Jr, Souza AG (2007) Thermoanalytical characterization of castor oil biodiesel. *Renew Sust Energy Rev* 11(5):964–975
- Das S, Bhattacharyya DK (2006) Preparation and surface-active properties of hydroxy and epoxy fatty acid-containing soy phospholipids. *J Am Oil Chem Soc* 83(12):1015–1020
- Haighton AJ (1959) The measurement of hardness of margarine and fats with cone penetrometer. *J Am Oil Chem Soc* 36(8):345–348
- Laia OM, Ghazalia HM, Cho F, Chong CL (2000) Physical and textural properties of an experimental table margarine prepared from lipase-catalysed transesterified palm stearin: palm kernel olein mixture during storage. *Food Chem* 71(2):173–179
- Litchfield C (1972) Extraction, isolation, measurement and fatty acid analysis. In: Litchfield C (ed) Analysis of triglycerides. Academic Press, New York, pp 17–35
- Nyankson E, Demir M, Gonen M, Gupta RB (2016) Interfacially-active hydroxylated soybean lecithin dispersant for crude oil spill remediation. *ACS Sustain Chem Eng* 4(4):2056–2067
- Ogunniyi DS (2006) Castor oil: a vital industrial raw material. *Bioresour Technol* 97(9):1086–1091
- Pande G, Akoh CC, Shewfelt RL (2013) Utilization of enzymatically interesterified cottonseed oil and palm stearin-based structured lipid in the production of trans-free margarine. *Biocatal Agr Biotech* 2(1):76–84
- Saha G, Bhattacharyya DK, Ghosh M (2018) Enzymatic interesterification of blend of soyphospholipid and coconut oil. *Asian J Chem* 30(7):1421–1423
- Schmidt JC, Orthoefer F (1985) Lecithin in baking applications. In: Szuhaj BF, List GR (eds) Lecithins. Am Oil Chem Soc Press, Champaign, pp 203–211
- Sudheesh S, Ahmad J (2013) Effect of Wilhelmy plate material on hysteresis of langmuir film isotherms. *Asian J Chem* 25(7):3535–3538
- Vijeeta T, Reddy JRC, Rao BVSK, Karuna MSL, Prasad RBN (2004) Phospholipase-mediated preparation of 1-ricinoleoyl-2-acyl-snglycero-3-phosphocholine from soya and egg phosphatidylcholine. *Biotechnol Lett* 26(13):1077–1080
- Yılmaz E, Ögütçü M (2014) Properties and stability of hazelnut oil organogels with beeswax and monoglyceride. *J Am Oil Chem Soc* 91(6):1007–1017
- Yu L, Perret J, Harris M, Wilson J, Haley S (2003) Antioxidant properties of bran extracts from “Akron” wheat grown at different locations. *J Agr Food Chem* 51(6):1566–1570
- Zhang X, Li L, Xie H, Liang Z, Su J (2013) Effect of temperature on the crystalline form and fat crystal network of two model palm oil-based shortenings during storage. *Food Bioprocess Tech* 7(3):887–900

Effect of Medicinal Plants on Biofilm-Forming *Staphylococcus aureus* from Tertiary Health Care Hospital and Characterization of Biofilm-Associated Extracellular Polymeric Substances (EPS)



Rimashree Baishya and Soma Banerjee

Abstract Biofilm formed by microorganism exhibits increased resistance to antimicrobial agents and to the host immune system due to the extracellular polymeric substance (EPS) matrix in which the microorganisms are engrained and act as a shield to the microbes. The present work focuses on the search of an alternative approach for biofilm inhibition using plant products. In the present study, anti-bacterial activity of *Allium sativum* (garlic), *Curcuma longa* (haldi), *Ocimum sanctum* (tulsi), *Zingiber officinale* (ginger), and *Azadirachta indica* (neem) ethanolic extracts was studied against 30 clinically strong biofilm-forming samples. All the strains were susceptible to *Curcuma longa*, *Azadirachta indica*. Two plants were then selected to study the anti-biofilm activity against the strong biofilm strain *Staphylococcus aureus* (QS1). The effect of the plant extracts on biofilm adherence was studied at concentration of 128**MIC*, 256**MIC*, and 512**MIC*. The major components of EPS were analyzed and compared with control. SDS-PAGE analysis showed the presence of different bands with distinct difference in the band size in the plant-treated samples. The biofilm adherences showed a dose-dependent increase of activity with 13–40% reduction. QS1 treated with *Curcuma longa* and *Azadirachta indica* extracts resulted in significant degradation of the EPS components. Thus, the commonly known antimicrobial plant hinders the formation of biofilm by degrading its EPS components with its potential anti-biofilm constituents.

Keywords Antimicrobial · Biofilm · Extracellular polymeric substance · *Staphylococcus aureus*

R. Baishya (✉) · S. Banerjee

Department of Biotechnology, Heritage Institute of Technology, Chowbaga Road, P.O. Anandapur, East Kolkata Township, Kolkata, West Bengal 700107, India
e-mail: reemaorbabu@gmail.com

S. Banerjee

e-mail: soma.banerjee@heritageit.edu

© Springer Nature Singapore Pte Ltd. 2021

D. Ramkrishna et al. (eds.), *Advances in Bioprocess Engineering and Technology*,
Lecture Notes in Bioengineering,
https://doi.org/10.1007/978-981-15-7409-2_19

1 Introduction

Biofilm is defined as community of cells irreversibly attached to any surface enclosed in a complex exopolymeric substance (EPS). Extracellular polymeric substances (EPS) produced by microorganisms are a complex mixture of biopolymers primarily consisting of polysaccharides, as well as proteins, nucleic acids, and lipids. EPS make up the intercellular space of microbial aggregates and form the structure and architecture of the biofilm matrix. The key functions of EPS comprise the mediation of the initial attachment of cells to different substrata and protection against environmental stress and dehydration (Vu 2009). Biofilm possess various problems in medicinal devices, food industry, water pipes, etc. as the biofilm-producing bacteria becomes resistant to antimicrobial agents due to prolonged use of antibiotics (Flemming and Wingender 2010). Hence, the development of environmentally friendly anti-biofilm molecules has gained major interest among researchers as an alternative approach for biofilm treatments.

Plant-based compounds have gained widespread interest in health care industry due to the unlimited ability to synthesize bioactive compounds as secondary metabolites with various pharmacological properties and its ability to boost the immune system. The present work focuses on the search of using plant products for biofilm inhibition from commonly known medicinal plants.

2 Materials and Methods

2.1 Materials and Bacterial Strains

All the chemicals used for the experiments were purchased from Himedia, India. The bacterial stains were collected from IPGMER, Kolkata and RGKAR Medical College and Hospital, Kolkata.

2.2 Preparation of Medicinal Plant Extracts

The plants *Allium sativum* (garlic), *Curcuma longa* (haldi), *Ocimum sanctum* (tulsi), *Zingiber officinale* (ginger), and *Azadirachta indica* (neem) were collected from college premise or purchased from the local market. The plant was identified from the Department of Botany, University of Calcutta, India. The matured leaves and fresh rhizomes were dried at room temperature and were powdered using a grinder to coarse powder, packed into Soxhlet column, and then extracted with 70% ethanol for 24 hours (h). The extracts were then filtered with WhatMan No. 1 filter paper

(24 cm). The filtrates were then concentrated and were evaporated to dryness in water bath. The obtained crude extract was stored in airtight container in the refrigerator at -4°C for further studies.

2.3 Antimicrobial Activity

The antimicrobial activities of the plant extracts were determined against 30 strong biofilm-forming clinical strains collected from tertiary health care hospital by agar well diffusion method. Mueller–Hinton Agar (MHA) plates were prepared and the sample cultures were swabbed uniformly using sterile cotton swabs. Plates were incubated at 37°C for 24 h with the plant extracts in the agar wells (Balouiri et al. 2015).

2.4 Study of Anti-biofilm Activity of Plant Extract

One of the strong biofilm strains, *Staphylococcus aureus* QS1, was further studied along with reference strain *Staphylococcus aureus* ATCC 25923. The effect of all the plant extracts on biofilm inhibition was studied at concentration of 128^*MIC , 256^*MIC , and 512^*MIC of the extracts. Bacterial cultures with 1×10^5 CFU/ml concentration were transferred to a 96-well polystyrene microtiter plate treated with different concentrations of plant extracts and incubated for 24 h at 37°C . Control was prepared in TSB without plant extracts. After 24 h, the culture medium was discarded, and the wells were washed twice with distilled water to remove the planktonic cells. Plates were completely dry, and 1% crystal violet solution was added to each well. The wells were then washed with distilled water and acetic acid was added to each well. The optical density (OD) was measured at 570 nm (Quave et al. 2008).

2.5 EPS Production

The selected strain of *Staphylococcus aureus* QS1 culture was added in freshly prepared sterile nutrient broth and was treated with *Curcuma longa* (haldi) and *Azadirachta indica* (neem) plant extracts of different concentrations, 128^*MIC , 256^*MIC , and 512^*MIC . Vancomycin was used as the standard antibiotic with control, i.e., without the addition of plant extracts. The samples were incubated at 37°C for 24 h at 120 rpm. Samples were centrifuged and the supernatants were collected to which ice cold isopropanol was added and incubated overnight. The incubated samples were centrifuged and EPS pellets were collected. The EPS of samples was air dried and stored for further analysis (Teapaisan et al. 2016).

2.6 Quantification of EPS Components

EPS was quantified by measuring proteins by Lowry's method and carbohydrates by Anthrone method (Teaupaisan et al. 2016).

2.7 Emulsifying Activity

The EPS solutions were heated and then cooled and volume was made up to 2 ml using then phosphate-buffered saline (PBS). Olive oil was added and vortexed for 1 min and absorbance was measured at 540 nm after 30 min (Kavita et al. 2014).

2.8 Protein Profile Analysis by SDS-PAGE

EPS proteins were analyzed by sodium dodecyl sulfate polyacrylamide gel electrophoresis (SDS-PAGE). Electrophoresis were performed in 5% stacking gel and 10% separating gel in Tris-Glycine-SDS buffer and was run with a constant voltage of 20 V/cm. The gels were then stained with Coomassie Brilliant Blue R-250 (Sambrook et al. 1989). The molecular weight of the proteins bands was compared with the standard protein ladder (10–245 kDa) to know its respective sizes.

3 Results and Discussion

3.1 Antimicrobial Activity

The antimicrobial potential of all the five plant extracts against 30 strong biofilm-forming clinical strains was evaluated according to their zone of inhibition. All the 30 strains were susceptible to *Curcuma longa* (haldi), *Azadirachta indica* (neem), 71% samples were found susceptible to *Ocimum sanctum* (tulsi) and *Zingiber officinale* (ginger), and 93.33% were susceptible to *Allium sativum* (Garlic) (Fig. 1).

3.2 Study of Anti-biofilm Activity of Plant Extract

The anti-biofilm activity of plant extracts on the selected strain *S. aureus* QS1 by crystal violet method is shown in Fig. 2. For tulsi, there is a gradual increase of anti-adherence activity from 10 to 38%; for neem, the anti-adherence activity was



Fig. 1 Number of strains susceptible to the minimum volume (50 μ l) of plant extracts

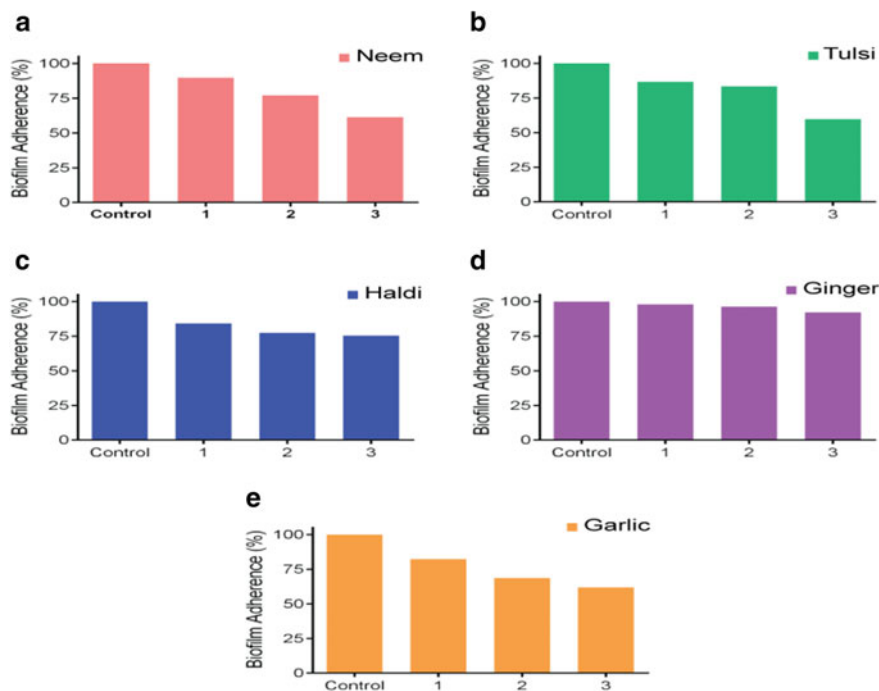


Fig. 2 Percentage inhibition of biofilm adherence of *S. aureus* QS1 treated plant extracts **a** Neem, **b** Tulsi, **c** Haldi, **d** Ginger, **e** Garlic at different concentrations (1—128**MIC*, 2—256**MIC*, 3—512**MIC*). ($n = 3$)

13 to 40%; for haldi, it shows an increase from 15 to 24%; and garlic has a 17–38% increase of anti-adherence activity with the increase in the concentrations from 128**MIC*, 256**MIC*, 512**MIC*. However, ginger showed the least anti-adherence activity from 2 to 7% increase.

A number of studies have confirmed the anti-biofilm effects of different plant extracts and its phytochemicals. Quave et al. 2008 established the inhibition effects of Italian medicinal plant extracts on planktonic growth, biofilm formation, and adherence of methicillin-resistant *Staphylococcus aureus* biofilm. Another group found

that grapefruit juice has an anti-biofilm effect against *E. coli* and *S. typhimurium* by interfering with quorum sensing (Truchado et al. 2015).

3.3 Quantification of EPS Components

The amount of the protein and carbohydrate of the control and treated EPS samples was measured at the optical densities of 660 nm and 620 nm, respectively. The inhibition percentage of the given samples was calculated and was observed that there was a gradual decrease in the amount of protein (Fig. 3) and carbohydrate (Fig. 4) in treated EPS compared to control with increase in plant extracts concentration.

Carbohydrate and proteins were the main components of EPS matrix. In the present study, the percentage of carbohydrate and protein present in the EPS was relatively less after treatment with plant extracts. Gandhi et al. 2017 reported similar results when *Sesbania grandiflora* extract was treated against *Staphylococcus aureus*.

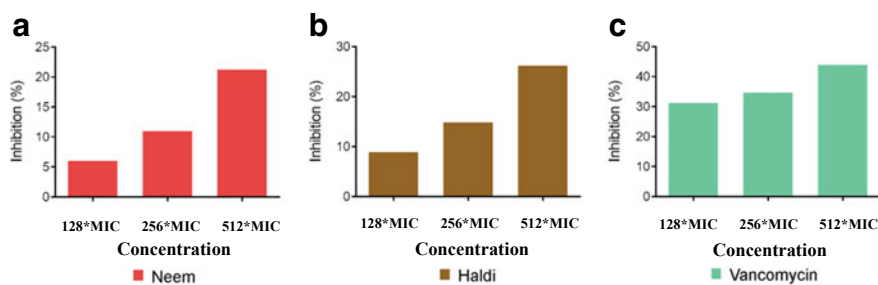


Fig. 3 Estimation of percentage reduction of protein with respect to control **a** neem, **b** haldi, **c** vancomycin ($n = 3$)

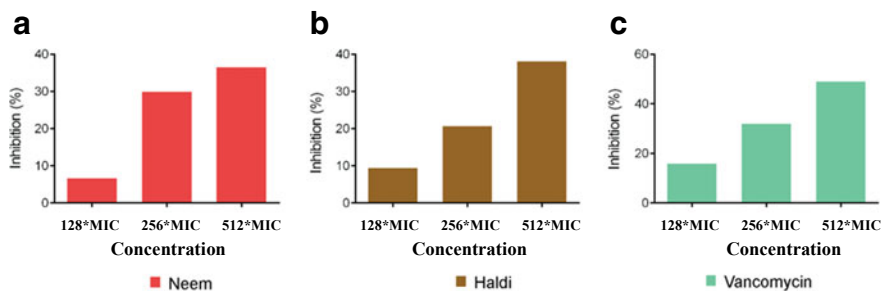


Fig. 4 Estimation of percentage reduction of carbohydrate content with respect to control **a** neem, **b** haldi, **c** vancomycin

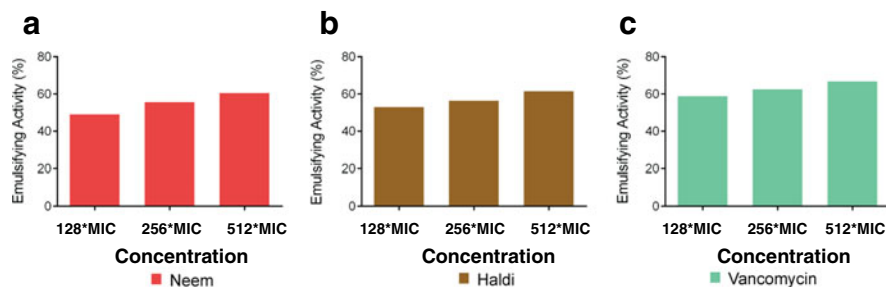


Fig. 5 Estimation of emulsification activity with respect to increasing dose concentration of **a** neem, **b** haldi, **c** vancomycin

3.4 Emulsifying Activity

The percentages of emulsifying activity are 49–60% for neem and 52–61% for haldi, respectively, as compared to 59–67% for vancomycin (Fig. 5).

3.5 Protein Profile Analysis by SDS-PAGE

A single band that migrated at a position corresponding to 240 kDa was reproducibly detected by SDS-PAGE of the EPS protein extract from the biofilm formed by bacteria strain *S. aureus* QS1 (lane 5) but not from the planktonic total protein of the cells of the same strain (lane 2). Bands of similar mobility were also detected in plant extracts treated (lane 3 and lane 4 respectively), however the expression level of the protein was negligible (Fig. 6).

Many protein members like Bap (Cucarella et al. 2001), Esp (Shankar et al. 2002), LapA (Hinsa et al. 2003), BapA (Latasa et al. 2006), etc. play an important role in early adhesion of *S. aureus* biofilm. In the present work, the protein at 240 kDa is mainly present in the EPS of the biofilm, explaining that these proteins are very important for biofilm formation. Without the presence of these proteins, biofilms cannot be formed as it has key role in intercellular interactions in the accumulation phase after the bacterial cells adhere to the surface. Thus, decreased protein expression might be an indication of decrease in biofilm formation.

4 Conclusion

This study suggests that all the five plant extracts possess phytochemicals with potential antimicrobial properties against biofilm-forming strains. The study showed evidence that the ethanolic extracts of *Curcuma longa* (haldi) and *Azadirachta*

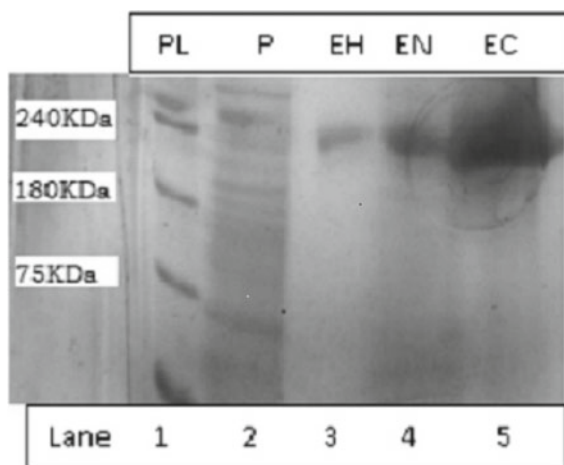


Fig. 6 SDS-PAGE of protein extracts of *Staphylococcus aureus* QS1 with PL-protein ladder (lane 1), P-planktonic total protein (lane 2), EH-EPS Haldi treated (lane 3), EN-EPS Neem treated (lane 4), and EC-EPS control (lane 5) (lanes from left to right)

indica (neem) have high anti-biofilm and anti-bacterial activity property against *S. aureus*. Thus, alternative agents can be identified to treat biofilm by elucidating the anti-biofilm agents from the two plant extracts.

Acknowledgements The authors wish to acknowledge the authorities of Heritage Institute of Technology for providing necessary technical support for this work. The authors are thankful to Department of Science and Technology and Biotechnology, West Bengal for financial support.

References

- Balouiri M, Sadiki M, Ibsouda SK (2015) Methods for in vitro evaluating antimicrobial activity: a review. *J Pharma Anal* 6:71–79
- Cucarella C, Solano C, Valle J, Amorena B, Lasa I, Penades JR (2001) Bap, a *Staphylococcus aureus* surface protein involved in biofilm formation. *J Bacteriol* 183:2888–2896
- Flemming HC, Wingender J (2010) The biofilm matrix. *Nat Rev Microbiol* 8:623–633
- Gandhi AD, Vizhia DK, Lavanyaa K, Kalpanab VN, Rajeswarib VD, Babujanathanam R (2017) *In vitro* anti-biofilm and anti-bacterial activity of *Sesbania grandiflora* extract against *Staphylococcus aureus*. *Biochem Biophys Rep* 12:193–197
- Hinsa SM, Espinosa-Urgel M, Ramos JL, O'Toole GA (2003) Transition from reversible to irreversible attachment during biofilm formation by *Pseudomonas fluorescens* WCS365 requires an ABC transporter and a large secreted protein. *Mol Microbiol* 49:905–918
- Kavita K, Singh VK, Mishra A, Jha B (2014) Characterisation and anti-biofilm activity of extracellular polymeric substances from *Oceanobacillus iheyensis*. *Carbohydr Polym* 101:29–35
- Lataca C, Solano C, Penades JR, Lasa I (2006) Biofilm-associated proteins. *C R Biol* 329:849–857

- Quave CL, Plano LRW, Pantuso T, Bennett BC (2008) Effects of extracts from Italian medicinal plants on planktonic growth, biofilm formation and adherence of methicillin-resistant *Staphylococcus aureus*. *J Ethnopharmacol* 118:418–428
- Sambrook J, Fritsch EF, Maniatis T (1989) *Molecular cloning: a laboratory manual*, 2nd edn. Cold Spring Harbor Laboratory Press, New York
- Shankar N, Baghdayan AS, Gilmore MS (2002) Modulation of virulence within a pathogenicity island in vancomycin-resistant *Enterococcus faecalis*. *Nature* 417:746–750
- Teanpaisan R, Kawsud P, Pahumunto N, Puripattanavong J (2016) Screening for antibacterial and antibiofilm activity in Thai medicinal plant extracts against oral microorganisms. *J Tradit Complement Med* 7(2):172–177
- Truchado P, Larrosaa M, Castro-Ibáñez I, Allendea A (2015) Plant food extracts and phytochemicals: their role as Quorum sensing inhibitors. *Trends Food Sci Technol* 43:189–204
- Vu B (2009) Bacterial extracellular polysaccharides involved in biofilm formation. *Molecules* 14:2535–2554

Synthesis and Characterization of MgO Nanoparticle and Its In Vitro Cytotoxic Effect on Erythrocytes



Bitopan Boro, Anup Kr. Nath, Manash Barthakur, and Pankaj Kalita

Abstract Nanomaterials have moved into modern biological and medicinal implications for the advancement of biomedical applications. Magnesium oxide is a basic oxide of interest that has many applications in catalysis, adsorption, and synthesis of refractory ceramics as well as in the biological system. Magnesium oxide nanoparticles are characterized with a wide variety of applications and are mass-produced throughout the world. However, questions remain regarding its safety. There has been paucity of toxicology research on its side effects, especially under in vivo conditions. The present paper aims at evaluating the toxicity of chemically synthesized magnesium oxide nanoparticles in erythrocytes or red blood cells (RBCs). The synthesized MgO nanoparticles were characterized using UV-Vis spectroscopy, DLS, FTIR, and TEM analysis. The synthesized MgO showed hemolytic activity in a dose-dependent sequence. Size and charge characteristics of MgO observed supposed to be the influencing factor for the toxicity to the erythrocytes. Functionalization and surface modification of the synthesized MgO will help in its better applicability in biomedical science.

Keywords Nanoparticle · MgO · Erythrocytes · Cytotoxicity

B. Boro · P. Kalita (✉)

Department of Biophysics, Pub Kamrup College, Baihata Chariali, Kamrup, Assam, India
e-mail: kalita.pankaj9@gmail.com

B. Boro

e-mail: bitopanboro@rediffmail.com

A. Kr. Nath

Department of Physics, Cotton University, Guwahati, Assam, India
e-mail: anup.tu@gmail.com

M. Barthakur

Department of Zoology, Pub Kamrup College, Baihata Chariali, Kamrup, Assam, India
e-mail: researchpkc@gmail.com

© Springer Nature Singapore Pte Ltd. 2021

D. Ramkrishna et al. (eds.), *Advances in Bioprocess Engineering and Technology*,
Lecture Notes in Bioengineering,
https://doi.org/10.1007/978-981-15-7409-2_20

1 Introduction

Nanoparticle research is a fascinating branch of science dealing with nanoscale level of materials at the dimension less than 100 nm (Yeh et al. 2012). Nanoparticles have gained a broad interest in recent years because of their distinctive physical and chemical properties such as mechanical stability, higher damping property, and high strength with good thermal conductivity (Gary and Luan 2001). Magnesium oxide (MgO) is a homomorphous chemical structure with rock salt structure (FCC), the Mg^{2+} occupies the octahedral sites within the anion closed packed structure, and its ionic constituents comprise a relatively small number of electrons. It has simple crystal arrangement and ideal ionicity, which leads MgO to form stunning foundation for the construction of efficient nanostructures (Wahab et al. 2007). Due to the high thermal, high surface reactivity and high chemical stability with the catalytic properties, the magnesium oxide nanoparticles make it a promising material for the application in therapeutic strategies like antibacterial, antithrombotic properties, etc. (Basit et al. 1998; Richard et al. 2000; Schram and Stehouwer 2005). Biodegradable and low-toxicity MgO NPs express highly desirable properties for cancer labeling (Di et al. 2012). Studies reveal that nanoparticles are having altered size, shape, and surface chemistry in comparison to that of parent compound. Moreover, among the metal oxide nanoparticles, MgO is particularly remarkable as an eco-friendly and cheapest material for large-scale use (Kumaran et al. 2015). In the present study, cytotoxicological effect of MgO nanoparticles was aimed to be evaluated in vitro in erythrocytes as it is the first line of interacting cells in the body system for accessing the sensitivity of external exposure. In the blood circulatory system, erythrocytes are abundantly present and due to its properties like biocompatibility, biodegradability, and long circulating half-life, the erythrocytes are broadly used as a biomarker for any foreign stimuli in the body system. In this paper, synthesis and characterization of MgO nanoparticles and its cytotoxic effects on erythrocytes are documented. This study will confirm the usability of MgO nanoparticle in further studies where animals including human being may come in contact with the MgO nanoparticles. Functionalization of MgO may be required for its enhanced usability.

2 Materials and Method

2.1 Synthesis and Characterization of MgO NPs

Magnesium oxide (MgO) nanoparticles were synthesized using magnesium nitrate ($MgNO_3 \cdot 6H_2O$) and sodium hydroxide (NaOH) as precursor compound as described by Wahab et al. (2007) with some modifications. Briefly, 100 ml of 0.2 M magnesium nitrate was vigorously stirred in a magnetic stirrer at temperature of 60 °C for 4 h and 0.5 M of NaOH solution was slowly added dropwise to the magnesium nitrate solution until the pH of the solution reaches 12. Temperature, concentration

of parent and stabilizing agent, and pH was maintained constantly as observed in standardization process. Occurrence of a white precipitate was observed indicating the completion of the reaction of MgO compound. The precipitate was filtered and washed with distilled water. The solution was centrifuged at 3000 rpm for 5 min and the precipitate was dried at 60 °C for 7 h. The white powder is grinded vigorously. However, the synthesis conditions were optimized for the current reaction by varying various parameters. Various concentrations of MgNO₃, ranging from 0.2 M to 0.5 M, were used with volume 50 ml. The mixture was stirred continuously using a magnetic stirrer varying the stirring duration from 3 to 5 h and the pH was maintained at values of 9, 10, 11, and 12 using 0.5 M NaOH solution. The reaction temperature was maintained at 60 and 80 °C. The same temperature at which synthesis was carried out was used for overnight drying at 60 °C of the precipitate obtained. The absorbance peak was observed using a UV-Vis spectrophotometer (Eppendorf Biospectrometer). The band gap (E_g) for this prepared nanoparticles is estimated by Tauc's equation $(\alpha h\nu)^2 = A(h\nu - E_g)$, where $h\nu$ is the photon energy, α is the absorption coefficient, and A is a constant relative to the material. The graph of $(\alpha h\nu)^2$ versus $h\nu$ was plotted by extrapolating the linear portion of the curve to horizontal axis in which $(\alpha h\nu)^2 = 0$ in Fig. 1 (inset). The curve indicates that the value of the direct band gap (E_g) is about 3.89 eV (Khanahmadzadeh et al. 2015). Further, particle size distribution pattern was observed using dynamic light scattering technique (DLS) (Malvern; Nano-zs90) and ethanol is used as a dispersant at temperature of 30 °C. Molecular and structural characterization of MgO nanoparticles was characterized by Fourier transform infrared (FTIR) spectroscopy and transmission electron microscopy (TEM).

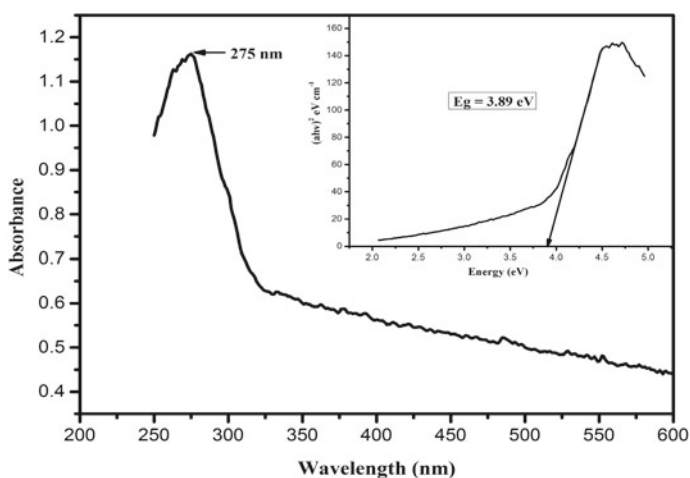


Fig. 1 UV-Vis spectrum of MgO nanoparticles. Absorption peak was observed at 275 nm and band gap was determined as 3.89 eV (as shown in inset figure)

2.2 Preparation of RBCs for the *in Vitro* Experiment

Blood samples were freshly collected from the medical laboratory technician course laboratory of Pub Kamrup College, Assam, India from five healthy human subjects. Erythrocytes were separated using standard procedure and kept in a special buffer as described in previous literature (Devi et al. 2016).

2.3 *In Vitro* RBCs Cytotoxic Evaluation of MgO NPs

RBC cells are separated by dissolving PBS buffer (pH = 7.4) with equal ratio and centrifuged at 3000 rpm for 5 min. Three different concentrations of MgO NPs, viz., 5, 15, and 25 mg/ml were treated with 500 μ l of RBCs in equal volume and incubated for 24 h at 37 °C. Water in PBS buffer is considered as negative control and dH₂O remains blank. The reaction mixture was centrifuged at 900 rpm for 5 min. and the supernatant was used for spectrophotometric measurement using UV-Vis spectrophotometer (Eppendorf Biospectrometer).

2.4 Microscopic Observation

After 24 h of incubation, precipitated erythrocytes were stained with Leishman stain using standard protocol for further microscopic observation. Briefly, treated blood smear was dried and working Leishman stain was used to stain the blood smear. Excess stain was washed out with distilled water and slides were dried and observed and microphotographs were taken by using a CCD camera attached microscope (Labomed LX300) (Devi et al. 2016).

3 Results and Discussions

3.1 Spectrophotometric Characterization of Prepared MgO Nanoparticles

Absorption of the synthesized MgO nanoparticles was measured in the range of 250–600 nm in the UV-Vis spectrophotometer and observed as shown in Fig. 1. A sharp absorption peak was observed at wavelength 275 nm and the linear curve indicates the uniformity of the synthesized nanoparticles. The band gap is found to be 3.89 eV and is shown in Fig. 1.

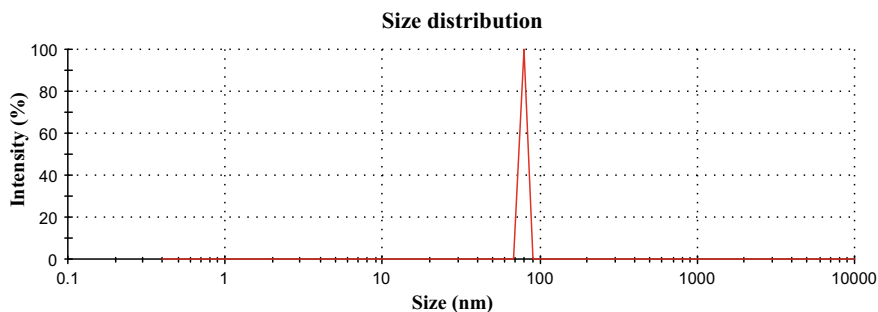


Fig. 2 Average particle size analysis of MgO NPs

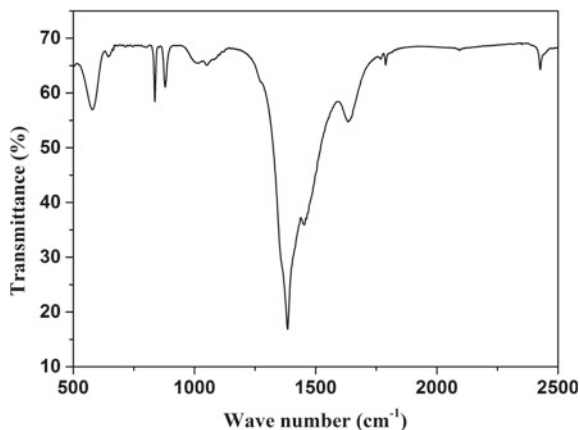
3.2 Particle Size Analysis

Particle size analysis was done by dynamic light scattering (DLS) technique as shown in Fig. 2. The particle size analysis has absolutely confirmed that the synthesized MgO nanoparticles are in the nano size form. The average particle size of synthesized MgO nanoparticles is 78.82 nm at intensity of 100%.

3.3 Fourier Transform Infrared (FTIR) Spectroscopy Analysis of MgO Nanoparticle

The formation of MgO nanoparticles has been confirmed from FTIR spectrum as shown in Fig. 3. The peak at 580 cm^{-1} is assigned to the Mg-O stretching vibration in $\text{Mg}(\text{OH})_2$. The absorption peak at 1400 cm^{-1} is due to the bending vibration of (OH) bond. The peak at 878 cm^{-1} signifies the out-of-plane aromatic stretching of MgO

Fig. 3 FTIR pattern of synthesized MgO nanoparticle



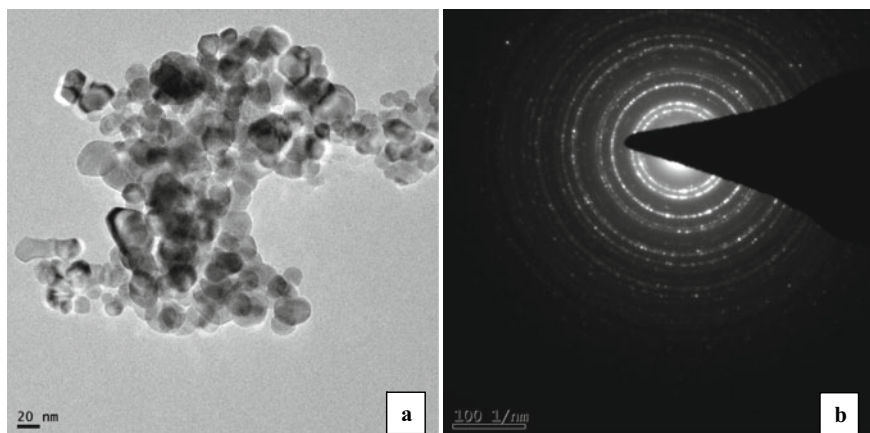


Fig. 4 **a** shows the formation of MgO nanoparticles. Figure shows nanoparticles of almost uniform size and shape having diameter 60–80 nm. The MgO nanoparticles are observed as served spherical shaped and uniform grains. **b** shows the selected area electron diffraction pattern (SAED) of MgO nanoparticles and the white array of spots confirms the crystalline nature of the nanoparticles. Thus, both the TEM micrographs confirm the formation of highly crystalline nanoparticles

nanoparticles. All these peaks confirm that MgO nanoparticles have been formed which corroborates the result shown by TEM micrographs.

3.4 *Transmission Electron Microscopy (TEM) Analysis*

See Fig. 4.

3.5 *Evaluation of Cytotoxic Effect of MgO NPs in RBCs—an in Vitro Assay*

RBCs are found affected by dose dependence of MgO NPs but in an inverse sequence. Lowest concentration (i.e., 5 mg/ml) of MgO NPs shows highest toxicity to the RBCs in comparison to the comparatively higher concentration (i.e., 15 and 25 mg/ml) of MgO NPs. Relatively lower cytotoxicity to the RBCs was observed at the concentration of 25 mg/ml MgO NPs.

In the present study, RBCs cytotoxicity was measured by both spectrophotometric analysis and microscopic observation. Table 1 shows the measurement of concentration of hemoglobin released by the RBCs upon incubation with MgO NPs. More the concentration of hemoglobin in the solution implies more absorbance shown by the spectrophotometric measurement reflecting more damage to the RBCs, thus

Table 1 Measurement of concentration of hemoglobin release by the RBCs

Conc. of MgO NPs	5 mg/ml	15 mg/ml	25 mg/ml	-ve control
Absorbance (Mean \pm SD)	46.76 \pm 0.37b	40.93 \pm 0.93b	17.87 \pm 0.68c	2.17 \pm 0.18a

Similar alphabets show non-significance and different alphabets show significance among the group

implying RBCs cytotoxicity. Present study reveals that there is a significant ($p < 0.1$) increase of cytotoxicity caused by MgO NPs. But toxicity is higher in lower concentration of MgO treatment in comparison to the higher concentration of MgO treatment.

According to Fig. 5, density of erythrocytes is less in highest concentration of MgO NPs treated slide as well as in the lowest concentration slide treated with MgO NPs in comparison to the control sample. On the other hand, among the MgO NPs treated slides, lower concentration of MgO nanoparticle treated sample shows lower density of erythrocytes and higher concentration treated sample shows higher density of erythrocytes implying destruction of erythrocytes is inversely proportional to the concentration of MgO NPs treatment. Figure 5 also reveals that in the highest concentration, treated slide shows relatively lower number of deformed (seen as oval/spindle shaped) erythrocytes in comparison to the lowest concentration treated slide as shown by white arrow in Fig. 5.

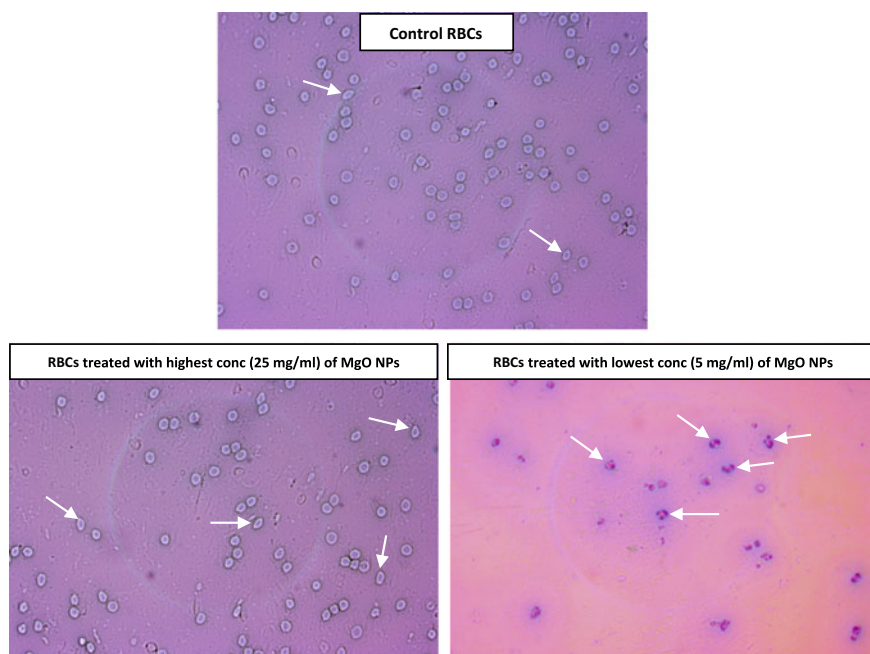


Fig. 5 Microphotographic view of negative control and highest concentration and lowest concentration treated with MgO NPs and deformity is indicated by the white arrows

With significant spectrophotometric and microscopic observation in RBCs, MgO NPs treatment is expected to yield a significant amount of hemolysis. However, there was no significant amount of hemolysis observed in higher concentration of MgO NPs. Nanoparticle can bind with the RBC membrane acting as a cementing material to the erythrocytes which enhance the RBC membranes to become stronger against the intracellular shock (Ghosh et al. 2013). But after binding the MgO nanoparticle with the RBC membrane component, functionality of the blood cell is still unclear. Because of surface characteristics, it may bind with the erythrocytes, thus preventing cell breakage. But deformed cellular morphology, as observed in Fig. 5, may be a clue to the abnormal functioning of the erythrocytes in MgO treated samples.

4 Conclusion

The present study reveals that after 24 h of treatment of MgO NPs to the RBCs the deformity of blood cell is high in low concentration of MgO NPs and low in high concentration of MgO NPs. But it is assumed that reduced incubation time may cause less harm to the RBCs. Functionalization of the MgO NPs may also eradicate the harmfulness of the MgO NPs. Further study, involving functionalization of MgO NPs with required bio-medically important bioactive molecules, may enhance the usability of MgO NPs in biomedical and pharmaceutical field of study for its advancement.

Acknowledgements Authors acknowledge the DBT sponsored Advanced Level Institutional Biotech Hub (Phase-II), Pub Kamrup College for giving full facility to perform this experiment. Thankfulness is also expressed in equal sincerity and spirit to the Principal of Pub Kamrup College. Authors also acknowledge the medical professional for helping the study in collecting the blood samples from human subjects.

Compliance with Ethical Standards

Conflicts of interest The authors declare that they have no conflict of interest.

Ethical approval All procedures performed in studies involving human participants were in accordance with the ethical standards of the Institutional Ethics Committee of Govt. Ayurvedic College, Assam, India and with the 1964 Helsinki declaration and its later amendments or comparable ethical standards.

Informed consent Informed consent was obtained from all individual participants included in the study.

References

- Basit AN, Kim HK, Blachere J (1998) Growth of highly oriented Pb(Zr, Ti)O₃ films on MgO-buffered oxidized Si substrates and its application to ferroelectric nonvolatile memory field-effect transistors. *Appl Phys Lett* 73:3941
- Devi C, Kalita P, Barthakur M (2016) An *in-vitro* study on the effect of citrate stabilized AuNP on RBC. *Mater Today Proc* 3(10):3439–3443
- Di DR, He ZZ, Sun ZQ, Liu J (2012) A new nano-cryosurgical modality for tumor treatment using biodegradable MgO nanoparticles. *Nanomed Nanotechnol Biol Med* 8(8):1233–1241
- Gary JE, Luan B (2001) Protective coatings on magnesium and its alloys—a critical review. *J Alloys Compounds* 336(1–2):88–113
- Ghosh M, Chakraborty A, Mukherjee A (2013) Cytotoxic, genotoxic and the hemolytic effect of titanium dioxide (TiO₂) nanoparticles on human erythrocyte and lymphocyte cells *in-vitro*. *J Appl Toxicol* 33(10):1097–1110
- Khanahmadzadeh S, Enhessari M, Solati Z, Mohebalizadeh A, Alipouramjad A (2015) Synthesis, characterization and optical band gap of the Co₂TiO₄ nanoparticles. *Mat Sci Semicon Proc* 31:599–603
- Kumaran R, Choi YK, Singh V, Song HJ, Song KG, Kim K, Kim H (2015) *In-Vitro* cytotoxic evaluation of MgO nanoparticles and their effect on the expression of ROS genes. *Int J Mol Sci* 16(12):7551–7564
- Richards R, Li W, Decker S, Davidson C, Koper O, Zaikovski V, Klabunde KJ (2000) Consolidation of metal oxide nanocrystals reactive pellets with controllable pore structure that represent a new family of porous. *Inorganic Mater J Am Chem Soc* 122(20):4921–4925
- Schram MT, Stehouwer CD (2005) Endothelial dysfunction, cellular adhesion molecules and the metabolic syndrome. *Hormone Metabolic Res* 37:49–55
- Wahab R, Ansari SG, Darl MA, Kim YS, Shin HS (2007) Synthesis of magnesium oxide nanoparticles by sol-gel process. *Mater Sci Forum* 558–559:983–986
- Yeh YC, Creran B, Rotello VM (2012) Gold nanoparticles: preparation, properties, and applications in bionanotechnology. *Nanoscale* 4(6):1871–1880

Formulation, Production, and Characterization of Nutritionally Enriched Spread Product with Blends of Fish Skin (*Labeo rohita*) Oil and Chia Seed (*Salvia Hispanica*) Oil



Nabanita Ghosh, Monalisa Roy, and D. K. Bhattacharyya

Abstract The work aims at the utilization of blends of Fish Skin Oil (FSO) and Chia Seed Oil (CO). The gluten-free Chia flour is utilized to formulate nutritionally enriched spreads. Among the three blending ratios 2:1 (CO:FSO) is nutritionally superior due to its higher antioxidative activity and lower tottox value. Four types of spreads were made by using raw chia flour (RC), defatted chia flour (DC), raw roasted chia flour (RRC), roasted defatted chia flour (RDC), followed by addition of blended oil, honey as natural sweetener, and egg lecithin as an emulsifier. The adaptation of roasted flour gives a nutty smell and attracting color that supports the masking of fishy smell in blended oils. All the formulated spreads are subjected to sensory evaluation and RRC spread is the most liked product. RRC spread is also subjected to antimicrobial assay followed by comparison with a market one. All these measures add a nutritional benefit to the spreads. These spreads are nutritionally enriched, gluten free, and protein rich.

Keywords Fish skin oil · Chia seed oil · Chiaflour · Breakfast cereal · Protein rich

1 Introduction

Chia (*Salvia hispanica*) is a plant belonging to the family of *Lamiaceae* loaded with healthy omega-3 fatty acids, fiber, polyunsaturated fatty acids, and protein including all essential amino acids, calcium, and several other minerals. Chia seed oil has a

N. Ghosh (✉) · M. Roy · D. K. Bhattacharyya
School of Community Science and Technology, Indian Institute of Engineering Science and Technology, Howrah, West Bengal 711103, India
e-mail: naba1990@gmail.com

M. Roy
e-mail: monalisaroy1997@gmail.com

D. K. Bhattacharyya
e-mail: dkb_oiltech@yahoo.co.in

variable chemical composition (Ayerza Jr et al. 1995). The seeds have about 25–38% oil by weight which contains the higher proportion of α linoleic acid (60%) (Palma et al. 1947). Chia seed oil has characteristics that are well suited for industrial applications, and they can contribute to healthy human diet (Vanesa et al. 2008).

The previous work of the authors Ghosh et al. (2019a, b) revealed that *Labeo rohita* skin oil (FSO) when blended with chia seed oil (CO) in 1:1, 1:2, and 2:1 ratio, becomes the most oxidative stable and antioxidant rich in 2:1 (FCO₃) ratio. In this study an attempt was made to utilize the FCO₃ for making nutritionally enriched spread products. Spread products are mainly produced from dairy products. Dairy spreads are deficient in some of micronutrients especially antioxidant. Moreover lactose intolerance patient cannot have it. Need for developing a nondairy spread product is increasing day by day Making spread from these blended oils utilizing chia flour will be an option to solve problems. In our study we have made four types of formulations for preparing the spread product utilizing blended oil and different chia flours. Blended oil has increased its nutritional quality while chia flour powder gives a gluten free, lactose free nutritional profile. For sweetness we have used honey as natural sweetener and egg lecithin as an emulsifier.

2 Materials and Methods

2.1 Materials

All reagent used are of analytical grade and all are brought from Sigma. Waste fish skin (*Labeo rohita*) from local market. Chia seeds (*Salvia hispanica*) were brought from Wild Forest brand.

2.2 Methods

2.2.1 Sample Preparation

2.2.1.1 Extraction of Fish Skin Oil and Chia Seeds Oil

Oil from fish skin was extracted according to the authors' previous work (Ghosh and Bhattacharyya 2019) and chia seeds were extracted by soxhlet method with n-hexane.

2.2.1.2 Preparation of Chia Flour

Four varieties of chia flour were prepared—roasted chia flour (RRC), roasted defatted chia flour (RDC), defatted chia flour (DC), and raw chia flour (RC). Roasting was conducted at a temperature of 50 °C for 30 min.

2.2.2 Proximate Composition Analysis of Chia Seed

Raw chia seed was subjected to proximate composition analysis to measure the amount of moisture, carbohydrate, protein, fat, and ash content of it via the following methods.

2.2.2.1 Moisture content:

5 gm sample was placed in a cover glass. Then the glass was placed in hot air oven at 60 °C. Weight was recorded at an interval of each 30 min till it to be constant. By the following formula moisture % was calculated. The result is mentioned in Table 1.

$$\text{Moisture(\%)} = \frac{\text{Weight of fresh sample} - \text{weight of dried sample}}{\text{weight of fresh sample}} \times 100$$

2.2.2.2 Ash content

5 gm sample was placed in Silica Porcelain Crucible and then the Crucible placed into Muffle Furnace at 600 °C for 6 h. It was determined by incinerating the sample. Ash percentage was calculated by the following formula. Result is mentioned in Table 1.

$$\text{Ash(\%)} = \frac{w_2 - w_1}{w_0} \times 100$$

where W_0 —Weight of sample (gm.), W_1 —Empty weight of Silica Porcelain Crucible (gm.), W_2 —Weight of Silica Porcelain crucible + Ash (gm.).

2.2.2.3 Protein content

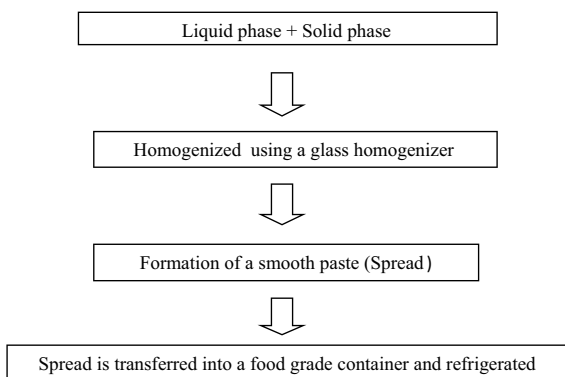
Protein content was determined by Folins test (Oh 1951). BSA solution was used as standard. The standard curve was fitted by plotting absorbance versus the corresponding concentration of BSA solutions. The absorbance value was converted into 100 g sample. The result is mentioned in Table 1.

2.2.2.4 Fat content

Total lipids were extracted by solvent extraction method. At first 15 gm sample was added to 300 ml hexane. After overnight soaking the mixture was filtrated by Whattman no. 1 filter paper. The filtrate was subjected to distillation. By the following formula fat (%) was calculated. The result is mentioned in Table 1.

$$\text{Fat(\%)} = \frac{\text{weight of crude fat(g)}}{\text{Weight of dry sample(g)}} \times 100$$

Fig. 1 Protocol for spread production



2.2.2.5 Carbohydrate content

Carbohydrate content was determined by Anthrone test (D.A.T. Southgate 1976). The absorbance was read at 630 nm. The standard curve was fitted by plotting absorbance versus the corresponding concentration of glucose. The absorbance value was converted into 100 g of sample. The result is mentioned in Table 1.

2.2.3 Preparation of Nutritionally Enriched Spread

Nutritionally enriched spread product was prepared according to the method described in Fig. 1 (Kar et al. 2014). Four Spread samples were prepared by mixing the solid phase and liquid phase. Solid phase contains different flour such as raw chia flour, defatted chia flour, roasted chia flour, roasted defatted chia flour, and named as RC, DC, RRC, RDC, respectively, whereas liquid phase contains FCO₃ oil. The process for making the spread is represented in Fig. 1. The proximate composition of all the formulations is given in Table 2. Pictorial view of RC, DC, RRC, RDC spread were represented in Figs. 2, 3, 4 and 5, respectively.

2.2.4 Determination of Spreadability of Spread Samples

0.5 g of the spread sample was placed between the two glass slides of equal weight, area, and thickness (3.9 mm). Thereafter the sample was loaded with a known weight of 5, 10, 15, 20 g on the upper slide for 30 s. To calculate the percent spreadability of spread, initial and final spreading diameters of the samples before and after the load were noted. The percent spreadability was calculated as per the equation:

$$\text{Spreadability}(\%) = \frac{D2 - D1}{D1} \times 100$$

where $D1$ is the initial diameter of the samples before the load and $D2$ is the final diameter of the samples after the load.

Table 1 Proximate composition of chia seed

Content	Amount (%)
Moisture	5.18 ± 0.032
Carbohydrate	46 ± 0.01
Protein	20 ± 0.03
Fat	24 ± 0.41
Ash	4.82 ± 0.025

All tests were performed in triplets. Data is expressed as mean ± SD

3 Results and discussions

3.1 Proximate Composition of Chia Seed

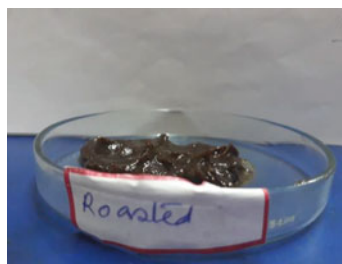
Chia seed was subjected to determine its protein, carbohydrate, and fat content. From the Table 1 it can be seen that dry chia seed contains higher amount of protein (21.5%). The average protein content varies from 15 to 23% according to the location when the seeds have grown (Cahill and Provance 2002). The total fat content of chia seed was 24% of which 17.3% contains omega-3 fatty acids (Di Sapio et al. 2012; Josephine Nirmala and Sarasvathi 2016). In the present study, the insoluble dietary fiber content of chia seed has nearly 49.47% which is capable of retaining water, provides bulk, and prolongs the gastrointestinal transit time. Increased gastrointestinal time is directly related to gradual increase in post-prandial glucose levels and decrease in insulin resistance over a period of time (Jeong et al. 2010). The inorganic material present in chia seed is 1.82% which is determined by ash content.

3.2 Preparation of Nutritionally Enriched Spread

The formulations of each spread is mentioned in Table 2. Honey is used as natural sweetener, egg lecithin as natural stabilizer, sodium benzoate as preservative. RC and

Table 2 Composition of spread formulation

Ingredients	RRC	RDC	DC	RC
Chai flour	100 gm	100gm	100gm	100gm
FCO ₃	30 ml	30 ml	30 ml	30 ml
Honey	20 gm	20 gm	20 gm	20 gm
Egg lecithin	10 gm	10 gm	10 gm	10 gm
Sodium benzoate	Pinch of	Pinch of	Pinch of	Pinch of
Salt	Pinch of	Pinch of	Pinch of	Pinch of

Fig. 2 RC spread**Fig. 3** DC spread**Fig. 4** RRC spread

DC spread does not form the smooth paste-like structure whereas RDC spread form a little closure to smooth paste-like structure. RRC spread forms the exact smooth paste-like structure. All the formulations were subjected to sensory evaluation among 10 research scholar of SOCSAT lab. The most liked spread was subjected to proximate composition.

3.3 Sensory Evaluation

Consumers are attracted by the positive attributes of food products. So, for the best quality products, sensory evaluation is a major criterion for judging the acceptability of it. Sensory quality is a combination of all the senses of perception applied for

Fig. 5 RDC spread**Table 3** Sensory evaluation of all spread formulations

Parameter	RRC	RDC	DC	RC
Color	8.85 ± 0.37	7.57 ± 0.53	5.25 ± 0.690	4.71 ± 0.755
Odor	8.85 ± 0.377	7.57 ± 0.53	7.42 ± 0.534	7.42 ± 0.534
Texture	8.85 ± 0.377	8.00 ± 0.577	4.714 ± 0.487	4.28 ± 0.487
Taste	8.57 ± 0.535	8.14 ± 0.377	6.714 ± 0.951	5.85 ± 0.690
Spreadability	8.42 ± 0.534	7.85 ± 0.377	7.147 ± 0.690	6.28 ± 0.487
Overall acceptance	8.85 ± 0.377	7.857 ± 0.37	6.57 ± 0.53	6.142 ± 0.690

All tests were performed in triplets. Data is expressed as mean ± SD

selecting and eating foods. The main ingredients of the prepared food product chia seed and fish skin oil are of edible food-grade quality as established by previous works (Susana et al. 2015; Rana 2019; Savedboworn et al. 2017; Vera et al. 2015; Ghosh and Bhattacharyya 2019) so, organoleptic evaluation of freshly prepared nondairy spread and the control one (chocolate spread) was done by the research scholar of SOCSAT lab who are conducting their research in food science background, to assess the acceptability of the product based on the various sensory attributes like color, texture, test, aroma, spreadability, and overall acceptability and the panelist must be applied the spread on a piece of bread while test. The evaluation was done on a 9 point hedonic scale method where 9 is like extremely and 1 is dislike extremely and the results were mentioned in Table 3.

3.4 Spreadability Properties of Spread

Spreadability is one of the important factors for spread-like products. It signifies how smoothly the product can spread on bread and other food products. Among all the spread formulations RRC spread shows the maximum spreadability properties followed by RDC, RC, and DC spreadability (Table 4).

Table 4 Spreadability properties of different types spread product

Product	Spreadability (%)
RRC	85
RDC	75
DC	65
RC	75

3.5 Optimization

The prepared spreads were exposed to sensory evaluation. Different testers are provided with the formulated spreads and they tested the product according to the taste, color, odor, appearance, and texture. The results are expressed in Table 3. Spread formulated with roasted chia flour is the most acceptable product among all the formulated spread.

4 Conclusion

In the last few years, a few no of workers have drawn a sequence of experiments on chia seeds with an outcome on proximate composition, describing various methods of oil extraction and its limited application to food products. In general the fish processing industries generate a large amount of waste with fish skin being the major component. Hence these works try to put forward the upshots obtained after blending the extracted chia seed oil and fish skin oil, which have been formulated in preparation of spreads. The raw roasted chia (RRC) spread gives the best result when compared to the RDC, DC, and RC spreads. The conversion of raw chia flour to its roasted variety adds a nutty smell and attracting color to the final product. In terms of all the aspects including color, texture, spreadability, sensory evaluation, overall acceptability, and antimicrobial analysis RRC suits the tasters. It is gluten free, protein rich, and also antioxidant rich.

Conflict of Interest The authors hereby declare that there is no conflict of interest.

Authors Contribution All the authors had contributed equally to the work. This is a part of Nabanita Ghosh's Ph. D. work and Master's degree dissertation work of Monalisa Roy and D.K. Bhattacharyya is the Principle investigator (PI) of the work.

Authors Funding Research contingency fund is provided by the School of Community Science and Technology (SOCSAT) lab, Indian Institute of Engineering Science and Technology (IEST), Shibpur.

References

- Ayerza R Jr (1995) Oil content and fatty acid composition of chia (*Salvia hispanica*L.) from five northwestern locations in Argentina. *J Am Oil Chem Soc* 72:1079–1081
- Cahill JP, Provance MC (2002) Genetics of qualitative traits in domesticated chia (*Salvia hispanica* L.). *J Heredity* 93(1):52–55
- D.A.T. Southgate (1976) Determination of food carbohydrates. Applied Science Publication Ltd.
- Ghosh N, Ghosal S, Bhattacharyya DK (2019a) Phytochemical screening and antioxidant activity of oil extracted from fish skin (*Labeo rohita*). *Int Res J Eng Technol (IRJET)* 06(02):1414–1420. <https://doi.org/10.13140/RG.2.2.33457.22884>
- Ghosh N, Roy M, Ghosh M, Bhattacharyya DK (2019b) Study on physicochemical and antioxidant properties of blend of fish skin (*Labeo rohita*) oil and chia seed (*Salvia hispanica*) oil. *Biotechnol Biol Sci*. ISBN 978-0-367-43161-7
- Ghosh N, Bhattacharyya DK (2019) Effect of heating time and heat on the physicochemical and antioxidative properties of fish (*Labeo rohita*) skin oil. *Int J Pharm Sci*, 11(9):87–89. <https://doi.org/10.22159/ijpps.2019v11i9.32917>
- Josephine Nirmala M, Sarasvathi V (2016) Analysis of chia seed—physiochemical and proximate analysis. *Res J Recent Sci* 5(8):39–41
- Jeong SK (2010) Effectiveness of topical chia seed oil on prutitus of end stage renal disease patients and healthy volunteers. *Ann Dermatol* 22(2):143–148. <https://doi.org/10.5021/ad.2010.22.2.143>
- Kar S, Sahu S, Ghosh M, Bhattacharyya DK (2014) Technology development for producing bitter and flavor free mustard spreads. *J Int Acad Res Multidiscipl* 2(6):250–263
- Oh L et al (1951) Protein measurement with the folin phenol reagent. *J Biol Chem*
- Palma F, Donde M, Lloyd WR (1947) Fixed oils of Mexico, I. Oil of chia—*Salvia hispanica*. *J Am Oil Chem Soc* 24:27–28. <https://doi.org/10.1007/BF02645767>
- Rana M (2019) Characterization of chia seed flour and wellbeing endorsing possessions. *Int J Food Sci Nutr Diet* 68(5):419–426
- Sapio Di O, Bueno M, Busilacchi H, Quiroga M, Severin C (2012) Morphoanatomical characterization of *Salvia hispanica*. *Boletín Latinoamericano Y Del Caribe De Plantas Medicinales Y Aromaticas*, 11(3):249–2268
- Savedboworn W, Kittiphattanabawon P, Benjakul S, Sinthusamran S, Kishimura H (2017) Characterization of collagen from rohu (*Labeorohita*) skin. *J Aqua Food Prod Technol* 26(3):248–257. <https://doi.org/10.1080/10498850.2015.1133747>
- Susana R, Patrícia F, Paulina M, Anabela R (2015) Assessing gelling properties of chia (*Salvia hispanica* L.) flour through rheological characterization. *J Sci Food Agric* 97(6). <https://doi.org/10.1002/jsfa.7971>
- Vanesa Y. Ixtaina, Susana M. Nolasco, Mabel C. Tomás, (2008) Physical properties of chia (*Salvia hispanica* L.) seeds. *Ind Crops Prod* 28(3):286–293
- Vera L, Vianado N, Victória MSB, de Oliveira ALL, Maurício et al (2015) Characterization of hydrolysed oil obtained from fish waste for nutraceutical application. *Food Sci Technol* 35(2):321–325. <https://doi.org/10.1590/1678-457x.6583>

Application of Used Tea as Solid Matrix for Immobilization of Alkaline Protease by OVAT Method



Tapasi Polley and Uma Ghosh

Abstract Enzyme immobilization on a solid matrix is nowadays widely employed, particularly in the food and pharmaceutical industries, in biomedical applications such as biosensors, immunological test systems, and in the production of fine chemicals. The conventional method of enzyme immobilization includes adsorption due to electrostatic and hydrophobic adhesion and covalent binding by internal cross-linkage of enzymes on a solid support. The immobilization of enzymes can offer several advantages including repeated usage of enzyme thereby reducing the cost of the enzyme, ease of product separation, and improvement in enzyme stability. The used tea, an abundant renewable source, can be applied as solid matrix for enzyme immobilization. In the present investigation, the immobilization of alkaline protease was studied on used tea. Immobilized enzyme showed better thermal stability than the free enzyme. Optimum conditions of immobilization investigated include temperature, pH and storage stability, and also reusability. The best result of immobilization yield (34%) and immobilization efficiency (45%) was found with 300 mg of solid matrix. The immobilized enzyme was activity even after eight cycles of repeated use.

Keywords Alkaline protease · Immobilization · Thermostability · Solid matrix

1 Introduction

Enzyme has been immobilized on several natural and synthetic supports (Naghshbandi et al. 2018). For effective immobilization, the carrier solid matrix should have very good inertness, regenerability, physical strength and resistance to microbial attack, thermal stability, and huge accessible surface area (Santos et al. 2015). The main advantage of enzyme immobilization is improved stability and resistance of

T. Polley · U. Ghosh (✉)

Department of Food Technology and Bio-Chemical Engineering, Jadavpur University, Kolkata 700032, India

e-mail: ughoshftbe@yahoo.co.in

T. Polley

e-mail: tapasipolley@gmail.com

© Springer Nature Singapore Pte Ltd. 2021

D. Ramkrishna et al. (eds.), *Advances in Bioprocess Engineering and Technology*,

Lecture Notes in Bioengineering,

https://doi.org/10.1007/978-981-15-7409-2_22

an immobilized enzyme to harsh environmental conditions such as large ranges of pH and temperature (Cipolatti et al. 2014). In the last decades, several methods have been used for immobilization of enzymes. These techniques are commonly classified into four wide categories; that is, covalent binding, adsorption, entrapment, and cross-linking (Dwevedi et al. 2016). In general, the chemical and physical properties of the supports used in combination with the biochemical properties of the enzyme play a key role in selecting the most appropriate immobilization technique (Mateo et al. 2007).

Immobilized enzymes offer more advantages, when compared to free enzymes, like enhanced stability against various denaturing conditions, higher catalytic activity, easier product and enzyme recovery, continuous operation of enzymatic processes, reusability, and reduced susceptibility to microbial contamination (Asftraf et al. 2010). However, limitations in applications of immobilized enzymes include high cost and low yield (Matto et al. 2007). The effective support materials for an immobilized enzyme should be low cost and provide an adequate large surface area, together with the least diffusion limitation in the transport of substrate and product (Krajewska et al. 2004). Natural polymers used as carrier materials in immobilization technology, such as alginate, carrageenan, agarose, chitin, and chitosan, along with their application in the treatment of various pollutants, have the advantages of being nontoxic, biocompatible, and biodegradable (Zille et al. 2003). Used tea is cheap, easily available, and nontoxic biological waste material. The utilization of used tea as solid matrix will not only reduce the disposal as well as pollution problem but will also help the immobilized enzyme to be cost-effective. The present study deals with

- i. Immobilization of alkaline protease using polyphenol extracted used tea as solid matrix.
- ii. Characterization of immobilized enzyme to temperature & pH optima, storage stability, and reusability.
- iii. Comparative study of thermal stability and pH stability of free and immobilized enzyme.

2 Materials and Methods

2.1 *Microorganism and Inoculum Preparation*

Alternaria alternata TUSGF1 strain was originally isolated from poultry farm soil and identified as producer of alkaline protease according to Polley et al. (2018). For inoculum preparation, the strain was grown on PDA agar slant at 30 °C for 7 days incubation.

2.2 Solid-State Fermentation

SSF was carried out in 250 ml conical flask containing 5 gm of substrate with 5 ml of distilled water (w/v) and it was autoclaved at 121 °C for 15 min. After sterilization, the flasks were inoculated with 5 ml of inoculum and incubated at 30 °C for 7 days. At the end of fermentation, fermented substrate was extracted with 50 ml distilled water for 2 h. The filtrate obtained was centrifuged at 4000 rpm for 20 min at room temperature. The supernatant was used as crude enzyme extract.

2.3 Partial Purification of the Enzyme

The crude enzyme obtained after centrifugation was concentrated to half of its initial volume using rotator vacuum evaporator (EYELA CCA-1110). Ammonium sulfate precipitation was done according to Abidi et al. 2011. To remove the high amount of salt from the precipitated protein, dialysis of the precipitate was performed. The 80% ammonium sulfate precipitate was used for dialysis against 1 mM Tris Hcl buffer (pH 8.0) till removal of sulfate from the protein fraction. The dialyzed protein was then subjected to further purification. The partially purified enzyme was used for further studies.

2.4 Preparation of Solid Matrix

The tea residues obtained after preparation of tea beverage were treated for polyphenol compound extraction (Pavlovic et al. 2013). The solid separated out of extraction process was collected and further treated with chlorine dioxide solution (1:6 w/v) as an oxidizing agent. The oxidation reaction was continued for 30 min. After this reaction the treated used tea was separated by filtration washed thoroughly with distilled water and dried at 80 °C for overnight. This polyphenol extracted used tea was employed as solid matrix in the immobilization process.

2.5 Immobilization of Alkaline Protease by Used Tea

1gm of used tea was mixed with a predetermined initial concentration of enzyme (1:20 w/v). Then the immobilized samples were collected after filtration, washed with distilled water, and enzyme activity was measured.

2.6 *Protease Assay*

Activity was determined according to the method described by Polley et al. using casein as substrate (Polley et al. 2016). The proteolytic unit was defined as the amount of enzyme that released 1 μg of tyrosine per minute under the assay condition.

2.7 *Immobilization Yield*

Initial activity of enzyme used for immobilization and is expressed as follows.

$$\text{Yield(\%)} = \frac{\text{Total Immobilized activity} \times 100}{\text{Starting activity}} \quad (1)$$

Total activity of immobilized enzyme was calculated by subtracting the residual enzyme activity remaining in the enzyme solution after immobilization.

$$\text{Efficiency(\%)} = \frac{\text{Observed activity} \times 100}{\text{Immobilized activity}} \quad (2)$$

2.8 *Optimization of Amount of Solid Matrix on Immobilization of Alkaline Protease*

Effect of amount of solid matrix on immobilization of protease was studied by carrying out immobilization with (100, 200, 300, 400, and 500 mg) of used tea. Each case the enzyme yield was determined.

2.9 *Optimization of Incubation Time on Immobilization of Alkaline Protease*

This effect was studied by incubating the mixture for the time period (2, 4, 6, 8, and 10 h) and for each sample enzyme assay was done.

2.10 Optimal Temperature and pH for Enzyme Activity

The temperature activity profile of the immobilized enzyme was studied by incubating the immobilized enzyme in 100 mM Tris Hcl buffer (pH 8.0) for 30 min with casein as substrate. The temperature range at temperatures (30, 35, 40, 45, 50, 55 and 60 °C), and enzyme activity was measured at each temperature.

Alternatively, the pH activity profile was studied incubating the enzyme substrate solution at 37 °C and at different pH from 7.5–10. Then enzyme activity was determined for various pH values.

2.11 Thermal Stability and pH Stability

Thermal stability of the free and immobilized enzyme was determined by 2 h of incubation enzyme over the temperature range (30, 35, 40, 45, 50, 55, and 60) °C at (pH 8.0). Residual activity was measured under standard conditions and expressed as percentage of the relative protease activity.

The pH activity profile for partially purified free and immobilized enzyme was determined at 37 °C for 2 h by incubating the enzyme with substrate at various pH ranges from 3 to 8. The pH of the reaction mixture was varied using different buffers (pH 7.5–9 and 10) and enzyme activity was calculated.

2.12 Storage Stability and Reusability

The immobilized alkaline protease was stored at Tris Hcl buffer (100 mM, pH 8.0) at 4 °C for 30 days. The activity was measured every 6 days.

The immobilized alkaline protease was repeatedly used for hydrolysis in each experiment. After each runs the immobilized enzyme was washed with distilled water followed by Tris Hcl buffer and stored in the same buffer.

3 Results and Discussion

3.1 Effect of Amount of Solid Matrix on Immobilization of Alkaline Protease

The amount of solid matrix for immobilization was optimized on the basis of immobilization yield and efficiency. Out of different amount of solid carrier used for immobilization of protease, maximum enzyme yield (34%) and efficiency (45%) was observed with 300 mg of matrix (Fig. 1). On increasing the amount of solid

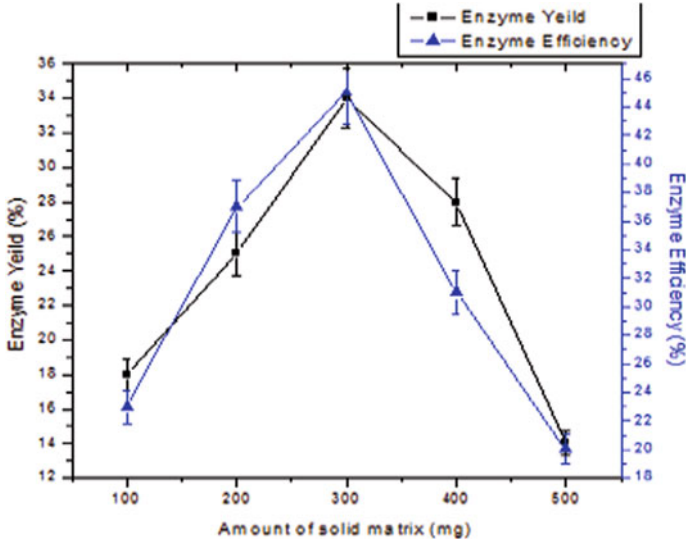


Fig. 1 Effect of amount of solid matrix on protease

matrix, enzyme binding did not improve. Hence, 300 mg of used tea was the matrix for further studies. Puri et al. (2005) reported that the maximum amount of solid matrix for enzyme activity of immobilized naringinase was 600 mg.

3.2 Effect of Incubation Time on Immobilization of Alkaline Protease

Maximum enzyme yield (40%) and efficiency (52%) binding of protease was observed at 6 h of incubation time, with no increase in binding thereafter (Fig. 2). The decrease in enzyme activity after 6 h was due to lengthy exposure of incubation time with enzyme. Enzyme activity was sustained up to 6 h and thereafter enzyme concentration was inhibitory.

3.3 Optimal Temperature and pH

The activity of immobilized protease at different temperatures is shown in Fig. 3. From the result it is clear that optimum activity was obtained at 45 °C. This increase of the optimum temperature is probably a significance of enhanced enzyme production. The optimum temperature for enzyme activity of immobilized phytases was 55 °C and similar to some studies (Das et al. 2016).

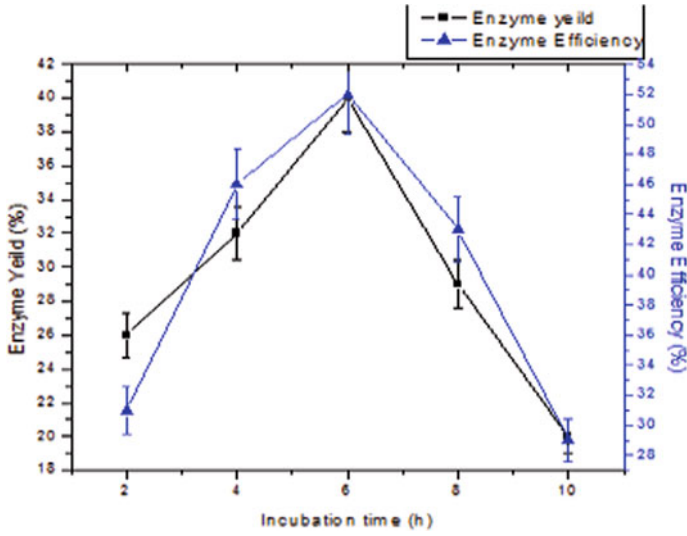


Fig. 2 Effect of incubation time on immobilization of protease

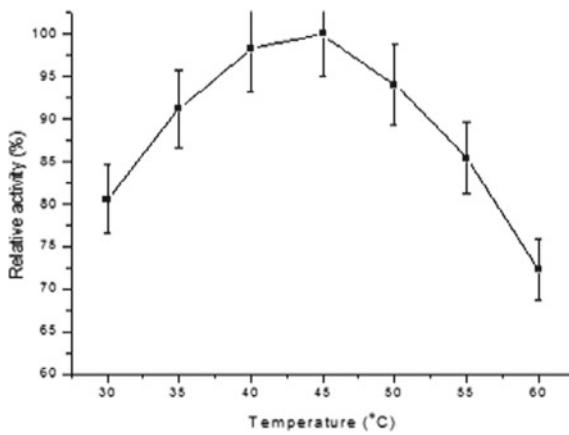


Fig. 3 Optimum temperature of immobilized protease

The result of the effect of pH on the immobilized is shown in Fig. 4. The optimum pH for the immobilized protease was 8.5. pH values ranging from 8.0 to 9.0, indicating that the immobilized alkaline protease was more resistant to alkaline conditions. They showed that in addition to the shift of the pH optimum from 7.5 to 9, more resistant to the alkaline environment was obtained (Dutta et al. 2017).

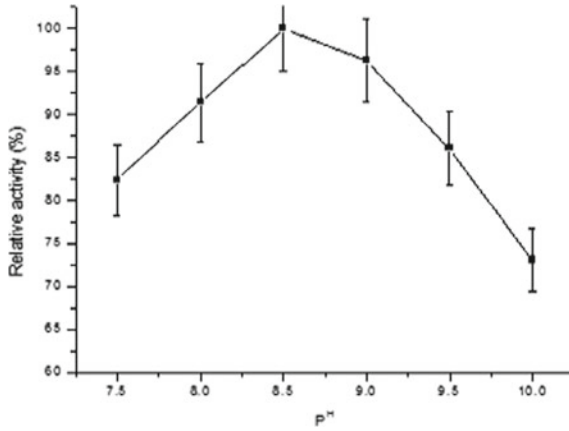


Fig. 4 Optimum pH of immobilized protease

3.4 Temperature and pH Stability

The thermal inactivation of free and immobilized enzyme was represented in Fig. 5. The results indicated that the immobilized enzyme was stable at (35–60 °C). This may be due to preservation of the struct of the enzyme by the matrix. An enhancement of enzyme thermal stability due to the immobilization process was reported by other authors (Kumar et al. 2015).

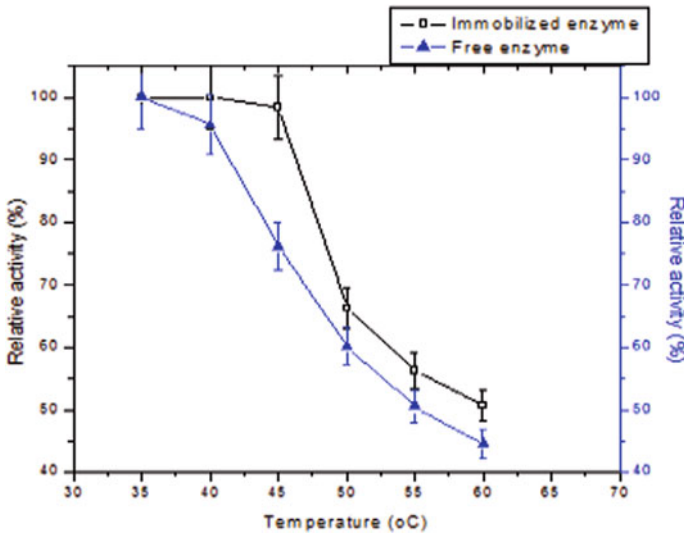


Fig. 5 Thermal stability of free and immobilized protease

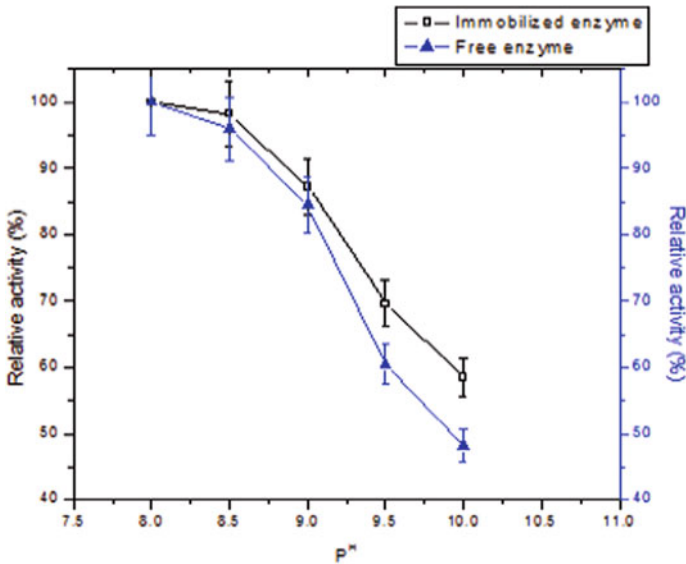


Fig. 6 pH stability of free and protease

The pH stability of free and immobilized protease is shown in Fig. 6. The maximum activity of both free and immobilized protease was found at pH 8.5. This increase in the optimum pH is probably a consequence of enhanced pH stability. El-Tanash et al. reported that a slight increase or decrease in optimal pH after immobilization.

3.5 Reusability and Storage Stability

The result of immobilized enzyme on solid matrix is shown in Fig. 7. The relative activity of immobilized enzyme retained 100–90% activity from first cycle to eight cycles and decrease from fourth cycle. *A. niger* tannase immobilized on sodium alginate beads without cross-linking with glutaraldehyde was used repeatedly for 7 cycles with 77% relative activity (Srivastava et al. 2010).

Protease stability was measured after a month of storage at 4 and 30 °C. The immobilization yield on 30th day was found 69% at 4 °C. Figure 8 showed that immobilized enzyme is more stable at 4 °C than 30 °C. β -galactosidase immobilized on alginate- gelatin fiber treated with glutaraldehyde was active for 35 days (Tanriseven et al. 2002).

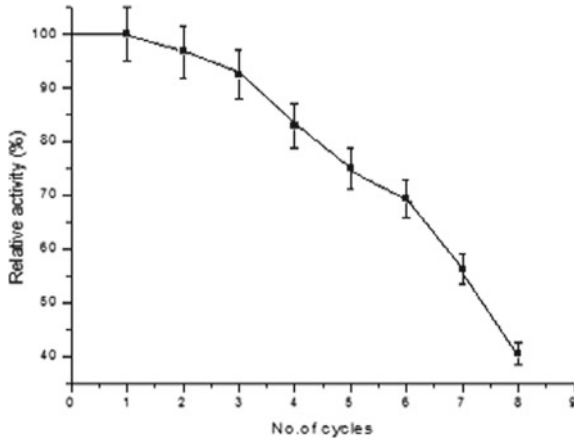


Fig. 7 Repeated use of immobilized protease

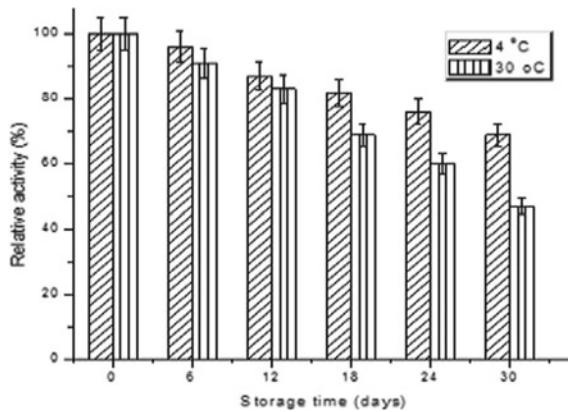


Fig. 8 Storage time of immobilized protease

4 Conclusions

In the present experiment, the potential application of this matrix in enzyme immobilization is reported. These results have shown that used tea may be effectively applied as a good supporting carrier for immobilization of alkaline protease. The successful application of this matrix not only reduces the disposal and environmental pollution problem as well as will make the process cost-effective.

Acknowledgements The authors gratefully acknowledge the financial assistance by University Grants commission, New Delhi for this study.

References

- Abidi F, Chobert JM, Haertle T, Marzoukia MN et al (2011) Purification and biochemical characterization of stable alkaline protease prot-2 from *botrytis cinerea*. *Process Biochem* 46:2301–2310
- Asftraf H, Husain Q et al (2010) Stabilization of DEAE cellulose adsorbed and glutaraldehyde crosslinked white radish (*Raphanus sativus*) peroxidase. *J Sci Ind Res* 69:613–620
- Cipolatti EP et al (2014) Current status and trends in enzymatic nano immobilization. *J Mol Catal B Enzym* 99:56–67
- Das R, Hamid SBA, Annuar MSM et al (2016) Highly efficient and stable novel nanobiohybrid catalyst to avert 3,4-dihydroxybenzoic acid pollutant in water. *Sci Rep* 6:33572
- Dutta N, Raj D, Biswas N et al (2017) Nanoparticle assisted activity optimization and characterization of a bacterial phytase immobilized on single layer graphene oxide. *Biocatal Agric Biotechnol* 9:240–247
- Dwevedi A et al (2016) Basics of enzyme immobilization. *Enzyme immobilization*. Springer, Switzerland, pp 21–44
- Krajewska B et al (2004) Application of chitin- and chitosan-based materials for enzyme immobilizations: a review. *Enzyme Microb Technol* 35:126–139
- Kumar S, Beniwal V, Kumar N, Kumar A, Chhokar V, Khaket TP et al (2015) Biochemical characterization of immobilized tannase from *Aspergillus awamori*. *Biocatal Agric Biotechnol* 4(3):398–403
- Mateo C, Palomo JM, Fernandez-Lorente G et al (2007) Improvement of enzyme activity, stability and selectivity via immobilization techniques. *Enzyme Microb Technol* 40:1451–1463
- Matto M, Husain Q et al (2007) Peroxide and redox mediators decolorization of direct dyes by salt fractionated turnip proteins enhanced in the presence of hydrogen. *Chemosphere* 69:338–345
- Naghsbandi MP, Moghimi H, Latif B et al (2018) Covalent immobilization of phytase on the multi-walled carbon nanotubes via diimide-activated amidation: structural and stability study. *Artif Cells Nanomed Biotechnol* 46(S1):S763–S772
- Pavlovic MD, Buntic AV, Siler-Marinkovic SS, Dimitrijevic-Brankovic SI et al (2013) Ethanol Influenced fast microwave-assisted extraction for natural antioxidants obtaining from spent filter coffee. *Sep Puri Technol* 118:503–510
- Polley T, Ghosh U et al (2016) Statistical optimization of alkaline protease production using isolated strain by submerged fermentation. *JABB* 7(4):2394–1081
- Polley T, Ghosh U et al (2018) Isolation and identification of potent alkaline protease producing microorganism and optimization of biosynthesis of the enzyme using RSM. *Indian Chem Eng* 60(3):285–296
- Puri M, Kaur H, Kennedy JF et al (2005) Covalent immobilization of naringinase for the transformation of flavonoid. *J Chem Technol Biotechnol* 80:1160–1165
- Santos JCS, Barbos O, Ortiz C et al (2015) Importance of the support properties for immobilization or purification of enzymes. *Chem Cat Chem* 7:2413–2432
- Srivastava A, Kar R et al (2010) Application of immobilized tannase from *Aspergillus niger* for the removal of tannin from myrobalan juice. *Ind J Microbiol* 50(1):545–552
- Tanriseven A, Dogan S et al (2002) A novel method for the immobilization of β -galactosidase. *Process Biochem* 38:27–30
- Zille A, Tzanov T, Gubitz GM, Cavaco-Paulo A et al (2003) Immobilized laccase for decolorization of reactive black 5 dyeing effluent. *Biotechnol Lett* 25:1473–1477

Environment and Agriculture

Isolation and Characterization of Arsenic Tolerant Bacteria from Industrial Soil and Analysing Its Metal Removal Potency



Aishwarya Das, Ranjana Das, and Chiranjib Bhattacharjee

Abstract Heavy metals are typically categorized as unavoidable contaminants of environment and arsenic is the most crucial heavy metal of concern. Arsenic appears in nature in different oxidation state and trivalent one, As(III) is reported as the component responsible for toxicity to animal and human as this form is more persistent in nature and cannot be broken down completely in non-toxic form. The present study aims to introduce the concept of microbiology to neutralize/eliminate the toxicity of As (III). Seven bacteria were isolated from two soil samples collected from the industrial zone of district Howrah and district South 24 Paraganas, West Bengal. The MIC values of the isolated bacterial systems experimentally observed and a consortium was prepared based on MIC values to achieve optimum removal efficiency. The consortium was found to tolerate up 200 mM of As(III) concentration and highest arsenic removal potency of 92% was observed. The plasmid DNA isolation and degradation were also performed to confirm the presence of desired genes promoting survival of the bacteria in stress conditions. Hence, with proper design and tuning, the isolates bioremediation of As(III) contaminated effluents may be achieved with immense societal benefits.

Keywords Arsenic · Bioremediation · Arsenic tolerant bacteria · Industrial soil · Metal removal potency

A. Das · R. Das · C. Bhattacharjee (✉)
Chemical Engineering Department, Jadavpur University, Kolkata 700032, India
e-mail: c.bhatta@gmail.com; chiranjib@jadavpuruniversity.in

A. Das
e-mail: signhereaish09@gmail.com

R. Das
e-mail: ranjanads78@gmail.com

1 Introduction

Arsenic is a metalloid element which is widely distributed on surface of the earth. Arsenic is 20th most abundant element in earth's crust, 14th in seawater and 12th in human body (Woolson 1975). Arsenic is a highly toxic pollutant that is released in the environment due to the natural calamities and anthropogenic actions. The indiscriminate release of the heavy metal into the soil and water is a major health concern worldwide, as it cannot be broken down into non-toxic form and therefore has long-lasting effects on ecosystem (Dixit et al. 2015). Arsenic is found in almost 20 minerals but the free metal is rare. The major forms of arsenic in environment exist in several oxidation states, As(V), As(III), As(0), and Arsenide(-III). The most common forms encountered in the soil are As(V) and As(III); i.e. arsenate and arsenite. Arsenite is the most toxic form of arsenic salt. Arsenic is exposed in the environment through the pedogenic process of weathering and also through human activities. The most significant natural source is weathering of minerals, erosion and volcanic activities (Dixit et al. 2015). The anthropogenic activities which release arsenic in the environment are mining, industries, agrochemicals, waste disposal and atmospheric disposal. Toxicity of Arsenic varies amongst the nature of species as well as with the oxidation state of the metal ion (Acharya et al. 1999). The probable reason has been explained as the expression of genes which are involved in the synthesis of AQP9 enzymes (Acharya et al. 1999). The toxicity of the arsenite is due to its affinity for closely-related spaced cysteine thiolates, it inactivates enzymes and receptors by binding to active site of cysteine residue, formation of disulphide bonds and production of reactive oxygen species by binding to reduced glutathione (Bhattacharjee et al. 2008). The industries such as paint, mining, agrochemicals are the major source of arsenic pollution. The groundwater is contaminated heavily due to effluents released by these industries. This has been recognized as one of the major catastrophic proportions. One doesn't normally associate arsenic with life, but it is now apparent that various types of microorganisms gain energy for growth from these toxic metals (Oremland and Stolz 2005). Microorganisms and their enzymes are actively involved in the arsenic cycle. They are involved in oxidation, reduction and methylation reactions. Usually, microbes have two types of uptake system, one is non-specific and the other is highly substrate specific. Bioremediation is the microbial-based cleaning mechanism of contaminants which may include toxins like hydrocarbons, agrochemicals and other organic toxicants. The heavy metals are not entirely rendered harmless by microbes and their enzymes but this is the technology they use to get rid of the arsenic. Potent metal sorbent bacteria are under the genera of *Bacillus*, *Pseudomonads*, *Streptomyces* and *P. Aeruginosa*. The mechanism that involves tolerating the metal in their cell has been reported as, (i) Exclusion of the metal ions by keeping away from the target sites; (ii) extrusion of the metals by pushing out of the cell through chromosomal/plasmid-mediated events; (iii) accommodation of metal form complex with the metal-binding proteins or other cell components; (iv) biotransformation: toxic metal is reduced to less toxic forms and (v) methylation and demethylation. This study aims to isolate,

characterize arsenic tolerant bacteria from arsenic polluted areas and to analyse the arsenic removal potency.

2 Materials and Method

2.1 Sampling and Preparation of Metal Solutions

The present study selected two industrial zones where arsenic is used for manufacturing their products. Two soil samples were collected from the industrial waste disposal area (5–6 cm) depth. Control sample was collected from region free of any arsenic contamination. The simulated arsenite and arsenate solution was prepared from the salts sodium arsenate and sodium arsenite, respectively, in 1 mM concentration.

2.2 Isolation of Metal (Arsenic) Resistant Bacteria, Screening and Characterization

The metal resistant bacteria were isolated from the collected soil sample by spread plate method. The media used was minimal media [M9 salts: 20 ml, MgSO₄ (1 mM)–200 µl, CaCl₂ (1 mM)–10 µl] and TSB agar media supplemented with 0.5 mM of arsenite solution. Pure culture was done by streak plate method.

The MIC at which no colony growth occurred for arsenite solution was performed by broth dilution method. Minimal media was prepared supplemented with different concentrations of arsenite solution (0.1–150 mM/L). The tubes were inoculated aseptically and incubated at 35 °C for 48 h. Minimum concentration of arsenite allowing growth of the isolates was an indication of positive tolerance.

The bacterial isolates that could tolerate the arsenic concentration were selected and characterized physically, biochemically and molecular. Gram nature was observed, silver nitrate test was performed as described by Simeonova et al. (2004). Biochemical tests were performed, the MRVP test, catalase test, starch hydrolysis, TSI, respectively, to characterize the bacteria isolated. Molecular characterization was done by isolation of plasmid DNA and confirming that the bacterial isolates contain plasmid.

2.3 Preparation of Consortium and Plasmid Curing

A consortium is defined as two or more microbial groups living symbiotically. They could be endosymbiotic or ectosymbiotic. The concept of consortium was first introduced by Johannes Reinke in 1872. In this study, the consortium was prepared using the bacterial isolates having high metal (arsenic) tolerance.

Plasmids are defined as extrachromosomal structure that replicates independently. Most of the essential genes required for the normal survival of bacteria are found in chromosomes. Many bacteria also carry different mobile genetic elements (MGE), that contribute to specialized functions as antibiotic resistance, metal resistance, etc. Thus, plasmid curing is a method to substantiate the relationship between the genetic trait and carrying that specific trait in the plasmid. Numerous agents Viz. chemical and physical are used, namely, acridine orange, acriflavin, SDS, etc. In this study ethidium bromide is used as the curing agent. The nutrient broth was prepared and filter sterilized ethidium bromide was added at concentrations ranging from 1.0–100 µg. Then the culture was added and incubated at 37 °C. The highest turbidity showing tube was used for plating and testing for survivability check.

2.4 Removal of Arsenic from Simulated Solution

The metal biosorption study of selected isolates was performed by measuring the As removal by the bacterial cells using methods proposed by Pazirendeh et al. (1998) and Bhakta et al. (2012). Fresh bacterial culture was harvested in 2mL centrifuge tube, tubes were centrifuged (13000 g/min) and the cells were washed three times with sterilized MiliQ water. Pellets of the cell (40 mg wet weight) of each bacterial isolates were resuspended in 5 ml sterilized As (1 mg/L) solution. Samples were incubated for 4 h at 37 °C. After incubation, the samples were centrifuged 13000 g/min and the supernatants were filtered through a 0.25 µm filter paper. The As content was measured using spectrophotometer using safranin O as a reagent at 532 nm. The metal removal percentage was calculated using equations described by Bhakta et al. (2012).

3 Results and Discussion

3.1 Isolation of Metal Resistant Bacteria

Seven arsenite resistant strains were isolated from sample 1 and sample 2 after cultured in minimal salt media and TSB media. The isolates are AsR1 AsR2, AsR3, AsR4, AsR(i), Asr(i), AsR(iii) (Fig. 1). The minimum inhibitory concentration of all the isolates has been presented in Table 1. The higher MIC values indicated that the

Fig. 1 Isolation of bacteria from arsenic-contaminated soil sample

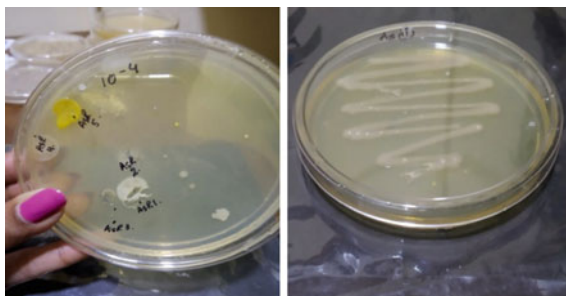


Table 1 Minimum inhibitory concentration

Bacterial isolates	MIC values (mM)
AsR1	10
AsR2	25
AsR3	70
AsR4	50
AsR(i)	10
AsR(ii)	150
AsR(iii)	150

bacterial isolates can tolerate a high concentration of arsenite salt. Thus the selected isolates can be used for efficient bioremediation process. Characterization profile of all the arsenic tolerant isolate has been presented in Table 2. This is to characterize the bacterial isolates based on morphological character. Amongst the seven bacterial isolates four were Gram positive in nature and three were Gram negative in nature. A brief of the observations of biochemical test has been presented in Table 3, to demonstrate the biochemical nature of the bacterial isolates. Table 3 represents the sugar utility of the isolates (TSI test), their capability to neutralize the toxic effects of oxygen metabolites, the ability to hydrolyse starch and to IMV test to characterize if any of the isolates were enteric in nature.

Table 2 Characterization of arsenic tolerant isolates

Characteristics of strains	AsR1	AsR2	AsR3	AsR4	AsR(i)	AsR(ii)	AsR(iii)
Colony colour	Off-white	Off-white	White	Yellow	White	Pale brown	Off-white
Colony shape	Circular	Irregular	Ovoid	Circular	Punctiform	Irregular	Circular
Surface	Smooth	Smooth	Rough	Smooth	Granular	Smooth	Smooth
Elevation	Convex	Flat	Raised	Convex	Raised	Convex	Convex
Margins	Entire	Undulate	Entire	Entire	Entire	Undulate	Entire
Opacity	Opaque	Opaque	Opaque	Opaque	Transparent	Transparent	Opaque

Table 3 Observation of biochemical tests

Biochemical tests	AsR1	AsR2	AsR3	AsR4	AsR(i)	AsR(ii)	AsR(iii)
Catalase test	+	+	+	+	+	+	+
Indole test	–	–	–	–	–	–	–
Methyl red test	+	+	+	–	+	+	+
VP test	–	–	–	–	–	–	–
Citrate test	–	–	–	–	+	+	–
Starch hydrolysis	–	–	+	+	–	+	+
TSI test	–	–	+	+	+	+	–

Table 4 Arsenic removal potency of the selected bacterial isolates and the consortium prepared

Selected bacterial strains	Arsenic removal(%)
AsR1	77
AsR2	65
AsR3	82
AsR4	85
AsR(i)	78
AsR(ii)	92
AsR(iii)	89

Table 3 represents the sugar utility of the isolates (TSI test), their capability to neutralize the toxic effects of oxygen metabolites, the ability to hydrolyse starch and IMV test to characterize if any of the isolates were enteric in nature. Arsenic removal potency of the selected bacterial isolates has been presented in Table 4, which represents the efficiency percentage of the isolates, showing AsR(ii) to produce the highest removal efficiency percentage. The present study has revealed the high metal tolerance capability of the isolated bacteria. The MIC values of the isolated bacteria can tolerate up to 100 mM of arsenite. The arsenic removal percentage of the selected isolates was more than 50% and amongst the seven selected bacteria AsR(ii) has shown the highest removal percentage of 92, the consortium has the removal percentage of 94. The plasmid curing of the selected isolates revealed that plasmid is an important factor that is associated with the arsenic resistance.

3.2 Molecular Characterization

AsR3, AsR4, AsR(ii) and AsR(iii) showed band under UV-transilluminator. Plasmid was then cured and it was checked by further running gel and the survivability test was done on TSB media. The four solates AsR3, AsR4, AsR(ii), AsR(iii) was plated and observed after 24 hr, no visible growth was observed. The result revealed that the

Fig. 2 No colony growth observed after plasmid curing



heavy metal resistance (Arsenic) mechanism is plasmid mediated. Figure 2 illustrates the absence of any colony growth after plasmid curing.

4 Summary of Overall Work

Bioremediation is an innovative technology in removal of heavy metals and the present study based on similar concept of microbial capacity to tolerate heavy metals and the removal percentage of them has illustrated significant removal percent. Further studies regarding the technology development based on such process are expected to be supportive to the community suffering from arsenic toxicity.

References

- Acharya SK, Chakraborty P, Lahiri S et al (1999) *Nature* 401:545–547
- Bhakta JN, Ohnishi K, Munekage Y, Iwasaki K, Wei M (2012) Characterization of lactic acid bacteria based probiotics as heavy metal sorbents. *J Appl Microbiol* 112:1193–1206
- Bhattacharjee H, Mukhopadhyay R, Thiyagarajan S, Rosen BP (2008) Aquaglyceroporins: ancient channels for metalloids. *J Biol* 7:33
- Dixit R, Wadiullah MD, Pandiyan K, Singh BS, Sahi A, Shukla R, Singh BP, Rai JP, Sharma PK, Lade H, Paul D (2015) Bioremediation of heavy metals from soil and environment: an overview of principles and criteria of fundamental process. *Sustainability* 7:2189–2212
- Oremland RS, Stolz JF (2005) Arsenic, microbes and contaminated aquifers. *Trends Microbiol* 1:45–49
- Pazirendeh M, Wells BM, Ryan RL (1998) *Appl Environ Microbiol* 64:4068–4072
- Simeonova DD, Lièvreumont D, Lagarde F, Muller Daniel AE, Groudeva Veneta I, Claire Lett M-C (2004) *FEMS Microbiol Lett* 237:249–253
- Woolson EA (1975) The persistence and chemical distribution of arsenic acid in the soils. *J Food Chem* 28:667–681

Application of *Bacillus* sp. NITD 19 for Utilization of Cyanide as Nutrient Source



Abhilasha Rai, Sanket Mukherjee, Agradeep Mukherjee, Jitamanyu Chakrabarty, Pinaki Bhattacharya, and Susmita Dutta

Abstract Cyanide is highly toxic to our ecosystem. The main contributor of cyanide to the environment is the untreated or improperly treated wastewater coming from various industries like steel, metallurgical, mining, tanning, etc. Bioremediation is an inexpensive yet effective measure, compared to physico-chemical methods, for removal of cyanide from industrial effluents. In the present study, one indigenous bacterial strain was collected and isolated from the outfall of nearby coke-oven plant and identified as *Bacillus* sp. NITD 19 through 16S rRNA gene sequencing. The test strain was used for removal of cyanide from synthetic solution. Lethal dose analysis was performed and the strain was found to grow up to 100 mg/L initial cyanide concentration. One factor at a time (OFAT) analysis was performed to get the effective operational parameters for maximum removal by varying pH (6–10), inoculum load (1–4%), temperature (25–37 °C), and initial concentration

A. Rai · S. Dutta (✉)

Department of Chemical Engineering, National Institute of Technology Durgapur, Mahatma Gandhi Avenue, Durgapur, West Bengal 713209, India
e-mail: susmita.dutta@che.nitdgp.ac.in

A. Rai

e-mail: abhilasharai.ra@gmail.com

S. Mukherjee · A. Mukherjee

Department of Biotechnology, Heritage Institute of Technology, Anandapur, Kolkata 700107, India
e-mail: smukherjee109@gmail.com

A. Mukherjee

e-mail: agra4mukherjee@gmail.com

J. Chakrabarty

Department of Chemistry, National Institute of Technology Durgapur, Mahatma Gandhi Avenue, Durgapur, West Bengal 713209, India
e-mail: jitamanyu.chakrabarty@ch.nitdgp.ac.in

P. Bhattacharya

Department of Chemical Engineering, Heritage Institute of Technology, Anandapur, Kolkata 700107, India
e-mail: pinaki.bhattacharya@heritageit.edu

© Springer Nature Singapore Pte Ltd. 2021

D. Ramkrishna et al. (eds.), *Advances in Bioprocess Engineering and Technology*,
Lecture Notes in Bioengineering,
https://doi.org/10.1007/978-981-15-7409-2_24

241

(20–100 mg/L) in a judicial manner. Time variation study of cyanide removal was carried out then. FTIR study was performed for biomass characterization.

Keywords Cyanide · Bioremediation · Lethal dose · *Bacillus* sp.

1 Introduction

Cyanide has been found as one of the most toxic chemicals for aquatic and terrestrial ecosystem (Razanamahandry et al. 2016, 2019). Anthropogenic sources of cyanide include the emission from industries like mining, metallurgical, steel, leather, paper, etc. (Sharma et al. 2019). Cyanide is one of the most hazardous chemicals which can deteriorate the environment day by day. The cyanide laden industrial effluents should be treated properly before being discharged to the environment. Though there are several methods for treatment of cyanide, the selection of suitable one depends on different factors such as its contamination level, cost of the method, environmental effect of the methods, etc. Among physical, chemical, and biological methods, the last one is found to be fascinating owing to its capability of removal in ppm level, low cost, and environment-friendly nature. Bacterial treatment of cyanide loaded wastewater is one of the most attractive techniques over the other remediation methods (Tiong et al. 2015). As per literature, microbes use cyanide as the nutrient source for their growth (Luque-Almagro et al. 2016). In the present work, one bacterial strain, collected and isolated from contaminated site and identified as *Bacillus* sp. NITD 19, was found effective in removal of cyanide from synthetic solution.

2 Materials and Methods

2.1 Collection, Isolation, Identification, and Growth of Bacterial Sample

Bacterial sample was collected from outfall of nearby coke-oven plant. Molecular identification was done by 16S rRNA gene sequencing (Eurofins Genomics India Pvt. Ltd., Bengaluru, India). Test strain was cultured with cyanide containing minimal medium [$\text{K}_2\text{HPO}_4 \cdot 2\text{H}_2\text{O}$ (1.0 g/L), $\text{MgSO}_4 \cdot 7\text{H}_2\text{O}$ (0.2 g/L), $\text{CaCl}_2 \cdot 2\text{H}_2\text{O}$ (0.01 g/L), NaCl (0.01 g/L), $\text{MnSO}_4 \cdot 4\text{H}_2\text{O}$ (0.2 g/L), $\text{CuSO}_4 \cdot 5\text{H}_2\text{O}$ (0.2 g/L) and $\text{ZnSO}_4 \cdot 7\text{H}_2\text{O}$ (0.2 g/L), and glucose (0.2 g/L)]. The growth of isolated strain was studied in terms of its cell biomass content.

2.2 *Lethal Dose Analysis*

Test strain was grown on minimal media with varying concentration of cyanide from 20–100 mg/L with inoculum load 2% at pH 7. The culture was kept in BOD shaker (Modern Equipment, M/s Atlanta Drugs and Chemicals, India) at temperature 37 °C and shaking speed 120 rpm under aseptic condition for 72 h. Samples were collected after incubation period. The samples were centrifuged at 5000 rpm for 15 min. Supernatant was analyzed with selective ion meter (Thermo scientific, Orion Dual Star, pH/ISE) for measuring residual cyanide concentration. Pellet was washed twice with deionized water and kept for drying at 65 ± 2 °C overnight for getting cell biomass concentration.

2.3 *One Factor at a Time (OFAT) Analysis and Time Variation of Cyanide Removal*

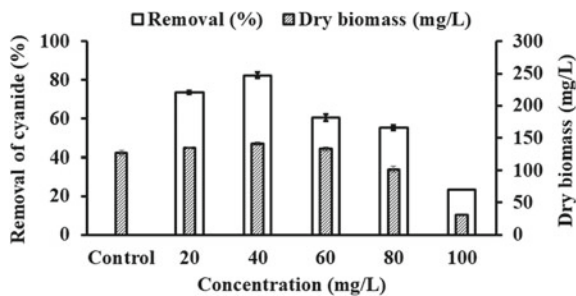
In order to know the effects of the different parameters like pH, inoculum load, temperature, and initial cyanide concentration on removal of cyanide, OFAT study was performed by varying the pH (6–10), inoculum load (1–4%), temperature (25–37 °C), and initial concentration (20–100 mg/L) individually in a judicial manner (Uppendar et al. 2018). Test strain was grown in minimal media for 72 h at a particular operating condition and samples were collected and analyzed for cell biomass concentration and residual cyanide concentration.

After assessing suitable operating conditions corresponding to maximum cyanide removal, time variation study was performed. Test strain was grown in cyanide loaded minimal media at pH 8 with inoculum load 4%, and at temperature 37 °C for 72 h. Samples were collected after every two hours intervals and were analyzed for residual cyanide concentration and cell biomass content.

2.4 *Characterization of Cell Biomass*

Fourier Transform Infrared spectroscopy (FTIR) study of both treated and untreated dry biomass of test strain was done using Fourier Transform Infrared spectrophotometer (Instrument Model: NEXUS-870).

Fig. 1 Lethal dose analysis of *Bacillus* sp. NITD 19 for cyanide removal



3 Results and Discussions

3.1 Collection, Isolation, Identification and Growth of Bacterial Sample

Bacterial isolate has been identified as *Bacillus* sp. NITD 19. Growth study has been performed in minimal media. Preparatory phase of the test strain has been found large which might be due to nitrogen deficiency and limited amount of carbon source in the present culture medium (figure is not shown).

3.2 Lethal Dose Analysis

Bacillus sp. NITD 19 has been found to grow up to 80 mg/L cyanide concentration and beyond this value, growth has been restricted (Fig. 1). High concentration of cyanide affects the microbial growth. This is in line with the observations made by other scientists (Kandasamy et al. 2015). From the diagram, maximum dry biomass has been obtained as 141 ± 0.97 mg/L at initial cyanide concentration of 40 mg/L.

3.3 One Factor at a Time (OFAT) Analysis and Time Variation of Cyanide Removal

Maximum cyanide removal and maximum cell biomass content have been obtained at a particular value of each varying parameters such as at pH 10 ($85 \pm 1.05\%$, 150 ± 1.91 mg/L), with inoculum load of 4% ($92.5 \pm 0.13\%$, 157.4 ± 2.5 mg/L), at temperature 37°C ($92.5 \pm 0.13\%$, 157.4 ± 2.5 mg/L) (Fig. 2a–c). Maximum cyanide removal ($98.6 \pm 0.1\%$) has been obtained with initial concentration of 20 mg/L while maximum biomass (157.4 ± 2.5 mg/L) has been obtained at initial concentration of 40 mg/L (Fig. 2d). Suitable operating condition has been chosen based on maximum

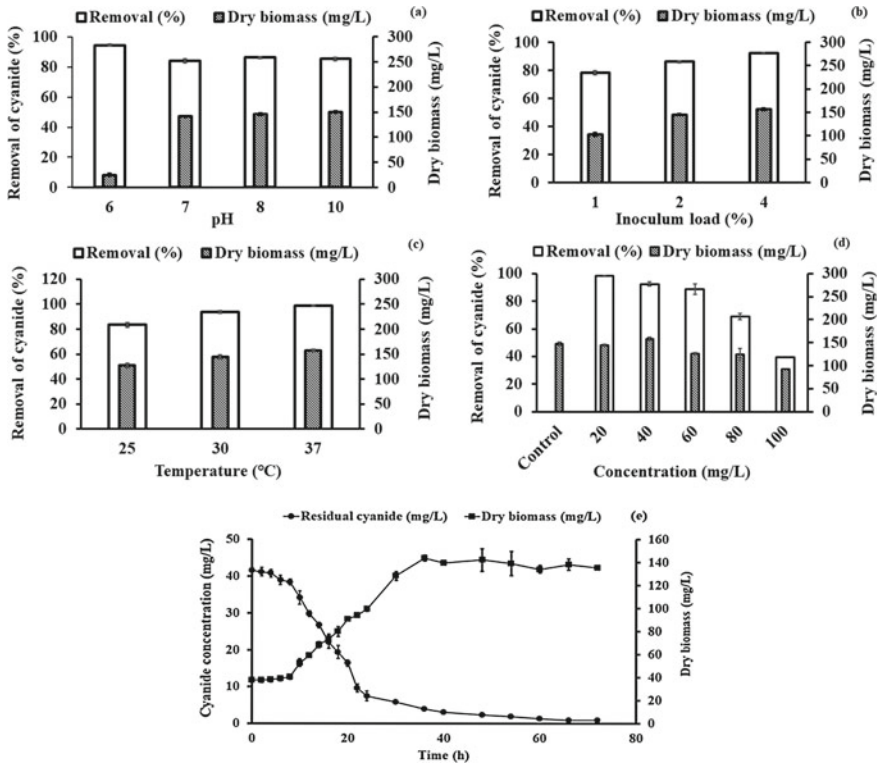


Fig. 2 Cyanide removal using *Bacillus* sp. NITD 19 at different **a** pH, **b** inoculum load, **c** temperature, **d** initial cyanide concentration, and **e** time variation study for removal of cyanide and dry biomass concentration using *Bacillus* sp. NITD 19

biomass production. Maximum cyanide degradation was observed at pH 10 but from economic point of view, pH 8 has been selected for further studies because both removal and growth at pH 8 are found nearly same to that obtained at pH 10. Further, loss of cyanide due to volatilization is also less at pH 8. Therefore, the most effective condition has been found as follows: pH 8, inoculum load 4%, temperature 37 °C, and initial concentration 40 mg/L.

Variation of removal of cyanide has been shown in Fig. 2e. From the diagram, it can be stated that cyanide has been utilized as a carbon and nitrogen sources by *Bacillus* sp. NITD 19.

3.4 Characterization of Cell Biomass

The FTIR spectra of naive and pollutant loaded *Bacillus* sp. NITD 19 biomass with wave numbers ranging from 4000 to 400 cm^{-1} have been shown in Fig. 3. The both

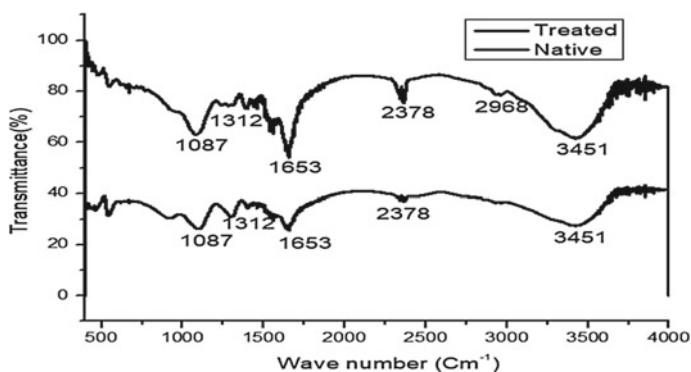


Fig. 3 FTIR spectra of native and treated cell biomass

naïve and treated bacterial biomass comprise of the characteristic bonds such as C–O stretch, C=C stretch, C–N stretch, N=O, C–H stretch, and N=H at the wavenumbers of 1087, 1653, 2378, 1312, 2978, and 3451 cm^{-1} , respectively. From the diagram, it can be stated that treated biomass has sharp and intense peaks as compared to the native cell biomass which might be due to nitrogen and carbon incorporation in the cell biomass.

4 Conclusion

The study has demonstrated the potential of *Bacillus* sp. NITD 19 to remediate cyanide, by consuming it as a carbon and nitrogen source under aerobic condition. OFAT analysis provides the suitable operational parameters for the maximum cyanide removal such as pH 8, inoculum load 4%, temperature 37 °C, and initial concentration 40 mg/L. Therefore, the present strain can efficiently be used for treatment of cyanide laden industrial wastewater in environment-friendly and cost-effective manner. However, the continuous study with real wastewater is scope of the future work.

Acknowledgements The authors are thankful to IMPRINT, Government of India [Sanction order no. F.No.3-18/2015-T.S.-I (Vol. III), dated April 24, 2017], and the National Institute of Technology Durgapur (Sanction order no. NITD/Regis/702/17, dated February 15, 2017) for providing the project funds to carry out this research work.

Conflict of Interest The authors declare that they have no conflict of interest.

Research Involving Human Participants and/or Animals This chapter does not contain any studies with human participants or animals performed by any of the authors.

Informed Consent Informed consent was obtained from all individual participants included in the study.

References

- Kandasamy S, Dananjeyan B, Krishnamurthy K, Benckiser G (2015) Aerobic cyanide degradation by bacterial isolates from cassava factory wastewater. *Braz J Microbiol* 46(3):659–666. <https://doi.org/10.1590/S1517-838246320130516>
- Luque-Almagro VM, Moreno-Vivián C, Roldán MD (2016) Biodegradation of cyanide wastes from mining and jewellery industries. *Curr Opin Biotechnol* 38:9–13. <https://doi.org/10.1016/j.copbio.2015.12.004>
- Razanamahandry LC, Onwordi CT, Saban W, Bashir AKH, Mekuto L, Malenga E, Manikandan E, Fosso-Kankeu E, Maaza M, Ntwampe SKO (2019) Performance of various cyanide degrading bacteria on the biodegradation of free cyanide in water. *J Hazard Mater* 380:120900. <https://doi.org/10.1016/j.jhazmat.2019.120900>
- Razanamahandry LC, Andrianisa HA, Karoui H, Kouakou KM, Yacouba H (2016) Biodegradation of free cyanide by bacterial species isolated from cyanide-contaminated artisanal gold mining catchment area in Burkina Faso. *Chemosphere* 157:71–78. <https://doi.org/10.1016/j.chemosphere.2016.05.020>
- Sharma M, Akhter Y, Chatterjee S (2019) A review on remediation of cyanide containing industrial wastes using biological systems with special reference to enzymatic degradation. *World J Microbiol Biotechnol* 35(5):1–14. <https://doi.org/10.1007/s11274-019-2643-8>
- Tiong BE, Bahari ZM, Lee NS, Jaafar J, Ibrahim Z, Shahir S (2015) Cyanide degradation by *Pseudomonas pseudoalcaligenes* strain W2 isolated from mining effluent. *Sains Malays* 44(2):233–238. https://www.ukm.my/jsm/pdf_files/SM-PDF-44-02-2015/10BelindaTiong.pdf
- Upendar G, Singh S, Chakrabarty J, Chandra Ghanta K, Dutta S, Dutta A (2018) Sequestration of carbon dioxide and production of biomolecules using cyanobacteria. *J Environ Manag* 218:234–244. <https://doi.org/10.1016/j.jenvman.2018.04.031>

Degradable Plastic Composite Film—A Comparison Between Photocatalytic and Biodegradation



Parbatee Nag, Aniruddha Mukhopadhyay, Amrita Debnath, Anirban Roy, and Sampa Chakrabarti

Abstract Due to the non-biodegradable and impervious nature, accumulation of plastic wastes in the environment poses an ecological threat. Plastics are generally littered into soil and water bodies. Microorganisms play a crucial role in biodegradation of plastics. They sometimes utilize these plastics as the substrate. It is also known that sunlight degrades plastic to some extent and the degradation is enhanced by adding semiconductors in the polymer matrix to promote solar photocatalysis. In this work, composite film comprising of polyvinyl chloride (PVC), polycaprolactone (PCL, for facilitating biodegradation), and Zinc Oxide (ZnO, a semiconductor photocatalyst active under sunlight) was subjected to photocatalytic and bio-degradation separately. The microbial strain capable of degrading PVC was isolated from soil and was identified as *Bacillus altitudinis*. Degradation in both cases was monitored by weight loss. Maximum degradation obtained by photodegradation was 17.8% whereas maximum biodegradation was about 10%. Photodegradation was a fast process (2 h) whereas biodegradation was a complex and slow process (25 days). The degradation by photocatalytic process followed pseudo first-order kinetics.

P. Nag · A. Mukhopadhyay

Department of Environmental Science, University of Calcutta, 35, Ballygunge Circular Road, Kolkata 700019, India

A. Debnath · S. Chakrabarti (✉)

Department of Chemical Engineering, University of Calcutta, 92, A. P. C. Road, Kolkata 700009, India

e-mail: sampac.2008@gmail.com

A. Roy

Department of Material Science and Technology, Maulana Abul Kalam Azad University of Technology, Kolkata, West Bengal 741249, India

© Springer Nature Singapore Pte Ltd. 2021

D. Ramkrishna et al. (eds.), *Advances in Bioprocess Engineering and Technology*, Lecture Notes in Bioengineering,

https://doi.org/10.1007/978-981-15-7409-2_25

1 Introduction

Environmental pollution is one of the most serious problems that the ecosystem is facing today. Increased use of plastic in every fields of life is nowadays considered as the most dangerous threat to the environment. Accumulation of waste plastic on the land is greater and more concentrated than that in the water. As per the estimate by Central Pollution Control Board (CPCB) the plastic consumption in India is 8 million tons per annum and about 5.7 million tons of plastic is converted into waste annually (Rathi 2006; Chakrabarty et al. 1995).

These waste plastics are generally littered into soil and water bodies and cause serious damage to the environment. Due to the non-biodegradable and impervious nature of plastics, if disposed in the soil, they create resistance to the recharging of groundwater aquifers in addition to polluting soil. Traditional methods for plastic waste handling are often creating new environmental difficulties. Incineration is one conventional way of treating plastic wastes but complete and incomplete combustion of waste plastics generates hazardous greenhouse gases, carcinogenic compounds, and acidic gases along with soot and ash. These combustion products are toxic, mutagenic, and endocrine disruptors (Lee et al. 1995). With the excessive use of plastics and increasing need for efficient plastic waste disposal, the demand for developing material which does not burden the environment significantly has been increased in the recent years. Many scientists advocate for the development of biodegradable plastics. But recently several disadvantages of biodegradable plastics are noticed; moreover, they are still not economical and widely available. So the need for invention of easily degradable plastic material is a demand of the day. Research is going on throughout the world to develop synthetic plastic films that can undergo degradation by several natural conditions like sunlight, ambient temperature, humidity, and microorganisms. According to different studies, soil microbial populations play crucial role in biodegradation of plastics. The polymer is first converted to its monomers during degradation then the monomers are absorbed into microbial cells and biodegraded (Goldberg 1995). The characteristics of polymer such as mobility, crystallinity, molecular weight, functional groups, and substituents present in its structure, and plasticizers or additives, all play significant roles in its degradation (Artham and Doble 2008; Gu et al. 2000). Campos et al. (2011) showed that plastic-blended films were achieved significant biodegradation in a very short incubation time. Ishigaki et al. (1999) have studied the mechanism of biodegradation of the blended film. It is also true that light energy generally degrades plastic. Solar photodegradation of plastics can be enhanced using semiconductor photocatalysis (Cho and Choi 2001; Zhang et al. 2004). Cho and Choi (2001) reported 27% loss in weight for PVC-TiO₂ film (1.5 wt% TiO₂) under 200 W mercury lamp (1.5 mW/cm² between 300 and 400 nm wavelength) after 300 h of exposure. On the other hand, Zhang et al. (2004) observed about 50% weight loss with TiO₂-PVC film under a 250 W lamp (2.0 mW/cm²) in 250 h. Chakrabarti et al. (Chakrabarti and Dutta 2008; Sil and Chakrabarti 2010; Chakrabarti et al. 2011) reported photocatalytic degradation of polymer-ZnO composite materials. In another study, they showed 12.29%

of degradation of PVC nanocomposite film comprising sonochemically synthesized Fe-doped ZnO nanoparticles in 3.5 h when exposed to the sunlight (Das et al. 2016).

The aim of this work is to develop a plastic composite film comprising polyvinyl chloride (PVC), zinc oxide (ZnO, a semiconductor photocatalyst), and polycaprolactone (PCL, a biodegradable organic compound) and to compare photocatalytic and biodegradation of the film. The source of light was sunlight and the source of microbes was contaminated soil.

2 Materials and Methods

2.1 Materials

PVC powder (free from plasticizers) was obtained from Reliance Industries Ltd. (trade name—Reon-grade 67–01), with k value 67 ± 1 . Cyclohexanone ($C_6H_{10}O$, Mol. Wt. 98.15) was obtained from E. Merck, Mumbai. Zinc oxide (ZnO-extra pure AR grade) was obtained from Sisco Research Laboratories Pvt Ltd Mumbai, India and Polycaprolactone (PCL-Sigma-Aldrich, USA).

2.2 Methods

2.2.1 Preparation of Plastic Composite Film Comprising PVC, PCL & ZnO

The plastic composite film was prepared by adding 0.625 gm of PVC powder in 25 ml of cyclohexanone using a magnetic stirrer to obtain a clear viscous solution. Then 0.125 gm polycaprolactone and finally 0.025 gm ZnO was added into it with continuous stirring for about 3 h to facilitate biodegradation and photodegradation, respectively. The suspension was then cast on a clean glass petridish (15 cm diameter) and air dried at ambient condition. Thickness of the film was about 50 μ m. Samples of approximately 7 cm \times 2 cm were cut from the film.

2.2.2 Photocatalytic Degradation of the Film Under Sunlight

Weighed samples of composite film were exposed horizontally in the photocatalytic reactor to the sunlight in presence of air and water. The reactor was a jacketed stainless steel (SS) box filled with water. The top cover was a quartz sheet for allowing sunlight. Air was bubbled through water in the reactor for supplying oxygen. The intensity of solar radiation inside the reactor was measured using a digital luxmeter (Dispart & Coalescent digital lux meter LX-101). The sample was withdrawn from the reactor

at specific time intervals and the degradation was monitored by weight loss of the sample using weighing balance (model no. BT 224 S, Max 220 gm, $d = 0.1$ mg, made by Sartorius) as described by Sil and Chakrabarti [2010](#).

2.2.3 Collection of Soil Sample

Soil sample was collected from a depth of 4–5 cm from Captain Bhery Eco & Aquatic Hub located at Tapuriaghata, E. M. Bypass Road, Kolkata-700105 for microbial isolation that was used for biodegradation of plastics. The site was used for dumping municipal solid waste along with huge amount of plastic materials either openly or partially buried in the soil. Sample was collected using a sterile spatula and aseptically taken to the laboratory for further analysis.

2.2.4 Isolation and Identification of PVC-Degrading Microbes from Soil

A stock solution of the collected soil sample was prepared by mixing 1 gm soil with 10 ml of normal saline water (0.9%). Single colonies were obtained after 24 h incubation at 37 °C temp. Single colonies were further subcultured on freshly prepared nutrient agar slant to obtain pure cultures. Mineral Salt Media (MSM) was used for screening bacteria from the isolated pure culture those were able to degrade PVC. PVC was used in the media as a major carbon source because MSM contain all nutrients except carbon necessary for bacterial growth for 4–8 weeks at 37 °C for isolating PVC-degrading bacteria. A control set was maintained (bacterial inoculation on media without polymer) simultaneously. The culture was identified by MTCC (CSIR), Chandigarh for 16S rRNA gene sequencing (1434 bases) and Blast search.

2.2.5 Biodegradation of the Film Using Isolated Microorganisms

Accurately weighed and sterilized plastic composite films were aseptically transferred to the 250 ml conical flasks having 50 ml of sterile MSM broth with 0.1% yeast extract in the laboratory. Except control each conical flask was inoculated with 5% of isolated PVC-degrading bacteria at approximately the same time. All the flasks were then incubated in a temperature-controlled shaker at 160 rpm at 37 °C for 25 days. After every 5 days, the films were recovered from the media and adhered bacterial cells, if any, were washed off from the surface of the film with 2% (v/v) SDS (sodium dodecyl sulphate) and further washed with distilled water (Gilan et al. [2004](#)). The washed films were then dried overnight at 60 °C and finally the degradation was monitored by loss of weight.

2.2.6 Characterization of the Film Before and After Degradation

Characterization of all the films was done by Scanning Electron Microscopy (SEM; Model No. S3400N, VP SEM, Type- II, Hitachi, Japan) along with Fourier Transformed Infra-Red Spectroscopy (FTIR; Perkin Elmer 1- Spectrum-2, Singapore) before and after photocatalytic degradation in addition to biodegradation. SEM was used for determining surface morphology whereas FTIR was used for functional group study.

3 Results and Discussion

3.1 Isolation of PVC-Degrading Strains

22 morphologically different isolates were obtained from the collected soil sample. Among these 22 isolates only 5 strains (FS1, FS2, FS3, FS4, and FS5) were able to degrade plastic composite film comprising PVC, PCL, and ZnO. The present work has been conducted by FS1 strain only and therefore FS1 is only identified.

3.2 Identification of Strain FS1

On the basis of 16 s rRNA gene sequencing method the FS1 strain was characterized as *Bacillus altitudinis*. Highlights of the colony morphology are: irregular configuration and margin, rough surface with raised elevation; gram-positive spore forming bacteria and can form pigment; spores are oval and centrally positioned. Growth characteristics indicate its positive growth in the temperature range 15–50 °C, pH range 5–9, and salt concentration of 3–9%. Biochemically they are positive in Casein, gelatin hydrolysis, catalase, and Esculine hydrolysis.

3.3 Photodegradation and Biodegradation of Plastic Composite Film

Maximum degradation obtained by photocatalysis was 17.8% after 120 min as it is a fast process whereas after 25 days maximum 10% microbial degradation was achieved because any biological process is actually a complex and slow process. For comparison, blank experiments with PVC, PVC-ZnO composite, and PVC-PCL composite films were subjected to the same experimental conditions (Figures not shown). The observed data have been represented in Fig. 1a, b. Average intensity of light was 341×100 lx in case of solar degradation. From Fig. 1a, b, it is observed

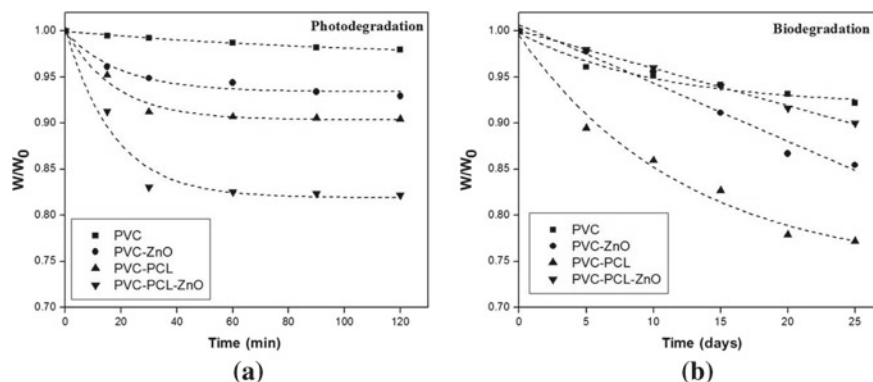


Fig. 1 Typical time-weight profile for **a** photo and **b** biodegradation of composite films

that PVC-PCL-ZnO had experienced the maximum photodegradation by sunlight whereas maximum biodegradation occurred for PVC-PCL composite film. Hydroxyl radical was generated on the surface of ZnO photocatalyst and it attached the PVC and PCL molecules in the former case and for the later case, presence of the biodegradable component PCL is responsible for the maximum biodegradation (Hoffmann et al. 1995; Turchi and Ollis 1990). PVC-ZnO composite film also degraded considerably by bacteria since ZnO acted both as a micronutrient and as a support for the biofilm (Brown et al. 2017).

3.4 Characterization

3.4.1 Scanning Electron Microscopy (SEM)

The untreated PVC-PCL-ZnO film showed almost plain surface. Since photodegradation was rapid and much higher, surface of the film after photodegradation was more rough and ruptured compared to the same after biodegradation which is a slow process degrading less amount of the film. This change in the morphology is due to the mechanical or physical action of microorganisms on PVC surface (Webb et al. 2012). Surface morphology of the other films is not shown (Fig. 2).

3.4.2 Infra-Red with Fourier Transform (FTIR)

After FTIR analysis some common peaks were observed in PVC, PVC-ZnO, and PVC-ZnO-PCL along with specific peaks. In PVC few specific peaks were present at approximately 2552, 2399, 2243, 2087, and 1936 cm^{-1} those were not found in other two samples; this may be due to the presence of $\text{C}\equiv\text{C}$ stretch or $\text{C}=\text{C}=\text{C}$ antisym

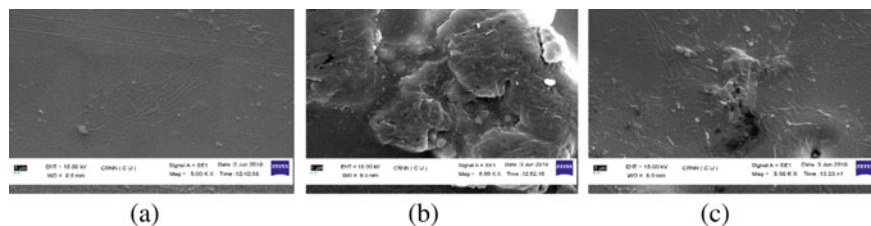


Fig. 2 SEM images of PVC-PCL-ZnO film **a** untreated **b** after photodegradation **c** after biodegradation

stretch or O–H stretching of carboxylic acid group. Similarly in PVC-ZnO, due to C–Cl stretch and presence of CH_2 group in methylene chain two new peaks were found at $\sim 853\text{ cm}^{-1}$ and $\sim 749\text{ cm}^{-1}$, respectively. But none of them were found in PVC and PVC-ZnO-PCL. On the other hand, two unique peaks were observed in PVC-ZnO-PCL due to the presence of chromophore group (at $\sim 1353\text{ cm}^{-1}$) and C–O stretch (at $\sim 1067\text{ cm}^{-1}$).

4 Conclusion

In this work, various composite films comprising PVC, PCL, and ZnO particles have been subjected to photocatalytic and biodegradation separately. Degradation of PVC-PCL-ZnO film by solar photocatalysis with ZnO catalyst in 120 min was the maximum (17.8%). Biodegradation was accomplished by a microbe isolated from contaminated soil. The microbe was later identified as *Bacillus altitudinis* by 16S rRNA gene sequencing method. Biodegradation after 25 days was maximum for the PVC-PCL film (22.81%) whereas PVC-PCL-ZnO film experienced 10% biodegradation. A sequential photo- and biodegradation may be tried so that the overall degradation may be enhanced. A photo-bio-degradable film may be developed in this way.

Acknowledgements Informed consent was obtained from all individual participants included in the study. The authors are especially grateful to the authorities of Captain Bhery Eco & Aquatic Hub located at Tapuriaghata, E. M. Bypass Road, Kolkata-700105 for their kind gift of the soil sample for isolating microbial strain.

References

- Artham T, Doble M (2008) Fouling and degradation of polycarbonate in seawater: field and lab studies. *J Polym Environ* 17:170–180
- Brown LR, Caulkins RC, Schartel TE et al (2017) Increased zinc availability enhances initial aggregation and biofilm formation of *Streptococcus pneumoniae*. *Front Cell Infect MI* 7:233

- Campos A, Marconato JC, Franchetti M et al (2011) Biodegradation of blend films PVA/PVC, PVA/PCL in soil and soil with landfill leachate. *Braz Arch Biol Technol* 54:1367–1378
- Chakrabarti S, Bhattacharjee S, Sil D, Chaudhuri B et al (2011) Comparison of the photocatalytic degradation of polyvinyl chloride and polystyrene with zinc oxide semiconductor catalyst under tropical sunlight. *CTAIJ* 6:58–64
- Chakrabarti S, Dutta BK (2008) Advanced technology in environmental remediation. *Int J Environ Technol Manage* 9:34–46
- Chakrabarty P, Srivastava VK, Chakrabarti SN et al (1995) Solid waste disposal and the environment—a review. *Indian J Environ Prot* 15:39–43
- Cho S, Choi W (2001) Solid-phase photocatalytic degradation of PVC-TiO₂ polymeric composites. *J Photochem Photobiol A* 143:221
- Das P, Roy A, Chakrabarti S et al (2016) Photocatalytic degradation of the nanocomposite film comprising polyvinyl chloride (PVC) and sonochemically synthesized iron-doped zinc oxide: a comparative study of performances between sunlight and UV radiation. *J Polym Environ* 25:1231–1241
- Gilan I, Hadar Y, Sivan A et al (2004) Colonization, biofilm formation and biodegradation of Polyethylene by a strain of *Rhodococcus ruber*. *Appl Microbiol and Cell Physiol* 65:97–104
- Goldberg P (1995) Product differentiation and oligopoly in international markets: the case of the U.S. *Automob Indus J Econom* 63:891–951
- Gu JD, Mitton DB, Mitchell R et al (2000) Microbial degradation of polymeric materials. *Uhlig Corrosion Handbook* 3:439–460
- Hoffmann MR, Martin ST, Choi W, Bahenemann DW et al (1995) Environmental applications of semiconductor photocatalysis. *Chemb Rev* 95:69–96
- Ishigaki T, Kawagoshi Y, Ike M, Fujita M et al (1999) Biodegradation of a polyvinyl alcohol—starch blend plastic film. *World J Microb Biot* 15:321–327
- Lee H, Wang L, Shin JF et al (1995) Mutagenicity of particulates from the laboratory combustion of plastics. *Mutat Res* 346:135–144
- Rathi S (2006) Alternative approaches for better municipal solid waste management in Mumbai, India. *J Waste Manag* 26:1192–1200
- Sil D, Chakrabarti S (2010) Photocatalytic degradation of PVC–ZnO composite film under tropical sunlight and artificial UV radiation: a comparative study. *Sol Energy* 84:476–485
- Turchi CS, Ollis DF (1990) Photocatalytic degradation of organic water contaminants: mechanisms involving hydroxyl radical attack. *J Catal* 122:178–192
- Webb HK, Arnott J, Crawford RJ, Ivanova EP et al (2012) Plastic degradation and its environmental implications with special reference to poly(ethylene terephthalate). *Polym* 5:1–18
- Zhang K, Cao W, Zhang J et al (2004) Solid-phase photocatalytic degradation of PVC by tungstophosphoric acid—a novel method for PVC plastic degradation. *Appl Catal* 276:67

Optimization of Energy-Proficient Infrared Radiated Rapid Hydrolysis of Pineapple Skin to Reducing Sugar



Swapnendu Chatterjee, Sayan Kumar Bhattacharjee, Rajdip Roy, and Rajat Chakraborty

Abstract Waste pineapple skin (WPS) has been hydrolyzed into reducing sugar (RS) using Amberlyst 15 catalyst. The effects of the application of infrared radiation on the intensification of hydrolysis of WPS have been evaluated. The Taguchi orthogonal design determined optimal values of process factors, viz., 70 °C reactor temperature, 30 min batch time, water to WPS ratio (w/w) of 35, and 2 wt% catalyst concentration, corresponding to maximum 86.78% RS yield employing an infrared radiated batch reactor (IRRBR). Remarkably, the RS yield in IRRBR was significantly greater than that obtained (45.62%) using a traditional batch reactor (TBR) at the derived optimal conditions.

Keywords Energy-proficient hydrolysis · Waste pineapple skin · Amberlyst 15 catalyst · Taguchi optimization · Infrared radiation

1 Introduction

Lignocellulosic biomass (LB), comprises cellulose (40–50%), hemicelluloses (30–40%), and lignin (20–30%). Cellulose hydrolysis plays an important key technology for the synthesis of RS from naturally abundant LB such as wood waste, agricultural crops, and fruit processing industries, i.e., waste pineapple skin (WPS) (Seker and Zain 2014; Zain et al. 2010), and cotton straw (Yang et al. 2013). Many industrially important chemicals such as bioethanol, furfural, HMF, and levulinic acid can be derived from RS (Limayem and Ricke 2012; Huber et al. 2006; Palmqvist and Hahn-Hägerdal 2000).

Homogeneous alkaline hydrolysis has some disadvantages, viz., long reaction time and high alkali concentrations (Kucuk and Demirbas 1999). Hydrolysis catalyzed by homogeneous acid for synthesis of RS from cellulose suffers from several drawbacks, i.e., leaching, handling, corrosions and generation of hazardous waste streams, and long reaction time (Orozco et al. 2007). In the last few years,

S. Chatterjee · S. K. Bhattacharjee · R. Roy · R. Chakraborty (✉)
Chemical Engineering Department, Jadavpur University, Kolkata 700032, India
e-mail: rajat.chakraborty@jadavpuruniversity.in

© Springer Nature Singapore Pte Ltd. 2021

257

D. Ramkrishna et al. (eds.), *Advances in Bioprocess Engineering and Technology*,
Lecture Notes in Bioengineering,
https://doi.org/10.1007/978-981-15-7409-2_26

some works on ionic liquids demonstrated higher yield of RS (Φ_g); however, higher costs made the overall process economically unattractive (Rinaldi et al. 2008; Zhang and Zhao 2009).

To overcome these difficulties, many researchers have shown much interest in the application of heterogeneous solid acid catalysts for LB hydrolysis (Suganuma et al. 2008). Recently, Meena et al. (2015) used Amberlyst 15 as solid acid catalyst for rice straw hydrolysis, but owing to higher mass transfer resistance between insoluble cellulose and solid acid, this method demonstrated poor hydrolysis efficiency.

In the last decade, microwave irradiation was applied to hasten the LB hydrolysis for RS synthesis (Vani et al. 2012; Chakraborty and Sahu 2014). Nonetheless, the yield was relatively low (20–45%) using HY zeolite in a microwave reactor (400 W) for 4 min (Zhang and Zhao 2009). Vani et al. (2012) reported a maximum Φ_g of 0.495 g/g applying 300 W power input for 6 min (108 kJ). Notably, high-pressure pretreatment (180 °C, 100 rpm for 45 min) repeated for 5 times, consumed approximately 540 kJ energy.

Recent work has exhibited the energy-efficient and time-saving application of infrared radiation (IRR) to intensify the trans-esterification reaction of waste tallow to produce ecologically benign cost-effective biodiesel (Chakraborty and Sahu 2014). Notably, no scientific report is available on the application of IRR especially for intensification of hydrolysis of WPS for production of RS.

Taguchi L_9 orthogonal array has been used to evaluate the optimal process conditions to achieve maximum Φ_g (Chakraborty and RoyChowdhury 2013).

This article reports the synthesis of RS by hydrolysis of pretreated WPS (PWPS) using commercial Amberlyst 15 catalyst in an infrared radiated batch reactor (IRRBR). The pretreatment of WPS, traditional Ammonia fiber explosion (AFEX) pretreatment has been modified through the application of IRR. Taguchi orthogonal experimental matrix (TOEM) was employed to evaluate the effects of four process factors, viz., PWPS to catalyst ratio(w/w), IRRBR Temperature (°C), water to PWPS ratio(w/w), and reaction time (min) and to evaluate the optimal factorial values corresponding to maximum Φ_g .

2 Materials and Methods

2.1 Materials

The WPS was collected from a local market and analytical reagent (AR) grade chemicals, viz., DNS (di-nitro salicylic acid) and aq. NH_4OH (25 wt%) were procured from Merck (India); Amberlyst 15 catalyst was sourced from SIGMA-ALDRICH.

Table 1 Experimental factors and levels for hydrolysis of PWPS

Process factors	X_{pc} (W/W)	X_T (°C)	X_{wp} (W/W)	X_t (min)
Level 1	1	60	15	30
Level 2	2	70	25	45
Level 3	3	80	35	60

2.2 Pretreatment

In the present study, the conventional AFEX pretreatment process has been modified through the incorporation of IRR replacing the traditional heating method.

2.3 Experimental Design and Optimization of RS Hydrolysis

The individual process factors and their levels are tabulated in Table 1 and the experimental runs were performed in triplicate employing different combinations of the four process factors, viz., PWPS to catalyst ratio (X_{pc}), IRRBR temperature (X_T), water to PWPS ratio (X_{wp}), and batch time (X_t) as per TOEM (Table 2). TOEM was employed to assess the interactions among process factors and to determine a set of optimal process factors corresponding to maximum Φ_g through computation of corresponding signal-to-noise (S/N) ratios using the software MINITAB-16 (Minitab Inc. USA for Windows 7).

The S/N ratio values corresponding to the maximum Φ_g were calculated, using “larger the better” characteristics. The S/N ratio for any run was computed using the yield of RS, i.e., y_i of the corresponding run (Eq. 1):

$$S/N = -10 \log \left(\frac{1}{n} \sum_{i=1}^n \frac{1}{y_i^2} \right) \quad (1)$$

where, i is the number of replicates and n is the number of trial experiments performed in any particular factorial combinations as per Table 2.

2.4 Hydrolysis Procedure of PWPS

Hydrolysis of PWPS was carried-out in an IRRBR consisting of a 0.5 L three-neck flask under IR irradiation (150 W; wavelength: 15 μm to 1 μm) equipped with a mechanical stirrer (speed 700 rpm), and a PID temperature controller was used to maintain the isothermal condition corresponding to the set point. A similar design was applied in TBR excepting that, a traditional heating mantle (as a heat

source, 500 W) was provided instead of FIR. The traditional AFEX pretreatment was modified by employing FIRR. In a representative hydrolysis run, a measured amount of PWPS and Amberlyst 15 (Table 2) were initially loaded in the IRRBR reactor followed by addition of distilled water (taken as the zero time) at fixed water to PWPS ratio (35 w/w, pH = 6.7). After the specified time, the reaction mix was filtered to separate the solid catalyst and PWPS residue. Additionally, the yield of RS (mol%) was evaluated according to Girisuta et al. (2013). The concentration of each compound in hydrolysis product was determined through calibration curves prepared by analyzing standard solutions of respective compounds of known concentrations. The superiority of IRRBR over TBR in the hydrolysis of PWPS was evaluated by comparing the RS concentration obtained in TBR at the TOEM derived optimal process conditions. Furthermore, hydrolysis of PWPS was conducted in absence of Amberlyst 15 using IRRBR and TBR at the optimal conditions. The resulting RS yields were analyzed and compared with that of the catalytic hydrolysis to study the effects of the catalyst on the PWPS hydrolysis.

3 Results and Discussion

3.1 TOEM Analysis

The design of hydrolysis experiments as per TOEM and mean of three experimental values of Φ_g along with the computed S/N ratio (Eq. 1) are presented in Table 2.

Summary results of the ANOVA (Table 3) indicate that the p values of X_T and X_t are significant ($P < 0.05$) among the other process parameters.

Table 2 L9 orthogonal experimental matrix at different operating conditions and corresponding mean Φ_g and signal-to-noise (S/N) ratio

Trial No	X_{pc} (w/w)	X_T (°C)	X_{wp} (w/w)	X_t (min)	Φ_g (mol/mol)	S/N ratio(dB)
1	L_1	L_1	L_1	L_1	75.67 ± 0.12	37.58
2	L_1	L_2	L_2	L_2	84.19 ± 0.23	38.50
3	L_1	L_3	L_3	L_3	79.51 ± 0.14	38.01
4	L_2	L_1	L_2	L_3	73.84 ± 0.21	37.37
5	L_2	L_2	L_3	L_1	86.78 ± 0.19	38.77
6	L_2	L_3	L_1	L_2	82.23 ± 0.22	38.30
7	L_3	L_1	L_3	L_2	74.87 ± 0.34	37.49
8	L_3	L_2	L_1	L_3	81.68 ± 0.13	38.24
9	L_3	L_3	L_2	L_1	80.27 ± 0.41	38.09

Table 3 Analysis of variance (ANOVA)

Source	DF	Adj SS	Adj MS	F-value	p-value
X_{pc}	1	1.084	1.0837	0.05	0.838
X_T	1	51.803	51.8028	49.27	0.014
X_{wp}	1	0.416	0.4161	0.02	0.899
X_t	1	9.856	9.8560	30.43	0.036
Error	4	91.383	22.8458		
Total	8	154.542			

Table 4 S/N ratios at different levels of the process factors and delta values (difference of the S/N values between highest and lowest levels of process factors)

Level	X_{pc}	X_T	X_{wp}	X_t
1	38.03	37.48	38.04	38.15*
2	38.14*	38.51*	37.99	38.10
3	37.94	38.13	38.09*	37.87
Delta	0.21	1.03	0.10	0.27
Rank	3	1	4	2

*Optimal factorial levels corresponding to highest S/N ratio that results in highest RS yield

3.2 Optimal Process Conditions

The higher the difference between the minimum and maximum S/N ratios in each factor, the higher is its effect on the Φ_g (Table 4). The optimal conditions of hydrolysis were found to be 2 X_{pc} , 70 °C X_T , 35 X_{wp} , and 30 min X_t , that resulted in the highest S/N ratio (38.77) corresponding to highest Φ_g (86.78).

3.3 Interaction Among Process Factors for Hydrolysis Process

An increment in catalyst concentration at all values of reaction temperature rendered augmented Φ_g over the range of factorial values (Fig. 1a). Similarly, at any given catalyst concentration, an increase in temperature resulted in higher Φ_g . At the lowest X_{wp} values, any rise in catalytic concentration (X_{pc}) resulted in higher Φ_g (Fig. 1b). On the other hand, due to increment in hydrolysis time (X_t) above 40 min resulted in lower Φ_g owing to the conversion of RS into undesired products (Fig. 1c). From Fig. 1d, the interaction between X_{wp} and X_T indicated that for any given X_{wp} over factorial range considered in the present study an increase in hydrolysis temperature resulted in greater Φ_g . From Fig. 1e an interesting observation between X_T and X_t could be observed for a given hydrolysis time. Any augmentation in IRR temperature

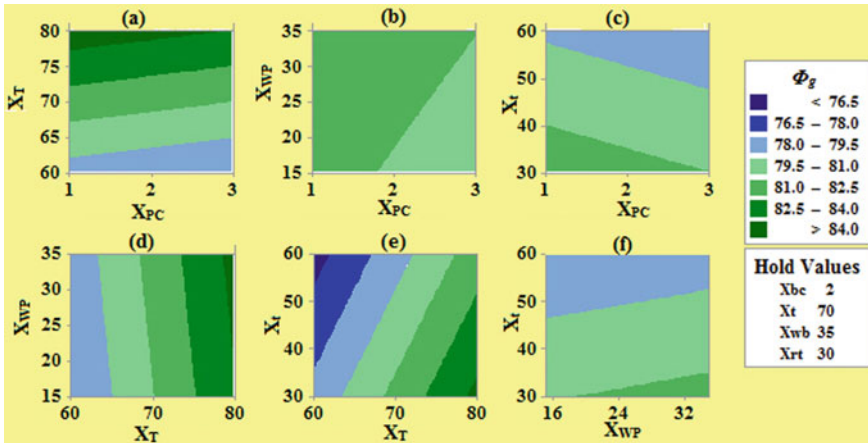


Fig. 1 Interaction plots depicting factorial effects on RS yield

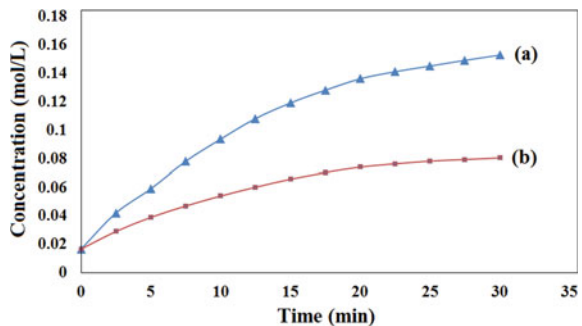
could facilitate greater Φ_g . Furthermore, it could be evident from Fig. 1f that for any X_{wp} over the experimental range, has a negative influence on Φ_g .

The optimal process conditions derived through Taguchi analysis were (Run NO. 5): 2 X_{pc} , 70°C X_T , 30 min X_t , 35 X_{wp} (Table 4). The hydrolysis conducted at the optimal conditions, exhibited a standard deviation in the range from ± 0.167 to ± 0.452 .

3.4 Effect of Infrared Radiation on Hydrolysis Kinetics at Optimal Conditions

A comparative assessment of the time evolution of RS concentrations in IRRBR and in TBR is depicted in Fig. 2. In case of IRR, it can be concluded that as the time proceeds from 0–30 min the concentration of RS could be increased rapidly and

Fig. 2 Comparative assessment of time evolution of RS concentration using a IRRBR and b TBR



reached a maximum value of 0.1527 mol/L corresponding to max Φ_g (86.78 mol%). Whereas, using traditional heating system, the RS yield increased slowly and reached its maximum value ($\Phi_g = 45.62$ mol%) at 30 min. Notably, in absence of catalyst, a lower RS yield of 75.43 mol% was observed in comparison with that obtained (86.78 mol%) in catalytic hydrolysis of PWPS by keeping all other factors at optimum level.

Thus, it was found that IRR could accelerate the hydrolysis of pretreated WPS (PWPS) significantly and also shortened the conversion time to obtain the maximum Φ_g as compared to the traditional heating method as IRR could penetrate hydrolysis mix more intensely to disrupt cellulosic-crystalline structures. The impingement of IRR causes accelerated stretching vibration of reactant molecules rendering rigorous molecular collisions, thus, enhancing hydrolysis conversion of PWPS.

4 Conclusion

The present study demonstrates an energy-efficient novel hydrolysis process to convert waste pineapple skin into RS using infrared radiated reactor. A significant saving in batch time, and higher yield of RS at a considerably lower temperature could be achieved compared to the traditional batch reactor. A significant amount of energy could be saved through the application of infrared radiation (150 W) in comparison with the traditional heating system (500 W). The present study also demonstrates effective valorization of waste pineapple skin through the preparation of RS by a cost-effective and environmentally benign process. The method may also be exploited in the future for hydrolysis of other lignocellulosic biomass for the synthesis of RS.

References

- Chakraborty R, Sahu H (2014) Intensification of biodiesel production from waste goat tallow using infrared radiation: process evaluation through response surface methodology and artificial neural network. *Appl Energy* 114:827–836
- Chakraborty R, RoyChowdhury D (2013) Fish bone derived natural hydroxyapatite-supported copper acid catalyst: Taguchi optimization of semibatch oleic acid esterification. *Chem Eng J* 215–216:491–499
- Girisuta B, Dussan K, Haverty D, Leahy JJ, Hayes MHB (2013) A kinetic study of acid catalysed hydrolysis of sugar cane bagasse to levulinic acid. *Chem Eng J* 217:61–70
- Huber GW, Iborra S, Corma A (2006) Synthesis of transportation fuels from biomass: chemistry, catalysts, and engineering. *Chem Rev* 106:4044–4098
- Kucuk MM, Demirbas A (1999) Kinetic study on hydrolysis of biomass (*Ailanthus altissima chips*) by using alkaline-glycerol solution. *Energ Convers Manage* 40:1397–1403
- Limayem A, Ricke SC (2012) Lignocellulosic biomass for bioethanol production: current perspectives, potential issues and future prospects. *Prog Energ Combust* 4:449–467

- Meena S, Navatha S, Devi BLAP, Prasad RBN, Pandey A, Sukumaran RK (2015) Evaluation of amberlyst 15 for hydrolysis of alkali pretreated rice straw and fermentation to ethanol. *Biochem Eng J* 102:49–53
- Orozco A, Ahmad MNM, Rooney D, Walker GM (2007) Dilute acid hydrolysis of cellulose and cellulosic bio-waste using a microwave reactor system. *Process Saf Environ* 85:446–449
- Palmqvist E, Hahn-Hägerdal B (2000) Fermentation of lignocellulosic hydrolysates. II. Inhibitors and mechanisms of inhibition. *Bioresour Technol* 74:25–33
- Rinaldi R, Palkovits R, Schuth F (2008) Depolymerization of cellulose using solid catalysts in ionic liquids. *Angew Chem Int Ed* 47:8047–8050
- Seker DC, Zain NAM (2014) Response surface optimization of glucose production from liquid pineapple waste using immobilized invertase in PVA–alginate–sulfate beads. *Sep Purif Technol* 133:48–54
- Suganuma S, Nakajima K, Kitano M, Yamaguchi D, Kato H, Hayashi S, Hara M (2008) Hydrolysis of cellulose by amorphous carbon bearing SO₃H, COOH, and OH Groups. *J Am Chem Soc* 130:12787–12793
- Vani S, Binod P, Kuttiraja M, Sindhu R, Sandhya SV, Preeti VE, Sukumaran RK, Pandey A (2012) Energy requirement for alkali assisted microwave and high pressure reactor pretreatments of cotton plant residue and its hydrolysis for fermentable sugar production for biofuel application. *Bioresour Technol* 112:300–307
- Yang Z, Kang H, Guo Y, Zhuang G, Bai Z, Zhang H, Feng C, Dong Y (2013) Dilute-acid conversion of cotton straw to sugars and levulinic acid via 2-stage hydrolysis. *Ind Crop Prod* 46:205–209
- Zain NAM, Suhaimi MS, Idris A (2010) Hydrolysis of liquid pineapple waste by invertase immobilized in PVA–alginate Matrix. *Biochem Eng J* 50:83–89
- Zhang Z, Zhao ZK (2009) Solid acid and microwave-assisted hydrolysis of cellulose in ionic liquid. *Carbohydr Res* 344:2069–2072

Value Addition of Agricultural Wastes for Improved Production of Industrially Important Enzymes by Employing Co-cultivation of Fungi



Sayari Majumdar and Jayati Bhowal

Abstract The aim of the present work was to evaluate the potential of cauliflower wastes for the cost-effective production of industrially important enzymes using mono and co-culture of *Aspergillus niger*, *Aspergillus oryzae* and *Candida intermedia* under submerged fermentation. All fungal strains were able to use cauliflower wastes as sole carbon source for producing enzymes such as cellulases and xylanase. Organosolvent pretreatment of cauliflower wastes relatively removed more hemicelluloses and lignin in lignocellulosic waste residues than acid and alkali treatment. Co-cultivation produced higher amount of lignocellulose degrading enzyme system than the mono-culture used. Crude cellulases and xylanase of mono and co-culture produced on the organosolvent pretreated cauliflower wastes with the highest cellulose content were further tested for the release of reducing sugar during the saccharification process of same pretreated waste biomasses. According to our results, fungal filtrate harvested from submerged fermentation was more efficient for lignocellulolytic biomass hydrolysis than the commercial enzymes.

Keywords Cauliflower wastes · Pretreatment · Cellulases · Xylanase · Filamentous fungi

1 Introduction

High production cost of pure lignocellulose degrading enzymes is the major obstacle in the widespread commercialization of enzymatic lignocellulosic biomass hydrolysis and also contributes to our environmental pollution problem. One potential

S. Majumdar · J. Bhowal (✉)
School of Community Science and Technology, Indian Institute of Engineering Science and Technology, Shibpur, Howrah, India
e-mail: jayatibhowal@gmail.com

S. Majumdar
e-mail: sayari.majumdar@gmail.com

© Springer Nature Singapore Pte Ltd. 2021
D. Ramkrishna et al. (eds.), *Advances in Bioprocess Engineering and Technology*,
Lecture Notes in Bioengineering,
https://doi.org/10.1007/978-981-15-7409-2_27

approach to decrease the production cost as well as to offer safe and better environment could be through the utilization of cheap, abundant and renewable lignocellulosic biomass, especially agricultural waste residues as nutrient source for the polysaccharide-degrading enzyme-producing microbes. Although a variety of lignocellulosic substrates were tried for production of enzymes relevant to degradation of lignocellulosic biomass (Sridevi et al. 2015), there is only a scanty published literature available on the use of cauliflower wastes (Dhillon et al. 2011). India is the second-largest producer of cauliflower (Khedkar et al. 2017). Cauliflower has the highest waste index (Stojceska et al. 2008) among the other vegetables belonging to *Brassicaceae* family. Cauliflower wastes consist of good protein (16.1%), cellulose (16%) and hemicelluloses (8%) (Wadhwa et al. 2015). Thus, besides the low cost and higher biomass availability, cauliflower waste could serve as a very promising substrate for microbial production of industrially important enzymes. The use of this cheap agro-waste in the production of these enzymes will bring down their production cost and at the same time reduce environmental pollution due to the wastes accumulation. Filamentous fungi produce appreciable levels of polysaccharide-degrading enzymes (Ferreira et al. 2018). *Aspergillus* genus, namely, *Aspergillus niger* and *Aspergillus oryzae*, are the two most important fungi frequently used in the release of enzymes for degradation of recalcitrant biomass (Hu et al. 2011). Most literature cited *Candida albicans*, *Candida utilis*, *Candida lipolytica* and other novel strains capable of generating hydrolytic enzymes (Kuhad et al. 2011; Bansal et al. 2012). We have not yet come across any published literature reporting commercial production of cellulase and xylanase from *Candida intermedia*. This study is the first direct comparison of *C. intermedia* with two important enzyme-producing fungi *A. niger* and *A. oryzae*. There has been an increasing interest in co-cultivation or synergistic action of microbial strains for efficient metabolism of feedstock and release of enzymes in substantial amount (Cavka and Jönsson 2014). In the present study, an attempt has been made to utilize inexpensive and easily available agrowastes such as cauliflower waste as substrate for enzymes production. Searching for new fungal strain suitable for efficient production of industrially important enzymes is another objective of the present study.

2 Materials and Methods

2.1 Microorganisms

Lyophilized three filamentous fungal strains *Aspergillus oryzae* MTCC 3782, *Aspergillus niger* MTCC 9687 and *Candida intermedia* MTCC 1404 were purchased from Microbial Type Culture Collection (MTCC, Chandigarh, India). A small amount of pellet of each fungal strain was dissolved in 100 ml Erlenmeyer flasks containing 30 ml of sterilized growth medium (Czapek yeast extract agar, malt extract agar and malt yeast extract agar for *A. oryzae*, *A. niger* and *C. intermedia*, respectively). All the

flasks were placed at 30 °C for 48 h to activate the fungi. All the media components were purchased from Himedia Laboratories Pvt. Ltd., India (Mumbai, India). All the chemicals used were of analytical grade and were procured from Merck, India.

2.2 Lignocellulosic Biomass Collection and Pretreatment

Cauliflower wastes (stalk and leaf) were collected from local market of Shibpur, Howrah, West Bengal, India. They were first washed with deionized water to remove dirt and impurities. Finely crushed cauliflower wastes were pretreated separately with 1% (v/v) 0.1 N dilute HCl and 1% (w/v) 0.1 N alkali (NaOH). For organosolvent pretreatment, 10 gm of cauliflower stalk and leaf were suspended separately in 100 ml of methanol with 0.1 M sodium acetate as catalyst. Pretreatment was carried out in autoclave at 121 °C for 15 min. The solution was centrifuged and the solid portions were collected and washed with distilled water and the solution was adjusted to pH 7 with 0.1 M HCl. The pretreated cauliflower wastes were dried in oven at 50 ± 5 °C and stored in airtight container for further use.

2.3 Inoculum Preparation

The inoculum was prepared by growing the fungal strains under submerged fermentation in 150 ml Erlenmeyer flasks containing 50 ml of sterile Czapek Yeast extract (for *A. oryzae*) and Malt extract and Malt Yeast extract media (for *A. niger* and *C. intermedia*), respectively. Fungi were co-cultivated by inoculating 2 µl of spore suspension on PDA plate with a distance of 3 cm by mixing the spores and inoculating it in the centre. The plates were incubated at 29 °C for 7 days.

2.4 Evaluation of Cauliflower Wastes for Extracellular Enzyme Production by Submerged Fermentation

In the first set of experiment, fermentation was carried out in 250 ml of Erlenmeyer flasks containing 5 gm (dry weight) of each above-mentioned pretreated wastes as substrate was dissolved in distilled water and autoclaved at 121 °C for 15 min, cooled and then inoculated with spore suspension containing 1×10^7 spores/ml of actively growing mycelia of *A. oryzae*, *A. niger* and *C. intermedia*. In another set of experiment, fermentation was carried out using spore suspension of co-cultures of the above fungi (in the ratio of 1:1:1) under the same conditions as described above. All the flasks were incubated under static condition at 30 °C and enzymatic extraction

was carried out after 7 days of fermentation. All the submerged fermentations were carried out in triplicate.

2.5 *Extraction of Enzyme*

After 7 days of incubation, enzymes secreted during submerged fermentation were extracted with sodium acetate buffer (0.1 M, pH 5) under shaking at 150 rpm for 1 h at room temperature. Solids were separated through centrifugation at 3000 rpm for 20 min. Supernatants were collected, freeze-dried and stored at $-30\text{ }^{\circ}\text{C}$ for subsequent enzymatic [cellulase (endoglucanase and exoglucanase), β -glucosidase] and xylanase activities.

2.6 *Enzyme Assay*

Endo- β 1, 4 D-glucanase (carboxymethylcellulase, CMCase) and Exo- β 1, 4 D-glucanase (cellobiohydrolase) in the culture supernatants were analysed according to Ghosh (1987) using 2% carboxymethyl cellulose and 1% microcrystalline cellulose (Merck Pvt. Ltd. Darmstadt, Germany) as substrate. The absorbance was recorded at 540 nm using Spectrophotometer (JASCO V620 UV Vis spectrophotometer, Maryland, USA) (Miller 1959). β -glucosidase (cellobiase) activity was evaluated according to Herr (1979) using 2 mM *p*-nitrophenyl- β -D glucopyranoside (pNPG) (Merck Pvt. Ltd. Darmstadt, Germany) as substrate. Xylanase activity was assayed according to Bailey et al. (1992) using 1% corncob xylan as substrate.

All the assays were carried out in triplicates.

2.7 *Enzymatic Saccharification with Crude Fungal Enzymes and Commercially Available Enzymes*

Enzymatic hydrolysis of organosolvent pretreated cauliflower stalk and leaf was carried out according to Sindhu et al. (2012). The commercially available enzymes and crude enzymatic extracts obtained from mono-culture of *A. niger* and co-culture cultivations as described previously were used for carrying out the biomass saccharification of cauliflower waste biomasses. In the first substrate batch, a suspension of organosolvent pretreated (5 gm) waste biomass in 50 mM citrate buffer was incubated separately with 1 ml of commercial cellulases [Celluclast[®] from *Trichoderma reesei* (700 EGU/g)] and xylanase, [recombinant *A. oryzae* ($\geq 2500\text{ U/g}$)] in screw-capped tubes. In another set of experiment, crude fungal cellulases obtained from mono-culture of *A. niger* [Endoglucanase ($160 \pm 0.69\text{ IU ml}^{-1}$) Exoglucanase

(105 ± 2.39 IU ml⁻¹), β -glucosidase (72.31 ± 2.38 IU ml⁻¹) respectively] and co-culture (Endoglucanase (151.34 ± 0.16 IU ml⁻¹), Exoglucanase (108.33 ± 0.26 IU ml⁻¹), β -glucosidase (109.21 ± 2.31 IU ml⁻¹)), respectively, cultivations were used as enzyme source for aforementioned enzymatic saccharification process. The crude xylanase used for saccharification was obtained from mono-culture of *A. niger* (158.67 ± 3.18 IU ml⁻¹) and co-culture (164.67 ± 0.31 IU ml⁻¹) cultivation. The reaction was carried out in magnetic stirrer with hot plate (REMI Q19A, Mumbai, Maharashtra, India) at 165 rpm by maintaining the temperature at 50 °C for 5 h at pH 4.8 for cellulase and pH 5.4 for xylanase, respectively. The resultant supernatants (hydrolysates) were analysed for reducing sugar content by DNS method using glucose and xylose as the standard (Miller 1959).

The saccharification yield (hydrolysis efficiency) for both commercial and crude cellulase and xylanase enzymes

$$\text{Hydrolysis efficiency \%} = \frac{\text{Formed TRS} \times 0.9}{\text{cellulose content of pretreated substrate}} \times 100 \quad (1)$$

$$\text{Hydrolysis efficiency \%} = \frac{\text{Formed TRS} \times 0.88}{\text{hemicellulose content of pretreated substrate}} \times 100 \quad (2)$$

where TRS = Total reducing sugar content, 0.9 is the anhydro correction factor for glucose and 0.88 is the anhydro correction factor for xylose.

All the hydrolysis experiments were conducted in triplicate and the data are represented as the mean \pm SD.

Statistical Analysis

All experiments are done in triplicate and standard deviation was determined. To determine the significance, the data was analysed by one way ANOVA using Origin 2018 software. Tukey test was performed for p value determination. Values of $p < 0.05$ were considered as significant value.

3 Results and Discussion

3.1 Proximate Chemical Composition of Substrates

Proximate analysis of untreated cauliflower wastes was presented in Table 1 indicates that both stalk ($18.52 \pm 0.082^a\%$) and leaf ($17.71 \pm 0.186^{ab}\%$) were good sources of cellulose that could be further converted to fermentable sugars. However, the high hemicellulose ($13.6 \pm 0.82^b\%$ and $15.1 \pm 0.01^{a,d}\%$ for leaf and stalk, respectively) and lignin content ($11 \pm 0.22^a\%$ and $8.3 \pm 0.62^{a,d}\%$ for leaf and stalk, respectively) of both the waste substrates inhibited the bioconversion rate of cellulose indicating the

Table 1 Determination of cellulose yield, hemicellulose yield, acid soluble and insoluble or Klason lignin yield of the solid residues after pretreatment

Substrate	Pretreatment methods	Cellulose yield (% DM)	Hemicellulose yield (% DM)	ASL (% DM)	AIL (% DM)
Cauliflower stalk	Untreated	17.71 ± 0.186 ^a	13.6 ± 0.01 ^b	Negligible	8.3 ± 0.62 ^{a,b}
	Alkali (NaOH)	63.29 ± 0.40 ^a	7.54 ± 0.80 ^b	5 ± 0.29 ^c	3.3 ± 0.051 ^{a,b}
	Acid (HCl)	42.19 ± 0.27 ^a	10.36 ± 0.62 ^b	6.26 ± 0.55	2.04 ± 0.67 ^{a,b}
	Organosolvent (methanol)	77.85 ± 0.58 ^a	1.071 ± 0.71 ^b	7.11 ± 0.69 ^c	1.19 ± 0.26 ^{a,b}
Cauliflower leaf	Untreated	18.52 ± 0.082 ^a	15.1 ± 0.01 ^b	Negligible	11 ± 0.31 ^{a,b}
	Alkali (NaOH)	66.75 ± 0.57 ^a	10.39 ± 0.69 ^c	8.6 ± 0.32 ^c	2.42 ± 0.12 ^{a,b}
	Acid (HCl)	46.87 ± 0.31 ^a	12.56 ± 0.45 ^c	6.52 ± 0.46	4.48 ± 0.52 ^{a,b}
	Organosolvent (methanol)	74.97 ± 0.39 ^a	6.84 ± 0.81 ^b	9.51 ± 0.39 ^c	1.49 ± 0.68 ^{a,b}

ASL Acid soluble lignin, AIL Acid Insoluble lignin Sample evaluation is done in triplicate. Values are calculated as Mean ± SD ($n = 3$). Lowercase letters indicate significant differences ($p \leq 0.05$). Values followed by the same letter are not significantly different ($p \leq 0.05$)

requirement of pretreatment of both the biomasses. Changes in chemical composition of waste biomasses after the pretreatments were shown in Table 1 indicating that among the various pretreatment methods, organosolvent process recorded maximum recovery of cellulose content for both cauliflower leaf ($74.97 \pm 0.39^a\%$ of dry weight) and stalk ($77.85 \pm 0.58^a\%$ of dry weight) followed by alkali and acid pretreatment. Pretreatment renders cellulose more accessible by increasing porosity of substrate and accessibility of enzymes for digestibility of cellulosic biomass by disrupting cell wall physical barrier (Maurya et al. 2015). There were only $1.071 \pm 0.71^b\%$ and $6.84 \pm 0.81^b\%$ remaining hemicellulose in stalk and leaf, respectively, after organosolvent (with 0.1 M Na acetate as catalyst) pretreatment at 120 °C. Low lignin content of pretreated cauliflower wastes (Table 1) indicated that pretreatment efficiently removed lignin content by breaking ether bonds and maximal removal of lignin was observed with organosolvent treated biomasses.

3.2 Evaluation of Cauliflower Wastes for Extracellular Enzyme Production by Submerged Fermentation

In the present study, individual culture and co-culture of three selected fungal strains were aim to investigate fungal growth and subsequent enzyme production. These results were then compared with fermentations using untreated biomasses and were presented in Table 2.

Table 2 Extracellular enzyme activities on pretreated cauliflower wastes by mono and co-culture fungal strains

Microorganisms	Substrate	Pretreatment methods	Endoglucanase (IU ml ⁻¹)	Exoglucanase (IU ml ⁻¹)	β -glucosidase (IU ml ⁻¹)	Xylanase (IU ml)
<i>A. niger</i>	CS	IN-CS	43.33 \pm 0.161 ^{de}	15.56 \pm 0.161 ^c	23.67 \pm 1.28 ^{de}	54.67 \pm 0.92 ^{c,d}
		Ac-CS	107.78 \pm 0.10 ^{ae}	33.89 \pm 0.87 ^c	45.17 \pm 2.71 ^{de}	108.67 \pm 0.29 ^{c,d}
		Alk-CS	137.56 \pm 0.35 ^{de}	58.89 \pm 1.48 ^c	56.19 \pm 1.29 ^{de}	138 \pm 0.14 ^c
		Os-CS	148.56 \pm 0.69 ^{de}	105 \pm 2.39 ^c	72.31 \pm 2.38 ^{de}	141.67 \pm 0.45 ^c
	CL	IN-CL	50.56 \pm 0.23	20.89 \pm 0.23 ^c	19.15 \pm 0.49 ^b	49.34 \pm 0.99 ^c
		Ac-CL	121.67 \pm 1.74 ^{de}	47.78 \pm 0.48 ^c	39.17 \pm 0.89 ^b	85.34 \pm 0.77 ^c
		Alk-CL	132.78 \pm 1.66 ^{de}	78.89 \pm 0.58 ^c	51.19 \pm 1.21 ^b	105.34 \pm 0.428 ^c
		Os-CL	160 \pm 2.87 ^{de}	107.23 \pm 0.36 ^c	70.28 \pm 1.37 ^b	146.67 \pm 0.743 ^c
<i>A. oryzae</i>	CS	IN-CS	32.78 \pm 0.17 ^{de}	29.45 \pm 0.13 ^{b,c}	16.78 \pm 0.76	40.67 \pm 0.67 ^c
		Ac-CS	82.78 \pm 0.194 ^{b,c}	58.78 \pm 0.48 ^{b,c}	34.57 \pm 1.09	79.34 \pm 0.72 ^c
		Alk-CS	91.12 \pm 0.72 ^{b,c}	78.89 \pm 0.58 ^{b,c}	45.17 \pm 0.93	58 \pm 0.78 ^c
		Os-CS	117.23 \pm 0.79 ^{b,c}	105.23 \pm 0.36 ^{b,c}	63.26 \pm 1.17 ^{cd}	84.67 \pm 0.656 ^c
	CL	IN-CL	23.89 \pm 0.25 ^{ad}	17.31 \pm 0.55 ^{b,c}	12.39 \pm 0.69 ^{cd}	32 \pm 0.29 ^{b,c}
		Ac-CL	77.23 \pm 0.31 ^{ad}	47.23 \pm 0.89 ^{b,c}	26.54 \pm 0.78 ^{cd}	65.34 \pm 0.75 ^{b,c}
		Alk-CL	88.78 \pm 0.26 ^{ad}	69.78 \pm 0.58 ^{b,c}	44.56 \pm 1.29 ^{cd}	92 \pm 0.34 ^{b,c}
		Os-CL	106.12 \pm 0.38 ^{ad}	97.78 \pm 0.82 ^{b,c}	53.42 \pm 1.26 ^{cd}	98 \pm 0.38 ^{b,c}
<i>C. intermedia</i>	CS	IN-CS	75.56 \pm 0.53 ^c	29.24 \pm 0.25 ^{c,d}	18.72 \pm 0.34	45.34 \pm 0.272 ^{ad}
		Ac-CS	95.56 \pm 0.55 ^c	64.52 \pm 0.267 ^{c,d}	41.23 \pm 0.38	74.67 \pm 0.15 ^{ad}
		Alk-CS	109.45 \pm 0.38 ^c	78.34 \pm 0.35 ^{c,d}	63.24 \pm 0.73	89.34 \pm 0.26 ^{b,c}
		Os-CS	113.89 \pm 0.71 ^c	102.12 \pm 0.39 ^{c,d}	87.28 \pm 0.78	111.34 \pm 0.59 ^{b,c}
CL	IN-CL	61.12 \pm 0.78	26.32 \pm 0.72 ^{de}	20.21 \pm 0.56 ^{ad}	40 \pm 0.61 ^{ad}	

(continued)

Table 2 (continued)

Microorganisms	Substrate	Pretreatment methods	Endoglucanase (IU ml ⁻¹)	Exoglucanase (IU ml ⁻¹)	β -glucosidase (IU ml ⁻¹)	Xylanase (IU ml)
Co culture	CS	Ac-CL	82.78 \pm 0.54 ^e	59.48 \pm 0.82 ^{d,e}	43.26 \pm 0.47 ^{a,d}	70.34 \pm 0.69 ^{a,d}
		Ak-CL	109.45 \pm 0.91 ^c	70.28 \pm 0.77 ^{d,e}	55.61 \pm 0.31 ^{a,d}	91 \pm 0.65 ^{a,d}
		Os-CL	119.45 \pm 0.63 ^c	95.68 \pm 0.84 ^{d,e}	73.41 \pm 0.57 ^{a,d}	94.34 \pm 0.76 ^{a,d}
CL	CL	IN-CS	52.78 \pm 0.61 ^c	20.56 \pm 0.22	32.18 \pm 1.31 ^{c,d}	37.34 \pm 0.52
		Ac-CS	89.45 \pm 0.88 ^c	49.44 \pm 0.08	56.17 \pm 2.10 ^{c,d}	80 \pm 1.11 ^{c, d}
		Ak-CS	118.45 \pm 0.79 ^c	70.56 \pm 0.13	87.17 \pm 2.37 ^{c,d}	106 \pm 1.14 ^{c, d}
CL	CL	Os-CS	151.34 \pm 0.16 ^c	108.33 \pm 0.26	109.21 \pm 2.31 ^{c,d}	158.67 \pm 3.18 ^{c, d}
		IN-CL	48.34 \pm 0.35 ^c	26.45 \pm 0.52 ^{d,e}	29.18 \pm 1.25 ^c	56.67 \pm 0.21 ^c
		Ac-CL	92.78 \pm 0.61 ^c	50.56 \pm 0.56 ^{d,e}	67.81 \pm 1.38 ^c	84.67 \pm 0.65 ^c
CL	CL	Ak-CL	122.78 \pm 0.58 ^c	71.12 \pm 0.33 ^{d,e}	92.131 \pm 2.38 ^c	104 \pm 0.16 ^c
		Os-CL	142.23 \pm 0.41 ^c	106.45 \pm 0.47 ^{d,e}	115 \pm 2.47 ^c	164.67 \pm 0.31 ^c

CL Cauliflower leaf, CS Cauliflower stalk, IN In Natura, Ac Acid pretreated substrate, AK Alkali pretreated substrate, Os: Organosolvent pretreated substrate. Sample evaluation is done in triplicate. Values are calculated as Mean \pm SD ($n = 3$). Lowercase letters indicate significant differences ($p \leq 0.05$). Values followed by the same letter are not significantly different ($p \leq 0.05$)

3.2.1 Endoglucanase and Exoglucanase Activities

In mono-culture cultivation, organosolvent pretreated cauliflower leaf exhibited highest amount of endoglucanase activity ($160 \pm 2.87^{\text{d,e}}$ IU ml⁻¹) by *A. niger* while maximum exoglucanase activity was achieved with organosolvent pretreated cauliflower stalk by the same fungus ($107.23 \pm 0.36^{\text{b,c}}$ IU ml⁻¹). However, there is hardly any report on the production of cellulases by *C. intermedia* and according to our results *C. intermedia* exhibited significant endoglucanase ($119.45 \pm 0.63^{\text{c}}$ IU ml⁻¹) and exoglucanase activities ($102.12 \pm 0.39^{\text{c,d}}$ IU ml⁻¹) while cultivated on organosolvent pretreated cauliflower wastes. According to our results for pretreated cauliflower stalk, co-cultivation of the three selected fungal strains resulted in an increase in endoglucanase activity and produced a little less exoglucanase activity than individual culture of *A. niger*. From these findings, it could be inferred that presence of *A. niger* in any combination led to increase in the enzymatic activity. Thus, the other fungal strains may be considered as ‘helper strain’ and *A. niger* as the main enzyme-producing strain.

3.2.2 β -glucosidase

It was evident from Table 2 that the three fungi used in this study showed different β -glucosidase profiles. *C. intermedia* exhibited the highest amount of β -glucosidase activity (87.28 ± 0.78 IU ml⁻¹) with organosolvent pretreated cauliflower wastes under submerged fermentation. We observed higher β -glucosidase activity with the co-culture cultivation of organosolvent pretreated cauliflower wastes ($115 \pm 2.47^{\text{c}}$ IU ml⁻¹) in comparison to the independent culture. Co-culture cultivations have yielded maximum β -glucosidase activity which acts as the positive inducer for the release of endoglucanase and exoglucanase in significant quantity (Kumar et al. 2016).

3.2.3 Xylanase Activity

Among mono-culture fermentation, highest extracellular xylanase activity of $146.67 \pm 0.743^{\text{c}}$ IU ml⁻¹ by *A. niger* was shown in organosolvent pretreated cauliflower leaf. Biosynthesis of xylanase was regulated by the activation of gene transcription to xylanase by the transcriptional activator XYR1. Co-culture cultivation of pretreated cauliflower wastes had shown maximum amount of extracellular xylanase activity of $164.67 \pm 0.31^{\text{c}}$ IU ml⁻¹ and $158.67 \pm 3.18^{\text{c}}$ IU ml⁻¹ for leaf and stalk, respectively, (Table 2). Co-culture manifestation held promise because it had potential in exerting synergistic effects by cohabiting and degradation of plant polysaccharides by secretion of enzyme mixture extracellularly (Dhillon et al. 2011; Hu et al. 2011).

Table 3 Comparative analysis of crude enzymes activities of fungal extracts produced on pretreated cauliflower wastes by mono and co-culture in comparison to commercially available enzymes

Media	Endoglucanase (IU ml ⁻¹)	Exoglucanase (IU ml ⁻¹)	β -glucosidase (IU ml ⁻¹)	Xylanase (IU ml ⁻¹)
CS (<i>A. niger</i>)	160 \pm 0.69 ^{d,e}	105 \pm 2.39 ^c	72.31 \pm 2.38 ^{d,e}	141.67 \pm 0.45 ^c
CL (<i>A. niger</i>)	155.65 \pm 2.87 ^{d,e}	107.23 \pm 0.36 ^c	70.28 \pm 1.37 ^b	146.67 \pm 0.743 ^c
CS (Co culture)	151.34 \pm 0.16 ^c	108.33 \pm 0.26	109.21 \pm 2.31 ^{c,d}	158.67 \pm 3.18 ^{c,d}
CL (Co culture)	142.23 \pm 0.41 ^c	106.45 \pm 0.47 ^{d,e}	115 \pm 2.47 ^c	164.67 \pm 0.31 ^c
Commercial cellulase	150 \pm 1.56	45 \pm 1.19	64.25 \pm 1.17	–
Commercial Xylanase	–	–	–	128 \pm 1.29

CL Cauliflower leaf, CS Cauliflower stalk Sample evaluation is done in triplicate. Values are calculated as Mean \pm SD ($n = 3$). Lowercase letters indicate significant differences ($p \leq 0.05$). Values followed by the same letter are not significantly different ($p \leq 0.05$)

3.3 Comparison Between Extracted and Commercially Available Enzyme Activity Analysis

In our study, crude fungal extract from mono-culture cultivation of *A. niger* also showed better activities of lignocelulosic degrading enzymes using pretreated cauliflower wastes as substrates than other mono-culture fermentation except the activity of exoglucanase obtained from *A. oryzae*. Activities of the hydrolytic enzymes that are relevant for the degradation of lignocellulose produced in our lab from mono-culture (*A. niger*) and co-culture (*A. niger* + *A. oryzae* + *C. intermedia*) microbial sources were compared with those of commercial cellulase and xylanase. The activities of endoglucanase, exoglucanase, β -glucosidase and xylanase obtained from crude fungal extract of co-culture cultivation on organosolvent pretreated cauliflower leaf were 142.23 \pm 0.41^c IU ml⁻¹, 106.45 \pm 0.47^{d,e} IU ml⁻¹, 115.67 \pm 2.47^c IU ml⁻¹ and 164.67 \pm 0.31^c IU ml⁻¹, respectively, while those obtained from commercial cellulase and xylanase were 150 \pm 1.56 IU ml⁻¹, 45 \pm 1.19 IU ml⁻¹, 64.25 \pm 1.17 IU ml⁻¹ and 128 \pm 1.29 IU ml⁻¹, respectively. These results (Table 3) clearly indicated that except endoglucanase, all of the enzyme activities in the fungal extract (from both mono and co-culture) were higher than the available commercial enzymes.

3.4 Pretreated Cauliflower Waste Hydrolysis

Enzymatic saccharification is the penultimate as well as the most important step for the conversion of pretreated lignocelulosic substrates into the production of reducing

Table 4 Saccharification yield of crude enzymes of fungal extracts produced on pretreated cauliflower wastes by mono and co-culture in comparison to commercially available enzymes

Enzymes	Saccharification yield (%)	
	Os CS	Os CL
Crude cellulase <i>A. niger</i>	71.15 ± 1.58 ^{a,d}	69.87 ± 2.31 ^{a,d}
Crude cellulase Co culture	76.23 ± 0.78 ^{a,d}	70.87 ± 1.26 ^{a,d}
Commercial cellulase	70 ± 0.62 ^{a,d}	59.4 ± 0.78 ^{a,d}
Crude xylanase <i>A. niger</i>	68.16 ± 1.58	71.89 ± 2.31
Crude xylanase Co culture	75.61 ± 1.34	93.24 ± 1.27
Commercial xylanase	57.52 ± 0.56 ^{a,d}	87.62 ± 1.24 ^{a,d}

sugars and other value-added products. Table 4 gave the saccharification yields achieved in the bioconversion of pretreated lignocellulosic substrates for production of fermentable sugars. Results here obtained clearly indicated higher saccharification efficiency was recorded with in-house-produced cellulases and xylanase on pretreated waste biomasses than those of commercial cellulases and xylanase.

Os Organosolvent pretreatment, *CS* Cauliflower stalk, *CL* Cauliflower leaf Sample evaluation is done in triplicate. Values are calculated as Mean ± SD ($n = 3$). Lower-case letters indicate significant differences ($p \leq 0.05$). Values followed by the same letter are not significantly different ($p \leq 0.05$).

4 Conclusion

The present study highlighted the feasibility of utilization of cheap and readily available kitchen wastes as substrate for production of industrially important enzymes under submerged fermentation, with a view to developing a low-cost production system. Organosolvent treated cauliflower waste residues with the highest cellulose content induced maximum production of extracellular enzyme components in comparison to untreated one. Compared to commercial lignocellulolytic enzymes, the in-house enzymes from fungal extracts exhibited better hydrolytic efficiency under the same hydrolytic condition.

Acknowledgements Authors are thankful to Indian Institute of Engineering Science and Technology, Shibpur (Formerly Bengal Engineering and Science University, Shibpur), West Bengal, India for providing facilities for the completion of this research work. Research Scholar (S. Majumdar) is grateful to UGC for providing financial support as Senior Research Fellowship.

References

- Bailey MJ, Biely P, Poutanen K (1992) Inter laboratory testing of methods for assay of xylanase activity. *J Biotechnol* 23(3):257–270
- Bansal N, Tewari R et al (2012) Production of cellulases from *Aspergillus niger* NS-2 in solid state fermentation on agricultural and kitchen waste residue. *Waste Manag* 32:1341–1346
- Cavka A, Jönsson LJ (2014) Comparison of the growth of filamentous fungi and yeasts in lignocellulose-derived media. *Biocatal Agric Biotechnol* 3(4):197–204
- Dhillon GS, Oberoi HS, Kaur S et al (2011) Value addition of agricultural wastes for augmented cellulase and xylanase production through solid-state tray fermentation employing mixed-culture of fungi. *Ind Crops Prod* 34(1):1160–1167
- Ferreira FL, Dall'Antonia CB, Shiga EA et al (2018) Sugarcane bagasse as a source of carbon for enzyme production by filamentous fungi. *Hoehnea* 45(1):134–142
- Ghosh TK (1987) Measurement of cellulase activities. *Pure Appl Chem* 59:257–268
- Herr D (1979) Secretion of cellulase and β -glucosidase by *Trichoderma viride* ITCC-1433 in submerged culture on different substrates. *Biotechnol Bioeng* 21(8):1361–1371
- Hu HL, Van den Brink J, Gruben GS et al (2011) Improved enzyme production by co-cultivation of *Aspergillus oryzae* and with other fungi. *Int Biodeterior Biodegradation* 65:248–252
- Kumar A, Gautam A, Dutt D (2016) Co-cultivation of *Penicillium sp.* AKB-24 and *Aspergillus nidulans* AKB-25 as a cost-effective method to produce cellulases for the hydrolysis of pearl millet stover. *Fermentation* 2(2):12
- Khedkar MA, Nimbalkar PR, Chavan PV et al (2017) Cauliflower waste utilization for sustainable biobutanol production: revelation of drying kinetics and bioprocess development. *Bioprocess Biosyst Eng* 40(10):1493–1506
- Kuhad RC, Gupta R, Singh A (2011) Microbial cellulases and their industrial applications. *Enzyme Res* 2011:1–10
- Miller LG (1959) Use of Dinitrosalicylic acid reagent for determination of reducing sugar. *Anal Chem* 31(3):426–428
- Maurya DP, Singla A, Negi S (2015) An overview of key pretreatment processes for biological conversion of lignocellulosic biomass to bioethanol. *3 Biotech* 5(5):597–609
- Stojceska V, Ainsworth P, Plunkett A et al (2008) Cauliflower by-products as a new source of dietary fibre, antioxidants and proteins in cereal based ready-to-eat expanded snacks. *J Food Eng* 87(4):554–563
- Sindhu R, Binod P, Janu KU et al (2012) Organosolvent pretreatment and enzymatic hydrolysis of rice straw for the production of bioethanol. *World J Microbiol Biotechnol* 28(2):473–483
- Sridevi A, Narasimha G, Ramanjaneyulu G et al (2015) Saccharification of pretreated sawdust by *Aspergillus niger* cellulase. *3 Biotech* 5(6):883–892
- Wadhwa M, Bakshi MPS, Makkar HPS (2015) Wastes to worth: value added products from fruit and vegetable wastes. *CAB International*, 1–25

Cost-Effective and Eco-Friendly Method for Decolorization of Malachite Green by *Kocuria marina* DAGII



Daiji Brahma and Debjani Dutta

Abstract This study aims for eco-friendly removal of Malachite green (MG) by 'biosorption' process. In our study, *Kocuria marina* DAGII isolated from soil could effectively decolorize MG approximately up to 99% in continuous study. Column study was performed for MG removal at different parameters to know the probable applicability of bacterial cells in industries. Column adsorbent bed was prepared by immobilizing bacterial cells in alginate. Response surface methodology (RSM) was performed to screen and optimize different physical parameters to yield maximum dye removal percentage. Analysis of variance (ANOVA) test was performed to study the interactive effect of different parameters and adequacy of the quadratic model in dye removal. From ANOVA test, $PreR^2$ of 0.9914 and $AdjR^2$ of 0.9844 obtained indicated good agreement between experimental and predicted value and generated a reliable quadratic model for MG removal. The final parameters optimized to get maximum dye removal in continuous mode were bed height 15 cm, flowrate 0.5 ml min^{-1} , initial MG concentration 50 mg l^{-1} , and alginate concentration of 2.5% (w/v).

Keywords Malachite green · Biosorption · Column study · Response surface methodology

1 Introduction

Malachite green (MG) is a synthetic triphenylmethane dye which is widely used in several industries for dyeing purposes (Chen et al. 2011). Excessive amounts of malachite green in wastewater cause water pollution which affects water transparency and gas solubility in water. Malachite green can cause severe irritation and pain to

D. Brahma · D. Dutta (✉)

Department of Biotechnology, National Institute of Technology Durgapur, MG Avenue, Durgapur, West Bengal 713209, India

e-mail: debjani.dutta@bt.nitdgp.ac.in; debs_2000in@yahoo.com

D. Brahma

e-mail: daijibrahma.rose@gmail.com

© Springer Nature Singapore Pte Ltd. 2021

D. Ramkrishna et al. (eds.), *Advances in Bioprocess Engineering and Technology*, Lecture Notes in Bioengineering,

https://doi.org/10.1007/978-981-15-7409-2_28

human eyes and skin upon chronic exposure. Due to its several negative impacts on the ecosystem it is banned worldwide since 2006 by Food and Drug administration, United States. But MG is still used in some of the industries due to the unavailability of cheap substitute (Daneshvar et al. 2007; Bera et al. 2016; Wu et al. 2018; Lv et al. 2013). Hence, removal of MG from industrial effluent by an economically feasible method is necessary to reduce the harmful effects of MG contamination. Biological method for dye removal has gained more attention over several physical and chemical methods due to inexpensive, highly specific, and ecologically friendly nature (Srinivasan and Viraraghavan 2010). Biosorption process has several advantages over other conventional treatment methods like low capital investment, inexpensive, low operational cost, high efficiency, production of biological or chemical sludge is less, etc. (Wang et al. 2015). In recent years biosorption using micro-organisms were mostly employed for removal of contaminants due to low cost, availability in large quantities, and high efficiency nature. Among the micro-organisms bacteria could make excellent biosorbent for dye removal due to their high surface to volume ratio, high content of potential active sites, high abundance, and diverse nature. Batch operations are frequently applied for dye removal study (Volesky 2007; Parmar and Shukla 2018). Column study was performed to understand the applicability of adsorbent in dye removal. Free cells are not suitable to be used in column due to its low size, density, and tendency to plug the column (Pons and Fuste 1993). Immobilization of cells in support matrix offers advantages such as increased stability, reduced cell loss, easier solid–liquid separation, and allows more efficient utilization of the capacity of adsorbent (Adhikari et al. 2012; Bayat et al. 2015). Recently, more research is focused on the application of live microbial biomass for wastewater treatments because they do not require pre-treatments which further save operational costs (Parmar and Shukla 2018).

In our study, we aimed to effectively decolorize malachite green dye by using *Kocuria marina* DAGII cells in continuous mode. Spectrophotometric analysis was carried out to know the process of dye removal. Column study was performed at different operating conditions using immobilized *K. marina* DAGII cells as packing material. Screening and optimization of physical parameters were done by Response Surface Methodology to obtain maximum removal.

2 Materials and Methods

2.1 Microorganism and Chemicals

The gram positive bacterial strain *K. marina* DAGII was isolated from the soil of NIT Durgapur, West Bengal. Growth of bacterium was done as described (Mitra et al. 2015). The strain was aerobically maintained in brain heart infusion (BHI) agar slants for regular use by subculture method and stored at 4 °C for further use. Inoculum was prepared as described (Mitra et al. 2016, 2017). All the chemicals

used during the study were obtained from Merck, Germany. A stock solution of MG was prepared at a final concentration of 100 mg l^{-1} . An inoculum of 1.2% (v/v) was used.

2.2 Dye Decolorization Study

Dye decolorization study by live cells of *K. marina* DAGII was performed in UV-Vis spectrophotometer (TECHCOMP UV 2310) by using the formula given in Eq. 1:

$$\frac{C_o - C_t}{C_o} * 100 = \text{Dyeremoval\%} \quad (1)$$

where C_o is the initial concentration of MG (mg l^{-1}) and C_t is the final concentration of MG (mg l^{-1}).

2.3 Malachite Green Removal in Continuous Study

In batch study concentration of decolorized dye by *K. marina* DAGII cells was measured at an equal interval of one hour for 8 h. Samples were taken and centrifuged at 10,000 rpm for 10 min. The supernatant was collected and absorbance was measured at 617 nm. In column study adsorbent was prepared by immobilizing whole live cells of *Kocuria marina* DAGII in alginate with dropwise addition in calcium chloride solution was done (100 mM, Merck) as described (Bera et al. 2016). Fixed bed column of 1.5 cm diameter and length 30 cm was used during the study. Treated MG solution was collected at an outlet at regular time intervals and the concentration was measured at 617 nm. All experiments were carried out at ambient room temperature (25°C).

2.4 Optimization of Column Parameters Using RSM

Design-Expert Software (Version 8.0.7.1, Stat-Ease, Minneapolis (USA) was used for optimization and screening. Based on changing one variable at a time (COVT) experiment response surface methodology (RSM) was conducted to identify significant factors for an optimal response of MG removal by *K. marina* DAGII cells. The four independent factors studied were alginate concentration (A) (2.5–3.5%), column bed height (B) (10–15 cm), influent flow rate of MG solution (C) ($0.5\text{--}1 \text{ ml min}^{-1}$), and initial MG concentration (D) ($30\text{--}50 \text{ mg l}^{-1}$). The variables were set at fixed levels

based on results of COVT experiments. Coded values of +1, 0, and -1 correspond to high, medium, and low levels of factors.

3 Results and Discussion

3.1 Dye Removal Process in Column Study

Decolorization study was carried out in continuous mode to study efficiency of *K. marina* DAGII cells in MG removal. Spectrophotometric analysis of MG removal showed a single characteristic absorption peak at wavelength of 617 nm as shown in Fig. 1. From the analysis, no change occurred in the pattern of UV-Vis spectrum of dye during the decolorization process which suggests that dye did not undergo degradation to form other toxic metabolites. Similar observations were made by (Almeida and Corso 2014). Therefore, our results indicate that the removal process might be controlled by biosorption process.

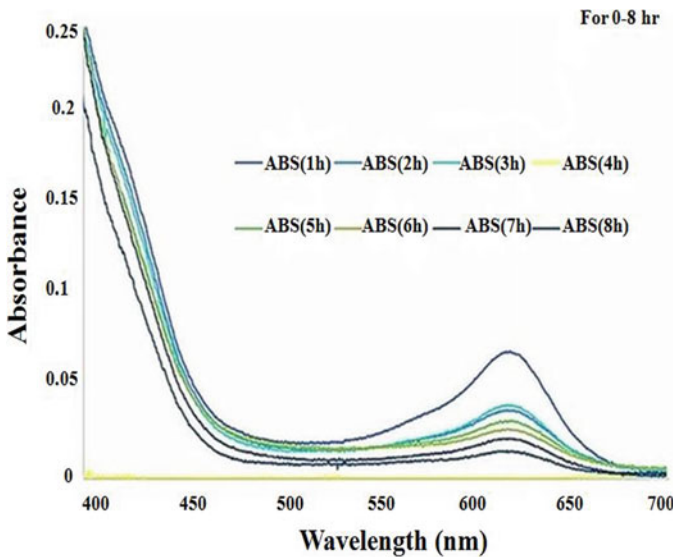


Fig. 1 Spectral scan of MG removal from 400 to 700 nm with adsorption peak at 617 nm

3.2 Application of RSM and ANOVA in Column Study

COVT experiment of dye removal by immobilized cells showed 99% removal. RSM was done to study the influence of different parameters contributing to maximum dye removal as shown in Table 1. From the data provided by ANOVA (Table 2) quadratic model was found to be significant ($p < 0.0001$). The lack of fit of model was non-significant ($p = 0.2416$). Also significant values were obtained for different parameters and their interactive effect on dye removal. In our study values of R^2 (0.9914) and R^2_{Adj} (0.9844) are highly acceptable (Fig. 2). Adequate precision of 38.197 suggested that the model can be adequately used to navigate the design space (Almeida and Corso 2014). The final model equation in terms of coded factors governing the dye removal by *K. marina* DAGII was represented as given in Eq. 2:

$$\begin{aligned} \text{MG removal (\%)} = & 98.27 + 0.012*A - 0.23*B - 0.083*C - 0.071*D \\ & + 0.033*A*B - 0.35*A*C - 0.37*A*D \\ & - 0.089*B*C + 0.21*B*D - 0.34*C*D \\ & + 0.055*A^2 - 0.055*B^2 - 0.35*C^2 - 0.024*D^2 \end{aligned} \quad (2)$$

3.3 Effect of Different Parameters on MG Removal

3.3.1 Alginate Concentration

The effect of alginate concentration in MG removal was studied. From Fig. 3 it was observed that when alginate concentration was increased from 2.5 to 3.5% (g ml^{-1}) at flow rate of 1 ml min^{-1} , removal of dye decreased from 98.3193 to 97.8572%. Results obtained by Mokhtar et al. 2017 predicted that increasing the adsorbent concentration increases removal efficiency due to more available actively binding sites and large surface area. However further increasing concentration leads to reduced removal due to aggregation of biomass (Mokhtar et al. 2017).

3.3.2 Flow Rate

The effect of flowrate on MG removal was studied. In Fig. 3b it was observed that increasing flow rate from 0.5 to 1 ml min^{-1} at initial MG concentration of 50 mg l^{-1} reduced the removal from 98.2017 to 97.565%. Ebraheim et al. (2018) reported similar results and explained that increasing flow rate decreased the service time of bed which reduces the removal of dye. Also Negrea et al. (2019) explained that increasing flow rate reduces contact time and leads to poor distribution of adsorbate inside the column which decreases removal capacity.

Table 1 Optimization using CCD in RSM for MG removal in continuous mode

Run	Factor A: Alginate concentration (g ml ⁻¹)	Factor B: Bed height(cm)	Factor C: Flow rate (ml min ⁻¹)	Factor D: Initial MG concentration (mg l ⁻¹)	Response: Removal %
1	2.5	10	0.5	50	98.14
2	3	12.5	0.75	60	97.97
3	3	12.5	0.25	40	97.11
4	2.5	10	0.5	30	97.4
5	3	12.5	1.25	40	96.66
6	3.5	10	0.5	50	98.2
7	3	12.5	0.75	40	98.29
8	3	12.5	0.75	40	98.37
9	2.5	15	1	30	97.56
10	3	7.5	0.75	40	98.47
11	3.5	10	1	50	96.81
12	2.5	15	1	50	98.04
13	3.5	10	1	30	98.8
14	3.5	15	1	50	96.58
15	3	12.5	0.75	20	98.39
16	2.5	15	0.5	50	98.25
17	2	12.5	0.75	40	98.54
18	3.5	15	1	30	97.8
19	3	12.5	0.75	40	98.23
20	3	12.5	0.75	40	98.3
21	4	12.5	0.75	40	98.45
22	3.5	10	0.5	30	98.7
23	3.5	15	0.5	30	98.1
24	3	12.5	0.75	40	98.2
25	2.5	15	0.5	30	96.51
26	3.5	15	0.5	50	98.38
27	2.5	10	1	50	98.55
28	3	12.5	0.75	40	98.22
29	2.5	10	1	30	98.69
30	3	17.5	0.75	40	97.64

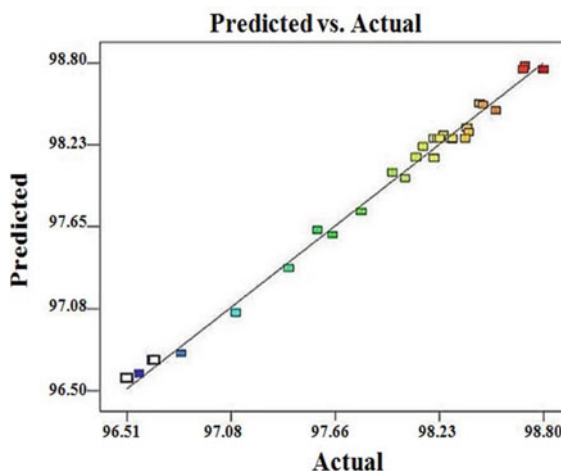
MG Malachite green

Table 2 ANOVA for MG removal in continuous study

Source	Sum of squares	DF	Mean square	F-value	p-value	
Model	12.13	14	0.87	131.61	<0.0001	Significant
A-Alginate concentration	3.75E-03	1	3.75E-03	0.57	0.4621	
B-Bed height	1.25	1	1.25	190.03	< 0.0001	
C-Flow rate	0.17	1	0.17	25.31	0.0001	
D-MG concentration	0.12	1	0.12	18.29	0.0007	
AB	0.017	1	0.017	2.57	0.13	
AC	2.02	1	2.02	306.24	<0.0001	
AD	2.25	1	2.25	341.71	< 0.0001	
BC	0.13	1	0.13	19.14	0.0005	
BD	0.73	1	0.73	111.02	<0.0001	
CD	1.81	1	1.81	274.74	<0.0001	
A ²	0.082	1	0.082	12.41	0.0031	
B ²	0.084	1	0.084	12.79	0.0028	
C ²	3.32	1	3.32	504.24	<0.0001	
D ²	0.016	1	0.016	2.43	0.1397	
Residual	0.099	15	6.58E-03			
Lack of fit	0.078	10	7.85E-03	1.93	0.2416	Non-significant
Pure error	0.02	5	4.06E-03			
Cor total	12.23	29				

DF Degree of freedom

Fig. 2 Predicted versus actual plots in continuous study



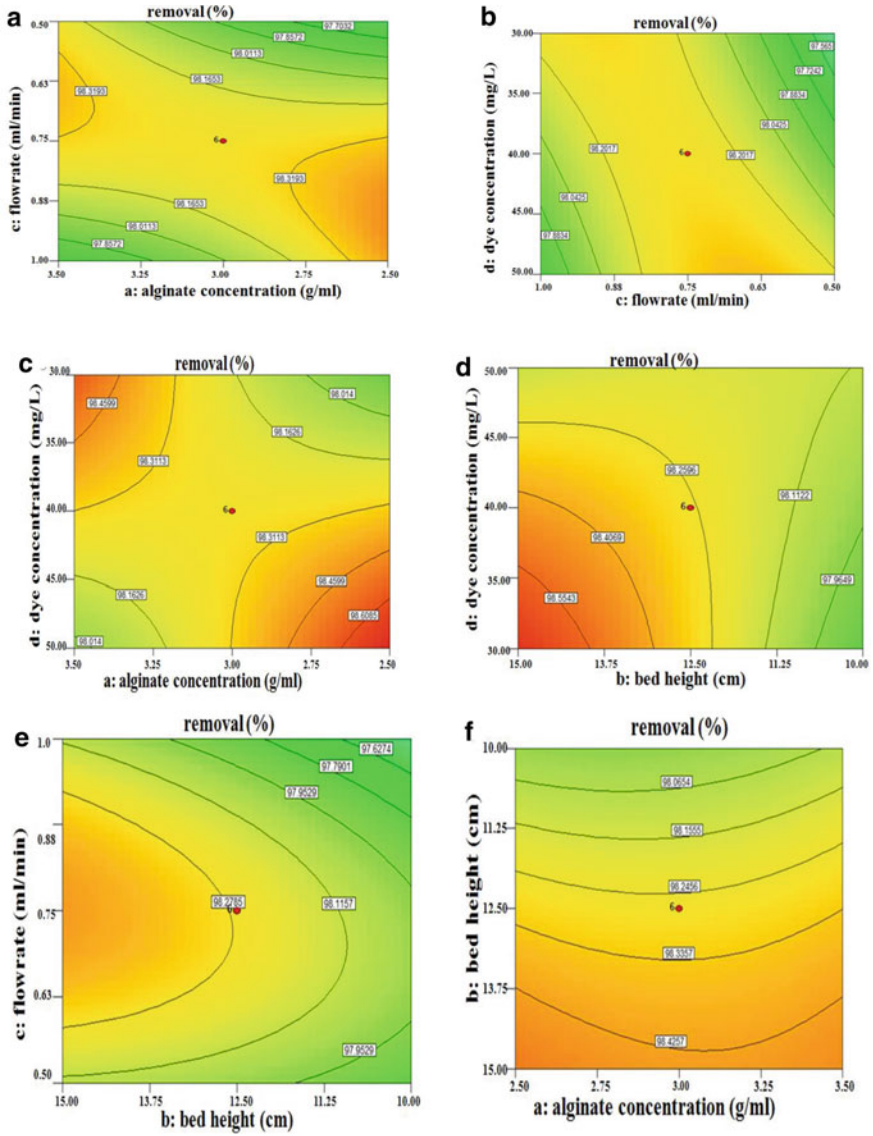


Fig. 3 **a** Contour plot image of effect of alginate concentration and flow rate on MG removal. **b** Contour plot image of effect of dye concentration and flow rate on MG removal. **c** Contour plot image of effect of dye concentration and alginate concentration on MG removal. **d** Contour plot image of effect of dye concentration and bed height on MG removal. **e** Contour plot image of effect of flow rate and bed height on MG removal. **f** Contour plot image of effect of alginate concentration and bed height on MG removal

3.3.3 Initial Malachite Green Concentration

From Fig. 3c it was observed that increasing the dye concentration from 30 to 50 mg L⁻¹ at fixed alginate concentration of 3.5% reduces the MG removal from 98.6085 to 98.014%. Similarly MG removal decreased from 98.5543 to 97.9649% at fixed bed height of 15 cm and is shown in Fig. 3d. Experiments by Kaviani et al. (2012) suggested that at higher initial concentration, the bed saturation was faster which led to earlier breakthrough and exhaustion of column biosorbent.

3.3.4 Bed Height

The effect of bed height on dye removal was studied. From Fig. 3e it was observed that decreasing the bed height from 15 to 10 cm at fixed flow rate of 0.5 ml min⁻¹ reduces the MG removal from 98.2785 to 97.6274%. Similarly in Fig. 3f it was observed that MG removal decreases from 98.4257 to 98.0654% on decreasing the bed height at fixed alginate concentration. Shadeera and Nagapadma (2015) reported that when the bed height was increased the adsorbate had more time to be in contact with the adsorbent which resulted in increased dye removal. Thus the different parameters optimized for dye removal are bed height 15 cm, flowrate 0.5 ml min⁻¹, alginate concentration 2.5%, and MG concentration 50 mg l⁻¹.

4 Conclusion

The present work was designed to study the removal of Malachite green by *K. marina* DAGII. Spectrophotometric analysis study showed that the dye removal did not undergo degradation process and was controlled by sorption process. Optimization of different parameters was done by RSM to obtain the maximum MG removal. ANOVA study of column showed the influence of different parameters and their interactive effect contributing to MG removal. The quadratic model was found to be significant and adequate which suggests that the model can be used to study the dye removal process.

Acknowledgements I express my thanks to National Institute of Technology Durgapur, West Bengal, India for supporting this work.

References

- Adhikari S, Chattopadhyay P, Ray L (2012) Continuous Removal of malathion by immobilised biomass of *Bacillus species S₁₄* using a packed bed column reactor. Chem Speciat Bioavailab 24:167–175

- Almeida EJR, Corso CR (2014) Comparative study of toxicity of azo dye Procion Red MX-5B following biosorption and biodegradation treatments with the fungi *Aspergillus niger* and *Aspergillus terreus*. *Chemosphere* 112:317–322
- Bayat Z, Hassanshahian M, Cappello S (2015) Immobilization of Microbes for Bioremediation of Crude Oil Polluted Environments: A Mini Review. *Open Microbiol J* 9:48–54
- Bera S, Sharma VP, Dutta S, Dutta D (2016) Biological decolorization and detoxification of malachite green from aqueous solution by *Dietzia maris* NIT-D. *J Taiwan Inst Chem Eng* 16:271–284
- Chen Y, Zhang Y, Chen L, Lu A, Zhang W (2011) Photodegradation of malachite green by nanostructured Bi₂WO₆ visible light-induced photocatalyst. *Int J Photoenergy* 2012:e510158
- Daneshvar N, Ayazloo M, Khataee AR, Pourhassan M (2007) Biological decolorization of dye solution containing malachite green by microalgae *Cosmarium* sp. *Bioresour Technol* 98:1176–1182
- Ebrahiem EE, Altaher H, Abdelghany EA, Magdy Y (2018) Packed bed column for adsorption of aqueous phenols on cement kiln dust. *J Hazard Toxic Radioactive Waste* 22(3):04018009
- Iman K, Pliieger PG, Kandile NG, Harding DRK (2012) Fixed-bed column studies on a modified chitosan hydrogel for detoxification of aqueous solutions from copper. *Carbohydr Polym* 90:875–886
- Lv GY, Cheng JH, Chen XY, Zhang ZF, Fan LF (2013) Biological decolorization of malachite green by *Deinococcus radiodurans* R1. *Bioresour Technol* 144:275–280
- Mitra R, Samanta A.K, Chaudhuri S, Dutta D (2015) Growth kinetics and carotenoid production of a newly isolated bacterium on glucose as a carbon source during batch fermentation. In: 5th annual conferences on advances in biotechnology, ISSN 2251-2489
- Mitra R, Samanta AK, Chaudhuri S, Dutta D (2016) Impact of carbon source on β-cryptoxanthin production by *Kocuria marina* DAGII: a classical approach. *Mater Today Proc* 3:3269–3275
- Mitra R, Chaudhuri S, Dutta D (2017) Modelling the growth kinetics of *Kocuria marina* DAGII as a function of single and binary substrate during batch production of β-Cryptoxanthin. *Bioprocess Biosyst Eng* 40:99–113
- Mokhtar N, Aziz EA, Aris A, Ishak FW (2017) Biosorption of azo-dye using marine macro-alga of *Euchema Spinosum*. *J Environ Chem Eng* (5):5721–5731
- Negrea A, Lupa L, Mihaela C (2019) Experimental and modelling studies on As (III) removal from aqueous medium on fixed bed column. *Chem Bull* 56(70):89–93
- Parmar ND, Shukla SR (2018) Decolourisation of dye wastewater by microbial methods: a review. *Indian J Chem Technol* 25:315–323
- Pons MP, Fuste MC (1993) Uranium uptake by immobilized cells of *Pseudomonas* strain EPS 5028. *Appl Microbiol Biotechnol* 39:661–665
- Qu W, Liu T, Zhao J (2018) Metagenomics-Based Discovery of Malachite Green-Degradation Gene Families and Enzymes from Mangrove Sediment. *Front Microbiol* 9:2187
- Shadeera R, Nagapadma M (2015) Modeling of fixed bed column studies for adsorption of azo dye on chitosan impregnated with a cationic surfactant. *Int J Sci Eng Res* (6). ISSN 2229-5518
- Srinivasan A, Viraraghavan T (2010) Decolorization of dye wastewaters by biosorbents: a review. *J Environ Manage* 91:1915–1929
- Volesky B (2007) Biosorption and me: a review. *Water Res* 41:4017–4029
- Wang MX, Zhang QL, Yao SJ (2015) A novel biosorbent formed of marine-derived *Penicillium janthinellum* mycelial pellets for removing dyes from dye-containing wastewater. *Chem Eng J* 259:837–844

Isolation of a Most Potent Bacterial Strain from Soil for Bioremediation of Phenol



Debapriya Maity, Pradyut Kundu, and Sunita Adhikari (Nee Pramanik)

Abstract Phenol is present as the basic structural compound of many synthetic organics. This pollutant generates from different sources such as herbicides, wood preservatives, petroleum industries, pharmaceuticals, etc. US Environmental Protection Agency marked it as the priority pollutant. The objective of this study is to isolate a potent bacterial strain from soil which is capable to remove phenol from wastewater. For this, soil sample was collected from the hospital area and enriched with 500 ppm phenol for 10 days. After serial dilution of the soil sample, colonies were developed in petri plate on nutrient agar medium. The isolated colonies were transferred to the slant and screening was done to select the most potent strain in liquid nutrient medium containing 500 ppm of phenol. The most efficient strain, P25, was able to reduce almost ~99.44% of phenol concentration in 24 h, 37 °C temperature, pH 6.8. The isolated strain was acclimatized in MSM (minimum salt medium) for 2 months and habituated to remove 700 mg/L phenol concentration. Simultaneously the strain was biochemically characterized and identified by 16S rDNA sequence analysis.

Keywords Phenol · Pollutant · Minimum salt medium (MSM) · 16S rDNA

D. Maity · S. A. (Nee Pramanik) (✉)
Department of Food Technology & Biochemical Engineering, Jadavpur University, Kolkata
700032, India
e-mail: sunitapramanik@gmail.com

D. Maity
e-mail: debapriyamaity552@gmail.com

P. Kundu
Department of Food Processing Technology, Mirmadan Mohanlal Government Polytechnic,
Plassey, Nadia, India
e-mail: kundupradyut@yahoo.co.in

1 Introduction

Many pollutants that are very hazardous for the nature are discharged from chemical, pharmaceuticals and oil refinery industries including many aliphatic and aromatic hydrocarbons (Taghreed and El-Naas 2014). Phenol is one of them, which has the capacity to damage the gastrointestinal tract, irritation of respiratory tracts, muscle tremors. Damage of liver, kidney, and nervous system are the adverse effects of phenol. Also phenol is very much hazardous to the aquatic ecosystems (Szczyrba et al. 2016). Therefore, it is mandatory to treat the phenol and phenolic wastes properly before disposal into the nature (Szczyrba et al. 2016; Kumar et al. 2005). The maximum permissible level of phenol in land water is 1 ppm according to the Central Pollution Control Board (CPCB) and IS:2490-1974 (Cheela et al. 2014; Lathasree et al. 2004; Saravanan et al. 2009). As per World Health Organization (WHO), the safety limit of phenol in drinking water should not exceed 1 mg/L (Bakhshi et al. 2011; Saravanan et al. 2008; Wang et al. 2010).

Several treatment methods are there to treat phenol such as adsorption, chlorination, ozonation as well as many physicochemical methods (Szczyrba et al. 2016; Tamer et al. 2010). Due to high cost effect of these methods and production of toxic intermediate compounds, involvement of biological processes is necessary in the treatment of phenol (Szczyrba et al. 2016). These biological treatments may be biosorption, biodegradation, bioaccumulation, etc., involving bacteria, algae, fungi, etc. Many such studies have been done previously as Mohanty and Jena (2017) did his experiment on biodegradation of phenol using *Pseudomonas* sp. NBM11 that was able to degrade up to 1000 ppm phenol completely in the temperature ranging between 30 and 32 °C and pH 6.8–7.2. Another study was done by Parvathy and Prabhakumari (2017) involving *Pseudomonas aeruginosa*, isolated from industrial soil to remove catechol.

The current study has been carried out aiming to isolate the most potent bacterial strain to degrade phenol and the identification of the strain.

2 Materials and Methods

2.1 Soil

Soil was collected from the local hospital area.

2.2 Reagents

Phenol-(analytical grade), 4-amino antipyrine, potassium ferricyanide, ammonium chloride and ammonium hydroxide solution. Our targeted concentration of phenol was prepared by mixing the properly weighed phenol to distilled water.

2.3 Bacterial Media

The nutrient agar medium with following composition was used for cultivation of bacteria.

Peptone—0.5%, beef extract—0.3%, agar—3.0%.

2.4 Isolation and Screening of Most Potent Bacterial Strain

The bacterial strain capable of removing phenol was isolated by soil enrichment and serial dilution plate count method. The soil was enriched with 500 ppm phenol for 10 days. After serial dilution and plate count isolated colonies were transferred in individual slant. A total of 29 isolated colonies were transferred to slant.

Screening was done to select most potent strain. Each of the isolated colonies was transferred to liquid medium and incubated 37 °C for 24 h in the presence of 500 ppm phenol. After fermentation, the fermented broth was centrifuged and the clear supernatant was used for spectrophotometric estimation of residual phenol content.

2.5 Estimation of Residual Phenol Content

Residual phenol concentration was measured in spectrophotometer at 510 nm wavelength followed by APHA method. Residual phenol content was calculated from the standard curve made with the known concentrations of phenol.

2.6 Morphological, Biochemical, and Phylogenetic Characterization of the Isolated Bacterial Strain

Morphological and biochemical characterization of the isolated bacterial strain was done as per Bergey's Manual of Determinative Bacteriology (Holt et al. 1993). Phylogenetic assay was made by 16s rDNA method.

3 Results and Discussion

3.1 Isolation and Screening of Most Potent Bacterial Strain

After serial dilution of the enriched soil sample and transfer of the diluted soil sample into nutrient agar medium, 29 isolated colonies were obtained. Colony characteristics of the isolated colonies are shown in Table 1.

After screening, it was found that the strain marked as P25 showed maximum phenol removal capability (~99.44%) (Table 1), so it was selected for further study.

3.2 Morphological, Biochemical, and Phylogenetic Characterization of the Isolated Bacterial Strain

Morphological characterization of the isolated bacterial strain P25 is shown in Tables 2 and 3. Gram characteristics and spore characteristics are shown in Figs. 1, 2, and 3. Physicochemical characteristics are shown in Table 4. The phylogenetic tree is shown in Fig. 4.

Table 1 Screening of the most potent bacterial strain

Sample strain number	Colony size	Colony pigmentation	Colony form	Colony margin	Colony elevation	% of phenol removal
P1	Moderate	White	Circular	Serrate	Flat	83.16
P2	Moderate	White	Irregular	Serrate	Flat	82.86
P3	Small	White	Irregular	Serrate	Flat	80.75
P4	Large	White	Circular	Entire	Flat	80.15
P5	Moderate	White	Circular	Entire	Flat	84.36
P6	Small	Light yellow	Circular	Entire	Raised	81.35
P7	Small	White	Circular	Serrate	Umbonate	80.15
P8	Pinpoint	White	Circular	Serrate	Flat	80.45
P9	Small	Light yellow	Circular	Serrate	Flat	79.25
P10	Moderate	White	Circular	Serrate	Raised	77.44
P11	Moderate	White	Circular	Entire	Flat	82.86

(continued)

Table 1 (continued)

Sample strain number	Colony size	Colony pigmentation	Colony form	Colony margin	Colony elevation	% of phenol removal
P12	Moderate	Light yellow	Circular	Entire	Flat	82.56
P13	Large	Yellowish	Irregular	Entire	Flat	84.06
P14	Small	Reddish yellow	Circular	Undulate	Flat	84.06
P15	Small	White	Circular	Serrate	Flat	83.76
P16	Moderate	White	Irregular	Serrate	Raised	84.36
P17	Large	White	Circular	Serrate	Raised	84.06
P18	Moderate	Yellowish	Circular	Entire	Umbonate	84.06
P19	Small	Light yellow	Circular	Entire	Raised	83.46
P20	Pinpoint	White	Irregular	Entire	Flat	64.51
P21	Small	Light yellow	Irregular	Serrate	Raised	80.15
P22	Small	White	Circular	Serrate	Flat	83.46
P23	Moderate	White	Circular	Entire	Flat	83.16
P24	Large	Light yellow	Circular	Serrate	Flat	98.84
P25	Large	White	Circular	Serrate	Flat	99.44
P26	Large	Light yellow	Irregular	Serrate	Raised	98.83
P27	Large	Light yellow	Circular	Serrate	Flat	98.68
P28	Large	White	Circular	Serrate	Flat	98.83
P29	Large	White	Circular	Entire	Flat	98.48

Bold indicates the corresponding organism removes maximum amount of phenol

Table 2 Colony characterization of the isolated bacterial strain

Colony characteristics	P25
a. Size	1 mm
b. Opacity	Opaque
c. Surface growth	Smooth
d. Edge	Sharp
e. Consistency	Good
f. Pigmentation	Nil

Table 3 Growth characterization on slant

Colony characteristics	D25
a. Opacity	Opaque
b. Surface growth	Smooth
c. Consistency	Sharp
d. Color	Good
e. Pigmentation	Nil

Fig. 1 Simple staining

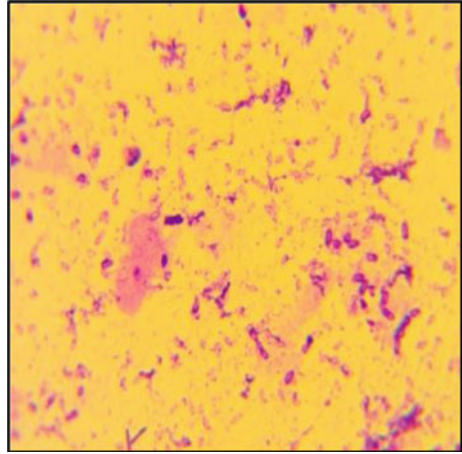


Fig. 2 Gram staining

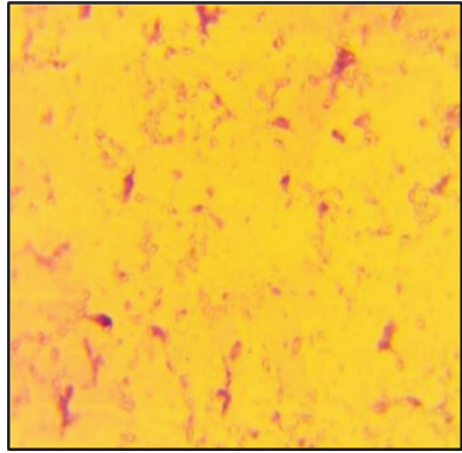


Fig. 3 Spore staining

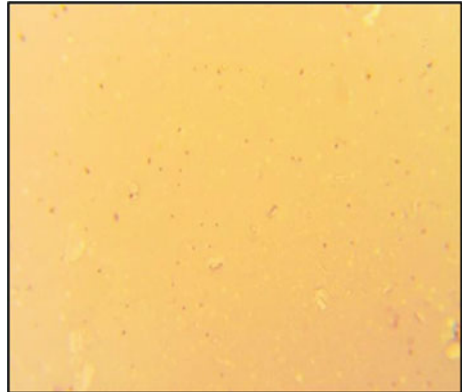


Table 4 Physicochemical characteristics of the isolated bacterial strain P25

Parameters	Characteristics of P25	
1. Ammonia from arginine	+	
2. Arginine used as sole source of energy	+	
3. Nitrate reduction	+	
4. Catalase reduction	—	
5. Carbohydrate fermentation	Acidity	Gas formation
a. Fructose	+	+
b. Arabinose	—	+
c. Galactose	+	+
d. Xylose	Not done	Not done
e. Glucose	+	+
f. Lactose	+	+
g. Raffinose	+	+
h. Sucrose	—	+
i. Maltose	+	+
j. Dextrin	+	+
k. Salicin	+	+
l. Mannitol	+	+
m. Glycerol	+	+
n. Inositol	—	+
6. Indole formation	+	
7. Litmus milk test	+	
8. Starch hydrolysis test	—	
9. Urease test	Incubation	
10. Voges—Proskauer test	Incubation	
11. Growth under anaerobic condition	Not done	
12. Growth at different temperatures	+	
13. Growth at extreme pH and NaCl concentration	+	

4 Conclusion

The isolated most potent bacterial strain was identified as *Brevibacillus formosus* strain NRRL NRS-863, which was able to reduce almost 99.44% of phenol. However, the mechanism of removal of phenol by the isolated strain i.e. whether the strain degrades it or accumulates it is not known till now. Our further study will reveal it.

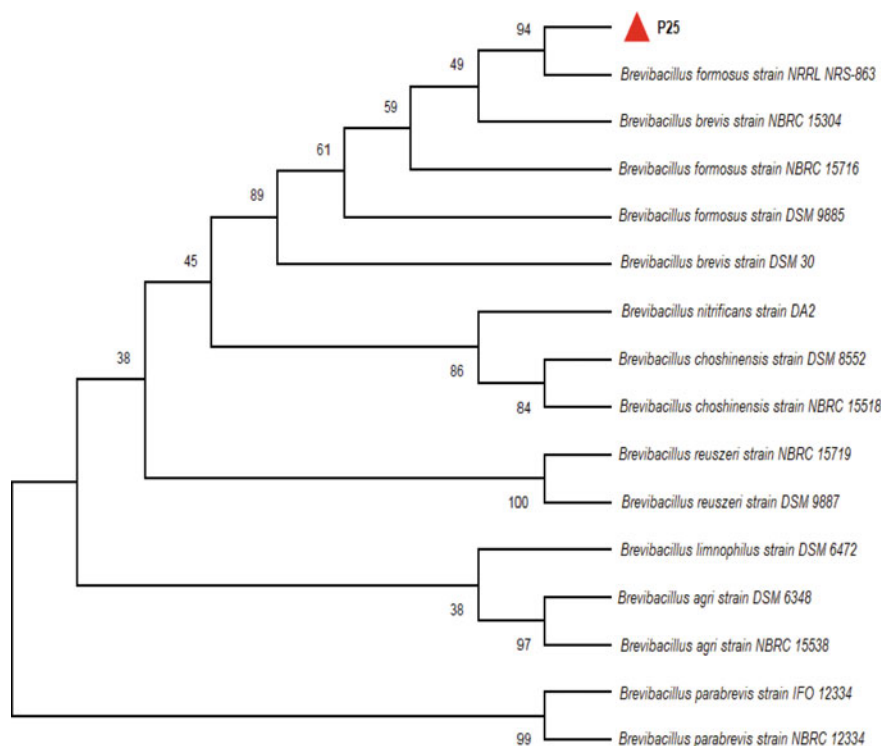


Fig. 4 Phylogenetic tree of the strain P25

References

- Bakhshi Z, Najafpour G, Kariminezhad E et al (2011) Growth kinetic models for phenol biodegradation in a batch culture of *Pseudomonasputida*. *Environ Technol* 32(16):1835–1841
- Cheela VRS, Kumar GS, Padma DV et al (2014) Biodegradation of Phenol using pure and mix culture Bacteria. *e-J Sci and Technol (e-JST)* 2(9):91–95. https://hypatia.lb.teiath.gr/bitstream/11400/6242/1/Cheela_35.pdf
- Holt JG, Kreig NR, Sneath JT, Williams ST (1993) *Bergey's manual of determinative bacteriology*, 9th edn. Wolters Kluwer
- Kumar A, Kumar S, Kumar S (2005) *Biochem Eng J* 22:151–159
- Lathasree S, Rao AN, Sivasankar B, Sadasivam V, Rengaraj K (2004) Heterogeneous photocatalytic mineralization of phenols in aqueous solutions. *J Mol Catal A-Chem* 223:101–105
- Mohanty SS, Jena HM (2017) Biodegradation of phenol by free and immobilized cells of a novel *Pseudomonas sp.* NBM11. *Braz J Chem Eng* 34(01):75–84
- Parvathy G, Prabhakumari C (2017) Isolation, characterization and optimization of catechol degrading *Pseudomonas aeruginosa* from Cashew Industrial soil. *Int J Adv Biotechnol Res* 7(1):13–23
- Saravanan P, Pakshirajan K, Saha P (2009) Degradation of Phenol by TiO_2 -based heterogeneous photocatalysis in presence of sunlight. *J Hydro-Environ Res* 3(1):45–50
- Saravanan P, Pakshirajan K, Saha P (2008) Growth kinetics of an indigenous mixed microbial consortium during phenol degradation in a batch reactor. *Bioresour Technol* 99:205–209

- Szczyrba E, Szczotka A, Bartelmus G (2016) Modelling of aerobic biodegradation of phenol by *Stenotrophomonas maltophilia* KB2 strain. Proc ECO Pole 10(2)
- Taghreed Al-Khalid T, El-Naas MH (2014) Biodegradation of phenol and 2,4 dichlorophenol: the role of glucose In biomass acclimatization. Int J Eng Res Technol 3(1):1579–1586
- Tamer E, Amin MA, El Tayeb O, Mattiasson B, Guieysse B (2010) Kinetics and metabolic versatility of highly tolerant phenol degrading *Alcaligenes* strain TW1. J Hazard Mater 173(1–3):783–788
- Wang L, Li Y, Yu P et al (2010) Biodegradation of phenol at high concentration by a novel fungal strain *Paecilomyces variotii* JH6. J Hazard Mater 183:366–371

Study on Application of Novel Synthesized Silver Metallosurfactant for Membrane Cleaning



Ankita Mazumder, Zinnia Chowdhury, Dwaipayan Sen,
and Chiranjib Bhattacharjee

Abstract Membrane separation technology used for the treatment of emulsified oily wastewater generating from different industries faces an intrinsic fouling problem that occurs either due to the adsorption of oil on the surface or pore blocking. For cleaning oil-clogged membrane, ionic surfactant sodium dodecyl sulfate (SDS) can be used as a cleaning agent for solubilizing the oil droplets by dispersion. However, with SDS, satisfactory permeate flux recovery was not achieved. Moreover, owing to the high critical micelle concentration (CMC), a high dosage of SDS is required, which promotes foaming and thereby negatively affects the cleaning process. Thus, a novel metallosurfactant where transition metal ions are incorporated in the surfactant through coordination chemistry is being investigated. Our work primarily focuses on the development of novel silver-based metallosurfactant by mixing silver nitrate (AgNO_3) and SDS as ligand at three different ratios. Among the three formulated metallosurfactants, the MS3 metallosurfactant showed the lowest CMC along with superlative surface tension reduction ability. Owing to the attributes like increased micellization and surface activity at a low concentration of MS3, satisfactorily high flux recovery of around 98% was found. Thus, this novel synthesized metallosurfactant can be used as a promising membrane-cleaning surfactant solution.

Keywords Fouling · Membrane cleaning · Metallosurfactant

A. Mazumder · Z. Chowdhury · C. Bhattacharjee (✉)
Department of Chemical Engineering, Jadavpur University, Kolkata, India
e-mail: c.bhatta@gmail.com

A. Mazumder
e-mail: chemical.ankita91@gmail.com

Z. Chowdhury
e-mail: chowdhuryzin@gmail.com

D. Sen (✉)
Department of Chemical Engineering, Heritage Institute of Technology, Kolkata, India
e-mail: dwaipayan.sen@heritageit.edu

1 Introduction

For the last three decades, membrane separation technology has gained popularity as an advanced separation method and is presently considered to be one of the expedient separation processes in the field of wastewater treatment. A wide range of industries including chemical, pharmaceutical, biotechnological, automobile, dairy industries, etc. have adopted this technology as their wastewater treatment method. Major benefits of membrane technology over other conventional separation technologies include selective separation, recovery of valuable by-products, nonrequirement of additional chemical dosage, reduction in the number of unit operations, easy operability, and low space requirement (Putatunda et al. 2019). However, the major hurdle associated with any membrane process is membrane fouling. In the case of fouling, permeate flux declines due to gradual pore blockage and cake layer formation during operation under constant transmembrane pressure (TMP). Reversible membrane fouling and irreversible membrane fouling are the two major categories of fouling. Reversible membrane fouling occurs due to the evolution of the cake layer on the membrane surface and can be removed by backwashing. In the case of irreversible one, membrane pore blockage occurs and is challenging to remove (Guo et al. 2012). Frequent membrane replacement being an expensive process, appropriate membrane cleaning strategy is utmost required. To eradicate irreversible membrane fouling, different chemical cleaning agents are utilized, which include acids, alkalis, surfactants, oxidants, enzymes, and chelating components. Moreover, the development of biofilms on the membrane surface owing to the presence of a high load of organic components is an unwanted common phenomenon and is commonly controlled to some extent by the addition of disinfectants (Shi et al. 2014). But complete removal and mitigation of biofouling need special cleaning solutions having antimicrobial activities. Thus, the optimization of membrane cleaning through the use of low-cost and effective chemical cleaning agents is a strenuous assignment. In this context, the present study concentrates on the development of a new cost-effective cleaning agent (metallo-surfactant) having the ability to remove sticky oil foulants from the membrane during the membrane separation of oily wastewater.

2 Overview on Metallosurfactant

Metallosurfactant has grasped the enormous attention of worldwide research communities by their exclusive surface activity. It represents an advanced class of surfactant where a central metal is induced in the polar head group of the conventional surfactant molecule as an intrinsic structural part. The embodiment of d-or-f block metal ions into the polar head of the surfactant system by coordination bond forms metallo-surfactant, which enriches different properties of ordinary surfactants by increasing the surface-active efficiency (Kumaraguru and Santhakumar 2009). The coordination bond is formed by the transition metals with ligands by accepting electron pairs.

Metallosurfactant can be synthesized by three types of reactions namely metathesis reaction, ligand substitution, and ligand insertion reaction. In the metathesis reaction, ion exchange occurs between cations and anions in the presence of a polar solvent. Substitution of a less-labile ligand in place of more labile ligand occurs for ligand substitution reaction, whereas the insertion of ligand without elimination takes place in case of ligand insertion reaction. The primary mode of action of any surfactant relies on the adsorption of its molecules at the boundary of a hydrophilic–hydrophobic medium, which thereby reduces the interfacial surface tension and shows its effective surface activity. On metal coordination, the molecular geometry of surfactant (ratio of head group area to tail volume) and electrostatic charge distribution gets modified. Bridging of a central metal counterion with multiple surfactant head groups can either promote attraction between the polar head groups and thereby bring them closer, or push the head groups far apart through repulsive force, based on the chemical structure of the metallosurfactant. Thus, the propensity of self-aggregation and micellization is affected along with the substantial deviation in the aggregate morphology. Metal incorporation helps to tune the characteristics of amphiphilic surfactant through inducing new properties to the system as of the attributes (such as acidic, basic, magnetic, and redox) of the attached metal (Brom et al. 2010). The self-aggregation activity of a metallosurfactant can be controlled by tuning the type of metal ion fused with a surfactant molecule. Other properties such as antibacterial, antimicrobial, catalytical, and magnetic properties can also be induced into the surfactant system by the selection of an appropriate central metal. Therefore, the property of the metallosurfactant is mostly characterized by the nature of the metal incorporated in the surfactant molecule.

3 Recent Trends on Applications of Metallosurfactant

Conventional surfactants are mostly inadequate in the case of chemical reactivity. Their properties are largely dependent on the hydrophobic/hydrophilic balance of the nonpolar and polar moieties of its molecular structure. The introduction of transition metal ions into amphiphilic structures is attracting significant attention as the variable charge, catalytic activity, and magnetic properties of metal deliver a way of concentrating these potential features at interfaces (Kaur et al. 2016). Though such metallosurfactants are comparatively rare than conventional surfactants, these compounds have recently found their application in diverse prospects such as homogeneous catalysis, interfacial photophysics, magnetic resonance imaging, thin-film optoelectronics, templating of mesoporous materials, drug delivery, antimicrobial activities, and anticancerous treatment (Griffiths et al. 2006). However, metallosurfactant has not been much explored as a cleaning agent.

4 Materials

All chemicals were purchased from Merck (Mumbai, India). Deionized water (DI) was collected from the hybrid Arium RO unit and the Arium 611 DI ultrapure water system (Made: Sartorius). The membrane operations were carried out by polysulfone (PSf) membrane procured from Sterlitech Corporation, USA.

5 Methods

SDS was blended with 175 mg of silver nitrate (AgNO_3) at the (w/w) ratio of 4:1, 3:1, and 2:1 in 100 mL of distilled water at room temperature and the mixtures were designated as MS1, MS2, and MS3, respectively. These mixtures were then stirred for 1 h at 550 rpm at 80 °C. After cooling it to room temperature, critical micelle concentration (CMC) of each formulated mixture was determined by conventional the conductivity method (Domínguez et al. 1997). The surface tension of these solutions was also evaluated by the stalagmometric method at 25 °C (Donald and Bulloch 1915).

Primarily PSf membrane was fouled with emulsified oily wastewater till the permeate flux drops to 10% of the original flux value of the new membrane. The fouled membrane was then dipped in each of the formulated mixtures and was rested for stirring up to 1 h at room temperature. After the accomplishment of the cleaning operation, the permeate flux value was reevaluated at constant transmembrane pressure of 3 kgf. Foulant removal performance was analyzed by calculating the flux recovery ratio as shown in Eq. 1 (Zhang et al. 2015).

$$F_R = \frac{J_C - J_F}{J_I - J_F} \times 100 \quad (1)$$

where J_C , J_F , and J_I are the permeate flux of cleaned membrane, fouled membrane, and new membrane, respectively.

6 Results and Discussion

By the conductivity method, the CMC values of formulated MS1, MS2, and MS3 were found to be 1580 mg/L, 1345 mg/L, and 525 mg/L, respectively, as represented in Fig. 1. It can be observed that the CMC of MS3 was found to be 66.77% and 60.97% lower than MS1 and MS2, respectively. Moreover, in comparison with the traditional surfactant SDS, the micellization tendency of MS3 metallocomplex was markedly intense owing to the 4.38 times less CMC than of SDS. The decrease in CMC value in the case of MS3 metallosurfactant is possibly due to increment in

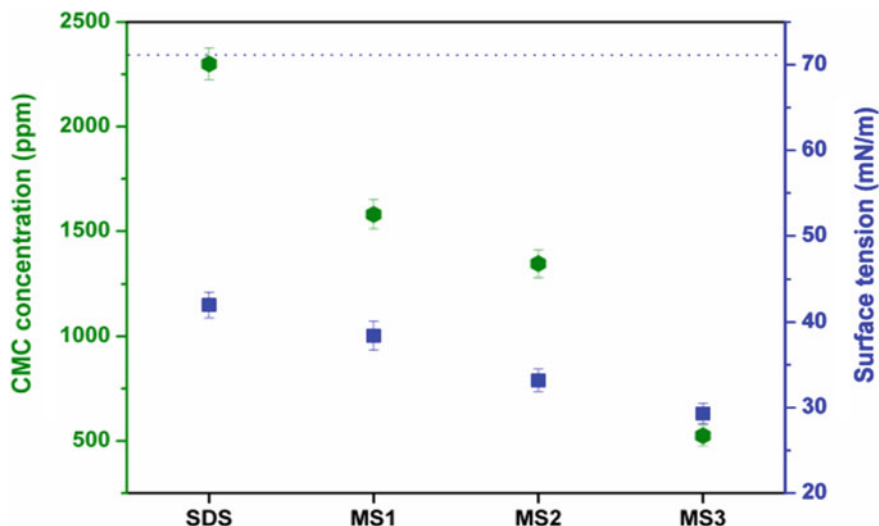


Fig. 1 Critical micellization concentration (CMC) (●) and surface tension (■) of studied cleaning agents; (represents the surface tension of DI water)

the presence of metallic counterions around the polar head group of the surfactant. This consecutively increases attractive interaction between polar head groups of the surfactant molecules favoring the micellization phenomenon and thus lowering CMC (Wagay et al. 2016). Moreover, surface tension values of MS1, MS2, MS3, and SDS solutions at CMC concentration were evaluated as 38.4 mN/m, 33.18 mN/m, 29.3 mN/m, and 42 mN/m, respectively. This result clearly indicates that the ability to reduce interfacial surface tension with respect to the control (DI water) was highest for MS3 compared with other studied cleaning agents.

Cleaning of the fouled membrane with all the surfactant solutions showed a recovery in the permeate flux values. Flux recovery ratio was found maximum for solution MS3 followed by MS2 and MS1. Around 98% of permeate flux recovery was achieved with MS3 metallosurfactant. With the increase in the availability of metal ions surrounding the hydrophilic polar head of the surfactant, both micellization and interfacial surface tension reduction at the interfaces are promoted. This eventually helps in the removal of sticky oil molecules from the membrane surface. Therefore, the formulated metallosurfactant can be a novel and promising cleaning agent for effective membrane cleaning (Fig. 2).

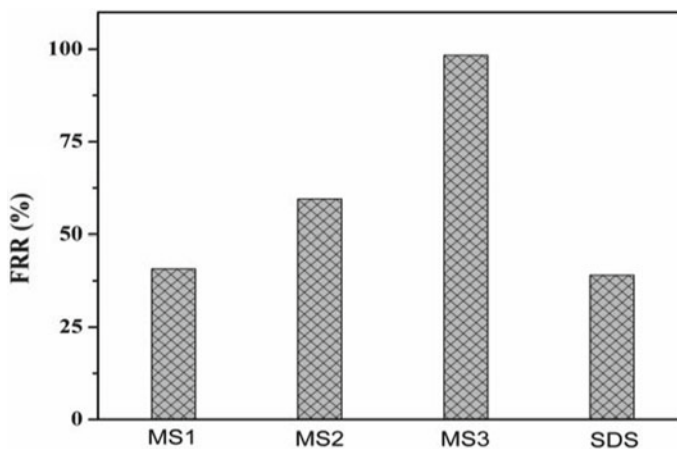


Fig. 2 Cleaning efficiency of the cleaning agents in terms of flux recovery ratio (FRR) %

7 Conclusion

The complexation of silver metal with the conventional surfactant at different weight ratios has resulted in superior cleaning performance. Enhanced binding of metal counterions with the polar head groups in MS3 metallocomplex has resulted in 77% reduction in CMC compared with SDS. Also, the surface activity of the MS3 metallosurfactant is 30% higher than SDS because of its capacity to reduce the interfacial surface tension markedly at the membrane and oil interface. On cleaning the fouled membrane with MS3, 98% flux recovery was achieved owing to its increased micellization and surface activity. Thus, MS3 can be considered as a promising cleaning agent showing satisfactorily better cleaning efficiency in cleaning the heavily fouled membrane.

Acknowledgements The authors thankfully acknowledge the Department of Science & Technology (DST), GOI for sponsoring the project (vide sanction letter no. DST/TSG/AMT/2015/276 dated 11.06.2016) and All India Council for Technical Education (AICTE) for providing the GATE fellowship.

Conflict of Interest None.

References

- Brom CR, Wagner M, Enkelmann V et al (2010) Alkylsulfides of Ag (I) and Au (I) as metallosurfactants. *Langmuir* 26(20):15794–15801. <https://doi.org/10.1021/la1027543>
- Domínguez A, Fernandez A, Gonzalez N et al (1997) Determination of critical micelle concentration of some surfactants by three techniques. *J Chem Educ* 74(10):1227–1231. <https://doi.org/10.1021/ed074p1227>

- Donald R, Bulloch W (1915) A method of drop-measuring liquids and suspensions: (rough practical notes). *Lancet* 186(4814):1243–1245. [https://doi.org/10.1016/S0140-6736\(01\)20384-5](https://doi.org/10.1016/S0140-6736(01)20384-5)
- Griffiths PC, Fallis IA, Chuenpratoom T et al (2006) Metallosurfactants: interfaces and micelles. *Adv Colloid Interfac* 122(1–3):107–117. <https://doi.org/10.1016/j.cis.2006.06.010>
- Guo W, Ngo HH, Li J (2012) A mini-review on membrane fouling. *Bioresour Technol* 122:27–34. <https://doi.org/10.1016/j.biortech.2012.04.089>
- Kaur G, Kumar S, Kant R et al (2016) One-step synthesis of silver metallosurfactant as an efficient antibacterial and anticancer material. *RSC Adv* 6(62):57084–57097. <https://doi.org/10.1039/C6RA09677H>
- Kumaraguru N, Santhakumar K (2009) Synthesis, characterization, critical micelle concentration determination, and antimicrobial studies of some complexes of chromium (III) metallosurfactants. *J Coord Chem* 62(21):3500–3511. <https://doi.org/10.1080/00958970903118053>
- Putatunda S, Bhattacharya S, Sen D et al (2019) A review on the application of different treatment processes for emulsified oily wastewater. *Int J Environ Sci Technol* 16(5):2525–2536. <https://doi.org/10.1007/s13762-018-2055-6>
- Shi X, Tal G, Hankins NP et al (2014) Fouling and cleaning of ultrafiltration membranes: a review. *J Water Process Eng* 1:121–138. <https://doi.org/10.1016/j.jwpe.2014.04.003>
- Wagay TA, Dey J, Kumar S et al (2016) Aggregation, adsorption, counterion binding, thermal and scattering behavior of metallosurfactant cis-[Co(en)₂(C₁₂H₂₅NH₂)Cl](NO₃)₂. *Colloid Surf A Physicochem Eng Asp* 503:61–69. <https://doi.org/10.1016/j.colsurfa.2016.05.030>
- Zhang B, Shi W, Yu S et al (2015) Optimization of cleaning conditions on a polytetrafluoroethylene (PTFE) microfiltration membrane used in treatment of oil-field wastewater. *RSC Adv* 5(127):104960–104971. <https://doi.org/10.1039/C5RA23980J>

Effect of Calcium Salts on Salinity Stress on Morphology and Biochemical Estimation of Rice Seedlings



Banhishikha Singh and Soma Banerjee

Abstract Soil salinity is one of the major abiotic stresses affecting plant growth and productivity globally as well in the Sunderban area of West Bengal. The study comprises comparison of the effect of the combined action of sodium chloride (NaCl) and three types of calcium salts calcium chloride (CaCl_2), calcium sulphate (CaSO_4) and calcium carbonate (CaCO_3) on three rice varieties ('Chinsurah Nona-2', 'Dudherswar' and 'Pratiksha') both morphological and biochemical estimations, i.e. shoot growth, chlorophyll, proline, starch and reducing sugar content and antioxidants expressions. The results show maximum recovery of shoot growth in 15 mM- CaSO_4 with 200 mM NaCl treatment set with respect to seedlings stressed with only 200 mM NaCl, i.e. 32% in variety 'Chinsurah Nona-2' and 10.5% in variety 'Pratiksha', whereas 'Dudherswar' variety shows 1.2 times recovery in 10 mM- CaCO_3 set. In case of chlorophyll content in the following sets, 5 mM CaCl_2 , 15 mM CaSO_4 and 10 mM CaCO_3 are showing best recovery. Similarly, for proline, starch and reducing sugar content, 10 mM CaSO_4 and 15 mM CaCO_3 sets show best results against 200 mM NaCl. For antioxidant expression in 'Chinsurah Nona-2' variety, the catalase activity increased 4.7 times in 5 mM CaCO_3 set followed by three times increase in ascorbate peroxidase activity in 10 mM CaCO_3 , and for lipid peroxidation, 79% decrease observed in 10 mM CaCl_2 . In 'Pratiksha' variety, 28% increase in catalase activity in 5 mM CaCO_3 set and 86% decrease in ascorbate peroxidase activity in 15 mM CaSO_4 , 1.4 times increase in glutathione reductase activity, 5 mM CaCO_3 and lipid peroxidation activity showed 59% decrease in 10 mM CaSO_4 . 'Dudherswar' variety showed marked response in all the antioxidant estimations in comparison with the other varieties, 5.5 times increase in superoxide dismutase activity in 15 mM CaCl_2 set, 11 times increase in catalase activity in 5 mM CaSO_4 , 89% increase in ascorbate peroxidase activity in 5 mM CaCO_3 the glutathione reductase activity highest increased (103%) in 10 mM CaCl_2 and 65% decrease in lipid

B. Singh · S. Banerjee (✉)

Department of Biotechnology, Heritage Institute of Technology, Kolkata, India

e-mail: soma.banerjee@heritageit.edu

B. Singh

e-mail: banhi.biotech@gmail.com

© Springer Nature Singapore Pte Ltd. 2021

D. Ramkrishna et al. (eds.), *Advances in Bioprocess Engineering and Technology*,

Lecture Notes in Bioengineering,

https://doi.org/10.1007/978-981-15-7409-2_31

peroxidation activity in 10 Mm CaSO_4 . The study reveals that CaCO_3 followed by CaSO_4 is better than CaCl_2 to combat NaCl stress.

Keywords Rice · Sodium chloride · Calcium ion · Reducing sugar · Starch · Chlorophyll · Proline · Antioxidants

1 Introduction

Rice is considered as a major food crop across worldwide and India is one of the largest producers of that. Rice plant (*Oryza sativa* L.) is a salt-sensitive crop for which soil salinity is a major factor limiting yield throughout the coastal areas of Africa and South Asia and Southeastern Asia (Flowers and Yeo 1981). In India, the Sunderban area of West Bengal falls under this. However, rice genotypes show wide variations in salt tolerance (Sahi et al. 2006). Rising sea levels, salt accumulation, erosion and human activities lead to increase the salinity in the rice fields rapidly (Maclean et al. 2002). Salinity effects on rice both in morphological and physiological ways (Khatun and Flowers 1995). Reactive oxygen species (ROS) are produced by the plant during photosynthesis and respiration. Stress situations lead to the formation of ROS in higher amount, causing cell death (Gupta and Huang 2014).

The important antioxidant enzymatic components of the defence mechanism are superoxide dismutase (SOD), catalase (CAT), ascorbate peroxidase (APX) and glutathione reductase (Ahmad 2014). It has been observed that there are several signalling molecules such as abscisic acid, salicylic acid, brassinosteroids and calcium (Ca) that can mitigate the adverse effects of salinity through activating the defence mechanisms (Cha-um et al. 2015; Gupta and Huang 2014; Popova et al. 1995; Fragnire et al 2011; Clause and Sasse 1998).

Ca has been reported to restrict the entry of Na^+ into the plant cells (Kader and Lindberg 2008; Hussain et al. 2010) and improve the soil physical conditions (Qadir et al. 2001). This study comprises comparison of the effect of the combined action of sodium chloride (NaCl) and three types of calcium salts, calcium chloride (CaCl_2), calcium sulphate (CaSO_4) and calcium carbonate (CaCO_3), on three rice varieties ('Chinsurah Nona-2', 'Dudherswar' and 'Pratiksha') both morphological and biochemical estimations.

2 Materials

Three varieties of rice seeds, 'Chinsurah Nona-2' (CN2), 'Dudherswar' (DDH) and 'Pratiksha' (PAT), locally cultivable at salted soils of Gosaba (Sunderban) were collected from Gosaba Rice Research Centre, Gosaba, South 24-Parganas, West Bengal.

3 Methodology

3.1 Experiment Designing and General Morphological

Seeds were grown with Hoagland media (Hoagland and Arnon 1950). The 15-day-old seedlings were treated with 200 mM of NaCl solutions with the three different calcium salts CaCl_2 , CaSO_4 and CaCO_3 in 5 mM, 10 mM and 15 mM concentration, respectively. Rice seedlings from each concentration were randomly selected after 7 days for the measurements of shoot length, biochemical estimations and estimations of antioxidant activities.

3.2 Estimations of Chlorophyll Content

Chlorophyll content was measured by using the method of Arnon (1949) at 645 nm and 663 nm and calculated using the following equation: Chlorophyll a: $12.7(A_{663}) - 2.69(A_{645})$ and Chlorophyll b: $22.9(A_{645}) - 4.68(A_{663})$.

3.3 Estimations of Proline Content

Proline content was analysed by acid ninhydrin according to the modified procedure of Bates et al. (1973). Reacted compound was extracted by toluene and measured at 520 nm.

3.4 Estimations of Carbohydrates

Reducing sugars were extracted with hot 80% ethanol and then estimated by using dinitrosalicylic acid reagent calorimetrically at 540 nm wavelength and starch was extracted with perchloric acid and then estimated with 'Anthrone reagent' (Miller 1972).

3.5 Estimations of Lipid Peroxidation Rate

The level of lipid peroxidation is expressed as $\mu\text{g/g}$ malondialdehyde content extracted with thiobarbituric acid–trichloroacetic acid (Agarwal 2007).

3.6 Antioxidant Activity Estimations

For the CAT assay, the enzyme activity was expressed in mmol of hydrogen peroxide consumed per minute (Clare et al. 1984).

The APX activity, one unit of the APX was measured as 1 μ M of ascorbate oxidized per minute (Nakano and Asada 1981).

In the glutathione reductase activity, the one unit of GR activity is defined equals to oxidation of 1 μ mol of NADPH (Schaedle and Bassham 1977).

4 Results and Discussion

4.1 Chlorophyll Content and Shoot Growth

The Chlorophyll a content was reduced by 82%, 75% and 80% and Chlorophyll b content was reduced by 81%, 84% and 83% in CN2, PAT and DDH variety, respectively, in the salt stress set (200 mM NaCl concentration.) (Fig. 1). The best recovery of Chlorophyll a was found in the following treatment sets i.e. 5 mM CaCl_2 (1.1 times), 5 mM CaSO_4 (48%) and 15 mM CaCl_2 (2.1 times) in CN2, PAT and DDH variety respectively with respect to the. On the other hand, best recovery of Chlorophyll b was found in the following treatment set of 15 mM CaCO_3 (1.1 times), 5 mM CaSO_4 (1.1 times) and 15 mM CaCl_2 (2.4 times) in CN2, PAT and DDH variety, respectively, with respect to stress control set. Similar results have found by Lutts et al. (1996) and Tahjib et al. (2018), where CaCl_2 treatments at 5 mM significantly increased Chl-a, Chl-b and Chl-(a + b) contents under salt stress conditions in early vegetative stages of rice seedlings. Gaballah et al. (2007) showed that CaCO_3 helped to increase chlorophyll content in sesame plants.

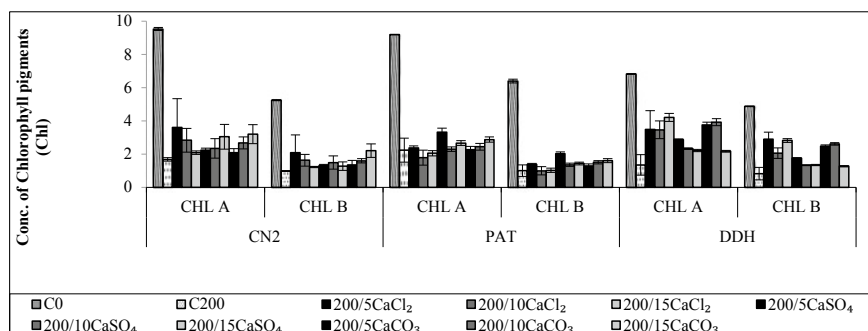
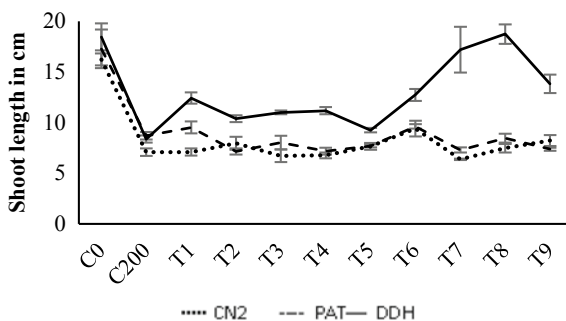
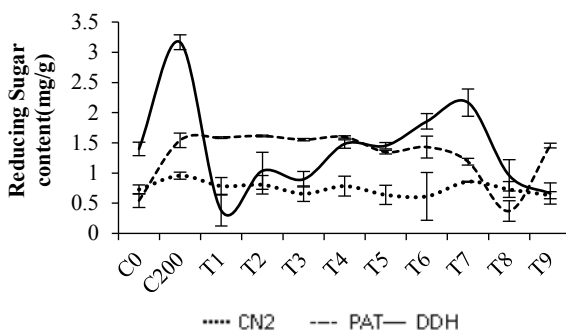


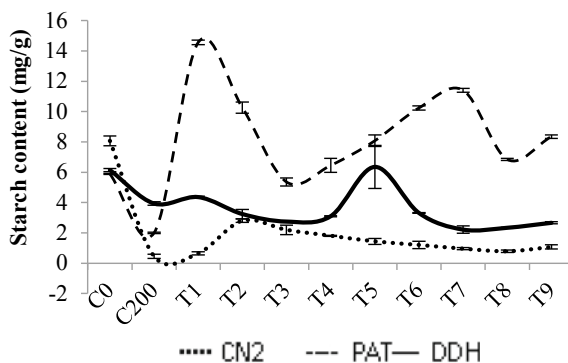
Fig. 1 Chlorophyll a and Chlorophyll b contents

Fig. 2 Comparative Shoot growth**Fig. 3** Reducing Sugar content

In seedlings, shoot growth was decreased 55%, 49% and 55% in CN2, PAT and DDH variety, respectively, in 200 mM NaCl with respect to control (Fig. 2). The results show that the maximum recovery of shoot growth was found in 15 mM CaSO_4 treatment set and 32% in CN2 variety, with respect to the seedlings stressed only with 200 mM NaCl; whereas, the shoot growth of DDH variety was markedly restored in 10 mM CaCO_3 set (1.2 times). This result matches the findings of Lutts et al. (1996) and Tahjib et al. (2018), where salinity decreased growth of rice leaves and they have also found that shoot length can increase through supplementation with CaCl_2 to the salt-treated seedlings. Ornami and Hammes (2006) have found that CaSO_4 showed stronger ameliorative effect than CaCl_2 during the growth rate study of salt-stressed amaranth. Although Bassett (1980) has found that CaCO_3 has an ameliorative effect on salt-stressed *Bromus mollis* (Fig. 3).

4.2 Proline Content

Proline accumulation (Fig. 4) was markedly increased in CN2 (10 times), PAT (3.1 times) and DDH (4.6 times) variety in 200 mM NaCl set. The highest reduction in proline accumulation was found in the treatment set of 10 mM CaSO_4 (81%), 15 mM CaCO_3 (73%) and 5 mM CaCO_3 (98%) in CN2, PAT and DDH variety, respectively,

Fig. 4 Starch content

with respect to the salt-treated seedlings. Rahman et al. (2016) observed in their work on CaCl_2 application reduction of proline content in comparison with the seedlings treated with NaCl alone.

4.3 Carbohydrate Content

The reducing sugar accumulation was increased 31%, 1.9 times and 1.2 times in CN2, PAT and DDH variety, respectively, in stressed set seedlings. The considerably best decrease in reducing sugar accumulation was found in the treatment set of 15 mM CaSO_4 (36%), 5 mM CaCO_3 (75%) and 5 mM CaCl_2 (88%) in CN2, PAT and DDH variety, respectively, with respect to the 200 mM NaCl -treated seedlings (Fig. 3). Similar result was found by Hakim et al. (2014) in the rice varieties of MR52 and Pokkali.

On the contrary, starch content was decreased 16.6 times, 1.9 times and 56% in CN2, PAT and DDH variety, respectively, in stressed set (Fig. 5). However, the

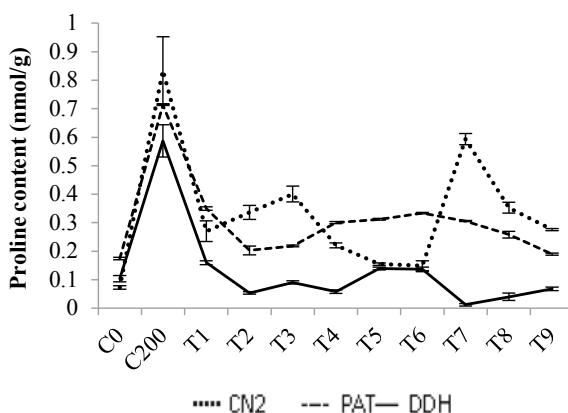
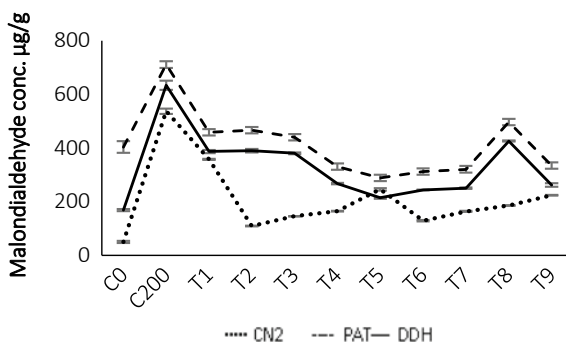
Fig. 5 Proline content

Fig. 6 Lipid peroxidation activity



starch accumulation was significantly restored in the treatment set of 10 mM CaCl_2 (5.1 times), 5 mM CaCl_2 (6.3 times) and 10 mM CaSO_4 (61%) in CN2, PAT and DDH variety, respectively, with respect to stressed set. The findings of Amirjani (2011) also revealed that starch concentration decreased in rice seedlings under salt stress. Dubey and Singh (1999) showed that accumulation of sugars along with other compatible solutes contributes to an osmotic adjustment under salt stress and probably this high storage helps in basal metabolism under stress (Hurry et al. 1995). According to Krapp and Stitt (1995), in their work, they showed starch may not play any important role in salt tolerance but metabolic alteration may cause reduction in starch content under salt stress.

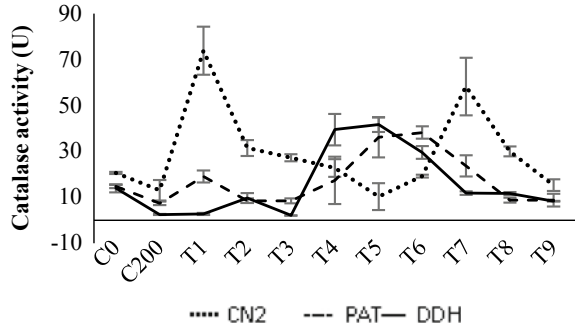
4.4 Rate of Lipid Peroxidation

In case of lipid peroxidation, malondialdehyde content was higher 9.6 times, 76% and 2.7 times in CN2, PAT and DDH variety, respectively, in the stress set. The highest reduction in lipid peroxidation activity has found through the treatment of 10 mM CaCl_2 (79%), 15 mM CaSO_4 (59%) and 15 mM CaSO_4 (66%) in CN2, PAT and DDH variety, respectively, with respect to the stressed set (Fig. 6). Rahman et al. (2016) have also found that exogenous application of CaCl_2 reduced the membrane damage, indicated a noticeable reduction of malondialdehyde content in the CaCl_2 treatment sets in comparison with the salt-treated rice seedlings.

4.5 Antioxidant Enzyme Activity

CAT activity is decreased in all three rice varieties under salt stress, viz., 37%, 49% and 82% in CN2, PAT and DDH variety, respectively, in 200 mM NaCl stressed control set. The significant increase in CAT activity was found with the treatment of 5 mM CaCl_2 (4.6 times), 10 mM CaSO_4 (4.1 times) and 10 mM CaSO_4 (15.8

Fig. 7 Catalase activity



times) in CN2, PAT and DDH variety, respectively (Fig. 7). Similar result was found in the work of Lee et al. (2001) where catalase activity is significantly decreased in salt stress. Tahjib et al. (2018) showed that on application of CaCl_2 , increased CAT activity in salt-stressed rice plants.

Unlike CAT activity, the APX activity was increased in all three rice varieties under salt stress, viz., 34%, 6.8 times and 3.6 times in CN2, PAT and DDH variety, respectively. Shim et al. (2003) were also found that salt stress has significant effect in enhancing the APX activity as compared with controls. The highest decrease in APX activity was found in ‘the treatment of 5 mM CaCO_3 (67%), 5 mM CaSO_4 (97%) and 15 mM CaCO_3 (82%) in CN2, PAT and DDH variety, respectively, with respect to stressed set (Fig. 8). Similar results have found by Tahjib et al. (2018), where CaCl_2 treatments significantly increased CAT activity, whereas decreased APX activities compared with the salt-stressed plants. Rahman et al. (2016) showed the application of CaCl_2 -reduced APX activity in the CaCl_2 treatment sets in comparison with the salt-treated rice seedlings.

For glutathione reductase, activity was increased 3.6 times, 14% and 26.3% in CN2, PAT and DDH variety, respectively, in 200 mM NaCl with respect to control. The highest decrease in glutathione reductase activity was found through the treatment of 15 mM CaSO_4 (72%), 15 mM CaCO_3 set (6%) and 15 mM CaCl_2 (42%) in

Fig. 8 Ascorbate peroxidase activity

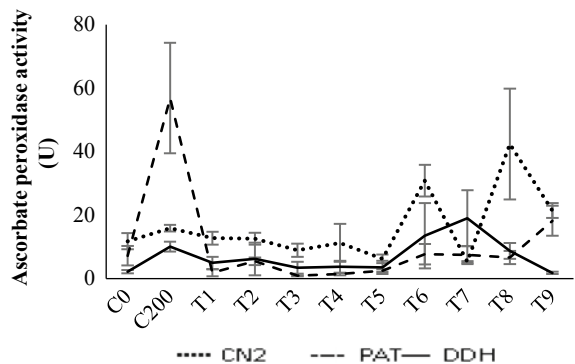
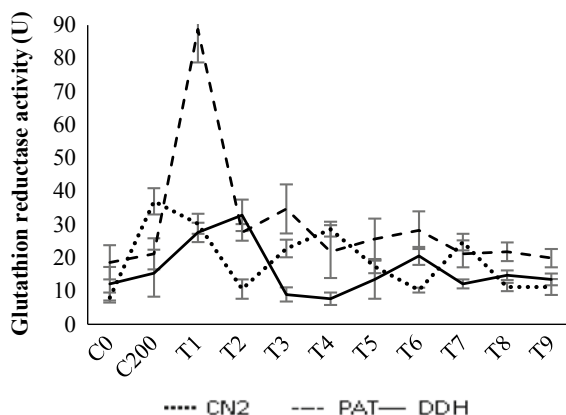


Fig. 9 Glutathione reductase activity



CN2, PAT and DDH variety, respectively, with respect to the 200 mM NaCl-treated seedlings (Fig. 9). Mishra et al. (1995) have also found that glutathione reductase was induced by salt stress. Similar result was found by Rahman et al. (2016), where application of CaCl_2 -reduced glutathione peroxidase activity in the Ca treatment sets in comparison with the salt-treated rice seedlings.

Results of experiments of CN2, PAT and DDH. Different combinations of NaCl and Ca salts are marked as (C0—neither NaCl nor Ca salts added, C200—only 200 mM of NaCl is applied, T1—5 mM of CaCl_2 , T2—10 mM of CaCl_2 , T3—15 mM of CaCl_2 , T4—5 mM of CaSO_4 , 10 mM of CaSO_4 , 15 mM of CaSO_4 , 5 mM of CaCO_3 , 10 mM of CaCO_3 and 15 mM of CaCO_3) (standard deviations are shown as bars).

5 Conclusion

The results showed that rice varieties Dudherswar (DDH) and Pratiksha (PAT) are very susceptible to NaCl than a salt-tolerant variety of Chinsurah Nona-2 (CN2). This study showed that exogenous Ca can alter the salt stress in rice seedlings and also reveals that application of CaCO_3 and CaSO_4 is better than CaCl_2 to combat salinity for the cultivation of rice.

Acknowledgements The authors would like to acknowledge the University Grants Commission for The Maulana Azad National Fellowship for funding and Gosaba Rice Research Centre under Chinsurah Rice Research Station for supplying the scientifically certified rice seeds. The authors wish to acknowledge the authorities of Heritage Institute of Technology for providing necessary technical support for this work.

References

- Agarwal S (2007) Increased antioxidant activity in Cassia seedlings under UV-B radiation. *Biol Plant* 51:157–160
- Ahmad P (2014) Oxidative damage to plants: antioxidant networks and signaling, 1st edn. Elsevier Science, Academic Press, Amsterdam, p 672
- Amirjani MR (2011) Effect of Salinity Stress on growth, Sugar content, pigments and enzyme activity of rice. *Int J Bot* 7(1):73–81
- Arnon DI (1949) Copper enzymes in isolated chloroplasts polyphenoloxidase in *Beta vulgaris*. *Plant Physiol* 24:1–15
- Bates LS, Waldren RP, Teare ID (1973) Rapid determination of free proline for water stress studies. *Plant Soil* 39:205–207
- Bassett PA (1980) The effect of soil salinity and calcium levels on the growth of *Bromus mollis* in the Camargue, France. *Oikos* 35(3):353–358
- Cha-um S, Singh H P, Samphumphuang T et al (2015) Calcium-alleviated salt tolerance in indica rice (*Oryza sativa* L. spp. *indica*): physiological and morphological changes. *Asian J Crop Sci* 6(1):176–182
- Clare DA, Duong MN, Darr D et al (1984) Effects of molecular oxygen on the detection of superoxide radical with nitroblue tetrazolium and an activity stain for catalase. *Anal Biochem* 140(2):532–537
- Clause SD, Sasse JM (1998) Brassinosteroids: essential regulators of plant growth and development. *Ann Rev Plant Biol* 49:427–451
- Dubey RS, Singh AK (1999) Salinity induces accumulation of soluble sugars and alters the activity of sugar metabolising enzymes in rice plants. *Biol Plantarum* 42:233–239
- Flowers TJ, Yeo AR (1981) Variability in the resistance of Sodium chloride salinity within rice (*Oryzasativa* L.) varieties. *New Phytol* 88:363–373
- Fragnire C, Serrano M, Abou-Mansour E et al (2011) Salicylic acid and its location in response to biotic and abiotic stress. *FEBS Lett* 585(12):1847–1852
- Gaballah MS, Abou Leila B, El-Zeiny HA et al (2007) Estimating the performance of salt-stressed sesame plant treated with antitranspirants. *J Appl Sci Res* 3(9):811–817
- Gupta B, Huang B (2014) Mechanism of salinity tolerance in plants: physiological, biochemical, and molecular characterization. *Int J Genomics* 2014:1–18
- Hakim MA, Juraimi AS, Hanafi MM et al (2014) Biochemical and anatomical changes and yield reduction in rice (*Oryza sativa* L.) under varied salinity regimes. *Hindawi BioMed Research Int* 2014:1–11
- Hasegawa PM, Bressan RA, Zhu JK et al (2000) Plant cellular and molecular responses to high salinity. *Ann Rev Plant Physiol Mol Biol* 51:463–499
- Hoagland DR, Arnon DI (1950) *Calif Agr Exp Stat Circ* 347:1–32
- Hurry VM, Strand A, Tobiaeson M et al (1995) Cold hardening of spring and winter wheat and rape results in differential effect of growth carbon metabolism and carbohydrate content. *Plant Physiol* 109:697–706
- Hussain K, Nisar MF, Majeed A et al (2010) What molecular mechanism is adapted by plants during salt stress tolerance? *Afr J Biotechnol* 9:416–422
- Kader MA, Lindberg S (2008) Cellular traits for sodium tolerance in rice (*Oryzasativa* L.). *Plant Biotechnol* 25:247–255
- Khatun S, Flowers TJ (1995) Effects of salinity on seed set in rice. *Plant Cell Env* 18:61–67
- Krapp A, Stitt M (1995) An evolution of direct and indirect mechanisms for the “sink-regulation” of photosynthesis in spinach: changes in gas exchange, carbohydrates, metabolites, enzyme activities and steady-state transcript levels after cold-gridling source leaves. *Planta* 195:313–323
- Lee DH, Kim YS, Lee CB (2001) The inductive responses of the antioxidant enzymes by salt stress in the rice (*Oryzasativa* L.). *J Plant Physiol* 158:737–745
- Lutts S, Kinet JM, Bouharmont J (1996) NaCl-induced senescence in leaves of rice (*Oryza sativa* L.) cultivars differing in salinity resistance. *Ann Bot* 78(3):389–398

- Maclean JL, Dawe DC, Hardy B et al (2002) Rice Almanac III Edition, 3rd edn. CABI Publishing, Wallingford, Oxon, p 253
- Miller GL (1972) Use of DNS reagent for determination of reducing sugar. *Anal Chem* 31:426–428
- Mishra NP, Mishra RK, Singhal GS (1995) Changes in the activities of anti-oxidant enzymes during exposure of intact wheat leaves to strong visual light at different temperatures in the presence of protein synthesis inhibitors. *Plant Physiol* 102:903–910
- Nakano Y, Asada K (1981) Hydrogen peroxide is scavenged by ascorbate peroxidase in spinach chloroplasts. *Plant Cell Physiol* 22(5):867–880
- Ornami E Nand Hammes PS (2006) Ameliorative effects of calcium on growth and mineral uptake of salt-stressed amaranth. *S Afr J Plant Soil* 23(3):197–202
- Parida AK, Das AB (2005) Salt tolerance and salinity effects on plants: a review. *Ecotoxicol Environ Saf* 60:324–349
- Popova LP, Stoinova ZG, Maslenkova LT (1995) Involvement of abscisic acid in photosynthetic process in *Hordeum vulgare* L. during salinity stress. *J Plant Growth Regul* 14(4):211–218
- Qadir M, Schubert S, Ghafoor A, Murtaza G (2001) Amelioration strategies for sodic soil: a review. *Land Degrad Dev* 12:375–386
- Rahman A, Nahar K, Hasanuzzaman M et al (2016) Calcium supplementation improves Na⁺/K⁺ ratio, antioxidant defense and glyoxalase systems in salt-stressed rice seedlings. *Front Plant Sci* 7(609):1–16
- Sahi C, Singh A, Kumar K et al (2006) Salt stress response in rice: Genetics, molecular biology and comparative genomics. *Func Integr Genomics* 6(4):263–284
- Schaedle M, Bassham JM (1977) Chloroplast glutathione reductase. *Plant Physiol* 59:1011–1012
- Shim IS, Momose Y, Yamamoto A et al (2003) Inhibition of catalase activity by oxidative stress and its relationship to salicylic acid accumulation in plants. *Plant Growth Regul* 39(3):285–292
- Tahjib UA, Roy PR, Sohag AAM, Afrin S, Rady MM, M. Hossain A (2018) Exogenous calcium supplementation improves salinity tolerance In Brri Dhan28; A salt-susceptible high-yielding *Oryza sativa* Cultivar. *J Crop Sci Biotech* 21(4):383–394

Synthesis and Characterization of TiO₂ Nanoparticle and Checking Its Antimicrobial Activity Against *Escherichia coli* and *Staphylococcus aureus*



Ram Singh Purty, Ishant Shakya, and Sayan Chatterjee

Abstract The aim of the experiment was to produce the conjugated nanoparticles and optimize its production that can be replicated at industrial level. The primarily used chemical from which TiO₂ nanoparticle was made is titanium isopropoxide (C₁₂H₂₈O₄Ti). The primary dopant used was urea CO(NH₂)₂. Ammonium chloride NH₄Cl was used as a secondary nitrogen dopant. Different molar ratios of these dopants were used while synthesizing the nanoparticle. The nanoparticle synthesized was characterized by the help of UV–vis spectrophotometer and DLS (dynamic light scattering). The synthesized NP was able to degrade the bromothymol blue dye under the action of UV received by the direct sunlight proving its photocatalytic property. The nanoparticles were tested for its antimicrobial property on the gram-negative bacteria *Escherichia coli* and gram-positive bacteria *Staphylococcus aureus*. Broth dilution method was used to study the antimicrobial effect. The results were further confirmed with the help of agar diffusion assay. The synthesized nanoparticle was able to inhibit the growth of the bacteria in both the assays successfully.

Keywords TiO₂ nanoparticle · Antimicrobial activity · *Escherichia coli* · *Staphylococcus aureus* · Synthesis of nanoparticle · Characterisation

1 Introduction

Nanotechnology is the technology that is aimed at synthesizing and getting new products that have some novel functionality. This in particular is the new branch of study

R. S. Purty · I. Shakya · S. Chatterjee (✉)
University School of Biotechnology, Guru Gobind Singh Indraprastha University, New Delhi,
India

e-mail: sayan@ipu.ac.in

R. S. Purty
e-mail: rspurty@ipu.ac.in

I. Shakya
e-mail: shakyaishant97@gmail.com

that has got a vast range of applications from industrial processes to biomedical and production of energy. In our current work, we were interested in the biological applications of nanoparticles particularly in removing the bacterial strains from different places under different conditions (Drexler 2007).

There are various studies related to TiO₂ NP that shows the effect of these nanoparticles on various strains of bacteria and its dye-degrading effect under the influence of direct sunlight and UV light. The bandgap of TiO₂ nanoparticle was found to be around 3.2 eV, which is not suitable for the solar application and for the dye degradation process. To overcome this problem, we used ammonia and ammonium chloride as dopants to make conjugated nanoparticle and lower the bandgap between the valence and conduction bands. Lower the bandgap, less will be the energy required for the electron to jump from the conduction band to valence band (Lusvardi et al. 2017).

The main aim of the experiment is to synthesize and improve the quality of TiO₂ nanoparticle in an economic way in the lab condition. The base materials used for the synthesis of TiO₂ nanoparticle were titanium dipropoxide and titanium chloride.

There are various types of nanoparticle oxides such as iron oxide, zinc oxide, oxides of gold and silver, titanium oxide. Out of these, TiO₂ nanoparticles are most widely used. The various functions of TiO₂ are being known such as degradation of various dyes in aqueous solution and its special property of reducing inorganic ions. TiO₂ nanoparticles have got a special property of photocatalysis and are the most used photocatalyst oxide (Gupta and Tripathi 2011). TiO₂ nanoparticles have large surface area and exhibit antimicrobial properties and having certain amount of thermal and chemical stabilities. It also shows low toxicity and has antimicrobial properties.

2 Materials and Methods

2.1 Synthesis

Based on the previous research paper, we have tested and reproduced some of the protocols in our laboratory. In order to produce TiO₂ nanoparticles, available protocols were optimized and improved keeping in mind the requirement of the markets. Reagents used were titanium isopropoxide 99.8%, urea 99%, and ammonium chloride 99.5%. Around 0.4 g of urea was added to 80 ml of double-distilled water in a beaker and mixed well for 5 min. To this, 1.8 g of ammonium chloride and 20 ml of titanium isopropoxide were added dropwise and stirred for 30 min. The suspension was incubated in the water bath set at 90 °C for 1 h. The separated product was dried at 80 °C for 12 h using hot air blower incubator. All samples were tested at room temperature.

2.2 Characterization

Before drying the solution, the supernatant was collected that contained suspended nanoparticles. The collected supernatant was centrifuged at 10,000 rpm for 10 min, around 200 μ l of this was added to 1800 μ l of double-distilled water. The diluted solution was further analyzed using DLS (dynamic light scattering) for the estimation of average nanoparticle size. The same solution sample was used in the UV–vis spectrophotometer for absorption studies.

2.3 Dye Degradation

For dye degradation test, around 1 ml of bromothymol blue (BPB) dye was diluted with 50 ml of double-distilled water and aliquoted to three 1.5-ml microcentrifuge tubes each containing 2 ml of diluted dye solution. To this dye solution, 20 mg of nanopowder was added to two tubes, whereas the third was mentioned as control without nanopowder. Out of three tubes, two were exposed to sunlight (one having nanopowder and one without) and the third was put in the dark having nanopowder. In another set of experiments, different concentrations of nanopowder, i.e., 20 mg, 40 mg, 60 mg, were added to three tubes each containing 2 ml of diluted dye solution to check the effect of concentration of nanopowder on the degradation of dye.

2.4 Antimicrobial Test

2.4.1 Antimicrobial Effect of TiO₂

The antimicrobial effect of TiO₂ was analyzed using *Escherichia coli* and *Staphylococcus aureus*. Overnight-grown culture of *E. coli* and *S. aureus* was added to 100 ml of LB nutrient broths without and with various concentrations of TiO₂ nanoparticles, i.e., 0 μ g/ml, 10 μ g/ml, 20/ml, 40 μ g/ml, 60 μ g/ml, 80 μ g/ml, 100 μ g/ml and incubated at 37 °C. The optical density was taken after the time interval of 25 min at 600 nm and a graph was plotted.

2.4.2 Antimicrobial Efficiency of TiO₂ Nanoparticle by Agar Diffusion Assay

On LB agar plate, 100 μ l of bacterial culture was spread plated and five round disks were placed. To each disk, 10 μ l of different concentrations of TiO₂ nanoparticles, i.e., 0%, 1%, 1.5%, 2%, and 2.5% was added. The zone of inhibition was measured after 24 h of incubation of plates at 37 °C.

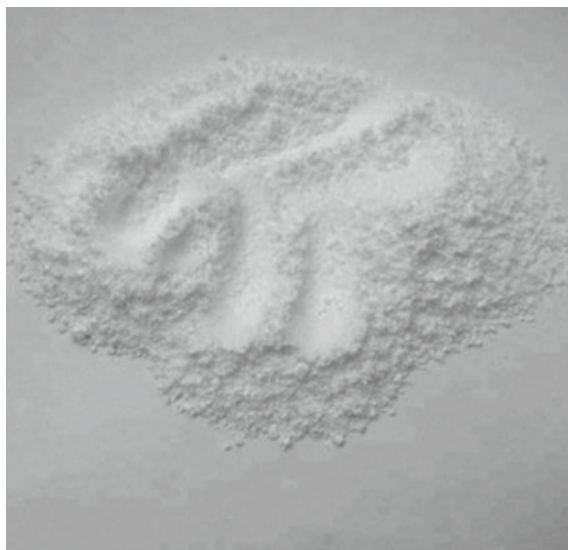


Fig. 1 Synthesized white titanium oxide nanopowder

3 Results and Discussion

3.1 Synthesis

After 12 h of incubation under 80 °C, there was the formation of white-colored nanopowder that was further grinded and stored in 4 °C away from any source of light or further usage and testing (Fig. 1).

3.2 Characterization

3.2.1 UV-Vis Spectrophotometry

Here the two red dots depict the formation of two peaks according to the table. The two broadening peaks were formed confirming the formation of the TiO₂ nanoparticle. The absorption spectra formed were founded to be similar to that of TiO₂ as reported in the literature (Kavitha et al. 2013).

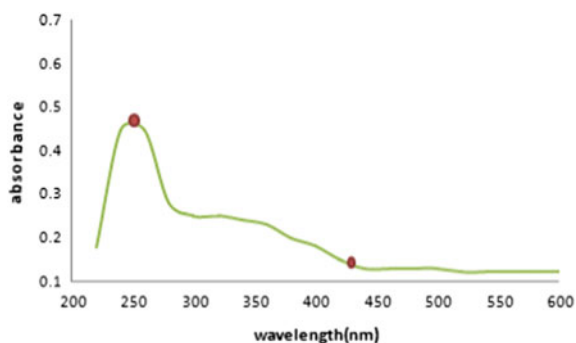


Fig. 2 Absorbance versus wavelength graph of TiO₂ conjugate nanopowder

3.2.2 Dynamic Light Scattering

Dynamic light scattering (DLS) is a technique in physics that can be used to determine the size distribution profile of small particles in suspension. In Fig. 3, the size of the nanoparticle was more than the expected. The peak was formed at 279.2 d. nm depicting the diameter of the synthesized TiO₂. The PDI value was found to be around 0.4511. In Fig. 4, the size of the particle increased to 372 d.nm, which was no longer a nanoparticle (Figs. 2 and 5).

3.3 Dye Degradation

Dye in all the three samples was degraded in almost equal time showing that there were no significant changes by altering the concentration of TiO₂ nanopowder. No color change was observed in the control as it had no nanopowder. The color of

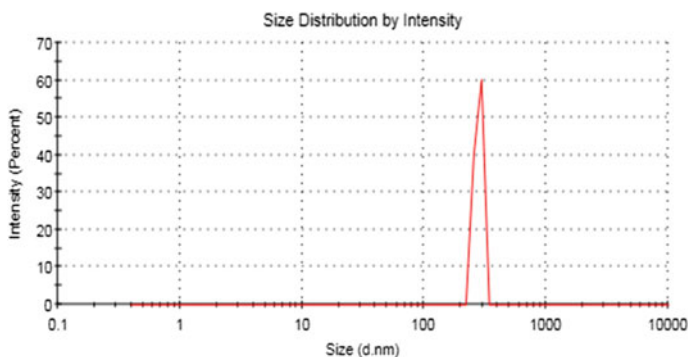


Fig. 3 DLS result for supernatant nanoparticle

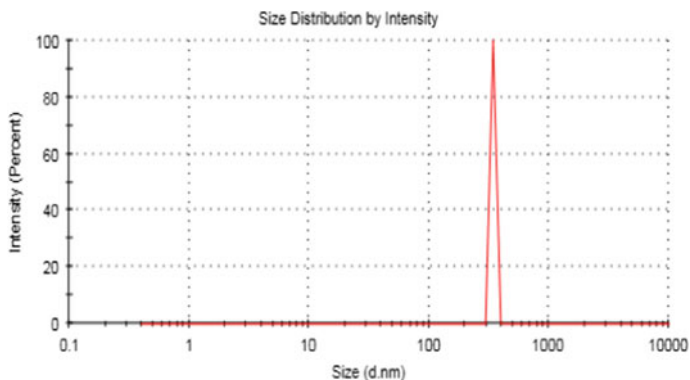


Fig. 4 DLS result for suspended nanopowder



Fig. 5 Degradation of dye

the two other tubes changed to pale yellow just after adding nanopowder to it. The second tube was kept in the dark and no color change was observed. The color change was observed in the third tube where color of the dye changed from pale yellow to colorless, showing that the process of dye degradation was successful by photocatalysis under the effect of direct sunlight. This was in accordance with the popular reports on this test for nanoparticles (Konstantinou and Albanis 2004).

3.4 Antimicrobial Test

3.4.1 Antimicrobial Effect of TiO₂ in Liquid Media

The continuous decrease in absorbance was noticed showing the decrease in bacterial colony with all the concentrations used. There was continuous growth of bacterial

colony in the control, where no nanopowder was added. From this, it was concluded that the addition of TiO₂ nanopowder was able to control the growth of *E. coli* and *S. aureus*.

3.4.2 Antimicrobial Efficiency of TiO₂ Nanoparticles by Agar Diffusion Assay

There was the formation of the inhibition zone around the disks present on the outer side. The size of inhibition did vary according to the concentration used but cannot clearly be depicted. No such zone was formed around the central disk, where only distilled water without any nanopowder was poured. Zone of inhibition meant that there was no growth of bacteria in that particular zone. There was the formation of inhibition zone around the disks present on the outer side. This was reported in similar work by other researchers (Damodar et al. 2009). The size of inhibition did vary according to the concentration used but cannot clearly be depicted. No such zone was formed around the central disk, where only distilled water without any nanopowder was poured (Figs. 6).

Among various types of nanoparticles, titanium dioxide was used because it can be economically produced as compared with the other nanoparticle material. Primary aim was to synthesize the TiO₂ nanoparticle and use in the biological/biotechnology field. The nanoparticles acting at nanolevel have the ability to alter the biological



Fig. 6 Zone of inhibition for *E. coli*

function of an organism. A carefully and efficiently synthesized nanoparticle size varies from around 20–150 nm. The size of the synthesized nanoparticle was found to be around 279.2 nm that is bit large as compared with the expected size but still was in nanometer range and can perform all the characteristic nanoparticle properties. Dye degradation test was such an example, where the activity of the nanoparticles degraded the dye although the time of degradation was more as compared with the time mentioned in other manuscripts (Nasikhudin et al. 2018). Also the synthesized nanoparticles were able to stop the growth of the bacterial colonies by interfering with the survival mechanism of bacterium and ultimately causing their death. Further, it could be said that nanoparticles in future could possibly replace the chemical methods to kill different microbes, specially the microbes related to cash crops and food industry. Antimicrobial clothes can also be reproduced by the process of nanocoating.

We were able to synthesize the TiO_2 nanoparticle, though not of desired size, but it had all the properties of a nanoparticle. The qualitative dye degradation was successfully performed as it was able to degrade the dye which is seen in Fig. 7. The result of UV–vis spectrophotometer was found to be good from which we concluded that it is of nanosize. DLS reading confirmed the same by giving the exact size of the nanoparticle that found to be around 342 nm. The decreasing number of bacterial colonies helps to conclude that the nanoparticles were able to kill or slow down the growth rate of bacteria. This result was further proven by diffusion assay in which there was the formation of zone of inhibition where bacterial colonies were unable to grow.

Acknowledgements RSP, IS and SC would like to thank GGS Indraprastha University, New Delhi for all the laboratory space and financial support provided.

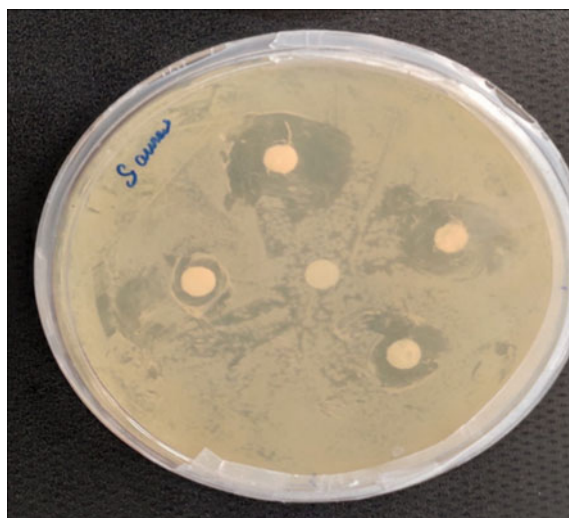


Fig. 7 Zone of inhibition for *S. aureus*

References

- Damodar RA, Sheng-Jie Y, Hui-Hsiang C (2009) Study the self cleaning, antibacterial and photocatalytic properties of TiO₂ entrapped PVDF membranes. *J Hazard Mater* 172(2–3):1321–1328
- Drexler KE (2007) *Engines of creation: the coming era of nanotechnology*. Publisher Doubleday, USA
- Gupta S, Tripathi M (2011) A review of TiO₂ nanoparticles. *Chinese Sci Bull* 56:1639–1657
- Kavitha KS, Syed B, Rakshith D, Kavitha HU, Yashwantha Rao HC, Harini BP, Satish S (2013) Plants as green source towards synthesis of nanoparticles. *Int Res J Biol Sci* 2(6):66–76
- Konstantinou IK, Albanis TA (2004) TiO₂-assisted photocatalytic degradation of azo dyes in aqueous solution: kinetic and mechanistic investigations: a review. *Appl Catal B-Environ* 49(1):1–14
- Lusvardi G, Barani C, Giubertoni F, Paganelli G (2017) Synthesis and characterization of TiO₂ nanoparticles for the reduction of water pollutants. *Materials* 10(10):1208
- Nasikhudin, Diantoro M, Kusumaatmaja A, Triyana K (2018) Study on photocatalytic properties of TiO₂ nanoparticle in various pH condition. *J Phys Conf Ser* 1011(1):012069

Taguchi-Based Process Optimization for Improving Iron Removal from Water Using Electrocoagulation Technique



Krishti Biswas and Mehabub Rahaman

Abstract The objective of this study is to remove iron from the aqueous solution by electrocoagulation (EC) process due to its simple setup and cost-effectiveness. Aluminum was chosen as the suitable material for the electrodes. In this study, the effect of different process parameters (viz. the initial concentrations of iron, the current intensity, the conductivity of the aqueous solution, the inter-electrode distance, and the initial pH of solution) was studied. Taguchi experimental design with an L_{16} orthogonal array was utilized to determine the optimal conditions for iron removal. The experiments were conducted at four different levels with the five process parameters. The ranges of the experimental parameters were chosen as an initial iron concentration: 15–30 ppm, current intensity: 0.50–1.25 A, inter-electrode distance: 8–14 mm, conductivity: 345–375 μS , and initial pH: 5–8. The processing time of the study was kept constant for all the experiments. The percentage of removal of iron was taken as the response for Taguchi analysis. The optimized conditions were found to be 15 ppm of initial concentration, 1.25 A of current intensity, and 8 mm of inter-electrode distance with insensitive to the range of values carried out for conductivity and initial pH of the solution. The decreasing order of sensitivity of the process parameters was found to be as initial concentration, inter-electrode distance, current intensity, pH of the solution, and conductivity.

Keywords Iron removal · Electrocoagulation · Optimization · Taguchi method

1 Introduction

Water is an essential natural resource for sustaining life and environment that we have always thought to be available in abundance and free gift of nature. Over the past few

K. Biswas · M. Rahaman (✉)
Department of Chemical Engineering, Jadavpur University, Kolkata, India
e-mail: mehabub@gmail.com

K. Biswas
e-mail: krisss.26910@gmail.com

© Springer Nature Singapore Pte Ltd. 2021
D. Ramkrishna et al. (eds.), *Advances in Bioprocess Engineering and Technology*,
Lecture Notes in Bioengineering,
https://doi.org/10.1007/978-981-15-7409-2_33

decades, the ever-growing population, urbanization, industrialization, and unskilled utilization of water resources have led to degradation of water quality and reduction in per capita availability in various developing countries. Iron is one of the most common elements in nature as it represents about 5% of the earth's crust (Hashim et al. 2017), and it can be found in freshwaters at a concentration of 0.5–50 mg/L. In addition to the natural occurrence of iron, many industries, such as mining and steel industries, contribute to the occurrence of iron in the water. However, iron represents an essential element for human health, where the daily intake of iron is recommended to be between 10 and 50 mg depending on the person's gender, age, physiological status, and the bioavailability of iron. Based on these considerations, the World Health Organization (WHO) limits their own concentration in drinking water to 0.3 mg/L (Vasudevas et al. 2009). Electrocoagulation has been suggested as an alternative to chemical coagulation in the treatment of waters and wastewaters (Balasubramanian et al. 2009; Chaturvedi and Dave 2012). In this technology, metal cations are released into the water by dissolving metal electrodes. Electrochemistry, coagulation, and flotation are identified as the key elements in the electrocoagulation process (Kobyas et al. 2003; Al-Qodah et al. 2017).

The electrocoagulation (EC) has been considered as a suitable process to remove iron in drinking water treatment because it lowers the amount of sludge and also provides some significant advantages such as quite compact and easy operation, no chemical additives needed, and high flow rates (Fu and Wang 2011). In this study, Taguchi method was implemented to investigate the effect of different parameters (viz. initial concentrations of heavy metal, current intensity, conductivity of solution, inter-electrode distance, and initial pH of solution) affecting EC process in the removal of iron from wastewater. The experiments were conducted at four different levels with five process parameters.

2 Materials and Methods

2.1 Materials

All the reagents used were analytical grade and were used without further modification. Iron sulfate heptahydrate ($\text{FeSO}_4 \cdot 7\text{H}_2\text{O}$) was procured from Merck, India. Sodium hydroxide (NaOH), sodium chloride (NaCl), and sulfuric acid (H_2SO_4) were also procured from Merck, India. Double distilled water was used to prepare the various solutions of iron. Aluminum sheets (~98% purity) for electrode fabrication were procured from local market.

2.2 Experimental Matrix Designing by Taguchi Method

Influential parameters affecting EC process were studied from various literatures. Parameters like the initial concentration of iron, current intensity, inter-electrode distance, conductivity, and initial pH were chosen. Taguchi method was implemented to analyze the effects of these parameters and to obtain the regression equation (Tir et al. 2015; Irdemez et al. 2006). In this work, orthogonal array OA₁₆ (4⁵) with five different parameters (P) of four different levels (L) were implemented. The level of each of the chosen parameters is shown in Table 1. N is the number of runs required for the orthogonal array, which is recognized using Eq. (1):

$$N = (L - 1)P + 1 \tag{1}$$

There are 16 experiments (L₁₆) to be carried out as per the Taguchi methodology and are shown in Table 2 (Karmakar et al. 2018). Minitab-17 software was utilized to implement Taguchi method for obtaining the optimized parameter values, the effectiveness of the parameters, and the regression equation. Each experiment was repeated at least three times to obtain the experimental removal efficiency (Martinez-villafane and Montero-Ocampo 2010). To evaluate the effect of parameters and to obtain their optimized value a response is chosen. In this study, the percentage removal of iron is chosen as the response of the Taguchi method, and experimental data were analyzed using the signal-to-noise (S/N) ratio. Since better the removal of iron from the solution, the “larger is better” characteristic has been chosen.

$$\frac{S}{N} = -10\log_{10}\left(\frac{1}{n} \sum_{i=1}^n \frac{1}{y_i^2}\right) \tag{2}$$

where S/N is the sound to noise ratio, n is the number of repetitions for one experimental combination, and y_i is the performance value of the ith experiment (Asghari et al. 2012).

Table 1 Experimental parameters and levels for the removal of iron using electrocoagulation

Variables	Levels			
	1	2	3	4
Initial concentration (ppm)	15	20	25	30
Current intensity (A)	0.5	0.75	1	1.25
Inter-electrode distance (mm)	8	10	12	14
Conductivity (μS)	345	355	365	375
Initial pH	5	6	7	8

Table 2 L₁₆ experimental matrix from Taguchi method

Experiment number	Initial concentration (ppm)	Current intensity (A)	Inter-electrode distance (mm)	Conductivity (μ S)	Initial pH	Percentage removal of iron
1	15	0.50	8	345	5	73.02
2	15	0.75	10	355	6	74.98
3	15	1.00	12	365	7	74.05
4	15	1.25	14	375	8	72.08
5	20	0.50	10	365	8	67.03
6	20	0.75	8	375	7	71.99
7	20	1.00	14	345	6	66.08
8	20	1.25	12	355	5	74.95
9	25	0.50	12	375	6	63.97
10	25	0.75	14	365	5	60.07
11	25	1.00	8	355	8	69.02
12	25	1.25	10	345	7	70.04
13	30	0.50	14	355	7	55.06
14	30	0.75	12	345	8	63.05
15	30	1.00	10	375	5	66.08
16	30	1.25	8	365	6	70.02

2.3 Experimental Setup and Procedure

A 5-L beaker was used for the electrocoagulation setup (Fig. 1). A 3-L of iron solutions of different concentrations were made for each of the experiments. Aluminum

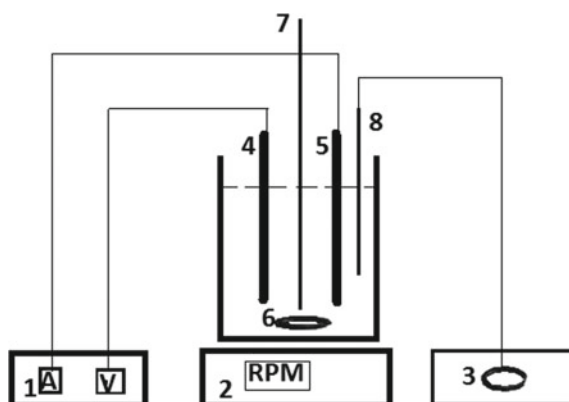


Fig. 1 Schematic diagram of electrocoagulation setup: (1) digital DC power, (2) magnetic bar stirrer, (3) multimeter meter, (4) anode, (5) cathode, (6) magnetic bar, (7) temperature probe, and (8) pH meter

plates were used as electrodes with dimensions of 100 mm × 30 mm × 1.5 mm. A perplex rod was used to support the anode and cathode. The inter-electrode distance varied from 8 to 14 mm. A DC power supply (Make: Aplab L6410 S) was connected to maintain a steady flow of current. A constant speed was maintained in the EC setup using a magnetic stirrer (Make: Remi 5 MLH Plus). The experiments were conducted at ambient temperature (25 ± 1 °C). The pH was varied for the experiments using 0.1 M solution of H₂SO₄ and NaOH. NaCl was used as the electrolyte. Each experiment had a fixed time span of 40 min. Samples were withdrawn at the end of the experiment and filtered through filter paper (Whatman Cat No 1001-110) and electrodes were cleaned by dilute HCl after each experiment.

The filtered sample was analyzed using ICP–OES spectrometry (Make: Perkin Elmer Optima 8000). The percentage removal of iron was calculated using the following equation:

$$\text{Removal efficiency} = \frac{C_i - C_f}{C_i} \times 100 \quad (3)$$

where C_i and C_f are the initial and final concentrations of iron solutions in mg L⁻¹, respectively (Hashim et al. 2019). Conductivity and pH were measured by multimeter meter (Make: EUTECH Instruments PC2700).

2.4 Analysis of Variance

Electrocoagulation of iron solution was performed in accordance with the set of parametric conditions acquired by experimental matrix design using L₁₆ orthogonal array methodology. The removal efficiency of iron using monopolar electrocoagulation process was analyzed statistically for an assessment of the importance of the model selected for optimization and the effects of separate process parameters on the response by means of ANOVA studies. ANOVA is a dynamic technique used to inspect the importance of a discrete parameter and selected the optimization model for the establishment of a mathematical model equation. It emphasizes on the analysis of the variance around the mean of the performance features and is accomplished by assessing the Fischer's test value (F -value). The influence of any parameter is elucidated by its F -value and the corresponding sum of squares (Shah et al. 2017). Higher F -value and sum of squares of any parameter specify its comparative importance in the procedure of the response. Contrariwise, the extents of acquired values of these tests are entirely owed to response signals and are assured by a p -value. The p -value simplifies the probability of attaining an F -value of this order due to noise values below 0.05 or 5% confirms the significance of the specific process parameter (Pundir et al. 2018).

3 Results and Discussion

3.1 Analysis of Iron Removal and Determination of Condition

The electrocoagulation process of iron solution was performed with a set of parametric conditions obtained by experimental matrix design using L_{16} orthogonal array approach. The percentage removal efficiency of iron was as a response and is shown in Table 2. In order to determine the effective parameters and their significance levels on removal efficiency, a statistical analysis of variance (ANOVA) was performed. The results of ANOVA are given in Table 3. The obtained adjusted sum of squares for the model was 479.299 and total degree of freedom (DF) was obtained to be 15. The F -value for initial concentration of iron was 71.26 which is the most significant but conductivity and pH were 0.03 and 0.62, which were least significant parameters. The F -value of the other parameters, current intensity and inter-electrode distance were found out to 30.32 and 33.97, respectively. These values can be assured from the P -value. Except conductivity and initial pH, other three parameters play a significant role in the removal of iron using electrocoagulation. Table 4 shows the priority of

Table 3 Analysis of variance (ANOVA) of the parameters

Source	DF	Adjusted SS	Adjusted MS	F -value	P -value
Regression	5	446.514	89.303	27.24	0.000
Initial concentration	1	233.620	233.620	71.26	0.000
Current intensity	1	99.391	99.391	30.32	0.000
Inter-electrode distance	1	111.368	111.368	33.97	0.000
Conductivity	1	0.109	0.109	0.03	0.859
pH	1	2.026	2.026	0.62	0.450
Error	10	32.785	3.278		
Total	15	479.299			

Table 4 Delta-rank of various parameters

Level	Initial concentration (ppm)	Current intensity (A)	Inter-electrode distance (mm)	Conductivity (μ S)	Initial pH
1	37.33	36.18	37.02	36.64	36.68
2	36.89	36.55	36.83	36.65	36.73
3	36.34	36.74	36.75	36.60	36.56
4	36.03	37.12	35.99	36.71	36.61
Delta	1.30	0.93	1.04	0.11	0.17
Rank	1	3	2	5	4

the parameters affecting in EC. From Delta-Rank, we can see that initial concentration of iron is the most significant parameter followed by electrode distance, current intensity, initial pH, and conductivity (initial concentration > inter-electrode distance > current intensity > initial pH > conductivity).

3.2 Effect of Various Parameters

To investigate the effect of various parameters like initial concentration of iron, current intensity, pH, inter-electrode distance, and conductivity on the removal efficiency of iron by electrocoagulation process, L_{16} experiments were carried at a fixed time.

3.2.1 Effect of Initial Concentration of Iron

Effect of initial concentration of iron is one of the most significant factors affecting the electrocoagulation process. Under reaction conditions of reaction temperature = 30 °C, reaction time = 40 min, monopolar connection of aluminum electrodes and agitation speed = 400 rpm, maximum removal efficiency of iron was obtained at 15 ppm of initial iron concentration, as demonstrated in Fig. 2. Figure 2 reveals that with an increase in initial concentration of iron the removal efficiency decreases. This is due to the fact that the time of each electrocoagulation was limited to 40 min and as the amount of iron increased the S/N ratio decreased. The maximum removal was observed at 15 ppm (S/N ratio: 37.33) and the least was at 30 ppm (S/N ratio: 36.03). At lower concentration (up to 15 mg/L), available aluminum hydroxide complexes are adequate to remove the Fe(II) molecules within 40 min with appropriate oxidizing

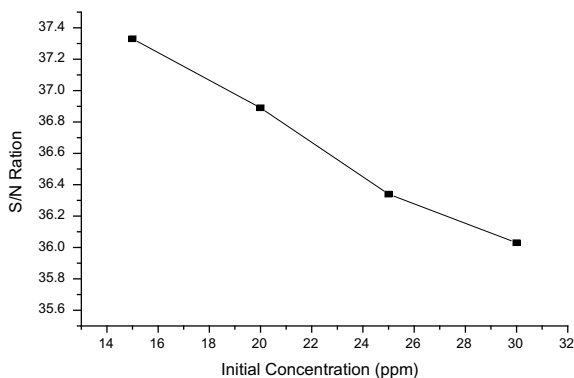


Fig. 2 Removal efficiency of iron versus initial concentration of iron by monopolar electrocoagulation process

environment. The rate of generation of aluminum hydroxide complexes is not sufficient to remove high Fe(II) concentration (>15 mg/L) within 40 min of operation. Therefore, longer residence time is required for electrocoagulation process of high Fe(II) concentration.

3.2.2 Effect of Current Intensity

The increase in current intensity increases the removal efficiency of iron. The amount of coagulants formed in electrocoagulation process depends greatly on the current passed and the time. Choice of electrode material is also an important factor affecting the cell voltage (different oxidation potential for different electrode materials) and the separation attained. In our work, aluminum was carefully chosen as the electrode material because of its cheapness, ready availability, nonharmfulness and it requires comparatively less oxidation potential. Here a sorption coagulation mechanism follows resulting in the creation of loose aggregates. As time progresses, further aluminum cation accumulation results in amorphous aluminum hydroxide precipitation that stimulates pollutant aggregation through a sweep coagulation followed by precipitation mechanism. During the final stages, coagulated aggregates act together with bubbles and float to the surface or settle to the bottom of the reactor. The size of the H_2 bubbles formed and the coagulant production rate is adjusted by varying the current intensity that also determines the floc growth in the system. Thus high efficiency of electrocoagulation is obtained using high current intensity. From Fig. 3, it can be seen that an increase in current intensity increases the S/N ratio (i.e., removal efficiency of iron). At 1.25 A, maximum S/N ratio was observed at 37.12 and at 0.5 A, the least removal of iron was determined at S/N ratio of 36.18.

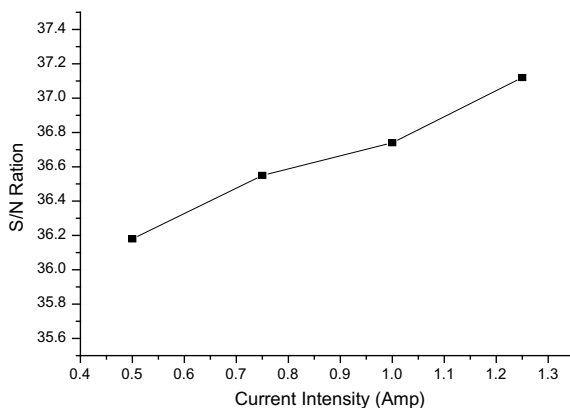


Fig. 3 Removal efficiency of iron versus current intensity (A) by monopolar electrocoagulation process

3.2.3 Effect of Inter-electrode Distance

The effective electrode area along with the inter-electrode distance between the cathode and the anode has a significant role in the electrocoagulation process. Increase in inter-electrode distance decreases the S/N ratio and it is shown in Fig. 4. This is due to the fact that as the applied voltage is constant as the inter-electrode distance increases the resistance for the applied current also increases leading to poor coagulation formation. The maximum S/N ratio was observed at 8 mm (S/N ratio: 37.02) and the least of 35.99 at 14 mm. The electrode setup plays a significant role in the effective surface area and also the inter-electrode distance. The equation that governs the variation in the voltage drop (ηIR) is:

$$\eta IR = I \cdot \frac{d}{s * k} \quad (4)$$

where, I = current (A), d = distance between two electrode (m), S = active anode surface (m^2), k = specific conductivity (103 mS/m) (Ghosh et al. 2008). From the above equation, it can be inferred that at constant anodic surface area and conductivity of the solution, voltage drop increases with the increase in inter-electrode distance. The resistance between the electrodes and the distance between them are directly related. Thus, with the increase in the inter-electrode distance the electric current decreases and to achieve the required current intensity, the voltage had to be increased.

3.2.4 Effect of pH

The solution pH plays a significant role in the autocatalytic disappearance of aqueous Fe(II) with the incentive of iron removal in slightly basic ($pH > 7$) range. Electrocoagulation is believed to be a satisfactory technology due to the formation of more OH^- ions in the electrolysis of water. In electrocoagulation where Al electrode is used, it has been witnessed that at somewhat basic ambience $Al(OH)_3$ precipitation occurs and the sweep-flock mechanism dominates (Fig. 5).

From Fig. 5, we can evaluate that initial pH has not much effect on the removal of iron from the solution. The S/N ratio lies from 36.56 to 36.73. However, maximum removal was obtained at pH 6 with S/N ratio of 36.73.

3.2.5 Effect of Conductivity

In this study, conductivity was maintained using sodium chloride (NaCl) salt. Conductivity increases the mobility of the ions present in the electrocoagulation process. Addition of salt increases the conductivity of the solution, which was directly influenced the cell voltage, energy consumption, and current efficiency in the electrolytic cell. The use of NaCl was also accompanied by the production of chloride

Fig. 4 Removal efficiency of iron versus inter-electrode distance by monopolar electrocoagulation process

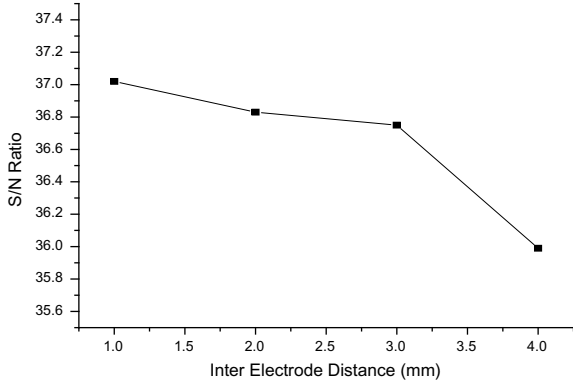
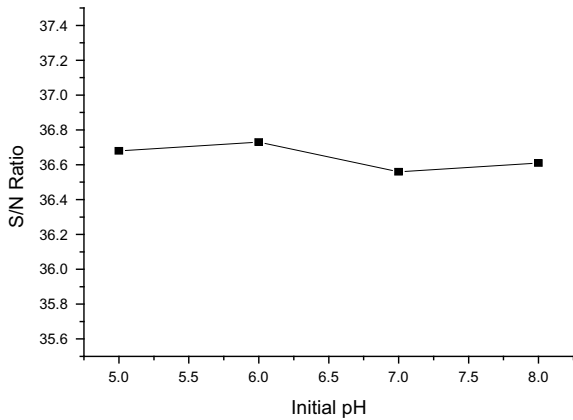


Fig. 5 Removal efficiency of iron versus initial pH by monopolar electrocoagulation process

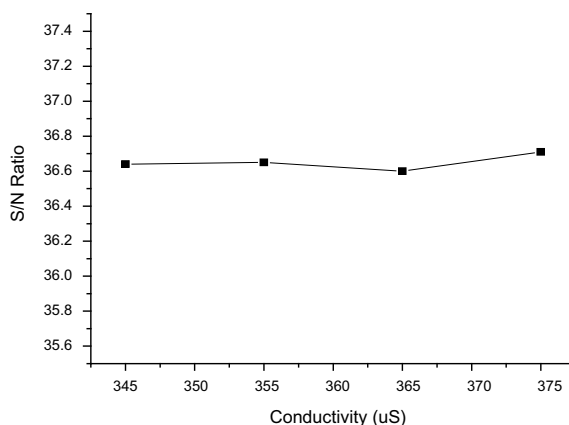


ions that reduces the effects of other anions, such as bicarbonate and sulfate which may lead to the precipitation of Ca^{2+} leading to the high-ohmic resistance of the electrochemical cell. Hence no significant effect is noticed with varied conductivity. The *S/N* ratio varies from 36.60 to 36.71 (Fig. 6).

4 Conclusion

From the above study, we can interpret that electrocoagulation is a suitable process for iron removal from wastewater. The regression equation obtained from the Taguchi method has an R^2 value of 93.16. The optimized conditions were found to be 15 ppm initial concentration, 1.25 A current intensity, 8 mm inter-electrode distance with conductivity at 360 μ S, and pH of solution at 5. From Delta-Rank, we can see

Fig. 6 Removal efficiency of iron versus conductivity by monopolar electrocoagulation process



that initial concentration of iron is the most significant parameter followed by electrode distance, current intensity, initial pH, and conductivity (initial concentration > electrode distance > current intensity > initial pH > conductivity).

References

- Al-Qodah Z, Al-Shannag M (2017) Heavy metal ions removal from wastewater using electrocoagulation processes: a comprehensive review. *Sep Sci Technol* 52(17):2649–2676
- Asghari A, Kamalabadi M, Farzinia H (2012) Electrochemical removal of methylene blue from aqueous solutions using Taguchi design. *Chem Biochem Eng Q* 26(2):145–154
- Balasubramanian N, Kojima T, Basha CA, Srinivasakannan C (2009) Removal of arsenic from aqueous solution using electrocoagulation. *J Hazard Mater* 167(1–3):966–969
- Chaturvedi S, Dave PN (2012) Removal of iron for safe drinking water. *Desalination* 303:1–11
- Fu F, Wang Q (2011) Removal of heavy metal ions from wastewaters: a review. *J Environ Manage* 92:407–418
- Ghosh D, Solanki H, Purkait MK (2008) Removal of Fe(II) from tap water by electrocoagulation technique. *J Hazard Mater* 155:135–143
- Hashim KS, Shaw A, Khaddar RA, Pedrola MO, Phipps D (2017) Iron removal, energy consumption and operating cost of electrocoagulation of drinking water using a new flow column reactor. *J Environ Manage* 189:98–108
- Hashim MA, Kundu A, Mukherjee S, Ng Y, Mukhopadhyay S, Redzwan G, Gupta BS (2019) Arsenic removal by adsorption on activated carbon in a rotating packed bed. *J Water Process Eng* 30:100591
- Irdemez S, Yildiz YS, Tosunoglu V (2006) Optimization of phosphate removal from wastewater by electrocoagulation with aluminum plate electrodes. *Sep Purif Technol* 52:394–401
- Karmakar B, Dhawane SH, Halder G (2018) Optimization of biodiesel production from castor oil by Taguchi design. *J Environ Chem Eng* 6:2684–2695
- Kobya M, Can OT, Bayramoglu M (2003) Treatment of textile wastewaters by electrocoagulation using iron and aluminum electrodes. *J Hazard Mater* 100:163–178
- Martinez-villafane JF, Montero-Ocampo C (2010) Optimization of energy consumption in arsenic electro-removal from groundwater by the Taguchi method. *Sep Purif Technol* 70:302–305

- Pundir R, Chary GHVC, Dastidar MG (2018) Application of Taguchi method for optimizing the process parameters for the removal of copper and nickel by growing *Aspergillus* sp. *Water Resour Ind* 20:83–92
- Shah AR, Tahir H, Kifayat Ullah HM, Adnan A (2017) Optimization of electrocoagulation process for the removal of binary dye mixtures using response surface methodology and estimation of operating cost. *Open J Appl Sci* 7:458–484
- Tir M, Moulia-Mostefa N, Nedjhioui M (2015) Optimizing decolorization of methylene blue dye by electrocoagulation using Taguchi approach. *Desalin Water Treat* 55(10):2705–2710
- Vasudevas LJ, Sozhan G (2009) Studies on the removal of iron from drinking water by electrocoagulation—a clean process. *Clean* 37(1):45–51

Kinetics Study of a Suspended Growth System for Biological Treatment of Bakery and Confectionery Wastewater



Biswajit Chakraborty, Pradyut Kundu, Joydeep Mukherjee, and Somnath Mukherjee

Abstract The effluent of bakery and confectionery production unit mainly contaminated with oil, fat, nitrogen, glucose, starch, etc. These industries use plentiful water for proper functioning and operating of the production unit and simultaneously it emanates a huge amount of wastewater. A laboratory investigation was undertaken to explore the feasibility of biodegradation of bakery and confectionery wastewater along with kinetic study. The experimental studies were done with simulated real-life bakery and confectionery wastewater in batch-fed reactor. Necessary characterization was done after collecting wastewater from the outlet of the real-life plant. It was found that COD value was within a range of 1300–1400 mg/L and BOD/COD ratio between 0.68 and 0.71. The microbial seed was acclimatized for 3 months. Necessary batch kinetic studies were performed with preacclimatized seed mixture in different proportions to the simulated sample. It was noticed that about 90% removal of COD could be achieved after a contact period of 26 h in corresponding to 1320 mg/L of the initial COD concentration. Similarly, 76% ammoniacal nitrogen ($\text{NH}_4^+ - \text{N}$) removal was also found with respect to initial $\text{NH}_4^+ - \text{N}$ concentration of 75.38 mg/L after a contact period of 30 h. Finally, experimental dataset was utilized to determine various kinetic coefficients such as K , Y , k_d , K_s for designing a real-life activated sludge reactor system for the treatment of bakery and confectionery wastewater.

B. Chakraborty · J. Mukherjee

School of Environmental Studies, Jadavpur University, Kolkata 700032, India
e-mail: chakrabortyjit007@gmail.com

J. Mukherjee

e-mail: joydeep.mukherjee@jadavpuruniversity.in; joydeep_envstu@school.jdvu.ac.in

P. Kundu

Department of Food Processing Technology, Mirmadan Mohanlal Government Polytechnic, Plassey, Nadia, West Bengal 741156, India

e-mail: kundupradyut@yahoo.co.in

S. Mukherjee (✉)

Environmental Engineering Division, Civil Engineering Department, Jadavpur University, Kolkata 700032, India

e-mail: mukherjeesomnath19@gmail.com

© Springer Nature Singapore Pte Ltd. 2021

D. Ramkrishna et al. (eds.), *Advances in Bioprocess Engineering and Technology*,
Lecture Notes in Bioengineering,

https://doi.org/10.1007/978-981-15-7409-2_34

Keywords Suspended growth batch reactor · Bakery and confectionery wastewater · COD removal · NH_4^+ -N removal · Kinetic constants

1 Introduction

Large commercial bakery and confectionery producing products including cakes, pies, cookies, biscuits, brownies, rolls, and a variety of other desserts. These plants generate wastewater with loads of contaminants too high, made unsuitable for municipal discharge without pretreatment. Bakeries use large volumes of butter, flour, shortening, eggs, fillings of various types that produce the high level of BOD, suspended solids and fats, oils, and grease in the wastewater. For purposes of wastewater characterization, the bakery industry may be divided into two groups: dry baking such as bread, bun, and roll baking and production of cakes, pies, doughnuts, cookies, and sweet rolls. In dry baking, production equipment such as mixing vats and baking pans are typically cleaned dry and floors are swept prior to wash down. Wastewater is produced from general cleanup operations and is of low strength. Its major contaminants are flour and some grease. The second type of baking operation such as cake production generates wastes of much higher strength containing grease, sugar, flour, filling ingredients, and detergents. Most of the production equipment, such as baking pans and trays, mixing vats, mixers, milk, and other liquid containers, are water cleaned. Pans and trays are washed with hot detergents and greased after each baking. The spent liquid from pan washers constitutes one of the most important sources of wastewater. Confectionery industry also generates high amounts of wastewater, which contains high concentrations of readily biodegradable organic materials characterized by high COD and BOD values (Beal and Raman 2000). The average wastewater qualities of bakery and confectionery production units found by Yim et al. (1975) are shown in Table 1.

The objective of the present study was to perform a treatability study in a laboratory-scale batch reactor for the treatment of simulated bakery and confectionery wastewater containing both organic carbon and ammoniacal nitrogen and also to evaluate kinetic constants for designing a suitable suspended growth bioreactor using experimental data.

Table 1 Wastewater quality of bakery and confectionery industries

Type of confectionery plant	pH	BOD ₅ (mg/L)	Suspended solid SS (mg/L)	Total solid TS (mg/L)	Oil and grease (mg/L)
Bread plant	6.9–7.8	155–620	130–150	708	60–68
Cake plant	4.7–8.4	2240–8500	963–5700	4238–5700	400–1200
Variety plant	5.6	1600	1700	–	630
Unspecified	4.7–5.1	1160–8200	650–13,430	–	1070–4490

2 Materials and Methods

2.1 Collection of Real-Life Sample

Real-life sample of bakery and confectionery wastewater was collected from local bakery and confectionery plants. The concerned bakery and confectionery plant use large volumes of butter, flour, shortening, eggs, fillings of various types for production of patties, sandwich, burger, pastry, cake, etc. The samples were collected at different times from plant outlets and were analyzed for various characteristic parameters like pH, COD, BOD, TSS, TDS, and ammoniacal nitrogen following the protocols as described in American Public Health Association (2000).

2.2 Preparation of Simulated Feed Solution

Simulated feed solution was prepared for the purpose of acclimatization of microbial seed collected from nearby local sewage treatment plant. The constituents feed solution consist of dextrose, peptone, beef extract, yeast extract, ammonium sulfate, ammonium chloride, dipotassium hydrogen phosphate, potassium dihydrogen phosphate as concentration of 12.5, 1.0, 0.8, 0.8, 0.4, 1.5, 1.0, and 1.0 g/L, respectively. The stock feed solution was diluted as per requirement for maintaining COD and ammoniacal nitrogen values of 1350 ± 50 and 70 ± 10 mg/L, respectively, during seed acclimatization and batch kinetic study.

2.3 Seed Acclimatization for Carbon Oxidation and Nitrification Study

The seed acclimatization study was carried out in a measuring cylinder of 1.0 L capacity as a reactor. About 100 mL of nonacclimatized seed collected from nearby local sewage treatment plants mixed with 700 mL of diluted simulated wastewater and 50 mL of micronutrient mixed solution to make a total volume of 850 mL in the cylinder. The micronutrient solution contains the following components (g/L), EDTA 0.01; $\text{ZnSO}_4 \cdot 7\text{H}_2\text{O}$ 0.001; $\text{CaCl}_2 \cdot 2\text{H}_2\text{O}$ 0.1; $\text{MnCl}_2 \cdot 2\text{H}_2\text{O}$ 0.008; $\text{FeCl}_3 \cdot 6\text{H}_2\text{O}$ 0.71; $(\text{NH}_4)_6\text{Mo}_7\text{O}_{24}$ 0.0011; $\text{CuSO}_4 \cdot 5\text{H}_2\text{O}$ 0.001; $\text{CoCl}_2 \cdot 6\text{H}_2\text{O}$ 0.2. The COD was maintained in the range of 1350 ± 50 mg/L and NH_4^+-N was 70 ± 10 mg/L. Aeration was done continuously by means of diffused air system with the help of aquarium pumps. The acclimatization was continued for an overall period of 3 months. The biomass growth was indicated by the magnitude of sludge volume index (SVI) and MLSS concentration in the cylinder. pH in the reactor was maintained in the range of 6.8–7.5 by adding required amount of sodium carbonate (Na_2CO_3) and phosphate buffer.



Fig. 1 Experimental setup of suspended growth batch reactor

2.4 Experimental Setup and Procedure for the Treatment of Wastewater in Batch Reactor

Batch kinetic studies for the treatment of stimulated bakery and confectionery wastewater for carbon oxidation and nitrification have been performed in 1 L volume measuring cylinder separately as shown in Fig. 1. After seed acclimatization, about 800 mL volume of sample was taken in each cylinder with necessary diluted feed solution. Each cylinder was facilitated with aeration system by inserting stone sparger fitted with laboratory-scale compressor. The graduation marked in the cylinder helped for determining sludge volume for each cylinder in more convenient manner.

3 Results and Discussion

3.1 Characterization of Real-Life Bakery and Confectionery Wastewater

The wastewater samples as characterized in the laboratory with respect to the following parameters are shown in Table 2. The COD and $\text{NH}_4^+\text{-N}$ values were found within a range of 1350 ± 30 and 65 ± 10 mg/L, respectively. The average pH and TSS of real-life composite sample wastewater were found to be 7.4 ± 0.2 and 550 ± 30 mg/L, respectively. The temperature during collection of sample was observed in the range of 25–32 °C. As regards to the high TDS value, the reason can be

Table 2 Characterization of real-life bakery and confectionery wastewater

S. No.	Parameters	Values
1	COD (mg/L)	1350 ± 30
2	BOD ₅ (mg/L)	905 ± 30
3	TSS (mg/L)	550 ± 30
4	Ammoniacal nitrogen (mg/L)	65 ± 10
5	pH	7.4 ± 0.2

attributed to the presence of different ions which generally are major constituents of the different cleansing agents and disinfectants used during the operation and maintenance stages. BOD₅ of the real-life wastewater was found to be 905 ± 30 mg/L that indicates the presence of biodegradable organic matter in wastewater.

3.2 Carbon Oxidation Study of Simulated Bakery and Confectionery Wastewater in Batch Reactor

The time concentration study for organic (COD) reduction with respect to the initial COD concentration value of 1352.16 mg/L is shown in Fig. 2. From Fig. 2, it was observed that the concentration of COD decreases with the progress of reaction time. The plot also reveals that within a 22 h of contact time, maximum COD removal was achieved (96.58%) beyond which the removal percentage was found to be marginal and the curve becomes asymptotic in nature, which indicates maximum stabilization of organic matter of wastewater within the above reaction period. Figure 3 demonstrates that there is a steady ascending in MLSS concentration up to a time period of 22 h, from initial MLSS concentration 2025 mg/L. After 22 h, the rate of increase

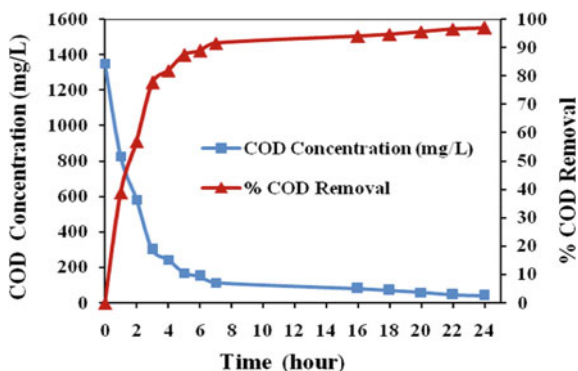


Fig. 2 COD removal profile during carbon oxidation study in batch reactor for simulated wastewater sample [Initial COD concentration = 1352.16 mg/L]

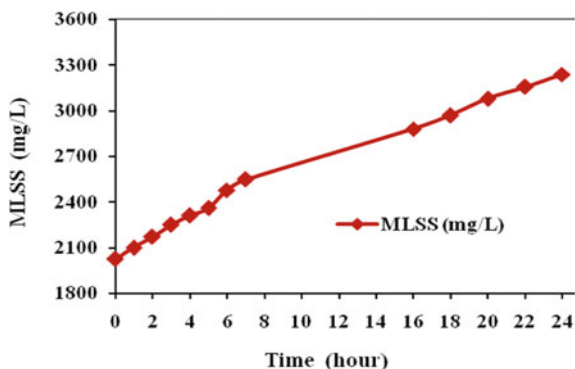


Fig. 3 MLSS concentration profile during carbon oxidation of simulated wastewater sample in batch reactor [Initial MLSS = 2025 mg/L]

of MLSS concentration was found to be ceased and a steady-state condition was achieved, which indicates that enzymatic activity of carbonaceous microorganisms in the mixed culture is exhausted and fully utilized.

3.3 Kinetics for Carbon Oxidation Study in Batch Reactor

The values for the reciprocal of specific substrate utilization rate ($1/U_C$), obtained from the results were plotted against the reciprocal of effluent COD ($1/S$) and substrate removal kinetics was evaluated using simple linear equation $1/U_C = [(K_s/k)(1/S)] + (1/k)$. A best-fit graph was drawn by applying the least square approach using experimental data, as shown in Fig. 4. The slope and intercept of the straight line were K_s/k and $1/k$, respectively. The value of k was 9.09 per day, whereas the half velocity constant (K_s) was 350.69 mg/L for an initial COD of 1350 ± 30 mg/L. The value of K_s obtained for carbon oxidation was found to be higher

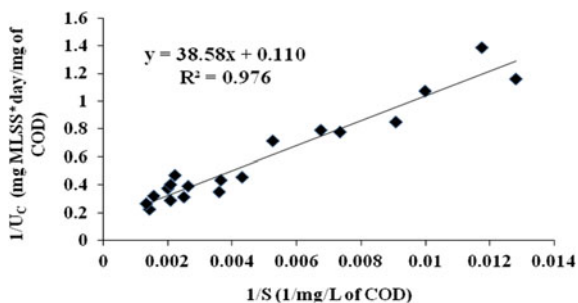
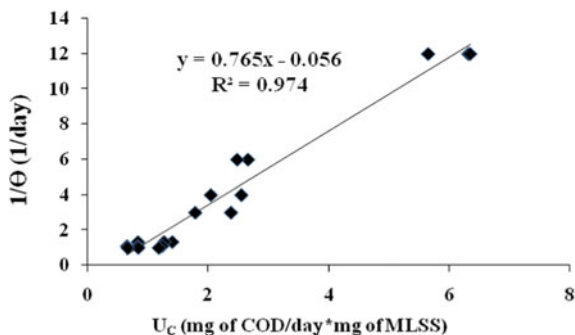


Fig. 4 Substrate utilization kinetic for carbon oxidation study of simulated wastewater sample in batch reactor

Table 3 Values of kinetic constants for carbon oxidation study

Serial number	Kinetic coefficients	Values from present study	Typical kinetic coefficient for municipal wastewater (Metcalf and Eddy Inc. 2000)
1	Y	0.765	0.4–0.8
2	K_d	0.056	0.025–0.075
3	K	9.09	2–10
4	k_s	350.69	25–100

**Fig. 5** Microbial growth kinetic for carbon oxidation study of simulated wastewater sample in batch reactor

than the standard value of kinetics coefficient of municipal wastewater treatment (Metcalf and Eddy Inc. 2000), may be due to higher initial concentrations of COD in the batch reactor, as shown in Table 3. Furthermore, the values of the reciprocal of the reaction time ($1/\theta$) were plotted against U_C as shown in Fig. 5. The yield coefficient (Y) was determined from the slope of the best-fit straight line and endogenous decay coefficient (k_d) was obtained from the intercept. The value of Y and k_d was found to be 0.765 mg of MLSS/mg of COD and 0.056 per day, respectively, for the COD value of 1350 ± 30 mg/L.

3.4 Nitrification Study of Simulated Bakery and Confectionery Wastewater in Batch Reactor

The results of the time course study of $\text{NH}_4^+\text{-N}$ removal are shown graphically in Fig. 6. From Fig. 6, it was observed that as time increases, $\text{NH}_4^+\text{-N}$ concentration decreases with respect to initial $\text{NH}_4^+\text{-N}$ concentration of 75.38 mg/L and ultimately after 30 h, the residual ammoniacal nitrogen concentration inside the batch reactor reaches to a minimum level of 17.58 mg/L which correspondence to 76.68% removal of $\text{NH}_4^+\text{-N}$ from wastewater sample. During nitrification process,

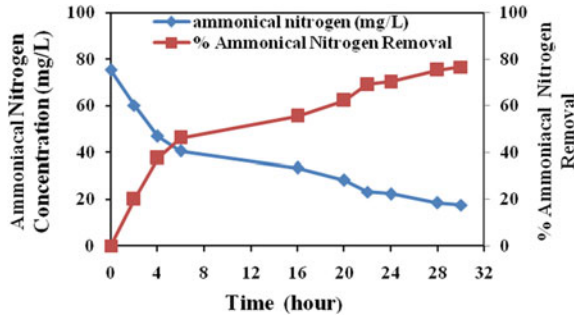


Fig. 6 Ammoniacal nitrogen removal profile during nitrification study in batch reactor for simulated wastewater sample [Initial $\text{NH}_4^+\text{-N}$ concentration = 75.38 mg/L]

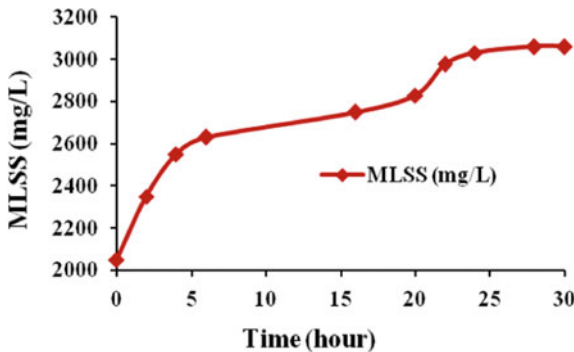


Fig. 7 MLSS concentration Profile during Nitrification of simulated wastewater sample in batch reactor [Initial MLSS = 2050 mg/L]

the MLSS concentration in the reactor increases up to 3060 mg/L from the initial MLSS concentration of 2050 mg/L within a period of 30 h of contact time. The increase of MLSS concentration is shown in Fig. 7. Temperature and pH level of wastewater during experiment maintained at 27–30 °C and 7–7.5, respectively, by controlling environmental condition.

3.5 Kinetics for Nitrification Study in Batch Reactor

The values for the reciprocal of specific substrate ($\text{NH}_4^+\text{-N}$) utilization rate ($1/U_N$) were plotted against the reciprocal of limiting $\text{NH}_4^+\text{-N}$ as substrate ($1/N$) and removal kinetics was evaluated using equation $1/U_N = [(K_s/k)(1/N)] + (1/k)$. A best-fit graph was drawn by applying a least square method using experimental data, which is shown in Fig. 8. The slope and intercept of the straight line were K_s/k and $1/k$, respectively. The value of k was 23.25 per day, whereas K_s was about 29.99 mg/L for initial

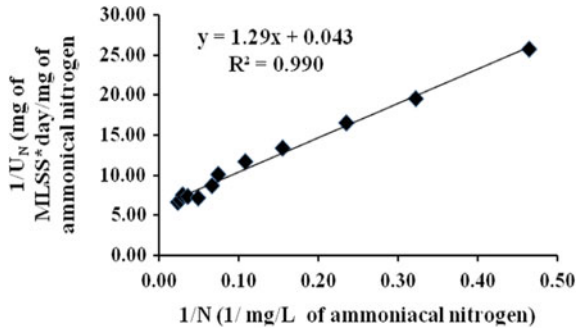


Fig. 8 Substrate utilization kinetic for nitrification of simulated wastewater sample in batch reactor

NH_4^+-N level of 65 ± 10 mg/L as N. Consequently, the magnitude of half velocity constant (K_s) value was corroborated with standard values as mentioned in Table 4, considered for nitrification of municipal wastewater stream (Metcalf and Eddy Inc. 2000). The values of the reciprocal of the reaction time ($1/\theta$) were plotted against specific substrate (NH_4^+-N) utilization rate (U_N) that are shown in Fig. 9. The value of Y and K_d was found to be 0.425 mg of MLSS/mg of NH_4^+-N and 0.063 per day, respectively.

Table 4 Values of kinetic constants for nitrification study

Serial number	Kinetic coefficients	Values from present study	Typical kinetic coefficient for municipal wastewater (Metcalf and Eddy Inc. 2000)
1	Y	0.425	0.1–0.3
2	K_d	0.063	0.03–0.06
3	k	23.25	1–30
4	k_s	29.99	0.2–5

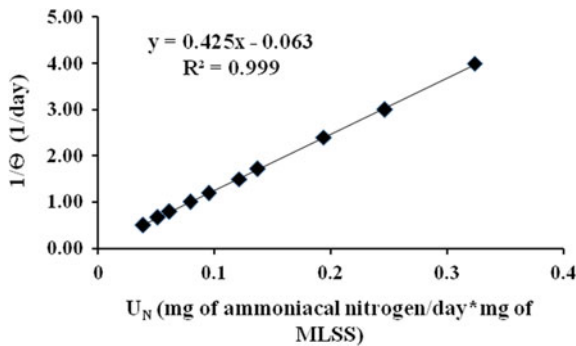


Fig. 9 Microbial growth kinetic for nitrification simulated wastewater sample in batch reactor

4 Conclusion

The batch study exhibited that both COD and ammoniacal nitrogen removal are possible by the mixed bacterial culture as developed in the laboratory under aerobic condition. Kinetic coefficients evaluated through experiments showed that the values are in congruence with those obtained by earlier researchers. The kinetic constants can be used for design of a field-scale suspended growth reactor for the treatment of real-life bakery and confectionery wastewater.

Compliance with Ethical Standards Informed Consent Wastewater sample was collected from the discharge outlet of a medium-sized bakery plant situated in Kasba Industrial Estate located near East Kolkata township area, Anandapur, Kolkata 700107, India. The plant authority did not object for sampling and analysis of their effluent for academic purposes. This study was submitted as M-Tech level thesis which was approved by the School of Environmental Studies, Jadavpur University. Informed consent was obtained from all individual participants and authors are included in the study.

Ethical Approval This chapter does not contain any studies with human participants or animals performed by any of the authors.

Conflict of Interest The authors declare that they have no conflict of interest.

References

- American Public Health Association (2000) Standard methods for the examination of water and wastewater. APHA, Washington, DC
- Beal LJ, Raman DR (2000) Sequential two-stage anaerobic treatment of confectionery wastewater. *J Agr Eng Res* 76(2):211–217
- Metcalf and Eddy Inc (2000) Wastewater engineering: treatment, disposal, reuse, 3rd edn. McGraw-Hill, Singapore
- Yim B, Young RHF, Burbank NC, Dugan GL (1975) Bakery waste: its characteristics, Part I. *Indust Wastes* 24–25

Role of Metallothionein and Phytochelatin in Combating Abiotic Stress Imparted by Copper-Induced Toxicity in Brinjal (*Solanum melongena*)



Pratik Talukder

Abstract Plants, though sessile, have various enzymatic and nonenzymatic antioxidant systems which help them in combating the heavy metal-induced oxidative stress and various other abiotic stresses. Metallothioneins (MTs) and Phytochelatins (PCs) are the two best characterized heavy metal-binding ligands in plants. In the present investigation, we made a comparative study on the role of metallothionein and PCs in combating copper-induced oxidative stress in brinjal (*Solanum melongena*), an important vegetable plant with immense nutritional value. Seedlings were exposed to various sublethal doses of copper and grew them for a period of 1 month. We studied the relative expression of these genes by reverse transcription PCR and real-time PCR techniques and the relative content of the major secondary metabolites and phytochelatins by High-Performance Liquid Chromatographic (HPLC) technique. In both cases, we find that 800 μM is the highest dose that the plants can withstand. On further increasing the dose to 1000 μM , a sudden drop in the expression of the genes, as well as polyphenolic and phytochelatin compound contents, was observed. This observation proves that phytochelatin and metallothionein function in a coordinated way to chelate, detoxify, and rendering the plant more tolerant to metal stress.

Keywords Abiotic Stress · Copper · Brinjal · *Solanum melongena* · Secondary metabolism · Polyphenols · Metallothionein · Phytochelatin

1 Introduction

Heavy metals are defined as those metals and metalloids which have atomic density 5 g cm^{-3} and above (i.e., greater than water) and atomic number >20 , and should possess properties of metals. A concentration $>0.1\%$ in soil becomes toxic to the plants. There are both essential and nonessential heavy metals present in the soil. Fe, Mn, Cu, Zn, Co, Mo are few important essential heavy metals, whereas Cd, Pb, Ur, Tl, Cr, Ag, Hg are considered as nonessential heavy metals (Wuana and Okieimen 2011).

P. Talukder (✉)

Department of Biotechnology, University of Engineering and Management, Kolkata, India
e-mail: pratiktalukder@gmail.com

© Springer Nature Singapore Pte Ltd. 2021

D. Ramkrishna et al. (eds.), *Advances in Bioprocess Engineering and Technology*,
Lecture Notes in Bioengineering,
https://doi.org/10.1007/978-981-15-7409-2_35

349

Plants and the metals in the soil have had a long and intimate evolutionary association that has resulted in many complex interactions. Copper is an essential micronutrient for plants. Plants maintain low copper concentration in the cells because at higher concentrations, it behaves as a cytotoxic stress factor by generating reactive oxygen species (ROS) and other free radicals (Cho and Seo 2005). Copper is an essential micronutrient. Being a redox-active metal, excess accumulation of copper generates reactive oxygen species (ROS) (Stohs and Bagchi 1995). Copper toxicity is accompanied with high rate of oxidative stress and lipid peroxidation (Díaz et al. 2001). Apart from producing ROS, heavy metals affect the plants either by binding to the essential –SH groups of enzymes and hence inactivates them and make them nonfunctional or they are also capable of replacing the essential functional elements in prosthetic groups of the enzymes and interrupts their ability of catalysis. Among the several mechanisms by which plants can cope with the ill-effects exerted by heavy metals is the activation of the genes responsible for metallothionein and phytochelatin production. Metallothioneins (MTs) are low molecular weight (7–8 kDa), Cysteine-rich, metal-binding proteins (Blindauer and Leszczyszyn 2010); they can bind to a variety of metals like zinc, copper, cadmium by forming mercaptide bonds. On the other hand, Phytochelatins (PCs) are nonprotein, cysteine-rich peptides which are biosynthesized enzymatically from the precursor Glutathione (GSH); heavy metals like Cd, Pb, Zn, Cu can induce PC biosynthesis metallothionein combats oxidative stress-induced heavy metals and phytochelatins, on the other hand, are involved in nullifying oxidative stress induced by heavy metals only (Ghoshal et al. 2015).

Food habit in human has evolved over the course of human evolution and human civilization. One of the main ingredients of our diet is vegetables. Brinjal [*Solanum melongena* L. (Solanaceae)] is known to be the chief vegetable source of our diet. It is the second most important vegetable in India after potato. In India, it is an important part of our daily diet as it is a rich source of macro- and micronutrients (Shishira et al. 2016). Being a fast-growing developing nation with such a huge population, it is of utmost importance to increase the production of agricultural products including vegetables such as brinjal. Due to rapid urbanization and industrialization, the amount of agricultural land is decreasing day by day and farmers are now growing vegetables in small hamlets nearer to the suburban areas. Unfortunately, the soil of those areas is highly contaminated with heavy metals including copper due to various industrial and anthropogenic activities. Hence, this present study is aimed to understand how the plants can mitigate the effect of heavy metal toxicity by enhancing the expression of the important genes of metallothionein and phytochelatin biosynthesis pathways and hence by higher production of MT and PC which are capable of quenching the heavy metals. This study would enable us to deduce a mechanism by which we can reduce the amount of heavy metal-induced toxicity in vegetables which we consume on a daily basis.

2 Materials and Methods

2.1 Plant Materials and Treatments

Brinjal [*Solanum melongena* L.] [Variety-BCO-1, Bidhan Chandra Krishi Viswavidyalaya, West Bengal, India] seeds were used for this study. About 500, 800, and 1000 μM solution of copper chloride (CuCl_2) (SRL, Mumbai, India) were used as treatment. LD_{50} was measured and it was found to be 1100 mM for Cu treatment. Hence all doses were taken lesser than the LD_{50} value.

2.2 Evaluation of Stress

2.2.1 Estimation of Chlorophyll and Carotenoid Content

The amount of chlorophyll was measured according to the method of Lichtenthaler (1987) with little modifications.

2.2.2 Lipid Peroxidation

The level of lipid peroxidation can be determined by measuring the amount of malondialdehyde (MDA). Method of Heath and Packer (1968) with little modifications (Ghoshal et al. 2015) was used to measure the extent of lipid peroxidation. The result was expressed as MDA equivalents in $\mu\text{M/g}$ fresh weight of tissue.

2.3 Preparation of Plant Extract

Plant extracts were prepared according to Brolis et al. (1998) with little modifications (Talukder et al. 2016).

2.4 Evaluation of Antioxidant Activity

2.4.1 Total Antioxidant Assay

This assay was performed according to Prieto et al. (1999).

2.4.2 DPPH Radical Scavenging Assay

The DPPH radical scavenging assay was done according to Brand-Williams et al. (1995), with few modifications (Talukder et al. 2016).

2.5 Gene Expression Analysis by Reverse Transcription PCR and Real-Time PCR

Thermal cycler condition for reverse transcription PCR was reverse transcription at 50 °C for 30 min, Initial denaturation step at 95 °C for 15 min followed by 40 cycles of denaturation at 94 °C for 1 min, primer annealing at 53 °C for 1 min, elongation at 72 °C for 1 min and 30 s, and the final extension was done at 72 °C for 10 min.

The reaction condition for real-time PCR was: an initial hold at 95 °C for 10 min, 40 cycles of denaturation at 95 °C for 30 s, annealing, and extension at 60 °C for 1 min. β -actin served as endogenous control. Three biological replicates were used for each reaction. Real-time PCR $2^{-\Delta\Delta CT}$ was performed according to the method of Livak and Schmittgen (2001) for the analysis of relative gene expression (Table 1).

2.6 Determination of Phytochelatin Content by HPLC

Plant extracts were prepared according to Sneller et al. (2000). Mobile phase was made up of solution A: 0.1% Trifluoroacetic acid (TFA) solution and solution B: 80% Acetonitrile (ACN) + 20% of 0.1% Trifluoroacetic acid (TFA) solution and the stationary phase was C18 reverse-phase column.

2.7 Statistical Analysis

All experimental results were represented as mean values \pm standard error of the mean. The data were analyzed by an analysis of variance (ANOVA) and means were compared by Student's t-test using KyPlot software (Version 3.0). All the experiments were performed in triplicates. Differences in the data at $p \leq 0.05$ were considered to

Table 1 Details of primers used in this study

Gene	Forward primer (5'-3')	Reverse primer (5'-3')
<i>MT 2</i>	5'ATGTCTTGCTGCAACGGAAACT3'	5'CTATTGCAATTGCATGGATTG3'
<i>β Actin</i>	5'ATCATGAAGTGTGATGTTGA3'	5'ACCTTAATCTTCATGCTGCT3'

be statistically significant. Level of significance was $p < 0.05$ (*); $p < 0.01$ (**); $p < 0.001$ (***).

3 Results

3.1 Evaluation of Stress

3.1.1 Chlorophyll and Carotenoid Content

The increases in chlorophyll a content in 500 and 800 μM Cu-treated plants were about 1.32 and 1.23 fold, followed by a drop in 1000 μM Cu-treated plants. The increase in chlorophyll b content in the 500 μM Cu-treated plants was more significant than that of 800 μM Cu-treated plants ($p \leq 0.001$ against $p \leq 0.01$). There has been significant increases ($p \leq 0.001$) of 1.34 and 1.22 fold in the total chlorophyll contents in 500 and 800 μM Cu-treated seedlings and an insignificant decrease in 1000 μM Cu-treated seedlings (Fig. 1).

Statistically significant increments in the carotenoid content have been observed in 500 and 800 μM Cu-treated seedlings ($p \leq 0.01$ and $p \leq 0.05$); however, in 1000 μM Cu-treated plants show an even more significant decrease ($p \leq 0.001$) in carotenoid content (Fig. 2).

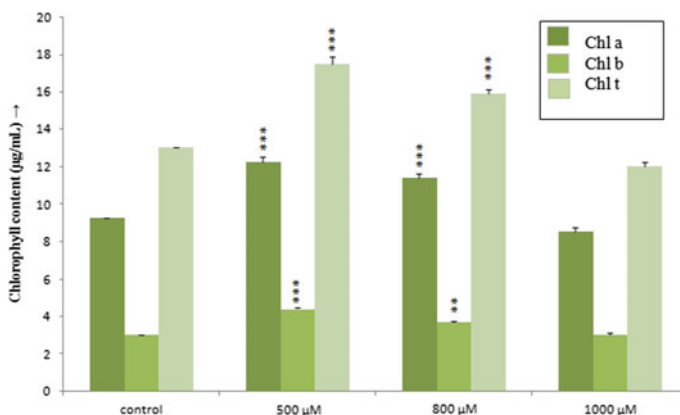


Fig. 1 Changes in total chlorophyll content

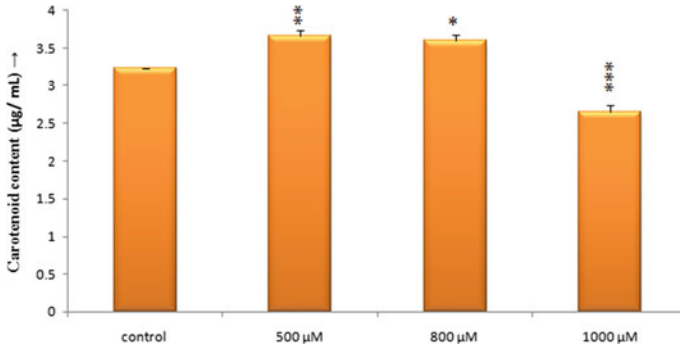
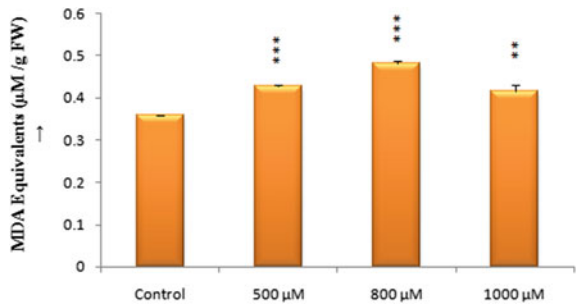


Fig. 2 Changes in total carotenoid content

Fig. 3 Change in lipid peroxidation



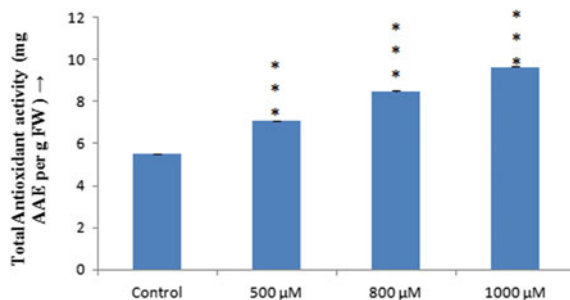
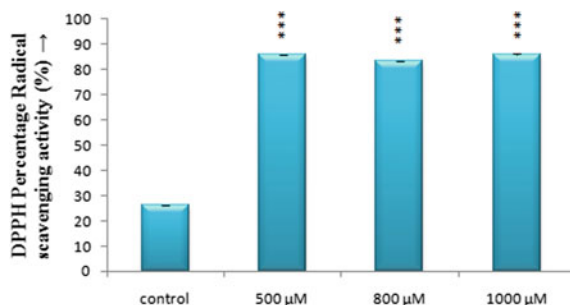
3.1.2 Amount of Lipid Peroxidation

Statistically significant increases ($p = 0.001$) of 1.2 and 1.35 fold have been observed in 500 and 800 µM Cu-treated samples whereas in 1000 µM Cu-treated samples, the increase in MDA production is 1.16 fold (significant at 1% level) (Fig. 3).

3.2 Evaluation of Antioxidant Activity

3.2.1 Total Antioxidant Activity

There have been 1.3, 1.5, and 1.8 fold increases in the total antioxidant activity with the addition of 500, 800, and 1000 µM Cu, respectively (Fig. 4).

Fig. 4 Change in total antioxidant activity**Fig. 5** Change in DPPH scavenging activity

3.2.2 DPPH Scavenging Activity

There has been a significant increase (about threefold) in the percentage DPPH radical scavenging activity in the Cu-treated plant extracts (Fig. 5).

3.3 Gene Expression Study by Reverse Transcription and Real-Time PCR, Respectively

MT2 is known to be expressed predominantly in shoot tissues. It is found that the expression of *MT2* has increased in Cu-treated plants with respect to untreated control. The densitometric analysis shows 1.36 and 1.38 fold increases in expressions of 500 and 800 μM Cu-treated samples, respectively, whereas a 1.66 fold increase in 1000 μM treated sample in comparison to untreated control (Fig. 6).

Real-time PCR of *MT2* gene was carried out by $2^{-\Delta\Delta C_T}$ method and observed 4.57 and 5.78 fold increases in the expressions of 500 and 800 μM Cu-treated samples, respectively, compared with untreated control. As we further increased the dosage to 1000 μM, we observed a drop (only 5.64 fold increase) in the relative gene expression of *MT2*. *β-actin* was taken as endogenous control (Fig. 7).

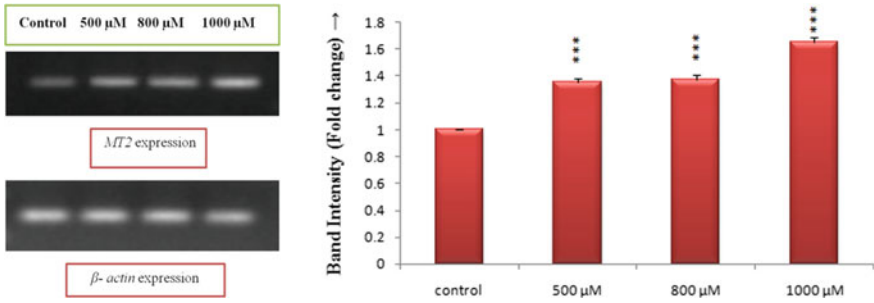
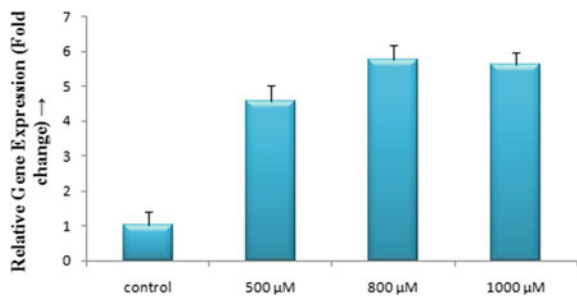


Fig. 6 Alterations in *MT2* gene expression by semiquantitative method

Fig. 7 Alterations in *MT2* gene expression by real-time PCR



3.4 Amount of Different Phytochelatins (by HPLC)

The results obtained from carrying out HPLC clearly implied that copper treatment stimulated the biosyntheses of Phytochelatin 2, 3, 4, 5, and 6 in the brinjal plants. About 800 μM Cu-treated samples showed the highest content of Phytochelatins 2, 4, 5, and 6; Phytochelatin 3, being the exception showed maximum concentration in 500 μM Cu-treated samples (Figs. 8 and 9).

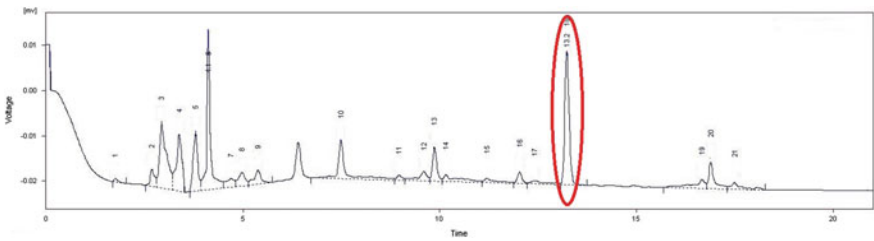


Fig. 8 HPLC chromatogram of phytochelation

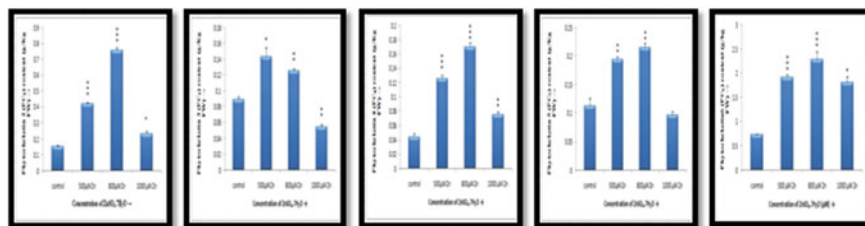


Fig. 9 Amount of PC2, PC3, PC4, PC5, PC6, respectively, under different doses of copper treatment

4 Discussion

Copper (Cu) is an essential trace element used as a micronutrient. Metal toxicity affects plant metabolism, growth, and development at various levels both directly and indirectly. Copper being an essential micronutrient plays a major role in photosynthesis, respiration, nitrogen fixation, protein metabolism, antioxidant activity, etc. Plants always maintain low copper concentration within the cell because at higher concentration it acts as a stress factor and generates high amount of reactive oxygen species (ROS) (Yruela 2005). Although copper acts as catalytic component of many enzymes, excess accumulation is cytotoxic and hence causes stunted growth and high rate of lipid peroxidation (Díaz et al. 2001). Excess copper causes toxicity; affects both terrestrial and aquatic life. Cu in excess is found to have genotoxic effects too, on plants. As effluents from metallurgical industries, copper smelters, that goes into the water bodies and agricultural fields. Metallothionein combats oxidative stress induced by not only heavy metals but also ionizing radiation like gamma rays, X-rays, heat shock, cold stress, drought, salinity, and biotic stress. Phytochelatin, on the other hand, are involved in nullifying oxidative stress induced by heavy metals only. Plant metallothionein is a stress-inducible protein, with antioxidant activities. Copper causes oxidative stress as evident from the biochemical assays. Plant metallothionein is a stress-inducible protein, with antioxidant activities. It is quite evident from the biochemical assays that the copper treatment has caused oxidative stress in brinjal plants. Metallothionein with the help of its antioxidative activity can protect the seedlings from the Cu-induced oxidative stress. The increase in the *MT2* gene expression in both semiquantitative and quantitative PCR techniques proved that the protein *MT2* is protecting the plant against the oxidative stress induced by copper and is acting as a nonenzymatic antioxidant. About 800 μM CuCl_2 is the highest dose that the plants can withstand. On the other hand, further increasing the dose to 1000 μM , a sudden drop in the expression of *MT2* gene was observed. PCs are more efficient heavy metal chelators and detoxifiers compared with the MTs in higher plants and bind more heavy metals on per cysteine residue basis. These results clearly showed MT and PC work in a coordinated manner to detoxify heavy metals such as copper in brinjal. Hence, this study on one hand would give a clear idea about the mechanism of phytoremediation of heavy metals by plants and also would be beneficial for human health.

Acknowledgements The author sincerely acknowledges the University of Engineering and Management, Kolkata for providing the facility to conduct the experiments and funding for this study.

References

- Blindauer CA, Leszczyszyn OI (2010) Metallothioneins: unparalleled diversity in structures and functions for metal ion homeostasis and more. *Nat Prod Rep* 27:720–741
- Brand-Williams W, Cuvelier ME, Berset C (1995) Use of a free radical method to evaluate antioxidant activity. *Lebensm-Wiss Technol* 28:25–30
- Brolis M, Gabetta B, Fuzzati N, Pace R, Panzeri F, Peterlongo F (1998) Identification by high-performance liquid chromatography–diode array detection–mass spectrometry and quantification by high performance liquid chromatography–UV absorbance detection of active constituents of *Hypericum perforatum*. *J Chrom* 825:9–16
- Cho UH, Seo NH (2005) Oxidative stress in *Arabidopsis thaliana* exposed to cadmium is due to hydrogen peroxide accumulation. *Plant Sci* 168:113–120
- Díaz J, Bernal A, Pomar F, Merino F (2001) Induction of shikimate dehydrogenase and peroxidase in pepper (*Capsicum annuum* L.) seedling response to copper stress and its relation to lignification. *Plant Sci* 161:179–188
- Ghoshal N, Talapatra S, Talukder P, Sengupta M, Ray SK, Chakraborty A, Sen Raychaudhuri S (2015) Cross-adaptation to cadmium stress in *Plantago ovata* by pre-exposure to low dose of gamma rays: effects on metallothionein and metal content. *Inter J Rad Biol* 91(8):611–623
- Heath RL, Packer L (1968) Photoperoxidation in isolated chloroplasts. I. Kinetics and stoichiometry of fatty acid peroxidation. *Arch Biochem Biophys* 125:189–198
- Lichtenthaler HK (1987) Chlorophylls and carotenoids: pigments of photosynthetic biomembranes. *Methods Enzymol* 148:350–382
- Livak KJ, Schmittgen TD (2001) Analysis of relative gene expression data using real-time quantitative PCR and the $2^{-\Delta\Delta CT}$ method. *Methods* 25(4):402–408
- Prieto P, Pineda M, Aguilar M (1999) Spectrophotometric quantization of antioxidant capacity through the formation of a phosphor molybdenum complex: specific application to the determination of vitamin E. *Anal Biochem* 269:337–341
- Shishira T, Nivedita P, D’souza Myrene R, Singh Kavitha G (2016) Antioxidant marker response of *Solanum melongena* to salinity stress. *J Chem Pharma Res* 8(7):533–539
- Sneller FEC, van Heerwaarden LM, Koevoets PLM, Vooijs R, Schat H, Verkleij JAC (2000) Derivatization of phytochelatin from *Silene vulgaris*, induced upon exposure to arsenate and cadmium: comparison of derivatization with Ellman’s reagent and monobromobimane. *J Agric Food Chem* 48(9):4014–4019
- Stoys SJ, Bagchi D (1995) Oxidative mechanisms in the toxicity of metal ions. *Free Radical Biol Med* 18(2):321–336
- Talukder P, Talapatra S, Ghoshal N, Sen Raychaudhuri S (2016) Antioxidant activity and HPLC analysis of phenolic compounds during *in vitro* callus culture of *Plantago ovata* Forsk and effect of exogenous additives on accumulation of phenolic compounds. *J Sci Food Agr* 96(1):232–244
- Wuana RA, Okieimen FE (2011) Heavy metals in contaminated soils: a review of sources, chemistry, risks and best available strategies for remediation. *Int Sch Res Netw ISRN Ecol* 2011:20 p, Article ID 402647
- Yruela I (2005) Copper in plants. *Braz J Plant Physiol* 17:145–156

Optimization of Process Parameters for Biodegradation of Resorcinol in Presence of Toxic Heavy Metals by Response Surface Methodology (RSM)



Sonali Hazra Das, Ayimiyaba R. Longkumer, Rayanee Chaudhuri, Srabanti Basu, Sudipta Dey Bandyopadhyay, and Bhaswati Chakraborty

Abstract Environmental pollution is caused by industrial effluents releasing toxic phenolics like phenol, cresol, resorcinol, etc. along with various heavy metals to the environment. It is difficult to degrade these pollutants by common soil microflora and persists for a long time in nature causing environmental pollution and adverse health conditions. Thus the objective of the present work is to study the biodegradation of resorcinol by a mixed bacterial culture isolated from the soil near to the outer limit of effluent discharge of tannery. The mixed bacterial culture was acclimatized to resorcinol by gradually increasing the concentration of resorcinol in the MS media to 500 mg/L. A batch kinetic study was carried out for the degradation of 500 mg/L of resorcinol by the mixed bacterial culture in the presence of different toxic heavy metals such as Mercury (Hg), Lead (Pb), and Chromium (VI) in concentrations of 5 ppm, 25 ppm, and 50 ppm. Removal efficiency of resorcinol in 20 h in presence of mercury was 44%, for lead was 68.8%, and for chromium (VI) was 86%. Optimization of the process parameters of the present system was done by Response Surface Methodology using DesignExpert11.0 software. The various physicochemical parameters viz. aeration (with/without) and concentration of the toxic metals were optimized for maximum degradation of resorcinol and removal efficiency of resorcinol. Removal efficiency of resorcinol as obtained under optimized conditions was 90.82%.

S. H. Das · A. R. Longkumer · R. Chaudhuri · S. Basu · S. D. Bandyopadhyay · B. Chakraborty (✉)
Department of Biotechnology, Heritage Institute of Technology, Anandapur, Kolkata, West Bengal 700107, India
e-mail: bhaswati.chakraborty@heritageit.edu

S. H. Das
e-mail: sonalihazra.das@heritageit.edu

S. Basu
e-mail: srabanti.basu@heritageit.edu

S. D. Bandyopadhyay
e-mail: sudipta.dey@heritageit.edu

Keywords Resorcinol · Heavy metals · Biodegradation · Response surface methodology

1 Introduction

Aromatic compounds are abundant in nature and have profound effect on environment. Among various aromatic compounds, phenolic compounds like phenol, cresol, resorcinol, etc. are present in the effluents of various industries including petrochemicals, coal coking, coal gasification, tanneries, etc. (Nasr et al. 2007). To maintain ecological balance, it is essential to reduce the concentrations of the above-mentioned pollutants to acceptable level. Industrial effluent consists not only of resorcinol but also significant quantity of toxic heavy metals (Tüfekci et al. 2007). Hence, it is necessary to check the removal of resorcinol by mixed bacterial culture in presence of heavy metals. Present study deals with the removal of resorcinol in the presence of different toxic heavy metals such as Mercury (Hg), Lead (Pb), and Chromium (VI) in concentrations of 5 ppm, 25 ppm, and 50 ppm by a mixed bacterial culture isolated from the soil of the outer limit of a tannery effluent discharge. Biodegradation usually involves the complete mineralization of the starting compound to simpler ones like CO_2 , H_2O , NO_3^- , and other inorganic compounds. Moreover, it has the advantages of being economic, eco-friendly and can be easily operated and scaled up (Chakraborty 2016). Chemical methods include stripping, solvent extraction, chemical oxidation, and coagulation. Though these methods are quite effective in removing pollutants from industrial effluent but are expensive and often cause disposal problem of toxic sludge generated. The chemicals used in the process may also cause secondary pollution problem. Physical method such as adsorption by activated charcoal could yield various toxic intermediates (Laura et al. 2016). While biodegradation does not suffer from the above-mentioned restrictions of the physicochemical methods, literature review shows that there are a limited number of microorganisms, especially bacteria, with the capability of aerobic degradation of resorcinol.

It has been observed that bacteria consortium is always more effective in removing various organic pollutants as compared to a pure strain. In a mixed culture, one microorganism may produce needed growth factors beneficial to a second microorganism. It may alter the pH of the medium, thereby improving the activity of one or more enzymes needed for biodegradation of the pollutant. Mixed cultures are able to bring about multistep transformations that would be impossible for a single microorganism. If the environmental conditions are maintained, it is easy to grow a mixed culture indefinitely and carry out repeated subculturing (Das and Chandran 2011).

2 Materials and Methods

2.1 Isolation of Mixed Bacterial Culture from Soil

10 g of the soil sample was collected from the outer limit of effluent discharge point of tannery. The soil, which was rich in microbial diversity, was suspended in 0.8% saline water and kept in a shaker overnight at 35 °C. The soil suspension was then centrifuged and the supernatant consisting of mixed bacterial culture was added to nutrient media. The culture was grown in the nutrient broth for 24 h at 35 °C. 100 ml of MS (Mineral salt) media was prepared and was inoculated with 10% of the culture from nutrient broth. Composition of the MS media (mg/L) was (KH₂PO₄: 680, K₂HPO₄: 1730, FeSO₄: 30, (NH₄)NO₂: 100, MgSO₄: 100, CaCl₂: 20, MnSO₄: 30). The mixed bacterial culture was allowed to grow in the MS media for 24 h with glucose as the sole carbon source.

2.2 Acclimatization of Mixed Bacterial Culture in Resorcinol

100 ml of MS media containing 1% glucose and 10 ppm of resorcinol was inoculated with 10 ml of the culture from the above bacterial media. The resorcinol concentration was gradually increased from 10 to 500 ppm and glucose concentration was decreased till resorcinol became the sole source of carbon for the bacterial consortium. The mixed bacterial consortium was allowed to grow in shaker at 100 rpm at 35 °C till stationary phase of the cells was reached or concentration of residual resorcinol dropped to below detection limit. Samples were collected at regular interval and cell biomass and residual resorcinol concentration were checked. The cell mass was obtained by spectrophotometer (Labman visible spectrophotometer LMSP V320) by measuring the absorbance at 600 nm. From the standard curve of A₆₀₀ against bacterial dry cell biomass (mg/ml), the cell O.D. was converted to dry biomass of bacteria. Residual resorcinol concentration was analyzed from the supernatant obtained by centrifugation of the above culture at 6000 rpm for 5 min. The resorcinol in the supernatant was checked by antipyrine assay. The absorbance of the above assay was checked at 490 nm.

2.3 Batch Kinetic Study of Removal of Resorcinol by the Mixed Bacterial Culture in Presence of Different Toxic Metals

Removal of resorcinol by mixed bacterial culture was studied in presence of different toxic metals such as Mercury (Hg), Lead (Pb), and Chromium [Cr (VI)]. MS Media

containing 500 mg/ml of resorcinol as sole carbon source for bacteria was prepared. Then each metal at different concentrations (5 ppm, 25 ppm, and 50 ppm) was added to separate flasks. Cell growth and resorcinol removal were measured and the maximum cell growth, maximum specific degradation rate, and percentage of removal efficiency were calculated for each run.

2.4 Optimization of Process Parameters for Removal of Resorcinol in Presence of Toxic Heavy Metals

The optimization of the process parameters for removal of resorcinol in presence of toxic heavy metals was done by Response Surface Methodology by using Design-Expert 11.0 software. The variable experimental parameters chosen were different concentrations of metals (Cr (VI), Hg, and Pb) and aeration condition. A set of forty experiments with varied values of process parameters were suggested by the software according to which the experiments were conducted. The resorcinol removal efficiency was measured for each run. This response was studied and analyzed by the software to predict the optimum operating conditions. All experiments were carried out for 24 h at 35 °C.

3 Results and Discussions

3.1 Kinetic Study of Growth of Bacteria in Presence of Resorcinol and Different Heavy Metals

From Fig. 1a–c, it was observed that the growth rate of bacteria was found to increase with the concentration of chromium (VI). This was probably because of the presence of chromium reductase in the bacterial system, which reduced Cr (VI) to less toxic form of Cr (III) (Anyanwu and Ezaka 2011; Focardi et al. 2013). Bacterial growth rate was found to increase with the increase of mercury concentration from 5 to 50 ppm due to bioaccumulation of mercury and production of methylated mercury (MeHg) by the bacterial consortium (Kucharzyk et al. 2015). Growth rate of the bacteria was found to remain same with the increase of lead concentration (Mishra and Mishra 2015).

From Fig. 2 it was noted that chromium (VI) and mercury in the media had enhanced the growth of bacteria while lead had interfered with the above process.

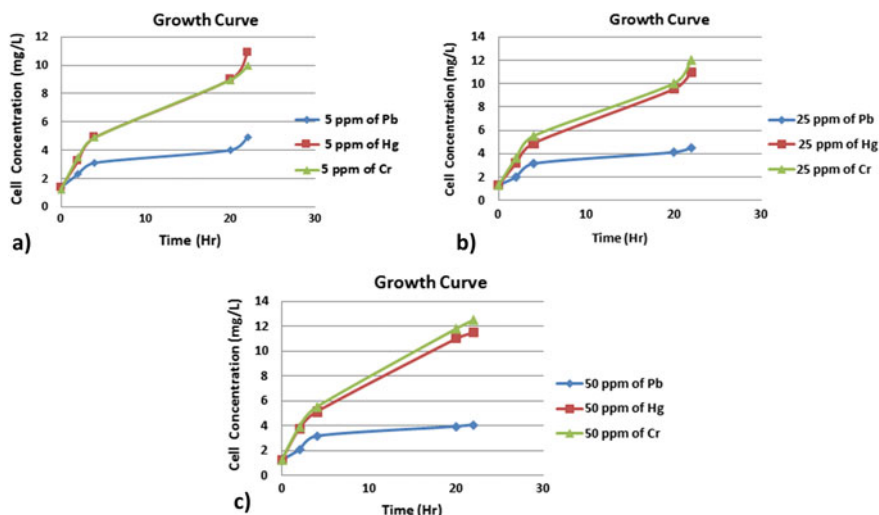


Fig. 1 a Growth curve of mixed bacterial culture in resorcinol in presence of 5 ppm of different metals. b Growth curve of mixed bacterial culture in resorcinol in presence of 25 ppm of different metals. c Growth curve of mixed bacterial culture in resorcinol in presence of 50 ppm of different metals

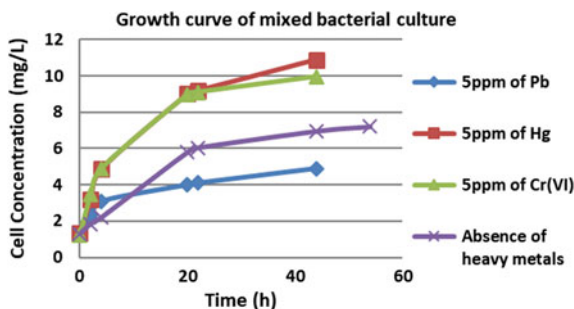


Fig. 2 Growth curve of mixed bacterial culture in resorcinol and in presence and absence of heavy metals

3.2 Kinetic Study of Removal of Resorcinol in Presence of Different Heavy Metals

From Fig. 3, degradation of resorcinol by mixed bacterial culture was maximum in presence of chromium (VI) as compared to the other metals. Moreover, resorcinol remediation was found to increase with the increase in chromium (VI) concentration. Thus it can be inferred that resorcinol acted as an electron donor for reduction of chromium (VI) (Shen and Wang 1995). Rate of resorcinol degradation in presence of mercury in the media was least in comparison to other two metals. The removal rate

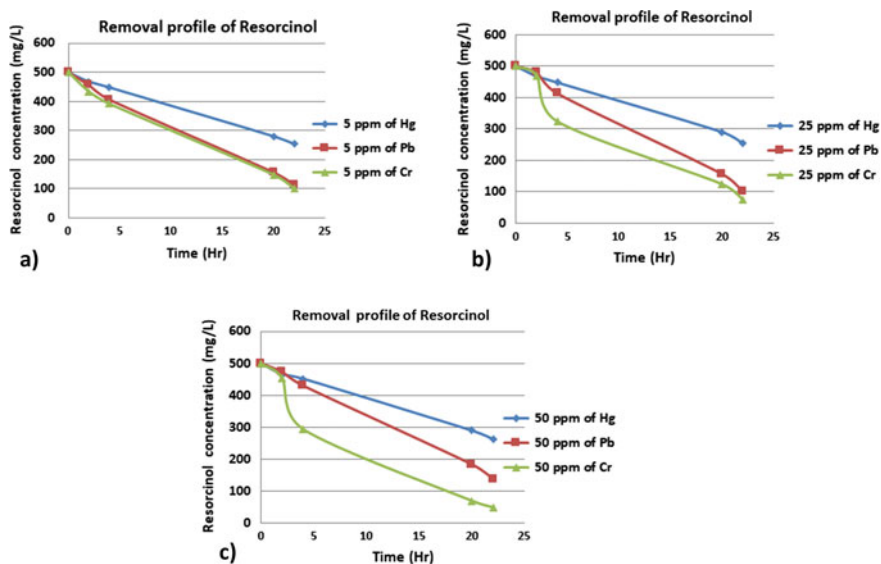


Fig. 3 **a** Degradation profile of resorcinol by mixed bacterial culture in presence of 5 ppm of different metals. **b** Degradation profile of resorcinol by mixed bacterial culture in presence of 25 ppm of different metals. **c** Degradation profile of resorcinol by mixed bacterial culture in presence of 50 ppm of different metals

remained the same when the mercury concentration was increased from 5 to 50 ppm, which stated that mercury in the growth media did not have much effect in resorcinol metabolism of bacterial consortium. Degradation rate of resorcinol was found to decrease slightly with the increase in lead concentration in the media, showing the interference of the metal with resorcinol degradation (Das and Chandran 2011). From Fig. 4, it can be observed that rate of biodegradation of resorcinol increased in presence of heavy metals.

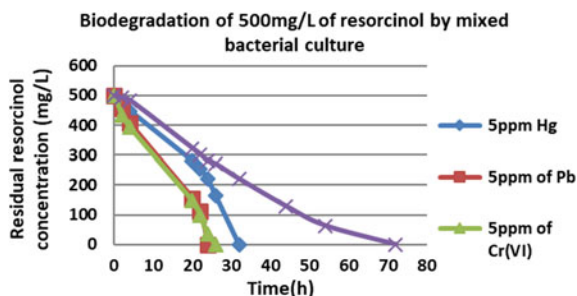


Fig. 4 Degradation profile of resorcinol by mixed bacterial culture in presence and absence of heavy metals

3.3 Comparative Study of Maximum Specific Growth Rate of Mixed Bacterial Consortium, Maximum Specific Degradation Rate of Resorcinol, and Removal Efficiency of Resorcinol in Presence of Heavy Metals

From Fig. 5, it was observed that the maximum specific growth rate (μ_{max}) of bacteria in presence of chromium (VI) and mercury (Hg) increased with the increase in the concentration of these heavy metals, showing its positive effect on the growth of bacteria. Lead (Pb), on the other hand, showed constant μ_{max} with the increase in lead concentration, showing its negligible effect on the growth of bacteria. Among the three metals, chromium (VI) in the culture medium has showed maximum specific growth rate of bacteria.

Figure 6 stated that the maximum removal rate of resorcinol by mixed bacterial culture was observed in presence of 5 ppm of chromium (VI) concentration. The removal rate in presence of mercury and chromium (VI) decreased with the increase in their respective concentrations, whereas conditions got reversed when lead was

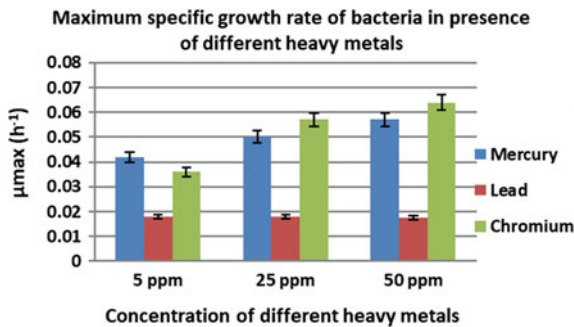


Fig. 5 Maximum specific growth rate of bacteria in presence of different heavy metals

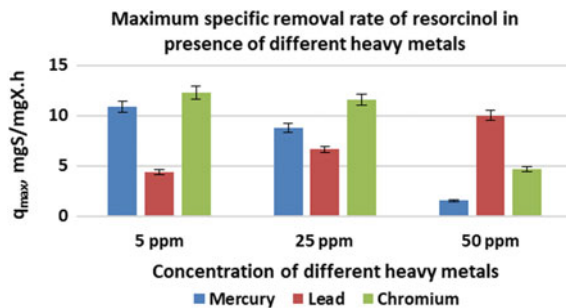


Fig. 6 Maximum specific removal rate of resorcinol in presence of different concentrations of heavy metals

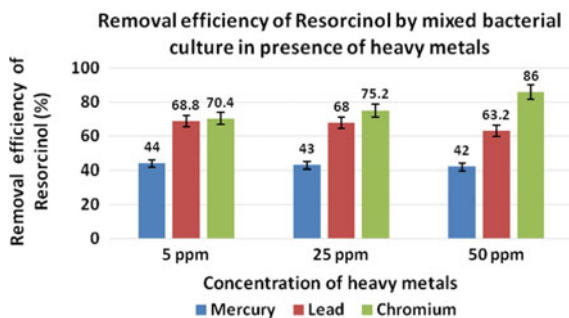


Fig. 7 Removal efficiency of resorcinol by mixed bacterial culture in presence of different concentrations of heavy metals

added in the medium at increasing concentrations. So it can be inferred that lead may abet removal rate of resorcinol (Kortessa and Vidyasagar 2007) (Fig. 7).

Removal efficiency of resorcinol by the mixed bacterial culture was found to increase with the increase in the chromium (VI) concentration and was observed to be maximum in presence of 50 ppm chromium (VI) in the media (Fig. 10), whereas removal efficiency in presence of mercury and lead showed insignificant change with the increase in the concentration of the above metals.

3.4 Optimization of Process Parameters Using Response Surface Methodology

Four experimental parameters such as Cr (VI) concentration, Pb concentration, Hg concentration, and condition of aerations were taken as input variables in Response Surface Methodology and percentage removal efficiency of resorcinol was chosen to be the response or output. DesignExpert 11.0 software analyzed the output and suggested linear model to be the best fit one. The model F -value of 48.70 implied the model was significant. There was only a 0.01% chance that an F -value this large could occur due to noise. P -value less than 0.05 indicated model terms were significant. In this case, P -value had been found to be <0.0001 (Figs. 8 and 9).

In un-aerated condition and at constant mercury concentration, removal efficiency of resorcinol by mixed bacterial culture was found to increase with the increase of chromium (VI) concentrations, with a maximum removal efficiency of 48%. Resorcinol remediation was seen to remain unchanged with the increase in lead concentration in the culture media. This might be due to the presence of chromium reductase in the bacteria which was able to convert chromium (VI) to chromium (III) (Fig. 10).

Similar observations had been seen in presence of chromium (VI) and mercury. Removal of resorcinol was more in presence of chromium (VI) as compared to mercury. Degradation of resorcinol increased with the increase of chromium (VI)

Std	Run	Factor 1 A:Cr(VI) concn mg/L	Factor 2 B:Pb concn mg/L	Factor 3 C:Hg concn mg/L	Factor 4 D:Aeration	Response 1 Removal Efficien... %
28	1	50	50	50	1	92.384
21	2	5	5	5	1	89.772
37	3	27.5	27.5	27.5	1	89.72
19	4	27.5	27.5	27.5	0	35.9
33	5	27.5	27.5	0	1	95.9
10	6	65.3403	27.5	27.5	0	44.5
1	7	5	5	5	0	45.96
40	8	27.5	27.5	27.5	1	89.72
30	9	65.3403	27.5	27.5	1	91.32
23	10	5	50	5	1	87.356
27	11	5	50	50	1	81.75
26	12	50	5	50	1	87.97
34	13	27.5	27.5	65.3403	1	86.57
32	14	27.5	65.3403	27.5	1	85.012
35	15	27.5	27.5	27.5	1	89.72
6	16	50	5	50	0	68.69
11	17	27.5	0	27.5	0	43.86
17	18	27.5	27.5	27.5	0	35.9
9	19	0	27.5	27.5	0	30.96
24	20	50	50	5	1	83.2
29	21	0	27.5	27.5	1	89.4
36	22	27.5	27.5	27.5	1	89.72
25	23	5	5	50	1	86.2
18	24	27.5	27.5	27.5	0	35.9
16	25	27.5	27.5	27.5	0	35.9
5	26	5	5	50	0	50.288
8	27	50	50	50	0	59.126
13	28	27.5	27.5	0	0	33.88
20	29	27.5	27.5	27.5	0	35.9
3	30	5	50	5	0	69.186
31	31	27.5	0	27.5	1	91.676
38	32	27.5	27.5	27.5	1	89.72
4	33	50	50	5	0	65.94
7	34	5	50	50	0	59.154
14	35	27.5	27.5	65.3403	0	49.27
15	36	27.5	27.5	27.5	0	35.9
2	37	50	5	5	0	61.136
12	38	27.5	65.3403	27.5	0	34.772
22	39	50	5	5	1	89.248
39	40	27.5	27.5	27.5	1	89.72

Fig. 8 Screenshot of experimental design by the DesignExpert software 11.0 and its response

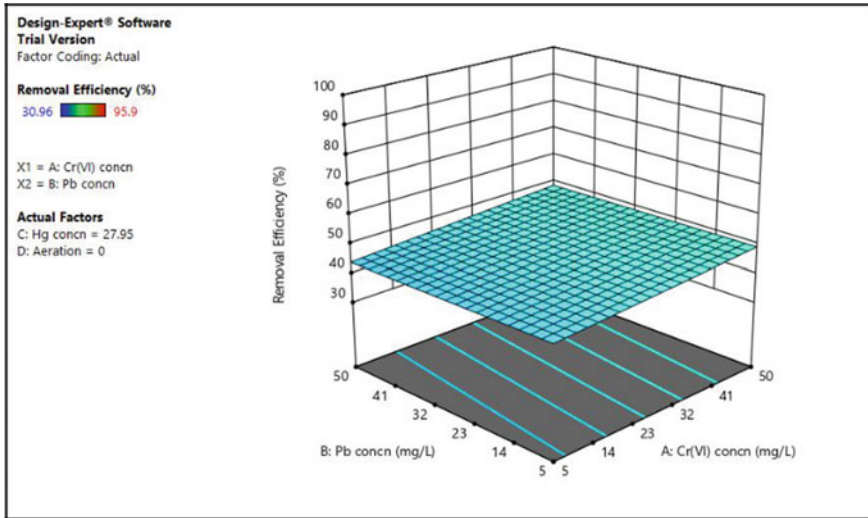


Fig. 9 3D surface view of removal efficiency of resorcinol versus Pb and Cr (VI) concentrations at constant Hg concentration without aeration

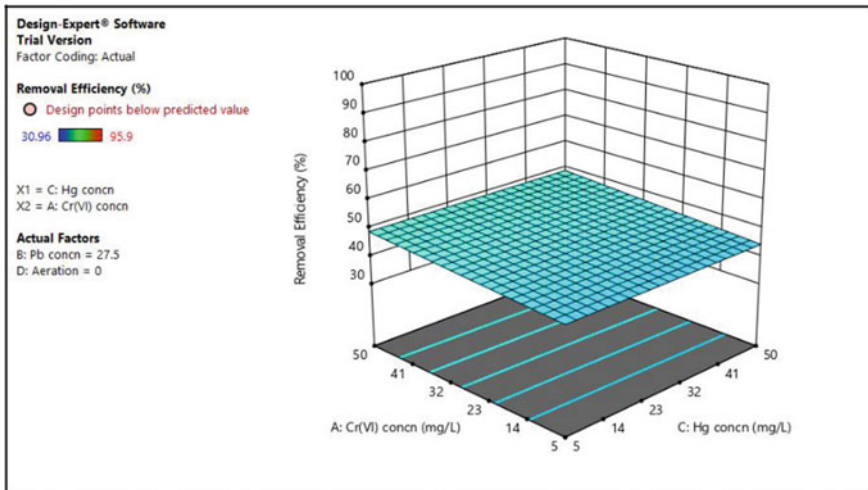


Fig. 10 3D surface view of removal efficiency of resorcinol versus Hg and Cr (VI) concentrations at constant Hg concentration without aeration

concentration in the media. However, increase in the concentration of mercury showed negligible changes in the removal of resorcinol.

When resorcinol removal optimization studies were done with external aeration by MBC in presence of chromium (VI) and lead or chromium (VI) and mercury, the maximum removal efficiency was found to be 90.8%. It could also be inferred from

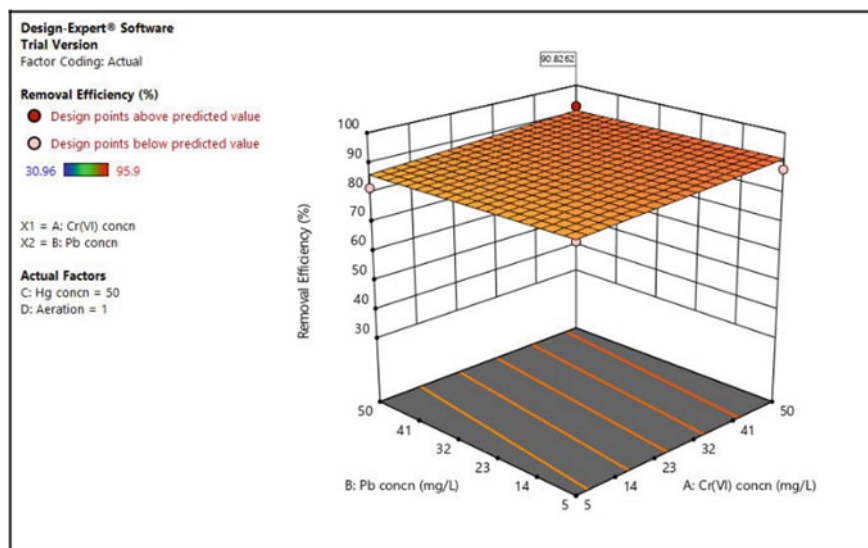


Fig. 11 3D surface view of removal efficiency of resorcinol versus Pb and Cr (VI) concentrations at constant Hg concentration under aerated condition

Fig. 11 that removal efficiency of resorcinol with aeration was almost twice than that without aeration. This was probably because continuous supply of air leads to increased growth rate of bacteria by enhancing the bacterial metabolic rate. Proper aeration was necessary for the bacteria to degrade resorcinol completely to carbon dioxide and water. In absence of oxygen, the process would become slow leading to incomplete mineralization of resorcinol. Turbulence caused by air might lead to uniform circulation of nutrients to the entire bacterial culture. The above observations showed that most of the species in the mixed bacterial culture in the present study were aerobic in nature (Malovanny et al. 2016) (Fig. 12).

The Predicted R^2 of 0.7933 was in reasonable agreement with the Adjusted R^2 of 0.8303, i.e., the difference was less than 0.2 (Fig. 13).

The optimum removal efficiency could be predicted by the following mathematical models:

For no aerated condition:

$$\begin{aligned} \text{Removal efficiency} = & 44.028 + 0.103 * \text{Cr(VI) concentration} \\ & - 0.01363 * \text{Pb concentration} \\ & + 0.002546 * \text{Hg concentration} \end{aligned}$$

For aerated condition:

$$\begin{aligned} \text{Removal efficiency} &= 86.22656 + 0.1030 * \text{Cr (VI) concentration} \\ &\quad - 0.013630 * \text{Pb concentration} \\ &\quad + 0.002546 * \text{Hg concentration} \end{aligned}$$

The optimum process parameters were 50 mg/l of Cr (VI), 50 mg/l of Pb, and 50 mg/l of Hg concentration under aerated condition. Maximum removal efficiency for the above design was found out to be 90.83%.

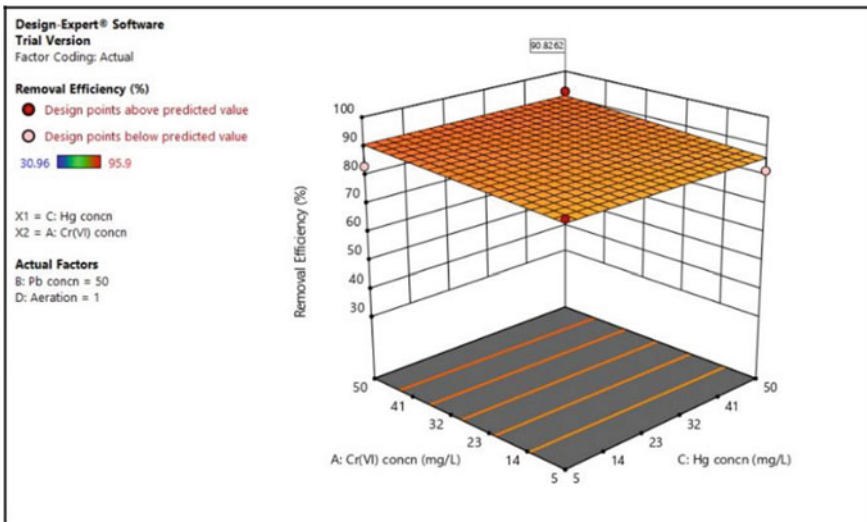


Fig. 12 3D surface view of removal efficiency of resorcinol versus Hg and Cr (VI) concentrations at constant Hg concentration under aerated condition

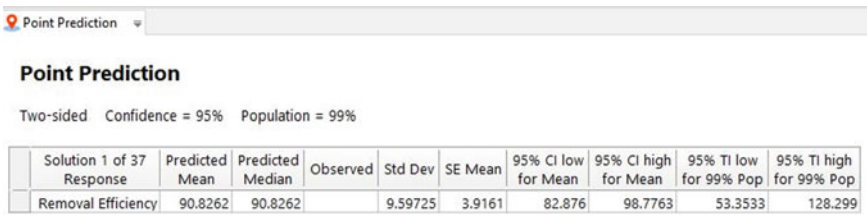


Fig. 13 Screenshot of the maximum removal efficiency of resorcinol as predicted by DesignExpert 11.0 for the given model

4 Conclusions

Mixed bacterial culture (MBC) in the present study was grown in a media containing resorcinol as the sole carbon source in presence of heavy metals (Cr (VI), Pb, and Hg). Chromium (VI) and mercury in the media had enhanced the growth of bacteria while lead had interfered with the above process. Growth of mixed bacterial culture was found to be maximum in the presence of Chromium (VI) in the media.

It was also observed that rate of biodegradation of resorcinol increased in presence of heavy metals. Removal efficiency of resorcinol by the mixed bacterial culture was found to be maximum in presence of 50 ppm chromium (VI) in the media, followed by lead and mercury.

The optimum process parameters as obtained from DesignExpert 11.0 were 50 ppm of Cr (VI), 50 ppm of Pb, 50 ppm of Hg under aerated condition. The optimum removal efficiency as obtained by the above design was 90.83%.

Compliance with Ethical Standards Research Involving Human Participants and/or Animals

This chapter does not contain any studies with human participants or animals performed by any of the authors.

Informed Consent Informed consent was obtained from all individual participants included in the study. The soil used in this study had been collected from the outermost discharge area of the treated tannery effluent, which was outside the tannery premises. Hence no formal permission was needed for collection of soil samples from plant authority.

Conflict of Interest The authors declare that they have no conflict of interest.

References

- Anyanwu CU, Ezaka E (2011) Growth responses of chromium (VI) tolerant bacteria to different concentrations of chromium. *Int J Sci Basic Appl Res* 11(5):41–44
- Chakraborty B (2016) Kinetic study of degradation of p-nitro phenol by a mixed bacterial culture and its constituent pure strains. *Mater Today Proc* 3(10):3505–3524
- Das N, Chandran P (2011) Microbial degradation of petroleum hydrocarbon contaminants: an overview. *Biotechnol Res Int* 2011:1–13
- Focardi S, Pepi M, Focardi SE (2013) Microbial reduction of hexavalent chromium as a mechanism of detoxification and possible bioremediation applications. *IntechOpen*. <https://doi.org/10.5772/56365>
- Kortsha D, Vidyasagar GM (2007) Isolation and characterization of phenol degrading pseudomonas aeruginosa MTCC 4996. *World J Biotechnol* 24:541–547
- Kucharzyk KH, Deshusses MA, Porter KA, Hsu-Kim H (2015) Relative contributions of mercury bioavailability and microbial growth rate on net methylmercury production by anaerobic mixed cultures. *Environ Sci Process Impacts* 17(9):1568–1577
- Laura G, Villegas C, Mashhadi N, Chen M, Mukherjee D, Taylor KE, Biswas N (2016) A short review of techniques for phenol removal from wastewater. *Curr Pollut Rep* 2:157–167

- Malovanyy M, Shandrovykh V, Malovanyy A, Polyuzhyn I (2016) Comparative analysis of the effectiveness of regulation of aeration depending on the quantitative characteristics of treated sewage water. *J Chem* 2016:1–9
- Mishra A, Mishra KP (2015) Bacterial response as determinant of oxidative stress by heavy metals and antibiotic. *J Innov Pharm Biol Sci* 2(3):229–239
- Nasr FA, Doma HS, Abdel-Halim HS, El-Shafai SA (2007) Chemical industry wastewater treatment. *The Environmentalist* 27:275–286
- Shen H, Wang Y (1995) Simultaneous chromium reduction and phenol degradation in a coculture of *Escherichia coli* ATCC 33456 and *Pseudomonas putida* DMP-1. *Appl Environ Microbiol* 61(7):2754–2758
- Tüfekci N, Sivri N, Toroz I (2007) Pollutants of textile industry wastewater and assessment of its discharge limits by water quality standards. *Turk J Fish Aquat Sci* 7:97–103

An Environmentally Benign Green Approach for the Reduction of Graphene Oxide by Apple Extract: Spectroscopic and Thermal Interpretation



Shweta Mitra, Saswata Bose, and Mehabub Rahaman

Abstract A simple, effective, and environmentally benign approach for the reduction of graphene oxide (GO) using apple juice as a reducing agent has been reported in this work. The advantage of this approach is that it eliminates the need for using toxic reducing agents or external stabilizers to carry out the chemical reduction of GO. The reduction, mediated by the extracted maleic acid from apple juice, was found to take place under mild conditions in the aqueous medium. The formation of layered graphitic structure and random orientation of graphene was confirmed by X-ray diffraction study. Appearance of a broad band at 24.9° , corresponds to d-spacing of ~ 0.342 nm) elucidates successful reduction. Successful reduction of GO was further confirmed by UV–visible spectroscopy. The plasmon peak at 230 nm has been red-shifted to 263 nm corroborating the electronic conjugation in MRGO nanosheets was restored. Raman spectroscopy revealed the formation of graphene with defects. Since the method proposed is economical, it can be used for the large-scale production of reduced GO.

Keywords Graphene · Apple extract · Reduction

1 Introduction

Graphene with its two-dimensional structure, high surface area, Young's modulus, thermal conductivity, and optical transmittance besides its chemical stability has been at the forefront of research in the field of nanoscience and technology over the past decade (Chabot et al. 2014). These unique properties of graphene have led to its

S. Mitra · S. Bose · M. Rahaman (✉)
Department of Chemical Engineering, Jadavpur University, Kolkata, India
e-mail: mehabub@gmail.com

S. Mitra
e-mail: shwtmtr@gmail.com

S. Bose
e-mail: saswataboseiit@gmail.com

application in a variety of different branches such as lithium-ion batteries (Wu et al. 2010), supercapacitors (Bose et al. 2017a, b), electronic devices (Guo et al. 2010), tribology (Eswaraiah et al. 2011), and fillers for nanocomposites (Bose et al. 2017a, b, 2018, 2019). Therefore, huge requisition for graphene and its peaking cost of large-scale production demands substantial reduction in the production cost associated with it. Compared to the preparation of graphene from graphite using various mechanical routes (Dikin et al. 2007), the reduction of graphene oxide (GO) offers a promising alternative for the mass production of graphene. Properties of the reduced graphene oxide (RGO) are affected by the characteristics of the GO used in the synthesis step (Subrahmanyam et al. 2009). The reduction of GO via electrochemical (Raj and John 2013), thermal (Liu et al. 2013), and photocatalytic (Akhavan 2011) routes have been explored in recent times. However, each of the afore-mentioned processes has major drawbacks, for example, electrochemical methods fail to remove inherent defects present in GO as well as lead to the formation of stable ether or carbonyl groups which are tough to eliminate (Aunkor et al. 2016). Moreover, the thermal and photocatalytic pathways are associated with complex multistep mode of operation and requirement of specially designed materials that can withstand uninterrupted ultraviolet radiation, respectively. These limitations coupled with the relatively fast and flexible nature of the chemical mediated reduction of graphene, researchers have widely regarded it as the easiest and most prudent route for the production of graphene with interesting morphological features (Low et al. 2015). Since the reduction of GO by chemical methods (hydrazine, NaBH_4 , hydroquinone, etc.) involves the problems associated with the production and disposal of toxic waste streams, researchers have turned their attention toward the conversion of GO to RGO by employing environmentally benign reducing agents. However, the reduction of GO via non-toxic routes involves reducing agents that are expensive, scarce, and prone to degradation during storage (Aunkor et al. 2016; Low et al. 2015). In the span of the last few years research efforts have been directed toward the identification and effectiveness of such green sources that can successfully reduce GO without interfering with the inherent structural properties. Previous works have shown the reduction of GO can be carried out using coconut water, clove extract, tea polyphenol, amino acids, pomegranate juice, and spinach extract as highlighted in some excellent review papers (Aunkor et al. 2016; De Silva et al. 2017). In this work, we have used the extract of apple (*Maluspumila*) to carry out the reduction of GO in aqueous medium. It is expected that the malic acid present in the apple extract will facilitate the reduction of GO as well as preventing the agglomeration of graphene into the pristine graphitic structure. The advantage of this process compared to other chemical reducing agents is the easy availability of the precursor involved and overall environmental consequences.

2 Experimental

2.1 Materials

All chemicals were of analytical grade and were used without further purification. Natural graphite flakes (LobaChemie) were used as the precursor for GO. Sulfuric acid (about 98%), hydrochloric acid (about 37%), and hydrogen peroxide (about 35%) were purchased from Merck. Potassium permanganate (KMnO_4) (Merck) was used as an oxidizing agent during the preparation of GO. Apples were purchased from a local market in Jadavpur, India.

2.2 Synthesis of GO

In the synthesis of GO the modified Hummers' method (Hummers and Offeman 1958), a weighed amount of natural graphite flakes was dissolved in concentrated H_2SO_4 in a round bottom flask placed in an ice bath at 0–5 °C (ice bath). Measured quantity of KMnO_4 was added slowly to the magnetically stirred mixture to avoid chances of explosion. The flask containing the reaction mixture was then put in an oil bath at 50 °C and stirred for 8 h, followed by the addition of deionized and stirring for further 2 h. 35% H_2O_2 was added dropwise to the mixture turning it brown to bright yellow. The excess of manganese salts was neutralized using a dilute solution of hydrochloric acid (5% v/v). A brown colored dispersion of GO was obtained in water. Finally, the GO dispersion was repeatedly washed using double distilled water till the pH of the mixture became neutral.

2.3 Reduction of GO by Apple Juice

To remove impurities, the apples were first washed with double distilled water a juicer (Bajaj Majesty 400-W Juice Extractor) was used to extract the juice. The juice was twice filtered using 0.2 μm Whatman Filter paper. Finally, in order to remove any heavy particles that may have still remained in the filtrate and centrifuged (Remi R-8C plus) at room temperature at 6000 rpm for 7 min to use the supernatant as the reducing agent. In a typical experiment, weighed amount of GO was dispersed in double-distilled water and exfoliated using an ultrasonic bath (Labman Instruments) which exhibited stability over a long time period. For reduction, fixed volumes of the exfoliated GO dispersion and apple extract taken in a round bottom flask were placed in an oil bath and refluxed at 90 °C while being continuously stirred at 350 rpm for 48 h. Visible changes in the color from the brown color of GO dispersed in water to black marked the end of the reaction. The product was washed copiously using

double distilled water till the pH of the mixture became neutral. Finally, it was dried in a vacuum oven at 60 °C and referred to as MRGO.

2.4 Measurements and Characterizations

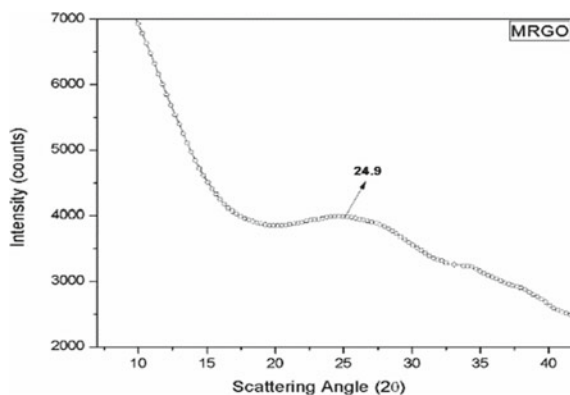
The GO and MRGO were dispersed in water and sonicated for 30 min in an ultrasonicator (Labman Scientific Instruments) to ensure their dispersion in the solvent. The dispersed samples were then analyzed using UV–Vis spectroscopy (Perkin-Elmer Lamda 8000). X-ray diffraction (XRD) studies were carried out at room temperature at a scan rate of 5°/min (Bruker D8 Advance) with Cu-K α targets ($\lambda = 0.154$ nm). Raman spectra of the prepared GO and MRGO samples were performed on a Raman Microscope (WITec Alpha 300R) in the range of 500–3000 cm⁻¹ using a He–Ne laser beam. Thermogravimetric analysis (TGA) was carried out at a heating rate of 5 °C/min from 50 to 600 °C in air. X-ray photoelectron spectroscopy (XPS) was carried out in PHI 5000 Versa Probe III using Al-K α X-ray source.

3 Results and Discussion

3.1 XRD Analysis

XRD spectra of MRGO in the range of 2θ from 5° to 45° are shown in Fig. 1. In the XRD pattern of MRGO, a broad band has appeared at 24.9° (d-spacing ≈ 0.342 nm). However, as observed in the earlier studies by Bose et al. (2012) GO showed a sharp peak at 11.02° with corresponding d-spacing of around 0.7997 nm. This shift in the d-spacing can be ascribed to the successful reduction of the GO and formation of graphitic structures. Decrement in interlayer spacing as compared to GO indicates

Fig. 1 X-ray diffraction pattern of MRGO



the removal of oxygen functionalities resulting in exfoliation of the layers in MRGO. The d-spacing of MRGO is considerably lower than that of GO but slightly higher than that of well-ordered graphite (0.3397 nm), implying reduction of GO. The appearance of the broad band is suggestive of the fact that the graphene flakes are randomly oriented in the stacking direction.

3.2 Raman Spectra Analysis

Raman spectroscopy is sensitive to the electronic configuration of “C=C” which exhibits high Raman intensities and therefore it is an important characterization tool of graphitic materials. The results of the Raman spectroscopy of GO and MRGO are shown in Fig. 2a, b. The spectra of pure GO (Fig. 2a) exhibited a relatively broad G-band centered at 1582 cm^{-1} that originated from the first-order scattering of the E_{2g} vibration mode of sp^2 carbon atoms and a prominent D-band at 1355 cm^{-1} due to the breathing mode of κ -point photons of A_{1g} symmetry (Bose et al. 2017a, b). The results suggested that the C- sp^2 character of graphite flakes was significantly reduced upon oxidation in addition to the introduction of defects in the GO sheets. The ratio of the intensity of the D-band to G-band was found to be almost similar both in case of GO ($I_D/I_G = 0.99$) and RGO ($I_D/I_G = 0.98$). The trend in the I_D/I_G ratio suggested that the GO and MRGO had similar defect density within their structure. In case of MRGO, the D-band shifted slightly to 1585 cm^{-1} while the G-band shifted to 1349 cm^{-1} . The change in peak position inferred the change in chemical atmosphere indicating that the apple extract could act as a reducing agent. The most important observation is that the appearance of 2D band for RGO at 2690 cm^{-1} (Fig. 2b). The appearance of weak 2D band in the Raman spectrum of MRGO ascribed to the second-order of the zone-boundary phonons generated by the double resonance Raman scattering with two-phonon emission. Generally, single Lorentzian peak fitting for the 2D band implies the formation of single-layer graphene at 2679 cm^{-1} . However, if the afore-mentioned 2D peak is broadened and

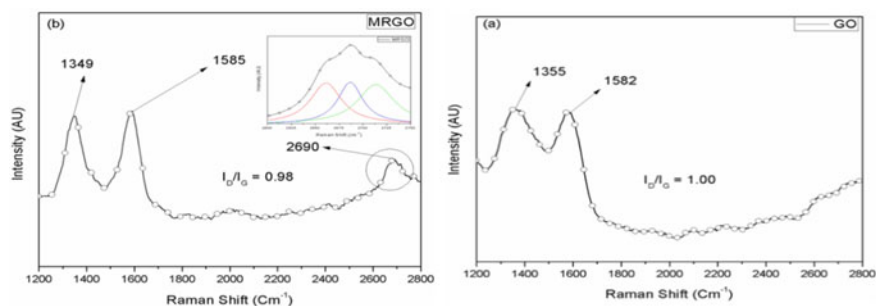


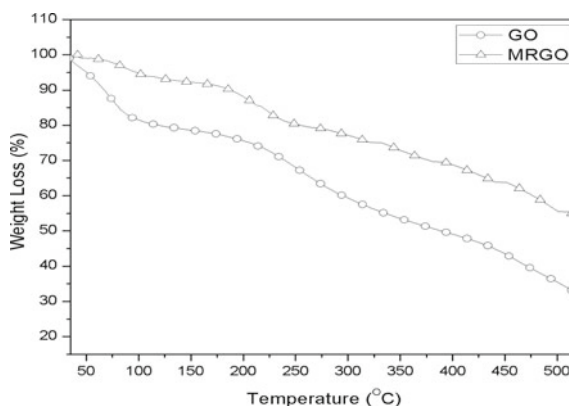
Fig. 2 Raman spectrum of **a** GO and **b** MRGO (Lorentzian fitting of the 2D band is shown in the inset)

shifted to a higher wavenumber, then we can infer that multilayer graphene is formed (Bose et al. 2012). In our current study, the 2D band is fitted with more than one Lorentzian function (shown in inset of Fig. 2b) and also the peak position is shifted toward higher wavenumber (2690 cm^{-1}). The band at 2690 cm^{-1} was absent in the spectra of GO suggesting the formation of a multilayered graphene (Ferrari 2007).

3.3 Thermogravimetric Analysis (TGA)

Figure 3 shows the TGA plots of pure GO and MRGO. It can be seen from the TGA curve of GO that there is a significant weight loss at $100\text{ }^{\circ}\text{C}$ which can be attributed to the elimination of the intercalated water molecules as well as the evaporation of adsorbed water from the surface of GO. The degradation occurring at $180\text{ }^{\circ}\text{C}$ was due to the removal of the oxygenated functional groups while the pyrolysis of the carbon backbone and residual oxygen-containing functional groups led to the degradation at $400\text{ }^{\circ}\text{C}$ (Jeong et al. 2009). At $520\text{ }^{\circ}\text{C}$ pure GO experienced a weight loss of 68.7% while the weight loss for the prepared MRGO was found to be 45.1%. Therefore, the results from the TGA analysis suggested that the majority of the reactive oxygenated moieties were absent in MRGO and thus confirming the partial but successful reduction of GO using apple extract. It is worth mentioning that our results are in close agreement with previous research concerning the reduction of GO using wild carrot root (Kuila et al. 2012) where it was found that refluxing favored the reduction of GO to RGO.

Fig. 3 TGA of GO and MRGO in air



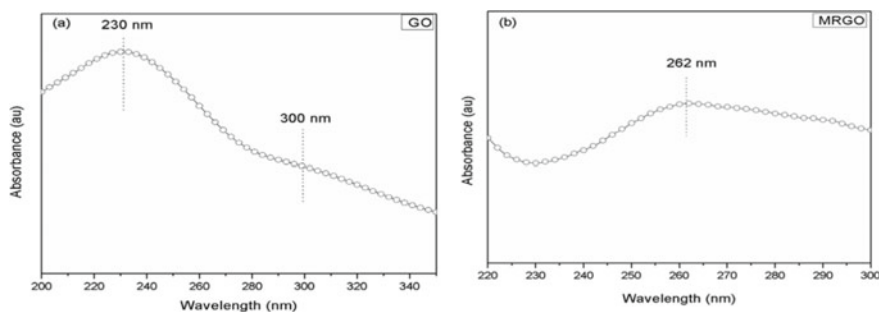


Fig. 4 UV-Vis spectra of **a** GO and **b** MRGO

3.4 UV-Visible Spectroscopy

Figure 4a, b shows the UV-vis spectra of the dispersions of GO and RGO in aqueous medium. The GO spectra revealed two characteristic features: the first broad shoulder at 300 nm has been assigned to the $n-\pi^*$ plasmon transition due to the presence of epoxide and acid groups. The second characteristic was the peak at 230 nm due to the $\pi-\pi^*$ transition of the C=C bonds which is similar to the values reported in literature (Mei et al. 2010). After reduction, the plasmon peak at 230 nm has been red-shifted to 263 nm corroborating an increase in π -electron density or in other words the electronic conjugation in MRGO nanosheets was restored to some extent. The results were in line with previously reported results concerning the reduction of GO by ascorbic acid (Zhang et al. 2010) and *Hibiscus sabdariffa* L. (Chu et al. 2014).

3.5 X-ray Photoelectron Spectroscopy (XPS)

To further exemplify the reduction, the binding energy was characterized using XPS to examine the removal of the oxygenated functional groups. FWHMs of GO and MRGO were shown in Fig. 5a, b, respectively. The reduction in peak intensity of O-1s in the XPS spectrum of MRGO (Fig. 5b) as compared to the FWHS spectrum of GO (Fig. 5a) suggests the successful reduction employing apple extract. Figure 5c, d shows the deconvoluted C-1s XPS patterns of GO and MRGO, respectively (Chu et al. 2014). The deconvoluted spectrum of GO contains four major peaks centered at 284.2, 286.2, 288.0, and 289.1 eV corresponding to the C-C/C=C bond in the aromatic rings, C-O, C=O, and O=C-OH bonds, respectively. However, upon reduction with apple extract, the slight shifting of the peak positions along with the noteworthy reduction in the peak intensities can clearly be attributed to the removal of oxygen moieties. Moreover, the peak at 289.1 eV, due to the presence of -COOH group, has been observed to diminish completely after reduction.

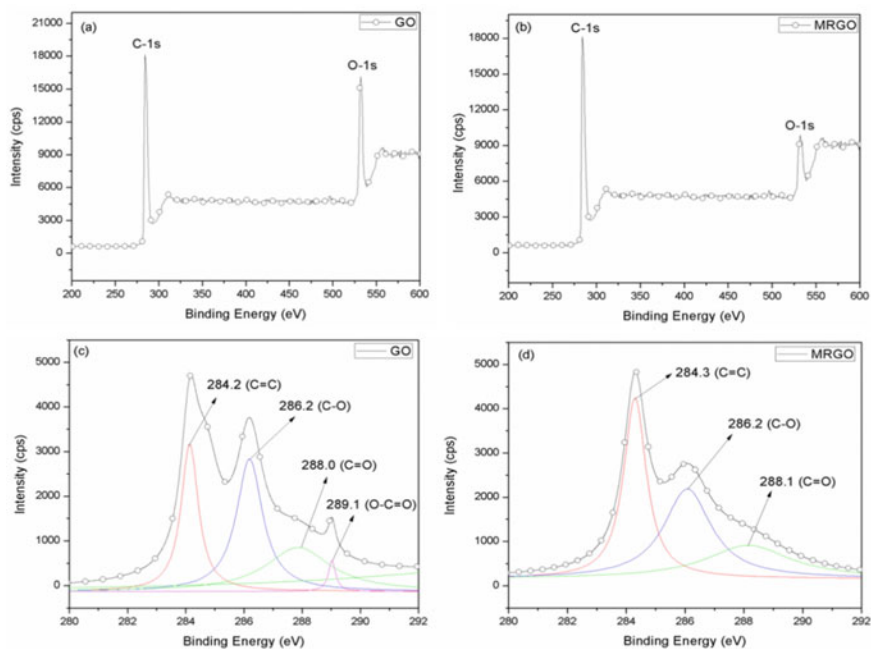


Fig. 5 FWHM X-ray photoelectron spectrum of **a** GO; **b** MRGO; **c** deconvoluted C-1s XPS spectrum of GO; and **d** deconvoluted C-1s XPS spectrum of MRGO

4 Conclusion

A green and environmentally benign approach has been described for the reduction of graphene oxide using apple juice extract. The reduction was carried out under reflux at 90 °C in aqueous medium. XRD of the final reduction product suggested the formation of few layers of graphene. The restoration of the sp^2 network and the introduction of defects into the GO and RGO during the course of the reaction was substantiated by Raman spectroscopy. The reduction in weight loss for RGO compared to GO also supported the de-oxygenation that took place during reduction. The UV-vis spectroscopy further confirmed the reduction. The benefits of using apple juice extract as a reducing agent compared to conventional chemicals are the green, economical, and straightforward approach.

References

- Akhavan O (2011) Photocatalytic reduction of graphene oxides hybridized by ZnO nanoparticles in ethanol. *Carbon* 49:11–18. <https://doi.org/10.1016/j.carbon.2010.08.030>
- Aunkor MTH, Mahbulul IM, Saidur R, Metselaar HSC (2016) The green reduction of graphene oxide. *RSC Adv* 6:27807–27828. <https://doi.org/10.1039/C6RA03189G>
- Bose S, Kuila T, Kumar Mishra A, Hoon Kim N, Hee Lee J (2012) Dual role of glycine as a chemical functionalizer and a reducing agent in the preparation of graphene: an environmentally friendly method. *J Mater Chem* 22:9696–9703. <https://doi.org/10.1039/C2JM00011C>
- Bose S, Basu S, Das A, Rahman M, Drzal LT (2017a) Fabrication of a sulfonated aramid-graphene nanoplatelet composite paper and its performance as a supercapacitor electrode. *J Appl Polym* 134:45099. <https://doi.org/10.1002/app.45099>
- Bose S, Das A, Basu S, Drzal LT (2017b) Edge stitching of graphene nanoplatelets (GnPs) and their effectiveness as a filler for epoxy nanocomposites. *Chem Select* 2:5769–5774. <https://doi.org/10.1002/slct.201701019>
- Bose S, Das A, Basu S, Drzal LT (2018) Covalent functionalization of graphene using polyacryloyl chloride and performance of functionalized graphene–epoxy nanocomposite. *Polym Compos* 39:3119–3128. <https://doi.org/10.1002/pc.24318>
- Bose S, Das A, Ghosh A (2019) Enhanced thermal and mechanical performance of functionalized graphene epoxy nanocomposites: effect of processing conditions, different grades and loading of graphene. In Sahoo P, Davim JP (eds) *Advances in materials, mechanical and industrial engineering*. Springer International Publishing, Berlin, pp 19–33
- Chabot V, Higgins D, Yu A, Xiao X, Chen Z, Zhang J (2014) A review of graphene and graphene oxide sponge: material synthesis and applications to energy and the environment. *Energy Environ Sci* 7:1564–1596. <https://doi.org/10.1039/C3EE43385D>
- Chu H-J, Lee C-Y, Tai N-H (2014) Green reduction of graphene oxide by *Hibiscus sabdariffa L.* to fabricate flexible graphene electrode. *Carbon* 80:725–733. <https://doi.org/10.1016/j.carbon.2014.09.019>
- De Silva KKH, Huang H-H, Joshi RK, Yoshimura M (2017) Chemical reduction of graphene oxide using green reductants. *Carbon* 119:190–199. <https://doi.org/10.1016/j.carbon.2017.04.025>
- Dikin DA, Stankovich S, Zimney EJ, Piner RD, Dommett GHB, Evmenenko G, Nguyen ST, Ruoff RS (2007) Preparation and characterization of graphene oxide paper. *Nature* 448:457–460. <https://doi.org/10.1038/nature06016>
- Eswaraiah V, Sankaranarayanan V, Ramaprabhu S (2011) Graphene-based engine oil nanofluids for tribological applications. *ACS Appl Mater Interfaces* 3:4221–4227. <https://doi.org/10.1021/am200851z>
- Ferrari AC (2007) Raman spectroscopy of graphene and graphite: disorder, electron–phonon coupling, doping and nonadiabatic effects. *Solid State Commun* 143:47–57. <https://doi.org/10.1016/j.ssc.2007.03.052>
- Guo CX, Yang HB, Sheng ZM, Lu ZS, Song QL, Li CM (2010) Layered graphene/quantum dots for photovoltaic devices. *Angew Chem Int Ed* 49:3014–3017. <https://doi.org/10.1002/anie.200906291>
- Hummers WS, Offeman RE (1958) Preparation of graphitic oxide. *J Am Chem Soc* 80:1339. <https://doi.org/10.1021/ja01539a017>
- Jeong H-K, Lee YP, Jin MH, Kim ES, Bae JJ, Lee YH (2009) Thermal stability of graphite oxide. *Chem Phys Lett* 470:255–258. <https://doi.org/10.1016/j.cplett.2009.01.050>
- Kuila T, Bose S, Khanra P, Mishra AK, Kim NH, Lee JH (2012) A green approach for the reduction of graphene oxide by wild carrot root. *Carbon* 50:914–921. <https://doi.org/10.1016/j.carbon.2011.09.053>
- Liu X, Kim H, Guo LJ (2013) Optimization of thermally reduced graphene oxide for an efficient hole transport layer in polymer solar cells. *Org Electron* 14:591–598. <https://doi.org/10.1016/j.orgel.2012.11.020>

- Low FW, Lai CW, Abd Hamid SB (2015) Easy preparation of ultrathin reduced graphene oxide sheets at a high stirring speed. *Ceram Int* 41:5798–5806. <https://doi.org/10.1016/j.ceramint.2015.01.008>
- Mei Q, Zhang K, Guan G, Liu B, Wang S, Zhang Z (2010) Highly efficient photo luminescent graphene oxide with tunable surface properties. *Chem Commun* 46:7319–7321. <https://doi.org/10.1039/C0CC02374D>
- Raj MA, John SA (2013) Simultaneous determination of uric acid, xanthine, hypoxanthine and caffeine in human blood serum and urine samples using electrochemically reduced graphene oxide modified electrode. *Anal Chim Acta* 771:14–20. <https://doi.org/10.1016/j.aca.2013.02.017>
- Subrahmanyam KS, Panchakarla LS, Govindaraj A, Rao CNR (2009) Simple method of preparing graphene flakes by an arc-discharge method. *J Phys Chem C* 113:4257–4259. <https://doi.org/10.1021/jp900791y>
- Wu Z-S, Ren W, Wen L, Gao L, Zhao J, Chen Z, Zhou G, Li F, Cheng H-M (2010) Graphene anchored with Co₃O₄ nanoparticles as anode of lithium ion batteries with enhanced reversible capacity and cyclic performance. *ACS Nano* 4:3187–3194. <https://doi.org/10.1021/nn100740x>
- Zhang J, Yang H, Shen G, Cheng P, Zhang J, Guo S (2010) Reduction of graphene oxide via L-ascorbic acid. *Chem Commun* 46:1112–1114. <https://doi.org/10.1039/B917705A>

Performance and Kinetic Studies of Dairy Effluent Using Mixed Culture in a Suspended Growth Batch Reactor



Dipankar Raha, Pradyut Kundu, and Somnath Mukherjee

Abstract A batch kinetic study was performed for examining potential application of microbial culture, for organic carbon oxidation, nitrification and denitrification from simulated real-life dairy wastewater. After necessary characterization of waste samples, it was found that SCOD, $\text{NH}_4^+\text{-N}$ and $\text{NO}_3^-\text{-N}$ were within the range of 1116.7–1361.2, 41.4–58.13 and 19.75–23.96 mg/L, respectively. Time concentration study showed that after 24 h of contact time, 93.80–97.30% reduction of SCOD, 80.27–90.99% reduction of ammonia nitrogen ($\text{NH}_4^+\text{-N}$) and 93.09–93.65% reduction of nitrate–nitrogen ($\text{NO}_3^-\text{-N}$) were achieved respectively in a separate suspended growth batch reactor. The kinetic constants for SCOD removal, nitrification and denitrification also evaluated from the results of batch study using Monod equation and Lineweaver–Burk plot for designing of a suitable pilot-scale bioreactor for treatment of real-life dairy wastewater.

Keywords Dairy wastewater · Suspended growth batch reactor · SCOD reduction · Nitrification · Denitrification · Kinetic coefficient

D. Raha

Lecturer in Civil Engineering, Maynaguri Government Polytechnic, Maynaguri, Jalpaiguri, West Bengal 735302, India

e-mail: dipankarraha.jal@gmail.com

P. Kundu

Lecturer, Department of Food Processing Technology, Mirmadan Mohanlal Government Polytechnic, Plassey, Nadia, West Bengal 741156, India

e-mail: kundupradyut@yahoo.co.in

S. Mukherjee (✉)

Professor, Civil Engineering Department, Jadavpur University, Kolkata, West Bengal 700032, India

e-mail: mukherjeesomnath19@gmail.com

© Springer Nature Singapore Pte Ltd. 2021

D. Ramkrishna et al. (eds.), *Advances in Bioprocess Engineering and Technology*,

Lecture Notes in Bioengineering,

https://doi.org/10.1007/978-981-15-7409-2_38

1 Introduction

The milk production unit and dairy plant emanate high volume of wastewater containing formidable amount of organics and nitrogenous substances (Tripathi and Upadhyay 2003). It is reported that dairy industry releases on an average of 0.2–10 L of effluent per litre of milk processing (Vourch et al. 2008). Wastewater emanates such plants contain high level of suspended solids, BOD, COD, nitrogen, oil, fat, grease contents along with varied pH levels due to different cleansing strategies, which necessitates a special treatment to minimize the environmental problems.

A high degree of wastewater treatment would be accomplished before its discharge in water environment to maintain ecological harness. Biological treatment is one of the alternative options for treatment of above wastewater because of high soluble BOD, high COD concentration and proven reliable processing technology. Furthermore, resulting end products emerge from this process are innocuous in nature. Biological treatment methods for treating dairy wastewater are advocated by Kargi and Dincer (1997) containing multi-substrates such as COD, N and P. The aim of the study was to perform a laboratory scale batch experiment to treat dairy plant effluent emphasis as COD and nitrogen removal to estimate kinetic constant using Monod's equation for designing reactor for a real-life application.

2 Materials and Methods

2.1 Seed Acclimatization

A glass cylinder of 1000 mL capacity was taken as an acclimatization unit. A non-acclimatized seed from nearby small-scale dairy industry was collected and mixed with waste samples and necessary air was supplied continuously with the help of small compressor unit. Seed acclimatization phase was continued for 2 months and considered to be complete when a steady performance was noted for a consistent COD removal and growth of biomass.

For acclimatization of nitrifiers, a separate synthetic solution was prepared in a cylinder of 1.0 L capacity, in which NH_4Cl and $(\text{NH}_4)_2\text{SO}_4$ of concentration of 0.10 g/L and 0.05 g/L, respectively, were added as nitrogen source to stimulate the appropriate environmental conditions. Necessary aeration was accomplished through a small compressor unit. pH within the cylinder was kept in the range of 7.5–8.0 by the addition of necessary doses of 0.1 N sodium bicarbonate (NaHCO_3) solution.

The denitrifying sludge was collected from a anaerobic digester unit. A separate denitrifying unit was employed, i.e. an aspirator bottle, kept on a magnetic stirrer, for mixing well in absence of oxygen. The seed was acclimatized by adding potassium nitrate (KNO_3) having NO_3^- -N concentration of 10–30 mg/L for a time period of

2 months. The pH value was maintained as 7.5–8 by adjusting with exact amount of acetic acid (0.01 N). During this acclimatization phase, biomass growth was noticed by checking SVI and also by gas formation aspect, which indicated that the biomass was in active stage.

2.2 Collection of Field Sample

Real-life dairy wastewater sample was also collected from a local dairy processing unit. Besides packaged milk, this dairy unit also produces curd, lassi, paneer butter-milk and ghee. The plant produces effluent with flow rate of 90–100 m³/d on daily average basis. Effluents were collected six times in different months during the study phase. The samples were brought to the Civil Engineering Department Laboratory, Jadavpur University and kept in a sample preservation unit at a temperature of 4 °C. Each sample was tested for the characterization of parameters viz. pH, alkalinity, DO, MLSS, SCOD, NH₄⁺-N, NO₃⁻-N as per 'Standard Methods' (APHA 1998).

2.3 Experimental Setup

The batch experiment for COD removal and nitrification was accomplished in plastic beakers of 1000 mL capacity as the photographs shown in Fig. 1. Diffused aeration systems were introduced for oxygen supply within the reactor. However, the batch denitrification was carried out in an aspirator bottle of 2000 mL capacity (Fig. 2)

Fig. 1 Photograph for batch reactor for COD removal and ammonia nitrification





Fig. 2 Photograph for batch denitrification

and kept over a magnetic stirrer for mixing well without any supply of oxygen and wrapped with a black plastic sheet to devoid any light to pass through for preventing any growth of algae.

3 Results and Discussion

3.1 Characterization of Dairy Wastewater

Analytical results on sample characterization are given in Table 1. The range of pH lies between 8.18 and 8.32, which corroborates the range found in the literature (Deshannavar et al. 2012). SCOD concentration was found between 1116.7 and 1361.2 mg/L, corroborating the finding of earlier researcher (Chaiudhari and Dhoble 2010). BOD₅ of the dairy wastewater was found to be 788.6–898.0 mg/L that is within the range, as observed by different other investigators (Pachpute et al. 2014).

Table 1 Characterization of dairy wastewater (pre-treated)

Parameters	Maximum	Minimum	Mean	SD
SCOD (mg/L)	1361.2	1116.7	1240.63	100.14
pH	8.32	8.18	8.25	0.06
TSS (mg/L)	1850.0	1520	1680.00	134.91
TS (mg/L)	5380	4300	4882.50	451.84
BOD ₅ (mg/L)	898.0	788.6	828.25	48.66
Alkalinity (mg/L as CaCO ₃)	593.0	562.0	577.50	12.82
NH ₄ ⁺ -N (mg/L as N)	58.13	41.40	49.95	7.01
NO ₃ ⁻ -N (mg/L as N)	23.96	19.75	21.54	1.76
DO (mg/L)	1.60	1.20	1.40	0.18

3.2 Performance Evaluation of Batch Reactor

This study was conducted for exploring the removal kinetics of COD and NH₄⁺-N with time, with the help of acclimatizing seed and also for determining the kinetic constants for designing of a prototype aeration tank for treatment of real-life dairy wastewater.

3.2.1 Time Course Study for Carbon Oxidation

The batch study was carried out with acclimatized seed and different initial MLSS concentration of 913–1352 mg/L to reduce SCOD from an initial SCOD concentration of 1250 ± 50 mg/L. Figure 3 represents the reduction of SCOD with time at different MLSS concentrations and observed that SCOD concentration decreases with time, for the activity of heterotrophic organic carbon oxidizing bacteria for maintaining their metabolic energy and cell synthesis. The figure also demonstrated that

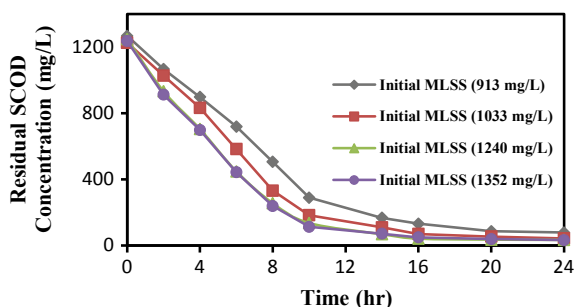


Fig. 3 SCOD removal profile during carbon oxidation study in batch reactor for different initial MLSS in the reactor [Initial SCOD concentration = 1250 ± 50 mg/L]

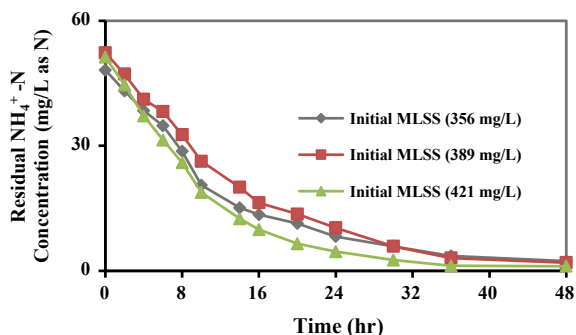


Fig. 4 Ammonia nitrogen concentration level during nitrification for different initial MLSS concentration [Initial $\text{NH}_4^+\text{-N}$ concentration = 50 ± 5 mg/L]

after 10 h of contact time, SCOD removal percentage is marginal and curve becomes asymptotic in nature. After 24 h of contact period, the residual SCOD concentration has been reduced to 50 ± 30 mg/L for all experimental sets.

3.2.2 Time Course Study for Nitrification

Nitrification study has been carried out in a plastic beaker of 1.0 L capacity for about 48 h. The results of the time-course $\text{NH}_4^+\text{-N}$ removal study for different initial MLSS concentrations are shown graphically in Fig. 4. The figure also demonstrates that the ammonia nitrogen level found to be decreasing in nature for an initial value 50 ± 5 mg/L as N, after 24 h, the concentration was found low. The maximum percentage of ammonia removal occurred within 16 h of reaction period, after that, the curve becomes asymptotic nature.

3.2.3 Time Course Denitrification Study

The batch denitrification study was carried out in an aspirator bottle, an anaerobic condition with acclimatized seed and different initial MLSS concentrations of 210–370 mg/L for reduction of nitrate in wastewater having $\text{NO}_3^-\text{-N}$ concentration of 40 ± 2.5 mg/L. The experimental results are plotted in Fig. 5. Figure 5 shows that initially some nitrate was there because the wastewater and the sludge already contained some amounts of nitrate; however, assimilation of nitrate could be occurred when the ammonia concentration was low during that time the nitrate converted to ammonia, which was consumed for biomass growth. Initially, nitrite was predominant, after some time when nitrite concentration reaches a high value, the oxidation of nitrite took place through the activity of nitrobacter and nitrate was formed. Within 10–12 h, maximum amount of nitrate was formed, after that time, the curve becomes nearly horizontal, i.e. no significant accumulation of $\text{NO}_3^-\text{-N}$ has been occurred.

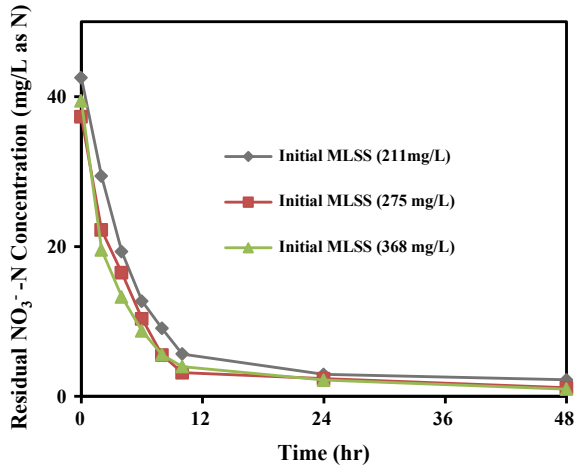


Fig. 5 Nitrate nitrogen concentration level during denitrification for different initial MLSS concentration [Initial NO_3^- -N concentration = 40 ± 2.5 mg/L]

3.3 Kinetics of Batch Reactor

Performance of any reactor would be properly evaluated and optimized by virtue of evaluation of reaction kinetics.

3.3.1 Kinetics for Carbon Oxidation

A linear plot was drawn with respect to the results found from the kinetic study with $(1/S)$, reciprocal of final substrate concentration and $(1/U_C)$, as ordinate value, reciprocal of specific substrate utilization rate. The graph is shown in Fig. 6. The value of half velocity constant (K_s) obtained from a straight-line equation $1/U_C = [(K_s/k)(1/S)] + 1/k$. The value of k is 14.49 per day, whereas K_s is 305.07 mg/L for carbon oxidation kinetic. The values of $(1/\theta)$, reciprocal of reaction time, were again plotted with U_C as shown in Fig. 7 to estimate the yield coefficient (Y) and endogenous decay coefficient (k_d) by applying equation $1/\theta = YU_C - k_d$. The value of Y is 0.509 mg of MLSS/mg of SCOD, whereas k_d is 0.028 per day for carbon oxidation kinetic.

3.3.2 Kinetics for Nitrification

The value of k is 23.25 per day, whereas the K_s is about 30.00 mg/L for nitrification study as shown in Fig. 8. K_s value for nitrification was found to be high than the standard values shown in Metcalf and Eddy Inc. (1991). The value of Y and k_d for

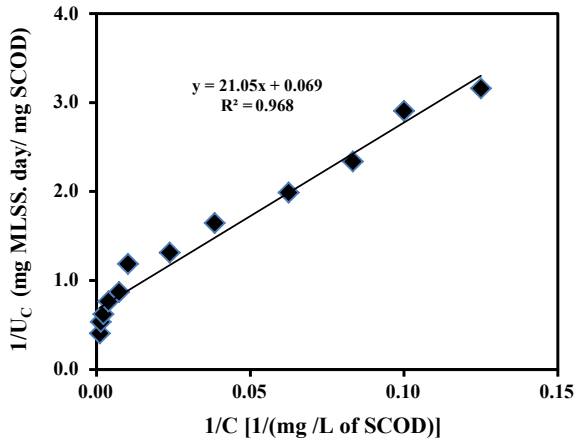


Fig. 6 Substrate utilization kinetics for batch carbon oxidation [SCOD = 1250 ± 50 mg/L]

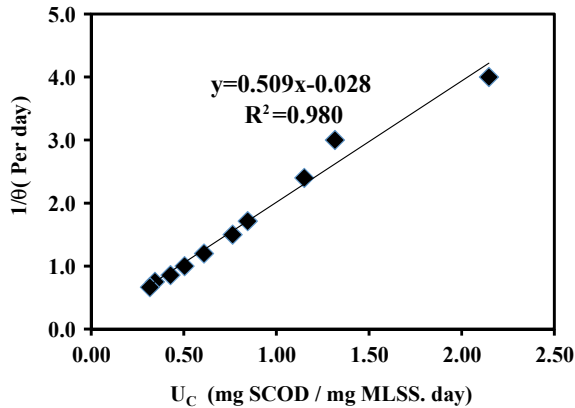


Fig. 7 Microbial growth kinetics for batch carbon oxidation [SCOD = 1250 ± 50 mg/L]

nitrification was found to be 0.273 mg of MLSS/mg of NH₄⁺-N and 0.052 per day, respectively as shown in Fig. 9.

3.3.3 Kinetics for Denitrification

The experimental value of (1/U_{DN}), the reciprocal of NO₃⁻-N utilization rate were plotted against (1/N'), reciprocal of NO₃⁻-N by using equation 1/U_{DN} = (K_s/k)(1/N') + 1/k as shown in Fig. 10. The values of 1/θ were also plotted against U_{DN} as shown in Fig. 11. The values of k, Y and k_d were found to be 0.937 per day, Y0.898 mg MLSS/mg NO₃⁻-N and 0.071 per day, respectively, for denitrification kinetics.

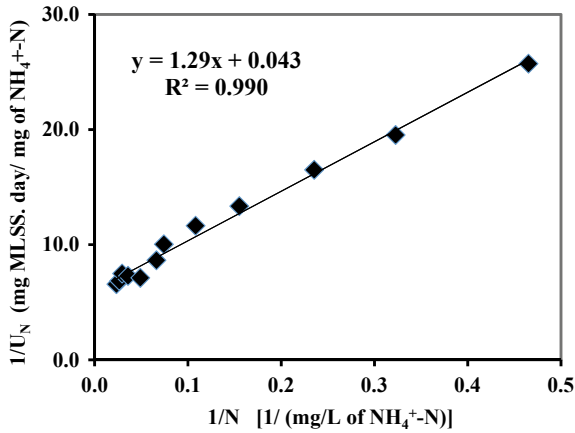


Fig. 8 Substrate utilization kinetics for batch nitrification [NH₄⁺-N = 50 ± 5 mg/L as N]

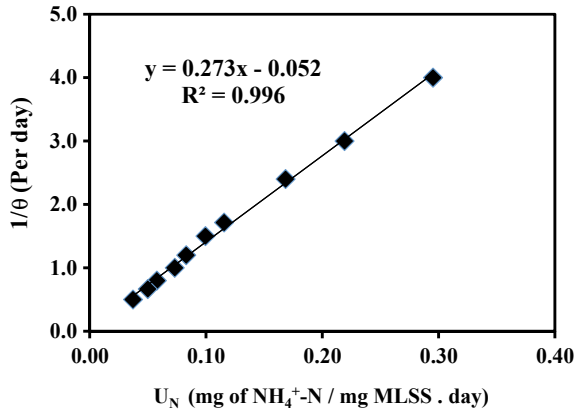


Fig. 9 Microbial growth kinetics for batch nitrification [NH₄⁺-N = 50 ± 5 mg/L as N]

4 Conclusion

Kinetic coefficients evaluated through experiments showed that the values were corroborated with those obtained by earlier researchers. The batch study data exhibited that both COD and nitrogen removal took place by the mixed bacterial culture grown in the laboratory under aerobic and anoxic conditions. The constants to be used for design of a practical aerobic reactor utilizing the kinetic values.

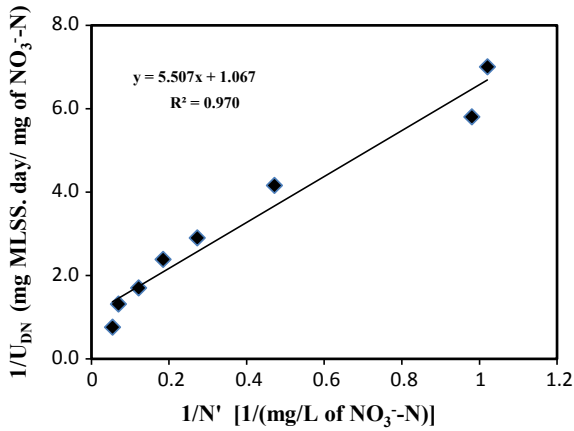


Fig. 10 Substrate utilization kinetics for batch denitrification [NO₃⁻-N = 40 ± 2.5 mg/L]

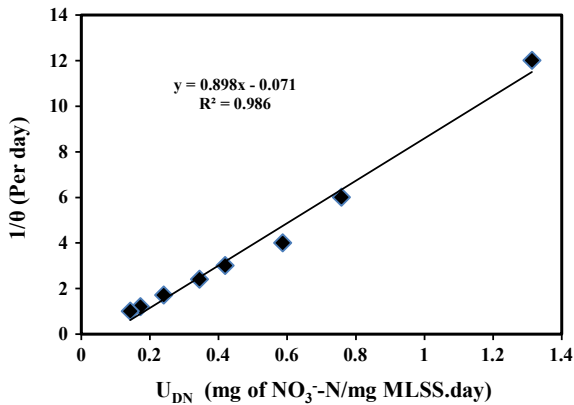


Fig. 11 Microbial growth kinetics for batch denitrification [NO₃⁻-N = 40 ± 2.5 mg/L]

Compliance With Ethical Standards Informed Consent Wastewater samples were periodically collected from the plant premises of M/S Meghna Dairy located at Sarisha, South 24 Parganas, West Bengal, India. Necessary permission and consent have been given by the plant authority for carrying out research investigation and academic pursuit not for any commercial/consultancy purpose. This study was endorsed and approved as master degree dissertation thesis by the Jadavpur University. All kinds of necessary consent were obtained from all individuals participated, including authors in the present study.

Ethical Approval This investigation does not contain any event with involving human participants or animals performed by any of the authors.

Conflict of Interest The authors declare that they have no conflict of interest.

References

- APHA, AWWA, WEF (1998) Standard methods for the examination of water and wastewater, 20th edn. Washington, D.C, USA
- Chaiudhari DH, Dhoble RM (2010) Performance evaluation of effluent treatment plant of dairy industry. *Curr World Environ* 5(2):373–378. <https://doi.org/10.12944/CWE.5.2.26>
- Deshannavar UB, Basavaraj RK, Naik NM (2012) High rate digestion of dairy industry effluent by upflow anaerobic fixed-bed reactor. *J Chem Pharm Res* 4(6):2895–2899
- Kargi F, Dincer AR (1997) Biological treatment of saline wastewater by fed-batch operation. *J Chem Technol Biot* 69:167–172. [https://doi.org/10.1002/\(SICI\)1097-4660\(199706\)69:2<167::AID-JCTB696>3.0.CO;2-C](https://doi.org/10.1002/(SICI)1097-4660(199706)69:2<167::AID-JCTB696>3.0.CO;2-C)
- Metcalf and Eddy Inc. (1991) Wastewater engineering: treatment and reuse, 3rd edn. McGraw-Hill Ltd., Singapore
- Pachpute AA, Kankal SB, Jadhav MV (2014) Use of artificial wetlands for treatment of dairy industry waste water for analysis of BOD and COD. *Int J Sci Eng Res* 2(6):38–41
- Tripathi BD, Upadhyay AR (2003) Dairy effluent polishing by aquatic macrophytes. *Water Air Soil Pollut* 143(1/4):377–385
- Vourch M, Balannec B, Chaufer B, Dorange G (2008) Treatment of dairy industry wastewater by reverse osmosis for water reuse. *Desalination* 219(1/3):190–202

Sustainable Energy

Optimization of TiO₂–KMnO₄ Composites with Natural Dyes for Solar Cell Application



Shyamal Datta and Subhasis Roy

Abstract Present study aimed to develop DSSC solar cell based on KMnO₄–TiO₂ composite active layer. To prepare KMnO₄–TiO₂ paste composite, the mixture of KMnO₄–TiO₂ powders was dispersed into a binder (benzyl alcohol). Uniform films of KMnO₄–TiO₂ composite were successfully prepared on the FTO glass substrate by doctor blade method. Different weight percentages of 0, 2, 6, and 10 wt% of KMnO₄ in TiO₂ were prepared for thin-film deposition on FTO substrate. Then the extracted natural dyes from *Mirabilis Jalapa* flower were successfully deposited on the coated films that act as light-harvesting materials. Optical properties, surface morphology, and crystal structure were investigated by UV–vis spectroscope, Scanning Electron Microscope (SEM), and X-ray diffraction (XRD). An electrolyte containing iodide/triiodide (I[−]/I₃[−]) was used to transport for redox mediator between two electrodes. This working electrode was assembled into a sandwich with graphite counter electrode. The performance of these cells was tested under simulated AM 1.5G solar illumination using 100 mW/cm² power. The highest optimized efficiency of 2.04% was achieved for 10 wt% KMnO₄ in TiO₂ composite films, which conclude that highest amount of MnO^{4−} consumed in TiO₂ matrix.

Keywords Thin film · Solar cell · Composite layer · Doping

1 Introduction

Solar energy is one of the clean and green energies that is abundant and easily can be converted to electricity by a solar photovoltaic cell. The first-generation solar cell was basically made with monocrystalline or polycrystalline of silicon wafer (Moyez and Roy 2018). Then second-generation solar cells came with its thin-film architecture and made with mainly amorphous silicon. A dye-sensitized solar cells (DSSCs) are considered as the third-generation solar cell that first fabricated invented

S. Datta · S. Roy (✉)

Department of Chemical Engineering, University of Calcutta, 92 A. P. C. Road, Kolkata 700009, India

e-mail: srchemengg@caluniv.ac.in

© Springer Nature Singapore Pte Ltd. 2021

D. Ramkrishna et al. (eds.), *Advances in Bioprocess Engineering and Technology*,

Lecture Notes in Bioengineering,

https://doi.org/10.1007/978-981-15-7409-2_39

by professor Michael Graetzel and it showed new direction (Ludin et al. 2014). This DSSC technology has attracted many researchers due to low-cost, easy fabrication process (Nair et al. 2012). Typically, a DSSC consists of one working electrode, dye, electrolyte, and a counter electrode. Titanium dioxide (TiO_2) is commonly used for layering on the working electrode and a sensitized adsorbed into the TiO_2 used to trap the sunlight and excite the TiO_2 molecules. An electrolyte containing iodide/triiodide is used as a redox mediator between two electrodes. TiO_2 is used in layering on the working electrode as it is chemically stable, nontoxic, and abundantly available. But TiO_2 has high bandgap (e.g. 3.6 eV) and absorbs a small fraction of solar light spectrum (Ye et al. 2015). Bandgap reduction is possible by adding other lower bandgap material with TiO_2 . The main objective of this research is to improve the efficiency of DSSC by adding KMnO_4 with TiO_2 on the active layer of the working electrode.

In this paper, different weight percentages of KMnO_4 in TiO_2 composite films were prepared and deposited on the conductive side of the FTO glass by the doctor blade method. Optical properties, surface morphology, and crystal structure were investigated by UV–vis spectroscope, scanning electron microscope (SEM), and X-ray diffraction (XRD). Moreover, the performance of the DSSC was tested under AM 1.5G solar illumination of having light intensity 100 mW/cm^2 .

2 Experimental Details

2.1 Materials

All the chemicals used in this experiment were purchased from Sigma-Aldrich, India.

2.2 Preparation of Natural Dye

Fresh *Mirabilis Jalapa* flower of 5 g was placed in 50 ml of ethanol and the mixed solution was heated up to $80 \text{ }^\circ\text{C}$ for 10 min to extract light-sensitive dye molecules. The liquor was then strained through a filter paper (200 nm) to obtain pure dye.

2.3 Preparation of the Working Electrodes

FTO glass having an area of $2 \times 1 \text{ cm}^2$ was washed with deionized water and then with ethanol. KMnO_4 – TiO_2 composite layer around 2000 nm was prepared by adding TiO_2 paste containing 20 wt% titanium dioxide, 65 wt% benzyl alcohol, and 15 wt% deionized water with KMnO_4 and deposited on the conductive side of the

FTO glass by the doctor blade method with an active area of $1 \times 0.5 \text{ cm}^2$. Then the FTO glasses were sintered at 450 °C for 1.5 h. This sintered FTO glasses coated with KMnO₄-TiO₂ films were immersed in the synthesized dye for 1 h. After heating around 80 °C, these films were gently washed in ethanol to remove any unadsorbed dye.

2.4 Preparation of the Graphite Counter Electrode

Graphite powder of 1.5 g is mixed with 0.1 g of ethyl cellulose and 10 g of terpineol was added into it to make a graphite paste for layering on the conductive side of the FTO. Graphite paste was deposited by the doctor blade method similarly like the working electrode fabrication process. Then the counter electrode was placed on hotplate keeping the conductive surface top at a temperature 90 °C for drying. When the paste was dried, it was sintered at 450 °C for 1 h.

2.5 Assembly of the DSSC

The working electrode and the graphite counter electrode were assembled into a sandwich-like structure. The electrolyte solution was added to the active area of the working electrode. Once the material of the working electrode absorbs the electrolyte, it was assembled with a counter electrode keeping the two conductive sides of the electrodes facing and hold this architecture with two binder clips. Figure 1 shows a schematic of the DSSC.

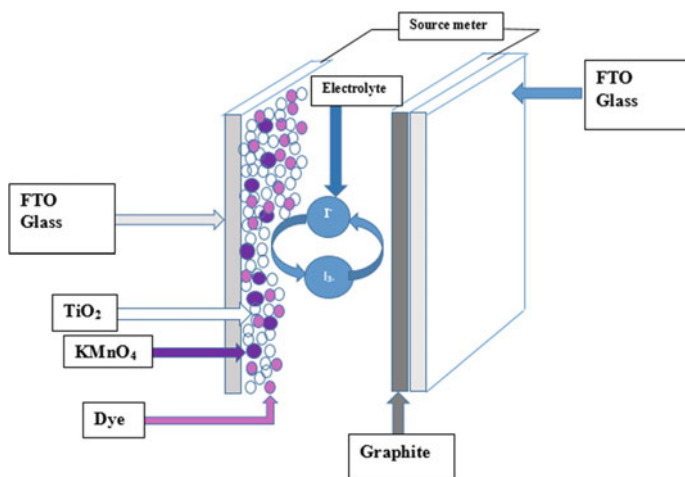


Fig. 1 Schematic of the DSSC

2.6 Characterization and Measurement

The optical properties of the films of $\text{KMnO}_4\text{-TiO}_2$ were observed by UV–vis spectroscope (Hitachi Spectrophotometer U-4100, Japan). The surface morphologies of the $\text{KMnO}_4\text{-TiO}_2$ films were investigated by scanning electron microscope (Zeiss EV 018, USA). The crystal structure of the $\text{KMnO}_4\text{-TiO}_2$ films was characterized using XRD (XPert PRO, USA) with a $\text{CuK}\alpha$ source (1.54 Å). Finally, all fabricated cell's electrical performance has been tested under simulated AM 1.5G solar illumination using 100 mW/cm^2 and this electrical measurement was done by a Keithley 2602A source meter (Keithley Instruments, USA).

3 Results and Discussion

SEM images of $\text{KMnO}_4\text{-TiO}_2$ (2, 6, 10 wt%) thin films are shown in Fig. 2. Lower particle size of TiO_2 with the addition of KMnO_4 leads to high adsorption of dye and less scattering of lights. It was observed that the lower particle size of TiO_2 increases the efficiency of the DSSC by forming suitable bandgap.

The chemical composition of the samples was investigated by EDS. EDS peaks at 5.4 keV, 4.31 keV, and 0.43 keV represent the presence of Mn, Ti, and O elements, respectively. The XRD pattern obtained for $\text{KMnO}_4\text{-TiO}_2$ (2, 6, 10 wt%) films are represented in Fig. 3. The strongest peaks 25.32° , 37.82° , 48.08° are corresponding to the plane (101), (004), and (200) of TiO_2 . It was observed from the figure that increase in the KMnO_4 percentage would decrease the d -spacing of the TiO_2 lattice plane.

The optical bandgap of all the samples was calculated by using Tauc equation from Fig. 4a (Hasan et al. 2010)

$$\alpha h\nu = A(h\nu - E_g)^n \quad (1)$$

where E_g is the optical energy gap, $n = 1/2$ for direct bandgap, which depends on the nature of transition and $h\nu$ is the photon energy (Mai et al. 2009). A graph between $(\alpha h\nu)^n$ versus $h\nu$ was plotted for bandgap calculation in Fig. 4b. It was observed that TiO_2 pure, $\text{KMnO}_4\text{-TiO}_2$ (2, 6, 10 wt%) film samples have approximately 3.6, 1.9, 1.7, and 1.45 eV.

Bandgap respectively which are the evidences of that the energy gap decreases with the increasing of KMnO_4 percentage in the $\text{KMnO}_4\text{-TiO}_2$ mixture. Figure 5a represents the current density–voltage ($J\text{-}V$) curve and (b) power–voltage curve of $\text{KMnO}_4\text{-TiO}_2$ (0, 2, 6, 10 wt%), which was tested under simulated AM 1.5G solar illumination having light intensity of 100 mW/cm^2 . From the tabulated data, it was found that the addition of KMnO_4 in the TiO_2 increases the photocurrent density as well as the overall efficiency of the DSSC (Table 1).

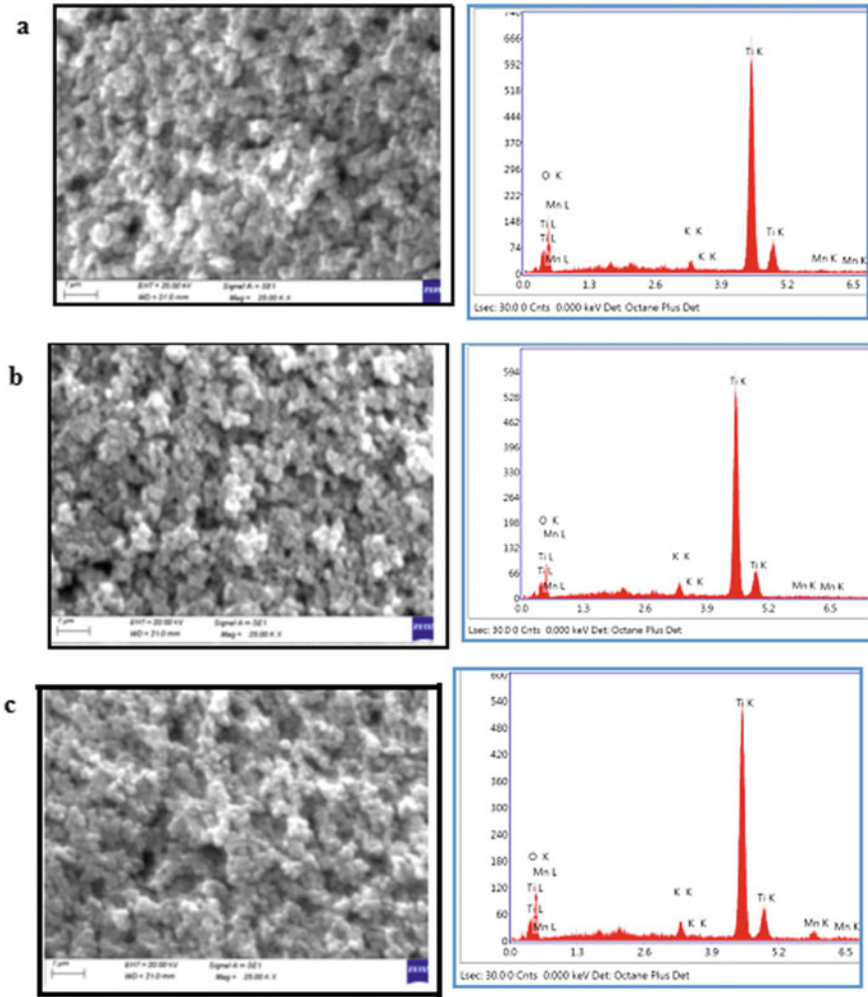


Fig. 2 SEM images and EDS result of the **a** KMnO₄-TiO₂ 2 wt%, **b** KMnO₄-TiO₂ 6 wt%, **c** KMnO₄-TiO₂ 10 wt%

4 Conclusion

KMnO₄-TiO₂ compact layers were successfully deposited on the conductive FTO glasses with a variable weight ratio. The addition of KMnO₄ in TiO₂ leads to minimizing the bandgap of TiO₂ and this lower bandgap is responsible to increase the performance of DSSC. Experimental results show that adding material like KMnO₄ in semiconductor increase more light-harvesting property due to more electron to flow. It was also observed that the optimized percentage of KMnO₄ doping enhances the electron conductivity of the composite thin film by shifting the conduction band

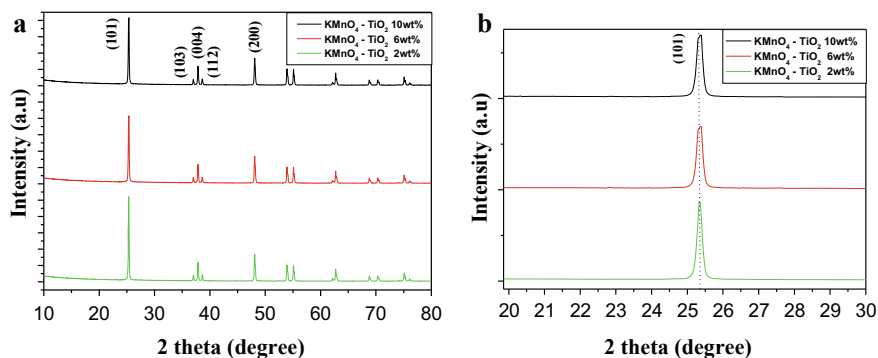


Fig. 3 XRD pattern of **a** $\text{KMnO}_4\text{-TiO}_2$ (2, 6, 10 wt%) **b** Shifting of d -space for $\text{KMnO}_4\text{-TiO}_2$ (2, 6, 10 wt%)

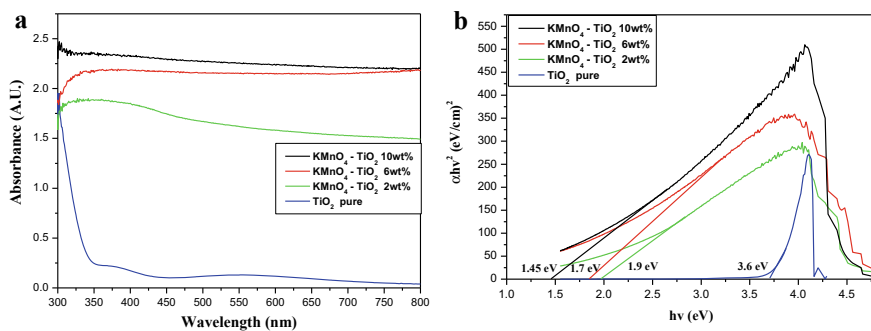


Fig. 4 **a** Absorbance–wavelength plot $\text{KMnO}_4\text{-TiO}_2$ (0, 2, 6, 10 wt%) **b** Tauc's plot of $\text{KMnO}_4\text{-TiO}_2$ (0, 2, 6, 10 wt%)

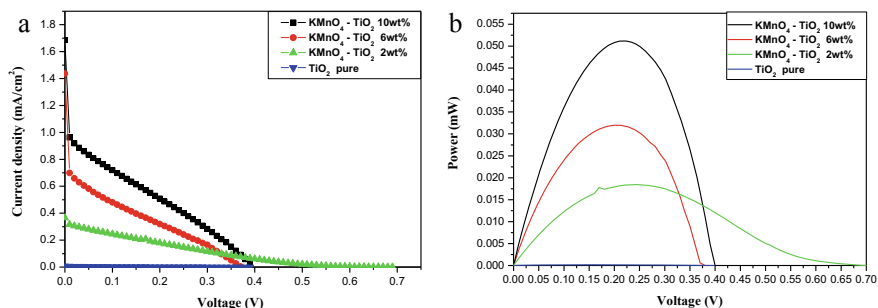


Fig. 5 **a** $J\text{-}V$ curve of $\text{KMnO}_4\text{-TiO}_2$ (0, 2, 6, 10 wt%) **b** $P\text{-}V$ curve of $\text{KMnO}_4\text{-TiO}_2$ (0, 2, 6, 10 wt%) DSSC cell

Table 1 Tabulated form of photovoltaic parameters of DSSCs with different wt% of KMnO₄ in KMnO₄-TiO₂ composite thin layer

Materials for photoanode	V_{oc} (V)	J_{sc} (mA cm ⁻²)	FF (%)	Efficiency (%)	P_{max} (mW)
Pure TiO ₂	0.39	0.007	10.78	0.006	0.000166
KMnO ₄ -TiO ₂ 2 wt%	0.69	0.364	14.63	0.736	0.018427
KMnO ₄ -TiO ₂ 6 wt%	0.37	1.437	15.36	1.633	0.040843
KMnO ₄ -TiO ₂ 10 wt%	0.39	1.685	15.57	2.047	0.051192

The active area of all the cells was 0.5 cm²

lower direction. Simultaneously, suitable doping increases the power output. It was also observed that heavy doping leads to the metallic property of the composite thin film which resulting in leakage formation. The optimized KMnO₄ 10 wt% in TiO₂ thin film based DSSC reaches the current density maximum. This cell also reaches maximum FF and PCE due to the highest amount of electron-hole generation in TiO₂ matrix. It was noted that due to the leakage problem, further increasing of KMnO₄ amount minimizes the efficiency of the fabricated cell. This electronic phenomenon of KMnO₄-TiO₂ compact layer will open new interests and opportunities in the field of solar cell technology. Further modification of the counter electrode with platinum is in progress to extract better performance of the DSSC.

Acknowledgements This work was supported by grants funded by the Department of Science and Technology (DST) under the Scheme “Innovation, Technology Development and Deployment” Central, Government of India through Mission Innovation Programme DST (DST/TMD(EWO)/IC5-2018/06(G)).

References

- Hasan M, Haseeb A, Saidur R, Masjuki H, Hamdi M (2010) Influence of substrate and annealing temperatures on optical properties of RF-sputtered TiO₂ thin film. *Opt Mater* 32:690–695. <https://doi.org/10.1016/j.optmat.2009.07.011>
- Ludin N, Mahmoud A, Mohamad A (2014) Review on the development of natural dye photosensitizer for dye-sensitized solar cells. *Renew Sust Energy Rev* 31:386–396. <https://doi.org/10.1016/j.rser.2013.12.001>
- Mai L, Huang C, Wang D, Zhang Z, Wang Y (2009) Effect of C doping on the structural and optical properties of sol-gel TiO₂ thin films. *Appl Surf Sci* 255:9285–9289. <https://doi.org/10.1016/j.apsusc.2009.07.027>
- Moyez A, Roy S (2018) Dual-step thermal engineering technique: a new approach for fabrication of efficient CH₃NH₃PbI₃-based perovskite solar cell in open air condition. *Sol Energy Mater Sol Cells* 185:145–152. <https://doi.org/10.1016/j.solmat.2018.05.027>
- Nair V, Balakrishnan A, Subramanian K, Anu A, Asha A, Deepika B (2012) Effect of TiO₂ nanotube length and lateral tubular spacing on photovoltaic properties of back illuminated dye sensitized solar cell. *Bull Mater Sci* 35:489–493. <https://doi.org/10.1007/s12034-012-0323-5>

Ye M, Wen X, Wang M, Locozzia J, Zhang N, Lin C, Lin Z (2015) Recent advances in dye-sensitized solar cells: from photoanodes, sensitizers and electrolytes to counter electrodes. *Mater Today* 18:155–162. <https://doi.org/10.1016/j.mattod.2014.09.001>

Production of Hydrogen by Steam Reforming of Methanol Over Novel Nano-Nickel Oxide-Based Catalyst



Barnali Bej, N. C. Pradhan, and Swati Neogi

Abstract The present investigation deals with the study of steam reforming of methanol for production of hydrogen over alumina (Al_2O_3)-supported nano-nickel oxide (NiO) in silica catalyst. Nano-NiO in silica was synthesized by sol-gel method. The catalyst was characterized using XRD, SEM, TEM, and BET surface area analyzer. The influence of catalyst activation temperature, reforming temperature, steam to methanol ratio, space velocity on methanol conversion, and product selectivity were studied to observe the contribution of methanol steam reforming, methanol decomposition, and water-gas shift reaction toward the yield of H_2 . The optimum process parameters established were reaction temperature $425\text{ }^\circ\text{C}$, steam to methanol molar ratio 1.8:1, and space velocity 0.14 kmol of methanol fed per kg catalyst per hour, and under these conditions, maximum 95% conversion of methanol was achieved. The comparative study of catalytic activity revealed that developed indigenous catalyst is superior over other commercial catalysts.

Keywords Hydrogen production · Steam reforming · Sol-gel method · Nano-catalyst · Calcination temperature · Water-gas shift reaction

1 Introduction

Increasing interest in hydrogen production for fuel cell-powered automobiles to avoid environmental pollution is a great challenge in the construction of a hydrogen-oriented society. Recently, global efforts are underway to minimize the emissions

B. Bej (✉)

Department of Chemical Engineering, Haldia Institute of Technology, Haldia, India
e-mail: bejbarnali@gmail.com

N. C. Pradhan · S. Neogi

Department of Chemical Engineering, Indian Institute of Technology Kharagpur, Kharagpur, India
e-mail: npc@che.iitkgp.ernet.in

S. Neogi

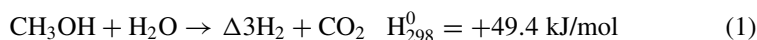
e-mail: swati@che.iitkgp.ernet.in

© Springer Nature Singapore Pte Ltd. 2021

D. Ramkrishna et al. (eds.), *Advances in Bioprocess Engineering and Technology*,
Lecture Notes in Bioengineering,
https://doi.org/10.1007/978-981-15-7409-2_40

of pollutants such as NO_x , SO_x , and greenhouse gases. In this context, hydrogen is considered as the best fuel because of its high fuel density and no emission of pollutants when it burns. It also offers high efficiency when used in polymer electrolyte membrane (PEM) fuel cells (Patel and Pant 2006). Fuel cell technology, one of the most promising sources of power generation, offers highly efficient conversion of chemical energy into electrical energy. However, hydrogen fuel cell as well as fuel cell vehicle presents some technological limitations with generation, storage, transportation, and distribution of pure H_2 . For safety, fuel cell vehicle would run on onboard H_2 generation by reforming of liquid fuel.

Among the liquid fuels to be reformed, methanol has been preferred as an appropriate source of hydrogen because of its low cost, high availability, low boiling point, and high ratio of H/C (4:1). Moreover, it can be converted to hydrogen at relatively low reforming temperature. It contains no C–C bonds, which in turn drastically reduces the risk of coke formation and catalyst fouling and makes its reactions energetically favorable. Among the various processes of hydrogen production, steam reforming of methanol (SRM) seems to be more attractive one to produce hydrogen as it produces theoretically higher H_2 yield and syngas with highest H_2/CO ratio.



A lot of research works have been performed on SRM over Cu-based catalyst, especially Cu/Zn or Cu/Zn/Al mixed oxide in previous years due to their high activity and selectivity, but their heat and oxidation resistance are poor. Therefore, deactivation of Cu-containing catalysts occurs at relatively low reforming temperature due to sintering and partial oxidation of Cu particles. To avoid this problem, efforts have been made to investigate the appropriate catalyst and operating conditions for SRM. Recently, several research works on precious metal catalysts and nanocatalysts in SRM show improved activity (Abrokwah et al. 2016; Bagherzadeh and Haghghi 2017; Deshmane et al. 2015a, b; Diaz-Perez et al. 2018; Kim et al. 2017; Pedrero et al. 2017; Lei et al. 2018; Tahay et al. 2018; Tian et al. 2017).

But less research works have been published on Ni-containing catalyst used in SRM. Some reports have been concentrated on the use of Ni/Al layered double hydroxides (LDH)-derived catalysts and nano-Ni catalyst for SRM because Ni is cheap and very active catalyst in steam reforming reactions (Lu et al. 2017; Qi et al. 2009; Shetty et al. 2007). The catalysts exhibited better stability and activity with high selectivity for CO_2 and H_2 and low level of CO and CH_4 depending on the experimental condition and pretreatment atmosphere.

The objectives of the present study include (i) experimental investigations to study the effects of process parameters such as reaction temperature, steam to methanol molar ratio, space velocity on catalytic activity, and product selectivity over synthesized alumina-supported nano-nickel oxide catalyst highly dispersed in silica and (ii) comparative study of activity of synthesized catalyst with commercial catalysts.

2 Materials and Methods

NiO/SiO₂ nanocomposite was prepared by sol–gel technique using nickel nitrate hexahydrate [Ni (NO₃)₂, 6H₂O, Merck] as precursor and tetra ethyl orthosilicate (TEOS, Merck) as silica matrix-forming agent with ethanol (absolute, 99%, Merck) solution. A certain amount of TEOS and ethanol solution was stirred using magnetic stirrer at room temperature. Nickel nitrate with intended Ni loading (5, 7, 10, 12.5, 15 wt% in the catalyst) dissolved in the aqueous ethanol solution was added slowly to the silica sol with constant stirring. The final solution was stirred at room temperature for about 5–6 h and allowed to age for 1 week. The obtained gel was dried in hot air oven at 110 °C for 24 h to remove water and other volatile compounds. Then the dried gel was calcined at 400 °C.

To prepare alumina-supported NiO/SiO₂ catalyst, alumina (SISCO), NiO–SiO₂, and bentonite powder (as binder, Merck) was mixed in an appropriate proportion and then the mixture was transformed into extrudates. The extrudates are finally dried in hot air oven at 110 °C. The catalysts were prepared with different Ni loadings of 5, 7, 10, 12.5, and 15 wt%.

2.1 Experimental Procedure

Steam reforming reaction was carried out in a fixed bed tubular reactor (10 mm inner diameter) placed inside a cylindrical furnace. The reactor was loaded with catalyst mixed with inert particles, so that the bed height was maintained at 60 mm. The remainder of the reactor was filled with inert ceramic material. The catalyst was reduced as well as activated by heating at 550 °C with the flow of hydrogen for 4 h. The thermocouple inserted into the thermowell of reactor recorded the catalyst bed temperature. After catalyst activation, the reaction temperature was fixed at a desired temperature and catalytic steam reforming reaction was performed at atmospheric pressure by introducing the flow of methanol–water mixture. The feed mixture was vaporized through the preheater before entering reactor inlet. The reactor outlet stream was passed through a condenser for separation of condensable components in the gas–liquid separator.

The product gas stream flow rate was measured using a wet gas meter. The gas mixture was periodically sent to gas–liquid chromatography (Model: Chemito GC 1000 DPR) for analysis using thermal conductivity detector (TCD) with packed. Nitrogen was used as carrier gas.

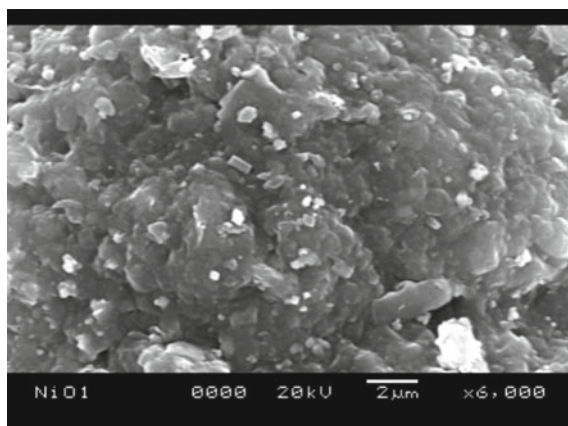


Fig. 1 SEM image of alumina-supported nano-NiO/SiO₂ before reaction

3 Results and Discussion

3.1 Catalyst Characterization

The detailed characterization results of the synthesized catalyst (XRD, SEM, TEM, BET surface area analysis) and optimum catalyst have been reported in the previous publication (Bej et al. 2013). The variation of physicochemical properties of synthesized catalysts with different calcination temperatures and different percent of Ni loadings has also been reported in the previous publication (Bej et al. 2013). The optimum catalyst has been shown as 10% Ni loading (actual Ni loading 8.84%) calcined at 400 °C. The BET surface area of the developed catalyst was measured at 268 m²/gm.

The scanning electron micrograph (SEM) shows that nickel oxide is uniformly dispersed in the catalyst. Figure 1 reveals the surface morphology of synthesized alumina-supported nano-NiO/SiO₂ catalyst. Figure 2 shows the surface morphology of the catalyst after reaction.

3.2 Effect of Temperature

In order to study the influence of reforming temperature on catalytic behavior of Al₂O₃-supported NiO/SiO₂ catalyst in SRM, experiments were carried out at different temperatures, ranging from 225 to 450 °C using steam to methanol molar ratio 1.4:1 and space velocity of 0.16 kmol methanol per kg catalyst per h. Figure 3 shows the effect of temperature on methanol conversion. As is seen from Fig. 3, conversion of methanol increases rapidly with an increase in temperature and almost

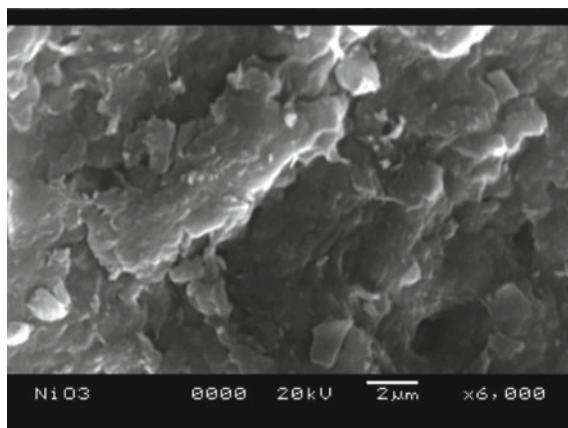


Fig. 2 SEM image of alumina-supported nano-NiO/SiO₂ after reaction (450 °C)

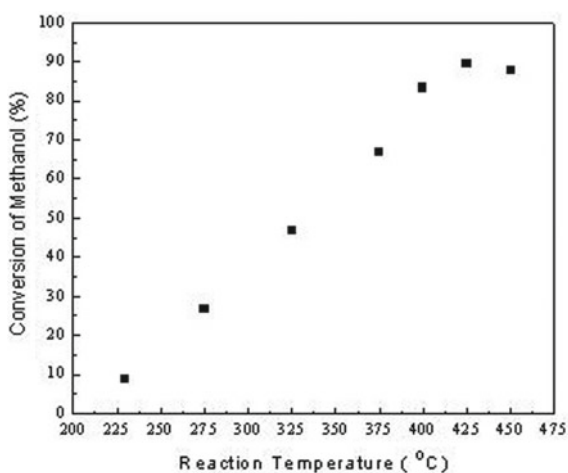
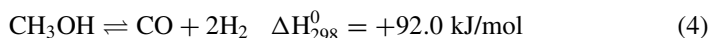
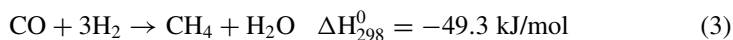
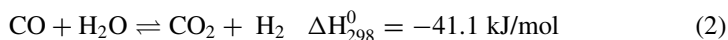


Fig. 3 Effect of temperature on conversion of methanol. Condition: H₂O: CH₃OH (molar), 1.4:1; space velocity, 0.16 kmol/kg catalyst h

89.3% conversion is obtained at 425 °C. The conversion of methanol decreases slightly beyond 425 °C may be due to the less stability of the catalyst at higher temperature. From our previous publication (Bej et al. 2013), it is reported that the crystallite size increases slightly due to the sintering of Ni particle at higher calcination temperature, and as a result, BET surface area decreases due to the blockage of pores. But the catalyst activity does not affect much up to 450 °C as same Ni loading presents in the catalyst. Therefore, catalyst is stable in the temperature range up to 450 °C. No intermediate products were detected in the product stream over the range of temperature studied.

The dry reformat stream contains gas mixture of H_2 , CO , CO_2 , and CH_4 , and selectivity of products dramatically changes with temperature. The experimental results predict the occurrence of water–gas shift reaction (WGS) (Eq. 2), methanation reaction (Eq. 3), reverse water–gas shift reaction, and methanol decomposition reaction (Eq. 4).



3.3 Effect of Feed Composition

As the highest conversion was obtained at 425 °C to find the optimum steam to methanol molar ratio, experiments were carried out at different steam to methanol molar ratio at 425 °C temperature and space velocity of 0.16 kmol methanol fed per kg catalyst per h. Figure 4 shows the effect of feed (steam:methanol) molar ratio on methanol conversion. It is evident from Fig. 4 that conversion of methanol increases remarkably with increasing steam to methanol molar ratio in feed, and a maximum 93% methanol conversion was achieved at 1.8:1 steam to methanol molar ratio. It is

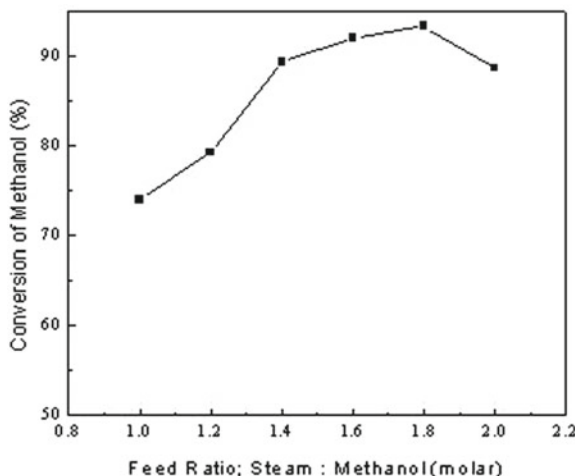


Fig. 4 Effect of feed composition on methanol conversion. Condition: temperature, 425 °C; space velocity, 0.16 kmol/kg catalyst h

clear from the figure that conversion of methanol decreases beyond steam to methanol molar ratio of 1.8:1.

It was observed that in product stream, H_2 selectivity increases gradually with the addition of more steam in feed, indicating the occurrence of WGS reaction. Moreover, suppression of methanation reaction with increasing steam to methanol molar ratio favors the enhancement of H_2 selectivity.

3.4 Effect of Space Velocity

Catalyst activity was found to be dependent on contact time of liquid feed. The reverse of contact time is known as space velocity. Therefore, to find optimum space velocity, catalytic tests were performed in the range from 0.12 to 0.25 kmol of methanol fed per kg catalyst per h by changing the feed flow rate at 425 °C with steam to methanol molar ratio 1.8:1. It is clearly seen from Fig. 5 that initially conversion of methanol is almost constant and then decreases rapidly with increasing space velocity.

Figure 6 illustrates the variation of product selectivity with space velocity. Initially, CO selectivity increases with increase in space velocity while CH_4 selectivity decreases slightly with almost constant selectivity of H_2 and CO_2 , indicating SRM via methanol decomposition becomes more dominant. On the other hand, H_2 selectivity increases significantly with increasing space velocity. This may be due to the occurrence of WGS reaction and steam reforming of methanol simultaneously. Maximum 95% of methanol conversion was obtained at 425 °C with H_2O /methanol ratio 1.8:1 and space velocity of 0.14 kmol of methanol fed per kg catalyst per h.

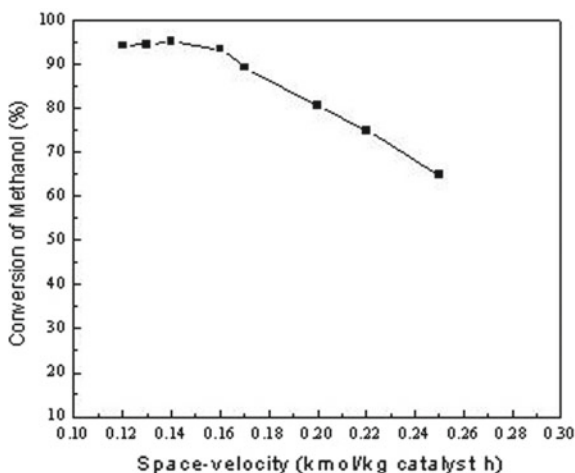


Fig. 5 Effect of space velocity on conversion of methanol. Condition: temperature, 425 °C; H_2O : CH_3OH (molar), 1.8:1

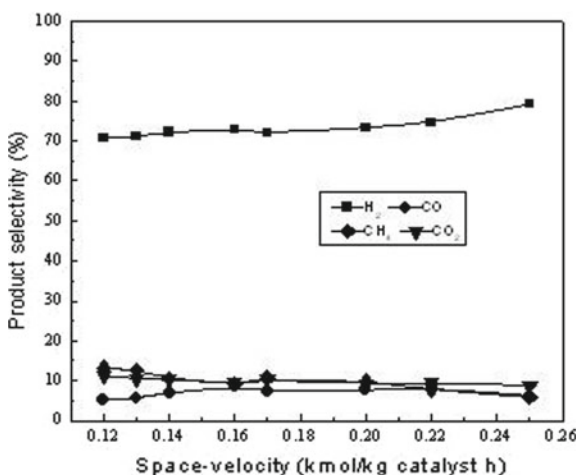


Fig. 6 Effect of space velocity on product selectivity. Condition: same as in Fig. 5

3.5 Activity Comparison with Commercial Catalyst

A comparative evaluation of catalyst activity was made from time on stream study of methanol conversion with commercial Ni-based catalyst, commercial Cu-based catalyst, and Al₂O₃-supported nano-NiO/SiO₂ (prepared) catalyst as shown in Fig. 7. Experiment was performed under optimum operating condition of 425 °C with steam to methanol molar ratio 1.8:1 and space velocity of 0.14 kmol of methanol fed per

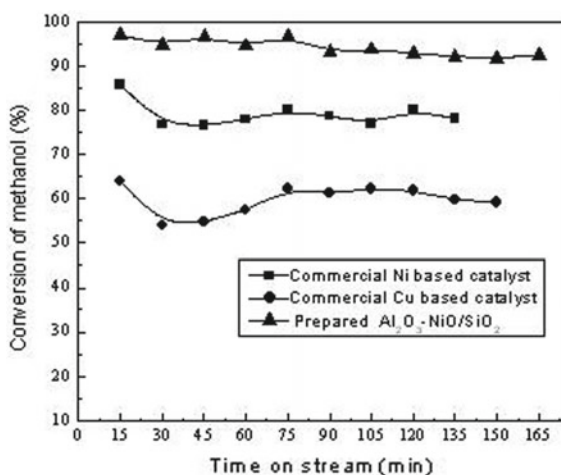


Fig. 7 Comparison of catalyst activity (TOS study). Condition: temperature, 425 °C; H₂O: CH₃OH (molar), 1.8:1; Space velocity, 0.14 kmol/kg catalyst h

kg catalyst per h. It is clear from the figure that higher conversion of methanol was obtained over indigenous nano-Ni-based catalyst and maintained almost constant catalytic activity for certain period of time (165 min) than other commercial catalyst. Moreover, at initial stage, methanol conversion drops rapidly due to extensive coke formation on catalyst surface for commercial Ni and Cu catalyst. Therefore, the prepared nano-NiO/SiO₂-Al₂O₃ catalyst is the best one over the commercial catalysts tested.

4 Conclusion

Sol-gel-derived nano-NiO/SiO₂-supported on alumina was prepared and successfully used in steam reforming of methanol. The catalyst containing 8.84% Ni calcined at 400 °C was observed to be optimum catalyst. The developed catalyst showed high catalytic activity and stability during the course of reaction. Extensive experimental investigations on SRM have been carried out over wide range of parameters such as reforming temperature, feed ratio, and space velocity. The distribution of dry reformate was also found to be significantly affected by process parameters. The optimum condition of SRM in terms of conversion was established at 425 °C with steam to methanol molar ratio of 1.8:1 and space velocity of 0.14 kmol of methanol fed per kg catalyst per h. Under this condition, conversion of methanol was about 95% and yield of hydrogen was 3 mol of H₂ per mole of methanol reacted.

Acknowledgements Authors are thankful to all the technical staff of the Department of Chemical Engineering of the Indian Institute of Technology, Kharagpur for their cooperation during execution of the research work.

References

- Abrokwah RY, Deshmane VG, Kuila D (2016) Comparative performance of M-MCM-41 (M: Cu, Co, Ni, Pd, Zn and Sn) catalysts for steam reforming of methanol. *J Mol Catal A Chem* 425:10–20
- Bagherzadeh SB, Haghghi M (2017) Plasma-enhanced comparative hydrothermal and coprecipitation preparation of CuO/ZnO/Al₂O₃ nanocatalyst used in hydrogen production via methanol steam reforming. *Energy Convers Manage* 142:452–465
- Bej B, Pradhan NC, Neogi S (2013) Production of hydrogen by steam reforming of methane over alumina supported nano-NiO/SiO₂ catalyst. *Catal Today* 207:28–35
- Diaz-Perez MA, Moya J, Serrano-Ruiz JC, Faria J (2018) Interplay of support chemistry and reaction conditions on copper catalyzed methanol steam reforming. *Ind Eng Chem Res* 57:15268–15279
- Deshmane VG, Owen SL, Abrokwah RY, Kuila D (2015a) Mesoporous nanocrystalline TiO₂ supported metal (Cu, Co, Ni, Pd, Zn, and Sn) catalysts: effect of metal-support interactions on steam reforming of methanol. *J Mol Catal A Chem* 408:202–213
- Deshmane VG, Abrokwah RY, Kuila D (2015b) Synthesis of stable Cu-MCM-41 nanocatalysts for H₂ production with high selectivity via steam reforming of methanol. *Int J Hydrogen Energy* 40:10439–10452

- Kim W, Mohaideen KK, Seo DJ, Yoon WL (2017) Methanol-steam reforming reaction over Cu-Al-based catalysts derived from layered double hydroxides. *Int J Hydrogen Energy* 42:2081–2087
- Lei Y, Luo Y, Li X, Lu J, Mei Z, Chen WPR, Chen K, Chen D, He D (2018) The role of samarium on Cu/Al₂O₃ catalyst in the methanol steam reforming for hydrogen production. *Catal Today* 307:162–168
- Lu J, Li X, He S, Han C, Wan G, Lei Y, Chen R, Liu P, Chen K, Zhang L, Luo Y (2017) Hydrogen production via methanol steam reforming over Ni-based catalysts: influences of Lanthanum (La) addition and supports. *Int J Hydrogen Energy* 42:3647–3657
- Patel S, Pant KK (2006) Influence of preparation method on performance of Cu(Zn)(Zr)-alumina catalysts for the hydrogen production via steam reforming of methanol. *J Porous Mater* 13:373–378
- Pedrero CM, Queiros S, Concepcion P, Mendes A (2017) Innovative ZrO₂-supported CuPd catalysts for the selective production of hydrogen from methanol steam reforming. *Appl Catal B Environ* 203:400–407
- Qi C, Amphlett JC, Peppley BA (2009) H₂ Production via the steam reforming of methanol over NiAl-layered double hydroxide derived catalysts. *Catal Surv Asia* 13:16–21
- Shetty K, Zhao S, Cao W, Siriwardane U, Seetala NV, Kuila D (2007) Synthesis and characterization of non-noble nano-catalysts for hydrogen production in micro-reactors. *J Power Sources* 163:630–636
- Tahay P, Khani Y, Jabari M, Bahadoran F, Safari N (2018) Highly porous monolith/TiO₂ supported Cu, Cu-Ni, Ru, and Pt catalysts in methanol steam reforming process for H₂ generation. *Appl Catal A* 554:44–53
- Tian J, Ke Y, Kong G, Tan M, Wang Y, Lin J, Zhou W, Wan S (2017) A novel structured PdZnAl/Cu fiber catalyst for methanol steam reforming in microreactor. *Renew Energy* 113:30–42

Performance Enhancement of Dye-Sensitized Solar Cell Using Extracted Photo-Sensitized Organic Molecules in Addition with Dielectric Nanomaterial



Argha Dey, Subhasis Roy, and Sourav Mondal

Abstract This research work illustrates the improvement in performance study of dye-sensitized solar cell (DSSC) in the presence of dielectric nanoparticles coupled with TiO_2 mesoporous film. Lanthanum-doped lead titanate (PLT15) was the chosen dielectric material used for this due to its strong field-effect passivation, screened columbic attraction, back reflector, and recombination inhibitor for solar cell. Natural dye extracted by a three-step drying and grinding process followed by solvent extraction from carrot is, namely, carotene. Postfiltration, the solution underwent through various absorption media for better purification. The synthesized dielectric nanoparticles were introduced into the TiO_2 matrix and coated on the FTO glass substrate by doctor blading technique followed annealing, and then dye depositional process was performed by dipping TiO_2 -PLT15-coated FTO glass in extracted organic dye solution for overnight. UV-Vis, FTIR spectroscopy, and SEM tools were used for the characterization of dyes. Finally the electrical performance of the fabricated cell was analyzed under simulated AM 1.5G solar illumination using 100 mW/cm^2 power.

Keywords Thin film · Dielectric · Natural dyes · Extraction · Nanoparticles

1 Introduction

Sun being the easily available renewable energy resource, energy is cultivated from sunlight. The performance of DSSC is dependent on the photosensitization process within the dyes in presence of mesoporous metal oxide semiconductors having

A. Dey · S. Roy (✉) · S. Mondal
Department of Chemical Engineering, University of Calcutta, 92 A. P. C. Road, Kolkata 700009,
India
e-mail: srchemengg@caluniv.ac.in

A. Dey
e-mail: deyargha11@gmail.com

S. Mondal
e-mail: mondalsourav939@gmail.com

wide bandgap. This sensitized light plays an important role for generating electrical energy through absorbing light from the sun and transforming it into energy. Among various inorganic dyes, Ru-based complex sensitizer is widely used due to their better photo conversion efficiency and high durability. But it possesses some demerits—their high cost, complicated synthetic routes, and lean towards degradation in presence of water (Zhang et al. 2008). In recent days, using natural pigments in the form of sensitizer for generating electricity has been started due to their various utilities—it is cost friendly as it is occurred naturally and also environmentally friendly (Kay and Graetzel 1993). Presently using of natural organic dyes in DSSC as sensitizer has become a new trend. In one of the previous works extracted, catechins from green tea leaves that have been used as sensitizer in DSSC (Dey et al. 2016) resulted improved photo conversion efficiency. Dey et al. (2017a) describes the photoconversion result of TiO_2 doped with graphene in association with bilayer of CdS. Whereas Dey et al. (2017b) describes the improved conversion efficiency observed for quantum dot solar cell, post addition of synthesized dielectric material lanthanum-doped lead titanate (PLT15).

In this paper, we report the performance improvement of DSSC through addition of synthesized dielectric material within the TiO_2 mesoporous film. The used dielectric material in this work is lanthanum-doped lead titanate (PLT15) due to its various beneficial factors: strong field–effect passivation, screened columbic attraction, back reflector, and recombination inhibitor for solar cell. Additionally, for the sensitization natural dye, carotene was extracted using carrot as rich source. The extraction involved three-step processes. Initially the chopped samples underwent for drying. Further the dried samples were grinded in the form of fine particles and finally the dye solution was prepared in presence of solvent. The fabrication of DSSC was then carried out using synthesized dielectric material within the TiO_2 matrix and hence the performance testing and other characterizations were carried out.

2 Experimental Details

2.1 Synthesis of TiO_2 Nanoparticles

Under continuous stirring of 0.1 M nitric acid solution, 5 ml of titanium isopropoxide (97% Sigma-Aldrich) was added dropwise at room temperature. Soon a white precipitate was generated that was heated at 80 °C. Further, at 1000 rpm stirring was continued for 8 h for achieving peptization. Then, nonpeptized agglomerates were removed through centrifugation at ~ 2000 rpm. Then by adding water to it, the final concentration was obtained as ~ 5 wt%. The solution was transferred to an autoclave. For 12 h, the stainless steel makes autoclave lined with Teflon was heated at 230–250 °C for the desired growth of 10–25 nm particles. Finally, the colloidal suspension was concentrated by employing of heating at 70 °C for 1 h.

2.2 *Synthesis of Dielectric Nanomaterial (PLT15)*

The preparation of 0.25 M lanthanum-doped lead titanate [$\text{Pb}_{0.85}\text{La}_{0.15}\text{TiO}_3$ (PLT15)] precursor sol, the used materials were lead acetate tri-hydrate [$\text{Pb}(\text{CH}_3\text{COO})_2 \cdot 3\text{H}_2\text{O}$] (99.99% Sigma-Aldrich), lanthanum nitrate hexahydrate [$\text{La}(\text{NO}_3)_3 \cdot 6\text{H}_2\text{O}$] (99.999% Sigma-Aldrich), and titanium butoxide [$\text{Ti}(\text{OC}_4\text{H}_9)_4$] (97% Sigma-Aldrich). Initially, lead acetate tri-hydrate and lanthanum nitrate in presence of warm acetic acid codissolving were taken place through rigorous stirring. Another three-neck flask was used that was containing of stoichiometric amount of titanium butoxide that was dissolved in glacial acetic acid (in 1:2 molar ratio) for reducing the moisture sensitivity of the alkoxide precursor. Finally, the prepared chelated sol was added dropwise into the mixed solution of lead acetate tri-hydrate and lanthanum nitrate under continuous stirring for 15–20 min for the preparation of PLT15 precursor sol.

2.3 *Extraction of Carotene*

Carrot has been chosen as raw materials for the extraction of carotene. After grinding the carrot bioparticles, these carrot materials were kept for drying in a hot air oven at 70 °C until they turned completely dried. Further the dried samples underwent for grinding to get fine powdered substance, which was preserved in culture tube. Then, 0.5, 1.0, and 2.0 g dried samples were taken from the powder samples, and further extraction process was carried out by dissolving them into benzene. Postdissolving into the solvent, the solution was allowed for sonication in presence of a bath-type sonicator for 45 min. Then the solution underwent for filtration using filter paper for the separation of undesired suspended particles. Finally, the filtrates were preserved into different culture tubes.

2.4 *Fabrication of Solar Cell*

Initially, the FTO glass substrate (15 Ω/cm , Pilkington) underwent for cleaning using detergent solution, water, and ethanol in an ultrasonic bath. Then the prepared titanium nanoparticles were deposited by means of thin layer of titanium oxide employing spin coating (model: spin NXG-P1, Apex Instruments make) at 3000 rpm for 30 s. Then the coated glass substrate underwent for heating at 450 °C for 30 min for removal of organic materials. After that the commercially available TiO_2 nanopaste coupled with synthesized dielectric nanomaterial (PLT15) was spin-coated followed by annealing. Then the glass substrate was allowed for dipping into the dye solutions for overnight. After 1 day, the glass substrate was subjected to atmospheric heating.

The spiro-OMeTAD (Sigma-Aldrich, 99%) was used as electrolyte and conductive silver paste was used as counter electrode.

2.5 Characterization of Materials and Solar Cells

X-ray diffraction (XRD, Ultima III, Rigaku, Japan) with Cu $K\alpha$ radiation was used for analyzing the crystal structure of the sample. For estimating the morphological characteristics, scanning electron microscopy (model: EVO 18 Special Edition, ZEISS make) was used. The absorption characteristics were analyzed using a HITACHI-make UV/vis spectrometer and Perkin–Elmer-make FTIR spectrophotometer. Finally, the electrical property, photovoltaic current–voltage (PVIV) nature, was analyzed using under simulated standard sunlight (100 mW/cm^2 , AM 1.5G) (model: 2400 High Current Source Meter, Keithley) (Compact 150W Solar Simulator, Zolix Instruments, China).

3 Results and Discussion

3.1 XRD Analysis

Figure 1 indicates the XRD pattern of TiO_2 coupled with PLT15 that was found to be similar in accordance with the reported literature (Dey et al. 2017b). From the XRD pattern, it is prominent that the presence of different planes has been identified having specification of (1 0 0), (1 1 0), (1 1 1), (2 1 0) for dielectric material.

Fig. 1 X-ray diffraction patterns of TiO_2 coupled with dielectric material PLT15

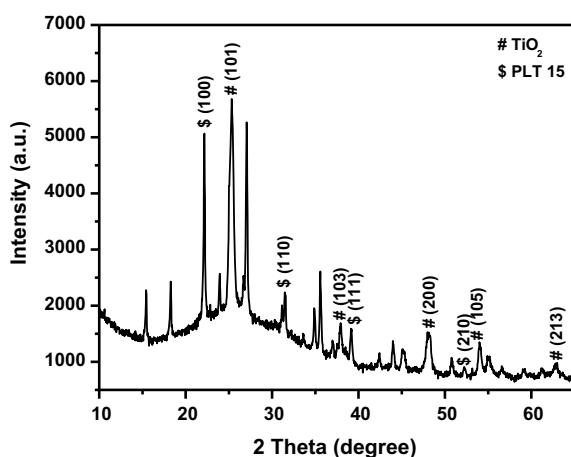
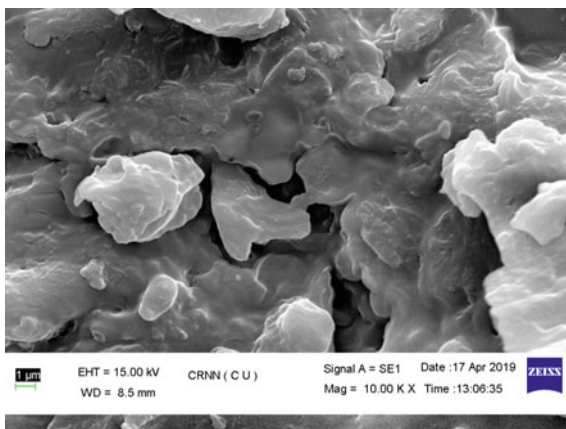


Fig. 2 SEM image of extracted carotene



3.2 Structural Observation

Figure 2 shows the Scanning Electron Microscope (SEM) micrograph of carotene extracted from carrot. From the figure, it is clear that the structure is distributed with small pores.

3.3 UV-Vis Spectroscopic Observation

The absorbance spectrum was obtained within the spectral range of 350–600 nm for carotene that was recorded using a HITACHI Spectrophotometer. This UV-vis absorption spectrum characteristics of carotene are shown in the following Fig. 3a having different concentrations. It was observed that high concentrated solutions are

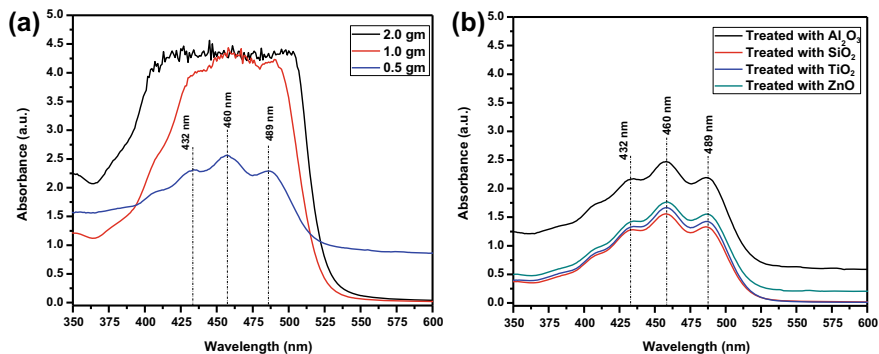


Fig. 3 UV-vis spectra of carotene **a** at different concentrations **b** treated with different absorption media

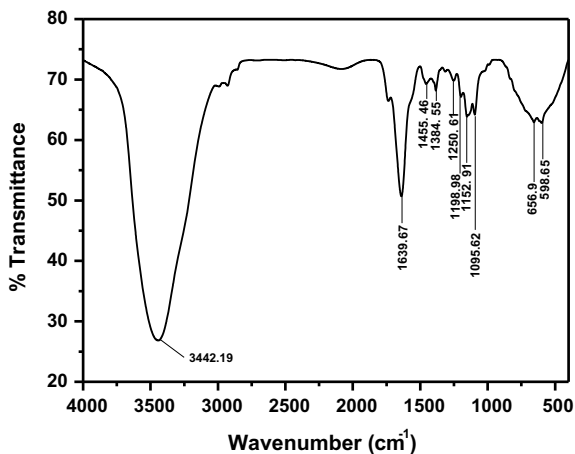
not showing proper peaks. The solution was diluted by keeping the solvent amount fixed and reducing the powder sample 2.0 gm to 0.5 gm. This time 0.5 gm powder containing sample showed peaks. Again the solutions were treated with various absorption medium starting from Al_2O_3 , SiO_2 , TiO_2 , ZnO with the 0.5 gm powder sample as shown in Fig. 3b. It reveals that the untreated sample is showing a sharp peak at 432 nm, 460 nm, and 489 nm. It was also observed that treating with different absorption medium peak absorbance became reduced. But interestingly treating with Al_2O_3 absorption medium showed a peak with greater absorption than the other treated materials. Further experimentation was carried with samples treated with Al_2O_3 .

3.4 FTIR Spectroscopical Observation

The FTIR spectroscopical analysis was carried out with carotene treated with Al_2O_3 absorption medium. Figure 4 illustrates the absorption spectrum of carotene treated with Al_2O_3 absorption medium.

It can be seen that within $3200\text{--}3600\text{ cm}^{-1}$ wavenumber region, the sample is showing broad absorption at 3442.19 cm^{-1} . This broad spectrum has been arisen may be due to the stretching of strong --OH group. During $1640\text{--}1820\text{ cm}^{-1}$, a broad absorption peak has been obtained at 1639.67 cm^{-1} that indicates the presence of C=O functional group for stretching mode of vibration may be due to the presence of carbonyl or amide group. At 1455.46 cm^{-1} , another peak has been obtained indicating for the presence of C=C stretching bond. Within $1000\text{--}1400\text{ cm}^{-1}$ region, five peaks have been obtained may be due to the presence of C-F group stretching vibration.

Fig. 4 FTIR spectra of carotene treated with Al_2O_3



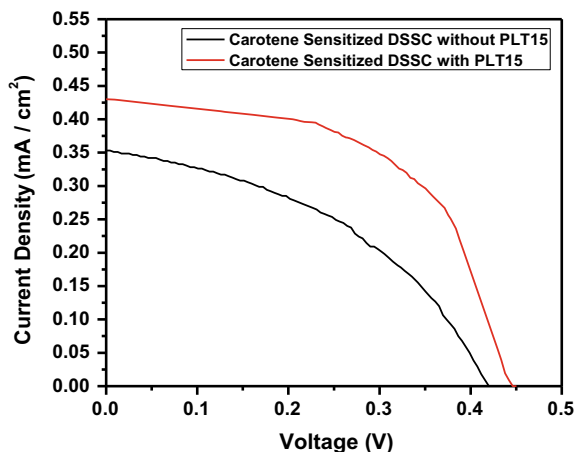


Fig. 5 The current–voltage (J – V) characteristics of carotene sensitized solar cell combining with and without PLT15 measured under simulated solar light (100 mW/cm^2 AM 1.5G)

Table 1 Photovoltaic parameters of the fabricated solar cell

Sample name	J_{sc} (mA/cm ²)	V_{oc} (Volt)	Fill factor (%)	Efficiency (%)
Carotene-sensitized DSSC in absence of PLT15	0.39	0.42	38.7	0.64
Carotene-sensitized DSSC in presence of PLT15	0.446	0.446	54	1.05

3.5 Electrical Characterization

The electrical characterization of the extracted organic sample in presence and absence of PLT15 was analyzed under simulated solar irradiation (1.5 sun). Figure 5 represents the current density versus voltage plot in the presence and absence of PLT15, respectively. From the obtained data point, the corresponding open-circuit voltage (V_{OC}), short circuit current (I_{SC}), fill factor (FF) and conversion efficiency have been obtained. Table 1 represents the tabulated form of electrical parameters. From the obtained data, it is clear that the presence of PLT15 has improved the efficiency of the fabricated solar cell.

4 Conclusion

The carotene-sensitized DSSCs in the presence and absence of synthesized PLT15 coupled TiO_2 have been analyzed using various tools. The XRD analysis of the thin films indicates impurity-free phase with desired peak in presence of necessary

coupling of TiO₂ and PLT15. The Scanning Electron Microscope (SEM) reveals that the extracted carotene is uniform in structure with lesser amount of pores. The UV–vis spectroscopy indicates the presence of absorption peaks under low concentration. Also purification was carried out using diluted dye solution in presence of various absorption media that reveals Al₂O₃-treated absorption is suitable for solar cell application. Hence, using Al₂O₃-treated sample underwent for FTIR spectroscopy that reveals the presence of various functional groups within the dye solution. Finally, electrical characterization was carried out with the dye in presence and absence of PLT15-coupled TiO₂ matrix. The result revealed that presence of PLT15 within the system has improved the photoconversion efficiency of the solar cell due to better charge collection properties and minimize the surface recombination.

Acknowledgements This work was supported by grants funded by the Department of Science and Technology (DST) under the Scheme “Innovation, Technology Development and Deployment” Central, Government of India through Mission Innovation Programme DST (DST/TMD(EWO)/IC5-2018/06(G)).

References

- Dey A, Moyez SA, Mandal MK, Roy S (2016) Fabrication of solar cell using extracted biomolecules from tea leaves and hybrid perovskites. *Mater Today Proc* 3(10):3498–3504
- Dey A, Das BC, Biswas AB, Sarkar P, Dhar A, Roy S, Moyez SA (2017a) Graphene co-doped TiO₂ nanocomposites for photocatalysis and photovoltaics applications. *Indian J Sci Tech* 10(31):1–6
- Dey A, Karan P, Sengupta A, Moyez SA, Sarkar P, Majumder SB, Pradhan D, Roy S (2017b) Enhanced charge carrier generation by dielectric nanomaterials for quantum dots solar cells based on CdS-TiO₂ photoanode. *Sol Energy* 158:83–88
- Kay A, Graetzel M (1993) Artificial photosynthesis. 1. Photosensitization of titania solar cells with chlorophyll derivatives and related natural porphyrins. *J Phys Chem* 97:6272–6277
- Zhang D, Lanier SM, Downing JA, Avent JL, Lum J, McHale JL (2008) Betalain pigments for dye-sensitized solar cells. *J Photochem Photobiol A* 195(1):72–80

Simulation of Biomagnetic Fluid Flow in a Lid-Driven Cavity Under Steady Localized Magnetic Field



Sumanta Banerjee and Ranjan Ganguly

Abstract The simulation study of steady, laminar, incompressible, and isothermal biomagnetic fluid flow within a lid-driven cavity is presented, under the influence of a time-independent localized external magnetic field. The mathematical model used for the problem formulation is consistent with the principles of FHD and MHD and therefore considers both the magnetic Kelvin force and the Lorentz force as body forces. The biomagnetic fluid is modeled as a homogeneous Newtonian continuum, which dually exhibits magnetization and its electrical conductivity. The numerical solution of the problem, described by a system of coupled, nonlinear system of PDEs with appropriate boundary conditions, is carried out using the SIMPLER algorithm. The solution is obtained by the finite volume method on a staggered grid. The results of the simulation, as visualized through the stream function plots, indicate the field–fluid interactions in laminar flow regimes.

Keywords Ferrohydrodynamics (FHD) · Magnetohydrodynamics (MHD) · Biomagnetic fluid · Lid-driven cavity · Magnetic number

1 Introduction

Biomagnetic Fluid Dynamics (BFD) investigates the dynamic behavior of magnetically susceptible biological fluids in the presence of magnetic fields. In simplified models, the biological fluids are considered as isothermal, Newtonian, and electrically nonconducting (Bashtovoy et al. 1988). These models, in line with the principles of Ferrohydrodynamics (FHD), attribute the driving Kelvin body force (KBF) in the flow field solely to fluid magnetization (Bashtovoy et al. 1988; Rosensweig 1985).

S. Banerjee (✉)

Mechanical Engineering Department, Heritage Institute of Technology, Kolkata 700107, India
e-mail: sumanta.banerjee@heritageit.edu

R. Ganguly

Power Engineering Department, Jadavpur University, Kolkata 700098, India
e-mail: rgangu2@yahoo.com

© Springer Nature Singapore Pte Ltd. 2021

D. Ramkrishna et al. (eds.), *Advances in Bioprocess Engineering and Technology*,
Lecture Notes in Bioengineering,
https://doi.org/10.1007/978-981-15-7409-2_42

A characteristic biomagnetic fluid is blood, as blood exhibits magnetic polarization in the presence of erythrocytes (Bashtovoy et al. 1988). The magnetic susceptibility of blood arises out of the complex biochemical interactions of the intercellular protein, cell membrane, and the hemoglobin (a form of iron oxide), which is present at high concentrations in mature red blood cells. Experimental observations indicate that erythrocytes preferably orient their disc plane parallel to the external magnetic field direction (Higashi et al. 1993). In addition, factors like the state of oxygenation influence magnetic behavior (Plavins and Lauva 1993), as blood exhibit diamagnetism when oxygenated and paramagnetism when deoxygenated. These attributes render different flow dynamics for venous and arterial blood under external magnetic fields.

A stable colloidal suspension of erythrocytes in plasma can be mathematically modeled as a homogeneous continuum that constitutes magnetic dipoles in a liquid carrier (Rosensweig 1985; Tzirtzilakis 2005). Realistic models based on blood constitution and rheology, as presented in (Tzirtzilakis 2005), also enable to model nonisothermal flows, whereby the field response of temperature-dependent fluid susceptibility can be studied and fine-tuned for practical applications. The Kelvin force then depends dually on the existence of a nonuniform magnetic and/or temperature fields.

In addition, blood exhibits appreciably high static electrical conductivity, which varies with temperature, hematocrit (ratio of the volume of red blood cells to total blood volume), and the flow rate (Jaspard and Nadi 2002). This warrants flow representations to consider the biofluid to be electrically conducting and incorporate the principles of MHD. In the presence of external magnetic field gradients, the fluid is then subjected to the Lorentz force (Davidson 2001; Farahbakhsh and Ghassemi 2010). However, the effect of the Lorentz force is significant only for strong magnetic fields; in situations of sharp field gradient and/or low magnetic field strength, the Kelvin force dominates (Rosensweig 1985).

As far as practical engineering applications are concerned, a prevalent technique is the release of artificially created nanoparticles in bloodstream, either attached to the erythrocytes or moving independently in accordance with the dynamics of flow. This enables the magnetization of blood to be augmented by several orders of magnitude and facilitates targeted transport of drugs using magnetic particles as drug carriers, reduction of bleeding during surgeries, promoting occlusion of the feeding vessels of malignant tumors, or development of magnetic tracers (Fuh et al. 2000). Moreover, biomedical applications based on the application of magnetic field directly on blood are proposed, like the development of magnetic devices for cell separation (Carlton et al. 2001), field-assisted treatment of internal wounds, or cancer treatment causing magnetic hyperthermia (Li et al. 2008; Voltairas et al. 2000; Haik et al. 1999).

Literature review presents numerical studies concerning basic BFD flow configurations for biofluids of diverse rheology. The studies all indicate the formation of recirculating flow-field vortices at the sites of high field intensities. The numerical studies introduce a magnetization term in the governing equations, which constitutes a source term that leads to irrotational flows under nonuniform external fields. A well-known classical, fundamental problem is that of isothermal flow within a rectangular

perpendicular to the cavity. The (normalized) magnetic field strength contours are also shown.

The fluid working medium is an electrically conducting magnetic fluid exhibiting paramagnetic behavior. The fluid rheology is Newtonian and conforms to the mathematical model proposed in Tzirtzilakis (2005) and Tzirtzilakis and Xenos (2012). The increment of viscosity due to external imposed field (or magneto-viscous effect) is neglected. The rotational forces acting on the erythrocytes, when entering and exiting the magnetic field, are also not taken into account (equilibrium magnetization). Finally, the electric field is neglected for the 2D flow field. Under the above assumptions, the mass and momentum conservation equations governing the flow (in coordinate-free form) are:

$$\nabla \cdot \vec{V} = 0 \tag{1}$$

$$\rho \nabla \cdot (\vec{V} \vec{V}) = -\nabla p + \underbrace{\mu_0 M \nabla H}_{\text{magnetic polarization force}} + \underbrace{\sigma [\vec{B} \times (\vec{B} \times \vec{V})]}_{\text{Lorentz force}} + \mu \nabla \cdot (\nabla \vec{V}) \tag{2}$$

The conservation equations in 2D rectangular Cartesian system are as follows:

$$\frac{\partial u}{\partial x} + \frac{\partial v}{\partial y} = 0 \tag{3}$$

$$\rho \left(u \frac{\partial u}{\partial x} + v \frac{\partial u}{\partial y} \right) = -\frac{\partial p}{\partial x} + \mu_0 M \frac{\partial H}{\partial x} - \sigma B_y^2 u + \sigma B_x B_y v + \mu \left(\frac{\partial^2 u}{\partial x^2} + \frac{\partial^2 u}{\partial y^2} \right) \tag{4}$$

$$\rho \left(u \frac{\partial v}{\partial x} + v \frac{\partial v}{\partial y} \right) = -\frac{\partial p}{\partial y} + \mu_0 M \frac{\partial H}{\partial y} - \sigma B_x^2 v + \sigma B_x B_y u + \mu \left(\frac{\partial^2 v}{\partial x^2} + \frac{\partial^2 v}{\partial y^2} \right) \tag{5}$$

The steady-state boundary conditions imposed on the square lid-driven cavity are:

Bottom Wall:	Left Wall:
$u = 0, v = 0 (0 \leq x \leq W, y = 0)$	$u = 0, v = 0 (x = 0, 0 \leq y \leq W)$
Top Wall:	Right Wall:
$u = U_0, v = 0 (0 \leq x \leq W, y = W)$	$u = 0, v = 0 (x = W, 0 \leq y \leq W)$

In the above Eqs. 1–5, the respective dimensional quantities are velocity $\vec{V} = (u, v)$, pressure p , (constant) top wall speed U_0 , fluid density ρ , electrical conductivity σ , dynamic viscosity μ , magnetic permeability of vacuum μ_0 , magnetic field strength (inside the fluid medium) $\vec{H} = (H_x, H_y)$, and the magnetic induction $\vec{B} (\vec{B} = \mu_0 \vec{H})$. The term $\mu_0 M \nabla H = (\mu_0 M \frac{\partial H}{\partial x}, \mu_0 M \frac{\partial H}{\partial y})$ represents the

(magnetic) Kelvin force density, which depends on (a) fluid magnetization and (b) the existence of the field gradient along coordinate directions (Rosenzweig 1985). The term $\sigma \left[\vec{B} \times \left(\vec{B} \times \vec{V} \right) \right]$ represents the Lorentz force per unit volume and arises due to the electrical conductivity of the fluid (Davidson 2001). The magnetic field inside the biofluid medium is (m : dipole strength of source):

$$\vec{H} = (1 + \chi_m)m \left(\frac{\sin \theta}{r^2} \hat{e}_r - \frac{\cos \theta}{r^2} \hat{e}_\theta \right) \quad (6)$$

The magnetization M is linearly related with the field intensity (magnitude) H through the magnetic susceptibility ($= \chi_m$), as shown in Eq. 7a (Banerjee et al. 2008). Moreover, the field induction \vec{B} conforms to Maxwell's equation in static form (Eq. 7b):

$$M = \chi_m H \quad (7a)$$

$$\left. \begin{aligned} \nabla \times \vec{H} &= \vec{0} \\ \nabla \cdot \vec{B} &= 0 \end{aligned} \right\} \quad (7b)$$

In order to obtain the numerical solution of the system (Eqs. 3–6), with the boundary conditions and the simplified assumptions (Eqs. 7a and 7b), the following nondimensional variables are introduced:

$$X = \frac{x}{W}; Y = \frac{y}{W}; U = \frac{u}{U_0}; V = \frac{v}{U_0}; P = \frac{p}{\rho U_0^2}; \tilde{H} = \frac{H}{(m/W^2)} \quad (8)$$

The conservation equations in nondimensional form are:

$$\frac{\partial U}{\partial X} + \frac{\partial V}{\partial Y} = 0 \quad (9)$$

$$\begin{aligned} \left(U \frac{\partial U}{\partial X} + V \frac{\partial U}{\partial Y} \right) &= -\frac{\partial P}{\partial X} + \text{Mn}_K \tilde{H} \frac{\partial \tilde{H}}{\partial X} - \text{Sn}_L (U \tilde{H}_Y^2 - V \tilde{H}_X \tilde{H}_Y) \\ &+ \frac{1}{\text{Re}_W} \left(\frac{\partial^2 U}{\partial X^2} + \frac{\partial^2 U}{\partial Y^2} \right) \end{aligned} \quad (10)$$

$$\begin{aligned} \left(U \frac{\partial V}{\partial X} + V \frac{\partial V}{\partial Y} \right) &= -\frac{\partial P}{\partial Y} + \text{Mn}_K \tilde{H} \frac{\partial \tilde{H}}{\partial Y} - \text{Sn}_L (V \tilde{H}_X^2 - U \tilde{H}_X \tilde{H}_Y) \\ &+ \frac{1}{\text{Re}_W} \left(\frac{\partial^2 V}{\partial X^2} + \frac{\partial^2 V}{\partial Y^2} \right) \end{aligned} \quad (11)$$

The nondimensional boundary conditions are correspondingly:

$$\begin{array}{ll}
 \text{Bottom Wall:} & \text{Left Wall:} \\
 U = 0, V = 0(0 \leq X \leq 1, Y = 0) & U = 0, V = 0(X = 0, 0 \leq Y \leq 1) \\
 \text{Top Wall:} & \text{Right Wall:} \\
 U = 1, V = 0(0 \leq X \leq 1, Y = 1) & U = 0, V = 0(X = 1, 0 \leq Y \leq 1)
 \end{array}$$

In Eqs. (10) and (11), the dimensionless group $Mn_K = (\mu_0 \chi_m m^2 / \rho U_0^2 W^4)$ denotes the magnetic number arising from polarization forces (due to external field gradients). Its magnitude varies inversely as the fourth power of the pertinent length scale ($= W$) of the system and can be quite significant for miniaturized enclosure geometries.

Likewise, the nondimensional group $Sn_L = \left[\mu_0 W^2 \left(\frac{\sigma}{\mu} \right)^2 \left(\frac{m}{W^2} \right)^2 / Re_W \right]$ is the Stuart number, which is the ratio of the square of the Hartman number to the Reynolds number (Tzirtzilakis 2005). It may be observed that when both of these magnetic numbers are zero, the problem is reduced to the problem of pure hydrodynamic flow in lid-driven cavity. For a given value of the Reynolds number, increasing the value of either of these magnetic numbers is equivalent to increasing the magnetic field strength.

A staggered grid arrangement has been used in the present study, which offers advantages over the collocated arrangement in convection-dominated flows (Patankar 1980). In addition, sinusoidal grid spacing has been applied, which has enabled (a) finer computational grid close to the walls and in vicinity of the magnetic source and (b) coarser grid close to the center of the cavity. The power-law scheme has been used to discretize the convection terms. The Semi-Implicit Method for Pressure Linked Equations Revised (SIMPLER) algorithm has been used to solve the system of the momentum and the pressure correction equations (Patankar 1980).

3 Results and Discussion

The stream function plot of lid-driven flow field within the cavity for purely shear-driven flow, in absence of magnetic field, has been presented in Fig. 2. The simulations are presented for values of $W = 0.05$ m, $U_0 = 5$ cm/s, $\nu \approx 3.1 \times 10^{-6}$ m²/s (Kalion et al. 2004). The stream Reynolds number is thereby evaluated as $Re_W \approx 8.1 \times 10^2$. The plots indicate crowding of contours near the (sliding) top wall, where velocity gradients are high. The flow rates flag off as the circulation descends down toward the bottom wall, under the effects of viscous forces. The wall shear effects create weak secondary vortices, fully conforming to physics of flow.

The stream function plots (in Fig. 3) show that applying the magnetic field below the bottom plate of the cavity results in bifurcation of the characteristic primary vortex obtained for pure hydrodynamic flow. This plot corresponds to

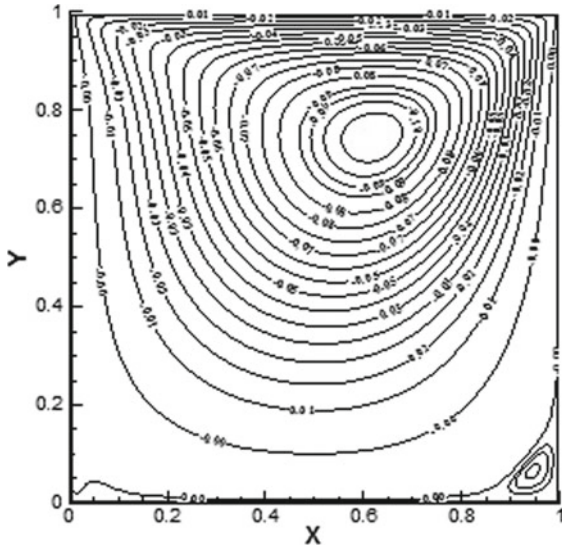


Fig. 2 Stream function plot of recirculation vortex in the absence of magnetic field

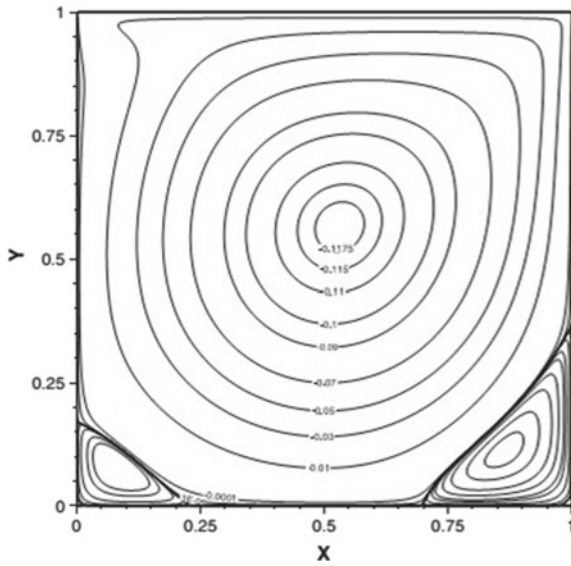


Fig. 3 Plots of primary and secondary vortices in the presence of magnetic field

$Mn_K \approx 10.21$, $Sn_L \approx 0.01$. For relatively weak magnetic field strengths, this splitting-up leads to the formation of other smaller vortices. The number of secondary vortices increases with rising values of magnetic field strength. For relatively strong magnetic fields, the increased number of vortices results in the reduction of flow-field velocities in close vicinity of the bottom plate. The application of the applied (magnetic) field gradient sets up strong circulation near the bottom plate, as evidenced by the two secondary, counter-rotating vortices. The primary vortex is largely influenced by the flow disturbance induced by the sliding top plate of the cavity, and to a lesser extent by the presence of the magnetic dipole.

References

- Banerjee S, Mukhopadhyay A, Sen S et al (2008) Optimizing thermomagnetic convection for electronics cooling. *Numer Heat Transfer Part A* 53:1231–1255
- Bashtovoy VG, Berkovsky BM, Vislovich AN (1988) Introduction to thermomechanics of magnetic fluids. Springer, Berlin
- Carlton JMR, Yowell CA, Sturrock KA et al (2001) Bio-magnetic separation of contaminating host leukocytes from Plasmodium-infected erythrocytes. *Exp Parasitol* 97:111–114
- Davidson PA (2001) An introduction to magnetohydrodynamics. Cambridge University Press, Cambridge
- Farahbakhsh I, Ghassemi H (2010) Numerical investigation of the Lorentz force effect on the vortex transfiguration in a two-dimensional lid-driven cavity. *Proc Inst Mech Eng Part C* 224:1217–1230
- Fuh CB, Lin LY, Lai MH (2000) Analytical magnetophoresis of magnetically susceptible particles. *J Chromatogr A* 874:131–142
- Haik Y, Pai V, Chen CJ (1999) Development of magnetic device for cell separation. *J Magn Magn Mater* 194:254–261
- Higashi T, Yamagishi A, Takeuchi T et al (1993) Orientation of erythrocytes in a strong static magnetic field. *J Blood* 82:1328–1334
- Jaspard F, Nadi M (2002) Dielectric properties of blood: an investigation of temperature dependence. *Physiol Meas* 23:547–554
- Kalion VA, Kazachkov IV, Shmakov YI (2004) Rheology of complex fluids. Div. Heat Power Tech., KTH Press, Stockholm, Sweden
- Li XL, Yao KL, Liu ZL (2008) CFD study on the magnetic fluid delivering in the vessel in high-gradient magnetic field. *J Magn Magn Mater* 320:1753–1758
- Patankar SV (1980) Numerical heat transfer and fluid flow. McGraw-Hill, New York
- Plavins J, Lauva M (1993) Study of colloidal magnetite binding erythrocytes: prospects for cell separation. *J Magn Magn Mater* 122:349–353
- Rosensweig RE (1985) Ferrohydrodynamics. Cambridge University Press, Cambridge
- Tzirtzilakis EE (2005) A mathematical model for blood flow in magnetic field. *Phys Fluids* 17(077103):1–15
- Tzirtzilakis EE, Xenos MA (2012) Biomagnetic fluid flow in a driven cavity. *Meccanica* 48:187–200
- Voltairas PA, Fotiadis DI, Michalis LK (2000) Hydrodynamics of magnetic drug targeting. *J Biomech* 35:813–821

Systems Biology Approach to Screen and Identify Algae-Based Alkaline Phosphatases as Heavy Metal-Detecting Biosensors



Dipankar Ghosh, Kalyanee Bera, Poulami Bera, Megha Bhattacharya, Bijaya Samanta, Somashree Mondal, Mamta Das, Bishal Maity, Sanjit Das, Surjata Haobam, Anwesa Das, and Pritha Mondal

Abstract Heavy metal has enormous toxicity on microbial metabolic pathways and its corresponding enzymes. Indiscriminate disposal of heavy metals in nature has a huge detrimental impact on the environment and ecosystem. Thus the minimal concentration of heavy metals should be maintained in environment with proper real-time monitoring. In general, ionic chromatography, mass spectrometry, inductively coupled plasma; polarography and usage of ion-sensitive electrodes are the most abundant approaches to detect the heavy metal contamination in nature. However, these current approaches suffer due to lower electrode selectivity, inaccurate response, and higher cost. Moreover, current avenues are not directly consociated with toxicity impact of these heavy metals. In general, algal alkaline phosphatases are a hydrolase (EC 3.1.3.1) class of enzymes, present in external membrane of microalgal regimes. Alkaline phosphatase enzyme transforms phosphoester molecules into soluble inorganic phosphate. However, its catalytic activity has strongly been inhibited in the presence of trace amount of heavy metals. This particular feature of algal phosphatase helps to detect these toxic heavy metals in nature even these are present in minute quantities. Based on this current global scenario, the current study is to focus on in silico screening and identification of algae-based alkaline phosphatases following systems biology approaches. The present study will help to (i) find out novel algae-based putative alkaline phosphatase protein sequences; (ii) bioinformatics and phylogenetic studies toward in silico characterizations, and (iii) algae-based alkaline phosphatase enzyme affinity toward diverse heavy metals especially cadmium and mercury. Therefore, this systems biology approach will accelerate the usage of algae-based alkaline phosphatase as a sustainable biosensor to detect the minute level of heavy metal toxicity in nature in the near future.

Keywords Heavy metal · Metabolic pathway · Biosensor · Systems biology · Alkaline phosphatase

D. Ghosh (✉) · K. Bera · P. Bera · M. Bhattacharya · B. Samanta · S. Mondal · M. Das · B. Maity · S. Das · S. Haobam · A. Das · P. Mondal
Department of Biotechnology, JIS University, Agarpara, Kolkata, West Bengal 700109, India
e-mail: d.ghosh@jisuniversity.ac.in

1 Introduction

Heavy metals are omnipresent in diverse chemical states in the ecosystem. The ecosystem has been contaminated by several anthropogenic activities likely municipal, agricultural, industrial, and mining waste effluent disposals, which are highly impoverished with toxic heavy metals. Animal and plants are both directly or indirectly intoxicated due to vulnerability of these heavy metals that are present in contaminated rhizosphere, water supplies, and foods, respectively (Mishra et al. 2017; Rana et al. 2018). Among several heavy metals, cadmium (Cd) and mercury (Hg) are considered as highly toxic threat to environment and human health (Chibuike and Obiora 2014; Henkler et al. 2010). Heavy metal stress induces several alterations in plant physiology and metabolic activities in a dose-dependent manner. These heavy metals especially cadmium and mercury compete with essential micronutrients (potassium, phosphorous, and zinc) absorption by root in plant bodies and cause nutrient deficiency (Zhuang et al. 2014). Cadmium heavily inhibits chlorophyll content, photosynthetic rate, photosystems II quantum yield, stomatal conductance, and intracellular carbon dioxide assimilation (hindering Rubisco enzymatic activity). It causes immense influence on nitrate metabolism by inhibition of nitrate uptake, nitrate transportation. Cadmium induces protease activity; it reduces metabolic efficacy of nitrate metabolizing enzymes (i.e., nitrate reductases, nitrite reductases) and ammonia-assimilating enzymes (i.e., glutamine synthetase, glutamine oxoglutarate aminotransferases, and glutamate dehydrogenase) (Singh et al. 2016). Cadmium generates reactive oxygen species (ROS) in respective organelles, i.e., chloroplast, mitochondria, and peroxisomes via reduction in the photosynthetic electron transport chain and disturbances in carbon dioxide sequestrations (Mittler et al. 2004). Mercury is abundant in nature and has enormous effect on kidney, causing proteinuria (Reyes et al. 2013). Extensive exposure to mercury can increase the possibility of immune, sensory, neurological dysfunctions having similar symptoms of autism spectrum disorders. Moreover, mercury affects antioxidants in the cellular system that enhances loss of membrane integrity and cellular necrosis (Abdel 2015). Mercury deposition induces ROS generation, mRNA expression of metallothionein, apoptosis, and proximal tubule damage (Agarwal et al. 2010). An alternative molecular mechanism includes an increase in hydrogen peroxide concentration after mercury exposure, which hampers glutathione antioxidant network. Moreover, mercury also increases hydrogen peroxide level in brain and lipid peroxidation (Farina et al. 2011).

Therefore, it is an urgent need for real-time monitoring of minimal level of heavy metals in our ecosystem to minimize heavy metal toxicity toward environment and human health hazards. Different spectroscopy, chromatography, and ion-sensitive techniques are in practice at present for heavy metal detections. However, these current approaches suffer due to lower electrode selectivity, inaccurate response, higher cost, and nonreal-time monitoring. Algal alkaline phosphatases (APs) (EC 3.1.3.1) are the class of hydrolase, which transform phosphoester molecules into soluble inorganic phosphate. However, catalytic efficacies of APs have strongly been inhibited in the presence of trace amount of heavy metals. This particular feature of

algal AP helps to detect least quantities of toxic heavy metals in nature. Hence, the current study focuses to tabulate novel putative algal APs through phylogenetic analysis and to predict heavy metals (i.e. cadmium and mercury) affinity on algal APs.

2 Experimental

In this current study, diverse ranges of algal APs (known and putative) protein sequences including EC 3.1.3.1 have been retrieved from KEGG, Uniprot protein databases including following unique protein Ids, i.e., Vca_Ph0 (*Volvox carteri*): XP_002958226.1; Cre_Ph0 (*Chlamydomonas reinhardtii*): XP_001702318.1; Lyn_Ph0 (*Lyngbya* sp. PCC 8106): ZP_01623784.1; Scy_Ph0 (*Synechocystis* sp.PCC 6803): BAA16956.1; Sco_Ph0 (*Synechococcus* sp.PCC 7942): AAA27331.1; Nos_Ph0 (*Nostoc* sp.PCC 7120): BAB76990.1; SynWH5_Ph0 (*Synechococcus* sp.WH5701): EAQ75607.1; SynWH8_Ph0 (*Synechococcus* sp. WH8120): NP_898480.1; Sel_Ph0 (*Synechococcus elongatus* PCC 6301): YP_170873.1; Cya_Ph0 (*Cyanothece* sp.ATCC 51142): B1WW62; Gci_Ph0 (*Gloeothecce citrififormis* PCC 7424): B7KHT5; Pma_Ph0 (*Prochlorococcus marinus* NATL1A): ABM75708; Cpa_Ph0 (*Calothrix parietina*): A0A0T7BMF5; Ava_Ph0 (*Anabaena variabilis* ATCC 29413): Q3M5K7; AhaA2_Ph0 (*Aphanothece halophytica* A2): F5HRA6; Aha_Ph0 (*Aphanothece halophytica*): F5HRA4. Retrieved protein sequences have been undergone multiple sequence alignment and phylogenetic studies using ClustalW and Molecular Evolutionary Genetics Analysis (MEGA 4.0) software considering NJ algorithm (Tamura et al. 2007). Putative protein 3D homology models have been generated using SWISS Model online server (Waterhouse et al. 2018) considering the most similar protein model in protein PDB database. Putative protein model qualities have been evaluated through Ramachandran plot, Global Model Quality Estimation (GMQE), MolProbity Score (Waterhouse et al. 2018). Afterward, transmembrane helices in protein sequences have been predicted to make sure which enzymes are secretory in nature (Krogh et al. 2001). Finally, putative protein models have been docked with two selected heavy metals, i.e., cadmium and mercury to predict the metal affinity and amino acid residues involvement in these interactions using MIB webserver (Lin et al. 2016).

3 Results and Discussion

Homology modeling using SWISS Model server has shown that most of algal AP models exist in the favored region in Ramachandran plot (average value of 82.5%) and MolProbity value around 2 having average sequence similarity

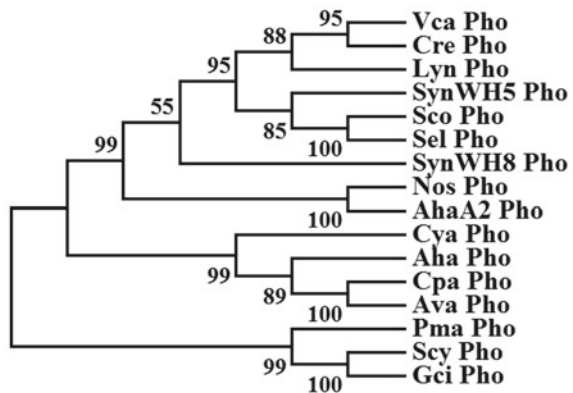
of about 50%. Phylogenetic study on algal APs has been carried out considering the following sequences Vca_Ph0 (*Volvox carteri*); Cre_Ph0 (*Chlamydomonas reinhardtii*); Lyn_Ph0 (*Lyngbya* sp.PCC 8106); Scy_Ph0 (*Synechocystis* sp.PCC 6803); Sco_Ph0 (*Synechococcus* sp.PCC 7942); Nos_Ph0 (*Nostoc* sp.PCC 7120); SynWH5_Ph0 (*Synechococcus* sp.WH5701); SynWH8_Ph0 (*Synechococcus* sp. WH8120); Sel_Ph0 (*Synechococcus elongatus* PCC 6301); Cya_Ph0 (*Cyanothecce* sp.ATCC 51142); Gci_Ph0 (*Gloeothecce citriformis* PCC 7424); Pma_Ph0 (*Prochlorococcus marinus* NATL1A); Cpa_Ph0 (*Calothrix parietina*); Ava_Ph0 (*Anabaena variabilis* ATCC 29413); AhaA2_Ph0 (*Aphanothecce halophytica* A2); Aha_Ph0 (*Aphanothecce halophytica*). Phylogenetic studies have shown that eukaryotic algae (Vca_Ph0 and Cre_Ph0) and prokaryotic algae, i.e., cyanobacterial exist in different clades (Fig. 1).

Metal ion binding (MIB) in silico studies have clearly shown that Sel_Ph0, Sco_Ph0, Aha_Ph0, and Lyn_Ph0 are the most predominant algal APs that can be used as biosensor enzyme to detect cadmium heavy metal toxicity in environmental samples in different habitats (Fig. 2). In cadmium-based Aps, affinities have been governed by aspartic acid, asparagine, and glutamate amino acids in protein chain A.

In the contrary, SynWH8_Ph0, Sel_Ph0, Sco_Ph0, and Cre_Ph0 are the most predominant algal APs that can be used as biosensor enzymes to identify mercury toxicity in environmental samples following in silico enzymatic affinity assay (Fig. 3). In mercury-based alkaline phosphatase, affinities have been governed by alanine, glycine, and serine amino acids in protein chain A.

Moreover, TMHHM analysis has shown that most of the algal APs are secretory in nature excluding Cre_Ph0, Nos_Ph0, Pma_Ph0, Cpa_Ph0, Ava_Ph0, and Aha_Ph0 (Fig. 4).

Fig. 1 Phylogenetic analysis of putative and known algal alkaline phosphatase (at 500 bootstrapping)



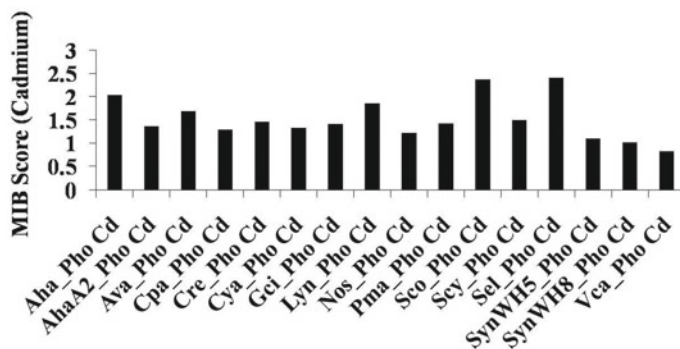


Fig. 2 Metal ion binding affinity prediction studies with cadmium (higher the metal ion binding affinity stands for higher degree of inhibition of alkaline phosphatase activity)

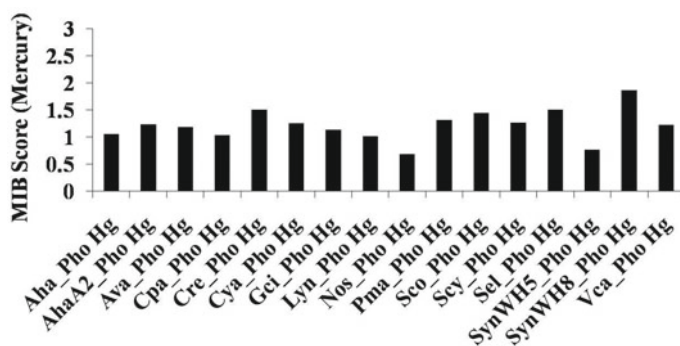


Fig. 3 Metal ion binding affinity prediction studies with mercury (higher the metal ion binding affinity stands for higher degree of inhibition of alkaline phosphatase activity)

4 Conclusion

Preliminary in silico prediction has clearly been shown that Sel_Ph0, Sco_Ph0, Aha_Ph0, and Lyn_Ph0 are the most predominant algal APs that can be used as biosensor enzymes to detect cadmium heavy metal toxicity in environmental samples in different habitats. On the other hand, SynWH8_Ph0, Sel_Ph0, Sco_Ph0, and Cre_Ph0 are the most predominant algal APs that can be used as biosensor enzymes to identify mercury toxicity in environmental samples. However, TMHMM analysis depicts Aha_Ph0 and Cre_Ph0 may not be useful enzymatic sensors as these putative enzymes having transmembrane domain where transmembrane segment may cause slow or no release of enzymes from algal species. Hence, Nos_Ph0, Pma_Ph0, Cpa_Ph0, Ava_Ph0, SynWH8_Ph0, Sel_Ph0, Sco_Ph0 could be the most promising choice as algal AP enzyme-based heavy metal-detecting biosensor in near future

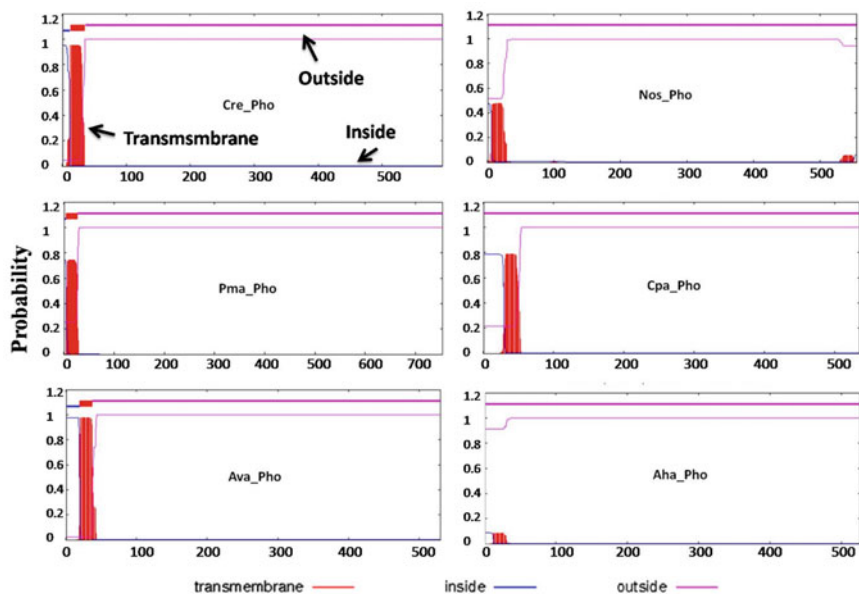


Fig. 4 TMHMM prediction studies using naive and putative algal alkaline phosphatases (red color bar indicates transmembrane segment, blue and pink lines indicate inside and outside the membrane, respectively)

after proper *in vitro* and *in vivo* validation of the aforementioned *in silico* prediction studies. However, putative protein PDB model needs to undergo crystal structure development, dynamic simulation analysis, and trajectory generations as future up-gradation studies to improve protein model accuracy and better data interpretation.

Acknowledgements Authors would like to thank JIS University and JIS Group of Educational Initiatives for financial support and help.

References

- Abdel MAE (2015) The neuroprotective effect of berberine in mercury-induced neurotoxicity in rats. *Metab Brain Dis* 30(4):935–942
- Agarwal R, Goel SK, Chandra R, Behari JR (2010) Role of vitamin E in preventing acute mercury toxicity in rat. *Environ Toxicol Pharmacol* 29:70–78
- Chibuikue GU, Obiora SC (2014) Heavy metal polluted soils: effect on plants and bioremediation methods. *Appl Environ Soil Sci* 2014:1–12
- Farina M, Rocha JB, Aschner M (2011) Mechanisms of methyl mercury-induced neurotoxicity: evidence from experimental studies. *Life Sci* 89(15–16):555–563
- Henkler F, Brinkmann J, Luch A (2010) The role of oxidative stress in carcinogenesis induced by metals and xenobiotics. *Cancers* 2(2):376–396

- Krogh A, Larsson B, von Heijne G, Sonnhammer ELL (2001) Predicting transmembrane protein topology with a hidden Markov model: application to complete genomes. *J Mol Biol* 305(3):567–580
- Lin YF, Cheng CW, Shih CS, Hwang JK, Yu CS, Lu CH (2016) MIB: metal ion-binding site prediction and docking server. *J Chem Inf Model* 56:2287–2291
- Mishra J, Singh R, Arora NK (2017) Alleviation of heavy metal stress in plants and remediation of soil by rhizosphere microorganisms. *Front Microbiol* 8:1706
- Mittler R, Vanderauwera S, Gollery M, Van Breusegem F (2004) Reactive oxygen gene network of plants. *Trends Plant Sci* 9:490–498
- Rana MN, Tangpong J, Rahman MM (2018) Toxicodynamics of lead, cadmium, mercury and arsenic-induced kidney toxicity and treatment strategy: a mini review. *Toxicol Rep* 5:704–713
- Reyes JL, Molina-Jijón M, Rodríguez-Muñoz R, Bautista-García P (2013) Tight junction proteins and oxidative stress in heavy metals-induced nephrotoxicity. *Biomed Res Int* 2013:1–14
- Singh S, Parihar P, Singh R, Singh VP, Prasad SM (2016) Heavy metal tolerance in plants: role of transcriptomics, proteomics, metabolomics, and ionomics. *Front Plant Sci* 6:1143
- Tamura K, Dudley J, Nei M, Kumar S (2007) MEGA4: molecular evolutionary genetics analysis (MEGA) software version 4.0. *Mol Biol Evol* 24(8):1596–1599
- Waterhouse A, Bertoni M, Bienert S (2018) SWISS-MODEL: homology modelling of protein structures and complexes. *Nucleic Acids Res* 46:W296–W303
- Zhuang P, Lu H, Li Z, Zou B, McBride MB (2014) Multiple exposure and effects assessment of heavy metals in the population near mining area in South China. *PLoS ONE* 9:e94484

Origin of Enantioselectivity: A Model Study of Sharpless Epoxidation



Nabanita Paul

Abstract An enantiomerically pure substance has paramount physiological importance. Synthetic chemists aimed to produce drug molecules primarily target to synthesize pure enantiomer. Enantiomers are optically active stereoisomers so in order to accomplish products with high enantiomeric excess, asymmetric synthesis must be designed judiciously. Mimicking nature's selective aptitude of biosynthesis is always considered a crucial challenge for synthetic chemists. The main target of drug designing is to attain skill in this specialized section. Racemization during asymmetric synthesis occasionally disappoints synthetic chemists by widely disrupting biophysical, biochemical characteristics of the synthesized compound. Kinetic resolution, however, is able to separate two enantiomers. Among innumerable synthesis, only a few are found to be associated with high enantiomeric excess yield. Contribution of enantioselective epoxide synthesis by Sharpless epoxidation is no less important in drug industry. Most striking feature of Sharpless epoxidation is materials used for producing enantiospecific epoxide are inexpensive. Product spread consisting of one predominating chiral epoxide is efficiently resolved. The current communication is aimed to analyse Sharpless epoxidation from analytical angle of a chemist using a model study of transition state structure using DIPT as chiral auxiliary and drives to find the underlying basis responsible for channelizing only one enantiomer at the suppression of other.

Keywords Diastereotopic TS · Kinetic resolution · Sharpless epoxidation

1 Introduction

The physiochemical activities are extremely specific. Almost all biochemical responses are enzyme-controlled processes. Enzymes are chiral substances. The degree of sensitivity is a function of chirality of the foreign moiety. In this circumstance, onus is on the synthetic chemists to synthesize enantiomerically pure

N. Paul (✉)

Department of Chemistry, A.P.C Roy Govt. College, Siliguri, India
e-mail: paulnabanita367@gmail.com

© Springer Nature Singapore Pte Ltd. 2021

D. Ramkrishna et al. (eds.), *Advances in Bioprocess Engineering and Technology*,
Lecture Notes in Bioengineering,
https://doi.org/10.1007/978-981-15-7409-2_44

compounds. In spite of all precautions, the reaction atmosphere often creates a portal that leads to racemization. To reach the target, a chemist is left with two options. Either by designing a method that perfectly proceeds through a specific reaction route that selectively siphoned specific chiral molecule or choosing a second option consisting of meticulous separation method that is able to separate two enantiomers. The second method is termed kinetic resolution (Martin et al. 1981). In 1980, K. B. Sharpless and T. Katsuki introduced a breakthrough epoxidation process which efficiently satisfies both criteria (Katsuki and Sharpless 1980). In the present context, origin of resolution is attempted to realize covering a model study of transition structure of the epoxidation based on data available on kinetic resolution method (Gao et al. 1987). Two enantiomeric allylic alcohols constitute two diastereotopic transition states with considerably higher difference of ΔG^\ddagger . This difference is reflected in relative rate difference, making separation of pure enantiomers feasible.

2 Experimental Section of Sharpless Epoxidation

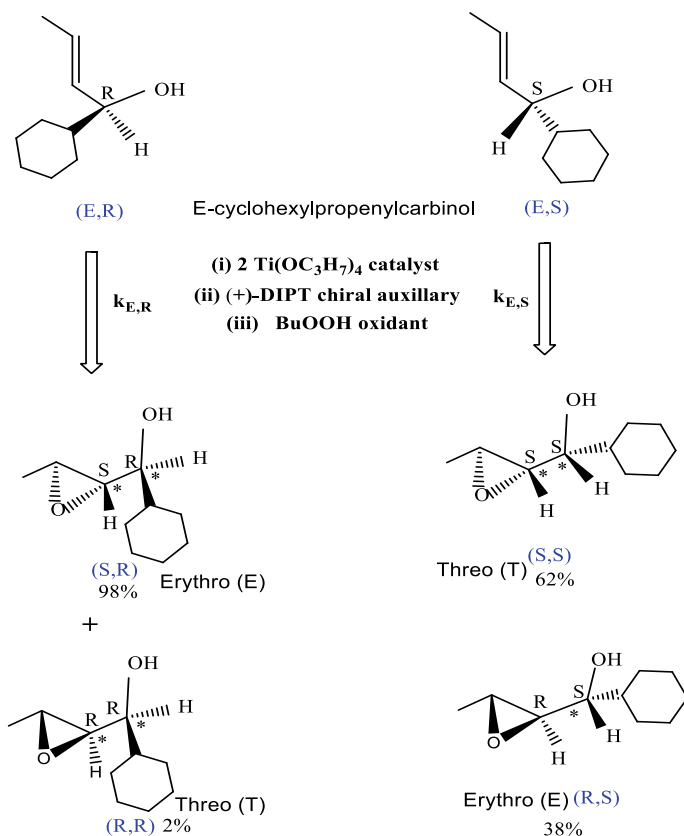
Katsuki et al. reported a reaction kettle is charged with dichloromethane (DCM) in ice-cold ($-20\text{ }^\circ\text{C}$) condition. Titanium (IV) tetraisopropoxide (1 equivalent), (+) DIPT (1.2 equivalent), 1 equivalent amount of racemic allyl alcohol, and 2 equivalent TBHP are injected by a syringe and stirred in ice-cold condition. After completion of the reaction, this cold mixture is introduced to another precooled ($-20\text{ }^\circ\text{C}$) acetone–water mixture. The homogeneous solution is kept for a stipulated period of time (Katsuki and Sharpless 1992). Tartrate hydrolysis and subsequent chromatographic separation resolve enantiomerically pure epoxide.

2.1 Description of Produced Enantioselective Epoxide with Specific Orientation

In Scheme 1, epoxide ring and lowest priority atom (hydrogen) of adjacent chiral centre are considered for Erythro (E) and Threo (T) designation.

3 Results and Discussion

Many instances are demonstrated by K. B. Sharpless, only four instances are considered in this article. The percentage of allylic alcohol consumption during epoxidation is not exactly known yet for some Z-alkenes, this is reported up to $55 \pm 1\%$. In Table 1, optical purity of epoxides and their erythro–threo orientation related to Sharpless asymmetric epoxidation are highlighted.

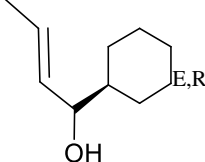
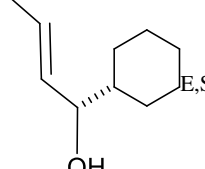
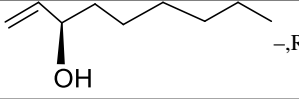
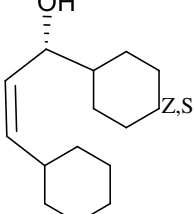


Scheme 1 Differential Aptitude leading to enantioselective products

This is clear allyl alcohol with E-geometry produced almost enantiomerically pure epoxide while allyl alcohol with Z-orientation fails to maintain optical purity. When resolution is performed epoxide of the first and second compound response to quick resolution (Katsuki and Sharpless 1992). The kinetics data sound a better tool for the current analysis. The rate of reaction is dependent upon chiral catalyst, substrate and oxidant. The expected third-order reaction is recorded as pseudo first-order since in the final workup schedule, two equivalent isopropyl alcohols are appeared as biproduct.

$$\text{Rate} = K \frac{[\text{Ti}(\text{tartrate})_2(\text{OR})_2][\text{TBHP}][\text{Allyl alcohol}]}{[\text{Isopropyl alcohol}]^2} \quad (1)$$

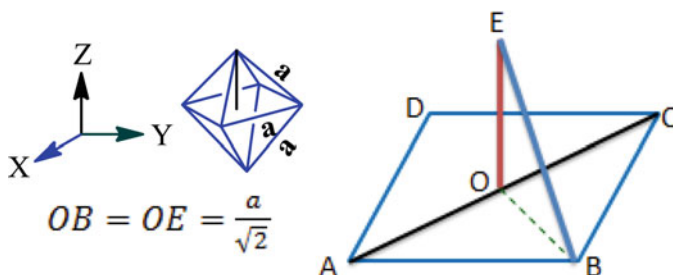
Table 1 Yield of epoxy alcohol by Sharpless asymmetric epoxidation

Configuration of alkene and chiral centre of allyl alcohol	Observed yield in % ee	E:T ratio of epoxyalcohol
	>95	98:2
	>96	38:62
	>96	99:1
	~10	2:98

3.1 A Proposed Model Based on Structure–Activity Concept

This section would deal with substrate, catalyst, oxidant and chiral auxiliary aggregate and attempt to sketch how geometry of participating entities regulates ultimate association resulting specificity. Molecular weight measurement suggests a dinuclear titanium–tartrate complex appears in the reaction (Katsuki and Sharpless 1980). In this article, the proposed model structure is constructed purely on the basis of geometry of constituent chemicals producing epoxide. In support of the proposed model, reported experimental technique is kept under strong vigil (Katsuki and Sharpless 1992). In the reported one pot synthesis, titanium (IV) tetra isopropoxide acting as the catalyst, chiral auxiliary (+)-tartrate ligand, substrate allyl alcohol and peroxidating reagent TBHP, were added sequentially in 1:1:1:2 ratio. It is obvious during synthesis, first interaction takes place between titanium (IV) tetra isopropoxide and tartrate ligand. These two together construct such an aggregate that allows further incoming chemicals in specific position. Tartrate ligand simultaneously links with two Ti(IV) by covalent and co-ordinate bonds and thereby forms a dinuclear coordination compound. The best structure commensurate with dinuclear geometry is edge fused two irregular octahedrons in which central positions are occupied by Ti(IV).

The basal plane of this fused octahedron is constructed by tartrate ligand. To avoid steric interaction to maximum extent, two tartrate ligands approach the basal plane from diametrically opposite side. Tartrate ligand has two different ligating sites of which alkoxy oxygen satisfies both covalent and co-ordinate valency and carbonyl oxygen of ester moiety initiates only co-ordinate linkage. In order to make the structure intact, alkoxy oxygens of tartrate ligand satisfy two consecutive covalent valencies of Ti(IV) making a five-membered chelate. Between two alkoxy oxygen atoms, one is positioned at fused corner. These oxygens show special bonding features by linking one Ti(IV) with covalent bond and connecting another Ti(IV) by coordinate linkage. In this way, three valencies of hexavalent Ti(IV) are fulfilled by chiral auxiliary. Remaining valency on equatorial plane is satisfied by initially attached isopropoxide ligand. One axial site is also linked with isopropoxide ligand by a covalent bond and its opposite axial site has a provision of linking with carbonyl oxygen by co-ordinate linkage. In this way, both primary and secondary valencies of Ti(IV) are satisfied. The role of ester moiety is vital since experiment carried out with ligand having no group capable of maintaining co-ordinate valency at axial site, losses enantioselectivity. In epoxidation experiment, optically pure tartrate is used so orientation of ester groups forces carbonyl groups to align in anti-parallel fashion. Carbonyl oxygen of ester group initiated co-ordinate linkage with Ti(IV) ion and as a consequence locks this site until and unless another ligand with co-ordinate bonding ability approaches. If the catalyst–chiral auxiliary aggregate is closely scrutinized, then each Ti(IV) nucleus is found associated with two isopropoxide ligands, one is in equatorial plane and other is in axial plane. In the one-pot synthesis, next step is the loading of allyl alcohol which under experimental condition easily generates alkoxide ligand which attempts to substitute similarly behaved isopropoxide ligand from catalyst surface. Two options are left with incoming allyl alkoxide ligand, either to replaced axially linked isopropoxide or equatorially attached isopropoxide. Among two possibilities, only axially anchored allyl alkoxide ion has the potential to generate specific epoxide. Final step of the synthesis is associated with the addition of peroxidating agent. TBHP has two vicinal oxygen atoms in which end oxygen has the ability to produce oxide linkage while intervening oxygen being attached to electron releasing tertiary butyl group has the ability of developing co-ordinate bond. These features together add a property within TBHP by which it can simultaneously shed two ligands from catalyst–chiral auxiliary substrate trio surface. End oxygen of peroxide gets connected with Ti(IV) using covalent linkage thereby displace isopropoxide ion from equatorial position while intervening oxygen is in a geometrically feasible position to initiate co-ordinate linkage with Ti(IV). Ester group linked with Ti(IV), carried out rotation around C1–C2 bond of tartrate ligand, deblocks the axial site of catalyst surface. This allows nice attachment of oxidant using one covalent and one co-ordinate bond. In short, two vicinal oxygen atoms of peroxide, anchored itself along one edge of the octahedron and this specific attachment suggests octahedron arrangement around one Ti(IV) has *Z*-in compressed geometry. This compression tendency is justified in Scheme 2. In this way, four chemicals together develop a chiral surface, which maintains a high degree of enantioselectivity during interaction between alkene moieties with peroxide. This geometry



Scheme 2 Morphology of catalyst surface

suggests substrate allyl alcohol and oxidant peroxide are attached with two axial sites of Ti(IV). Now, if non-linear distance of allyl alkoxide appears such that linear distance between axially bound alkoxide oxygen of substrate and mid-position of alkene is shorter than edge of octahedron constructed by Ti(IV)-centred aggregation, then alkene moiety always remains hanging top of peroxidating oxygen. Aggregate of four thus constructs a chiral surface which allows only Re-facial attack of oxygen during epoxidation when catalyst surface is tuned with (+) tartrate as chiral auxiliary. Tartrate in optically pure form locks one axial site from a specific direction scratching the route of specificity.

3.2 A Prediction for the Morphology of Catalyst

Performing a simple geometrical analysis, one can visualize morphology of catalyst surface. The height of a regular octahedron with edge **a** from basal plane is **0.707a**.

This is now correlated with chemical information. Peroxo linkage of oxidant is needed to be aligned with an edge, hence **a** is taken as 0.1807 nm. Thus height appears as 0.1278 nm. Titanium(IV) tetraisopropoxide is a basic component for catalyst. The ionic radius of Ti^{IV} is 0.064 nm and O^{2-} is 0.14 nm. The Ti–O bond length is likely to be 0.204 nm. This suggests considerable Z-in compression of octahedral unit lattice of catalyst. A distortion from regular octahedron assists acquiring the aggregate a dissymmetric outlook.

3.3 Resolution Strategy

A chiral auxiliary driven epoxidation opens an avenue towards the synthesis of optically active epoxide. The epoch-making Sharpless Asymmetric Epoxidation method efficiently executes the resolution method. Optically active diisopropyl tartrate (DIPT) is found to offer better assistance as a chiral auxiliary than diethyl

tartrate (DET) (Takano et al. 1991). The higher space-filling feature of isopropyl moiety may play a crucial role in etching a reaction route yielding product with high enantiomeric excess feature and thereby paves a fine way for resolution. In kinetic resolution, emphasis was given on three facts, viz, the extent of conversion, relative rate and enantiomeric enrichment achieved during resolution. Alkene having E-geometry is resolved as erythro epoxide in a better manner. In case of Z-stereoisomer, however, inclination of epoxide towards erythro form is abruptly less. The (E,R) form is reported to exhibit higher relative rate difference. Higher $\frac{K_{fast}}{K_{slow}}$ illustrates (E,R) stereoisomer is resolved at a faster rate.

3.4 Model Study Based on Structural Formula

The rate of epoxidation as well as ratio of purified enantiomers can be perceived by a model study. In this discussion, model structure is drawn on the basis of probable geometry of participating molecules. In dimeric form of homogeneous catalyst, titanium tetra isopropoxide, (+) DIPT is used as chiral auxiliary, the ligand isopropoxide directs Re-facial approach of epoxidating oxygen, exclusively produces (S,R) form. A model TS of allyl alcohol having (E,R) orientation is likely to be the structure as shown in Fig. 1.

In the TS, incipient epoxide ring and hydrogen of chiral alcoholic carbon are in same face. Space-filling moieties are so oriented that do not encourage repulsive interaction. When chiral carbon having alcoholic -OH group is in R-orientation, Re-facial approach of epoxidating oxygen seems very likely as hydrogen not cyclohexyl group is projected along this face. Moreover, electron-releasing effect of isopropyl group of tartrate can set an attractive interaction. All these decrease energies of TS specifically produce (S,R) epoxide at a faster rate. This TS produces epoxide with extremely high optical purity (96%). Rate enhancement and product selectivity together assist kinetic resolution. The approach from Si-face has a very low probability. The stepwise addition allows rotation about C-C bond prior to epoxide ring formation giving rise to (RR) product. This possibility is extremely low owing to highly energized TS. Now, the same reaction route is analysed with enantiomeric allyl alcohol in (E,S) form as shown in Fig. 2.

In TS, incipient epoxide ring and cyclohexyl group of chiral alcoholic carbon are in same face. The tartrate ligand-guided reaction route makes product spread of (E,S) isomer into 62% SS isomer and 38% RS isomer. First one, i.e. SS form is formed by Re-facial approach of epoxidating oxygen while second one, i.e. RS form is resulted from Si-facial attack. Interaction between more space-filling cyclohexyl group and epoxidating ring is mandatory in the Re-facial approach of epoxidating oxygen. Van der Waals repulsive interaction greatly hinders epoxidation resulting only 62% SS isomeric epoxide. This enhances the magnitude of $\frac{K_{T(S,S)}}{K_{E(R,S)}}$.

The alkyl group of tartrate ester group does offer an influence on the reaction course. Among several chiral auxiliary (+), DIPT is found to be best for kinetic

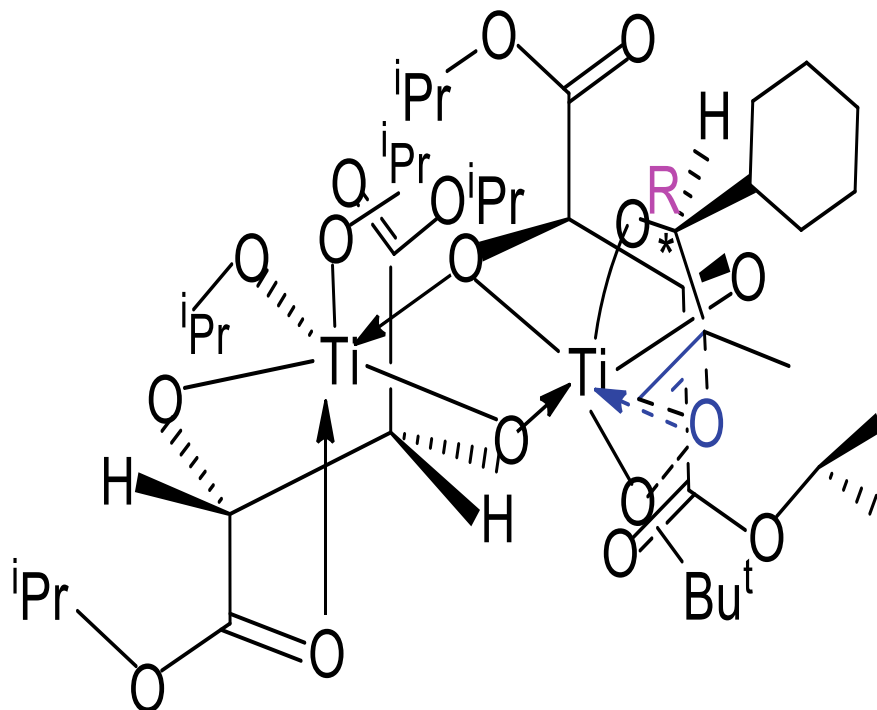


Fig. 1 A model structure of diastereotopic TS produced by Re-facial approach of epoxidating oxygen

resolution. Electron-releasing effect of alkyl group is supposed to be one feature for its selectivity. More space-filling group strongly imposes a geometrical constraint which siphones (E,R) alcohol more towards epoxide.

3.5 Justification of Scheme 1 by Model TS Structure

The discussion covered in this section considers allyl alcohol as starting compound in which carbon-bearing alcoholic hydroxylic group is a chiral centre and adjacent double-bonded carbon is a prochiral carbon. The product spread obtained from Scheme 1 is represented in Table 2.

The model based on stoichiometry ratio of reacting components clearly illustrates dimeric structure of catalyst. Attachment of chiral auxiliary allows trans coordination of substrate through alcoholic oxygen and oxidant peroxide. Chiral auxiliary when change from diethyl tartrate to diisopropyl tartrate, stereoelectronic factor of isopropyl group offers a stringent action on catalyst–substrate–epoxidating agent aggregate. And trans orientation of substrate–oxidant arrangement hardly allows

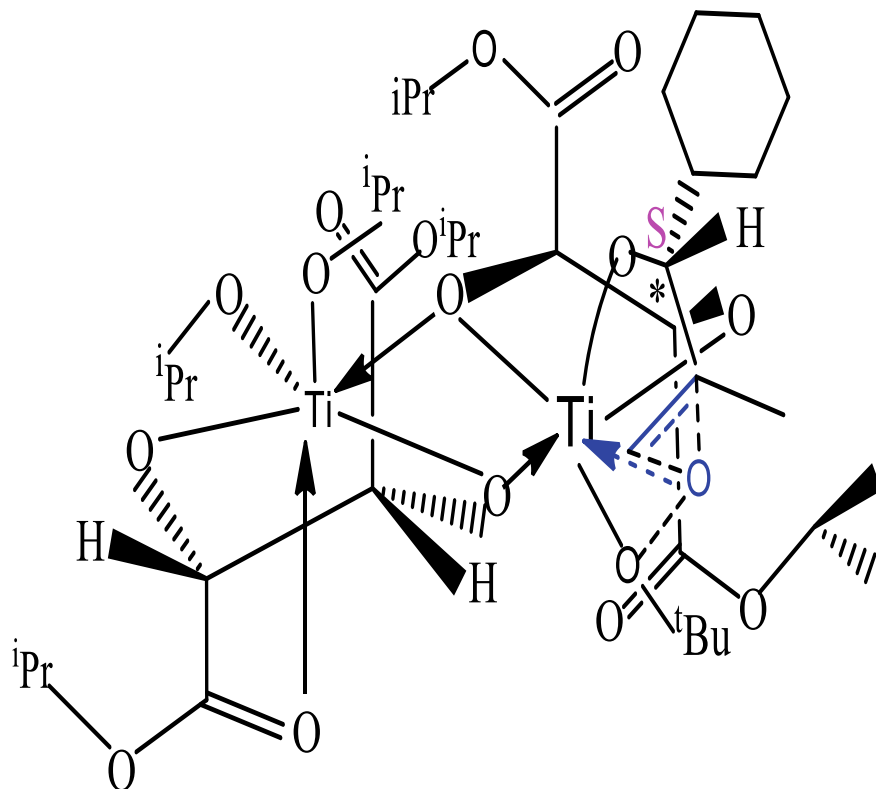


Fig. 2 A model structure of diastereotopic TS produced by Re-facial approach of epoxidating oxygen

Table 2 Orientation of existing and developing chiral centres

Approaching face	Substrate: optically active allyl alcohol		
	Chirality of alcoholic centre	R	S
Re-face	Prochiral centre appears S	SR (98%)	SS (62%)
Si-face	Prochiral centre appears R	RR (2%)	RS (38%)

epoxidating oxygen for Si-facial attack. As a result of Re-facial approach of epoxidating oxygen on (E,R) isomer of allyl alcohol, optically active epoxide bears a specific geometry showing (S,R) orientation for two chiral centres. Experimentally reported data suggest this isomer is almost enantiomerically pure with ee 96%. In case of S-configuration of starting alcohol, it projects more space-filling cyclopropyl group towards developing epoxide ring. And these two interact with bulky isopropyl group of chiral auxiliary which waived strict course of Re-facial approach of epoxidating oxygen and permits Si-facial attack to take place in lesser extent. As a result,

starting with (E,S)-allyl alcohol, Re-facial attack is recorded to yield 62% (S,S) isomer while Si-facial approach also left a considerable contribution like 38% for (R,S) isomer making product only 24% optically pure.

4 Conclusion

The model study states the origin of enantioselectivity in Sharpless epoxidation has been linked to geometrical constraint noticed in the aggregate of homogeneous catalyst, substrate and epoxidating reagent in transition structure. The analysis also points out best synthetic strategy for producing enantiomerically pure epoxide must start with an optically pure R-allyl alcohol and to direct predominating Re-facial epoxidation, tartrate-based chiral auxiliary must contain a more space-filling and more electron-releasing moiety. These epoxides appear as potential synthons for many drug molecules. Occasionally this is noticed that an in vitro active substance is almost inactive in in vivo atmosphere. Laborious attempts of synthetic chemists clinch enantiomerically pure substances in a substantial amount. The flavour of asymmetric synthesis is realized by performing resolution. The loss of more reactive half of enantiomers may often turn beneficial. Exclusion of one enantiomer from racemic mixture is a cherished target in synthetic chemistry. In this article, model based on geometry of structures meticulously illustrates dynamicity of the homogeneous catalysis leading to peerless resolution of enantiomerically pure epoxides in Sharpless asymmetric epoxidation. It is this enantioselectivity that plays a key role in providing characteristic features within molecules to attain bioselectivity.

Acknowledgements Authoress is indebted to Dr. Santanu Chakraborti, Dr. Sanjay Roy and Dr. Anjan Das for their constant encouragement.

References

- Gao Y, Hanson RM, Klunder JM, Masamune SY, Sharpless KB (1987) Catalytic asymmetric epoxidation and kinetic resolution: modified procedures including in situ derivatization. *J Am Chem Soc* 109(19):5765–5780
- Katsuki T, Sharpless KB (1980) The first practical method for asymmetric epoxidation. *J Am Chem Soc* 102(18):5974–5976
- Katsuki T, Sharpless KB (1992) The nature of the Katsuki-Sharpless asymmetric epoxidation catalyst. *J Org Chem* 57(24):6629–6635
- Martin V, Woodward S, Katsuki T, Yamada Y, Ikeda M, Sharpless KB (1981) Kinetic resolution of racemic allylic alcohols by enantioselective epoxidation. A route to substances of absolute enantiomeric purity? *J Am Chem Soc* 103(20):6237–6240
- Takano S, Iwabuchi Y, Ogasawara K (1991) Inversion of enantioselectivity in the kinetic resolution mode of the Katsuki-sharpless asymmetric epoxidation reaction. *J Am Chem Soc* 113(7):2786–2787

Electron Momentum Distribution Around Vacancy Cluster in CdO Nanoparticles



Anjan Das

Abstract Very small-sized cadmium oxide nanoparticles were prepared by sol–gel process using cadmium chloride and sodium hydroxide as precursor. Two solutions of 0.2 M CdCl₂ and 0.2 M NaOH were used with a mixture of 1:2 ethylene glycol and methanol. The particles are in the range 9–22 nm. X-Ray Diffraction (XRD) crystallography and High-Resolution Transmission Electron Microscopy (HRTEM) were carried out to characterize the samples. They are found polycrystalline in nature and possessed *fcc* (NaCl-type) structure with lattice parameter varying with annealing temperature. In the XRD spectra, the (111), (200), (220), (311), and (222) peaks of *fcc* structure can be seen without any other phases. HRTEM pictures show that the as-prepared samples are hexagonal in structure. Positron annihilation spectroscopy was carried out to investigate the Doppler-broadened spectra of the samples. The CDBS ratio curve showed a characteristic peak at $p_L = 18.7 \times 10^{-3} m_0c$ in the spectra of all the samples. It indicated the sites of positron annihilation inside the nanoparticles. The S and W parameters revealed the chemical surroundings and momentum distribution of the vacancy clusters varying with crystallite size. The lineshape (S) parameter showed a remarkable change and wing (W) parameter continuously increased with decreasing crystallite size.

1 Introduction

In this era, the nanomaterials have drawn much attention for its wide application and an increase in basic knowledge in material (Das et al. 2018) research. It is possible that structural, optical, and electrical properties of a metal oxide nanomaterial be changed with its particle size or thickness. Cadmium oxide (CdO) is a wide bandgap p-type semiconductor (Yao et al. 2013). Various methods have been adopted to synthesize CdO nanoparticles (Liu et al. 2002, 2003) in low cost to use

A. Das (✉)

Department of Physics, A.P.C. Roy Government College, Siliguri, Darjeeling 734010, West Bengal, India

e-mail: anjan802002@yahoo.co.in

© Springer Nature Singapore Pte Ltd. 2021

D. Ramkrishna et al. (eds.), *Advances in Bioprocess Engineering and Technology*,

Lecture Notes in Bioengineering,

https://doi.org/10.1007/978-981-15-7409-2_45

them in technological applications. Among the synthesis procedures, the sol–gel process is advantageous for its low cost, simple method, and production of high purity, size-controlled nanoparticles. The fabrication of three different CdO samples was achieved by sol–gel method followed by annealing in 400, 450, and 500 °C to obtain various crystallite sizes. The size, crystal structure, and morphology of the samples are discussed. Positron annihilation spectroscopy has been carried out to defect characterization and to closely observe the core electron structure with the changes in particle size.

2 Experimental Details: Synthesis of Samples

Two different solutions were prepared by dissolving 0.1 M CdCl₂ and 0.1 M NaOH in 40 ml and 200 ml distilled water. Another mixture of ethylene glycol and methanol was prepared in 1:2 ratio. Ethylene glycol mixture was added to NaOH solution and stirred for 1 h. Then CdCl₂ solution was added and stirred for 2 h. A milky white solution was obtained. The precipitate was formed by adding acetone to it. The precipitate was washed by methanol and heated to 70 °C to evaporate the methanol. Then the dried precipitate was annealed in a furnace at 300 °C. By changing the concentration of ethylene glycol, two other samples of different particle sizes were prepared. X-ray diffraction (XRD) patterns of the samples were recorded with Bruker D8 Advance diffractometer using Cu K α ($\lambda = 1.5406 \text{ \AA}$) radiation at 40 kV and 40 mA. All the samples were scanned from 20° to 85° with a scanning speed of 2° (2 θ) per minute. HRTEM images were taken with a JEOL (Model JEM 2200FS) microscope operating at 200 kV. To carry the Coincidence Doppler-Broadening measurements, a 10 μ Ci strong ²²Na source was used. The source was kept immersed inside a column of powdered sample taken in a glass tube. The source and sample were kept in a moisture-free condition. Coincidence Doppler-Broadening (CDB) measurements were done with two high-purity germanium detectors (HPGe) of energy resolutions 1.33 keV and 1.27 keV at 0.511 meV. Analysis was done with AMPS (Chatterjee et al. 2013). About 2.0×10^7 coincidence events were accumulated under CDB spectrum.

2.1 Result of X-Ray Diffraction Spectroscopy

Figure 1 shows the XRD patterns of three CdO nanoparticulate samples. Our peaks agree well with the standard values (JCPDS Card No. 05-0640) from which the purity of the samples is confirmed and face-centered cubic structure is clearly seen. The lattice constant of bulk CdO is 4.77 \AA (Yao et al. 2013). From the XRD data, we have measured the lattice constant of each sample. From the most intense broadened peak width, the average crystallite sizes of the different samples were estimated by

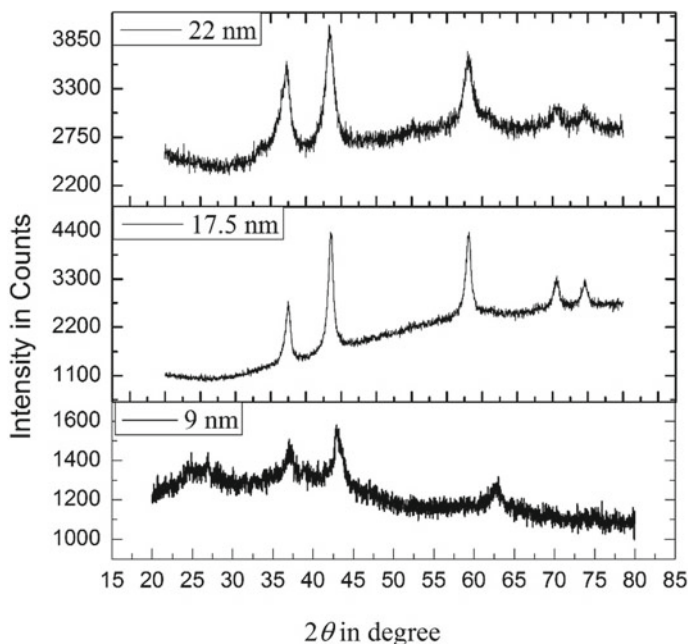


Fig. 1 X-ray diffraction spectra of synthesized samples

using the Debye–Scherrer equation (Cullity 1956) and they varied from 9 to 22 nm. Table 1 shows the crystallite size and their lattice constant.

It is seen from Table 1 that as particle size increases, lattice constant also increases. The decrease in lattice constant with decreasing particle size can result from strain induced by the increasing number of surface atoms (i.e., the atoms less surrounded by neighbor atoms) in an effort to minimize the surface free energy. Unlike in a bulk solid or coarse crystallite where the number of core atoms far outnumber the surface atoms and offer stiff resistance to surface reduction, the inner core of a nanoparticle is soft enough to contract in order to facilitate the minimization of surface energy.

Table 1 The crystallite size, lattice constant, and concentration of CdCl₂

Crystallite size (nm)	Lattice constant (Å)	Concentration of CdCl ₂ (M)
9	4.7986	0.10
17.5	4.8012	0.15
22.0	4.8052	0.20

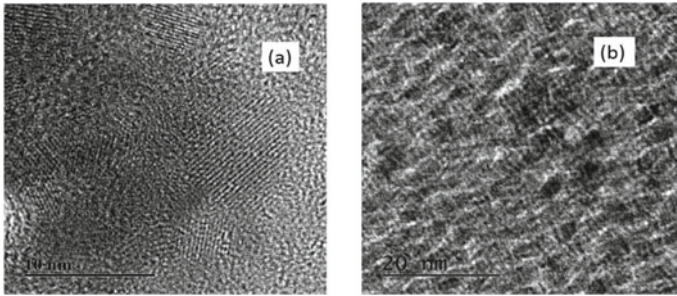


Fig. 2 HRTEM images of (a) 22 nm and (b) 9 nm samples

3 Results and Discussion

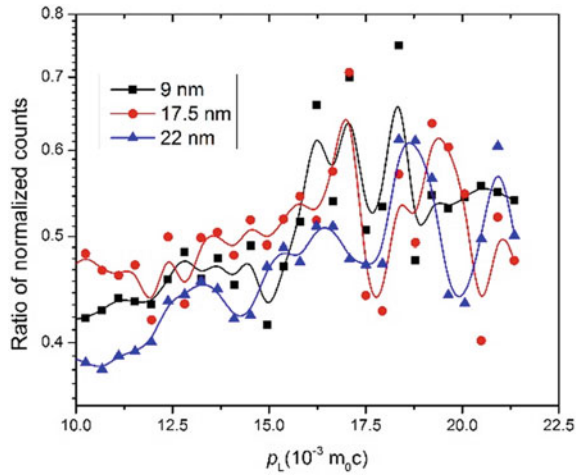
3.1 HRTEM Analysis

Figure 2 shows HRTEM images of two of the samples (Fig. 2a, b). The samples entirely consist of CdO nanoparticles of sizes 10 and 20 nm. The crystallites are hexagonal and uniform in shape and size. The crystallite sizes obtained from HRTEM images did not match exactly with the results from XRD data, and it is very natural for the experiments. The well-developed lattice fringes are also visible.

3.2 Coincidence Doppler-Broadening Analysis

The relative variation of positron annihilation parameters with electrons of the different elements present in a sample can be understood with coincidence Doppler-broadening measurements. The momentum conservation during the annihilation process gives a tool to study the momentum distribution of electrons in the solid. The momentum of the positron after thermalization is significantly smaller than that of most electrons. An advantage of the momentum distribution techniques is their sensitivity to the chemical environment of the annihilation site, which is higher compared with the positron lifetime spectroscopy. This is because the momentum distribution information is more influenced by the chemical surroundings (Das et al. 2016) than the electron density. The results of CDBS measurements are illustrated in Fig. 3. The figure shows the ratio curves obtained from the one-dimensional projection of Doppler-shifted energy distribution along the energy absorption channel and dividing the same by an identical distribution from a reference sample. A characteristic peak is observed at $p_L = 18.7 \times 10^{-3} m_0c$ in the spectra of all the samples. This is attributed to positron annihilation with the $2p$ electrons of O^{2-} ions and it indicates the trapping and annihilation of positrons in the cationic vacancies or vacancy clusters. The S -parameter is calculated from its definition—the ratio of the counts under central

Fig. 3 Peak-normalized positron lifetime spectra of samples



area of the 511 keV photopeak to the total counts under the whole spectrum. The *S*-parameter represents the fraction of positrons annihilating with the electrons of low momentum with respect to the total number of annihilated electrons. The *W*-parameter is the ratio of the counts in the wings of the curve of detected gamma radiation to the total, representing high momentum core electrons. When positron and electron annihilate inside a defect of a material, two gamma rays are usually produced, of approximate energy 511 keV each. Gamma-ray energy can be affected by the relative momentum of the particles. We have plotted the gamma photon versus channel number curve using the software AMPS. From the plot of *S* parameter versus crystallite size (Fig. 4), it can be seen that *S* increases when crystallite size increases, and the trend alters for 22 nm sample. The initial sharp increase in *S* indicates vacancy clustering inside the nanoparticles. On the other hand, the moderate decrease in *S* again emphasizes the different types of defects. The CDDBS ratio curve shows the peak again shifting toward higher momentum side for 22 nm sample. The *S* parameter decreases, which indicates the formation of phases other than CdO like Cd(OH)₂. When nanocrystallite size increases, the surface to volume ratio decreases as more and more molecules are gathered inside a particle and increases the volume. The variation of *S* may have been influenced by the formation of positronium states also inside the larger nanoparticles. I have taken the total count of six consecutive channels on each wing of the curve to calculate the *W* parameter. The increase in concentration of CdCl₂ forces the vacancy-type defects to agglomerate. The *W* parameter has shown an increasing trend with decrease in crystallite size.

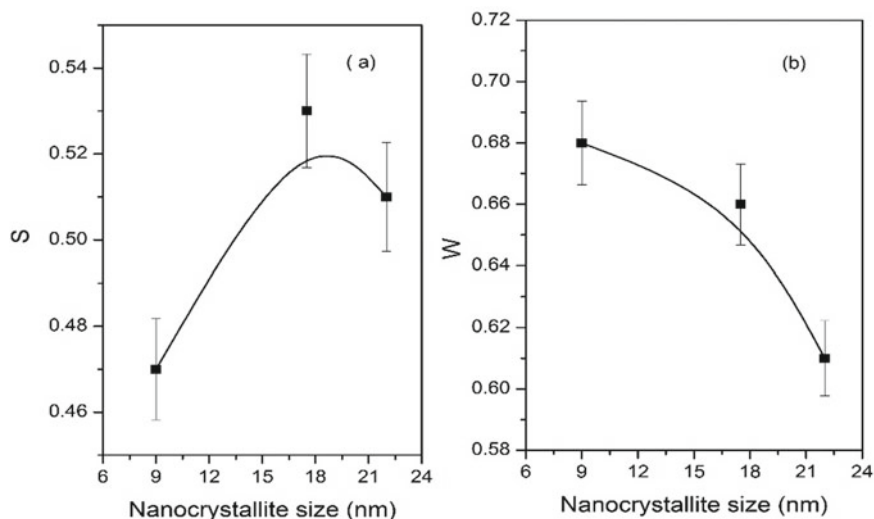


Fig. 4 Variation of S and W parameters of samples with nanocrystallite size

4 Conclusion

An understanding of size variation of cadmium oxide nanoparticles influences the crystal structure and defect characteristics have been studied in this report. Besides, the results of X-ray diffraction measurements and TEM studies are also reported. These showed lattice constant variation in one direction and similar shape and sharp lattice fringes. The positron annihilation spectroscopy showed the peak shift in lower momentum direction for 9 and 17.5 nm samples and toward higher momentum direction for 22 nm sample. In summary, the size variation successfully shows the agglomeration of defects.

References

- Chatterjee A, Ramachandran K, Kumar A, Behere A (2013) Linux advanced multiparameter system. Nuclear Physics Division, BARC. Available via <https://www.tifr.res.in/~pell/lamps.html>
- Cullity BD (1956) Elements of X-ray diffraction. Addison-Wesley Publishing Company Inc., Reading
- Das A, Mandal AC, Roy S, Nambissan PMG (2016) Mn-doping in NiO nanoparticles: defects-modifications and associated effects investigated through positron annihilation spectroscopy. *J NanoSci Nanotech* 83:4153–4163
- Das A, Mandal AC, Roy S, Nambissan PMG (2018) Internal defect structure of calcium doped magnesium oxide nanoparticles studied by positron annihilation spectroscopy. *AIP Adv* 8:095013-1–095013-13
- Liu Y, Yin C, Wang W, Zhan Y, Wang G (2002) Synthesis of cadmium oxide nanowires by calcining precursors prepared in a novel inverse microemulsion. *J Mater Sci Lett* 21:137–139

- Liu X, Li C, Han S, Han J, Zhou C (2003) Synthesis and electronic transport studies of CdO nanoneedles. *Appl Phys Lett* 82:1950–1959
- Yao G, An X, Lei H, Fu Y, Wu W (2013) Electronic and optical properties of Rocksalt CdO: a first-principles density-functional theory study. *Model Numer Simul Mater Sci* 3:16–19

Isolation, Screening, and Evaluation of Cellulase-Producing Bacteria from the Soil of Similipal Biosphere Reserve for Biofuel Production from Lignocellulosic Biomass



Manish Paul, Soumya Ranjan Meher, Subhadarshini Giri,
and Hrudayanath Thatoi

Abstract Lignocellulose is found in nature as an alternative source of energy and can be used for the production of bioethanol. Cellulose, one of the most abundant components of lignocellulose can be hydrolyzed using enzymes cellulase to produce glucose, which can be used for the production of ethanol. Cellulase production from cellulolytic bacteria is challenging. Hence, research has been focused on isolation and identification of efficient cellulolytic bacteria for their use in bioethanol production. In the present investigation, the most potent screened bacterial strain was subjected to optimization of its cellulase production by using response surface methodology taking four independent variables such as substrate concentration, pH, temperature, and incubation time. The optimization result showed that the bacteria had a maximum production of cellulase enzyme of 617.71 U/mL in an optimized condition at an incubation time of 42 h, pH 9, carboxy methyl cellulose (CMC) concentration of 15 gm/L, and temperature of 37.5 °C. The strain, SCB9, was identified as *Bacillus albus* based on the 16S rRNA sequencing and phylogeny analysis. Overall results from this study indicate that the cellulolytic bacteria SCB9 is a potent candidate for cellulase production, which can be exploited for bioethanol production from lignocellulosic biomass through adaptation of further appropriate biotechnological approaches.

Keywords Lignocellulosic biomass · Similipal biosphere reserve · Cellulolytic bacteria · Cellulase · Response surface methodology · Enzyme optimization

M. Paul · S. R. Meher · S. Giri · H. Thatoi (✉)

Department of Biotechnology, North Orissa University, Takatpur, Baripada 757003, Odisha, India
e-mail: hn_thatoi@rediffmail.com

M. Paul

e-mail: p.manish88@gmail.com

S. R. Meher

e-mail: soumyameher222@gmail.com

S. Giri

e-mail: www.shubhadarshini@gmail.com

© Springer Nature Singapore Pte Ltd. 2021

D. Ramkrishna et al. (eds.), *Advances in Bioprocess Engineering and Technology*,
Lecture Notes in Bioengineering,
https://doi.org/10.1007/978-981-15-7409-2_46

1 Introduction

Fossil fuel sources such as coal, oil, natural gas have contributed to the drastic increase in the level of greenhouse gases in the earth's atmosphere resulting in the need for alternative energy sources that are environmentally friendly, renewable, and sustainable (Ballesteros et al. 2006). Biomass is readily accessible around the world as residual wastes and agriculture biomass can be used as eco-friendly, renewable, and sustainable energy sources. The most important and abundant renewable biomass resources include crop residues such as corn straw, wheat straw, and rice straw. China has abundant biomass resources, as it is one of the largest agriculture-based economies in the world. China produces approximately 216 million metric tons of corn straw per annum and more than half of that remains utilized. Corn straw contains nonedible plant material so-called lignocellulose and is mainly composed of cellulose, hemicelluloses, and lignin.

Bioethanol produced from lignocellulosic biomass promises to achieve a great emphasis; however, the process has several challenges and limitations such as biomass transport, biomass handling, and efficient pretreatment methods for total delignification of lignocellulosic and appropriate fermentative organism. Conventionally, bioethanol is produced from the processing of starch and sucrose-based feedstock, utilizing enzymatic liquefaction and saccharification, leading to the production of relatively clean glucose pool. However, the food and feed crops for energy production crisis have promoted the need for bioethanol production from sources other than the feedstocks with direct food and feed values.

In the current study, soil sample was collected from Similipal Biosphere Reserve (SBR). Similipal Biosphere Reserve located in the northern part of Odisha and spreading over an area of 5578 km² is one of the prominent biological hotspots enriched in various floral, faunal, and microbial communities. The uneven geophysical condition of this biosphere reserve influences the diversity of floral and faunal distribution. Several studies in relation to flora and fauna diversity have been undertaken in this ecosystem. However, very less attempt has been made to assess the microbial diversity from this unique biosphere reserve. The soils of Similipal forests are associated with lignocellulosic waste materials and are good source of lignocellulolytic microorganisms. Hence, in the present study, an attempt has been made to isolate and identify some of the cellulose-degrading soil bacteria from this biosphere reserve and to assess the cellulose production ability for possible use in bioethanol production from lignocellulosic biomasses. There are attempts being made in the present study to isolate and screening of cellulose-degrading bacteria from the rhizospheric soil sample from SBR. Maximum cellulase enzyme production from the most potent bacterial isolates has also been conducted using various parameters such as temperature, pH, incubation time, and substrate concentration.

2 Materials and Methods

2.1 Collection of Soil Sample

The soil samples were collected from seven different locations of Sitakunda and Lulung regions of Similipal Biosphere Reserve.

2.2 Isolation of Cellulolytic Bacteria

Bacterial isolates were isolated by serial dilution method (Aneja 2007). 1 gm of each of the respective soil samples was homogenized in 9 mL of sterilized sterile distilled H₂O taken in test tube and the suspension was then serially diluted up to 10⁻⁵ and 10⁻⁶, respectively.

2.3 Screening of Cellulolytic Bacteria

Each bacterial isolates were screened for cellulolytic activity using CMCase plate assay (Muhammad et al. 2012). 10 µL of each bacterial broth was inoculated inside 4 mm pore made on the CMC agar plate. The CMC agar plates containing bacteria inoculums were then incubated at 37 °C for 72 h. After incubation, CMC agar plates were stained by 0.1% Congo Red solution for 1 h followed by distain using 1 N NaCl solution for the determination of cellulose hydrolyzing zone surrounding the bacterial growth on CMC agar plate.

2.4 Quantitative Assay of Bacterial Cellulase Activity

Quantitative assay of cellulase activity was estimated using DNS method (Miller 1959) by measuring the amount of reducing sugar hydrolyzed by individual bacterial isolates. Each selected bacterial strain was cultured in nutrient broth medium for overnight incubation at 37 °C. Incubated bacterial broths were individually transferred to sterilized 1-mL Eppendorf tube. Each Eppendorf tube was centrifuged at 10,000 rpm for 10 min at 4 °C. Substrate solution was prepared by adding 1% of CMC with phosphate buffer (0.1 M) at pH 6.8. 0.5 mL of substrate solution and 0.5 mL of each bacterial supernatant (crude enzyme) were taken in assay tube to form 1 mL reaction mixture. Assay tubes containing the reaction mixture were then incubated at 55 °C for 15 min in water bath. After the incubation of reaction mixture, 1.5 mL of DNS solution was added in each assay tube and boiled at 100 °C for 10 min in water bath to stop the reaction. Amount of reducing sugar released in the hydrolysis by

Table 1 Range of values for independent variables used in Box–Behnken design (BBD)

Independent variables	Symbols	Units	−1 (low value)	0	+1 (high value)
Incubation time	<i>A</i>	hour	12	42	72
pH	<i>B</i>	–	4.50	6.75	9.00
Substrate concentration	<i>C</i>	gm/L	2.0	8.5	15.0
Temperature	<i>D</i>	°C	30	37.5	45

each bacterial supernatant was measured using spectrophotometer at an absorbance value of 540 nm. During the spectrophotometric analysis, 1.5 mL DNS and 1 mL ddH₂O were taken as reference. 1 unit of cellulase activity was expressed as 1 μ/mol of glucose liberated per mL of enzyme per minute.

2.5 Optimization of Cellulase Enzyme

2.5.1 Experimental Design of Process Parameters for Cellulase Optimization Using RSM

For determining the optimum condition of cellulase activity, Box–Behnken designs (BBD) was used. Box–Behnken designs are used to generate higher order response surfaces using fewer required runs than a normal factorial technique. This technique essentially suppresses selected runs in an attempt to maintain the higher order surface definition. Using four independent variables and BBD approach, the combinatorial effects of the incubation time, pH, substrate concentration, and temperature were studied on cellulase enzyme production by the cellulolytic strain SCB9. Using Box–Behnken method, the first and higher order may be the effects of each factor and the interaction among them on cellulase activity was investigated. A total of 27 experimental conditions were designed using Design Expert 12 software optimization toolbox to perform response surface methodology (RSM). The minimum and maximum ranges of all the independent variables are given in Table 1.

Mathematical relationship of response (enzyme activity) and variables, i.e., *A*, *B*, *C*, and *D* was approximated by a quadratic polynomial model equation.

2.5.2 Preparation of Bacterial Growth Medium and Extraction of Crude Enzyme

Growth medium for bacterial isolates was prepared in 250-mL Erlenmeyer flask containing culture broth medium containing (gm/L) K₂HPO₄, 1.0, KCl, 0.2; MgSO₄·7H₂O, 1.0; yeast extract, 1.0; and pH adjusted to three different values (4.5, 6.75, and 15) with a range of substrate concentration of 2, 8.5, and 15 gm/L. All the flasks containing CMC culture broth were autoclaved at 121 °C for 15 min. After

sterilization, the flasks were set to cool in room temperature and placed under laminar flow keeping the UV light on. After few minutes, each flask was inoculated with 1% standard inoculum (V/V) of the SCB9 cellulolytic bacterial strain. The inoculated flasks were then incubated on a rotary shaker (120 rpm) at specific temperatures (30, 37.5, and 45 °C) and for specific time (12, 42, and 72 h) as given in the experimental design from the RSM calculation.

2.5.3 Quantitative Estimation of Cellulase Production

After incubation, according to the design experimental conditions, 1 mL of bacterial from each flask was taken in the Eppendorf tube. In this study, cellulase activity was measured in triplicate by preparing three Eppendorf tubes containing bacterial cultures for each experimental condition. Each Eppendorf tube containing 1 mL bacterial culture broth was centrifuged at 10,000 rpm for 10 min at 4 °C. After centrifugation, the bacterial supplements were collected to perform the DNS assay for the estimation of cellulase activity (Miller 1959). The predicted value of cellulase activity obtained from each experimental condition was then used to generate three-dimensional contour plots, regression analysis, and analysis of variance (ANOVA).

2.5.4 Statistical Analysis and Analysis of Variance (ANOVA)

Design Expert 12 (Stat Ease, Inc., Minneapolis, USA) was used for regression analysis of the experimental data to obtain working parameters and to generate polynomials and the surface contour plots. A second-order polynomial equation was established based on the analysis of variance, and the optimum ratio of experimental variable was found using the same software. Standard deviation, p value, F value, and R^2 value were also analyzed.

2.5.5 Molecular Identification and Phylogeny Analysis

The most potent cellulolytic bacterial strain was identified using 16S rRNA sequencing. The partial contig sequence obtained was further analyzed through phylogeny tree in MEGA 7 (Kumar et al. 2016).

2.5.6 Model Validation

The mathematical generated during RSM implementation was validated by conducting checkpoint studies. Experimentally obtained data were compared with the predicted one and the prediction error was calculated.

2.5.7 Molecular Identification of Cellulolytic Bacteria by 16S rRNA Gene Sequencing

Molecular identification of the bacterial strain SCB9 was performed using 16S rRNA gene sequencing of the DNA isolated from the bacterium. For the DNA extraction purpose, 1.5 mL of bacterial culture was centrifuged at 10,000 rpm to obtain bacterial cell pellets. The 16S rRNA gene was amplified using Applied Biosystem Verti Thermal Cycler. The primers for amplification were provided by Sigma-Aldrich. Universal primers, 27 forward (5AGAGTTTCCTGGCTCAG3) and 1492 reverse (5ACGGCTACCTTGTTACGATT3), were used for gene amplification. The presence of amplified gene products was determined by 2.5% agarose gel electrophoresis, and to analyze the size of amplified gene product, DNA markers of 100 bp were used that were provided by the Puregene. Amplified 16S rRNA gene was purified using a Gel DNA extraction kit (Qiagen, Seoul, South Korea) and sent for sequencing to Applied Bioscience Eurofins, Bangalore.

3 Results and Discussion

3.1 Quantitative Assay of Bacterial Cellulase Activity

In accordance with the cellulose hydrolyzing plate assay, bacterial isolates SCB7, SCB9, and SCB24 showed the highest cellulose-hydrolyzing activity as measured in DNS method. Obtained spectrometric absorbance values of the three bacterial isolates implied maximum amount of reducing sugar after the catalytic activity of cellulase on the substrate carboxy methyl cellulose (Fig. 1). Lynch et al. (1981) determined the cellulase activities of some aerobic microorganisms isolated from soil. Cellulose extracted from wheat straw, avicel, and CF11 cellulose powder contained 90% glucose, whereas filter paper and carboxy methyl cellulose contained 18% and 28% hemicelluloses, respectively. Among the microorganisms isolated, only fungi had cellulase activities and this activity was the greatest cultures of *Cladosporium cladosporoides*. Therefore, the current study is in well accordance with the above study conducted by Lynch et al. (1981) and it can be implied that bacterial strains with higher cellulolytic efficiency are abundant in the soil sample.

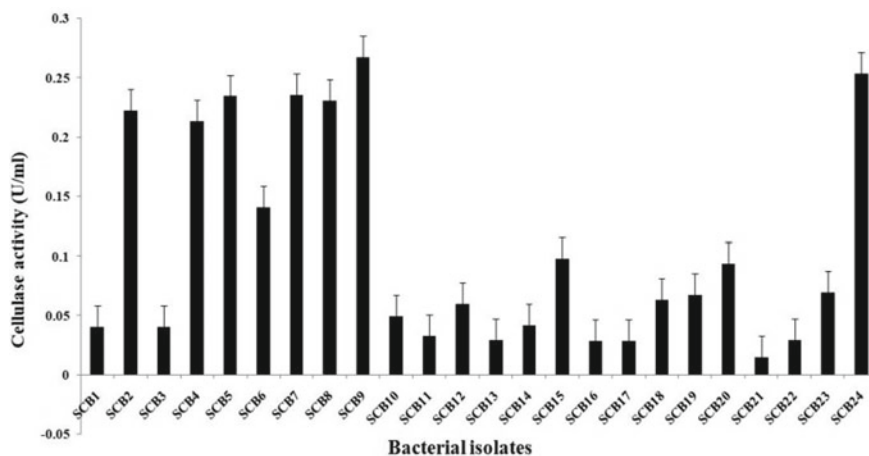


Fig. 1 Cellulase activity of Different Bacterial isolates

3.2 Optimization of Cellulase Enzyme from SCB9 Strain

3.2.1 Optimization of Physical Factors by Response Surface Methodology

From the RSM study, a highest cellulase activity for the cellulolytic bacterial strain SCB9 in an optimized condition when the independent variables were maintained at incubation time 42 h, pH 9, substrate concentration 15 gm/L and temperature 37.5 °C (Fig. 2).

3.2.2 Regression Analysis

Regression analysis was carried out to fit the mathematical model to the experimental data in order to determine the optimum conditions that result in the maximum enzyme activity. By applying multiple regression analyses, on the experimental data, a second-order polynomial equation was found to represent the relationship between enzyme activity, incubation time, pH, substrate concentration, and temperature adequately. This second-order polynomial equation obtained from multiple regression analysis is shown to explain cellulase activity of the cellulolytic bacterial strain SCB9 regardless of the significance of the coefficients. If Y is the response value of cellulase activity (Fig. 2), then the fitted response surface model is:

$$\begin{aligned} \text{Cellulase activity}(Y) = & +133.02 + 33.09 * A + 57.46 * B \\ & + 125.66 * C - 51.68 * D + 13.50 * AB \\ & + 116.91 * AC - 22.22 * AD + 184.23 * BC \end{aligned}$$

$$\begin{aligned}
 & - 10.04 * BD - 128.96 * CD - 46.05 * A^2 \\
 & - 3.76 * B^2 + 114.62 * C^2 - 35.94 * D^2
 \end{aligned}$$

3.2.3 Statistical Analysis

It is evident from the obtained statistical analysis that the cellulase activity model of SCB9 strain was highly significant, as suggested by the model F -value and low probability value. The model F -value of 230.17 as calculated from this system implies that the model is significant. There is only a 0.01% chance that an F -value larger than this could occur due to noise. The lack of fit F -value of 0.3782 implies that the lack of fit is not significant relative to the pure error. There is an 88.03% chance that a lack of fit F -value larger than this could occur due to noise. This nonsignificant lack of fit as represented from the ANOVA table evidences the optimization of model system. The coefficient of determination (R^2) was calculated as 0.9963 for enhanced cellulase activity, indicating that the statistical model can explain adequate variability in the response. Similarly, Doddapaneni et al. (2007) suggested that closer the value of R^2 to 1.0, stronger the model and better it predicts the response of tested enzyme activity according to the designed experimental conditions. The predicted R^2 value of 0.9831 was in reasonable agreement with the adjusted R^2 value of 0.9920. This indicated a good agreement between the experimental and predicted values for cellulase activity. If there are many terms in the model and the sample size is not very large, the adjusted R^2 value may be noticeably smaller than the R^2 . In the present study, in concur with the above statement, adjusted R^2 0.9920 is also less than the R^2 value 0.9963.

Saravanan et al. (2012) studied the optimization of cellulase production using *Trichoderma reesei* by RSM and comparison with genetic algorithm. The potential of *Trichoderma reesei* for cellulase production using pineapple waste as substrate has been investigated. A maximum cellulase activity of 569.23 U/mL is obtained under the optimum experimental conditions; pH 5.5, temperature 37 °C, initial substrate concentration 3%, inoculum concentration, and culture time. Box–Behnken design (BBD) statistical tool and genetic algorithm are used to optimize the process parameters. The BBD study of linear and quadratic interactive effects of experimental variables on the desired response of cellulase activity showed that the second-order polynomial is significant. Therefore, it can be depicted from the optimization of cellulase activity that both the current study and the study undertaken by Saravanan et al. (2012) that BBD is a suitable technique and it properly determines as well as validate the optimum condition for maximum enzyme activity.

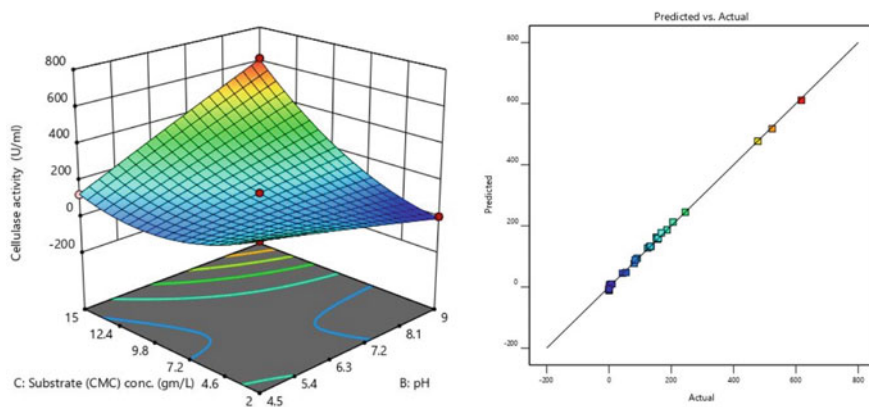


Fig. 2 3-D response surface contour plots of interaction between various experimental factors with cellulase activity (left). Predicted versus actual model of cellulase activity of SCB9 (right)

3.3 Identification of Cellulolytic Bacteria

The most potent cellulolytic strain SCB9 was identified as *Bacillus albus* by its 16S rRNA sequencing. Shajahan et al. (2016), in their study, identified high cellulose-producing thermophilic bacteria as *Bacillus licheniformes*. Therefore, the current study and the study of Shajahan et al. (2016) implied that the bacterial strains from the genera *Bacillus* are common with high cellulolytic activity and this bacterial class is diversified according to their habitat.

4 Conclusion

Cellulases are the most important enzymes that are responsible for the bioethanol production. It is one of the most widely used enzymes having great industrial application. Microorganisms are main source of cellulase for which research has been focused on isolation and identification of potent cellulose-producing bacterial to meet the growing demand for cellulases. In Similipal Biosphere Reserve, soil-decomposed plant biomasses are rich in lignocellulolytic bacteria. In this study, 24 cellulolytic bacteria were isolated from the Similipal soil samples that were screened for their cellulose-hydrolyzing capacity and cellulase activity. The screening of cellulase activity revealed that SCB9 strain has the highest turnover of glucose production by degrading CMC with a value of 73.94 U/mL in unoptimized condition. When subjected to optimization of parameters through RSM, the enzyme production showed (617.71 U/mL) cellulase activity over the unoptimized conditions with 8.35-fold increase. The present study reveals the potential for high cellulase production by the identified strain *Bacillus albus*. Further studies with regard to enzyme

characterization and the potential of the enzyme in bioethanol production need to be evaluated.

Conflict of Interest The authors declare that they have no conflict of interest.

Ethical Approval This chapter does not contain any studies with human participants or animals performed by any of the authors. Collection of soil sample from the buffer areas of Similipal Biosphere Reserve, Odisha with a condition that no plants and animals would be disturbed and following all the provision of Biodiversity Act has been permitted by Odisha Forest and Environment Department, Government of Odisha.

References

- Aneja KR (2007) Experiments in microbiology, plant pathology and biotechnology new age international 1-602
- Ballesteros I, Negro MJ, Oliva JM, Cabañas A, Manzanares P, Ballesteros M (2006) Ethanol production from steam-explosion pretreated wheat straw. *Appl Biochem Biotechnol Spring* 129–132:496–508
- Doddapaneni KK, Tatineni R, Potumarthi R, Mangamoori LN (2007) Optimization of media constituents through response surface methodology for improved production of alkaline proteases by *Serratia rubidea*. *J Chem Technol Biotechnol* 82(8):721–729
- Kumar S, Stecher G, Tamura K (2016) MEGA7: molecular evolutionary genetics analysis version 7.0 for bigger datasets. *Mol Biol Evol* 33(7):1870–1874
- Lynch JM, Slater JH, Jacqueline A, Bennett SH (1981) Cellulase activities of some aerobic microorganisms isolated from soil. *J Gen Microbiol* 127:231–236
- Miller GL (1959) Use of dinitrosalicylic acid reagent for determination of reducing sugar. *Anal Chem* 31(3):538–542
- Muhammad I, Asma S, Quratulain S, Muhammad N (2012) Isolation and screening of cellulolytic bacteria from soil and optimization of cellulase production and activity. *Tur J Biochem* 37(3):287–293
- Saravanan P, Muthuvelayudham R, Kannan RR, Viruthagiri T (2012) Optimization of cellulase production using *Trichoderma reesei* by RSM and comparison with genetic algorithm. *Front Chem Sci Eng* 6:443–452
- Shajahan S, Muthu GMI, Natesan S, Gopal S (2016) Statistical modeling and optimization of cellulase production by *Bacillus licheniformis* NCIM 5556 isolated from the hot spring, Maharashtra, India. *J King Saud Univ Sci* 29

Nanomaterials and Nanotechnology

Reduced Graphene Oxide (RGO)-Based Nanocatalyst for Inhibition of Pathogenic Bacteria Toward Enhancement of Water Purification



Shubhanwita Saha, Debashis Roy, and Chiranjib Bhattacharjee

Abstract Over the last few decades, various research concepts have been developed to inhibit the growth of waterborne pathogenic bacteria. Among them, antibacterial agent synthesis and application in water disinfection is one of the major challenges, nowadays. It was observed that metal nanoparticles, such as Zn, Ag, Ti, Fe, or metal-derived nanomaterials exhibited enhanced catalytic effect for water disinfection. The use of graphene or R-GO as a support material for the dispersion of metal nanoparticles provides new ways to develop advanced, cost-effective catalyst materials for the enhanced catalytic reaction. It is an attempt to generate a general overview regarding the role of graphene and RGO-based composites as disinfectant agents against waterborne pathogens.

Keywords Wastewater treatment · Graphene · RGO-based catalyst · Pathogen disinfection

1 Introduction

At present, the environment is getting affected by several effluences, harmful wastes, contaminants, among them, water pollution is one of the major problems that affected the natural habitat of the living being, directly. As per the report of WHO in 2015, almost 1.1 billion people were affected by the drinking water crisis caused by several environmental and climatic concerns, increasing population and higher cost of drinking water (Anjum et al. 2016). To get rid of the problem of water crisis, several projects have been launched all over the world. In our country, “Namami

S. Saha · D. Roy · C. Bhattacharjee (✉)
Chemical Engineering Department, Jadavpur University, Kolkata 700032, India
e-mail: c.bhatta@gmail.com

S. Saha
e-mail: shubhanwita.2007@gmail.com

D. Roy
e-mail: deebie_roy@yahoo.com

Gange Programme” is one of the examples of that kind of attempt by the government for the improvement of “Swachh Bharat Mission.”

For last few years, various strategies such as filtration, absorption, chlorination, and UV irradiation have been employed to remove contaminants from wastewater. Although some of the techniques are unsuccessful to completely disinfect harmful contaminants such as organic dyes, harmful chemicals, and aquatic pathogenic bacteria, viruses from wastewater as well as surface water and other techniques are very costly (Anjum et al. 2016; Collivignarelli et al. 2018). Recently, it is notified that several researchers are utilizing nanotechnology-based routes toward the enhancement of wastewater remediation, whereas nanomaterials, specifically graphene or reduced graphene oxide, carbon nanotube-based materials play very crucial role as adsorbent, catalyst-supporting agent, bactericidal agents, and so on (Yousefi et al. 2019; Saha et al. 2014; Han et al. 2019). More specifically, Graphene is a two-dimensional single-layer nanosheet consisting of sp²-hybridized C-atoms (Hass et al. 2008). Its unique planar nanostructure and wide-ranging extraordinary properties offer various potential applications in a large number of areas such as water purification, membrane preparation, sensor application, enhanced energy generation, storage, and so on. On the other hand, metal and semiconductive metal nanoparticles such as Zn, Ag, Ti, Fe, and their derivatives exhibited enhanced catalytic effect for water disinfection (Han et al. 2019; Akhavan and Ghaderi 2009).

In terms of pathogen disinfection, *Legionella*, *Salmonella typhimurium*, *Escherichia coli* (specific stain), *Vibrio cholera*, and *Campylobacter jejuni* are well-known bacteria causing various harmful diseases and their complete inhibition from water system is another major challenge in wastewater remediation, nowadays (Han et al. 2019). It is also revealed that graphene and its composites are very effective bactericidal agents and able to destroy bacterial cell walls as well as forming various reactive species (H⁺, O⁻, H₂O₂, OH⁻) in optimum condition. In this paper, we are reviewing the role of graphene and reduced graphene oxide-laden composites for the inhibition of pathogenic bacteria toward the enhancement of water purification.

2 Graphene as Antibacterial Agent

For the historical evolution of graphene-based materials, graphene oxide (GO) has been experimentally analyzed for the last 40 years (Boehm et al. 1962, 1994). More precisely, it is the oxidized form of graphite with various functional groups that converted as reduced graphite oxide (RGO) or graphene after reduction by the strong reducing agent like hydrazine hydrate. The basic structure of graphite and graphene is demonstrated in Fig. 1.

It was first reported in the year of 2010 that physical structure and sharp edges in graphene sheet are destroying cell walls in pathogen. Moreover, graphene sheets were more capable to destroy the bacteria than general antibiotic and graphite oxide also proficient to destroy the broad range of pathogens such as pathogenic bacteria, protozoans, fungi, and so on. Due to the presence of various functional groups such

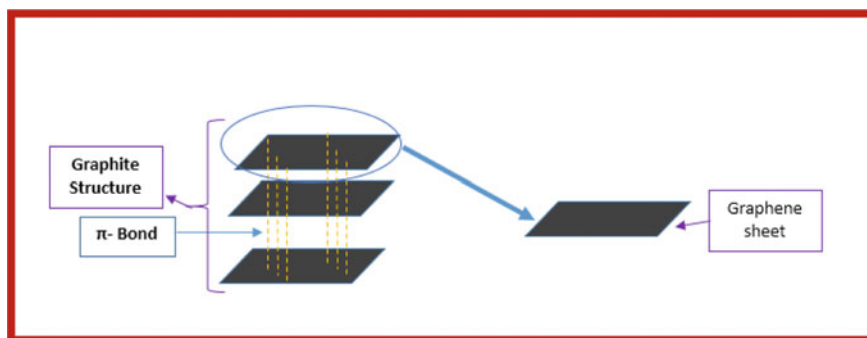


Fig. 1 Structure of graphite and 2D graphene

as $-OH$, $C=O$, in GO, it may have strong adsorption, cell membrane destruction capability helps to prevent the direct contact with other organelles as well as the cell death (Liu et al. 2011).

3 Graphene or RGO Metal-Based Nanocomposites as Antibacterial Agent

In the wide range of antibacterial agents, silver (Ag) is a very well-known metal used as an antibacterial agent from the past few decades. Recently, it is reported that functionalized graphene or RGO with Ag shows a better antipathogenic effect than only graphene and Ag, elaborated in Table 1. Particularly, RGO–Ag composite destroys the bacterial cell through two-step process, first, the nanocomposite interacts with the cell membrane and releasing Ag ions that able to destruct the cell membrane follows by the oxidation reaction.

In-situ reduction, microwave-assisted synthesis, immobilization-method are well-known chemical-based synthesis routes which are mainly employed by several researchers for RGO–Ag nano-composite synthesis purpose in recent past. The synthesis process is very important to enhance the bactericidal property in nanocomposite. In some cases, it was also found that the agglomeration of Ag reduces the efficiency of the composite. Therefore, the size of Ag nanoparticles, dispersion of Ag nanoparticles on graphene sheet, and structure of nanocomposite are the most crucial factors for synthesizing efficient nanocatalyst as well as enhancing the antibacterial property in wastewater remediation.

On the other hand, several metals and metal-based oxide nanocatalysts such as RGO–ZnO, RGO–Fe, RGO–CuO exhibited their enhanced antibacterial property due to their higher catalytic efficiency. Moreover, enhanced conductivity and electron transfer to oxygen contain group in GO result higher amount of ROS production than the nonmetal composite, which leads to cell damage.

Table 1 Comparative antimicrobial performance analysis of GO- and RGO-based nanomaterials

Name of nanomaterials	Concentration of nanomaterials (mg/ml)	Name of bacteria	Antibacterial performance	References
RGO	40,000	<i>E. coli</i>	45.9% in 2 h	Liu et al. (2011)
GO–Ag	0.045	<i>E. coli</i>	100% in 48 h	Bao et al. (2011)
RGO–Ag	0.025	<i>E. coli</i>	89% in 2 h	Shahriary et al. (2015)
Graphene–Fe	0.1	<i>E. coli</i>	90% in 1 h	Gonavelli et al. (2013)
GO–ZnO	0.05	<i>E. coli</i>	50–60% in 24hrs	Wang et al. (2014)
RGO–TiO ₂	0.1	<i>E. coli</i>	100% under sunlight in 1.5 h	Wanag et al. (2018)
GO–TiO ₂	0.18	<i>E. coli</i>	100% under sunlight in 30 min	Chang et al. (2015)

4 Graphene or RGO-Based Photocatalyst as Antibacterial Agent

Nowadays, the main objective of photocatalyst synthesis is to improve their photocatalytic performances in the presence of visible light irradiation. However, graphene or RGO plays a very vital role in increasing the amount of ROS and hydrogen peroxide production, which influences cell apoptosis as well as necrosis via cell oxidative stress. In the case of efficient photocatalyst, titanium dioxide (TiO₂) is a familiar example, able to enhance the photocatalytic performances in the field of water splitting, dye degradation, and so on. On the year of 2015, it was reported that GO–TiO₂ photocatalyst enhances the bactericidal property by almost 25% and 60% than the bare TiO₂ under solar light and UV light irradiation, respectively (Chang et al. 2015). Several RGO–TiO₂-based photocatalysts and their performances against *E. coli* have been tabulated in Table 1. It refers that only small amount of graphene enhances the photocatalytic efficiency of TiO₂ against gram-positive bacteria *E. coli* under visible light irradiation. Most recently, it was reported that TiO₂ functionalized RGO sheet able to inactivate the *E. coli* cell within 75 min under sunlight irradiation (Wanag et al. 2018).

5 Summary and Future Scope

In this article, we were focusing on the part of the antibacterial activity of graphene- or RGO-based composites for wastewater remediation. The effectivity of RGO metal nanocatalysts for *E. coli* inhibition was properly reviewed. Not only that the role graphene for effective photocatalyst development as well as antibacterial property enhancement was shortly described and explained. Bactericidal effect of RGO-based nanocatalyst, namely, RGO–Ag, RGO–Fe, RGO–Cu, RGO–ZnO, RGO–TiO₂ were evaluated and their comparative analysis was done based on their performance. Probable mechanisms in terms of nanocomposite–cell membrane interaction, ROS production, and electron transfer process were briefly elaborated and depicted in Fig. 2. Although the exact cell destruction mechanism of each catalyst for specific pathogens as well as their structural and functional correlation establishment are broad gap and future scope of research, till the date.

Acknowledgements Financial assistance for PostDoctoral Fellow received from RUSA 2.0 (Ref No.: R-11/397/19) is gratefully acknowledged.

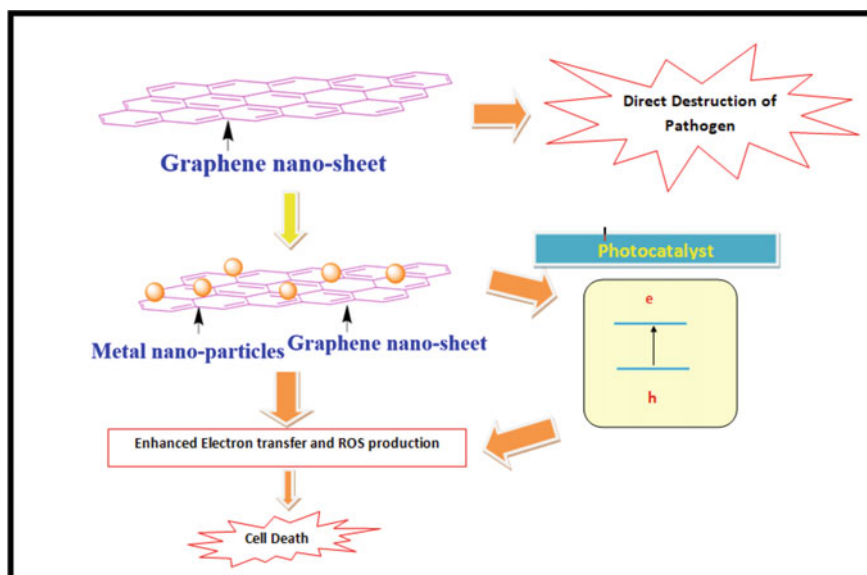


Fig. 2 Graphene and its composite and their effect on pathogen destruction

References

- Akhavan O, Ghaderi E (2009) Photocatalytic reduction of graphene oxide nanosheets on TiO₂ thin film for photo inactivation of bacteria in solar light irradiation. *J Phys Chem C* 113:20214–20220. <https://doi.org/10.1021/jp906325q>
- Anjum M, Miandad R, Waqas M et al (2016) Remediation of wastewater using various nano-materials. *Arabian J of Chem* 12:4897–4919. <https://doi.org/10.1016/j.arabjc.2016.10.004>
- Bao Q, Zhang D, Qi P (2011) Synthesis and characterization of silver nanoparticle and graphene oxide nanosheet composites as a bactericidal agent for water disinfection. *J Colloid Interface Sci* 360:463–470. <https://doi.org/10.1016/j.jcis.2011.05.009>
- Boehm HP, Clauss A, Fischer GO et al (1962) The adsorption behavior of very thin carbon films. *Zeitschrift Für Anorganische Und Allgemeine Chemie* 316:119–127. <https://doi.org/10.1002/zaac.19623160303>
- Boehm HP, Setton R, Stumpp E (1994) Nomenclature and terminology of graphite intercalation compounds. *Pure Appl Chem* 66:1893–1901. <https://doi.org/10.1351/pac199466091893>
- Chang YN, Ou XM, Zeng GM et al (2015) Synthesis of magnetic graphene oxide-TiO₂ and their antibacterial properties under solar irradiation. *Appl Surf Sci* 343:1–10. <https://doi.org/10.1016/j.apsusc.2015.03.082>
- Collivignarelli MC, Abbà A, Benigna I et al (2018) Overview of the main disinfection processes for wastewater and drinking water treatment plants. *Sustainability* 10:1–2. <https://doi.org/10.3390/su10010086>
- Gonavelli G, Chang CC, Ling YC (2013) Facile synthesis of smart magnetic graphene for safe drinking water: heavy metal removal and disinfection control. *ACS Sustain Chem Eng* 1:462–472. <https://doi.org/10.1021/sc300112z>
- Han W, Wu Z, Li Y et al (2019) Graphene family nanomaterials (GFNs)—promising materials for antimicrobial coating and film: A review. *Chem Engg J* 358:1022–1037. <https://doi.org/10.1016/j.cej.2018.10.106>
- Hass J, Heer WAD, Conrad EH (2008) The growth and morphology of epitaxial multilayer graphene. *J Phys Condens Matter* 20:323202–323229. <https://doi.org/10.1088/0953-8984/20/32/323202>
- Liu S, Zeng TH, Hofmann M et al (2011) Antibacterial activity of graphite, graphite oxide, graphene oxide and reduced graphene oxide: membrane and oxidative stress. *ACS Nano* 5:6971–6980. <https://doi.org/10.1021/nn202451x>
- Saha S, Basak V, Dasgupta A, Ganguly S, Banerjee D, Kargupta K (2014) Graphene supported bimetallic G-Co-Pt nanohybrid catalyst for enhanced and cost effective hydrogen generation. *Int J Hydrogen Energy* 39:11566–11577. <https://doi.org/10.1016/j.ijhydene.2014.05.131>
- Shahriari L, Nair R, Sabharwal S, Athawale AA (2015) One-step synthesis of Ag-reduced graphene oxide-multiwalled carbon nanotubes for enhanced antibacterial activities. *New J Chem* 39:4583–4590. <https://doi.org/10.1039/c4nj02275k>
- Wanag A, Rokicka P, Kusiak-Nejman E et al (2018) Antibacterial properties of TiO₂ modified with reduced graphene oxide. *Ecotoxicol Environ Saf* 147:788–793. <https://doi.org/10.1016/j.ecoenv.2017.09.039>
- Wang YW, Cao A, Jiang Y et al (2014) Superior antibacterial activity of zinc oxide/graphene oxide composites localized around bacteria. *ACS Appl Mater Interfaces* 6:2791–2798. <https://doi.org/10.1021/am4053317>
- Yousefi N, Lu X, Elimelech M, Tufenkji N (2019) Environmental performance of graphene based 3D macrostructures. *Nat Nano Technol* 14:107–119. <https://doi.org/10.1038/s41565-018-0325-6>

Wound Healing and Antimicrobial Property of Phytofabricated Silver Nanoparticle by *Saraca asoca* Bark Extract on Diabetic Wound In Mice



Baishakhi Bairagi and Debjani Nath

Abstract The phytochemicals can act as reducing agents as well as nontoxic capping materials of metal nanosilver. The objective of the present work was to fabricate the synthesis of silver nanoparticle using aqueous bark extract of *Saraca asoca* as reducing agent and testing the wound healing efficacy of the material by studying the level of wound contraction and re-epithelialization and expression of inflammatory factors like cytokines and different proinflammatory markers in diabetic mice. The biocompatibility of the synthesized silver nanoparticle was tested by cell cycle analysis, ROS generation, DAPI, comet assay. It was indicated that the synthesized silver nanoparticles were nontoxic to normal mice in vivo. Antibacterial properties of the silver formulation are comparable to different antibiotics and more effective against *Bacillus firmus* and *Staphylococcus gallinarum* of diabetic wound. SEM images and histopathological observations revealed that the healing process was accelerated in the silver nanoparticle treated group. The significant healing efficacy of phytofabricated nanoparticles was evident by the observations of downregulation of proinflammatory cytokines such as IL-1 β , IL-6, and TNF- α , and upregulation of anti-inflammatory cytokine, IL-10.

Keywords *Saraca asoca* · Silver nanoparticles · Diabetic wound · Wound healing · Antibacterial efficacy

1 Introduction

Diabetic wound is a challenging problem due to its delayed process of healing that needs a longer time for proper cure. Silver nanoparticles are best studied due to their antimicrobial activity and have the efficacy in bypassing mechanisms of drug

B. Bairagi · D. Nath (✉)
Department of Zoology, University of Kalyani, Kalyani, Nadia, West Bengal 741235, India
e-mail: nath_debjani@yahoo.co.in

B. Bairagi
e-mail: baisakhi91@yahoo.com

resistance found in diabetic wounds (Griffith et al. 2015; Pelgrift and Friedman 2013). Clinical uses include topical treatment of infected burns, open wounds, and chronic ulcers. In addition to its anti-inflammatory effects, it controls collagen deposition that accelerates wound healing (Chaloupka et al. 2010). Phytochemically protected silver nanomaterial is more sustainable and eco-friendly than the chemically synthesized one.

Diabetic wounds are characterized by a hyperinflammatory response characterized by infiltration of large number of neutrophils and macrophages capable of producing radical oxygen species as defense mechanisms against invading microbes. The effect can aggravate the inflammation and cytotoxicity of the microenvironment delaying wound healing (Wetzler et al. 2000; Dissemond et al. 2002; Robinson 2009).

Green synthesized silver nanoparticles using *Catharanthus roseus*, *Solanum xanthocarpum* L., *Solanum indicum*, *Ziziphus nummularia*, *Citrullus colocynthis*, *Kigelia Africana*, *Coriandrum sativum*, *Arnebia nobilis*, *Cassia auriculata*, *Virola oleifera*, *Viburnum trilobum*, *Tridax procumbens*, *Lansium domesticum*, *Azadirachta indica*, *Dimocarpus longan*, *Cucumis sativus* and *Orchidantha chinensis* have been shown by different investigators to have significant healing efficiency toward cut and burn wound and chronic wounds (Shinwari et al. 2006; Garg et al. 2014; Shankar et al. 2015; Pothireddy et al. 2016; Mohanta et al. 2017; Bhagavathy and Kancharla 2016; Pannerselvam et al. 2017; Wang et al. 2017; Al-Shmgani et al. 2017). Silver ion is considered as toxic toward biological system due to its biochemical reactivity but many investigators showed that phytoprotective silver nanomaterial possessed insignificant level of toxicity in cultures as well as in vivo system (Ovais et al. 2018). Phytoprotected silver nanoparticles have the capacity to kill multidrug-resistant bacterial populations leading to the fast healing of wounds (Gunasekaran et al. 2011). It exposes its reactive and catalytic sites for action during inflammation, cell proliferation, contraction and remodeling of skin during wound healing.

The bark extract of *S. asoca* was found to have significant analgesic and anti-inflammatory activity (Sharif et al. 2011). In this study, we have applied “green” method to synthesize silver nanoparticles using the aqueous bark extract of *Saraca asoca* as reducing agent. In this study, we have analyzed the efficacy of topically applied phytofabricated silver nanoparticle for the healing of diabetic wound in comparison with common silver sulfadiazine ointment.

2 Materials and Methods

2.1 Preparation of Plant Extract

Saraca asoca bark was collected from the garden of University of Kalyani, Kalyani, Nadia, and West Bengal, India. The voucher specimens (Deb.kly-60) were deposited and preserved in the Department of Botany. Bark was ground properly. 0.5 g of bark powder was mixed with 20 ml of distilled water and heated for 10 min.

2.2 Synthesis of Silver Nanoparticles

20 ml of 0.001 (M) silver nitrate solution was mixed with 1 ml of plant extract. The mixture was heated to 45 °C for 45 min in water bath and after that, it was kept at room temperature for 30 min to observe the color change from light yellow to brown. Then the mixture was incubated at room temperature for 48–72 h for completion of the reaction (Banerjee and Nath 2015). The change of color of the mixture was from pale yellow to light brown during the heating process and finally, the color became dark brown and indication for the synthesis of silver nanoparticles. The conical flask was incubated at room temperature for 48 h for the complete settling of the nanoparticles.

2.3 Characterization

Prepared silver nanoparticles were characterized by UV–vis spectroscopy at 400–450 nm after proper incubation. The hydrodynamic size of synthesized nanoparticle was characterized by DLS. Zeta potential was also observed. Proper size of nanoparticle was characterized by AFM and SEM images. To investigate the surface material of the nanoparticles, FTIR was done with the dried sample.

2.4 Biocompatibility

The level of biocompatibility was tested on the isolated lymphocytes. The spleen lymphocytes were obtained using Histopaque (Sigma-Aldrich, St. Louis, MO, USA) according to the method of Boyum (1976). The extent of nuclear damage was estimated by DAPI staining (Mollick et al. 2014), Comet assay (Sing et al. 1988), and cell cycle analysis by flow cytometry (Pozarowski and Darzynkiewicz 2004). The generation of ROS was detected by 2, 7-dichlorofluorescein di-acetate (DCFH-DA) fluorescence following the methodology of Roy et al. (2008).

2.5 Preparation of Diabetic Animal Model

Twenty-week-old mature Swiss albino male mice were taken. Diabetes was induced by one-time injection of streptozotocin at 150 mg/kg body weight. 180 mg/dl of blood glucose level was the indication of diabetes that was developed on the 11th day of streptozotocin injection. There were six groups of mice and three mice in each group.

Group 1: diabetic mice + thermal wound (untreated); Group 2: diabetic mice + thermal wound + SSD treated; Group 3: diabetic mice + thermal wound + AgNPs

treated; Group 4: normal + thermal wound (untreated); Group 5: normal + thermal wound + SSD treated; Group 6: normal + thermal wound + AgNPs treated. Silver nanoparticle was given at the rate of 15 mg/kg body weight one time to each mouse.

Thermal wound was developed with hot water. The wounds were covered with proper dressing prepared by SSD ointment and different concentrations of silver nanoparticles. After 5th, 10th, and 15th days of treatment, the skin samples were collected for histological analysis and PCR technique to see the cytokine levels (Bhagavathy and Kancharla 2016).

2.6 Reverse Transcription and Amplification

Skin tissue was homogenized and processed for isolation of RNA. Reverse transcription and real-time polymerase chain reaction were done by preparing the complementary cDNA using TaqMan reverse transcription with MultiScribe reverse transcription as per manufacturer's protocol. Then the reaction mixture was taken to thermal cycling in a real-time PCR system with the conditions: after incubating with hexamer at 25 °C for 12 min, the reverse transcription was continued for 58 min at 37 °C. Then the temperature was increased to 95 °C for 6 min to stop the reaction and to get the final cDNA product. cDNA product was stored at -20 °C until used for amplification.

2.7 Antibacterial Activity Testing

Wound swab was collected and bacterial colonies were cultured on nutrient agar plates. Nutrient agar was mixed with water (28 gm/L) and then slightly heated to dissolve the agar. The dissolved agar was poured into the Petri dishes. After 3–4 h, the agar plates were ready to culture the bacterial samples. After inoculating the plates with bacterial samples, the plates were kept in BOD incubator at 37 °C. Within 24–48 h, bacterial colony formation was observed. After proper growth of the bacterial colonies on agar plates, each type of colony was isolated and separately cultured on agar medium. To get a pure culture of each bacterial sample, 3–4 agar plate transfer was done. After getting pure culture, all the bacterial samples were identified by 16S rDNA-based molecular technique. DNA was isolated and evaluated on agarose gel. DNA sample was amplified by PCR technique and then subjected to Sanger sequencing. Then bidirectional DNA sequencing reaction of PCR amplicon was carried out. Consensus sequence of 16S rDNA was generated from forward and reverse sequence data using proper software. The 16S rDNA sequence was used to carry out BLAST alignment search tool of NCBI Genbank database.

The bacterial colonies on agar plates were used to measure the zones of inhibition with synthesized nanoparticles in comparison with antibiotics and standard synthetic drugs.

3 Results and Discussion

The average particle size calculated was found to be 3–10 nm using Dynamic Light Scattering measurements (DLS). It was observed that 45 °C was the optimal temperature for the conversion of silver metal to silver nanoparticle and the SPR peaks became sharper with an increase in optical density of the yellowish-brown solution after 30 min of incubation depending on increasing temperature from 25 to 45 °C. The SPR peak at 433 nm indicates the formation of silver nanoparticles. Further increase in temperature (up to 65 °C) showed a clear shift of SPR peak from 433 to 455 nm and an indication for the increase in AgNPs size (Banerjee and Nath 2015). Depending on the size of the nanoparticle, the sharpness in the absorbance peak can be determined, as at 45 °C temperature, the particle size may be smaller that results in sharpness of the plasmon resonance band of silver nanoparticles (Goia 2004). Increasing temperature up to 65 °C induced the crystal growth formation around the nucleus that results in decreasing the absorption as well as the intensity of synthesized nanoparticle.

The presence of spherical shaped particles within the size range of <5 nm was shown by AFM analysis. FTIR analysis indicated the involvement of carboxyl ($-C=O$), hydroxyl ($-OH$), and amine ($-NH$) functional groups of the phytochemicals in capping and stabilizing silver nanoparticles. The rapid electrokinetic behavior of the silver was evaluated using zeta potential (approximately -23.2 mV) confirmed its stability (Banerjee and Nath 2015). According to the GC–MS analysis, different phytochemicals or hydrocarbon groups are present on the surface of the synthesized nanoparticle. The hydrocarbons present on the synthesized silver nanoparticle are the capping agent of silver nanoparticles. These capping agents prevent the agglomeration of the particle and thus the synthesized nanoparticle was stabilized (Starlin et al. 2012).

Biocompatibility study by DAPI staining revealed no change in nuclear morphology and membrane integrity. The result of comet assay was also similar in both treated and control groups of cells and it produced no evidence of release of nuclear material and no disruption of the cellular membranes. Intracellular ROS levels were not altered significantly when compared with that of the control. Results of the tests conducted at the cellular and genetic levels indicated that the synthesized silver nanoparticle is not potentially toxic to induce any significant or harmful change (data not shown).

Without any treatment, the healing process continues but becomes accelerated by silver nanoparticles in case of both diabetic and normal mice (Fig. 1). Histological studies show that re-epithelialization almost complete within 15th day when it was treated with AgNPs (Fig. 2). For wound healing process, fibroblast cells are important. Scanning electron microscopy images (Fig. 3) show that proper fibroblast cells are formed by the treatment of AgNPs in relation to standard synthetic drug, SSD.

Results show that AgNPs are much more effective for healing of thermal wound. The results revealed that the percent of wound contraction was 90% at 15th day of treatment with the synthesized green silver nanoparticles of normal as well as

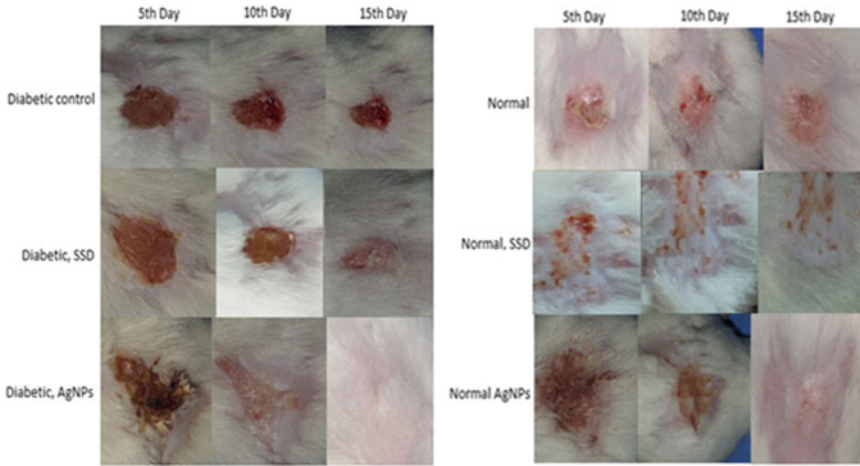


Fig. 1 Wound contraction in treated and untreated mice

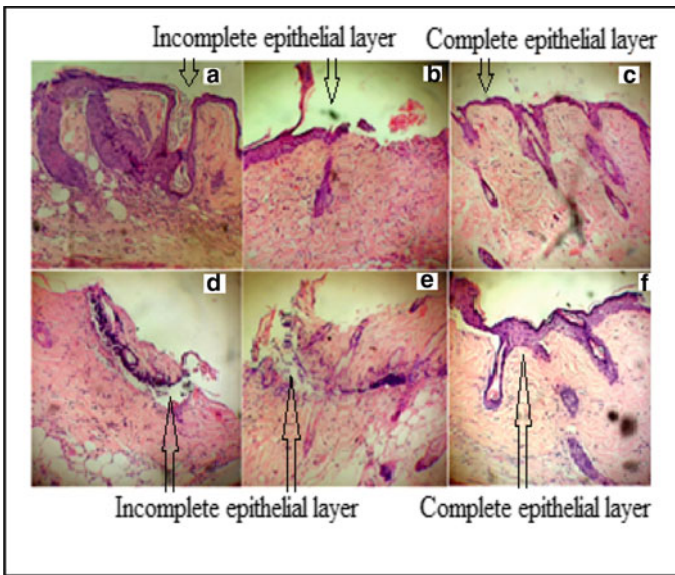


Fig. 2 Histology of skin tissues. a Normal, untreated, b normal, SSD, c normal, AgNPs, d diabetic untreated, e diabetic, SSD, f diabetic, AgNPs

diabetic wounds but on the same day, the percent of wound contraction was 75% in standard drug-treated group which clearly indicated that the silver nanoparticle synthesized using the bark extract had better potential in healing diabetic wound (Fig. 4) supported by both histological as well as SEM results.

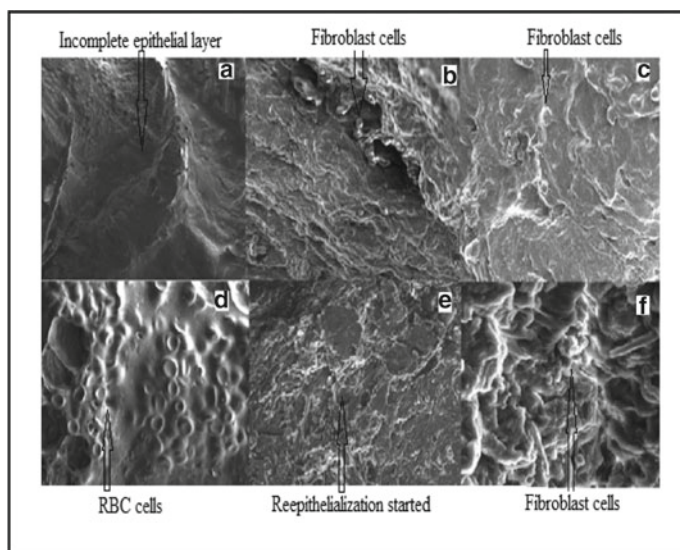


Fig. 3 SEM images of skin samples at 15th day. **a** Normal, untreated, **b** normal, SSD, **c** normal, AgNPs, **d** diabetic untreated, **e** diabetic, SSD, **f** diabetic, AgNPs

Bacterial inhibition zones show that AgNPs are effective antibacterial agents as they cause maximum inhibition zones in agar plates. It is mostly effective for *Staphylococcus gallinarum*, (28 ± 1.2 mm) and for *Bacillus firmus* (26 ± 1.2 mm), in comparison with antibiotic and standard drug (Table 1).

Inflammation is an important factor of wound healing. In case of diabetic mice, the time span becomes extended due to prolonged infection of different bacterial groups. So the potential of pro- and anti-inflammatory cytokines is important for speedy healing of wounds. A vital mediator of anti-inflammatory cascade is IL10. IL-6, TNF- α , IL-1 β are the initiators of events in the physiological alterations of inflammation after thermal injury (Tian et al. 2007). In our study, the graphical representation

Table 1 Zone of inhibition of different bacteria

S. No.	Name of bacteria	Zone of inhibition (approx. in mm)			
		Control	Antibiotic	SSD	AgNPs
1	<i>Staphylococcus soprophyticus</i>	6 ± 1.2	36 ± 11	34 ± 1	35 ± 1.2
2	<i>Bacillus firmus</i>	7 ± 1	10 ± 2.2	8 ± 1.2	26 ± 1.2
3	<i>Bacillus circus</i>	5 ± 1.3	34 ± 2	30 ± 0.5	34 ± 1
4	<i>Staphylococcus sciuri</i>	6 ± 2	36 ± 1.3	25 ± 1	35 ± 2
5	<i>Staphylococcus gallinarum</i>	5 ± 2.08	8 ± 1.2	9 ± 0.8	28 ± 1.2

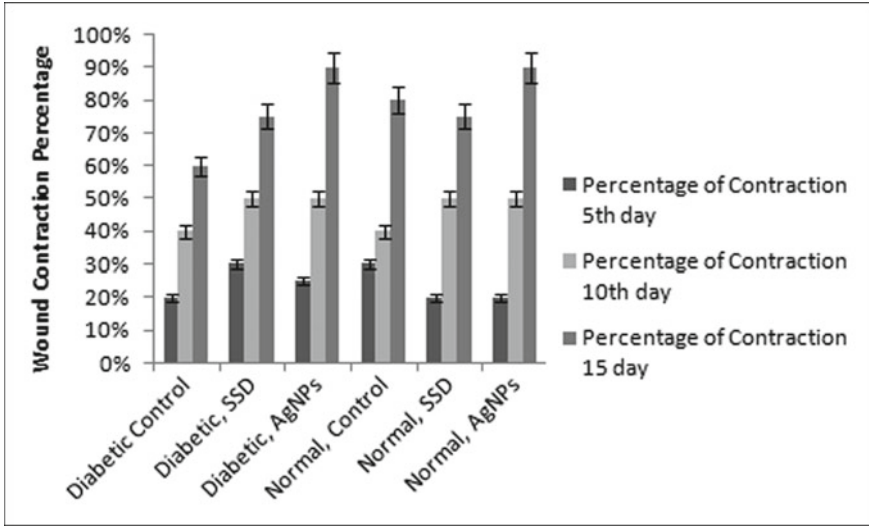


Fig. 4 Percentage of wound contraction

showed that pro-inflammatory cytokines, IL-6, TNF- α , IL-1 β remained downregulated and anti-inflammatory cytokine, IL-10 became upregulated in AgNPs-treated diabetic wound up to 3 days in comparison with standard drug. The lack of the activation process of inflammatory cytokines is important for the scar less quick healing of thermal injury (Fig. 5).

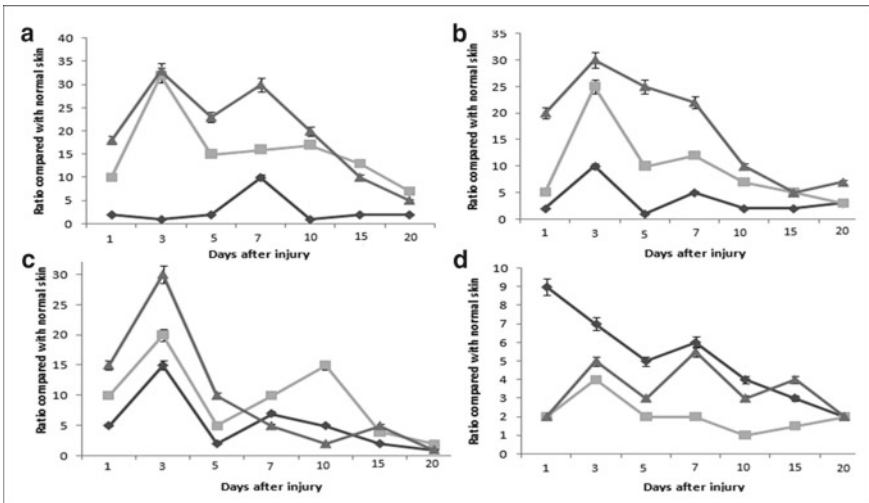


Fig. 5 Cytokine modulation by silver nanoparticle: mRNA levels of a IL-6, b TNF- α , c IL-1 β , d IL-10. \blacklozenge AgNPs \blacksquare SSD \blacktriangle No treatment

4 Conclusion

It can be concluded that silver nanoparticles that are prepared by *S. asoca* bark extract have the ability to heal burn wounds faster than the other synthetic drugs. It also has good antibacterial activity. Due to insignificant toxicity level, the green nanoparticle is eco-friendly and helpful for diabetic wound healing.

Acknowledgements The authors gratefully acknowledge the University of Kalyani for financial support for the research.

References

- Al-Shmgani HS, Mohammed WH, Sulaiman GM, Saadon AH (2017) Biosynthesis of silver nanoparticles from *Catharanthus roseus* leaf extract and assessing their antioxidant, antimicrobial and wound healing activities. *Artif Cells Nanomed Biotechnol* 45:1234–1240
- Banerjee P, Nath D (2015) A phytochemical approach to synthesize silver nanoparticles for non-toxic biomedical page 2 of 14 application and study on their antibacterial efficacy. *Nanosci Technol* 2(1):1–14
- Bhagavathy S, Kancharla S (2016) Wound healing and angiogenesis of silver nanoparticle from *Azadirachta indica* in diabetes induced mice. *IJHM* 4(5):24–29
- Boyum A (1976) Isolation of lymphocytes, granulocytes and macrophages. *Scand J Immunol* 5:9–15
- Chaloupka K et al (2010) Nanosilver as a new generation of nanoparticle in biomedical applications. *Trends Biotechnol* 28:580–588
- Dissemond J, Goos M, Wagner SN (2002) The role of oxidative stress in the pathogenesis and therapy of chronic wounds. *Hautarzt* 53:718–723
- Garg S, Chandra A, Mazumder A, Mazumder R (2014) Green synthesis of silver nanoparticles using *Arnebia nobilis* root extract and wound healing potential of its hydrogel. *J Pharmac* 8(2):95–101
- Goia DV (2004) Preparation and formation mechanisms of uniform metallic particles in homogeneous solutions. *J Mater Chem* 14:451–458
- Griffith M et al (2015) Anti-microbiological and anti-infective activities of silver. In: Alarcon EI (eds) *Silver nanoparticle applications: in the fabrication and design of medical and biosensing devices*. Springer, Berlin, pp 127–146
- Gunasekaran T, Nigusse T, Dhanaraju MD (2011) Silver nanoparticles as real topical bullets for wound healing. *J Am Col Clin Wound Spec* 3:82–96
- Mohanta YK, Biswas K, Panda SK, Bandhyopadhyay J, De D, Jayabalan R, Bastia AK, Mohanta TK (2017) Phyto-assisted synthesis of biofunctionalised silver nanoparticles and their potential anti-oxidant, anti-microbial, and wound healing activities. *IET Nanobiotechnol* 11:1027–1034
- Mollick MMR, Bhowmick B, Mondal D, Maity D, Rana D, Dash SK, Chattopadhyay S, Roy S, Sarkar J, Acharya K, Chakraborty M, Chattopadhyay D (2014) Anticancer (in vitro) and antimicrobial effect of gold nanoparticles synthesized using *Abelmoschus esculentus* (L.) pulp extract via a green route. *RSC Adv* 4:37838–37848
- Ovais M, Ayaz M, Khalil AT, Shah SA, Jan MS, Raza A, Shahid M, Shinwari ZK (2018) HPLC-DAD finger printing, antioxidant, cholinesterase and α glucosidase inhibitory potentials of a novel plant *Olox nana*. *BMC Complement Altern Med* 18(1):1
- Pannerselvam B, Dhamalingam Jothinathan MK, Rajenderan M, Perumal P, Pudupalayam Thangavelu K, Kim HJ, Singh V, Rangarajulu SK (2017) An in vitro study on the burn wound healing activity of cotton fabrics incorporated with phytosynthesized silver nanoparticles in male Wistar albino rats. *Eur J Pharm Sci* 100:187–196

- Pelgrift RY, Friedman AJ (2013) Nanotechnology as a therapeutic tool to combat microbial resistance. *Adv Drug Deliv Rev* 65:1803–1815
- Pozarowski P, Darzynkiewicz Z (2004) Analysis of cell cycle by flow cytometry. *Methods Mol Biol* 281:301–311
- Pothreddy S, Kaliki A, Yegireddy M, Pagadala EP, Prasad TNVKV (2016) Evaluation of wound healing efficacy of chemical and phytogetic silver nanoparticles. *IET Nanobiotechnol* 10:340–348
- Robinson JM (2009) Phagocytic leukocytes and reactive oxygen species. *Histochem Cell Biol* 131:465–469
- Roy A, Ganguly A, Bose Dasgupta S, Das BB, Pal C, Jaisankar P, Majumder HK (2008) Mitochondria-dependent reactive oxygen species-mediated programmed cell death induced by 3,3-diindolylmethane through inhibition of FOF1-ATP synthase in unicellular protozoan parasite *Leishmania donovani*. *Mol Pharmacol* 74:1292–1307
- Shankar S, Jaiswal L, Aparna RSL, Prasad RGSV, Kumar GP, Manohara CM (2015) Wound healing potential of green synthesized silver nanoparticles prepared from *Lansium domesticum* fruit peel extract. *Master Express* 5:159–164
- Sharif MK, Hossain M, Uddin ME, Farooq AO, Islam MA, Sharif MM (2011) Studies on the anti-inflammatory and analgesic efficacy of *Saraca asoca* in Laboratory animals. *Arch Pharm Pract* 2(1):47–52
- Shinwari Z, Renman M, Watanabe T, Yashikawa Y (2006) Medicinal and aromatic plants of Pakistan (a pictorial guide) Kohat University of Science and Technology, Kohat, Pakistan 969-8870-00-8
- Singh NP, McCoy MT, Tice RR, Schneider EL (1988) A simple technique for quantitation of low levels of DNA damage in individual cells. *Exp Cell Res* 175:184–191
- Starlin T, Arul Raj C, Ragavendran P, Gopalakrishnan VK (2012) Phytochemical screening, functional groups and element analysis of *Tylophora pauciflora* weight and arn. *Int Res J Pharm* 3:182–183
- Tian J, Wong KKY, Ho C-M et al (2007) Topical delivery of silver nanoparticles promotes wound healing. *ChemMedChem* 2(1):129–136
- Wang Y, Qiao Y, Wang P, Li Q, Xia C, Ju M (2017) Bio fabrication of silver nanoparticles as an effective wound healing agent in the wound care after anorectal surgery. *J Photochem Photobiol B* 178:457–462
- Wetzler C, Kampfer H, Stallmeyer B, Pfeilschifter J, Frank S (2000) Large and sustained induction of chemokines during impaired wound healing in the genetically diabetic mouse: Prolonged persistence of neutrophils and macrophages during the late phase of repair. *J Investig Dermatol* 115:245–253

Anti-adhering Property Study of Green Nanotechnology Based Modified Chitin Flakes: A Novel Approach Towards Biofilm Eradication



Anindita Chatterjee, Rimashree Baishya, and Soma Banerjee

Abstract Biofilms are complex, heterogeneous, integrated community of surface-attached microorganisms that remain encased within the self-producing extracellular polymeric matrix. In healthcare-associated infections, biofilms are linked to the survival of pathogenic bacteria—*Staphylococcus aureus*, showing antimicrobial resistance. The present work focuses on the anti-adhering property study of silver-coated green nanoparticles against biofilm-forming bacterial population of *Staphylococcus aureus* (ATCC 25923) on modified chitin model. The UV spectroscopy was used to monitor the formation of silver nanoparticles from *Curcuma longa* and *Azadirachta indica* extracts. The bacteria were seeded in TSB media with chitin as the substrate for the biofilm formation. Biofilm inhibition on chitin flakes coated with green nanoparticles and antibiotics (Vancomycin and Gentamycin) were studied and cell counts were observed at intervals from 24 h to 96 h. Morphology of the biofilm architecture on coated chitins was analyzed by SEM and the change in the chemical components was observed by FTIR. The results show the reduction of microbial adhesion by 81% at 24 h and 90–96% at 96 h when chitin flakes are coated with green nanoparticles.

Keywords Silver nanoparticles · Green nanotechnology · Biofilm · Chitin flakes · Anti-adhering activity

A. Chatterjee · R. Baishya · S. Banerjee (✉)
Department of Biotechnology, Heritage Institute of Technology, Anandapur, Chowbaga, Kolkata,
West Bengal 700107, India
e-mail: somabanerjee2005@gmail.com

A. Chatterjee
e-mail: aninditachatterjee.91@gmail.com

R. Baishya
e-mail: reemaorbabu@gmail.com

1 Introduction

Biofilm is a bacterial population that remains enclosed by an extracellular polymeric substance (EPS), which confers stability of the biofilm structure, inhibits the penetration of antibiotics through the biofilms and leads to the pathogenesis of biofilm-associated infections and antibiotic resistance (Davies 2003; Fux et al. 2005). Biofilms of *S. aureus* are difficult to treat with antibiotics due to the formation of EPS and play an important role in healthcare-associated infections and also those related to medical devices (Stoodley et al. 2004; Costerton et al. 1999; Khatoun et al. 2018). As increased tolerance of biofilms to antibiotics makes its eradication difficult therefore there is a need to develop an alternative therapeutic method for the treatment of various infections. Nanotechnology is an emerging technological advancement in the present years due to its applications in various science fields. Among the different types of nanomaterials produced, silver nanoparticles have proved to be an excellent antimicrobial agent. Green nanotechnology facilitates the manufacture of nanotechnology-based products that are eco-friendly with sustainable commercial viability. The present work aims at the simple and reproducible method of biofilm inhibition by coating the chitin flakes with green nanoparticles (*Curcuma longa* and *Azadirachta indica*) in the concentration range of 1 mg–50 mg/ml.

2 Materials and Methods

2.1 Materials and Bacterial Strains

All the chemicals used for the experiments were purchased from Himedia, India and silver nitrate from Merck India. The bacterial strain *Staphylococcus aureus* (ATCC) was purchased from Himedia.

2.2 Synthesis of Green Nanoparticles

Green nanoparticles were synthesized with *C. longa* and *A. indica* plant extracts using 0.01M AgNO₃ at 25 °C (Shameli et al. 2012) and 0.001 M AgNO₃ at 45 °C (Roy et al. 2017), respectively, and were characterized by UV–vis spectrophotometer and were confirmed by SEM analysis.

2.3 Determination of Minimum Inhibitory Concentration (MIC)

The MIC of antibiotics (Vancomycin and Gentamycin) against *S. aureus* ATCC 25923 was determined by CLSI (2019) guidelines while those of crude *C. longa* and *A. indica* plant extracts and the synthesized green nanoparticles were determined by Kirby–Bauer disk diffusion technique.

2.4 Modification of Chitin Flakes with Antibiotics and Green Nanoparticles

Based on the MIC, chitin flakes were encrusted with antibiotics, crude extracts of *C. longa* and *A. indica* and green nanoparticles at 1 mg–50 mg/ml concentration for a certain period of time and then used for testing.

2.5 Effect of Green Nanoparticle on Biofilm Formation

S. aureus ATCC 25923 biofilm was developed on chitin flasks by standard protocol (Anderl et al. 2000). The bacterial culture was inoculated into Tryptic Soy Broth and incubated overnight aerobically at 37 °C for 18 h. The overnight culture with a concentration of 1×10^6 CFU/ml was inoculated into sterile TSB with normal and encrusted chitin flakes and incubated at 37 °C for 24 h, 48 h, 72 h, and 96 h. The chitin flakes were then washed with 0.9% saline by agitation at 180 rpm for 2 min to remove non-adherent cells. Viable counts were determined by inoculating the biofilm cells on TSA plates and incubated overnight at 37 °C (Gomes et al. 2012). SEM was used to analyze the morphology of the biofilm structure on encrusted chitins and the change in the chemical components was observed by FTIR.

3 Result

3.1 UV Analysis of Synthesized Green Nanoparticles

Ultraviolet–visible (UV–vis) absorption spectroscopic analysis showed the formation of silver nanoparticles from *C. longa* and *A. indica* extracts at a range of 300–800 nm with a prominent peak at 429 and 420 nm (Fig. 1). Kumar et al. (2014) had reported similar peak of silver nanoparticles was around 420 nm, and in the present study, it was centered at 420–430 nm.

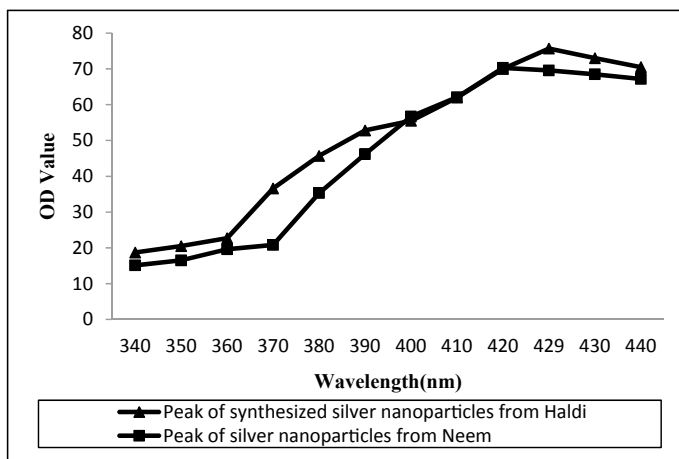


Fig. 1 UV-spectroscopic analysis of silver nanoparticles of *C. longa* and *A. indica*

3.2 Determination of Minimum Inhibitory Concentration (MIC)

The MIC of crude plant extracts was 150 mg for *C. longa* and 180 mg for *A. indica* whereas the MIC of synthesized green nanoparticles against the biofilm-forming *S. aureus* ATCC 25923 was 0.08 mg and 0.15 mg, respectively, for *C. longa* and *A. indica*. It was evident from the study that green nanoparticles showed significantly lower MIC values as compared with crude plant extracts.

3.3 Effect of Green Nanoparticle on Biofilm Formation

The biofilm inhibition of green nanoparticles of both *C. longa* and *A. indica* was compared from 24 h to 96 h old isolates. Microbial adhesion was reduced by 81% (8.78 log CFU/ml) at 24 h and 90–96% (7.51 log CFU/ml) at 96 h and by 72% (8.98 log CFU/ml) at 24 h and 80% (8.42 log CFU/ml) at 96 h when chitin flakes were coated with silver nanoparticles from *C. longa* and *A. indica* at 2 mg/ml concentration as compared with control and antibiotics (Fig. 2).

The Scanning Electron Microscopy (SEM) (Fig. 3) confirms the morphological variation of modified chitin flakes toward inhibition of biofilm formation. It shows the presence of various-shaped (tetragons, pentagons, hexagons) nanoparticles on the modified chitin flakes with size ranging from 10 to 80 nm (Fig. 3b). The FTIR spectra obtained for modified chitin (Fig. 4b) show a rapid increase in peak formation than the control (uncoated chitin) due to peaks at 1652 cm^{-1} (amide II band N–H

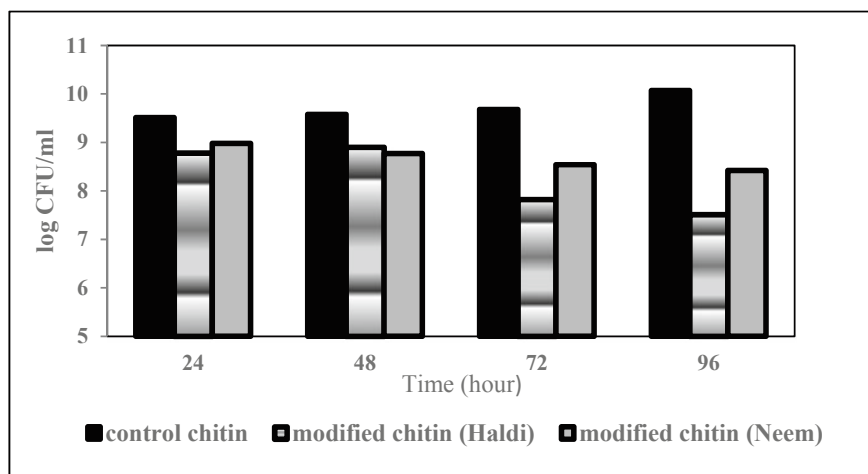


Fig. 2 Biofilm Inhibition by modified chitin at different time intervals

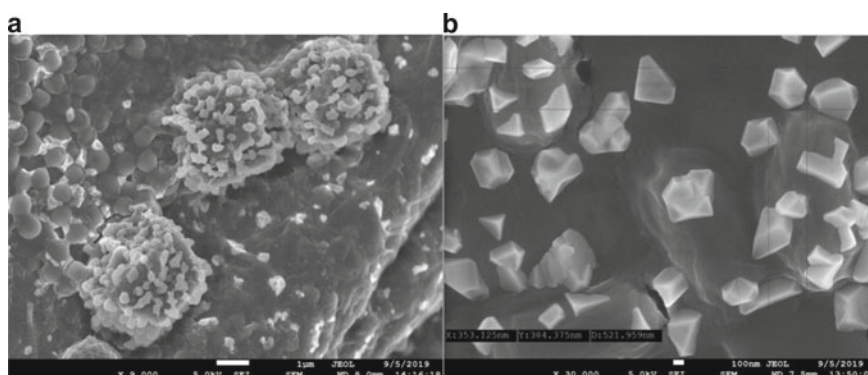


Fig. 3 SEM confirming biofilm formation on chitin flakes at 9000 \times (a) and the nanoparticle structure on coated chitin flakes at 30,000 \times (b)

stretching), 1425 cm^{-1} (asymmetrical C–H bending of the CH_2 group) and 1066 and 1024 cm^{-1} (O-bridge stretching) representing the glucosamine residue.

Antibiotic treatment is not sufficient enough to combat healthcare-associated infections (HAIs), especially those related to the implant of medical devices. Therefore, it is necessary to observe whether green nanoparticles are best suited for biofilm inhibition than antibiotics. It was observed that when *S. aureus* was incubated with chitosan-coated iron oxide nanoparticles, there was a sudden decrease in viable bacteria numbers and biomass formation (Shi et al. 2016), moreover, chitin/Ag NP composites have high bactericidal activity (Bguen et al. 2013). Silver nanoparticles itself have high antimicrobial activity against both Gram-positive (*S. aureus*) and Gram-negative bacteria (*E. coli*) (Vu et al. 2018). Similar results of minimum viable

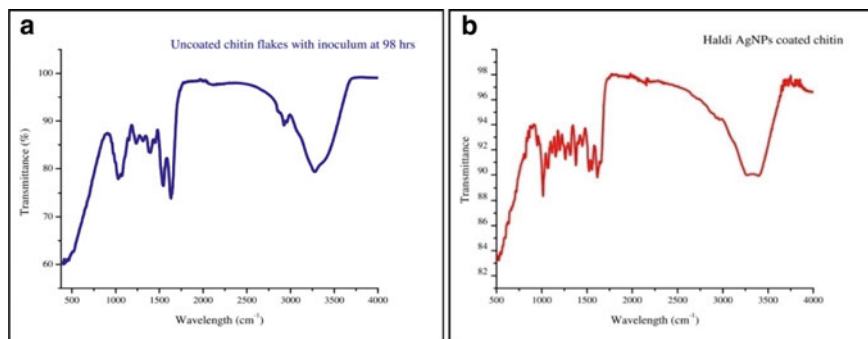


Fig. 4 FTIR confirming the change in chemical change of biofilm structure **a** uncoated chitin flakes and **b** modified chitin (Haldi AgNPs coated)

bacterial numbers were obtained in the present work when green nanoparticle-coated chitin flakes were used against biofilm-forming *S. aureus* ATCC 25923.

4 Conclusion

The results show that green nanoparticles synthesized from *C. longa* extracts are more effective in biofilm inhibition at a low dose than those synthesized from *A. indica* extracts. While on the other hand, antibiotics vancomycin and gentamycin require a high dose to inhibit biofilm formation. The following study helps us to study the biofilm inhibition pattern of antibiotics and green nanoparticles by a simple method. This study pattern can be applied to inhibit biofilm formation in medical devices with minimum cost effects.

References

- Anderl JF, Franklin MJ, Stewart PS (2000) Role of antibiotic penetration limitation in *Klebsiella pneumoniae* biofilm resistance to ampicillin and ciprofloxacin. *Antimicrob Agents Chemother* 44(7):1818–1824
- Bguen VQ, Ishihara M, Nakamura S, Hattori H, Ono T, Miyahira Y, Matsuri T (2013) Interaction of silver nanoparticles and chitin powder with different sizes and surface structures: the correlation with antimicrobial activities. *J Nanomater* 467534:1–9
- Costerton JW, Stewart PS, Greenberg EP (1999) Bacterial biofilms: a common cause of persistent infections. *Science* 284:1318–1322
- Davies D (2003) Understanding biofilm resistance to antibacterial agents. *Nat Rev Drug Discov* 2:114–122
- Fux CA, Costerton JW, Stewart PS (2005) Survival strategies of infectious biofilms. *Trends Microbio* 13:34–40

- Gomes F, Teixeira P, Ceri H, Oliveira R (2012) Evaluation of antimicrobial activity of certain combinations of antibiotics against in vitro *Staphylococcus epidermidis* biofilms. *Indian J Med Res* 135(4):542–547
- Khatoon Z, McTiernan CD, Suuronen EJ, Mah TF, Alarcon EI (2018) Bacterial biofilm formation on implantable devices and approaches to its treatment and prevention. *Heliyon* 4(12):e01067, 1–36
- Kumar DA, Palanichamy V, Roopan SM (2014) Green synthesis of silver nanoparticles using *Alternanthera dentata* leaf extract at room temperature and their antimicrobial activity. *Spectrochim Acta Part A Mol Biomol Spectrosc* 127:168–171
- Roy P, Das B, Mohanty A, Mohapatra S (2017) Green synthesis of silver nanoparticles using *Azadirachta indica* leaf extract and its antimicrobial study. *Appl Nanosci* 7(8):843–850
- Shameli K, Ahmed MB, Zamanian A, Sangpour P, Shabanzadeh P, Abdollahi Y, Zargar M (2012) Green biosynthesis of silver nanoparticles using *Curcuma longa* tuber powder. *Int J Nanomed* 7:5603–5610
- Shi SF, Jia JF, Guo XK, Zhao YP, Chen DS, Guo YY, Zhang XL (2016) Reduced *Staphylococcus aureus* biofilm formation in the presence of chitosan-coated iron oxide nanoparticles. *Int J Nanomed* 11:6499–6506
- Stoodley LH, Costerton JW, Stoodley P (2004) Bacterial biofilms: from the natural environment to infectious diseases. *Nat Rev Microbiol* 2:95–108
- Vu XH, Duong TTT, Pham TTH, Trinh DK, Nguen XH, Dang VS (2018) Synthesis and study of silver nanoparticles for antibacterial activity against *Escherichia coli* and *Staphylococcus aureus*. *Adv Nat Sci: Nanosci Nanotechnol* 9:025019, 7

Modern Advancement of Nanotechnology Over Conventional Drug Therapies



Tania Pal, Bhuban Ruidas, and Chitragada Das Mukhopadhyay

Abstract Conventional drug therapies have a lot of drawbacks such as limited drug solubility, poor biodistribution, lack of selectivity, and unfavorable pharmacokinetics. Nanotechnology has been proved to be an excellent platform for overcoming these challenges, which mainly deals with measuring, imaging, modeling, and manipulating matter at a length of nanometer scale. A zero-dimensional (0D) structure and small diameter (<10 nm) are the most desired nature of a matter for providing the significant biological as well as therapeutic results. Herein, we have discussed the importance of nanobiotechnology in targeted diagnosis and treatment against various diseases using nanoscale drug carriers. Some of the threatening diseases targeting by direct drug delivery are quite difficult due to the inability in specific target identification and carrying capacity. Based on proof of concept, the carbon nano-onions (CNO) is one of the most efficient nanocarrier systems as it is highly capable of acting as a platform for the attachment of several targeted drugs, ligands, or both to encounter the diseases more efficiently. Again, the CNO-conjugated drug and ligand delivery are less studied at the early stage of development. In this scenario, our primary goal is to explore the future possibilities of CNO along with our present findings. We have further elaborated and illustrated the art of this emerging field as the most promising carrier system for therapeutic target.

Keywords Conventional drug therapies · Pharmacokinetics · Nanobiotechnology · Carbon nano-onions · Therapeutic

T. Pal · B. Ruidas · C. Das Mukhopadhyay (✉)
Centre for Healthcare Science and Technology, Indian Institute of Engineering Science and
Technology, Shibpur, Howrah 711103, West Bengal, India
e-mail: chitragadadas@yahoo.com

T. Pal
e-mail: taniapal58@gmail.com

B. Ruidas
e-mail: bhubo18@gmail.com

© Springer Nature Singapore Pte Ltd. 2021
D. Ramkrishna et al. (eds.), *Advances in Bioprocess Engineering and Technology*,
Lecture Notes in Bioengineering,
https://doi.org/10.1007/978-981-15-7409-2_50

1 Introduction

Cancer is the leading cause of death costing millions of people their lives globally despite the efforts made to alleviate its preponderance. The conventional standard for cancer treatment includes surgical removal of the tumor along with chemotherapy, radiotherapy, etc., which have low efficiency and cause serious side-effects such as toxicity and limited biodistribution due to their poor pharmacokinetic characteristics (Naidu et al. 2004). To solve the concerns mentioned earlier, there is an exponential rise in the use of nanotechnology to develop effective diagnostic and therapeutic platforms. Nanomaterials made from organic, inorganic, protein, and lipids can incorporate a variety of bioactive agents and are capable of crossing biological barriers and selectively target the malignant cells and deliver anticancer drugs through the sustainable release of the drug. Pharmacokinetics and pharmacodynamics profiles can also be controlled, enhancing the accumulated drug concentration at tumor sites. Moreover, nanocarriers can be loaded with multidrug for synergistic activity (Navya and Daima 2016). When NPs enter the cell via receptor-mediated endocytosis avoids recognition by P-glycoprotein, one of the critical drug resistance mechanisms (Larsen et al. 2000). These are few reasons among the others that show nanotechnology is revolutionizing the field of drug delivery and cancer therapeutics.

Herein, we have tried to give a brief illustration of the advancement of nanotechnology over the conventional method used so far.

2 Nanotechnology and Future Possibilities

Nanotechnology mainly deals with the engineered functional system at a molecular scale. Sometimes, nanotechnology is quite capable to formulate new devices and materials with a broad range of applications, such as nanoelectronics, nanomedicine, biomaterials for energy productions, and so on. Also, the potential of nanomaterials for biomedical applications is largely dependent on its surface charge, shape, and size as it directly affects the nano–bio interface interaction and aids in internalization and cellular endocytosis of the nanocarriers. Again, designing nanocarriers is a sophisticated process that has to meet certain requirements to be an efficient drug delivery system. Further, negatively charged nanoparticles accumulate at tumor sites efficiently whereas positively charged nanocarriers are internalized more efficiently due to negatively charged cell membranes. Further, surface chemistry plays a crucial role in designing nanomaterial as the biological impact of the nanoparticle can be controlled by chemical modifications restraining cellular interactions, thus reducing potential side effects. Surface conjugation with ligands such as antibodies, aptamers, oligosaccharides, peptides, etc. can alter the fate of nanomaterial, hence it is important to carefully examine them after surface conjugation to measure the increased sensitivity and specificity as well as to avoid toxic effects postmodification (Sied et al. 2019). Therefore, the introduction of engineered nanomaterials is the best choice to

achieve target-specific action and avoid unwanted uptake by healthy cells without any major toxic effects. Further, nanotechnology enhanced the target specificity along with controlled and sustained drug release, which is one of the major advancements over conventional drug treatment.

3 Therapeutic Barrier and Targeting

Nanomaterials have to cross various barriers to reach their target, like intestinal barrier and blood–brain barrier. To solve this problem, nanocarriers must be soluble or colloidal in aqueous solution and be made of biocompatible material that can be easily functionalized. It should have a long half-life and shelf life with a low rate of aggregation and shows high intake in cancer cells compared with healthy cells. The treatment is effective only when the proper dose is provided and shows maximum activity in the tumor cells. Thus it can become inefficient since the effect of anticancer drugs is mitigated by increasing time for the drug to reach the target. The nanomaterials should be capable of delivering the drugs in and around the cancer cells and increase its local concentration, thus reducing toxicity toward normal cells. Thereby an effective target selection prior to disease treatment is always the top precedence in nanotechnology that can be achieved successfully via both active and passive targeting.

3.1 Active and Passive Targeting

Active targeting mainly indicates the direct action at targeted location that are well programmed to bind to specific receptor molecules such as proteins, carbohydrates, lipids expressed on the diseased cells, or molecules present in its microenvironment or the physicochemical environment surrounding the targeted disease or malfunctioning system. This approach also known as active targeting or ligand-mediated targeting that involves affinity-based recognition, facilitated intake, and retention in the cells. Taking into account the complexity of routes for nanoparticle administration and its interactions with various cells in the body, the differences in the affinity toward the cancerous and normal cells cannot be the basis for efficient and successful drug delivery to the target cells by the nanoparticles. Thus, a single nanocarrier is conjugated with multiple ligands for targeting multiple receptors. However, for using active targeted anticancer platforms, multiple factors including ligand density on the nanoparticle surface and affinity between the carrier and the target need to be optimized. Sometimes non-internalization of the nanocarrier is desired for bystander effect, due to which solid tumors lacking the specific receptors can be killed by the release of drug at the surface of neighboring cells that can bind with carriers. Contrary to the belief that a higher number of ligands will facilitate stronger binding, it has been observed that ligand density does not increase the affinity toward the target

due to improper ligand orientation, bond constraints, molecular saturation, steric constraints from neighboring cells. Similarly, higher binding affinity in solid tumors decreases binding efficacy due to the “binding site barrier” caused by a decrease in penetration of nanocarriers due to strong binding with the target (Rosenblum et al. 2018).

In passive targeting, drug-encapsulated nanocarriers are generally administered via intravenous injection circumventing absorption in intestinal epithelium that is imperative via oral administration for enhancement of permeability and retention effect (EPR effect), forms the basis of passive targeting. Generally, tumors are characterized by poor lymphatic function, which does not clear the accumulating nanoparticles rapidly in the tumor interstitium, and leaky vessels that enable the nanocarriers to extravasate into the tumor site (Rosenblum et al. 2018). Again, certain drugs are incapable of diffusing efficiently making it difficult to target cells within the target site. Thus, controlling the random nature of the approach is arduous, failing to which induces multiple drug resistance (MDR) leading to the failure of the treatment.

4 Nanomaterials and Drug Delivery

Nanoparticles consisted of organic and inorganic materials are being developed for a wide range of applications ranging from imaging to treatment. Here, we discuss various nanocarriers that are being widely used in nanotherapeutics.

4.1 *Organic Nanomaterials*

A significant characteristic of any nanomaterial for drug delivery is its biocompatibility and biodegradability, thus making organic nanomaterials a promising candidate for these systems.

The use of nanomaterials as a drug delivery vehicle was started with liposomes in 1965. They are spherical colloids made by self-assembling of lipid bilayers of either natural or synthetic phospholipids surrounding a central aqueous space, called liposome, which are truly advantageous for carrying desired drugs and other molecules in the aqueous core or lipid bilayer to the target site without any severe side effects. Various drugs have been delivered using PEGylated liposomes in the treatment of glioma and breast cancer. Newer generations of smart multifunctional liposomes are being developed despite extensive research and preclinical development, but FDA has approved very few drugs encapsulated in liposomes (Olusanya et al. 2018).

Further, drug delivery via active or passive targeting can be efficiently achieved using polymeric nanoparticles. Targeting cells using polymeric nanocarriers helps in drug delivery in high concentrations within the cell. Several studies using ligands such as peptides, antibodies, and aptamers to target tumor cells have been demonstrated to show higher anticancer activity. The outset of utilizing biodegradable polymer as a

delivery vehicle by conjugating with drugs started with Poly-L-glutamic acid (PGA). Several drugs that are used clinically have been conjugated with PGA and tested in vitro and in vivo and showed to have better effects than its free drug counterparts (Ekladiou et al. 2019). Polymer micelle is gaining tremendous interest as nanocarrier owing to their unique characteristics like increasing the solubilization of hydrophobic drugs, protecting cargos from degradation by enzymes, and sustained release of drugs. Temozolomide (TMZ) and anti-Bcl-2 siRNA were packed in a polymeric micelle conjugated with folic acid to surpass the blood–brain barrier and efficiently prevent growth in resistant glioma cells (Aziz et al. 2017).

The anticancer drugs are encapsulated in dendrimers (polymeric macromolecules) or are functionalized on their surface. They reduce toxicities toward normal cells and improve drug delivery and bioavailability and increase drug stability. In that regard, CXCR4-targeted dendrimer has been developed for breast cancer therapy. Polyamine amide dendrimer encapsulating doxorubicin and conjugated with the linear type of FC131 showed enhanced cytotoxicity against cancer cell lines (Anitha et al. 2018). For nanobiotechnological applications of drug delivery and tissue targeting, a variety of viruses and bacteriophages have been developed. Viruses such as canine parvovirus have a natural affinity for transferrin receptors present on various cancer cells. VLPs are a promising alternative drug delivery nanoparticle derived from protein coats of viral capsids typically lacking their natural genome and thus are noninfectious. They can pack and deliver anticancer drugs, proteins, siRNA, and RNA aptamers, having the potential to overcome the limitations of other nanomaterials. However, there are still challenges like stability and avoiding phagocyte mediated clearance (Aljabali 2018).

4.2 *Inorganic Nanoparticles*

Currently, the majority of drug delivery systems are using inorganic nanomaterials due to their meticulous control of shape and size, controlled surface chemistry, tunable physicochemical properties that can be functionalized using a variety of molecules. A large number of inorganic nanomaterials including metal and metal oxide-based nanoparticles and carbon-based nanomaterials have been developed and used in cancer treatment and management.

4.2.1 **Metal-Based Nanomaterial**

Metal-based antitumor drugs play a relevant role in antitumor chemotherapy. To target alternative mechanism of action, new metallodrugs that function in the biological systems were developed. The introduction of platinum-based metallodrugs cisplatin has paved the way for anticancer therapeutics (de Menezes et al. 2019). Although, long-time research has been done on copper compounds with the assumption that endogenous metals are less toxic and it can inhibit proteasome as well as

induce oxidative stress hampering several cellular processes. The Cu(II) compounds strongly promote the apoptosis of cancer cells through the intrinsic ROS-mediated mitochondrial pathway accompanied by the regulation of Bcl-2 family proteins. Thus, combining copper with organic compounds has shown high anticancerous properties (Mandal 2017). The metal nanostructure of Au, Ag, Zn, Mn is also widely used as a delivery vehicle. In a recent report, doxorubicin-loaded Au particles showed sustained and pH-dependent release of drugs and decrease in tumor size (Aminabad et al. 2019). Similarly, Ag nanoparticles are used as anticancer agents against multiple cancers, helping in delivering anticancer drugs to enhance the therapeutic index of the drug. Ag nanoparticles, when combined with phytopharmaceuticals, act as nontoxic contrast agents, photothermal agents, and delivery vehicles for cancer therapy (Burduşel et al. 2018).

4.2.2 Carbon-Based Nanomaterial

Carbon nanomaterials exhibit very intriguing properties among nanoparticles like lightweight, high chemical resistance, and exceptional mechanical properties and are thus widely used for imaging, delivery, and diagnosis purpose. They also have a great variety of morphologies ranging from 0D (carbon nano-onions) to 1D nanotubes and 2D nanosheets. Most commonly studied carbon nanomaterials are carbon nanotubes (CNT), carbon nanohorns, graphene and its derivatives, nanodiamonds, to name a few. CNTs are effective anticancer drug delivery vehicles and for co-delivery of drugs at cancer sites with the potential of treating multidrug-resistant cells. Multiwalled CNT nanoplatforms with prolonged circulation time and high-cargo capacity with active targeting have been developed showing potential multimodal platforms for cancer therapeutics. CNT-based phototherapies can be utilized for intracellular drug delivery. Graphene and its derivatives are widely used in cell imaging, biosensing, drug, and gene delivery. Paclitaxel-encapsulated PEG-GO showed higher toxicity against A549 cells compared with free paclitaxel (Patel et al. 2016).

Carbon nano-onions (CNO) are an emerging class of carbon nanomaterials that have gained interests due to its unique properties like large surface to volume ratio and low density. It is made up of multiple graphene layers surrounding a fullerene core with an interlayer distance of about 0.34 nm. CNOs showed excellent biocompatibility suggesting they are not cytotoxic and thus appropriate for biological applications. CNOs used in *in vivo* studies of prokaryotic and eukaryotic studies also revealed that it has no toxic effects on any of them thus affirming its biocompatibility. They can also cross the blood–brain barrier and thus can be used for neurobiomedicine. In one of the studies, CNOs conjugated with fluorescein were injected in the hippocampal region of mice brain and showed no significant increase in neuroinflammatory response. Cysteine-functionalized CNOs carrying maleimide demonstrated its ability to deliver protein and glycopeptides intracellularly without any adverse effect. Even in comparative studies against other carbon nanomaterials, carbon nano-onions showed better biocompatibility with better drug deliverance

capability, thus proving CNO to be an ideal imaging and drug-targeting vehicle (Camisasca and Giordani 2017).

5 Combinational Therapy

It has been evidenced that multiple-drug treatment is more efficient than single-drug treatment. It is predicted that when multiple drugs are administered in an optimized ratio, they show a synergistic effect on the cancer cells. They not only enhance drug targeting, but also prolong circulation time and reduce drug resistance in cancer cells. Recent advancements in this field have developed various nanocarriers for co-delivery of anticancer drugs (Pemovska et al. 2018). Thus, using a theranostic approach of combining both diagnosing and treating cancer is an emerging platform through which not only the drug released can be studied, but also its effects on the cancerous cells are visualized. These abilities can be potentially exploited to develop personalized medicines (Ahmed et al. 2012).

6 Conclusion

Since several factors affect the biodistribution and targeting, it is difficult to choose an appropriate nanocarrier based on a few existing comparative studies. To evaluate the ideal properties of nanocarriers, further studies need to be done based on various screening methodologies. Utilizing specific nanocarrier or targeting molecule for improved therapeutic outcomes and reduced costs may be available to the oncologists. Though we are far from Nobel Laureate Paul Ehrlich's 'magic bullet', it is possible to believe in an era of nanocarrier-based therapeutics and diagnostics.

References

- Ahmed N, Fessi H, Elaissari A (2012) Theranostic applications of nanoparticles in cancer. *Drug Discov Today* 17:928–934
- Aljabali AAA (2018) Viral nanoparticles: a drug delivery platform. *J Drugs Ecotoxicol* 1
- Aminabad NS, Farshbaf M, Akbarzadeh A (2019) Recent advances of gold nanoparticles in biomedical applications: state of the art. *Cell Biochem Biophys* 77:123–137
- Anitha P, Bhargavi J, Sravani G et al (2018) Recent progress of dendrimers in drug delivery for cancer therapy. *Int J Appl Pharm* 10:34
- Aziz ZABA, Ahmad A, Mohd-Setapar SH et al (2017) Recent advances in drug delivery of polymeric nano-micelles. *Curr Drug Metab* 18:16–29
- Burdușel A-C, Gherasim O, Grumezescu AM et al (2018) Biomedical applications of silver nanoparticles: an up-to-date overview. *Nanomaterials* 8:681
- Camisasca A, Giordani S (2017) Carbon nano-onions in biomedical applications: promising theranostic agents. *Inorganica Chim Acta* 468:67–76

- de Menezes BRC, Rodrigues KF, da Fonseca BCS et al (2019) Recent advances in the use of carbon nanotubes as smart biomaterials. *J Mater Chem B* 7:1343–1360
- Ekladious I, Colson YL, Grinstaff MW (2019) Polymer–drug conjugate therapeutics: advances, insights and prospects. *Nat Rev Drug Discov* 18:273–294
- Larsen AK, Escargueil AE, Skladanowski A (2000) Resistance mechanisms associated with altered intracellular distribution of anticancer agents. *Pharmacol Ther* 85:217–229
- Mandal A (2017) Copper nanomaterials as drug delivery system against infectious agents and cancerous cells. *J Appl Life Sci Int* 15:1–8
- Naidu MUR, Ramana GV, Rani PU et al (2004) Chemotherapy-induced and/or radiation therapy-induced oral mucositis—complicating the treatment of cancer. *Neoplasia* 6:423–431
- Navya PN, Daima HK (2016) Rational engineering of physicochemical properties of nanomaterials for biomedical applications with nanotoxicological perspectives. *Nano Converg* 3:1
- Olusanya TOB, Haj Ahmad RR, Ibegbu DM et al (2018) Liposomal drug delivery systems and anticancer drugs. *Molecules* 23:907
- Patel SC, Lee S, Lalwani G et al (2016) Graphene-based platforms for cancer therapeutics. *Ther Deliv* 7:101–116
- Pemovska T, Bigenzahn JW, Superti-Furga G (2018) Recent advances in combinatorial drug screening and synergy scoring. *Curr Opin Pharmacol* 42:102–110
- Rosenblum D, Joshi N, Tao W et al (2018) Progress and challenges towards targeted delivery of cancer therapeutics. *Nat Commun* 9:1410
- Sied M, Filli, Abdalla A et al (2019) The impact of physicochemical characteristics on therapeutic efficacy of anticancer nanomaterials: a review. *Int J Pharm Sci Drug Res* 11